BIOMECHANICS OF THE FOREFOOT

Thesis presented for the Degree of Doctor of Philosophy

by

Hilaire A.C. Jacob, Masch. Ing. HTL

Bioengineering Unit
University of Strathclyde
Glasgow

May 1989

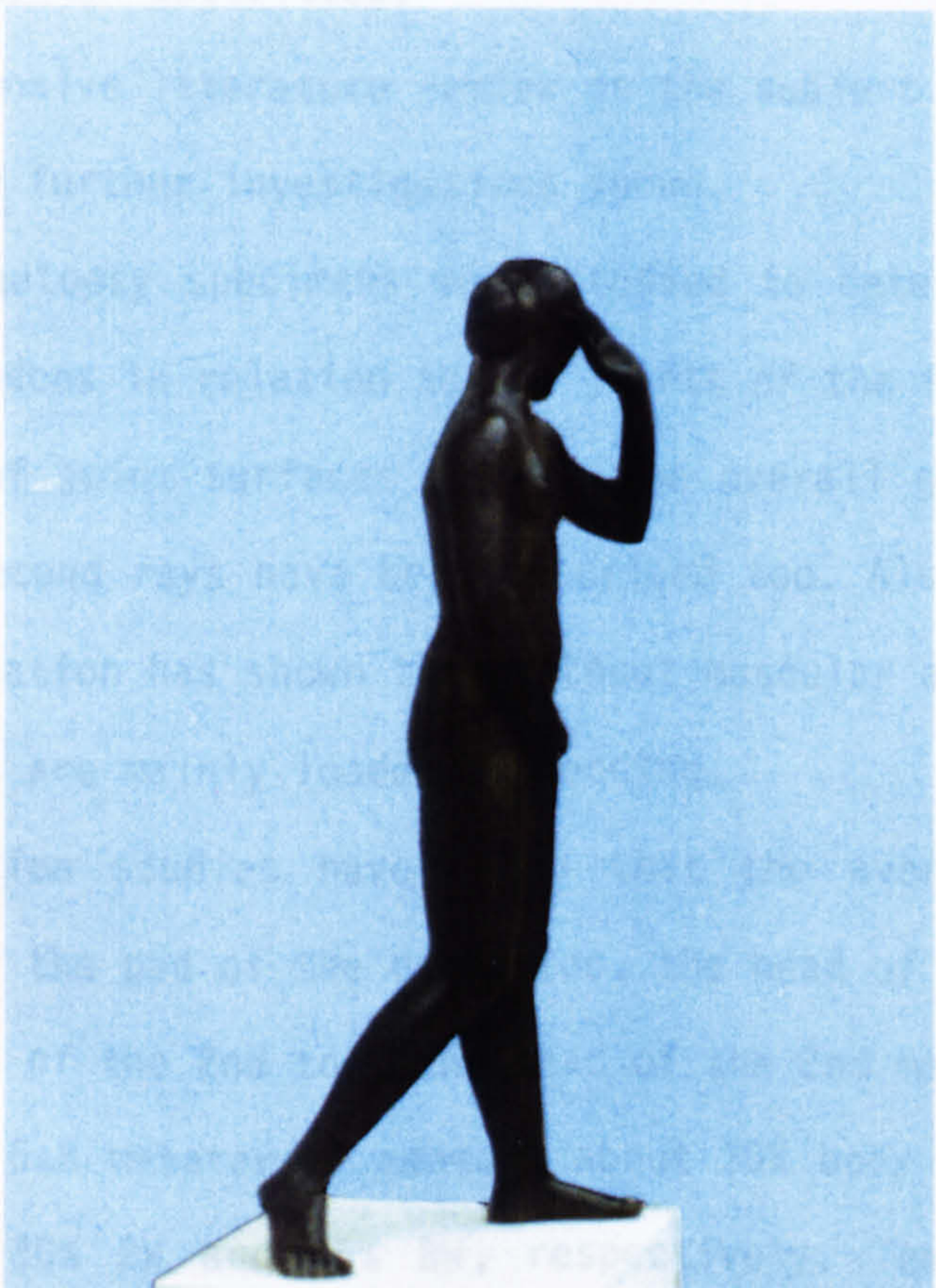

'Die Schreitende' or 'Striding woman'

Bronze sculpture by the impressionist
Hermann Haller (1880 - 1950)

Oskar Reinhart Art Collection, Winterthur

ABSTRACT

The work reported in this thesis was carried out to investigate the kinematic and dynamic behaviour of the forefoot during normal locomotion activities.

An extensive literature review on the subject is presented and the need for further investigations shown.

Fresh autopsy specimens were studied to determine the course taken by tendons in relation to the joints of the forefoot, and the topography of joint surfaces mapped. The overall geometries of the first and second rays have been described too. Also, an experimental investigation has shown that without muscular activity the metatarsal bones are mainly loaded in bending.

Locomotion studies have shown that the average peak ground forces under the pad of the great toe, the head of the 1st metatarsal, the pad of the 2nd toe, the head of the 2nd metatarsal and the head of the 5th metatarsal measure about 30% body weight (BW), 15% BW, 6% BW, 30% BW and 15% BW, respectively. Temporal graphs of these forces show their behaviour during the gait cycle. Furthermore, the magnitudes of these forces when wearing shoes with stiff soles, when climbing up and down stairs, as well as when walking up and down a slope of 15° are reported.

Based on the external forces measured, the internal forces acting along the flexor tendons and across joint surfaces of the 1st and 2nd rays during gait are estimated. The stresses that thereby develop in the shanks of the metatarsal bones indicate that the 1st metatarsal bone is subjected mainly to compression while the 2nd metatarsal bone is exposed to a high degree of bending.

The relationship between the results of this study and clinical problems is considered and especially a hypothesis has been advanced to explain how under edge-loading conditions localised necrosis of the metatarsal heads could occur, thus giving rise to Koehler-Freiberg's disease.

ACKNOWLEDGEMENTS

The work presented in this thesis was carried out in the Biomechanic Laboratories of the Department of Orthopaedic Surgery, Balgrist, University of Zurich, and I am very grateful to Professor A. Schreiber for the use of these facilities. It was also he who suggested that I embark on this project and gave me all the support I needed from this end.

Professor J.P. Paul and Dr. A.C. Nicol supervised the project and I am very thankful to them for all their advice and encouragement.

Thanks are also due to Mr. R. Richter and Mr. J. Steinmann for their assistance during the experimental work. I would also like to express my gratitude towards Mr. F. Lottenbach and Mr. M. Schaerlig who carried out part of the gait studies reported in this thesis.

To Mrs. H. Bilfinger I owe very special thanks for her untiring efforts in typing this thesis, a feat that can only be fully appreciated by those acquainted with my handwriting.

Dr. H. Zollinger needs special mention since it was through his ardent interest in the foot that I got introduced to this subject. I am also grateful to him for bringing me in touch with some of the clinical manifestations of foot disorders.

I would also like to thank all those physiotherapists of 'Balgrist' who readily volunteered as test subjects and thereby contributed significantly to the material reported.

Special thanks are due to my wife, Erika, without whose continuous encouragement and gentle pushing, this work might still not have been completed.

The project was financed partly by the Research Council of the Schweizerischer Verein Balgrist to whom I am particularly indebted.

May 1989

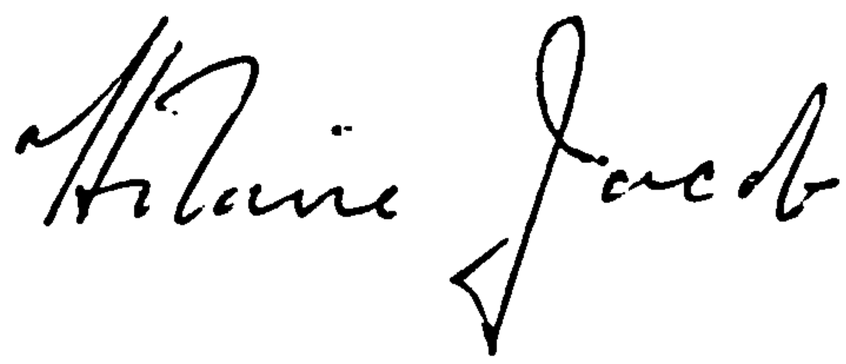

NOTATION

In general all terms have been defined when they first occur in the thesis, and several of them have been repeatedly defined when they reappear in a new chapter. Nevertheless, the following list of notations and abbreviations could be of assistance when quick reference is required.

It must be expressly mentioned that notations which according to convention would usually be written lower than the principal character, have been typed on the same line instead. For instance the point A_2, or the resultant in the metatarsal joint R_{mp}, would appear as A2 and Rmp, respectively.

Vectors have been designated $\underline{a}$, $\underline{b}$, $\underline{r}$, etc. and unit vectors are usually shown as $\hat{a}$, $\hat{b}$, $\hat{r}$, etc.

While capital letters standing alone denote points, dual combinations like BD, $\underline{EF}$, etc., refer to lines or even vectors.

Multiplication is usually shown by a dot (.), unless of course cross-multiplication of vectors is involved, in which case the cross (x) is used.

Throughout the thesis SI units have been employed except where it is specifically stated to the contrary. Abbreviations for measures, etc. that are in accordance with SI rules and also those that are generally known, have not been included in the following list:

a	axial, designation of axis
abd.	abductor
add.	adductor
ant.	anterior
A	area
b	bending
brev.	brevis
BW	body weight
c	cosine (only in matrices)

def	defective (unphysiological)
digit.	digitorum
db	digit.brev.
dl	digit.long.
di DIP	distal interphalangeal
ext.	extensor (muscle or its tendon)
E	Young's modulus of elasticity
EMG	electromyography
flex.	flexor (muscle or its tendon)
F	ground force (magnitude)
$\underline{F}$	force vector
$\underline{F}$---	force vector brought about by ---
GC	gait cycle (from heel-strike (0%) to following heel-strike of same foot (100%)
% GC	a particular instant in the gait cycle; absolute, not relative.(If a relative amount of the gait cycle is meant, for instance an interval of the gait cycle, then the abbreviation GC will not be used).
hall.	hallucis
hb	hall.brev.
hl	hall.long.
io	interosseus (interossei)
ip IP	interphalangeal
I	moment of inertia
k	ratio, factor, coefficient
l, l_n	lengths
lat.	lateral
long.	longus
med.	medial
mh	metatarsal head
mp	metatarsophalangeal
MP	metatarsophalangeal, but usually applying to the metatarsal head when referring to the ground force, as in MP-1, MP-2, etc.
n	index, any integer
p	vector showing direction of helical axis of motion

pl	peroneus longus
post.	posterior
PCSA	physiological cross-sectional area
pi PIP	proximal interphalangeal
R	resultant force
r	radius (curvature $\varsigma = \frac{1}{r}$)
s	distance, sine (only in matrices)
t	time, pitch, period, transverse
tr	transverse
T	toe
UTS	ultimate tensile strength
xyz	Cartesian coordinate system
rst uvw	Cartesian coordinate sub-system (usually contained within the global xyz one)
ε	strain (usually presented as 'μm/m' which is identical with $\times 10^{-6}$)
μ	micro ($\times 10^{-6}$)
σ	normal stress
τ	shear stress
-1, -2, -3, etc.	usually in reference to the corresponding ray of the forefoot (-1, ray comprising the great toe; -5, ray comprising the small toe)
Φ	angle of rotation about the helical axis of motion
+	tensile (with respect to σ, or ε)
-	compressive (with respect to σ, or ε)
$\equiv$	identical with
$\hat{}$	unit vector when used such as $\hat{p}$
$\hat{\equiv}$	corresponding to
$\tilde{\equiv}$	approximately
x	cross-multiplication
.	product

All other notations used in this thesis are either self-explanatory or have been defined in the immediate vicinity of their occurrence.

Finally, attention is drawn to the notation adopted with regard to appendices. Appendix g(k) is the g-th appendix of chapter k.

CONTENTS

CHAPTER 1

INTRODUCTION, AND REVIEW OF NORMAL ANATOMY OF THE FOREFOOT

1.1 Introduction

1.2 Objectives of the Investigation into the Biomechanics of the Toe Joints

1.3 Anatomy of the Forefoot

1.3.1 Introduction to the anatomy of the forefoot

1.3.2 Definition of general terms applied to directions in space and directions of movement

1.3.3 Bones and joints of the foot

1.3.4 Functional anatomy

1.3.5 Description of muscles and tendons involved

1.3.5.1 Muscles that produce dorsiflexion

1.3.5.2 Muscles that produce plantar flexion

1.3.5.3 Muscles that produce abduction and adduction

1.3.6 Description of ligaments and joint capsules of the forefoot

1.3.7 Description of the joint surfaces and movements

1.3.7.1 The tarsometatarsal joints

1.3.7.2 The metatarsophalangeal joints

1.3.7.3 The proximal interphalangeal joints

1.3.7.4 The distal interphalangeal joints

1.1 Introduction

There is probably no more fitting way to commence this chapter than to quote Frederic Wood Jones (1944) who, in his vivid treatise on the structure and function of the human foot, observes that 'for the most part we have but little pride in our feet and it is a pity that this is so for, Man's foot is all his own. It is unlike any other foot. ... It is the most distinctly human part of his anatomical make-up. It is his feet that confer upon him his only real distinction and provide his only valid claim to human status'. But even without being caught up and carried away in philosophical discourses on the human foot in phylogeny, one is urged to take an interest in this organ that both supports and enables bipedal locomotion of the body, especially when it becomes surprisingly evident that the foot has indeed not been given the same attention as other members of the human body have received up to now.

Whereas the tarsus, that includes the ankle joint, has increasingly attracted the attention of investigators in the recent past (Inman, 1976; Kimizuko et al., 1980; Procter, 1980), description of the forefoot beyond the metatarsal heads is very scanty and meagre. In "Movements of the Foot" to be found in the chapter on Arthrology of Gray's Anatomy, 1973, for example, not once are the phalanges even mentioned, and a search through available literature did not reveal any information on anthropometric data pertaining to the arrangement of the ligaments and tendons that cross the metatarsophalangeal joints, although the sensitive controlling action of the toes in standing and their assistance in propelling the body forward during walking and running, have long been recognized and appreciated.

Pathological affections of the toes and metatarsophalangeal joints such as the commonly known hallux valgus, hallux rigidus, hammer toes, etc., and also the less common diseases like Koehler-Freiberg's disease (an idiopathic necrosis of the metatarsal heads) surely call for more understanding of the biomechanics of the joints involved, an ardent desire often expressed at conferences on such themes (Blauth, 1986). In the meantime it has also become very evident that none of the artificial joints used for replacement of the articulations of the forefoot up to date could really be considered successful and this too further encourages looking into the mechanics of the toe joints more closely - an urgent necessity as reflected by the lack of information on this matter also in very recent reviews of biomechanical literature on the human foot (Debrunner, 1985).

In the present study, the biomechanics of the 'normal' forefoot, with special attention to the joints of the first two rays, are presented. The particular objectives of this investigation are formulated in 1.2.

1.2 Objectives of the Investigation into the Biomechanics of the Toe Joints

The objectives of this study are as follows:

- To establish the spatial kinematic and dynamic behaviour of the metatarsophalangeal and interphalangeal joints (rays I and II) during normal locomotion.
- To investigate the anatomy of the normal forefoot and identify such structures that probably influence mechanical function and to

collect anthropometric data relating to these structures.

- To estimate the magnitudes of forces in the structures crossing the above mentioned joints and in the joints themselves during normal locomotion.
- To identify in the results whatever criteria that might be of value in explaining the genesis of any known disorder.
- To supply information that might be of use in the design or estimation of artificial joints.

1.3 Anatomy of the Forefoot

1.3.1 Introduction:

A concise description of the foot in general and of the forefoot in particular is presented in this section. The main purpose is to recall some of the functional elements of the foot to the mind of the reader and to also define some of the terms relating to this structure, especially with regard to directions and movements, that have been used in this thesis. In this section, bracketed numbers that immediately follow the anatomical designation of bones have been included in the text to facilitate reference to figure 1.1. For the most part, the anatomical description of the foot in general has been based on the method adopted by Platzer (1984). The anatomical terminology too is the same. The term FOREFOOT itself calls for a closer definition and therefore before focusing on the specific area of interest, a brief description of the foot as a whole is first presented.

Anatomists have divided the skeleton of the foot into three segments: the tarsus, the metatarsus and the phalanges. The tarsus

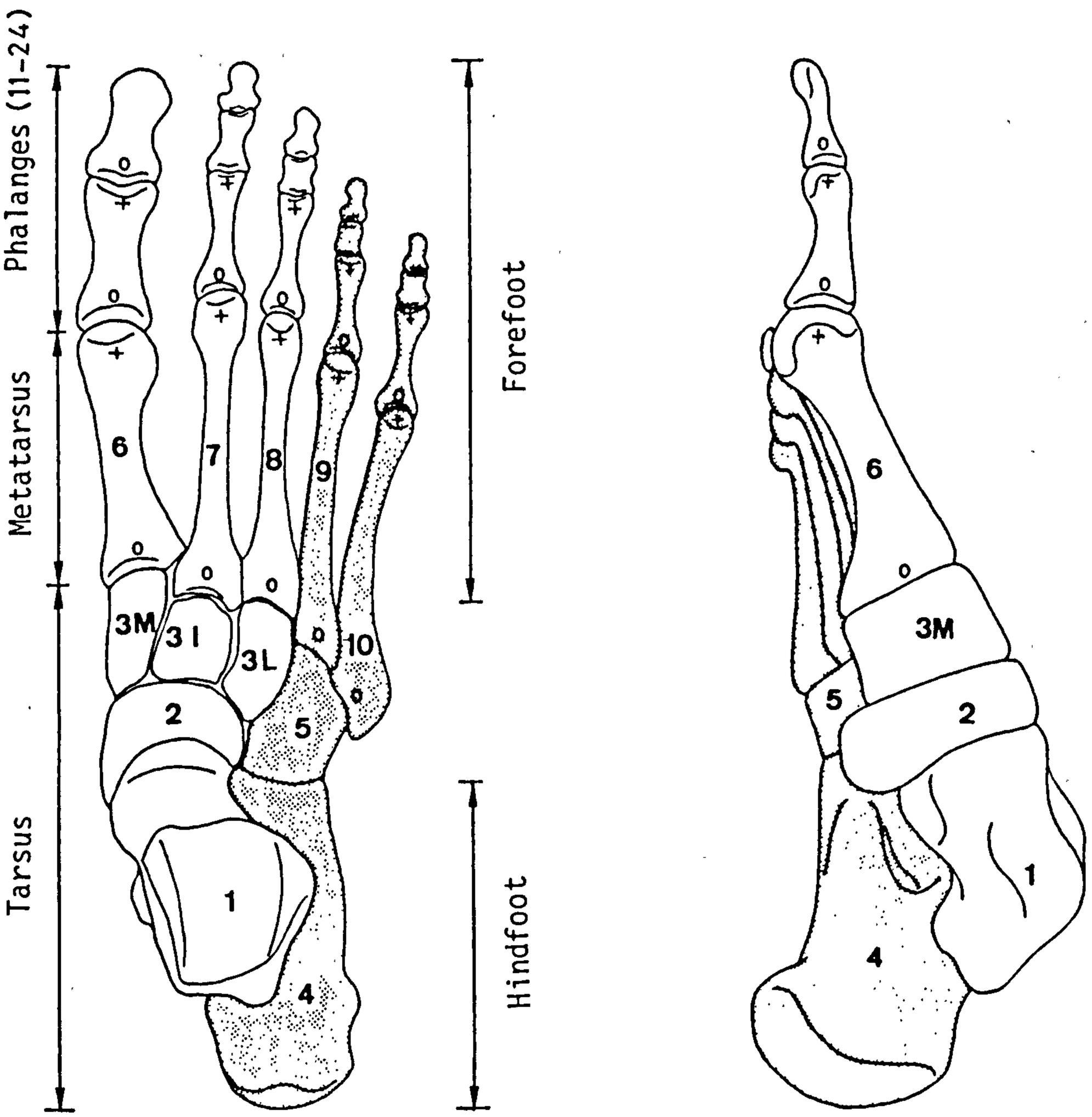

Figure 1.1 The bones of the foot

is the posterior part of the foot and consists of seven bones that exclude the five rays of metatarsals and the phalanges or digits (fig 1.1). Clinicians, however, refer to the talus (1) and calcaneous (4) as belonging to the back of the foot or hindfoot, while the other tarsals (2, 3M, 3I, 3L and 5) are regarded as the middle of the foot, and the metatarsal and phalangeal bones (6-10 and 11-24 respectively) as the forefoot. The term forefoot has been chosen in this sense.

1.3.2 Definition of general terms applied to directions in space and directions of movement:

The terminology used for describing position and direction, particularly when applied to the foot, is notoriously confusing. The terms used in this thesis are mainly in accordance with those employed by Platzer and, to obviate ambiguity, are defined with reference to figure 1.2 as follows:

Directions in space:

- Dorsal: toward the upper surface of the foot
- Plantar: toward the sole of the foot
- Medial: toward the median plane passing through the trunk
- Lateral: away from the median plane passing through the trunk
- Anterior: toward the front (toward the toes)
- Posterior: toward the back (toward the heel)

Directions of movement:

- Dorsiflexion (Extension): looking in the latero-medial direction at the right foot, motion in an anticlockwise direction.
- Plantar flexion (Flexion): looking in the latero-medial direction at the right foot, motion in a clockwise direction.

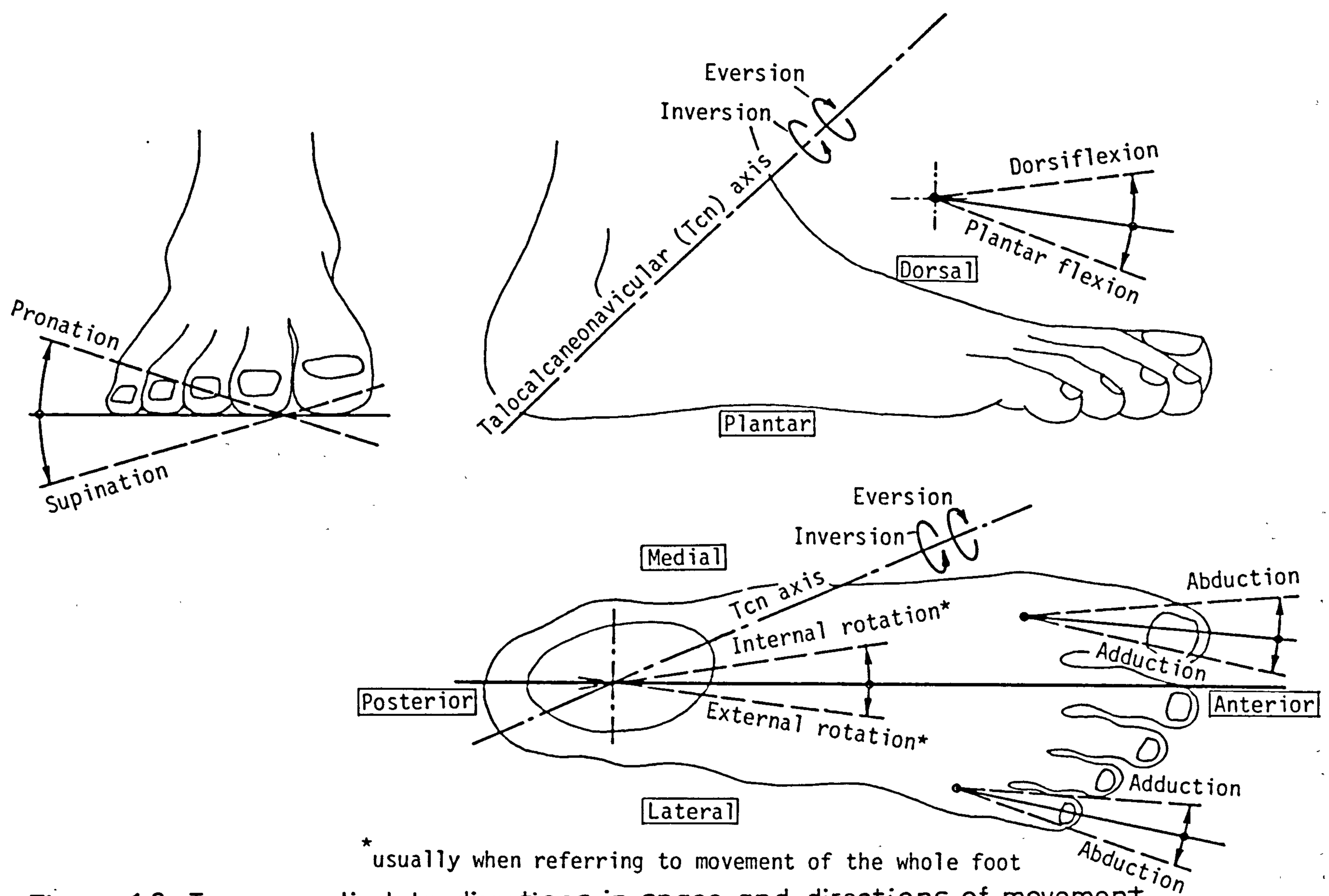

*usually when referring to movement of the whole foot

Figure 1·2 Terms applied to directions in space and directions of movement

- Internal rotation: looking in the dorso-plantar direction at the right foot, motion in an anticlockwise direction.
- External rotation: looking in the dorso-plantar direction at the right foot, motion in a clockwise direction.
- Abduction: rotational movement about a vertical axis such that all points situated anterior to the axis move away from a vertical plane of reference passing from the centre of the heel through the 2nd metatarsal head.
- Adduction: rotational movement about a vertical axis such that all points situated anterior to the axis move towards a vertical plane of reference passing from the centre of the heel through the 2nd metatarsal head.
- Eversion: on fixing the talus of the right foot and looking along the axis of the talocalcaneonavicular joint, which runs from the lateral side of the back of the heel, upwards, forwards and medially to emerge at the superior and medial aspect of the neck of the talus, motion in an anticlockwise direction.
- Inversion: motion in an opposite direction to that of eversion.
- Pronation: looking in a posterio-anterior direction, motion in an anticlockwise direction. This always involves combined angular movement in the talocrural and talocalcaneonavicular joints.
- Supination: looking in a posterio-anterior direction, motion in a clockwise direction. This too involves combined angular movement in the talocrural and talocalcaneonavicular joints.

1.3.3 Bones and joints of the foot

Referring to figure 1.1a and starting from the talus (1), a medial series of bones (unshaded) continues forwards, while a late-

ral series (shaded) proceeds from the calcaneous (4) also towards the front. Posteriorly, the talus (1) lies above the calcaneous (4) while in the middle and anterior region the adjacent bones lie side by side.

The medial series of bones consists of the talus (1), the navicular (2), the cuneiform bones (3M, 3I, 3L) and the three medial metatarsals (6,7,8) with their associated phalanges. The lateral series contains the calcaneous (4), the cuboid (5) and the two lateral metatarsals (9,10) with their corresponding phalanges. This results in the foot being wide in front and narrower at the back and also higher behind than in front.

Viewing the skeleton of the foot from the medial side (fig 1,1b) it becomes apparent that the medial bones rise as they proceed backwards until finally the talus (1) is seated over the calcaneous (4). This gives the appearance of an 'arch', a longitudinal curvature that is referred to as the medial arch. A lateral view of the foot also presents a longitudinal arch composed of the lateral series of bones. This lateral arch, however, is much lower than the medial one and not always visible. On application of vertical force to the ankle joint (upper bearing surface of the talus (1)) both longitudinal arches tend to flatten their curvature, this being opposed in static loading almost solely by the plantar ligaments and supposedly by the plantar aponeurosis (figs 2.15a and 4.28) (Basmajian and Stecko, 1963).

The only tarsal joints which contribute to any substantial movement within the foot are the talonavicular, the subtalar and the calcaneocuboid joint (Shephard, 1951). The remaining joints of the midfoot are so-called amphiarthroses that are restricted in their move-

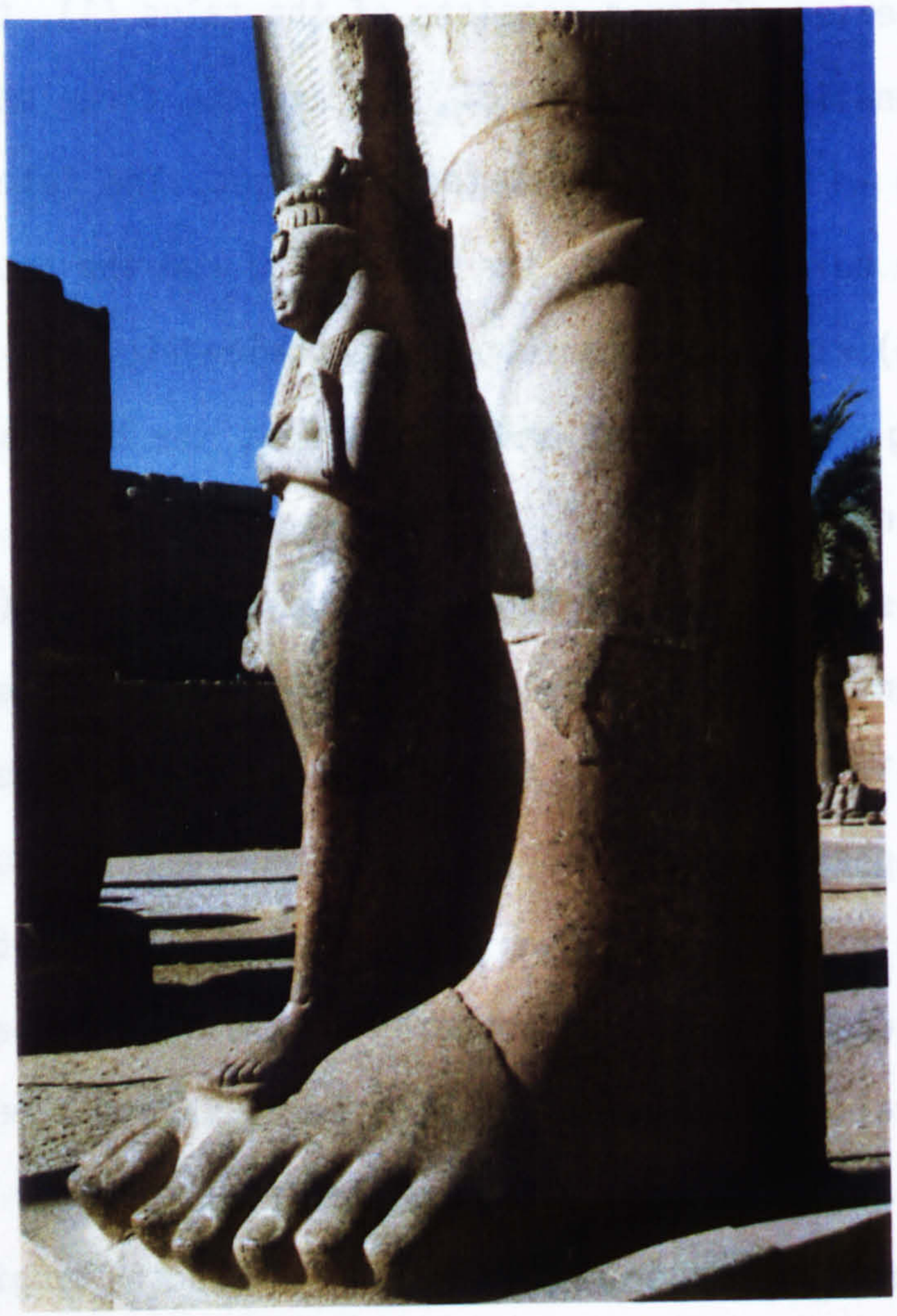

Figure 1·3 A granite colossus of Pharaoh Ramses II, exhibiting feet of the 'Egyptian' type (Karnak)

ment by the tense ligaments that interconnect the bones in this area. The five rays of metatarsals that proceed forwards are attached at their bases to the three cuneiform and cuboid bones of the mid-foot also by ligaments that, with the exception of the 1st metatarsal, allow only a very limited range of movement in these joints. The base of the 1st metatarsal, in contrast to that of the other metatarsals, is reported to have an appreciable amount both of up and down movement and of rotation (Gray, 1973).

The relationship of the metatarsal bones to each other is such that their bases are arranged in a somewhat jagged manner (see section 1.3.7.1) generally along an oblique line oriented posteriorly and laterally from the base of the 1st metatarsal. The distal projections of the metatarsals, however, follow a varying pattern, given by the so-called metatarsal formula. According to some, 1=2>3>4>5 is considered as belonging to the 'ideal' foot but the one accepted by most anatomists is 2>3>1>4>5 (Saraffian, 1983).

The configuration of the toes has led some anatomists to classify normal feet. Wood-Jones and others have used a digital formula that expresses the forward projection of each of the toes relative to each other. The so-called Grecian foot has a great toe that is shorter than the second toe; it occurs in 18% of the population (Trott, 1980). Also according to Trott, the so-called Egyptian foot is characterised by a great toe longer than the second, this occurring in 74% of people, while a third type has the great toe equal to the second in length and is known as a 'squared foot' that is seen in 8% of people. However, some authors refer to the 'squared foot' as being of the Egyptian type (Kubik, 1982) as shown in figure 1.3. No evidence, however, indicates that one type is more subject to

disease or mechanical disorders than another. It is also known that the relation in length of the great toe to the second toe is not necessarily the same with respect to the lengths of the metatarsals. Thus a Grecian foot can have a first metatarsal that is shorter or longer than, or equal to the length of the second metatarsal. The same relative relationship applies to the Egyptian foot.

The 1st metatarsal is the shortest and thickest. At its anterior end, the head which is roughly spherical exhibits two small grooves on the plantar surface that leave a ridge between them. In these two grooves are regularly found the two sesamoid bones which are embedded in the flexor tendon of the great toe that passes across the plantar aspect of the metatarsal head.

The 2nd, 3rd and 4th metatarsals are slimmer and their bases are wider dorsally than on their plantar sides. The heads of these three metatarsals bones are flattened medially and laterally so that they exhibit a barrelled shape.

The 5th metatarsal bone differs from the others in that it has a tuberosity on the lateral side of its base. The head of this metatarsal also appears more spherical than those of the 2nd, 3rd and 4th ones.

The 2nd-5th digits all have a proximal middle and distal phalanx, while the 1st digit only has two phalanges. Each phalanx bone has a base, a shaft and a head. The distal phalanx bone has a distal tuberosity.

The metatarsophalangeal joints and the interphalangeal joints may be referred to as the proximal, the middle, and the distal joints. The metatarsophalangeal or proximal joints are ball-and-socket joints although their mobility is limited by collateral li-

gaments. The middle and distal joints are described as pure hinge joints.

Apart from the bones of the foot already mentioned (a total of 28, including the two sesamoids under the 1st metatarsal head) there are other small bony elements occasionally present. These are usually termed accessory bones and will not further be dealt with in the present context.

1.3.4 Functional anatomy:

The function of the human foot has evolved through the necessity to walk, run and jump in serving the vital purposes of obtaining food or of escaping from danger. Several investigators have drawn attention to the probability that the human foot has been derived from an originally climbing organ and is still in the process of completely adapting itself to its present function (Weidenreich, 1921; Wood-Jones, 1944; Preuschoft, 1971). As Hohmann (1939) points out, the human foot is characterised by a substantial longitudinal arch, supported by strong ligamentous ties across its concave, plantar aspect, by a medial transversal arch composed of the three cuneiform bones and the cuboid in which, however, the medial cuneiform has descended in a plantar direction, and by a particularly strong 1st metatarsal bone that is not very mobile at its proximal end. The hind foot has retained some of its former characteristics as indicated by the direction of the axis of the talocalcaneonavicular joint which makes inversion and eversion of the foot - a prerequisite for arboreal life - possible. Thus, whereas the mid- and hind-foot still show an arrangement of bones in distinct supination, the forefoot has adopted a relatively pronated position. This has led to the concept of

the pedal skeleton as a twisted plate which may be untwisted (supination) or further twisted (pronation) during the maintenance of a plantigrade stance in various positions of the foot.

The toes are regarded as a forward extension of the foot with the ability to respond quickly to changes in the position of the body's centre of gravity so as to maintain balance. Nevertheless, they also are able to follow an uneven surface so as to distribute the weight over as large an area as possible. In addition to the dorsiflexion and plantar flexion that can obviously be effected through muscular activity in the joints of the toes, it should also be possible to execute abduction and adduction in the metatarsal joints of the 1st and 5th digits, the muscular system for this being present. However, as Last (1984) mentions, this is an action largely lost in boot-wearing races, but retained in the bare-foot peoples. In walking, as the heel leaves the ground, the ground force is shared by the ball of the foot and the toes. The toes assume an important role at this stage of the walking cycle and the load transmitted through the toes can reach 50% of body weight (Hutton et al., 1982). By virtue of their ability to flex their distal ends in a plantar direction, they can assist in propelling the body forwards by finding purchase on the underlying ground. It is also believed that through dorsiflexion in the metatarsophalangeal articulations, by means of a 'windlass' effect, the plantar apononeurosis is further tensioned, thus further bracing the longitudinal structure of the foot, making it more suitable to act as a lever during the push- off phase in walking, running and jumping (Hicks, 1953).

The functional behaviour of the foot might be broadly divided into conditions of static weight-bearing and those during movement.

In standing on both feet, the weight of the body is transmitted through the ankle joint to the talus from where part of the weight is taken by the calcaneous while the remainder acts on the heads of the metatarsal bones. It has been shown that in a neutral position, that is, with the centre of gravity neither too close to the balls of the feet nor just over the heels, negligible activity in the muscles of the foot (both extrinsic and intrinsic) is present (Basmajian and Stecko, 1963). This gives strong evidence that the ligaments and plantar aponeurosis must play a predominant role in the support of the static skeleton by supporting the arch. It has also been shown that no significant change in the form of the skeletal structure of the foot comes about on sustaining the full bodyweight (Carlsöö and Wetzenstein, 1968). A number of conflicting theories have been proposed regarding the distribution of body weight when standing. Investigations performed by Stott et al., 1973, have shown that the way in which the body weight is shared between heel and forefoot is quite variable, and a comfortable stance could be achieved with the heel carrying between one and three times the load of the forefoot. The load distribution across the forefoot was found to be fairly uniform and bore no relation to the size of the metatarsal bones. However, the pattern of distribution was observed to be subject to rapid alteration if called for in maintaining balance. The same investigators also reported that the toes carry 5-10% of the forefoot load in upright stance.

In walking, the magnitude and distribution of load under the feet is very different from that of static weight bearing. Before describing the movements and loading of the foot in walking, a brief explanation of the walking cycle, which will often be referred to,

is given as follows:

During normal walking each foot spends about 60% of time in contact with the ground (stance phase) while the remaining 40% is spent in swinging to adopt a new position ahead (swing phase). The period spent between heel-strike of one foot and the succeeding heel-strike of the same foot is termed the walking cycle. From the start of the cycle, for a duration of about 10% of the total cycle time, both feet are in contact with the ground. This occurs again in the middle of the cycle between 50 and 60% just following heel-strike of the other foot.

At heel strike, the leg is in its foremost position with the knee fully extended. The ankle joint might be at this moment in a neutral position. Immediately following heel strike, the ankle joint moves into plantar flexion thereby bringing the whole foot in contact with the ground. This phase of the gait cycle is accompanied by deceleration of the body-mass both forward and vertically. The vertical force under the foot at this time exceeds body weight by 10-20%. Simultaneously, a peak horizontal force opposing forward movement of the foot relative to the ground appears. Up to this moment, only the extrinsic muscles of the foot have been active, especially tibialis anterior and the long extensor muscles of the foot that oppose plantar flexion in the ankle joint when the heel strikes the ground. From now on, the intrinsic muscles become increasingly active. The intrinsic muscles brace the foot for transfer of load to the forefoot and for the subsequent push-off phase. In the meantime (20% of the walking cycle) the vertical force is distributed equally between the heel and the ball of the foot with the mid-foot taking very little load. The distribution across the

metatarsal heads according to Stott et al. (1973) shows a maximum load under the 1st with a continuous decrease towards the 5th. Finally, during the push-off phase (35-60% of the walking cycle) the ground load is entirely borne by the forefoot, the load on the heads of the 1st and 2nd metatarsals rapidly increasing to a maximum at about 45% of the walking cycle, with an increasing amount of load shared by the pads of the toes.

Movement within the skeletal structure of the foot during walking is only partially understood. According to Wright et al. (1964), just after heel strike, the ankle joint moves from a neutral position into plantar flexion. Simultaneously, subtalar rotation proceeds from inversion to eversion during the first 10% of the walking cycle. Following this, during the 'foot-flat' phase (10-45% of the walking cycle) dorsiflexion of the ankle joint increases and rotation in the subtalar joint gradually reverts from eversion fo inversion. At the end of this phase the heel begins to leave the ground and while the ankle joint moves from dorsiflexion into plantar flexion, the subtalar joint dwells in the adopted state of inversion. During this phase of walking (45-60% of the cycle) the foot is said to have changed from a mobile structure into a rigid lever that persists during push-off. The mechanism of this happening is complicated and not completely understood (Inman et al., 1981). Pronation of the foot during the last phase of push-off enables thrust to be largely transferred to the ball of the hallux before, finally, the foot leaves the ground.

The sole of the foot is a very important structure specially designed to meet with the severe requirements imposed upon it. Relaxed, the ball of the foot is a soft and pliable pad. The plantar

skin can be moved from side-to-side and, proximodistally. Dorsiflexion of the toes changes this situation; the ball becomes tense and mobility of the skin becomes greatly reduced. This stiffening ensures that shear forces resulting from accelerations, decelerations or twists are transferred to the skeleton, this being effected by numerous fibrous bands that bind the skin to the underlying aponeurosis.

1.3.5 Description of muscles and tendons involved:

The muscles of the foot may be broadly divided into extrinsic and intrinsic muscles. The extrinsic muscles are those whose tendons only extend into the foot; that is, the muscles proper are contained in the leg. The intrinsic muscles, on the other hand, are those located within the foot itself. There are basically various ways of classifying muscles. In the following, classification according to function has been chosen. This being considered more appropriate for a discourse on the biomechanics of the forefoot.

1.3.5.1 Muscles (extrinsic, A; and intrinsic, B) that produce dorsiflexion (extension) in the joints of the foot:

A. Extrinsic extensors:

- The TIBIALIS ANTERIOR arises from a wide area of the lateral surface of the tibia, the interosseous membrane and the crural fascia. The muscle ends in a tendon which passes beneath the superior and inferior extensor retinacula and then passes anteriorly and along the medial border of the foot to be inserted in the medial surface of the medial cuneiform and at the base of the 1st metatarsal bone. The tibialis anterior flexes the foot in the ankle joint (talocrural)

dorsally and is usually reported to lift the medial edge of the foot in supination (Platzer, 1984) or, as mentioned by Gray (1973) and Last (1984), invert the foot. This latter function attributed must certainly be accepted with some reserve since the line of action of the tendon passes very close to the axis of the talocalcaneonavicular joint and can therefore not exert any appreciable turning moment about this axis.

- The EXTENSOR HALLUCIS LONGUS arises from the medial surface of the fibula and the interosseus membrane. It continues as a tendon which runs in its own synovial sheath between the sheath for the tendon of the tibialis anterior and that for the extensor digitorum longus beneath the superior extensor retinaculum and inferior extensor retinaculum. It reaches across the 1st metatarsal to the dorsal aponeurosis of the great digit and is inserted into the terminal phalanx. The muscle flexes the great toe dorsally and aids dorsiflexion of the foot.

- The EXTENSOR DIGITORUM LONGUS has its origin along the lateral ledge of the tibial plateau, the head and anterior crest of the fibula as well as the interosseous membrane. The muscle proceeds far down the leg and terminates in a single tendon that, however, splits into two just under the superior extensor retinaculum. Both tendons continue their course below the inferior retinaculum from which they anteriorly emerge, each again divided into two tendons. The divided two lateral tendons reach the 5th and 4th toes and the medial two tendons reach the 3rd and 2nd toes, respectively. All four tendons enter a dorsal aponeurosis of the 2nd to 5th digits. This aponeurosis is formed in the dorsal aspect of the proximal phalanges, receiving contribution from the lumbrical and interosseous muscles.

This aponeurosis narrows as it approaches the proximal interphalangeal joint and divides into three slips that pass over the joint. The central slip inserts into the base of the middle phalanx while the other two reunite distally before becoming attached to the base of the distal phalanx. The muscle produces dorsiflexion of the digits and the foot.

- The PERONEUS TERTIUS muscle is sometimes present (in about 90% of feet) arising from the distal third of the anterior edge of the fibula and terminating in a tendon that runs alongside the extensor digitorum longus tendon. After passing beneath the inferior extensor retinaculum, the tendon proceeds anteriorly and laterally to insert in the dorsal surface of the base of the 5th metatarsal bone. In those cases in which the muscle is not present, the extensor digitorum longus tendon has an additional slip which takes the course described before. This tendon is said to effect pronation of the foot.

B. Intrinsic extensors:

- The EXTENSOR DIGITORUM BREVIS arises on the dorsum of the foot from the calcaneous and from the lateral side of the inferior extensor retinaculum. It extends with three tendons anteriorly to the dorsal aponeurosis of the 2nd to 4th digits. All of the three tendons meet the dorsal aponeurosis over the proximal digits and very often form the lateral slip of the tendon trifurcation that crosses the proximal interdigital joint (see extensor digitorum longus). Together with the extensor digitorum longus, this muscle enables dorsiflexion of the lesser toes. The 5th toe is not actuated by the extensor digitorum brevis.

- The EXTENSOR HALLUCIS BREVIS (sometimes considered as an integral part of the extensor digitorum brevis muscle, but with a fourth tendon) shares a common origin with the extensor digitorum brevis muscle and is located medially with respect to the latter. The tendon follows a course anteromedially along the dorsum of the foot and inserts in the dorsal aspect of the base of the proximal digit of the great toe.

1.3.5.2. Muscles (extrinsic, A; and intrinsic, B) that produce plantar flexion (flexion) in the joints of the foot:

A. Extrinsic flexors:

- The TRICEPS SURAE (calf) muscle consists of the SOLEUS, GASTROCNEMIUS and (when present) the PLANTARIS.

The soleus arises from the head and upper third of the tibia. The large terminal tendon of the muscle joins the tendon of the gastrocnemius and is inserted distally into the tuber calcanei as the "Achilles' tendon".

The gastrocnemius arises from just above the posterior aspect of the femoral condyles. It has two heads, one proximal to the lateral and one proximal to the medial femoral condyle. The two heads run distally along the back of the leg to join the tendon of the soleus.

The plantaris, if at all present (as in about 7% of all cases), is a slight, delicate muscle with a long terminal tendon. It arises just medial to the origin of the lateral head of gastrocnemius and its tendon proceeds distally between the soleus and gastrocnemius to terminate at the tuber calcanei, immediately medial to the Achilles' tendon.

The triceps surae muscle is the powerful plantar flexor of the ankle

joint. It is also considered to be the strongest to effect inversion (Platzer, 1984).

- The TIBIALIS POSTERIOR has its origin in the intrerosseous membrane and fibula, almost along the whole length of the leg. Its tendon passes distally and is diverted around a pulley formed by the malleolar groove behind the medial malleolus after which it runs towards the tuberosity on the plantar aspect of the navicular bone. Just before reaching the navicular, the tendon splits into two, a medial and a lateral extension. The medial part inserts into the navicular tuberosity and into the plantar surface of the 1st cuneiform bone while the lateral part proceeds under the arch of the foot to meet the 2nd and 3rd cuneiform and the cuboid bones.

- The FLEXOR DIGITORUM LONGUS arises from the posterior surface of the tibia and after crossing the tibialis posterior at its distal end, terminates in a tendon that passes underneath the flexor retinaculum, just posterior to the tendon of the tibialis posterior. This tendon takes a course parallel to that of the tibialis posterior tendon until it has assumed an antero-plantar direction. It now enters under the arch of the foot and divides into four terminal tendons which proceed to the terminal phalanges of the 2nd-5th digits on the plantar side.

- The FLEXOR HALLUCIS LONGUS has its origin along the distal two-thirds of the posterior surface of the fibula, the interosseous membrane and the posterior crural intermuscular septum. The muscle belly extends far distally before it is completely transformed into its tendon which lies in a groove in the talus and calcaneous. It proceeds beneath the flexor retinaculum to the sole of the foot where it is inserted into the base of the terminal phalanx of the great

toe. The tendon is crossed superficially by that of the flexor digitorum longus, just distal to the talus. It produces plantar flexion of the great toe.

- The PERONEUS LONGUS arises from the head of the fibula and along the lateral side of the proximal half of the latter. It ends in a tendon that runs behind the lateral malleolus and, together with the tendon of the peroneus brevis, it passes under the superior peroneal retinaculum in a common synovial sheath. After making almost a quarter of a turn under the lateral malleolus it proceeds to the lateral border of the cuboid bone where it enters a deep groove in the plantar surface of the latter, immediately behind the tuberosity of the 5th metatarsal base, before it traverses the sole of the foot to be inserted in the plantar surface of the 1st metatarsal base and in the medial cuneiform bone.

This, together with the peroneus brevis is a dorsiflexor of the ankle joint and is the strongest in effecting eversion of the foot.

- The PERONEUS BREVIS arises from the lateral surface of the fibula, along its middle third. Its tendon runs distally and then turns anteriorly on the pulley formed by the lateral malleolus. It adopts a position immediately dorsal to the tendon of the peroneus longus as it passes through the inferior peroneal retinaculum and then proceeds directly to insert laterally in the tuberosity at the base of the 5th metatarsal.

B. Intrinsic flexors:

These muscles, all located in the sole of the foot, are usually described in three groups - those contained in a medial compartment that serve the great toe, those in a central compartment that belong

to the 2nd, 3rd and 4th digits, and those in a lateral compartment that control the little toe. The three compartments are formed by longitudinal septa (partitioning walls of fibrous connective tissue) that arise from the plantar aponeurosis plate at the base of the foot and proceed dorsally to meet the 1st metatarsal, the medial cuneiform and the navicular bones in the case of the medial septum, and to meet the 5th metatarsal bone and long plantar ligament in the case of the lateral one.

- The FLEXOR HALLUCIS BREVIS in the medial compartment, arises from the medial cuneiform bone, the long plantar ligament and the tendon of tibialis posterior. It has two heads. The medial head extends to the medial sesamoid bone and to the base of the proximal phalanx, while the lateral one is inserted into the lateral sesamoid and into the base of the proximal phalanx too. This is the main plantar flexor of the metatarsophalangeal joint.

- The INTEROSSEI muscles contained in the central compartment of the sole of the foot are divided into plantar and dorsal groups. The three plantar interossei each arise by a single head from the medio-plantar side of the 3th-5th metatarsals and extend into the joint capsule below the heads of the corresponding metatarsalia after which the tendon fibres proceed antero-dorsally to be inserted into the medial aspect of the base of the proximal phalanges. The four dorsal interossei each arise by two heads from the opposing surfaces of all the metatarsals on their dorsally directed surfaces and from the long plantar ligament. The interosseus dorsales I only is inserted at its distal ends into the medial side of the base of the 2nd digit; all the other dorsal interossei are inserted into the lateral side of the 2nd-4th digits. The path ta-

ken by all the dorsal interossei muscles and their tendons is similar to that of the plantar interossei in that they extend into the joint capsule under the metatarsal heads before proceeding anteriorly and dorsally to be inserted in the base of the corresponding proximal phalanges.

The interossei, plantar and dorsal, when working together, are reported to act as plantar flexors at the metatarsophalangeal joint. However, as shown in Chapter 6, they probably serve primarily as ab- and adductors of the metatarsalia and only to a lesser extent as plantar flexors in the metatarsophalangeal joints.

- The FLEXOR ACCESSORIUS (or, QUADRATUS PLANTAE) arises with two heads from the medial and lateral margins of the plantar surface of the calcaneous and terminates into the lateral margin of the tendon of the flexor digitorum longus just where the latter splits into four parts.

- The LUMBRICAL muscles, four in number, arise from each of the four divisions of the flexor digitorum longus tendon within the central compartment. They extend to the medial margin of the proximal phalanges of the 2nd-5th digits and radiate into the extensor aponeurosis. The lumbrical muscles are sometimes totally absent.

- The FLEXOR DIGITORUM BREVIS, also in the central compartment, arises from the middle part of the tuber calcanei and as it proceeds anteriorly, it divides into four tendons which pass to the four lateral toes. Each of the four tendons are split in two just before they insert into the plantar aspect of the base of the corresponding middle phalanges. The tendons of flexor digitorum longus pass in-between these split terminals before the former progress further on.

- The OPPONENS DIGITI MINIMI that is contained in the lateral compartment, arises from the lateral side of the long plantar ligament and is inserted into the lateral aspect of the 5th metatarsal bone. It plantarflexes the 5th metatarsal. It is quite often absent.
- The FLEXOR DIGITI MINIMI BREVIS, also in the lateral compartment, arises from the base of the 5th metatarsal and the adjoining sheath of peroneus longus. Its tendon is inserted into the base of the proximal phalanx at its plantar aspect.

1.3.5.3 Muscles that produce abduction and adduction in the joints of the foot:

These muscles usually have a compound function, plantar flexion being often a considerable part of their total action.
- The ABDUCTOR HALLUCIS arises from the medial process of the calcaneous tuberosity and from the flexor retinaculum. It is inserted into the medial side of the proximal phalanx of the great toe and also in the area of the medial sesamoid. It acts as an abductor, and supposedly as a weak flexor.
- The ADDUCTOR HALLUCIS has two heads; one traverses the sole of the foot obliquely, while the other is arranged transversally. The oblique head arises from the cuboid and lateral cuneiform bones and from the bases of the 2nd and 3rd metatarsals. The transverse head arises from the capsular ligaments on the medio-plantar side of the metatarsophalangeal joints of the 3rd-5th digits. Both heads are inserted into the lateral sesamoid bone under the 1st metatarsal head.
- The ABDUCTOR DIGITI MINIMI forms the lateral border of the foot. It arises from both medial and lateral tubercles of the calcaneus.

Its tendon is inserted into the lateral side of the proximal phalanx of the small toe. Some medial fibres are attached to the tubercle of the 5th metatarsal bone.

Before terminating this section on the muscles and tendons involved, it must be expressly stated that the foregoing is only a very general description, and that no attempt has been made to include the diversity in physical forms and the variety of courses taken by the muscles and tendons of the foot occasionally encountered. The main purpose of this description is to offer a source of reference that would facilitate reading this thesis.

1.3.6 Description of ligaments and joint capsules of the forefoot:

In this section, the main interosseous ligaments and the joint capsules that lie distal to the cuboid and the three cuneiform bones are treated. Those ligaments that arise from the hindfoot and midfoot, but which reach forward into the forefoot, are described too.

The cuboid and cuneiform bones are interconnected by dorsal, plantar and interosseous ligaments. The synovial joints between the three cuneiforms and between the lateral cuneiform and cuboid all lie at the dorsal limits of their mating surfaces. The broad lower parts of these surfaces give strong fixation to the plantar and interosseous ligaments that bind the bones firmly together. The dorsal and plantar ligaments each consist of three transverse bands that interconnect the adjacent bones. The plantar ligaments are strengthened by slips from the tendon of the tibialis posterior. The articular capsules and synovial cavities are continuous with each other and with those of the cuneonavicular joint.

The tarsometatarsal articulations are bridged by dorsal, plan-

tar and interosseous ligaments. The dorsal ligaments are strong flat bands. The plantar ligaments consist of longitudinal and oblique bands disposed with less regularity than the dorsal ligaments. The strength of the ties diminishes towards the lateral side of the foot. The interosseous cuneometatarsal ligaments are three in number: The first, and the strongest, passes from the lateral surface of the 2nd metatarsal. The second connects the lateral edge of the lateral cuneiform with the adjacent side of the base of the 4th metatarsal. The third, that is inconstant, connects the lateral cuneiform with the 2nd metatarsal.

The metatarsophalangeal articulations are enclosed in fibrous capsules that are attached to the margins of the articular surfaces. Dorsally they are thin, but on the plantar side they are thick and are inseparable from the plantar ligaments of the joints and from the plantar aponeurosis. Also embedded in the plantar part of the capsules are the fibres of the deep transverse ligament that connects the plantar ligaments of adjoining metatarsophalangeal joints to one another. The capsule of the 1st metatarsophalangeal joint contains the two regular sesamoid bones embedded in the fibrocartilaginous pad through which force is transmitted to the ground. The remaining metatarsophalangeal joint capsules rarely have sesamoid bones but often exhibit sesamoid fibrocartilages instead. Collateral ligaments further connect the metatarsal heads with their corresponding phalanges. On each side of the metatarsal heads two ligaments arise, a metatarsophalangeal collateral ligament and a metatarsoglenoid suspensory ligament. The former is directed downward to insert on the plantar plate.

The interphalangeal joints exhibit collateral ligaments that

extend from the head of each proximal phalanx to the base of the distally located one. Each joint has an articular capsule, the plantar surface of which is strengthened to form a fibrous plate that is often referred to as the plantar ligament.

There now remain two important ligamentous structures that are directly responsible for maintaining the longitudinal arch of the foot: the long plantar ligament and the plantar aponeurosis.

The long plantar ligament extends from the calcaneal tuberosity to the cuboid and bases of the 2nd-4th (sometimes also the 5th) metatarsal bones.

The plantar aponeurosis is a complex framework which ties the pedal arches, anchors the skin to the skeleton, at the same time allowing the nerves, vessels and tendons to pass through the weight-bearing area below the metatarsal heads (Bojsen-Møller, 1979). This aponeurosis springs from the tuber of the calcaneous and proceeds anteriorly covering the central compartment. Proximal to the metatarsal heads the aponeurosis divides into superficial and deep fibres. The former insert in the skin of the anterior part of the ball of the foot while the latter penetrate between the flexor tendons to meet the plantar ligaments under the metatarsal heads. These plantar ligaments are connected loosely to the metatarsals by synovial folds, but are attached firmly to prominent facets on the bases of the proximal phalanges.

1.3.7 Description of the joint surfaces and movements:

1.3.7.1 The tarsometatarsal joints:

The three CUNEIFORMS are interposed between the navicular proximally, the first three metatarsals distally, and the cuboid

laterally. These three wedge-shaped bones articulate against each other, the cartilage bearing surfaces being situated toward their dorsal boundaries. Their proximal, or posterior cartilage surfaces bear against each of three corresponding facets on the anterior aspect of the navicular bone. Distally, the intermediate cuneiform is in proximal recess, by about 8 mm relative to the medial cuneiform and 4mm relative to the lateral cuneiform. This arrangement leads to the base of the 2nd metatarsal bone being held within the slot thus formed by the cuneiform bones and by virtue of the tense ligament ties across the joint, movement in this tarsometatarsal joint is very restricted.

The CUBOID is in juxtaposition with the calcaneous, the bases of the 4th and 5th metatarsals, and with the lateral cuneiform. All mating surfaces are cartilaginous. The posterior surface which is saddle shaped, articulates with the calcaneous. The medial face makes contact with the lateral cuneiform only in the middle third of its expanse. The anterior surface articulates with the base of the 4th and 5th metatarsals. The bearing surface in contact with the 4th metatarsal is quadrilateral, and that in contact with the 5th triangular in form.

The five metatarsals articulate with the three cuneiforms and the cuboid and form the tarsometatarsal or Lisfranc's joint. Proximally the bases of the metatarsals are arranged in a transverse arch matching the position taken by the cuneiforms and cuboid. The arch is high medially and low laterally with the apex corresponding to the base of the 2nd metatarsal.

The 1st metatarsal diverges slightly from the 2nd, the angle between the longitudinal axes of the bones being between 3° to 9°

(Saraffian, 1983). The BASE of the 1st METATARSAL has a kidney shaped articular surface in contact with the medial cuneiform. The lateral surface of the base establishes variable contact with the 2nd metatarsal.

The BASE of the 2nd METATARSAL is wedge-shaped with the crest directed downward. The three articular surfaces (medial, posterior and lateral) contact five bones: the base of the 1st metatarsal (in some cases), the medial cuneiform, the intermediate cuneiform, the lateral cuneiform, and the base of the 3rd metatarsal.

The Base of the 3rd METATARSAL is also wedge-shaped and is so positioned that the apex of the wedge points in a medio-plantar direction, the medial side of the wedge lying against the lateral side of the base of the 2nd metatarsal. The posterior aspect of the base articulates with the anterior surface of the lateral cuneiform while the latero-plantar side of the base contacts the 4th metatarsal.

The BASE of the 4th METATARSAL exhibits a posterior surface that is an oblique quadrilateral which bears on the corresponding anterior facet of the cuboid. Its medio-dorsal aspect contacts the 3rd metatarsal base distally, and the lateral cuneiform bone proximally while its latero-plantar side articulates with the base of the 5th metatarsal.

The BASE of the 5th METATARSAL articulates proximally with the cuboid by a triangular, oblique surface and medially with the 4th metatarsal bone.

It should be pointed out that little is known on the range of movement in the tarsometatarsal joints. Hicks (1953) reviews the opinions up to that time that ranged from 'slight flexion extension', 'slight contribution to inversion and eversion', 'rather insignifi-

cant', to 'appreciable up-and-down movement of the first metatarsal' with 'the other metatarsals moving in one piece'. This is because of the tight ligamentous cross-ties between the bases of the 2nd-5th metatarsals and the adjoining tarsal bones, and between each other. Saraffian (1983) refers to Hicks who measured the total range of motion from flexion-pronation to extension-supination in the 1st tarsometarsal joint to be 22° while that of flexion-supination to extension-pronation in the 5th joint amounted to 10°. Saraffian (1983) also refers to Kelikian who reported 10° to 15° passive 'up-and-down' movement in the 1st metatarsocuneiform with 'side- to-side' motion about half of that range. The 2nd metatarsal was reported to have 'limited mobility' while the 3rd had a range of flexion-extension of about 10°.

1.3.7.2 The metatarsophalangeal (MP) joints:

The heads of the MP joints not only bear against the proximal phalanges, but also against the plantar aspect of the joint capsule in transmitting force to the ground. This necessitates a specialised plantar bearing surface. As described in Section 1.3.6 the capsules of the MP joints are fibrocartilaginous in character on the plantar bearing surface in contact with the metatarsal heads. Since various tendons insert in the fibrous plantar plate that is anteriorly attached to the base of the proximal phalanges, movement in the MP joints is always associated with gliding motion between the plantar aspect of the metatarsal heads and the underlying capsule.

The HEAD of the 1st METATARSAL is an ovaloid with the large diameter in a transverse direction. The articular surface in contact with the phalanx is smooth and convex (more in the vertical direc-

tion than the transverse). The plantar articular surface is traversed by two parallel grooves, each running in a sagittal plane separated by an interval of about 6 mm from each other. The two regularly present sesamoid bones, partly embedded in the underlying fibrocartilaginous capsule, glide within these grooves. The medial groove is usually larger to accomodate the normally larger medial sesamoid. All articular surfaces are, as usual, lined with cartilage.

The HEADS of the 2nd-5th METATARSALS are barrel-shaped, being flattened transversely. The articular surface is condylar, extending more on the plantar aspect than on the dorsal. When observed in the lateral profile, the metatarsal heads have an elliptic articular contour.

The BASES of the PROXIMAL PHALANGES articulate with the metatarsal heads. The articular surface is a shallow socket sometimes described as a glenoid. The surface area of the socket is much less than that of the opposing mating surface, indicating a considerable range of possible relative motion.

The MP joints allow plantar and dorsal flexion as well as some abduction-adduction and some supination-pronation too. Relative to the axis of the metatarsal bone, the 1st proximal phalanx can be brought into 90° dorsal flexion whereas plantar flexion is limited to 'a few degrees' (Gray, 1973). Joseph (1954) reported active dorsiflexion of the great toe averaging 52° and active plantar flexion of about 24°. The amount of dorsiflexion in the 'neutral' position (foot flat on the ground) was observed to be about 16°. Debrunner (1982) however gives 70° dorsiflexion and 45° plantar flexion for the 1st MP joint, without mentioning whether this is in active or

passive motion. Debrunner also gives the range of movement for all the remaining MP joints as 60° to 80° dorsiflexion and 40° plantar flexion. No values for the range of motion (even passive) for abduction-adduction or supination-pronation could be found in the literature consulted for any of the MP joints.

1.3.7.3 The proximal interphalangeal joints:

The head of each of the proximal phalanges articulates with the base of the distally adjoining bones. The articulating surface of the heads is saddle-shaped, or trochlear, and mates with a reciprocally curved surface on the base of the neighbouring phalanx. The geometry of the joint surfaces therefore only permits dorsal and plantar flexion with no abduction-adduction or supination-pronation movement whatever. The range of movement in the proximal interphalangeal joint of the great toe is given by Debrunner (1982) as being 0° dorsiflexion and 80° plantar flexion, measured by the position of the axes of the neighbouring phalanges relative to each other. The range of movement given by the same author for the lesser toes is 0° dorsiflexion and 35° plantar flexion.

1.3.7.4 The distal interphalangeal joints:

These joints are similar in form to those of the proximal interphalangeal articulations and as such, exhibit hinge motion with no abduction-adduction or pronation-supination whatever.

The range of movement in the distal interphalangeal joints of the 2nd-4th toes is given by Debrunner (1982) as being 30° dorsiflexion and 60° plantar flexion. Debrunner points out that while the proximal interphalangeal joints can only be plantar flexed, the dis-

tal interphalangeal joints can be dorsally flexed too. Gray (1973) however mentions that extension (dorsiflexion) is limited generally and that movement in the proximal interphalangeal joints is 'freer' than in the distal ones. Saraffian (1983) mentions that in 37%, the distal and middle phalanges of the 5th toe are fused.

C H A P T E R 2

REVIEW OF BIOMECHANICAL AND OTHER LITERATURE RELATING TO THE FOREFOOT

a) Feet found at an excavation site in Sakkara

b) A strange foot in ancient Egypt. Does the prominent second toe bear evidence of Hellenic influence during the Ptolemaic period ?

Figure 2.1 Feet in ancient Egypt

2.1 Introduction

It is the purpose of this chapter to review literature relevant to the study of the biomechanics of the forefoot. Before proceeding with specific details of ground reaction forces, anatomy, muscle studies, gait characteristics, observation of movement, and the derivation of joint reaction forces, however, some of the general literature pertaining to the forefoot will be reviewed to reflect on the views expressed by earlier investigators.

2.2 General Literature

There can be no doubt that artists even in ancient times carefully investigated the foot (fig 2.1). However, it was Borelli (1680) who described the mechanics of gait, with special reference to the forefoot, in terms familiar to us. In his "De Motu Animalium"* he clearly states that the solei muscles are tightened, causing the foot to plantar flex at the ankle joint. This causes lengthening of the leg and the floor is pushed by the toes resulting in a forward movement of the whole body in a manner 'not unlike the way a small boat, pushed with a pole by the sailors, leaves the shore' (Translation by A. Cappozzo). Borelli also discusses the necessity for the centre of gravity of the body to fall within the base of support and illustrates the total contact area between the foot and the ground when standing and walking. In this manner, the role played by the forefoot, and especially the toes, not only

---

* an original version of a later edition (1685) is kept in the library of the Dept. of Orthop. Surg. BALGRIST, University of Zurich, Switzerland.

during the push-off phase but also in maintaining balance when standing, was clearly indicated.

After the advent of the industrial revolution it was, however, the Weber brothers - Wilhelm and Eduard - who, ardently dedicated to the science of gait, in 1836 wrote their famous 'Mechanik der menschlichen Gehwerkzeuge' or, 'The mechanics of the human walking implements. Not only did they attempt to analyse the movement of the lower limbs, but they even explained the individual function of all the major muscles of the leg and foot in effecting flexion, extension, abduction and adduction, and also movements of the toes. Apart from their interest in the longitudinal arches of the foot which they considered were maintained chiefly by the calcaneo-cuboid and calcaneo-metatarsal ligaments, they paid much attention to the great toe and the sesamoid bones, saying: "The main supporting point of the foot, when it has risen so as to stand on the ball, lies on the medial side of the foot, as proved by the greater size of the bones and muscles on this side. We find a special apparatus on this inner side of the foot too that serves this purpose. The first metatarsal bone does not rest directly on the ground, but has a partly cartilagenous, partly bony substrate formed by two little bones, the sesamoids... The body is thus supported at three points: the two sesamoid bones and the great toe, following contraction of the flexor halucis muscle".

However, it was only after the introduction of photography that exact observation of gait became possible (Carlet, 1872; Marey, 1873). The monumental work of Braune and Fischer (1895) and Fischer (1900, 1904), who employed the photographic techniques developed by Marey, was the first to present data on gait that was used to calculate ac-

celerations of moving masses and to estimate joint reaction forces during the swing phase of walking. Fischer's analysis of motion did not throw light on movements within the foot nor was any attempt made to determine the forces acting across the joints of the fore-foot.

R. Fick (1911) closely investigated anatomical details of the foot. He carefully looked into the biomechanics of the longitudinal and transverse arches of the foot, the role played by the plantar ligaments in maintaining the structural form, and made important observations relating to the load distribution under the foot in standing and during gait. Referring to the arches of the foot, he states that their function cannot be explained by simply comparing them to any of those encountered in engineering. He recognises five individual longitudinal arches in juxtaposition with a common member at one extremity, the calcaneous. All arches are sustained by means of strong ligamentous ties on their plantar aspect, and all take a share in maintaining the structural form of the foot under load; the one capable of taking the largest load being the 2nd arch (2nd metatarsal). He also denies the existence of a functional transverse arch at the level of the metatarsal heads, these lying almost in one horizontal plane when the foot is loaded in standing, but points out that the metatarsal bases, however, may well be described as forming one. Fick very definitely disagrees with the general opinion of that time that the foot, like a tripod, must rest on three points while standing: the tuber calcanei, the head of the 1st metatarsal and the head of the 5th, and discusses the information obtained from foot prints which disproves this. Finally, R. Fick examines the structures in the sole of the foot and, referring to L. Fick (1853),

notes that when the toes are dorsiflexed in the metatarsophalangeal joints (such as when 'standing on ones toes') the plantar aponeurosis effects plantar flexion of the toes, thereby causing the latter to also share in carrying the total load. This mechanism is often referred to in current literature as the 'Hicks windlass effect' presumably because Hicks (1954) was the first to investigate, in extenso, the arch supporting mechanism of the plantar aponeurosis and its capability to raise the arch without the action of any muscle.

It is therefore apparent that at the turn of this century, knowledge of the biomechanics of the forefoot had already progressed to a point which only just fell short of information that could solely be obtained by the most modern measuring techniques of today. With the development of electronics and fast, miniature transducers, the much wanted information has been gradually added so that, in the last five decades, most of the significant advances have been made mainly in this respect.

2.3 Studies of Pressure Distribution and Ground Reaction Forces

2.3.1 Earlier investigations (1882-1930):

It has long been recognised that measurement of the pressure distribution between the foot and ground can be of great value in understanding and treating disorders of the feet. Without this, one must depend upon one's own subjective impression, or upon the patients' statement.

The earliest investigator referred to in literature appears to be Beely (1882), who made his subjects step on a linen bag filled with quick-setting plaster of Paris. Beely thought that those por-

tions of the foot carrying the greater weight would make the deepest impressions, and concluded that, in standing, the heel and the heads of the 2nd and 3rd metatarsals were the points of support.

Seitz (1901) had the ingenious idea of observing changes in the blood flow through the capillaries of the sole of the foot, as an indication of magnitude of pressure. He made his test subjects stand on a plate of glass while, by means of a mirror, he observed the change in colour of the skin due to the ischaemia that resulted from the contact pressures that occurred.

In 1921, Milatz presented a quantitative measuring device consisting of rubber bulbs connected to manometers in which pneumatic pressure was made use of, to determine the pressure distribution under three selected areas of each foot. No results were given.

Frostell (1926) used a network of iron wires that was laid onto an inked pad. The net was covered by a paper and the subject made to step on the latter. The higher the pressure, the deeper the net sank into the elastic pad, enabling the paper in the meshes to bear more largely on the inked surface; thus producing a pressure diagram of the foot.

Another method was devised by Abramson (1927) who spread steel shot over a hard surface, placed a lead plate over the shot, and invited his subjects to stand on the lead plate. The depth to which the shot penetrated the plate was a measure of the weight carried by the parts of the foot. He observed that in standing on both feet, the toes only take about 1.8% of the total weight on the foot, half this amount being carried by the great toe alone. The whole forefoot takes 37% of the total load, the rest being taken by the heel. The highest force under the ball of the foot was found below the 1st me-

tatarsal head with the remaining heads sharing the load in a ratio of about 2:1:1:1:1.

In 1927, Basler reported the experiments performed by Seitz with the glass plate (vide supra) but attempted to quantify the results by determining the magnitude of pressure at which the skin becomes completely anaemic. He found this to occur at about 10 kPa (100 g/cm^2). Basler also described a harp-like machine that transferred the load borne by an upward projection on each of ten parallel, horizontal beams that were hinged at one end, to ten vertically suspended strings at the other. By observing the frequency of vibration of each string, the load acting on the corresponding beam was determined, and hence the load distribution across the foot.

Morton (1930) was the first investigator to make use of the elasticity of rubber in dealing with foot pressure. A rubber mat bearing longitudinal ridges was placed in contact with an inked ribbon and paper. As the subject walked over this combination, the ridges widened where the pressure was greatest, making a correspondingly wide impression on the paper.

All these investigations were performed to determine the load distribution under the sole of the foot and although it became universally accepted that the heel bore a large amount of the total load in standing, the manner in which the remaining load was distributed across the forefoot was still very much debated. Whereas Beely, Muskat and Momberg believed that the 2nd and 3rd metatarsal heads were more highly loaded than the others, Seitz was convinced of the 1st and the 5th being the ones that mainly supported the forefoot (Hohmann, 1939). Frostell (1926) was basically of the same opinion as Beely, Muskat and Momberg, but made allowance for some individu-

als in which the 1st metatarsal head definitely took the largest share. He also observed that in quick walking, the load distribution is readjusted to load the 1st metatarsal more than otherwise. The matter of load distribution during gait was still more difficult to deal with since, up to this time (1930), no one had yet conceived a device to register the variation of load distribution as a function of time.

The old question as to whether callosities and some forms of cellulitis often found under the second and third metatarsal heads are primarily due to an unphysiological loading pattern, or whether they are only evidence of the normal load distribution and hence particularly exposed to high bearing pressures, had still not found a unanimous answer in the middle of the 30's.

2.3.2 More recent investigations (1933-1985):

Staudinger (1933) was one of the first to carry out a fairly exact quantitative analysis of the pressure distribution under the sole of the foot, but, however, only in the standing position. He used a mirror with reflected ray and photosensitive paper to measure the deflection of a membrane that was subjected to the pressure under the foot. By moving the measuring cell in the horizontal plane, he mapped the pressure at various points and after interconnecting points of identical pressure values, obtained 'isobars'. Staudinger plotted these isobars onto an X-ray picture and showed a pressure distribution across the forefoot with a maximum under the 1st metatarsal head, and a continuous decline towards the 5th.

Elftman (1934) was however the first to make use of cinematography in conjunction with a rubber mat, similar to the one used by

Morton (1930). Elftman's rubber mat was studded with pyramidal projections that rested on a heavy glass plate. As the subject walks over the mat, the area of contact of each pyramid with the underlying glass increases in proportion to the pressure exerted by the overlying foot. A white fluid which filled the spaces between the pyramids of black rubber enhanced the contrast when viewed from below. Records were made with a motion picture camera at the rate of seventy-two frames per second, and for the first time delivered information on the distribution of pressure from moment to moment, instead of the composite pictures that had been obtained in the past. Elftman observed that following heel-strike, the pressure under the heel rises while it rolls forward until the ball of the foot comes into contact with the mat. As movement continues, the pressure under the heel diminishes while that under the ball of the foot increases. The toes are brought into play, until finally, they alone exert some pressure before the foot eventually leaves the ground. He also reported that the pattern of distribution of pressure in the ball of the foot varies with the relative length of the metatarsals and also with the amount of toeing in or toeing out. He observes that a line joining the area bearing the greatest pressure in the heel with the area bearing the greatest preasure in the ball of the foot tends to remain parallel to the direction of progression. The results were, however, more qualitative than quantitative in character, due to the difficulty in determining the exact area of contact between the flattened rubber pyramids and glass.

Schwartz and Heath (1947) demonstrated the first electric resistive load cell to be used to measure the force under the lateral and medial aspects of the heel, the 1st, 3rd and 5th metatarsal heads, and the great toe. The load cells, each consisting of a pile

of carbon discs, were secured with scotch tape to the plantar surface of the foot. Employing an oscillograph, they were probably the first to make time-dependent recordings of forces at multiple points under the foot. In 1964, Schwartz et al. reported on a quantitative analysis using the same configuration of transducer arrangement as in 1947, and showed that the head of the 3rd metatarsal bore the highest load in the forefoot. (The force under the 2nd metatarsal head had not been measured!)

In 1963, Baumann and Brand described a capacitive type load cell that was only 1 mm thick with a pressure-sensitive area of 1 cm^2. Such transducers were placed under the 1st, 2nd and 5th metatarsal heads, the great toe and the heel. They observed that during the forefoot phase, in a normal subject, the 2nd metatarsal head bore far more weight than the 1st, but remark, however, that this distribution varies from person to person. (Baumann , however, did not measure the load under the 3rd metatarsal head!)

Collis and Jayson (1972), using a semiconductor strain gauge, built a flat transducer (2 mm thick and 11 by 12 mm) that was attached to the foot underneath each of the metatarsal heads of ten subjects. The results were presented as ratios between the pressure measured under each metatarsal head and that under the heel. The highest pressure ratios were recorded under the 2nd and 3rd metatarsals, with low pressure ratios under the 1st and 4th, and the least under the 5th.

Stott et al. (1973) presented results of an extensive investigation of the forces under the foot using a series of twelve parallel beams that rested on load cells (with electric resistance strain gauges) that measured only the vertical force on each beam. By tak-

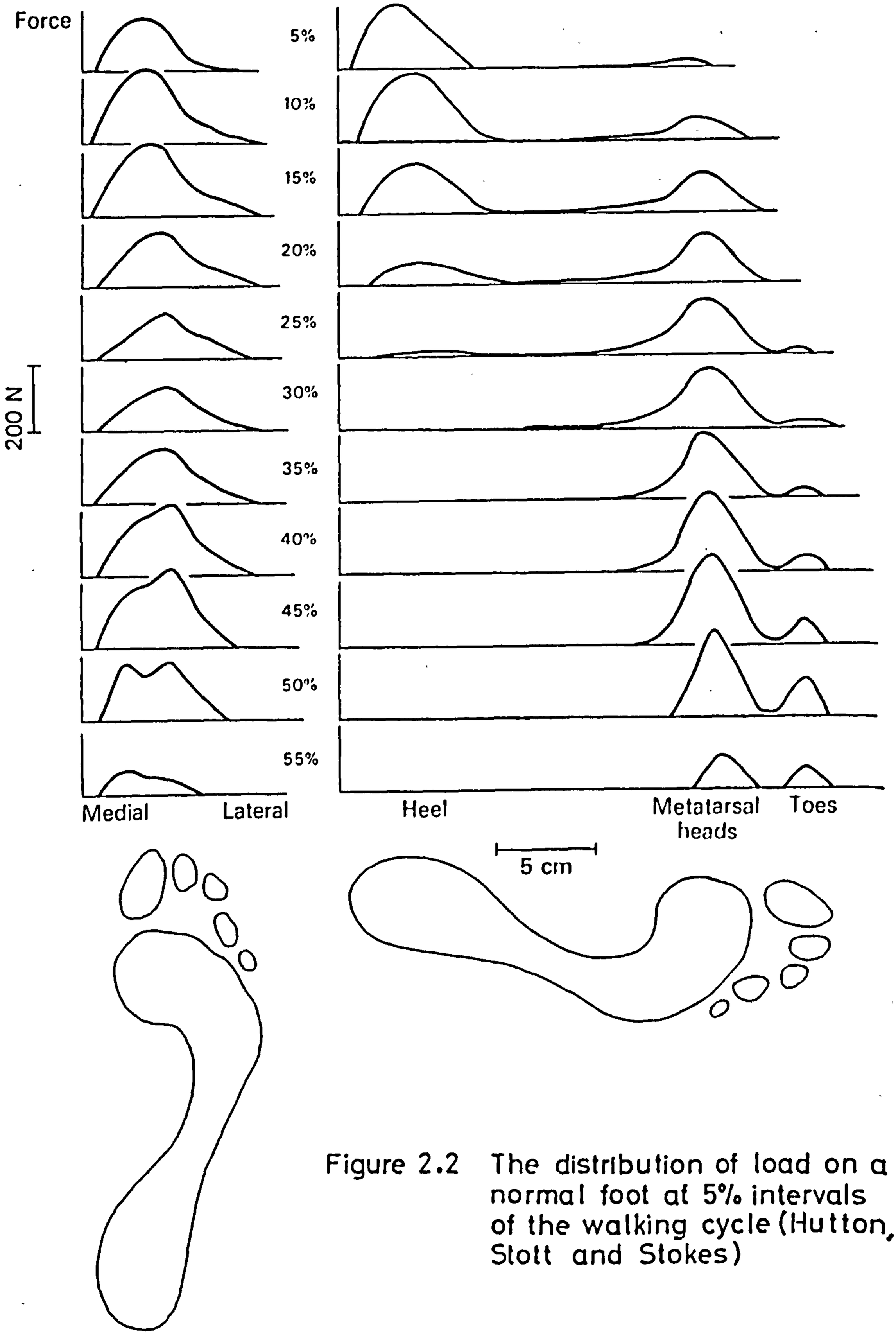

Figure 2.2 The distribution of load on a normal foot at 5% intervals of the walking cycle (Hutton, Stott and Stokes)

ing recordings with the beams, first arranged longitudinally and then transverse to the direction of walking, the force distribution in the longitudinal and transverse direction of the whole foot was obtained. However, because of the relatively small sensitive surface area of the set-up, it was not possible to accommodate the complete foot during any single test, and therefore several tests were necessary to build up a composite load distribution on the whole foot. Stott et al. observed that there is considerable variation in the way maximum loads are distributed across the forefoot in normal subjects during walking and that there is a marked step to step variability too. In some, the peak load falls on the first metatarsal 'segment' while in others this 'segment' of the foot carries low loads compared with the 2nd and 3rd metatarsal bones. Typical values obtained were as follows: about 40% body weight (BW) under the 1st metatarsal head with a decline to about 10% BW under the head of the 5th metatarsal. They also observe, that when the subject stands still the load is distributed fairly evenly across the forefoot but there is no indication of where the maximum loads occur during walking. A further interesting observation is that the forefoot distributes the load more to the lateral side of the foot at the slowest walking rate.

The same authors (Hutton, Stott and Stokes, 1982), using an improved force plate with 128 square areas, later on gave a more detailed account on the progression of forces under the foot in normal walking (fig 2.2). They observe: "because the line of the metatarsal heads is not transverse to the direction of walking, but inclines laterally and backwards by about 30°, as the foot tips forward on the metatarsal heads, the lateral metatarsal heads tend to leave the

ground and the centre of load moves medially". A diagram showing the pathway of the centre of load shows that this follows an almost straight line from the centre of the heel to an area occupied by the 2nd metatarsal head, thereafter curving slightly medially to terminate in the centre of the great toe. In standing, the centre of the load was found to vary between 1.5 and 5 cm in front of the ankle joint while the distribution of load across the forefoot was such that the central metatarsals were usually loaded more than the others. The normal midfoot was found to carry very little load.

In 1975, Grundy et al. used a force plate that not only permitted determination of the exact location of the centre of pressure beneath the foot, but also allowed simultaneous observation of the contact area between the foot and a glass plate. In comparing results obtained with normal bare feet, normal feet with various footwear, and with those suffering from disorders of the foot, they examine not only the course taken by the centre of pressure during stance, but also the velocity of the centre of pressure. They infer that the midfoot plays little part in transferring load, that the forefoot is much more important than the hindfoot in transferring force, and that the toes transmit 'very little' force.

Arcan and Brull, 1976, reported on a novel method to record the pressure distribution between each foot and the ground during standing or walking. They used a thin leather sole on which a number of hard hemispherical projections were firmly attached. The projections acted against a layer of photoelastic material that carried a reflective layer on its upper surface and which was supported by a glass plate beneath. By viewing the underside of the photoelastic material through the glass plate in polarised light, circular interference

fringes are seen due to the contact force, the diameter of the circles being a non-linear function of the force exerted. The authors examined a 'typical' case of standing on both feet and concluded that with both feet loaded equally (symmetric), the forefoot carries 37% of the load while 63% is carried by the heel. These results are identical with those obtained by Abramson in 1927.

Scranton and McMaster (1976) used a unique method to investigate the distribution of forces under the foot. They employed a liquid crystal technique in which shear-sensitive, cholesteric crystal encased in a flexible plastic sheet was used. A motion picture camera recorded the changes in color -from light to dark blue - that issued from the changes in specific shear forces. Only qualitative results were reported for walking and running: In both cases, forces were reported to shift smoothly to the lateral midfoot, lateral toes, great toe and finally to the metatarsals. Apart from the meagre information given on the use of liquid crystals, the article contains nothing of fundamental value.

Stüssi (1977), using a Kistler force plate, presented the resulting space vectors in 20ms intervals during the stance phase. The trace of the centres of pressure was, however, not correlated to anatomical details of the foot.

Nicol and Henning (1978) employed a matrix of 256 capacitors, made by applying 16 parallel conducting strips on each side of a rubber mat, the strips on one side being arranged in an orthogonal direction to those on the other, to determine the load distribution under the foot. A multiplexing system that incorporates each capacitor sequentially in a simple voltage divider circuit produced a display of varying light intensity from an array of light emitting

diodes, so arranged as to correspond to the arrangement of capacitors. The method might be described as semi-quantitative. The distribution of vertical forces under the foot in hopping and during the take-off phase in broad jump were illustrated.

Cavanagh and Michiyoshi (1980) took up the method used by Arcan and Brull and, using a motion picture camera operating at 100 frames per second, presented data obtained from an array of about 25 x 6 measuring points directly under the foot. The data was displayed in three-dimensional form incorporating perspective distortion (as first employed by Abramson in 1927!), the pressure estimate from each transducer being plotted as the component perpendicular to the plane of the foot outline. The investigation showed the anterior migration of pressure until, in slow barefoot gait, for example, the peak pressure under the first and second toes reached approximately 0.6 MPa, 550 ms after heel contact. The presentation, however, does not allow much quantitative information to be extracted. In 1985, Cavanagh and Rodgers reported on the pressure distribution when standing, walking and running. They mention that in most subjects the average peak pressure in the forefoot, while standing, was only 38% of the rearfoot values and that a tendency for the lateral three metatarsal heads to bear a larger load than the 1st and 2nd metatarsal heads was noticed.

In 1982, Duckworth et al. published very comprehensive results on pressures under the foot of normal subjects and compared the results with those obtained from patients with foot disorders. They used an optical method based on the original idea from Chodera (1957) in which a thin sheet of opaque reflective plastic is viewed through a glass plate. The subject stands on the plastic foil while illumina-

tion is effected through strip lights positioned along the edges of the glass plate. Total internal reflection at the glass-plastic boundary is affected by the contact pressure, resulting in a varying intensity of the impression when observed. When recorded in black and white, a scale of grey shades can be used to express the magnitude of pressure directly. Duckworth et al. found that the peak pressures under the 1st and 2nd metatarsal heads in normal walking were of the same level, of about 1 MPa ($1N/mm^2$), at approximately 62% of the gait cycle. A little later in the cycle, the great toe was also subjected to the same maximum pressure. The peak pressures under the remaining metatarsal heads were observed to lie along a gradient that declined to about 0.15 MPa under the 5th metatarsal head during gait.

Also in 1982, Diebschlag used a method similar to that first introduced by Elftman in 1934 (described earlier in this section). The extent of flattening of the pyramidal rubber studs of the mat was, however, determined by an automatic scanner that evaluated the grey intensity. The procedure of subsequent evaluation and presentation of results was very similar to that undertaken by Duckworth et al.. It is interesting to note that the highest values determined in the region of the metatarsal heads was in the order of only 0.4 MPa when walking at a rate of 5 km/h. Also, Diebschlag points out the existence of a three-point support: the heel, the head of the 1st metatarsal and that of the 5th! He also describes the pathway taken by the point of maximum pressure (centre of pressure?) as moving from the centre of the heel to the head of the 5th metatarsal and then on to the head of the 1st metatarsal, before terminating at the tip of the great toe; which stands in sharp contrast to that repor-

ted by several other investigators.

2.3.3 Concluding remarks on pressure distribution and ground reaction forces:

The literature review shows that basically all the attempts made to determine the loading pattern under the foot may be divided into three groups:

A. Pressure distribution

B. Force distribution

C. Location of centre of pressure

In particular, careful differentiation must be made between the groups A and B especially, since more often forces are primarily measured under discrete areas beneath the foot and subsequently, pressures mapped. Also, in considering results involving the magnitude and pathway taken by the centre of pressure, one should be fully aware of the momentary distribution about this 'centre' at every instant during the stance phase if wrong conclusions are to be avoided. Generally, recent developments are more successful at producing quantitative rather than just qualitative results. However, the tolerance limits of measurements are usually not mentioned so that the accuracy of the presented values is often questionable, especially where pressure distribution is concerned.

Some of the most comprehensive data collected belonging to group A (pressure distribution) is presented by Duckworth et al. (1982) while that of group B (force distribution) has been published by Hutton et al. (1982). In both cases, however, it is difficult to extract quantitative information about the forces acting between the ground and the heads of the metatarsals and at the pads of the toes;

in the first case, integration of pressure (N/mm^2) must be performed over a chosen area and in the second, the curves of load distribution (N) presented have first to be broken down into discrete steps that cover the bearing area of interest.

Hence, apart from some explicit but unfortunately incomplete information given by Baumann and Brand (1963) and Schwartz et al. (1964) on the loads under the metatarsal heads and pads of the toes, no specific useful data was found. This therefore made special investigations, reported in Chapter 5, necessary.

2.4 Muscle, Tendon, and Electromyographic Studies

2.4.1 Studies of muscles and tendons:

Some studies of the mechanical effects of muscle were certainly performed by Borelli three centuries ago. Probably this dates the beginning of scientific investigations into the mechanics of skeletal articulations and, after all, the effect of muscle forces acting across the joints. However, the Weber brothers (1836) were the first to suspect a direct relationship between the size of a muscle and the magnitude of force exerted by it. They weighed individual muscles of the lower limbs and after grouping them into two classes, extensors and flexors, observed that the mass of extensors was more than twice that of the flexors. (Those muscles crossing two articulations were recognised to be extensors of one joint and flexors of the other, and therefore one half of the total mass of these was added to that of each group that could be clearly classified, before arriving at the result mentioned). They expressly mentioned, however, that the weight of muscles is by no means alone a measure of their force potential, this being also dependent on 'chemical and organic

conditions'. About seven decades later, Strasser (1908) described the anatomy of muscle, including fibres and fibrils, mentioning that the fibrils contain the contractile substance. Also hypothesised, was that the fibrils could be further broken down into elements of shorter length (sarcomeres) that would still possess contractile properties. Most interesting, however, is that he specifically notes "through attaching several elementary particles behind each other in a row, or by connecting muscle fibres end to end, the change in length upon contraction can be vastly increased; not, however, the force. On arranging the functional elements (fibrils or fibres) side by side on the other hand, the change in length will not be increased but the total force exerted, instead". This assertion has only recently been repeated - in an almost identical form - by Wickiewicz et al. (1983).

During the last 80 years much research has been done to understand the contractile mechanism in muscle (a comprehensive review is given by Huxley (1974)) and yet, present prediction of force that would be exerted by a given muscle during a particular activity can still deviate up to 800% (Brand et al., 1986)! Active force generation in a muscle is known to depend upon several parameters, mainly: the muscle fibre (type, number, orientation, area of cross section and momentary length), the mode of contraction (isometric, lengthening or shortening), and whether the muscle is fatigued or at rest. Nevertheless, ever since the Webers first attempted to find a relationship between muscle weight and mechanical action 150 years ago, it has always been considered mandatory to include some measure of muscle size in predicting muscle force, even to the extent of excluding all other possible factors.

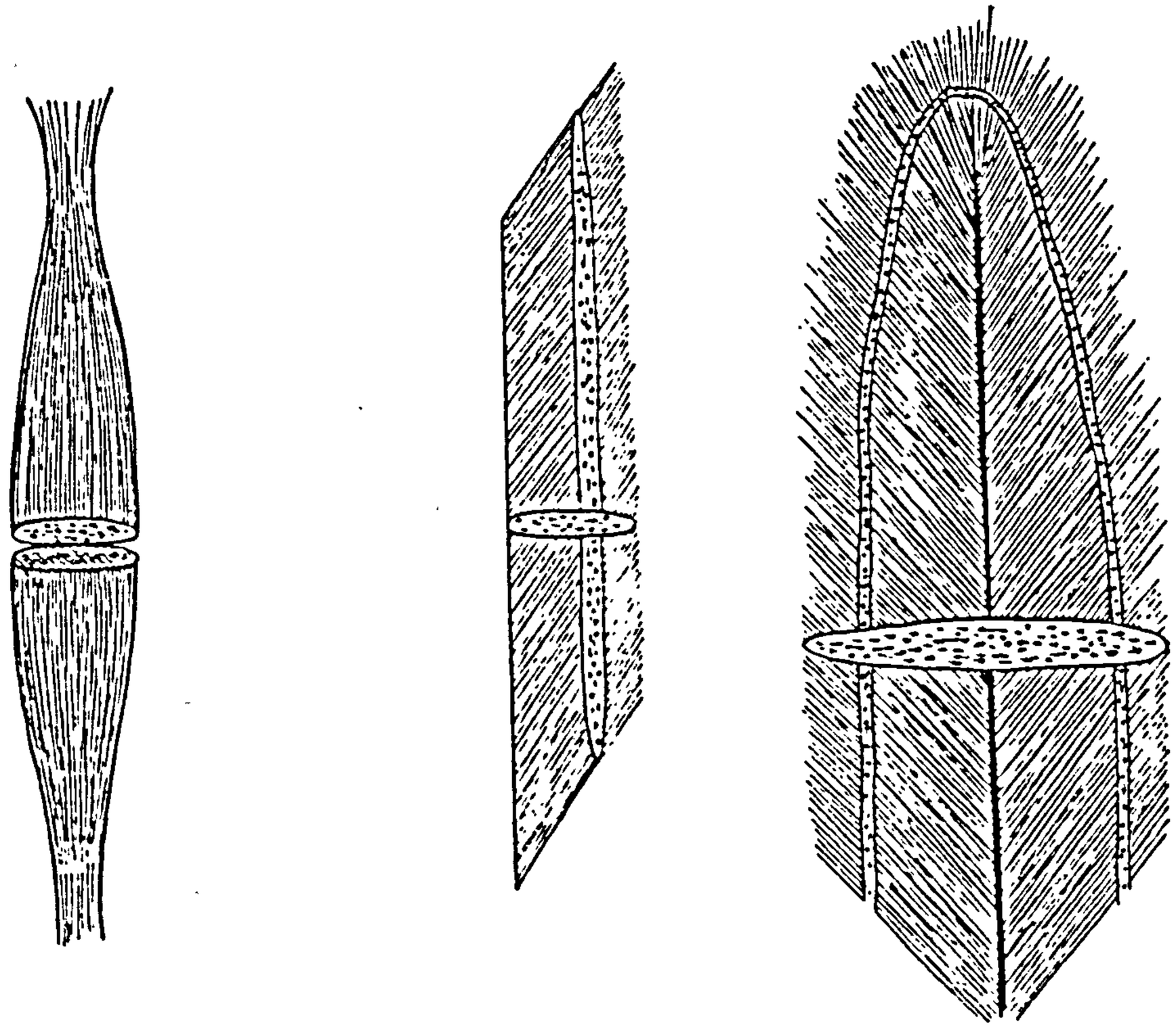

Figure 2.3 The physiological cross sectional area (PCSA) of parallel fibred and pennate muscles according to Fick (1910)

R. Fick (1910) was one of the first to apply the area of cross section of a muscle to estimate the magnitude of force that could be expected of it. Fick discussed the action of parallel fibred and pennate muscles, fig. 2.3, in extenso, suggesting the use of an 'oblique factor' (cos α) when calculating the pull on the tendon from the total muscular force that in turn is derived by multiplying the muscle's physiological cross sectional area (PCSA) by a factor representing force per unit area. The PCSA was defined as the area normal to the direction of every fibre. Fick, however, goes on to note that the obliquity of the fibres in a pennate muscle is usually such that this detail could be neglected and that, since the PCSA closely approaches the anatomical cross sectional area, the latter might be used instead. Referring to investigations carried out by J.V. Johnson, as reported by R. du Bois in 'Ergebn. d. Physiol., Bd. 2, 1903, Heft 2', Fick used a value of 0.98 MPa (10 kg/cm^2) for the factor representing force per unit area, which he termed the 'muscle force unit', to estimate the average peak force that a muscle could exert.

Several investigators have ever since used this approach which involved the PCSA of a muscle - however defined - to directly estimate the force exerted by it and to determine the resultant force acting at the joint (joints) it crosses (Haxton, 1944; Ikai and Fukunaga, 1968). Use of the PCSA can be also particularly convenient when dealing with statically indeterminate problems such as in determining conditions of equilibrium about a joint that involves the action of more than one muscle in balancing the effect of an external load. This application in which the ratios of PCSA rather than their absolute values are used, has been attempted by Alexander and Vernon

Table 2.1 Physiological cross sectional areas of muscle in cm^2 as determined by various investigators.

Muscle	Alexander and Vernon (1975)	Brand et al. (1986)		Wickiewicz et al. (1983)		
	1*	2*	3*	4*	5*	6*
Tib.ant.	14 (8)	17	9	13 (5)	8 (5)	9 (5)
Ext.dig.long.	8 (15)	8	4	4 (5)	6 (10)	6 (10)
Ext.hall.long.	-	7	2	2 (5)	2 (5)	2 (8)
Gastrocnem.(M)	22 (16)	51	17	29 (10)	39 (15)	29 (25)
Gastrocnem.(L)	13 (8)	14	9	-	-	-
Soleus	67 (20)	187	58	58 (30)	-	-
Tib.post.	17 (20)	26	19	25 (15)	15 (10)	23 (10)
Flex.dig.long.	-	6	6	6 (10)	5 (5)	4 (5)
Flex.hall.long.	-	19	9	6 (15)	5 (10)	4 (5)
Peron.long.	11 (11)	25	8	12 (10)	17 (10)	7 (10)
Peron.brev.	-	20	5	5 (5)	8 (5)	5 (5)
Peron.tertius	-	4	1	-	-	-

*
1: male specimen 1.66 m, 603 N, 48 yrs
2: male specimen, 1.83 m, 893 N, 37 yrs
3: female specimen, 1.63 m,579 N, 63 yrs
PCSA = volume/averaged fibre length.
4-6: details unknown
The values in parenthesis are the angles of pennation.

(1975). Amis et al. (1980) and by the author, Jacob et al. (1976). (Jacob et al. used the ratio of the PCSA of the glut. med. to that of the glut. min. in distributing the total pelvitrochanteric force over the lateral surface of the pelvis model in their experimental investigations). Ripperger et al. (1980) used a similar technique to calculate the relative contribution of shank muscles at the ankle but, as Procter (1980) points out, they used PCSA's on a basis of muscle volume divided by overall muscle length - instead of muscle fibre length - which gives correct values for parallel fibred but not for pennate muscles. PCSA's, as obtained by dividing the muscle volume by the average length of muscle fibres - not muscle length - were determined by Brand et al. (1986) who arrived at the results shown in Table 2.1. These investigators did not however, use the PCSA's directly to predict the force in each muscle but also took the time of contraction into consideration, believing that 'endurance' is the determining factor in the sharing of force amongst simultaneously cooperating muscles. Using a non-linear relationship between the time of contraction and the muscular force, a non-linear optimization technique (Crowninshield and Brand, 1981) was employed to predict the forces in the muscles of the lower limbs during locomotion.

Thus, the PCSA of muscle has been used in three main ways for the assessment of muscle forces: Firstly, by applying to it a 'muscle force unit', as Fick called it, to directly obtain the maximum force generated. (Table 2.1 shows the values of PCSA given by some authors and Table 2.2 shows stress values that have been estimated); secondly, by using ratios of PCSA's to weight the contribution of muscles cooperating in a particular activity; and thirdly, by using

Table 2.2 Maximum stress values estimated for human muscle in isometric contraction

Investigators	Max. stress [kNm^{-2}]
Alexander and Vernon (1975), combining their own anthropometric data with maximum forces estimated by Lindahl, Movin and Ringqvist, for the quadriceps :	380 - 210
Alexander and Vernon (1975), combining their data with that from Smidt. for the hamstring muscles :	400
Fick (1910), quoting Johnson for the elbow flexors :	1000
Haughton (1867), for the arm: for the leg:	654 760
Haxton (1944), for the gastrocnemi and soleus :	380
Ikai and Fukunaga (1968), for the elbow flexors :	600

the PCSA together with some other factor (e.g. time of endurance, which could also be a function of the PCSA) so as to satisfy conditions for some chosen optimizing criterion. The first two applications are based on the equal stress criterion that is hypothesised to apply to a strenuous situation in which muscles which are cooperating in a group are likely to have their fibres similarly stressed as their maximum strength is approached. However, since some simultaneous action from antagonists - especially across multiaxial joints - is to be expected (this being usually totally neglected) and in view of the fact that through training, muscle force can be increased by nearly 40% while an increase of PCSA of only 23% has been noted (Komi, 1975), one must be cautious when considering the validity of use of a muscle's PCSA in estimating the force generated.

Already in 1867, Haughton proposed that "the force of a muscle is proportional to the cross section of the tendon that conveys its influence to a distant point", and this presents a further alternative to using the muscle's PCSA. Because of the doubt surrounding calculation of PCSA, Procter (1980) made use of the tendon cross section as a participation factor in determining the force shared by cooperating muscles.

The tendons of the foot, especially those proceeding from the intrinsic muscles, have not yet been examined in any detail from a biomechanical point of view, as far as the author is aware. Apart from the details already given in the preceding chapter relevant to the general anatomy, no data on the size or exact position and direction taken by the tendons at their points of insertion are known. The only attempt, known to the author, at determining the forces acting on the metatarsals during normal walking was performed by

Stokes et al. (1979). These investigators, however, made such simplifications to the geometry of the metatarsophalangeal joints and to the course taken by the flexor tendons that their results appear questionable. The assumptions they made in describing the profiles of the metatarsal heads will be treated later in Section 2.6, but also the line of action of the flexor tendons with respect to the phalanges was taken to be parallel to the ground (fig 2.8), whereas actually, after passing around and below the metatarsal heads they proceed anteriorly and dorsally to meet the base of the phalanges at an angle of about 30° to the horizontal.

2.4.2 Electromyographic studies:

At the end of the eighteenth century, Galvani reported that skeletal muscles will contract when stimulated electrically and, conversely, that they produce a detectable current or voltage when they contract from any cause (Basmajian, 1976). While the first part of Galvani's discovery was made use of by the neurophysiologist Duchenne a hundred years ago to electrically stimulate intact muscles for the systematic determination of the dynamics of skeletal muscles, the second aspect, namely that muscles produce electricity, could only be reasonably exploited after voltage amplifiers with high input resistance, that were capable of amplifying the low-level signals from the rather high resistance sources became available. However, before this could be accomplished, the only way to determine the activity of muscles was by means of palpation. R. Scherb*

---

* R. Scherb, a pioneer of gait analysis, carried out these investigations while he was Director of the BALGRIST orthopaedic clinic, Zurich, from 1925-1952.

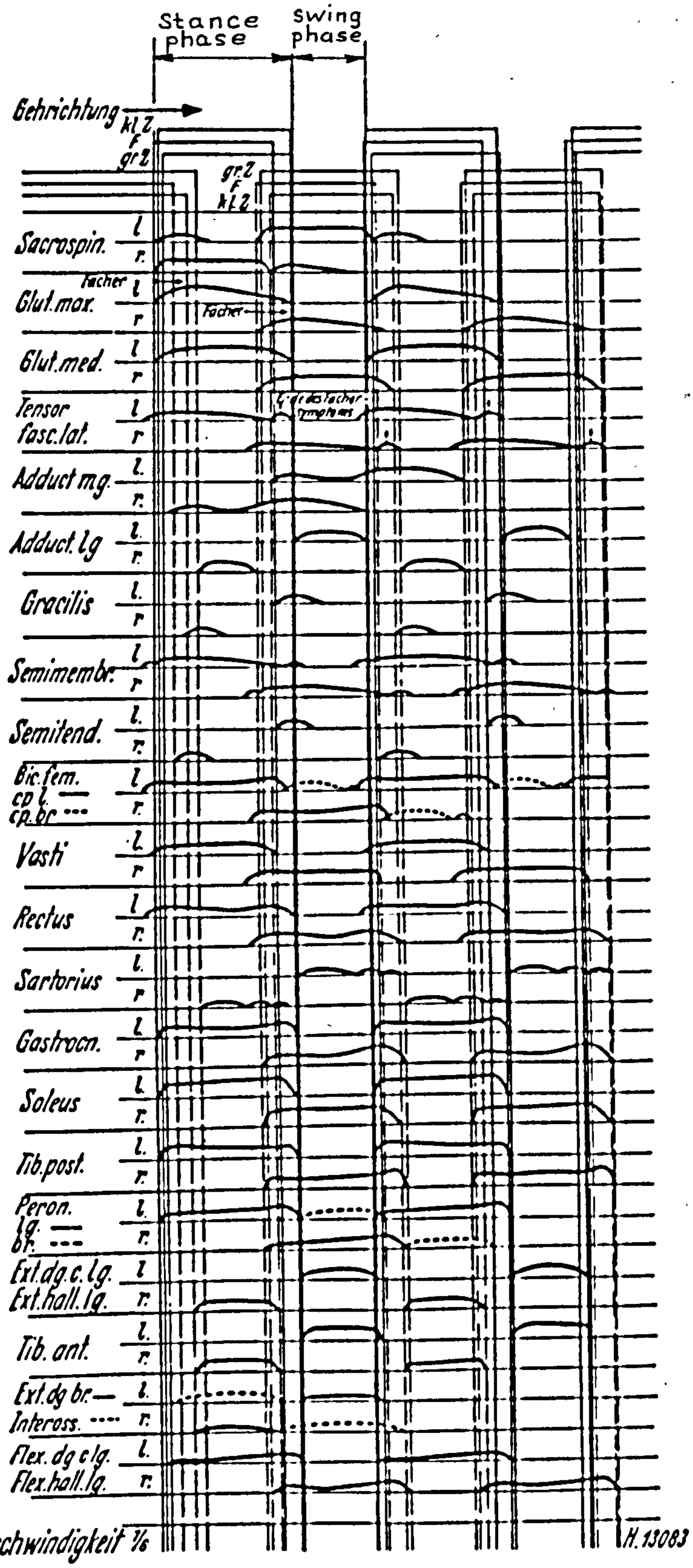

Myokinesigramm. Physiologische Verhältnisse

Figure 2.4 Scherb's myokinesigram (shown by Francillon, 1957)

(1926) used a hand-operated tread mill that allowed him to palpate all accessible muscles during gait. With the aid of a simple heel switch he recorded the phasic activity of almost every crural muscle and also some of the trunk (fig 2.4). During the last forty years, however, electromyography (EMG) has been used to study the activity of almost every muscle of the human body in kinesiological and psychophysiological investigations (Scherb and Arienti, 1945; Basmajian, 1978).

It would be beyond the scope of this thesis to enter into a discourse of muscle physiology in relation to the EMG signal and reference must be made to the specific literature on this subject (e.g. Basmajian, 1974). Yet a brief synopsis of some relevant details is given as follows:

When a single impulse reaches the muscle fibre through the axonal branch of the nerve, a brief twitch occurs as the fibre contracts. Immediately after this, rapid and complete relaxation follows. The duration of this twitch varies from a few milliseconds to as much as 0.2 seconds, depending on the type of fibre involved (fast or slow). During the twitch, as depolarisation propagates along the muscle fibre, an electromagnetic field is generated and a very low voltage is induced that lasts for only 1 to about 4 ms. Measurement of single fibre potentials has shown these to be in the order of 6 mV with a spike duration of about 470 μs (Basmajian, 1974, referring to investigations done by Ekstedt). Since all the muscle fibres of a motor unit do not contract exactly at the same time - there being a delay of several milliseconds between the first and the last - the motor unit potential recorded from a single twitch can last for 5 to 12 ms. In order to sustain a muscle contraction,

the motor units must be repeatedly activated, this being manifested by a train of impulses. When the force requirements increase, not only does the firing rate of individual motor units within the given muscle increase, but additional motor units within the muscle are also progressively recruited. The resulting signal composed of superimposed potentials, as picked up by electrodes during this period, then exhibits voltage peaks in the order of 0.5 mV but can vary on either side of this figure by a factor of ten, depending on the location and type of electrodes. The sensing electrodes for picking up the EMG signal may be applied in the form of surface electrodes attached to the surface of the skin, or by insertion into the muscle itself in the form of special needles or wires. The period of mechanical twitch lasts much longer than the electrical motor unit potential; this in the case of 'slow fibre motor units' that take as long as 100 ms or more to completely relax. The EMG signal is known to depend upon several parameters such as: external load, length of muscle, rate of contraction, age, sex, fatigue, type of muscle (slow or fast), and measuring technique. This makes quantitative determination of muscle force through EMG extremely difficult and a direct relationship of force to EMG is only possible under very restricted conditions of muscular excursion, load, and rate of contraction.

EMG is, however, a reliable indicator of the temporal activity of muscles and it is frequently used to characterise the phasic activity of the muscles of the leg during walking. However, the time-lag between EMG activity and muscle force generation must be taken into consideration when relating muscle activity to locomotion activities. Paul (1971) reviewed literature on leg muscle EMG and made the recommendation that EMG signals should not be interpreted in

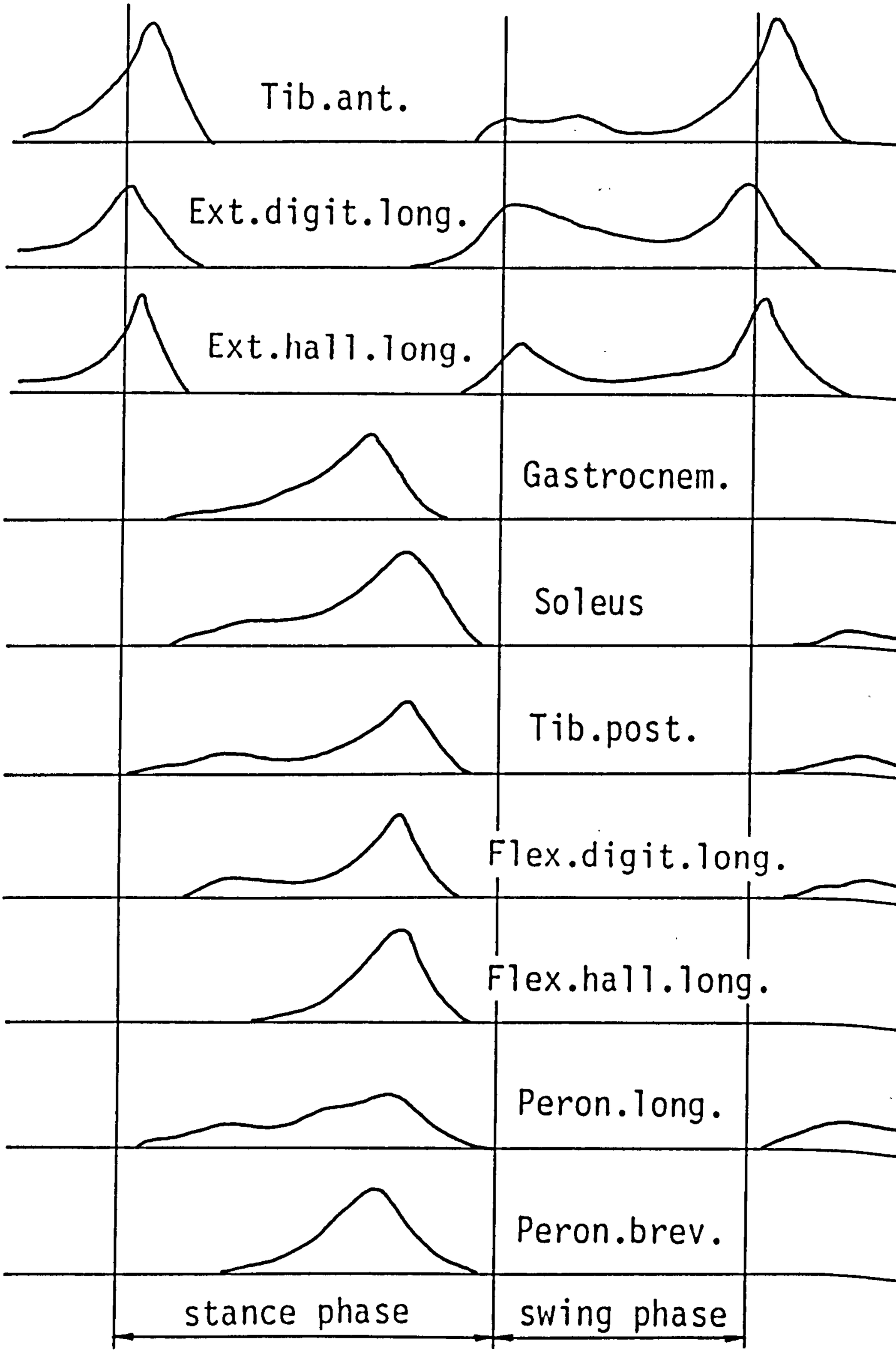

Figure 2.5a EMG patterns; normal level walking (Univ. of California)

TEXT BOUND INTO

THE SPINE

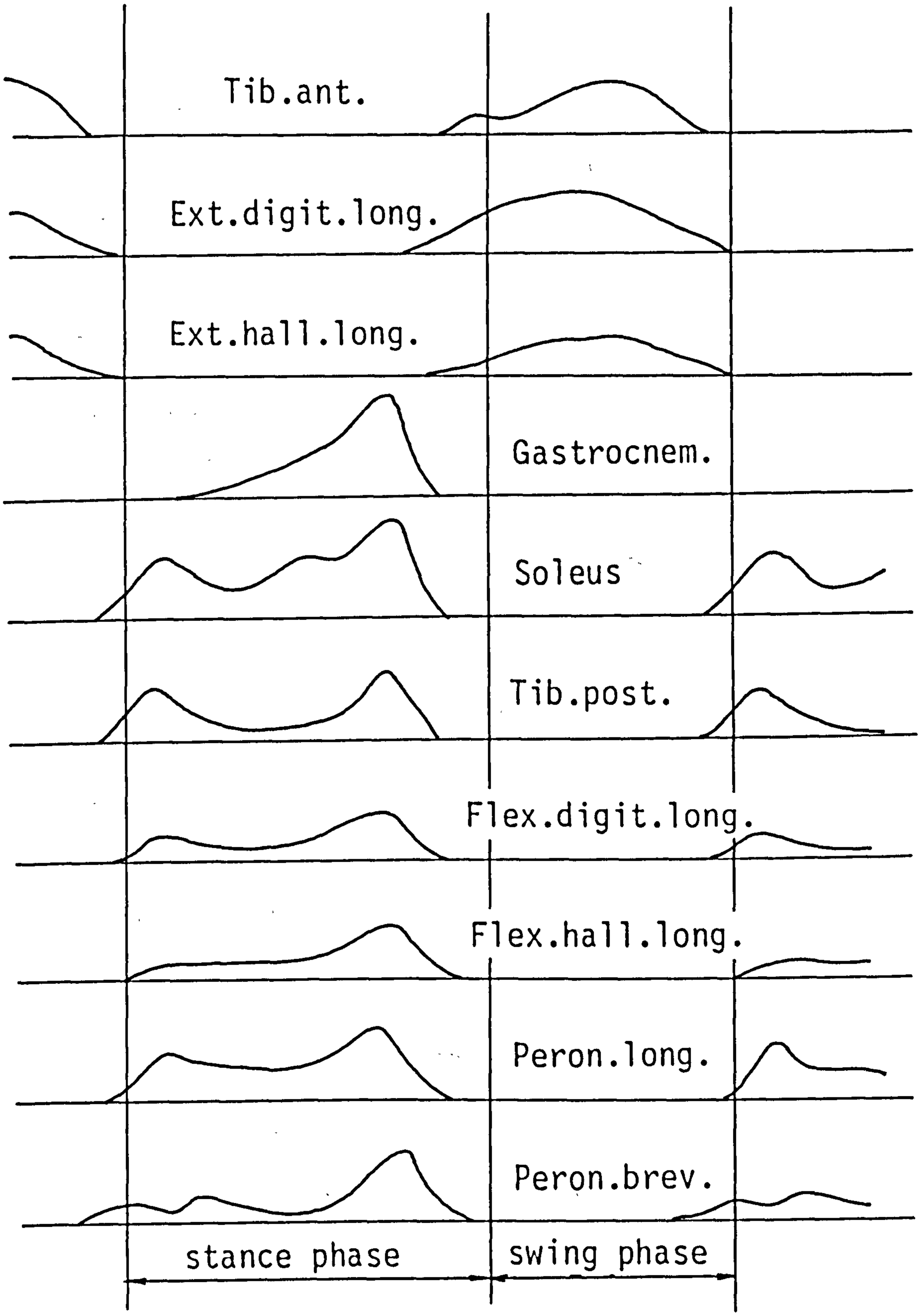

Figure 2.5b EMG patterns; walking up stairs (Univ. of California)

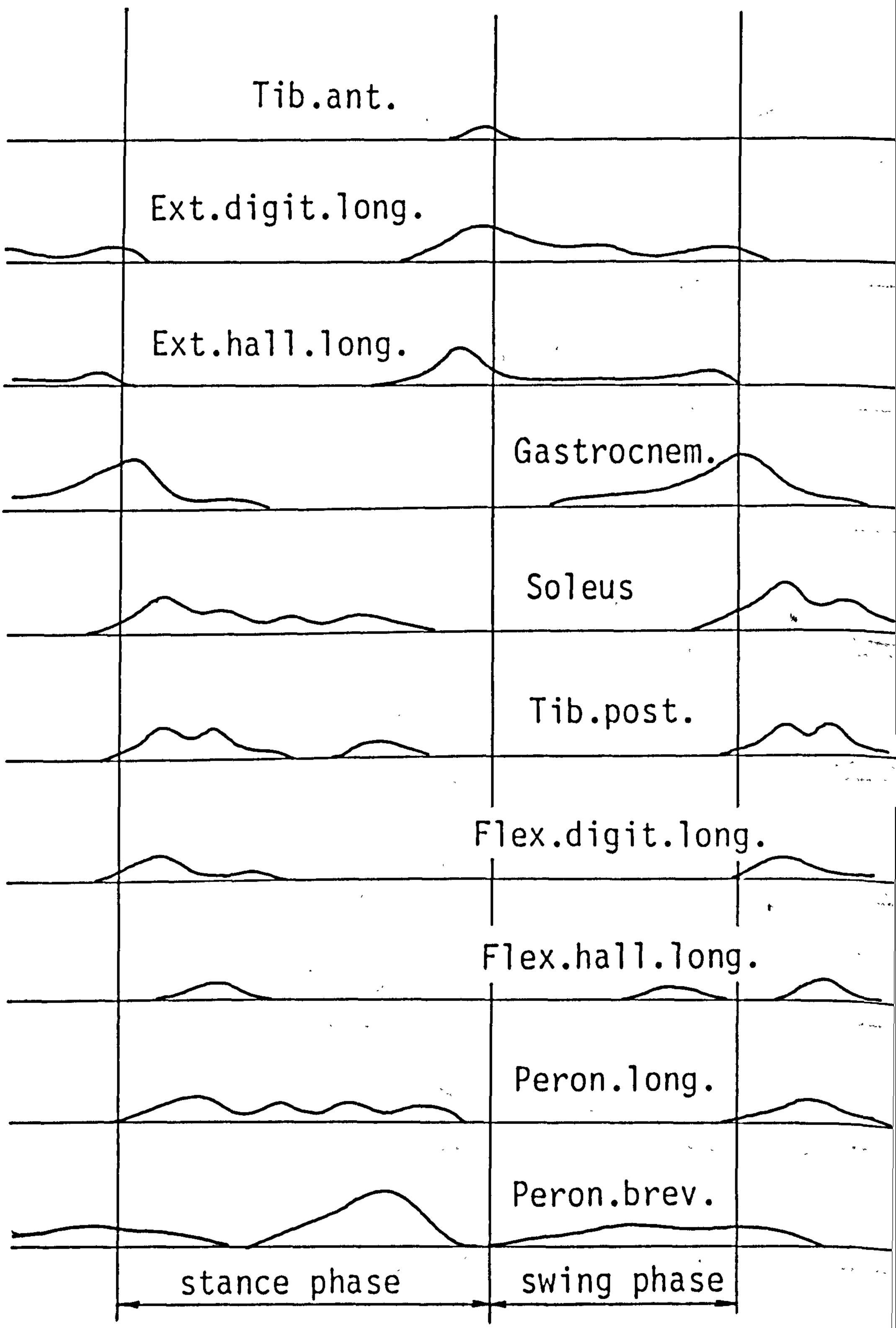

Figure 2.5c EMG patterns; walking down stairs (Univ. of California)

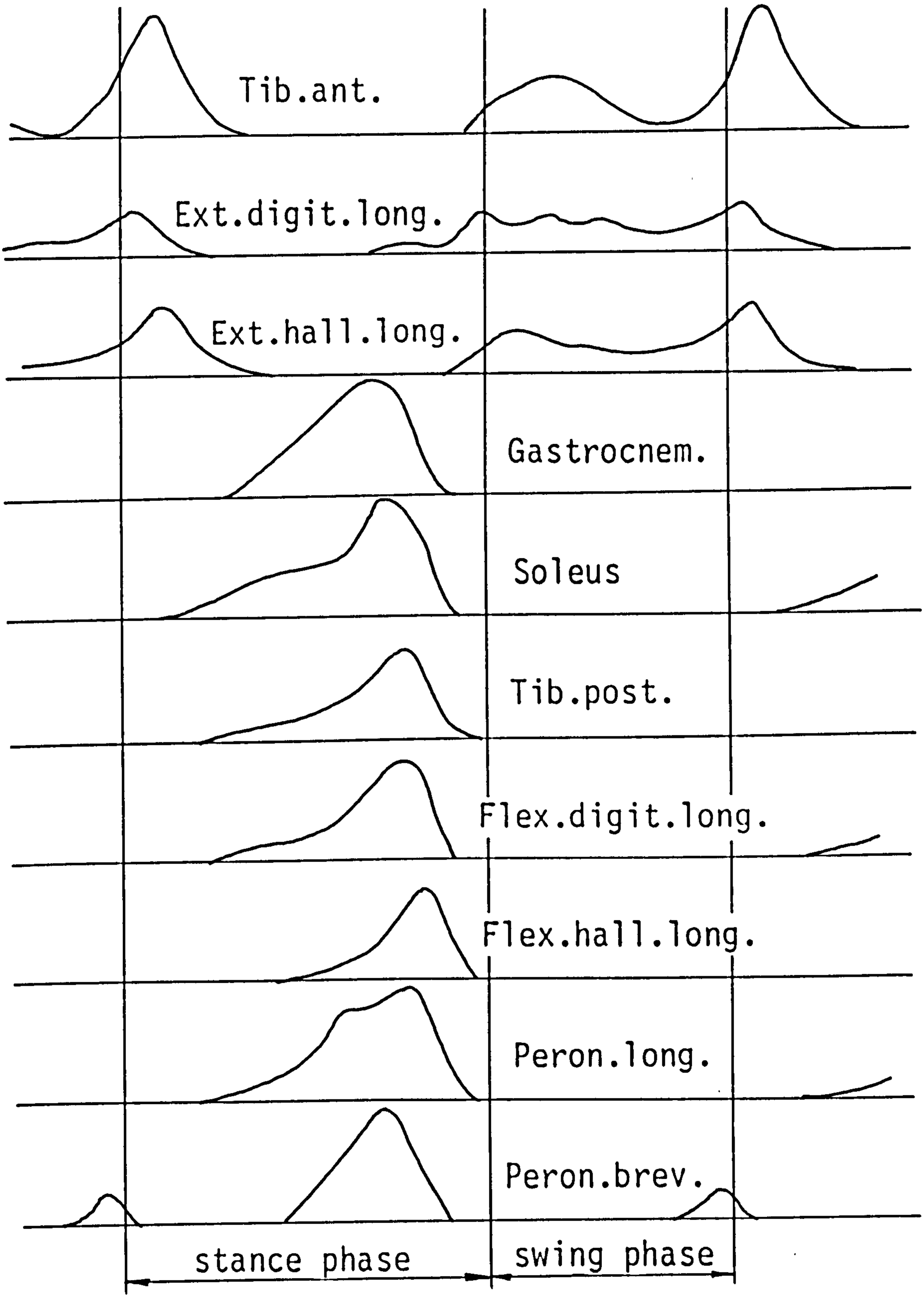

Figure 2.5d EMG patterns; walking up ramp
(Univ. of California)

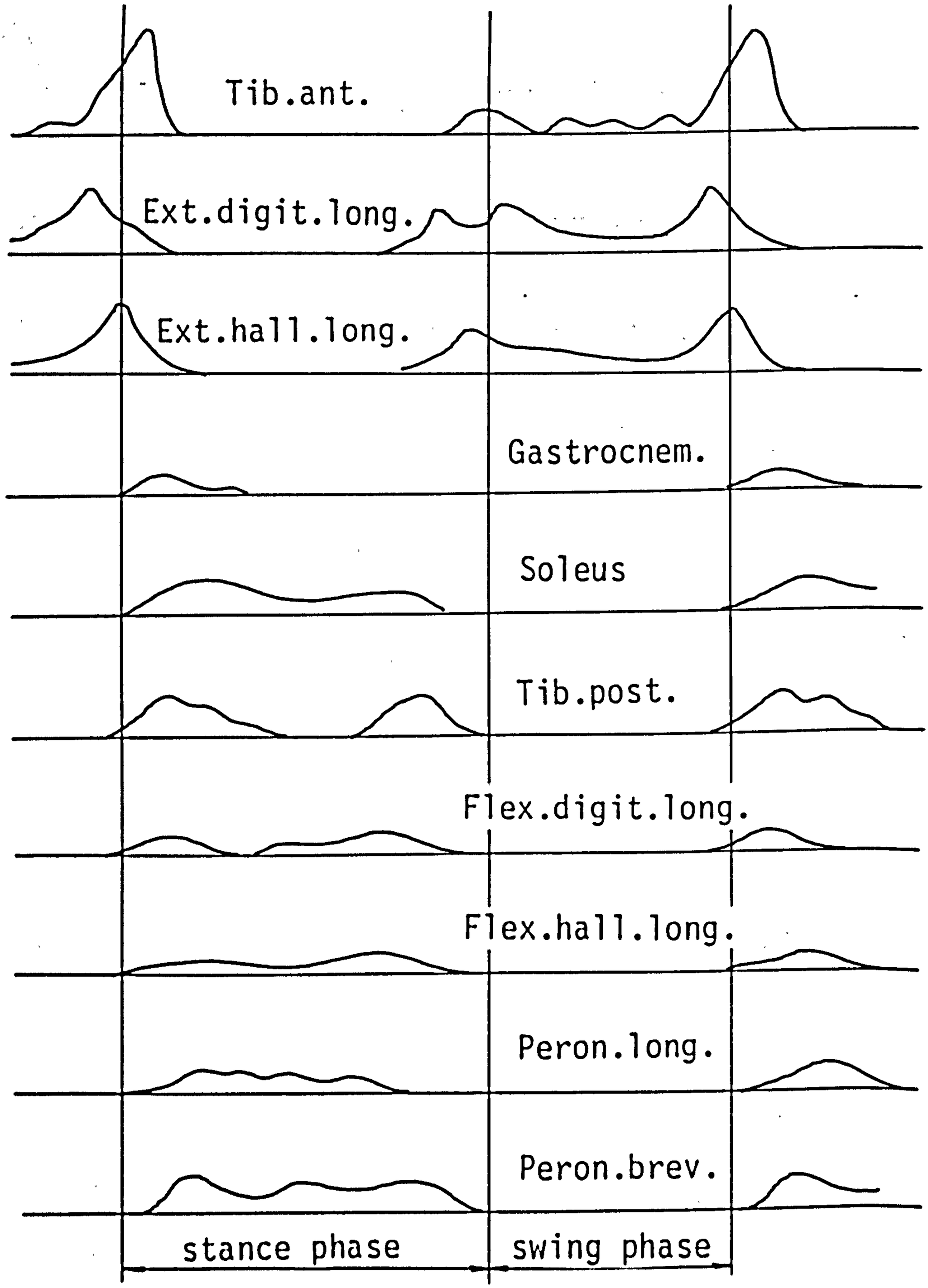

Figure 2.5e EMG patterns; walking down ramp
(Univ. of California)

isolation but only in relation to measured kinematics since they depend much more on the relevant dynamics.

One of the earliest comprehensive reports on muscular activity in the lower extremity during walking, as determined by means of EMG, was presented by the University of California in 1953. Wire electrodes, implanted in the belly of each muscle examined, were used. They presented the results of their examination of six subjects (five males and a female) in the form of rectified and filtered signals that were smoothed to give a trace which facilitated interpretation. Figures 2.5a-e show the average traces re-drawn for those muscles of the lower extremity that reach into the foot (ext.digit. long.; ext.hall.long.; flex.digit.long.; flex.hall.long.; gastroc.; peron.brev.; peron.long.; soleus; tib.ant.; and tib.post.). Some time later, Mann and Inman (1964) carried out a detailed study of the EMG activity of the intrinsic muscles of the foot. They not only observed the pattern of muscle action in normal feet (five subjects) but also in three cases that had asymptomatic bilateral flat-foot. The muscles mainly investigated were: ext.digit.brev.; abd.hall.; flex.hall.brev.; flex.digit.brev.; abd.digit.min.; and the dorsal interosseus. Simultaneously, the EMG's of tib.ant. and the gastroc. were also recorded. Observations were made during level walking, up and down stairs, and up and down a ramp (as also performed previously by the University of California). The results are shown in figures 2.6a-e. These results may be considered to be complementary to those obtained by the Californian group (figs 2.5a-e) but, one must exercise caution since, as Procter (1980) pointed out, a direct comparison of results is sometimes difficult to make when insufficient detailed information on the experimental technique adopted by

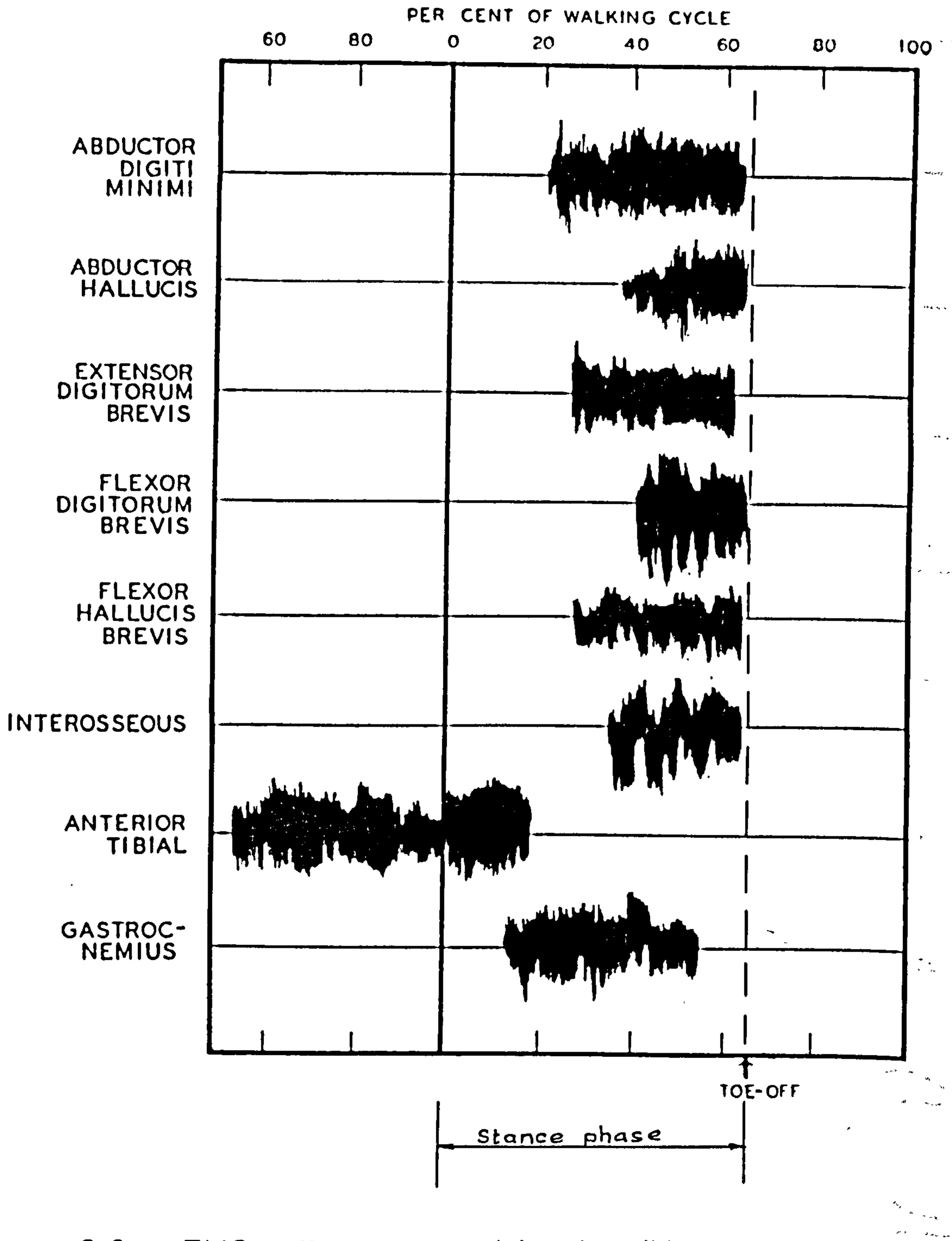

Figure 2.6a EMG patterns; normal level walking (Mann and Inman)

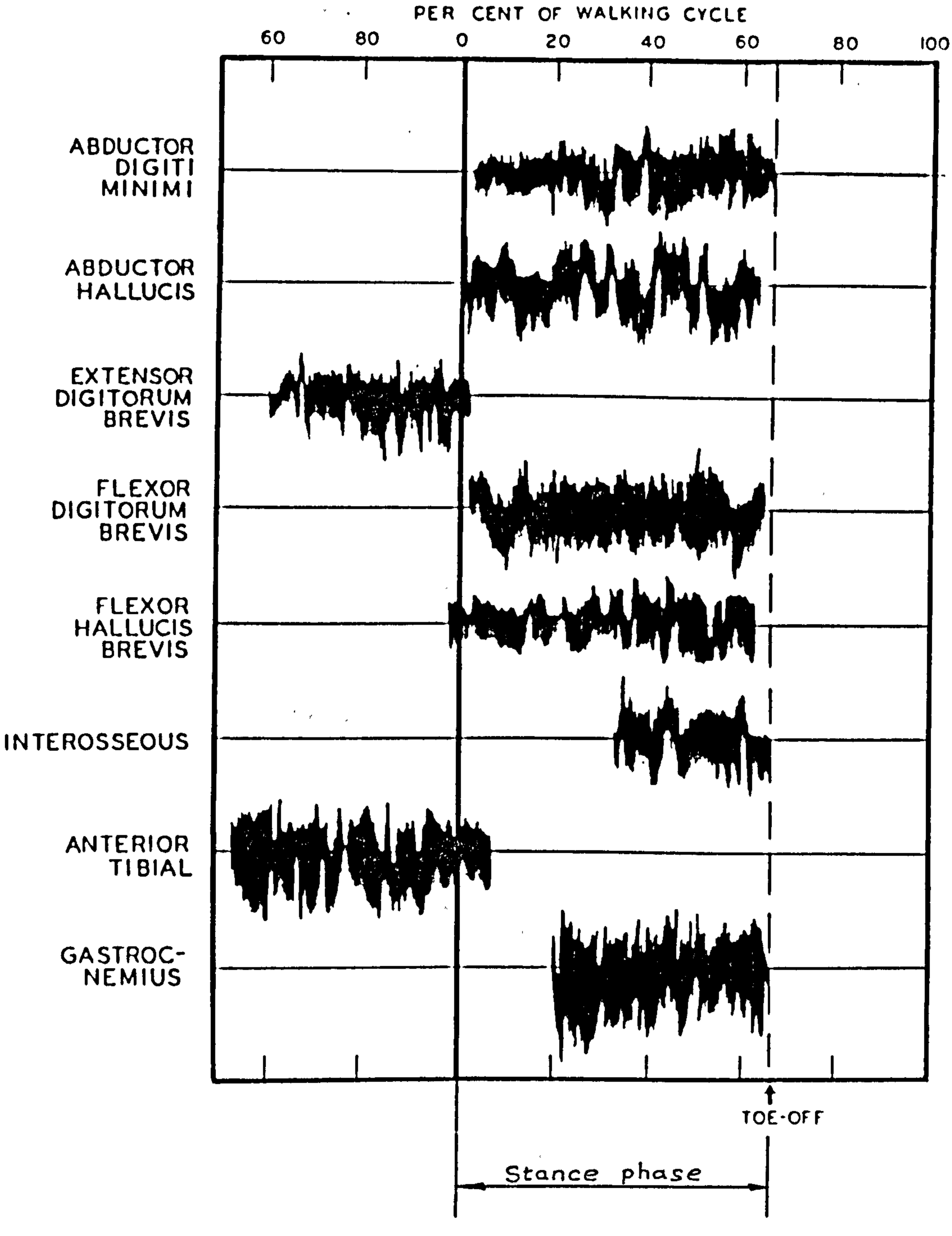

Figure 2.6b EMG patterns; walking up stairs (Mann and Inman)

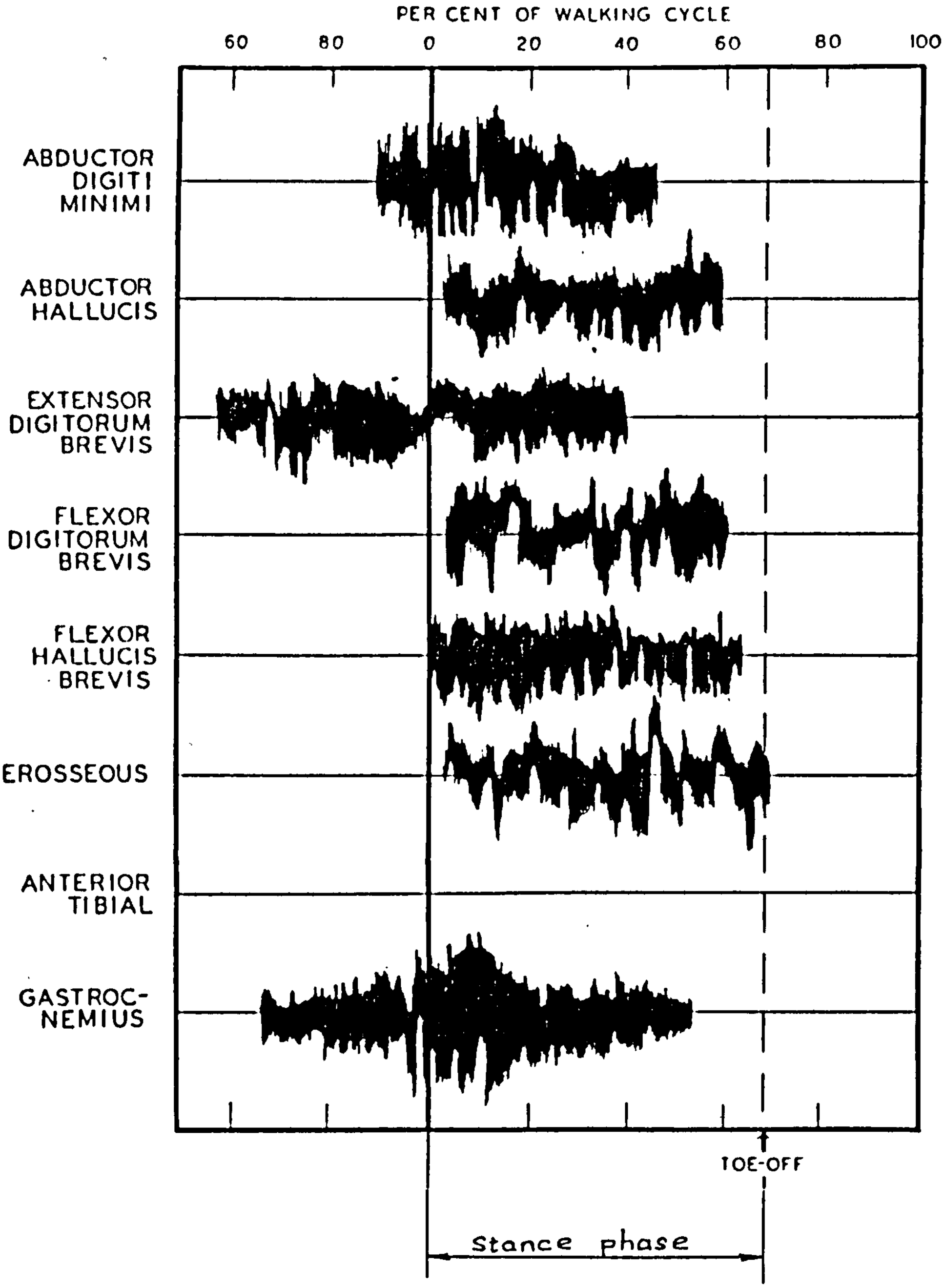

Figure 2.6c EMG patterns; walking down stairs (Mann and Inman)

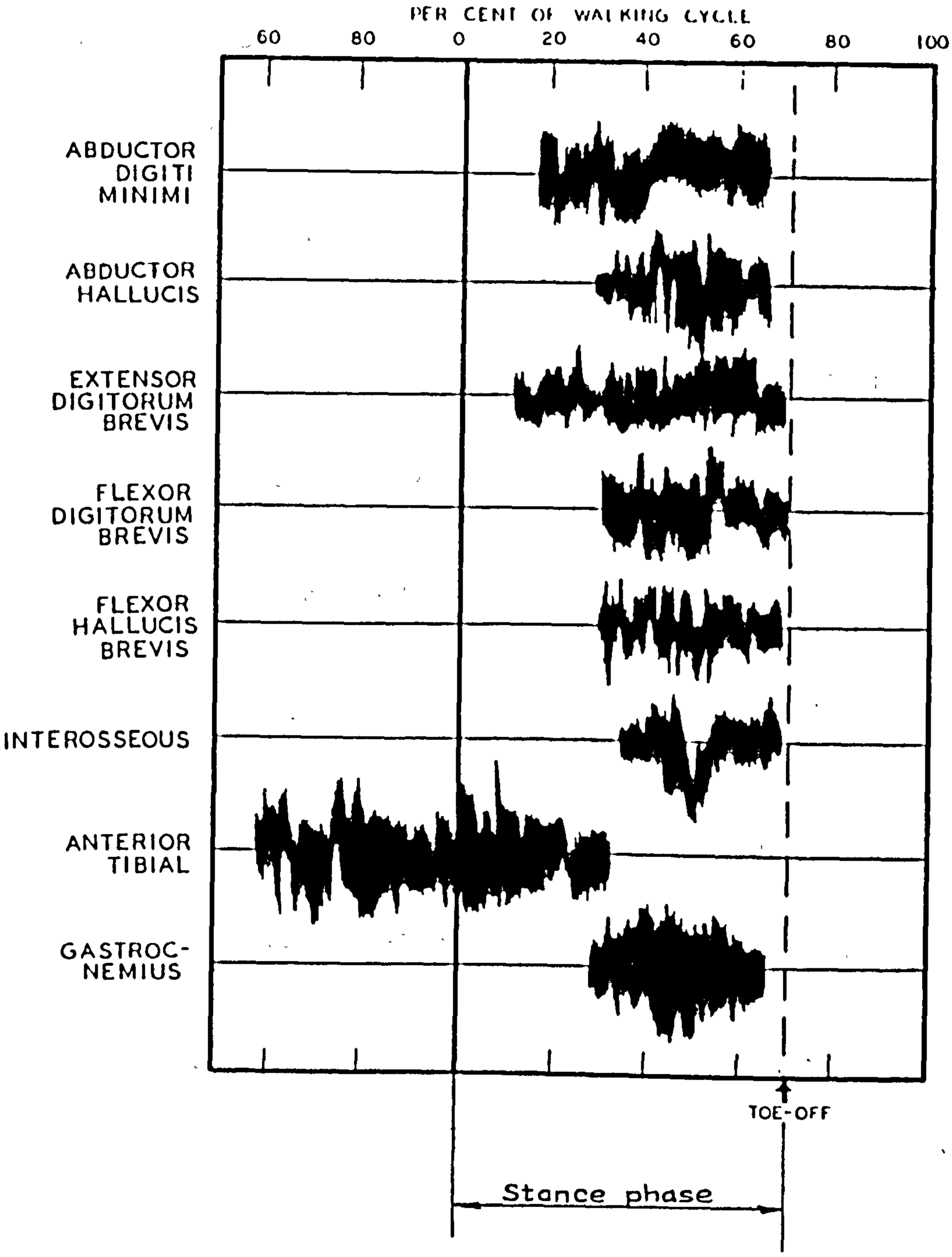

Figure 2.6d EMG patterns; walking up ramp (Mann and Inman)

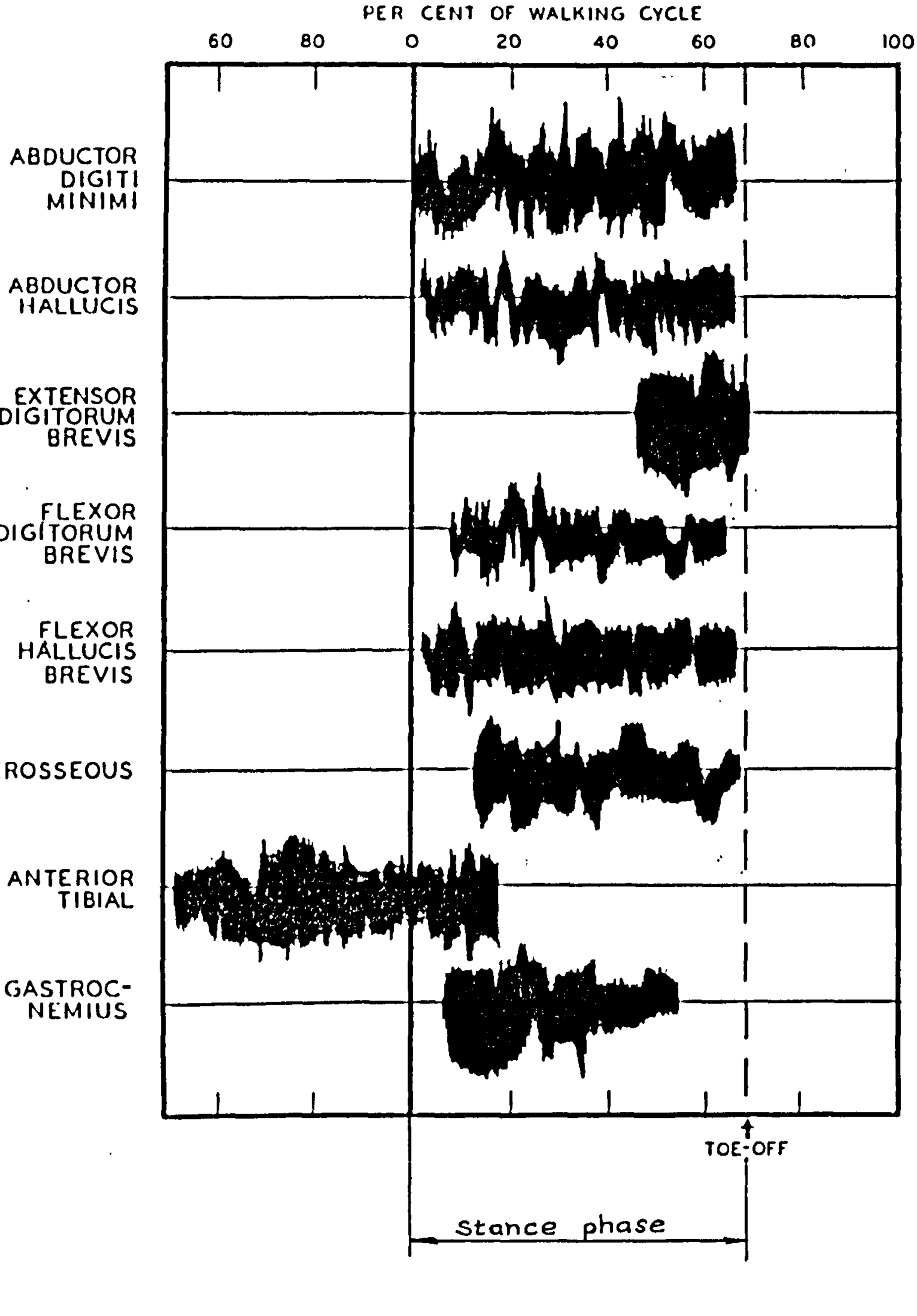

Figure 2.6e EMG patterns; walking down ramp (Mann and Inman)

the investigators is available. The variation in the point of toe-off or heel-strike in temporal EMG characteristics, for example, can sometimes be misleading. This depending upon the method of recognition used (heel switch, visual determination from cine film records, etc.). Nevertheless, the tracings obtained by both those research groups facilitate an understanding of the synergistic action of the muscles affecting the forefoot during level walking, walking up and down a slope, and when walking up and down stairs.

EMG investigations have also been performed to determine whether ligamentous structures alone bear loads in certain activities. Such an investigation is described in the next section, when dealing with the plantar ligaments and plantar aponeurosis of the foot.

2.5 Studies of the Ligaments of the Forefoot

Ever since the french anatomist Bertin in 1754 realised that the structure of the foot was something more specific than just flat terminal supports (Abramson, 1927), and for the first time described the 'vault' of the foot (la voûte du pied), the arch of the foot has continued to remain a matter of contention. No matter whether the 'key stone' of the arch some investigators were looking for was to be found in the talus or in the navicular, or whether there were in fact five longitudinal arches running side-by-side rather than a dome-like structure, it was unanimously accepted, already a century ago, that the ligamentous ties on the concave side of the foot must play an important part in maintaining the structural form under load. W. and E. Weber (1836) note: "two ties, the particularly strong calcaneocuboid ligament and the calcaneometatarsal ligament, are responsible for support of the hollow of the foot when bearing the

weight of the body". H. v. Meyer (1873) and R. Fick (1911) furthermore add to the opinion of the Weber brothers that the calcaneonavicular ligament and the plantar aponeurosis are also of paramount importance in supporting the longitudinal arch.

But, in spite of this long established view regarding the arch supporting effect of the plantar ligaments, some were of the opinion that it was mainly the muscles that were responsible (Henke, in contradiction to H. v. Meyer, 1858; Abramson, 1927; Keith, 1929; Lake, 1937).

R.L. Jones (1941) took this matter up and carried out elaborate in vivo and in vitro tests to determine the role played by the muscles and ligaments in the support of the arch. In his in vivo experiments he palpated the tendons to ascertain whether the muscles were active or not when the totally relaxed lower limb was made to support a load. He reported convincingly that: 'much the greater part of the tension stress of the longitudinal arch is borne by the plantar ligaments of the foot'. However, he did make room for 'the short plantar muscles also contributing to the support of the arch'.

Hicks, in 1954, investigated the relation between passive dorsiflexion of the big toe at the metatarsophalangeal joint and the accompanying rise of the longitudinal arch of the foot. Also, a tight band that appears in the region of the aponeurosis attracted his attention. He observed that the distal attachment of the aponeurosis to the bases of the phalanges has an important mechanical effect on the arch during dorsiflexion. 'When the toe was extended, the phalanx, sliding on to the dorsum of the metatarsal head, pulled after it the plantar pad which thereby came to lie anterior to the metatarsal head and this in turn pulled upon the attached process of

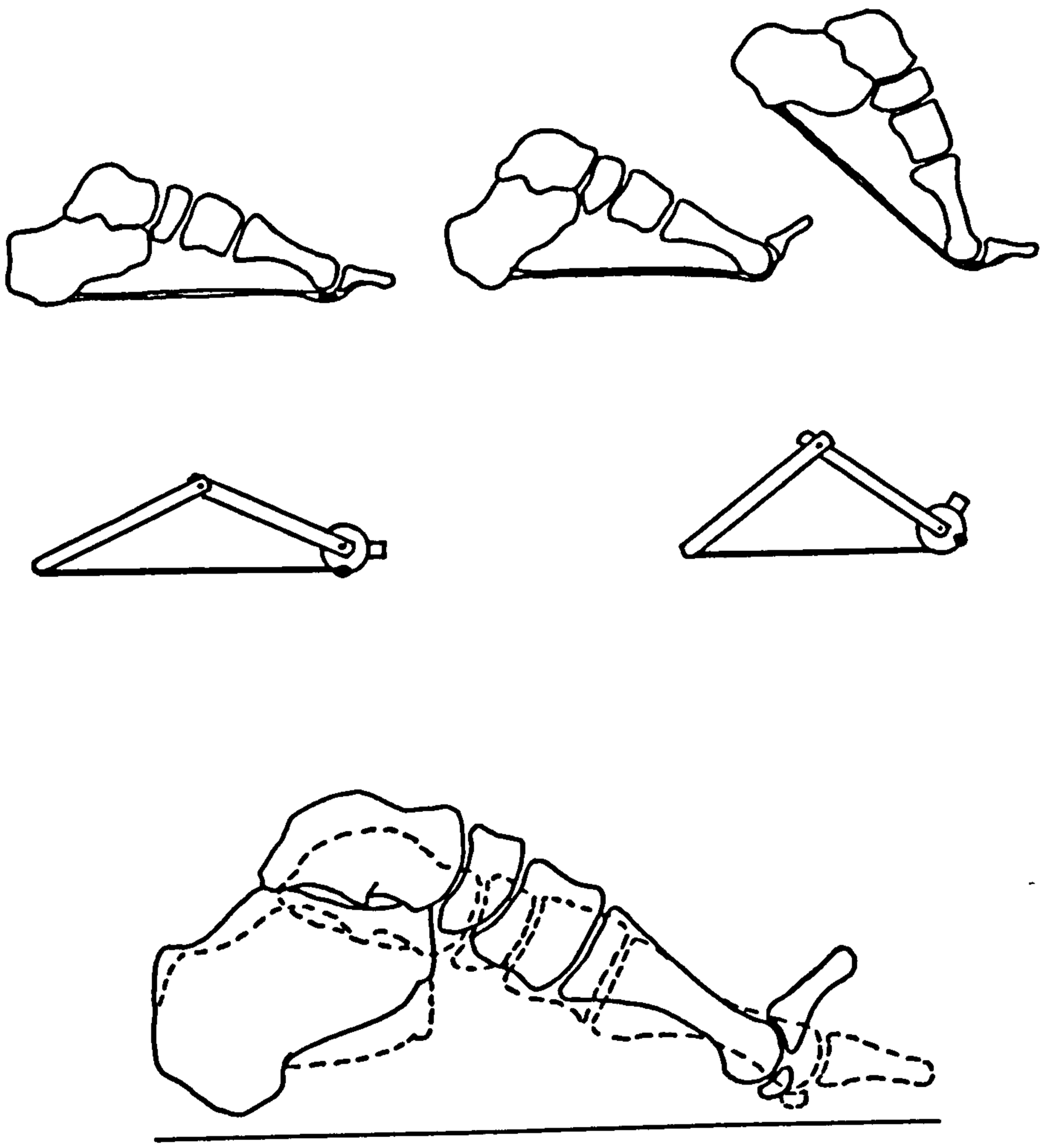

Figure 2.7 Hick's 'windlass' mechanism

the plantar aponeurosis (fig 2.7). The effect was as though a cable had been wound one-quarter of a turn on to the drum of a windlass, the drum of the windlass being the head of the metatarsal. The handle which does the winding being the proximal phalanx and the cable which is wound on to the drum being the plantar pad and the plantar aponeurosis! To confirm that the 'cable' is strong enough to perform this function, tests were made and it was found that the total breaking load of the mechanism to all five toes ranged from 1.7 to 3.4 times body weight. To clarify the role played by the muscles in the support of the arch, Basmajian and Stecko, 1963, carried out EMG studies on the extrinsic muscles - tibialis anterior, tibialis posterior, and peroneus longus and flexor hallucis longus - and the intrinsic muscles: abductor hallucis, and flexor digitorum brevis. Indwelling electrodes were used. With the foot flat on the ground, the tibia in a vertical position, and the knee flexed by 90°, weights were applied to the femoral condyles of the seated subject, similar to the procedure adopted by R.L. Jones. Up to a load of 200 pounds thus applied to the foot, hardly any EMG activity was exhibited. Basmajian and Stecko therefore concluded that: 'The first line of defense of the arches is ligamentous. The muscles form a dynamic reserve, called upon reflexly by excessive loads, including the take-off phase in walking'.

In order to determine the strength and elastic properties of plantar fascia, Wright and Rennels (1964) tested the stress-strain characteristics on four specimens. The specimens were gripped in special jaws of a materials testing machine and while the load was continuously increased, the elongation was recorded with the aid of a clip-on gauge (strain-gauged transducer). The modulus of elasti-

city was found to increase from an initial value of about 345 N/mm^2 (0.05 x 10^6 lb/sq.in) at low elongation to 829 N/mm^2 (0.12 x 10^6 lb/sq.in) at high elongations. The rupture point was estimated to lie above 21 N/mm^2 (3000 lb/sq.in) at over 4% strain. No information was given on the loading rate during testing. The same authors observed the in-vivo elongation of the plantar fascia when increasing loads were applied to the knee of a seated subject through X-ray examination, and estimated a unit elongation of 1.68% at a load of 200 lb. Using the stress-strain curves presented, this unit elongation corresponds to a stress of about 6 N/mm^2 assuming that the strain, or unit elongation, was constant throughout the length of the plantar aponeurosis. Also, employing a simple three bar truss with pin joints to simulate the arch of the foot and the plantar aponeurosis, they observe that the tensile force in the plantar aponeurosis must equal 0.47x weight applied to the ankle joint.

No further biomechanical studies on ligamentous structures of the forefoot were found, but mention must be made of Straub (1950) who is reported by Wright and Rennels (1964) to have observed that there is no difference histologically between other ligaments of the foot and the plantar fascia.

2.6 Studies of the Forefoot Articulations

2.6.1 Topography of joint surfaces:

An exact description of the geometry of articulating surfaces is absolutely necessary when determining the direction and magnitude of the forces that act across the bearing surfaces. Neglecting friction - an assumption invariably made when dealing with animal joints, justified by the very low value of the coefficient of friction - the

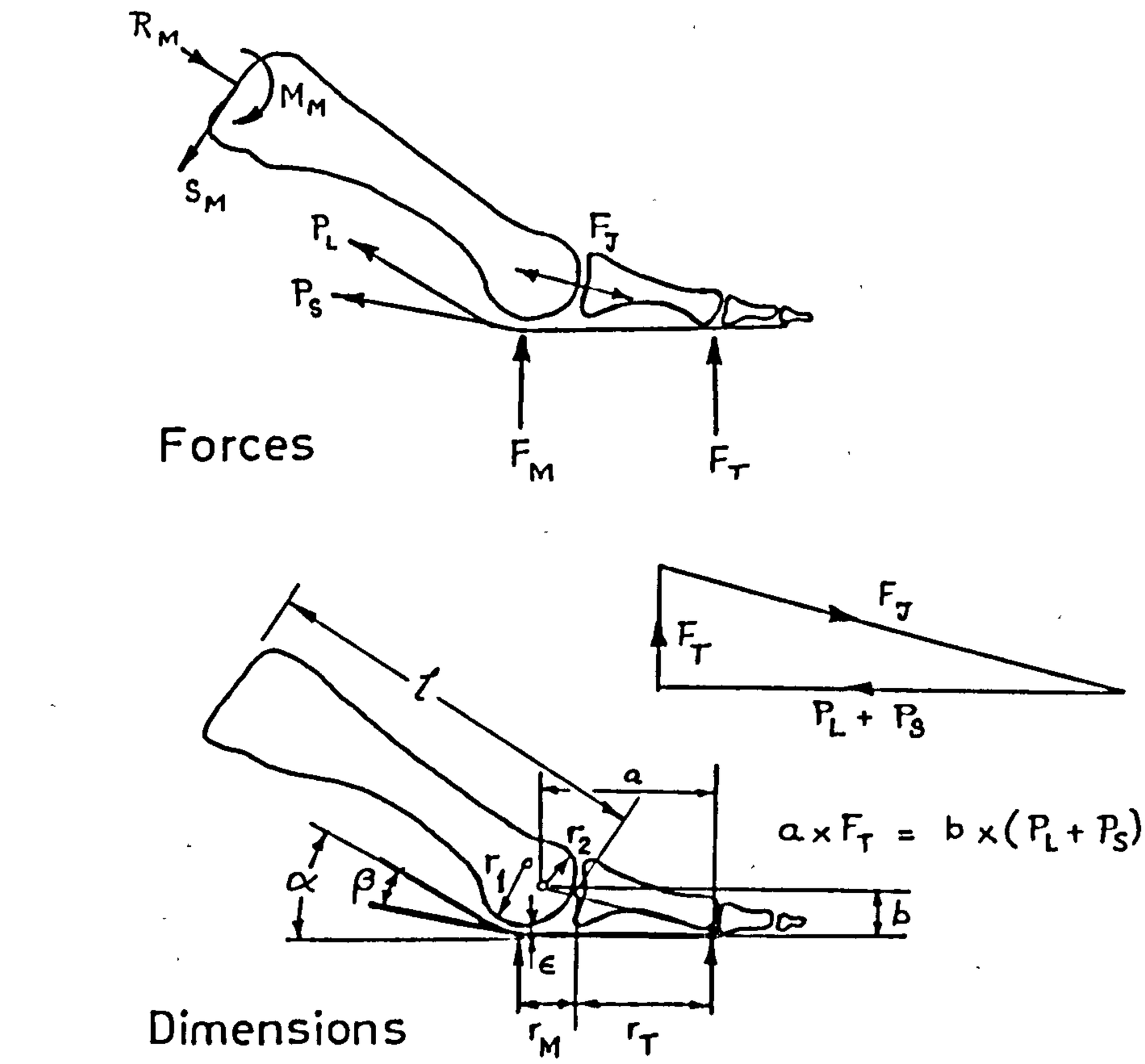

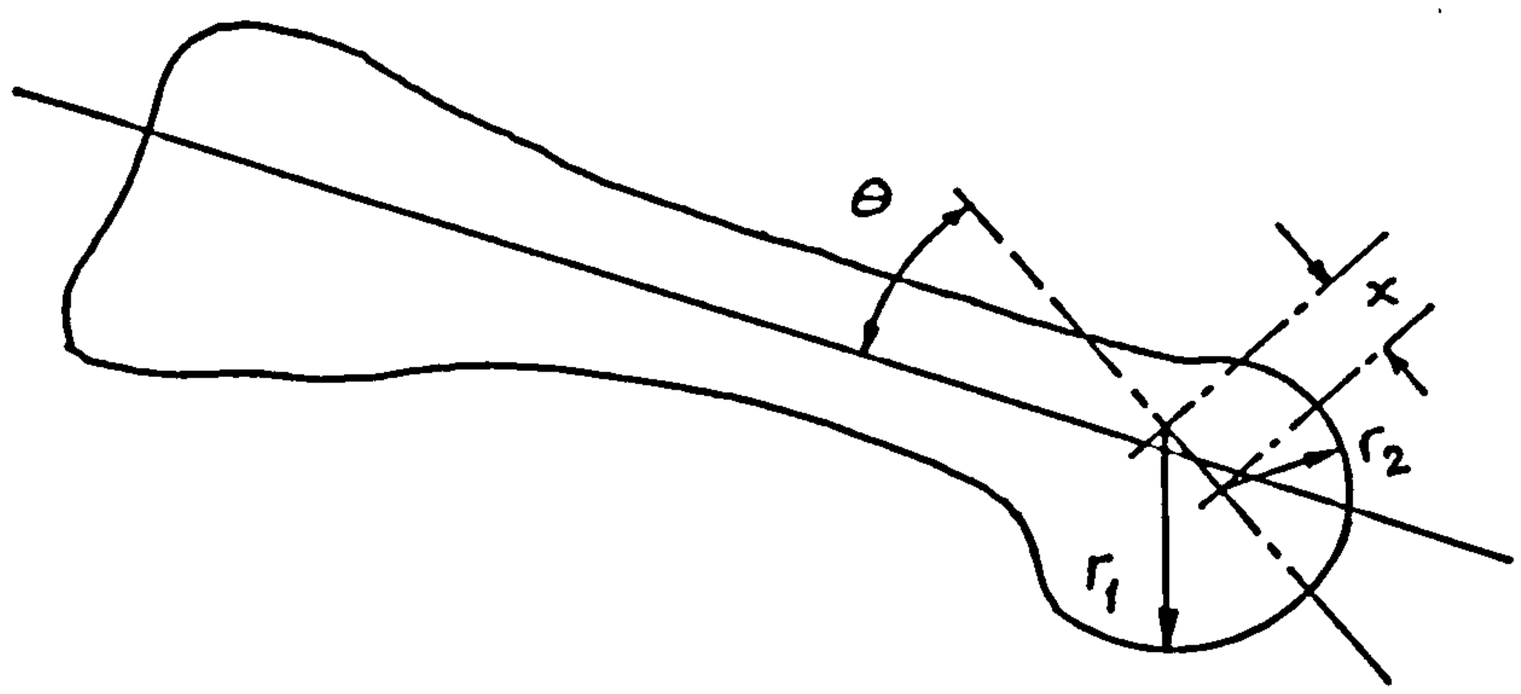

The profile of a metatarsal head described by two circular arcs

Figure 2.8 Determination of forces acting on the metatarsals (Stokes, Hutton and Stott)

resultant joint force can only act normal to the contact surfaces, and the position of the joint surfaces therefore determines the direction of joint force. This in turn usually sets the values of all the forces that come into play in order to maintain conditions of equilibrium about the joint. As far as the author is aware, only Stokes et al. (1979) have ever attempted to give a quantitative description of the sagittal profile of the metatarsal heads, as shown in figure 2.8. These values had been normalised by the use of scaling factors after measuring the radii of curvature from lateral photographs of metatarsals from six amputated feet. The data describing the profile of the metatarsal heads is, however, grossly simplified and could therefore lead to wrong results in certain applications. No data, whatever, is available on the geometry of the glenoid mating surfaces of the proximal phalanges, nor on the interphalangeal joint surfaces.

2.6.2 Range of movement in the forefoot articulations:

In Section 1.3.7 of this thesis explicit mention has already been made of current knowledge of the range of movement in the joints of the forefoot. Some investigations on the dorsiflexion of the toes during walking are reviewed in Section 2.7.3 since the observations are more specific to locomotion.

2.6.3 Concluding remarks on topography and range of movement:

The specific information required on the topography - or at least the geometry of the sagittal profile - of the metatarsophalangeal and interphalangeal joints, in order to estimate joint forces, is not available in the literature known to the author. Data on the

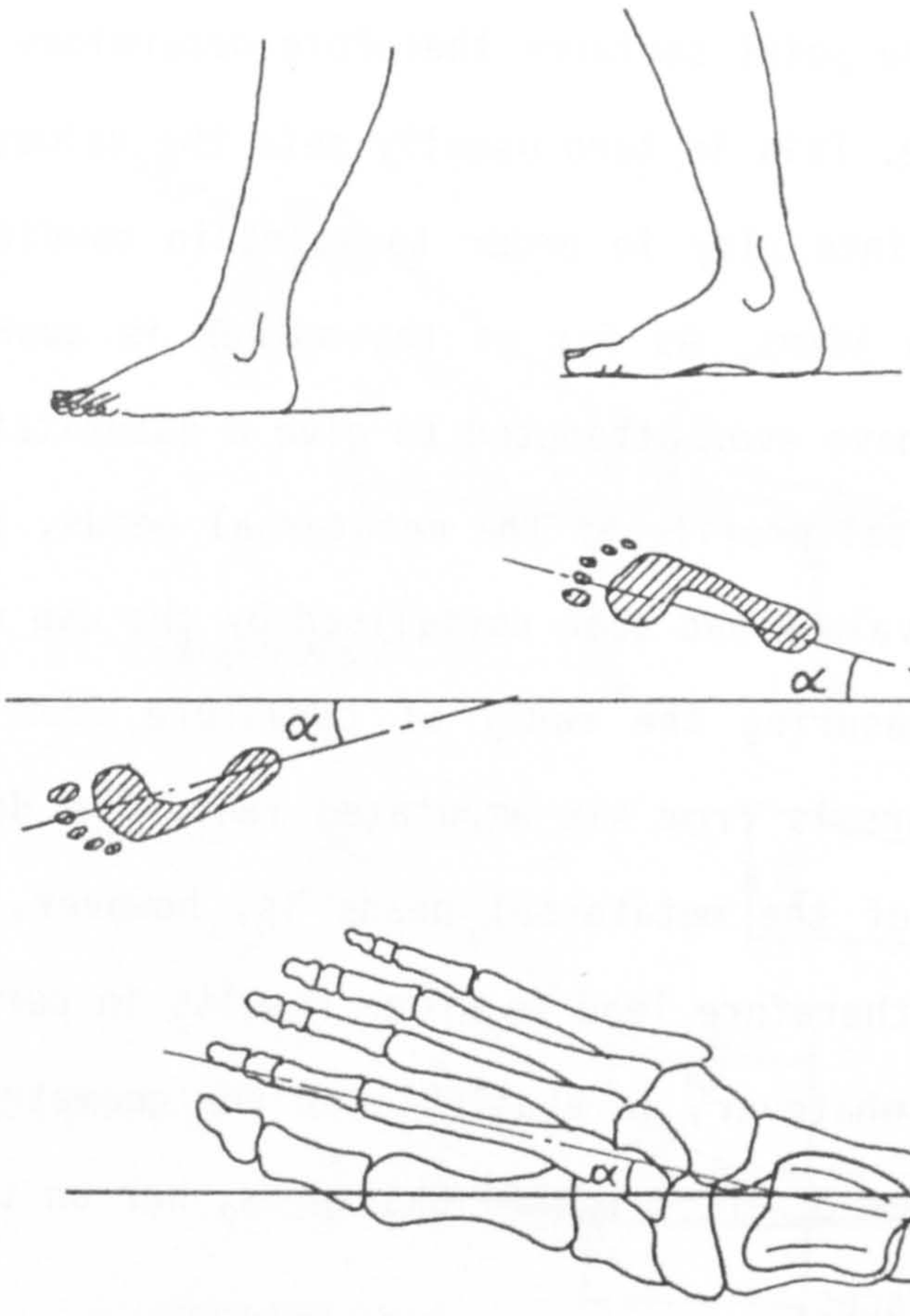

Figure 2.9 Toe-out, foot angle, or angle of gait

Ein Bild von Füßen, die nicht durch Schuhe verunstaltet sind.

Figure 2.10 Feet that have not been deformed through the use of shoes (Frostell, 1926)

range of movement of the articulations of the forefoot are sparse (see 1.3.7) and in many cases, the question arises as to how far could such information be legitimately applied to feet that have been only accustomed to wearing shoes.

2.7 Locomotion Studies

2.7.1 General remarks:

Obviously, any biomechanical study involving any part of the forefoot must take into consideration the walking pattern. The distribution of load on the ball of the foot, for example, is probably determined by the extent of supination/pronation, by the foot angle or toe-out (fig 2.9), by the terrain (level, slope, stairs, etc.), by the type of shoes worn and by the speed of progression. Some of these factors might again be due to certain inherent characteristics of the foot such as: the state of the foot's arch, the metatarsal formula, variations of muscle and tendon insertions and obviously, in the case of the pathological foot, the nature of the disorder. Although these influencing factors have been mentioned in literature on gait, the extent to which they influence the loads and movements within the structure of the foot are still unclear. Already in Section 1.3.4 on the functional anatomy of the foot, mention has been made of the general pattern of walking, but special attention will presently be drawn to a particular detail deserving consideration: toe-out, foot angle, or angle of gait.

2.7.2 Toe-out:

The toe-out, foot angle, or angle of gait (fig 2.9), is defined as the angle between the axis of the foot and the direction of pro-

gression during the foot flat phase. However, since the position of the longitudinal axis of the foot has been defined in several ways, as a line passing through a point in the hindfoot (centre of heel, or centre of the saddle shaped surface of the ankle joint) and some other point in the forefoot region (along the 1st, 2nd or 3rd metatarsal, or even in-between), one must be cautious when comparing values found in literature.

The relevance of toe-out with respect to load distribution under the ball of the foot has been described by Elftmann (1934), as follows: 'With toeing out, pressure is concentrated on the lateral portion of the heel at first and when transferred to the ball of the foot is concentrated on the inner portion, frequently resulting in a concentration of pressure under the head of the 1st metatarsal. When the second metatarsal is longer than the first, it participates in this increased pressure. On the contrary, when the individual toes in, the inner border of the heel bears the greater weight, and it is transferred to the outer border of the ball of the foot. In this case the lateral toes may be the last to leave the ground'. He also notes that with toeing in or out the distribution of pressure in the foot changes in such a fashion that a line joining the area of greatest pressure in the heel with the area bearing greatest pressure in the ball of the foot tends to remain parallel to the direction of progression.

Probably the first to examine this feature of human gait (fig 2.10) at length was Frostell (1926). Utilising his podobarometer that consisted of a wire mesh overlaying an elastic, inked pad (see Section 2.3.1), he investigated the toe-out of 54 test subjects. The angle of toe-out described by him was referred to a line that was

Table 2.3 Toe-out, angle of gait, or foot angle

Investigator	Average toe-out angle
Brinckmann (1981)	7^{o}
Ducroquet (1965)	11^{o}
Frostell (1926), slow gait, left foot	11^{o}
" " right foot	13^{o}
" fast gait, left foot	7^{o}
" " right foot	10^{o}
Klein-Vogelbach (1976)	11^{o}
Morton (1935)	$8 - 13^{o}$
Murray et al.(1964)	3^{o}

tangential to the medial border of the foot print. His results showed that in slow gait, the toe-out of the left foot was about 6° while that of the right one measured about 8°. In fast walking, these average values declined, becoming 2° and 5° respectively. The range of toe-out angles reported was very broad, being between 0° (or even negative) up to over 20°. Referring all these values to the longitudinal axis defined in accordance with Section 1.3.2, that is, as a line passing through the centre of the heel and through the 2nd metatarsal head, a value of 5° must be added to all the above figures (Table 2.3). Frostell remarked that when a large positive value of toe-out was adopted by his test subjects during walking, the pressure observed under the 1st metatarsal head was greatest while a steady decline towards the lateral side of the forefoot was recorded. On adopting negative toe-out values, the highest pressure moved to the 5th metatarsal head and now declined steadily towards the medial side of the forefoot.

Morton (1935) reported on the study of toe-out in a total of 379 American individuals and 147 Central African natives 'who had not been affected by the influences of civilization, such as shoe-wearing and well-intentioned advice as to proper foot posture'. The results obtained showed that all the feet were comparable with an average toe-out of 5° to 10° within a spread ranging from less than -10° to more than 20°. Morton's line of reference was what he termed the 'leverage axis', a line running from the centre of the heel and passing in-between the 1st and 2nd metatarsal heads. Therefore, to reduce his values to the common reference axis chosen here, an angle of 3° must be added (Table 2.3). Morton also observed a 'mild degree' of asymmetry whereby the angle of the right foot was slightly grea-

ter than that of the left. Furthermore, Morton remarked that the widest angle of toe-out is associated with standing or with a slow strolling stride, while the feet are turned forward toward a more parallel position as the pace becomes quickened.

Murray et al. (1964) looked at various features of gait among sixty normal subjects between twenty and sixty-five years of age and from 480 observations, noted that the mean toe-out angle was about 7°. No significant difference between left and right feet were found. However, they observed a greater degree of toe-out in subjects between sixty and sixty-five years of age than in younger ones. They believe it is to achieve additional lateral stability rather than a matter of slower walking rate. These authors referred the toe-out angle to a line passing through the middle of the shoe sole and therefore, to compare their values with the chosen standard, an angle of 4° must first be deducted from the above mentioned figures.

The Ducroquet's (1965) gave a toe-out angle of 15° as average normal, this axis passing from the centre of the heel to between the 2nd and 3rd toes, therefore necessitating a reduction of 4° before comparing. Klein-Vogelbach (1976) mentions 11°, referring the angle to the axis of the foot as presently chosen. Table 2.3 shows a comparison of values of toe-out given by the authors mentioned above. Brinckmann (1981) conducted an investigation on 10 adult male persons since he found it difficult to accept the value of 15° given by Ducroquet, and observed an average value of 7° instead.

All investigators have found in common that the angle of toe-out varies from less than -10° to over 25° and that even in a particular individual, the angle could vary widely from step to step. The angle of toe-out has also always been observed to vary with the

speed of walking with the greatest value at the slowest pace. Finally, the right foot has been shown, in some studies, to exhibit greater toe-out than the left one, but other studies again, have failed to confirm this.

The significance of toe-out becomes apparent when the line of the metatarsal heads relative to the direction of walking is considered since, because the line joining the lateral four metatarsal heads is inclined laterally and backwards by about 30° (fig 2.11), as the foot tips forward on the metatarsal heads, the lateral metatarsal heads tend to leave the ground and the centre of load moves medially (Hutton et al., 1982). To distribute the weight between all metatarsal heads, the foot supinates as the heel leaves the ground.

A review of some literature dealing with gross movements in the joints of the forefoot during locomotion is given in the following section.

2.7.3 Movements of the toes during walking:

Human walking, as already often mentioned, has been subject to extensive study for several centuries. Some of the more recent investigations dealing with locomotion have been presented by Barnett (1956), Murray et al. (1964), Weil and Weil (1966), Inman et al. (1981), and yet, the role played by the toes has received but very little attention. Preuschaft (1970) was probably one of the first to show that when the toes are acted upon by the digital flexors, causing them to dig into the ground, that active muscular support of the arch of the foot results. Bojsen-Møller and Lamoreux (1979) showed the significance of free dorsiflexion of the toes in walking by examining the skin and plantar fascia tightening effect produced

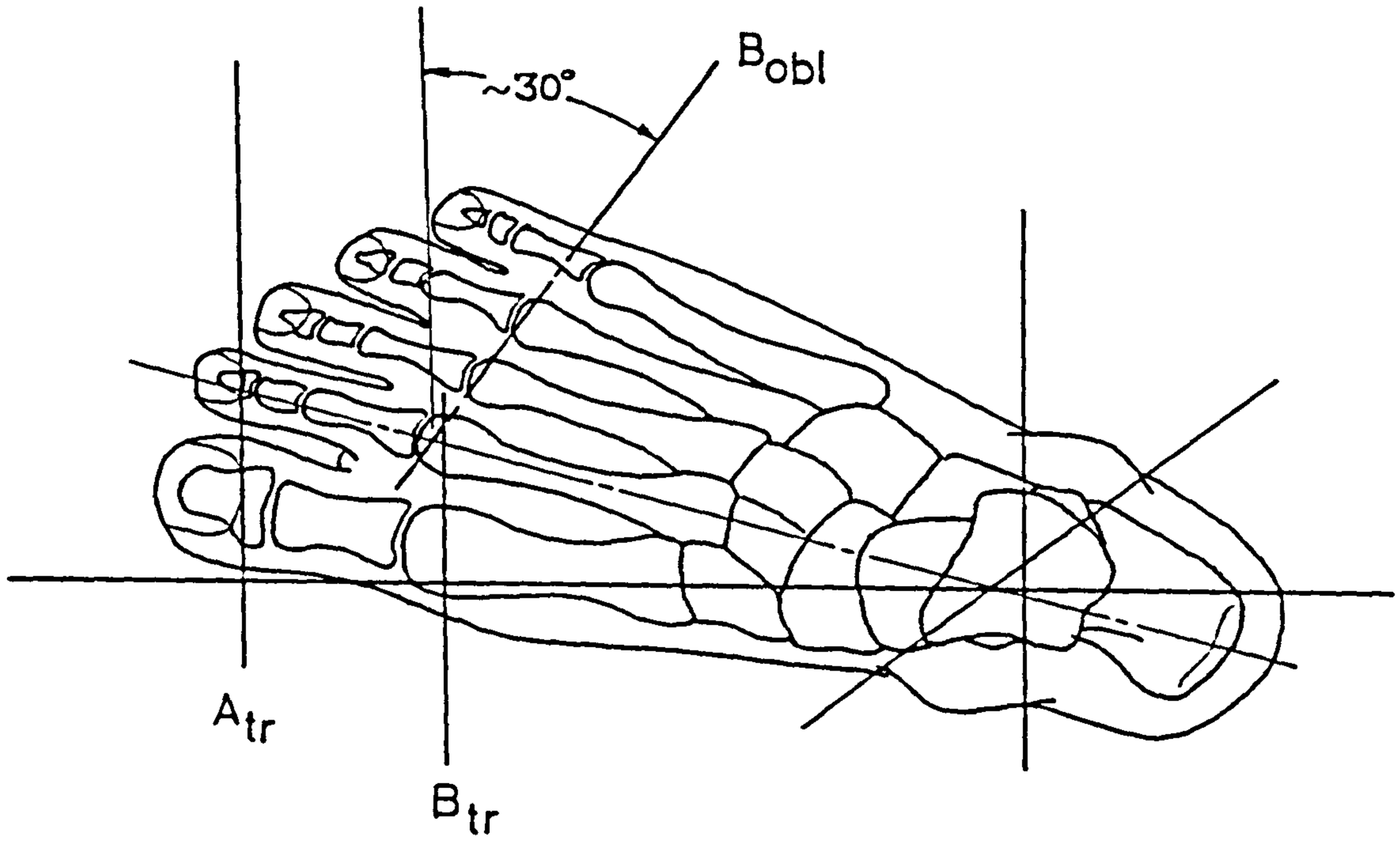

Figure 2.11 Location of axes in the forefoot during push off (Bojsen-Møller and Lamoreux)

by the toes in dorsiflexion. They observed the movements of the toes during walking on 21 subjects and reported as follows:

At heel strike the great toe was dorsiflexed 20-30° and reached the ground 40-120 ms later than the ball, which itself touched down 60-100 ms after heel strike. (The angle of dorsiflexion is probably the angle between the axis of the proximal phalanx and that of the metatarsal bone). Toe contact was established either by all five toes at the same time or by the first and fifth toes together with the ball followed by a delayed contact of the second, third and fourth toes. During the following plantigrade phase in which full contact was maintained with the ground, the leg rolled forward on the foot and reached a forward inclination of 10-25°. The plantigrade phase lasted on an average 375 ms or 45% of the total stance phase. After this, push-off started with rising of the heel. Using terms from comparative anatomy, these authors divided the push-off interval into a DIGITIGRADE and an UNGULIGRADE phase each lasting 32% and 14% of the stance phase, respectively. In the former phase the toes rested on the ground while the heel circled 60° about an axis at the metatarsophalangeal joints. [During a part of this phase, the authors observed rotation about an oblique axis (fig 2.11, axis B_{obl}) passing through the heads of metatarsals 1 and 5, followed by rotation about a transverse axis (fig 2.11, axis B_{tr}) passing through the heads of metatarsals 1 and 2]. The unguligrade phase then started with a sudden displacement of the axis to the tip of the great toe, and while the toe and the metatarsophalangeal joint circled 90° about this distal point (fig 2.11, axis A_{tr}), the relative dorsiflexion of the toes was undone, allowing the hindfoot to follow a more gently curved or straighter path. Finally, the foot continued forward and

slightly upward with a translatory movement into a new swing phase. During midswing the toes were slightly dorsiflexed to clear the ground.

The above account given by Bojsen-Møller and Lamoreux is not only very comprehensive, but is particularly interesting in that the authors see a three-stage leverage in the process. The first is a short 'load arm' (with highest mechanical advantage and lowest speed) extending from the ankle joint complex to the oblique metatarsal head axis, the second is from the ankle joint complex to the transverse metatarsal head axis and the third (with lowest mechanical advantage but with highest speed) from the ankle joint complex to the tip of the great toe. The 'power arm' remains constant, this being defined as the lever extending from the Achilles tendon to the ankle joint complex.

Mann and Hagy, also in 1979, investigated the function of the toes in walking, jogging and running. They note that the phalanges are dorsiflexed 20° from the axis of the metatarsals in the foot-flat position. After heel rise, which begins at 35% of the walking cycle, progressive dorsiflexion occurs until the ball of the foot leaves the ground. At this point in the walking cycle, a maximum of dorsiflexion has occurred, measuring 70 to 90°, depending upon the flexibility of the individual's metatarsophalangeal joints. During the swing phase there is approximately 30° to 40° of dorsiflexion at the metatarsophalangeal joint to prevent the toes from catching on the ground. Surprisingly, the authors, referring to electromyography of the extrinsic and intrinsic muscles about the foot and ankle, contend that "during walking there is no ankle plantar flexor or intrinsic muscle of the foot which causes push-off to propel the body for-

ward"!

Finally, mention may be made of an investigation reported by Fujita et al. (1983). These investigators used a strip-type goniometer that made use of electrical resistance strain gauges, similar to the type developed by Nicol (1987) of the University of Strathclyde. Recordings obtained for the 1st metatarsophalangeal joint only and on just one test subject, were presented. They report 10° dorsiflexion during the foot-flat phase, about 50° dorsiflexion during push-off, and 30 to 40° dorsiflexion during the swing phase. Electromyography of the extrinsic foot muscles was carried out with force plate measurements simultaneously. The conclusion arrived at was that the toes do not participate in the action of push-off in regular level walking, that is, the metatarsophalangeal joints move only passively during the end of the stance phase.

2.7.4 Concluding remarks on locomotion studies:

Locomotion studies of the forefoot have produced conflicting data. For instance, although it is generally agreed that the extent of toe-out during walking varies within broad limits amongst the normal population, and even does so in the case of a single individual from step to step, the values presented as average figures still vary considerably, that is, from 3° (Murray et al., 1964) to 11° (Ducroquet, 1965; Klein-Vogelbach, 1976). The manner in which toe-out affects load distribution in the forefoot has been well shown by Elftman (1934), and its effect on the movements in the metatarsophalangeal joints has been discussed by Bojsen-Møller and Lamoreux (1979). Therefore, this feature of human gait deserves attention and should be investigated more thoroughly.

Furthermore, some of the results of locomotion studies involving the toes (Mann and Hagy, 1979; Fujita et al., 1983) appear to be in sharp contrast with others (Bojsen-Møller and Lamoreux, 1979; Hutton et al., 1982) as far as participation of the toes in propulsion during the push-off phase is concerned. This important detail also requires clarifying.

2.8 Analysis of Forces within the Structure of the Foot

2.8.1 General remarks:

Mention has already been made in Section 2.5 of some of the concepts that have evolved in the past that relate the structure of the foot to that of an arch. How this arch retains its form under load has been a matter of speculation and contention for over a century and has made investigations into the function of muscles and ligamentous structures, especially those acting on the plantar side of the foot, inevitable. It has also been mentioned that while ligaments and the plantar fascia alone are quite capable of supporting the arch in a state of normal static loading, the flexor muscles certainly assist under dynamic conditions. How this supporting effect is shared between these soft structures is still unknown and probably varies individually, and is most certainly different in a flat foot than in a 'normal' one.

Generally, it is always assumed that bones are subjected primarily to compressive forces. How far the metatarsal bones are also exposed to some degree of bending is uncertain. Most commonly, the ties that support the arch are assumed to act at the two extreme ends of the latter - neglecting the possible effect of the short plantar ligaments and the muscles that insert at, or near the bases

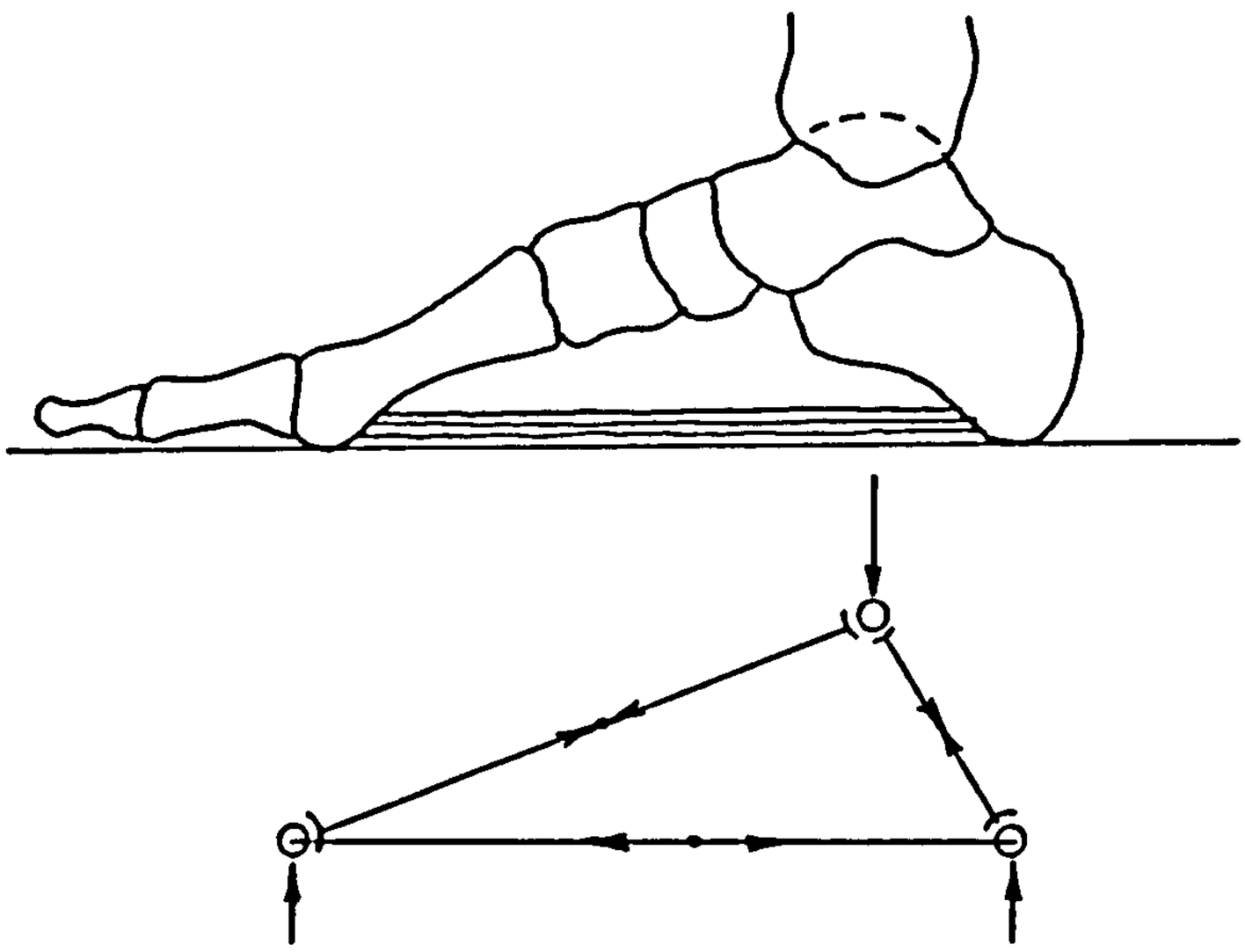

Figure 2.12 The truss theory of loading

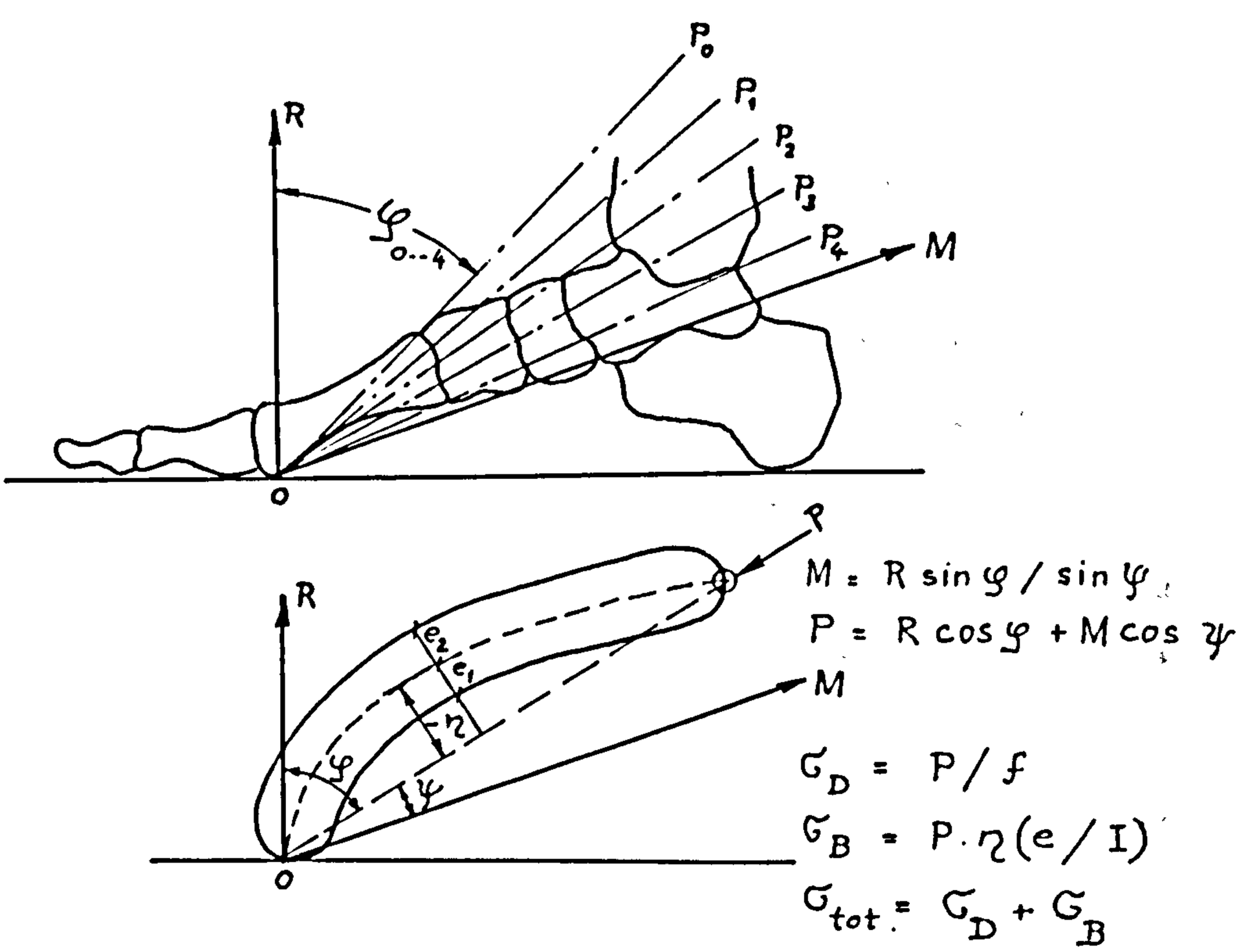

M=muscle force ; f=area of cross section ; I/e=modulus of section

Figure 2.13 Stresses in the metatarsals as derived by Abramson (1927)

of the metatarsals - thereby forming a simple three bar truss with purely compressive forces that act along the axis of the metatarsal bones (fig 2.12).

The following is a review of some of the experimental and theoretical analyses performed up to date:

2.8.2 Experimental and theoretical analyses:

One of the most interesting attempts at determining the forces acting in the structure of the forefoot was carried out by Abramson in 1927. He first obtained the ground reaction forces under the heads of the metatarsals in standing by positioning 3/8" steel balls directly under them (two balls were placed under the head of the 1st metatarsal and one under each of the others) and by measuring the indentation on the surface of a lead plate. Following this, and assuming that muscular action alone maintained equilibrium (the muscle force was assumed to act at the plantar aspect of the metatarsal head and in a direction parallel to the axis of the metatarsal bone) he then determined the resultant force P which would act along a line joining the plantar aspect of the head with the dorsal part of the metatarsal base (fig 2.13). Abramson went on to calculate the cross sectional areas and the moduli of section of the metatarsal bones and finally determined the normal and bending stresses acting in them. He concluded that the stresses were such that under unfavorable conditions the 2nd and 3rd metatarsal bones may well fracture, the ultimate tensile strength of 15 kg/mm^2 (150 N/mm^2) being easily reached.

R.L. Jones, as already mentioned in Section 2.5, performed a unique experiment in 1941 to determine whether the muscles or the

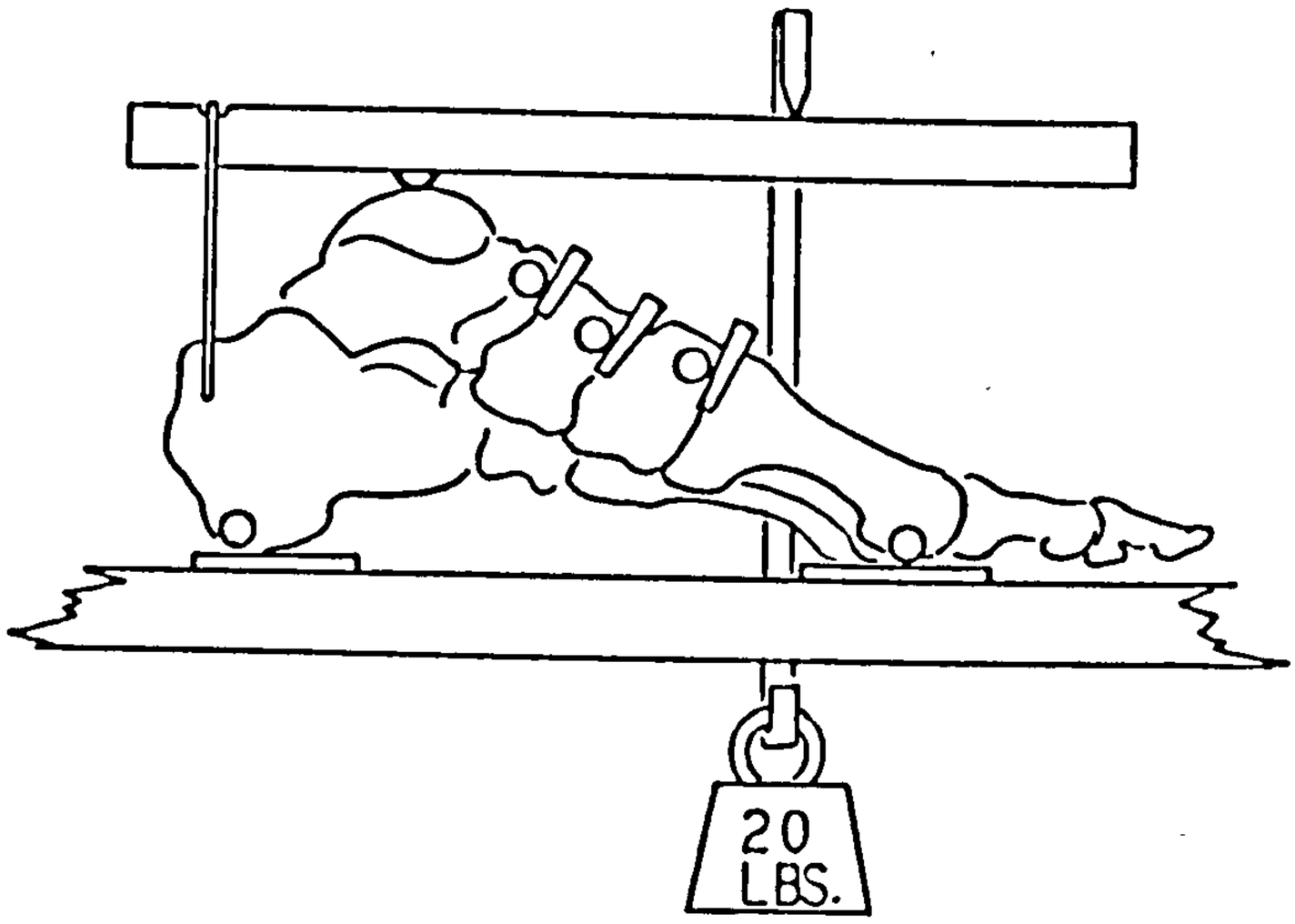

a) Method of loading foot

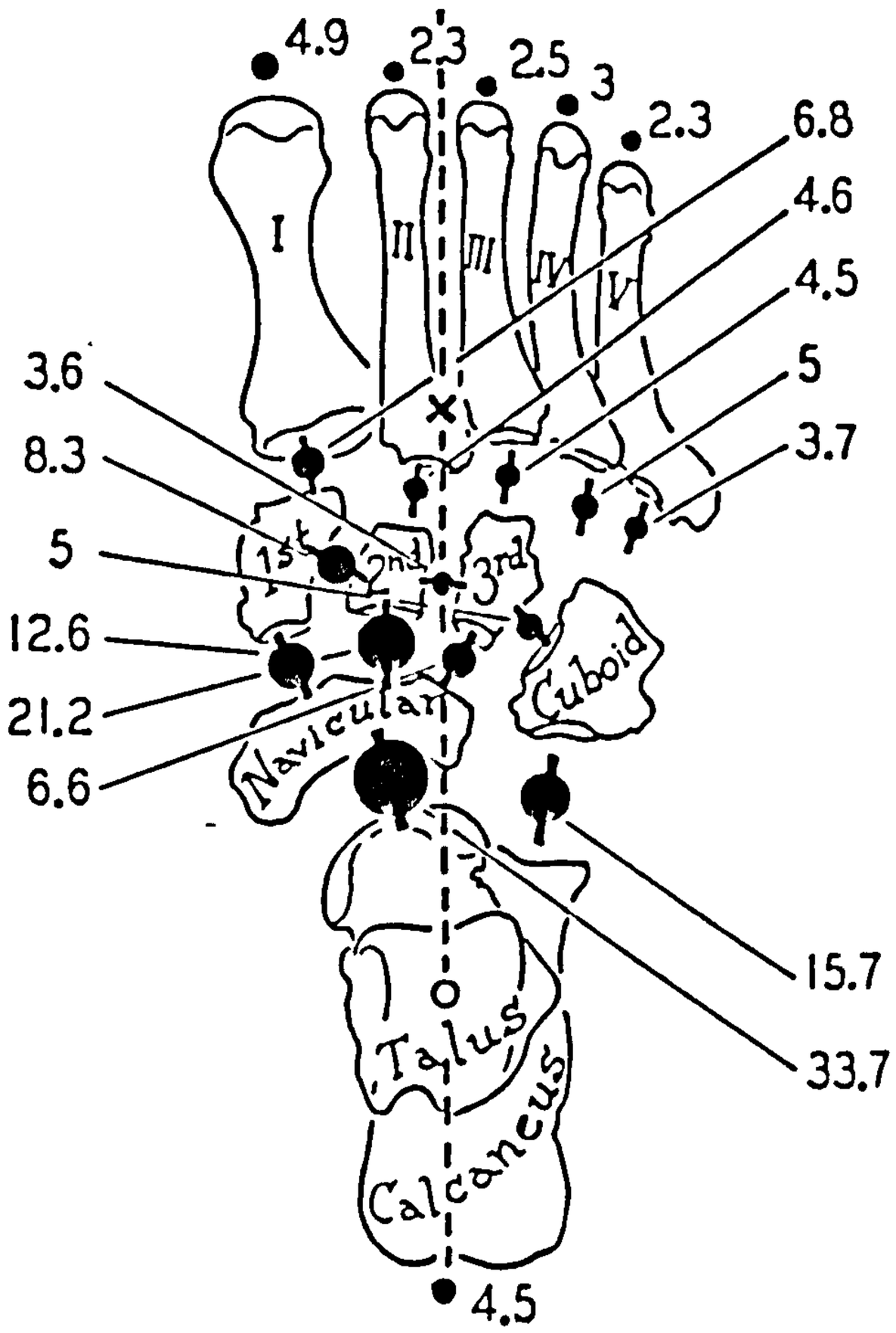

b) Distribution of compression at joints and reactions of support under the foot

Figure 2.14 Compression forces in the foot (Manter, 1946)

ligamentous structures were responsible for the support of the arch. In an in vivo investigation, the knee of a seated test subject was subjected to a load of 400 pounds with the tibia in a vertical position and the foot flat on the ground. The muscles were completely relaxed and nevertheless 'the arch was able to endure this load for over a minute with no pain or the slightest injury'. It was therefore shown that the ligaments were quite capable of supporting the arch and probably do so alone, without the aid of muscles. Even though no estimation of the forces in the structure of the foot was performed by Jones, the results of his investigations directed the undertakings of others, like, for example, Manter.

Manter (1946) set out to experimentally determine the forces that act across 13 joints of the tarsus and metatarsus regions of wet ligament preparations of the foot (fig 2.14a). Using a method to determine the forces similar to that employed by Abramson, he tightly embedded 5/16" steel balls flush with the tops of the joints. Lead plates hammered to the proper thickness were slipped into slots cut into the mating joint surfaces so that the balls engaged with the lead plates with a minimum of play in-between. Similar balls inserted under the heads of the metatarsals and under the calcaneous that rested on a lead sheet enabled the ground reaction forces to be determined when the specimen was loaded vertically through the top of the talus. Unfortunately, it is not clear from the report as to whether the plantar aponeurosis had been retained, or not. Manter found that the 1st cunei-metatarsal joint was most heavily loaded among the joints of the Lisfranc articulation. The next in turn was that of the 4th ray followed by the 2nd, 3rd and 5th. Figure 2.14b shows the results obtained. It was also observed that the ratio of

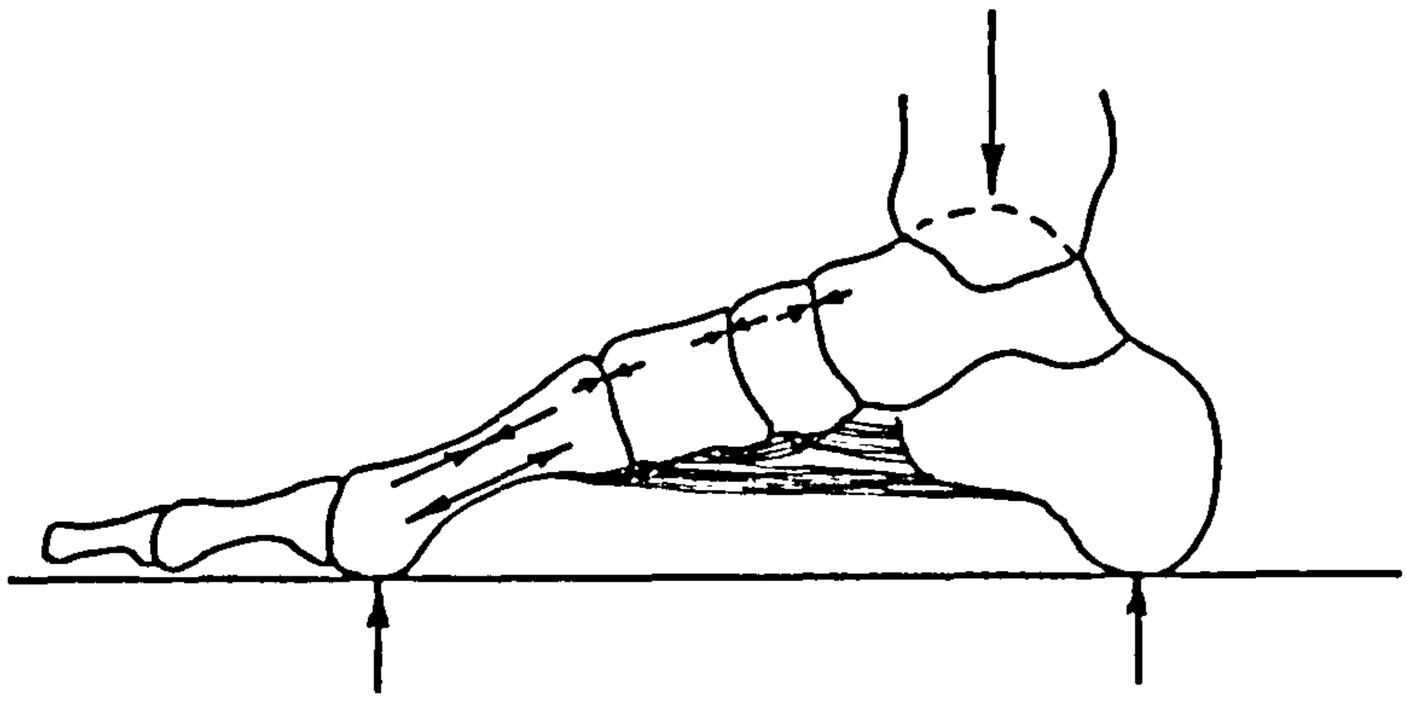

a) Structure behaving like a beam

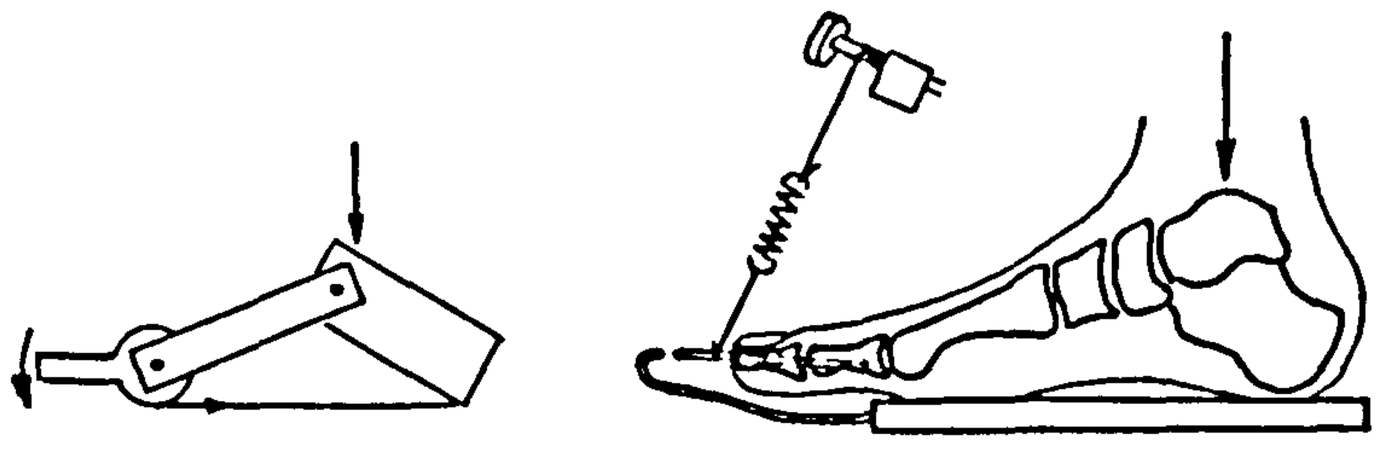

b) Principle of the measurement of plantar aponeurosis tension

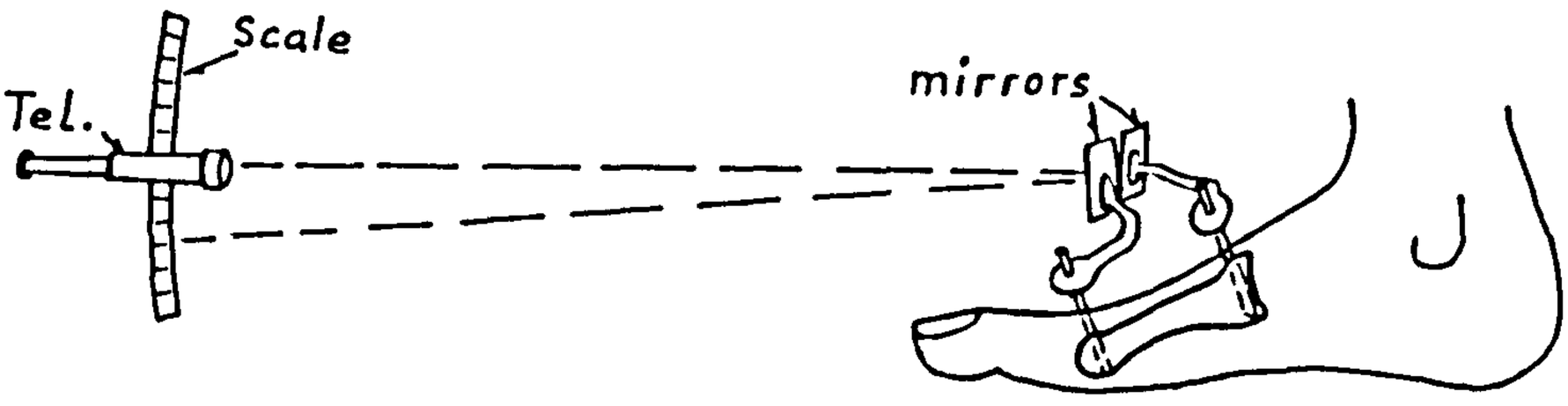

c) Method of measuring bend in a metatarsal

Figure 2.15 Hick's investigations of arch support with the toes in the straight position

force distribution among the heads of the metatarsals was roughly 2:1:1:1:1 when the 'lever axis' (dotted line in figure 2.14b) lay along the 2nd interdigital space. On moving it to lie within the 1st interdigital space, the head of the 1st metatarsal carried as much load alone as that taken by the others all together. The distribution among the four lateral metatarsal heads was not reported. Manter furthermore compared the bending moments produced by external loads with the internal resisting moment (product of interarticular forces measured and the distance to the 'plantar' ligaments) but details are not given. Finally, forces measured in a transverse direction, between the cuneiforms and across the cuneiform - cuboid junction showed that the transverse arch cooperates in maintaining the given structural form under load.

Hicks (1955), shortly after showing the role played by the plantar aponeurosis in raising the arch through a 'windlass' effect that comes into function when the toes are dorsiflexed in the metatarsophalangeal joints (see Section 2.5), carried out further experimental investigations to see whether the aponeurosis continued to act as a tie in supporting the arch after the toes had resumed their normal straight positions, or whether dorsiflexion of the rays would now be taken over by intersegmental ties becoming taut that would hence subject the metatarsal bones primarily to bending stresses (fig 2.15a). Specimens of feet were subjected to a vertical load that was applied between the heel and the ball of the foot. The flattening of the arch that resulted caused tension in the plantar aponeurosis which in turn tended to plantar flex the toes in the metatarsophalangeal joints. This was prevented by five spring balances that therefore gave an indication of the tension in the aponeu-

rosis (fig 2.15b). Simultaneously, bending of the metatarsal bones was measured with a mirror arrangement as shown in figure 2.15c. The results obtained showed that 2/3 to 3/4 of the load is taken by the structure behaving as an arch, or truss, that is, with the aponeurosis acting as a tie, while the remaining load is carried by the bones in bending, as in a beam.

Stokes et al. (1979) were probably the first to attempt estimating the forces that act across the metatarsophalangeal joints. Using geometrical data obtained from amputated feet, and by applying the ground reaction force that had been measured in six subjects, the total force in the flexor tendons was calculated. This was assuming that the joints are frictionless, no extensor muscles act on the toes while they press against the ground, and that the flexor muscles and the plantar aponeurosis act horizontally when the foot is flat on the ground. Following this, the joint force was calculated as the equilibrant of the measured ground reaction force under the toe and the corresponding force in the flexor tendons. Figure 2.8 shows the procedure adopted. The results obtained showed that the force across the metatarsophalangeal joint could amount to about 600 N in the 1st joint, 370 N in the 2nd, 200 N in the 3rd, 130 N in the 4th, and about 90 N in the fifth. In addition to this, they also estimated the axial metatarsal force, the bending moment, and shear force in the metatarsal bone. However, as already mentioned in Sections 2.4.1 and 2.6.1, these investigators made such simplifications to the geometry of the metatarsophalangeal joints and to the course taken by the flexor tendons, that their results appear questionable.

Preuschoft (1979), in a very extensive investigation involving the feet of various primates showed the importance of including the action of all the plantar flexors of the foot in determining the stresses to which the structure is exposed. He emphasises that the supporting effect of the aponeurosis plantaris and other plantar ligaments might well be adequate when considering the foot in standing, but that as soon as the moving foot is examined, the overall effect of the long and short flexors becomes indispensable. This is particularly so in the case of the apes that do not have a longitudinal arch as highly developed as in humans. Preuschoft treats the foot, similar to Hicks, as a beam and determines the bending moment diagram under various conditions of loading in the sagittal plane. Although he shows qualitatively how the bending stresses are distributed within the structure, no quantitative data corresponding to any loading condition is presented whatever. In compliance with the expected stress conditions at the tarsal-metatarsal transition, Preuschoft explains the wedge shaped form of the joint surfaces that are required to bear greater compressive forces towards their dorsal boundary and are hence wider in these areas, thereby enabling a more uniform pressure distribution over the bearing surface with values that would not overload the cartilage.

Kummer (1984) discussed the forces in the foot when standing with the foot flat, and with the heel raised. In the first case he mentions two systems of ties that support the arch: a superficial system consisting of the plantar aponeurosis and the short flexor muscles, and a deep system composed of the long plantar ligament and the long plantar flexor that include tibialis posterior and peroneus longus. On considering the centre of gravity of the body falling

between the ankle joint and the metatarsal heads, and taking into account the equilibrating action of the soleus muscles, he initially refers to the superficial system of ties that link the bases of the proximal phalanges with the heel. This, he shows, leads mainly to compression in the metatarsals with a negligible amount of bending. The deep system, however, that terminates much more proximal (at the bases of the metatarsals) when considered acting alone, must give rise primarily to bending stresses in the metatarsals. Therefore, Kummer concludes that the actual stresses that occur in the forefoot depend very much on how support of the arch is shared between the superficial and deep structures on the plantar side of the foot.

The second case which Kummer examines is with the heel raised. In this situation he sees primarily the passive extension of the aponeurosis plantaris as it wraps around the metatarsal heads and the action of the short flexors, both of which belong to the superficial system described above. Since the ties supporting the arch now act at the distal extremity, through the heads of the metatarsals, the metatarsal bones are exposed mainly to compressive forces and very little bending. Apart from these interesting views, no quantitative data was presented.

The most recent attempt at describing the structure of the foot through a mathematical model was made by Salathé et al. (1986). They modeled the foot as a statically indeterminate structure supporting its load at the heads of the five metatarsals and the tuberosity of the calcaneous. The distribution of support was determined through an analysis of the deformations caused in the structure as a result of the forces at these locations. The action of the toes in bearing some of the load was not taken into consideration. The action of

muscular forces was completely neglected so that only the intersegmental ligaments limited relative movement of the bones. The authors present the governing equations in the form of an 11x11 matrix but regret that a complete and reliable set of anatomical and biomechanical data necessary to solve the equations is not available at the present time.

2.8.2 Concluding remarks on analysis of forces in the structure of the foot:

Analysis of forces in the structure of the foot that have been performed up to now vary from treatment of simple three-bar-trusses (Morton, 1926; Abramson, 1927; Wright and Rennels, 1964; Hicks, 1955; Preuschoft, 1970; Kummer, 1984) to modeling of the foot as a statically indeterminate structure (Zitzlsperger, 1960; Salathé et al., 1984). How exactly the bones of the normal foot are loaded is still not known since controversial opinions still exist regarding the manner in which the longitudinal arch of the foot is supported by the muscles and ligamentous structures that span the arch on its plantar side. Whereas some, like v. Meyer (1886), Fick (1911), R.L. Jones (1941), Manter (1946), Hicks (1954, 1955) and Wright and Rennels (1964) believe that the plantar ligaments and aponeurosis play a major role in supporting the arch, others like Abramson (1927), and Preuschoft (1970) are of the opinion that the muscles are the main agents. Others, again, are convinced that both, ligaments and muscles play a complementary role, depending on the momentary situation of the foot, i.e., whether standing, raised on the toes, etc. Such opinions have been forwarded by Basmajian and Stecko (1963), Mann and Inman (1964), and Kummer (1984). Finally, depending

on what structures are considered in supporting the arch, the metatarsal bones might either be exposed to normal forces alone, or to bending forces, or to a combination of both. Preuschoft has shown that the action of the plantar flexors of the metatarsophalangeal and interdigital joints could have a powerful influence on the share of load taken by the plantar aponeurosis in supporting the arch and this deserves closer attention in all future attempts at analysing the forces in the structure of the foot. Stokes et al. (1979) are probably the only ones up to now to have attempted calculating the forces in the flexors of the metatarsophalangeal and interdigital joints, but further investigations of this kind involving more exact anatomical data are necessary to clarify the situation satisfactorily.

CHAPTER 3

MEASURING TECHNIQUES AND EQUIPMENT

3.1 Introduction

The review of published literature, as discussed in the preceding chapter, failed to disclose the anthropometric data required to enable analysis of forces in the structure of the forefoot to be performed. The topography of the joint surfaces and their relation to geometrical landmarks of the relevant bones, for instance, have been described only in a very incomplete manner, and the exact directions of the tendons that cross the metatarsophalangeal joints, just prior to their insertions, have not been reported at all. An anthropometric study was therefore undertaken (Chapter 4). In addition to obtaining the desired information mentioned above, the range of movement in the joints of the forefoot and the limiting effect imposed by the adjacent ligaments and surrounding capsule were also observed in order to appreciate the possibility of injury to these structures when a joint is forced against these constraining devices.

Also, gait studies were performed to determine ground reaction forces acting under the metatarsophalangeal joints and under the toes, especially of the first and second rays (Chapter 5). Furthermore, an investigation was conducted to observe the effect of toe-out on the force distribution under the forefoot and to gather information on the habitual toe-out of randomly selected individuals during normal level walking.

All this required application of special measuring and observation techniques which are described in this chapter in a general form. Adaptations of the general method for specific purposes are dealt with later in the relevant sections.

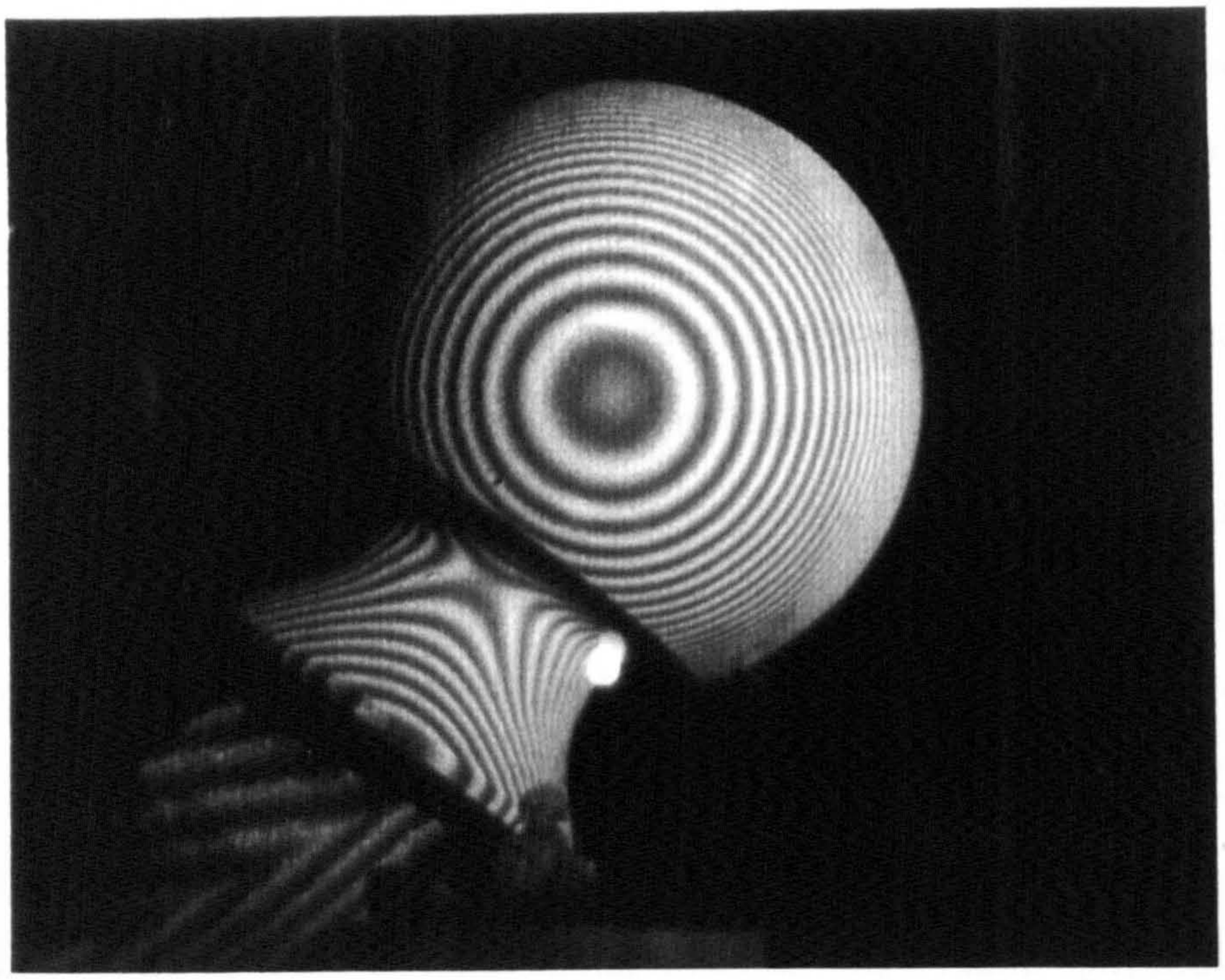

Figure 3.1 Moiré fringes on the spherical head of a hip prostheses

3.2. Topography, using the Moiré Technique

This technique was made use of to record the surface geometry of the cartilaginous joint surfaces. The principle is as follows:

When the shadow of a grid of parallel straight bars produced by a point light source falls on an irregular or undulating surface, the shadow cast on the surface is distorted. If this shadow be viewed through the bars, that is, with the eye on the same side of the grid as the source of light, the pattern which presents itself is again changed. What is now seen is the shadow on the surface interrupted by the bars themselves. The broken-up shadow appears to reunite into curved lines that join points of equidistance between the grid and the surface, thus producing a pattern of fringes like the lines of constant altitude on a geographic map. Figure 3.1 shows the appearance of the spherical head of a hip prosthesis when viewed in this manner. The geometric details on which calculation of the difference in 'altitude' between one fringe and the next is based, can be described with reference to figure 3.2, which shows the grid, G, of optically opaque and non-reflecting strips with pitch, t, that are arranged in a plane normal to that of the paper. Each strip, and the space in-between the strips, are of equal width. The light source, L, and the camera (eye), E, are in fixed positions relative to the grid. For ease of computation, the grid is considered to be along the y axis with one end at the origin of a Cartesian coordinate system. It will be appreciated that on viewing shadows cast on a white surface placed in any one of the positions marked D_1 to D_4, the shadows will completely fill in the spaces between the strips and therefore a dark field will be seen when viewed from E. However, on looking at a surface placed anywhere marked H_1 to H_3, the surface

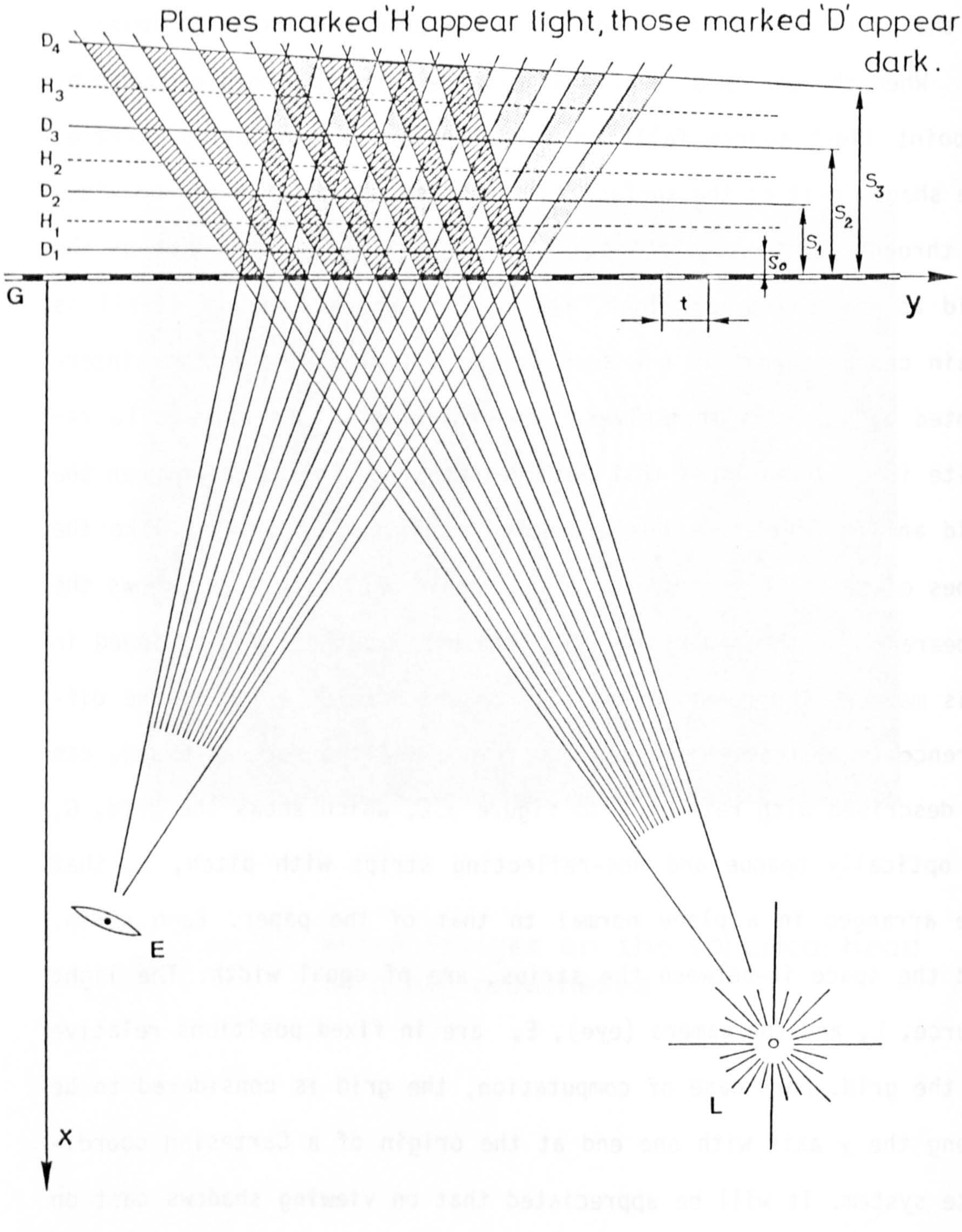

Figure 3.2 Principle of moiré fringe formation

will be seen illuminated and, apart from the strips of the grid being also viewed, the field will appear light. Now, if the grid alone were moved in its own plane, and along the y axis, the appearance of darkness or light on any plane as described above will remain unaltered, and therefore by moving the grid fast enough, the disturbing effect of the grid as directly seen by the eye can be eliminated. It now follows that if an object with a white surface of irregular, undulating form be placed in the position occupied by the planes D and H, then fringes will appear on its surface depending on the distances S_1 to S_n from the plane of the grid to points on the object surface. This explains the fringes on the spherical head of the hip prosthesis as seen in figure 3.1. The distances S_1, $S_2 - - - S_n$ (fig 3.2) are dependent on the pitch of the grid, and the spatial position of the light source and that of the camera in relation to the grid. Figure 3.2 shows the projection of all rays onto the x-y plane of the coordinate system, and therefore the diagram is obviously valid for all z positions of the light source and camera. Appendix 1(3) shows the manner in which the distances S_1, $S_2 - - - S_n$ are derived from the governing geometry of the optical set-up. It is important to note that the surface of an object appearing uniformly dark (or light) would not be a plane, but a curved surface. However, if the x distance between camera and grid, and between light source and grid are sufficiently large, and if the size of object is small, then the difference, $S_n - S_{n-1}$, might for practical purposes be considered constant and a single value may be used to describe the topography of the whole surface examined. The computer programme (see Appendix 1(3), however, gives the exact distances over any chosen range of width and depth of field. Further details regarding

the apparatus used and the calibration procedure exercised to determine the exact position of the camera and light source in the chosen Cartesian coordinate system, including the estimation of the size of object in the y and z directions from photographic records, will be presently treated as follows:

3.2.1 The moiré apparatus:

The optical grid employed for producing moiré patterns was a photographic negative exhibiting dense black strips of 0.3 mm width with 0.3 mm spacings that covers a rectangular area of 120 mm x 200 mm on a plastic foil of 0.3 mm thickness that was specially chosen for dimensional stability. The width of the strips and spaces, that run parallel to the 120 mm long edge, are asserted to be within a tolerance of +/- 0.015 mm (+/- 5%) and the pitch lies within a tolerance of +/- 0.5% of the total length of foil (manufacturer specifications of Grapho-Optik Ltd., Vaduz, Switzerland). The foil is sandwiched between two plane glass plates of 2 mm thickness each, that are held in a metal frame (fig 3.3). This frame is supported vertically between roller bearings and made to oscillate in a horizontal direction (parallel to the 200 mm edge), by means of a crank arrangement driven by an electric motor, at a frequency of 1 Hz, with a stroke of 15 mm.

A table of 72 cm height with a top of 160 cm x 80 cm and covered with a sheet of dimensionally stable plastic, ruled like 'graph paper', exhibiting mm square graduations, was used as a base. On checking the marked dimensions of the graduated sheet with a steel ruler no deviation could be detected along the overall length of 100 cm that was greater than 0.5 mm. This graduated sheet fixed rigidly

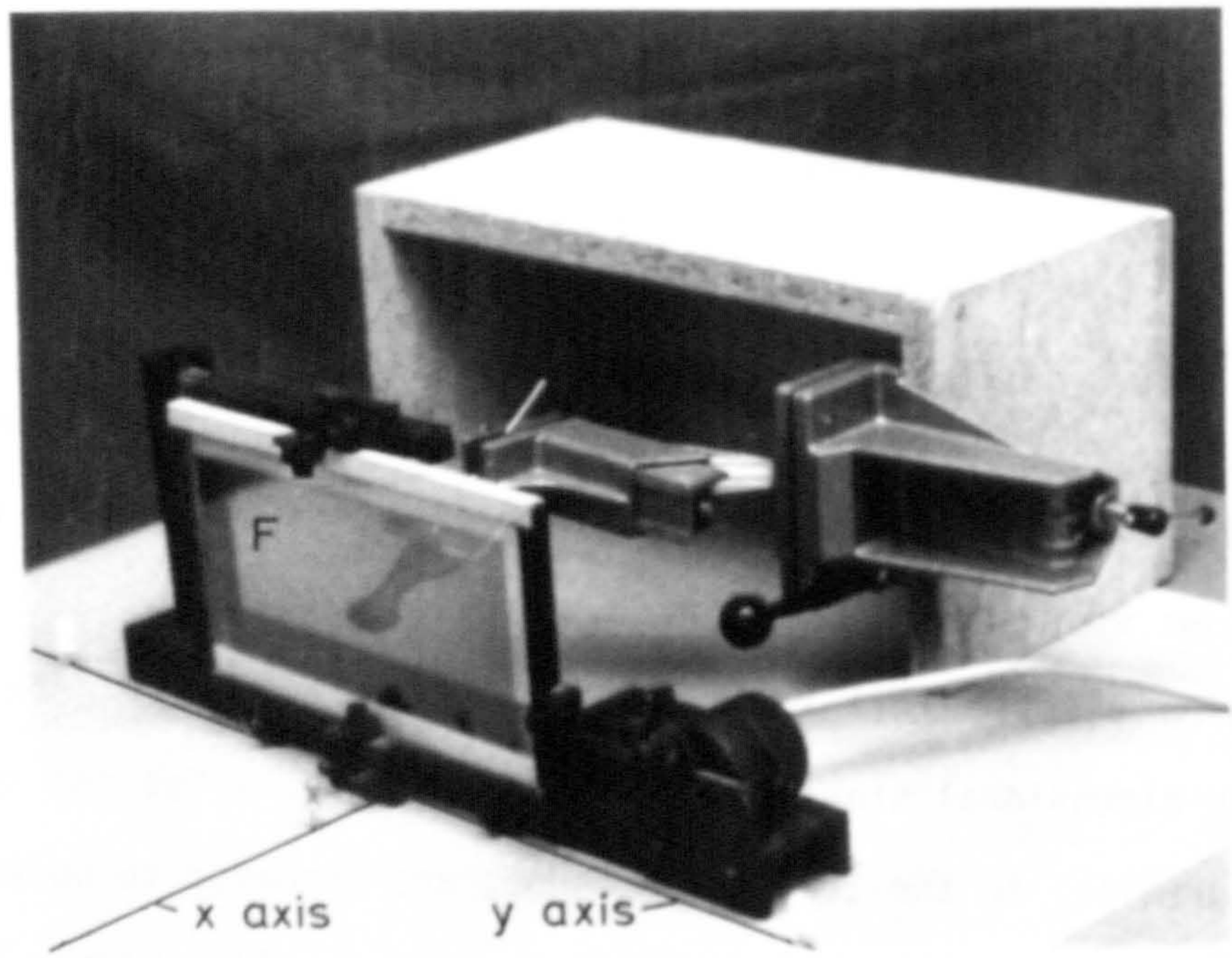

F: Frame with optical grid (grid lines run vertically)

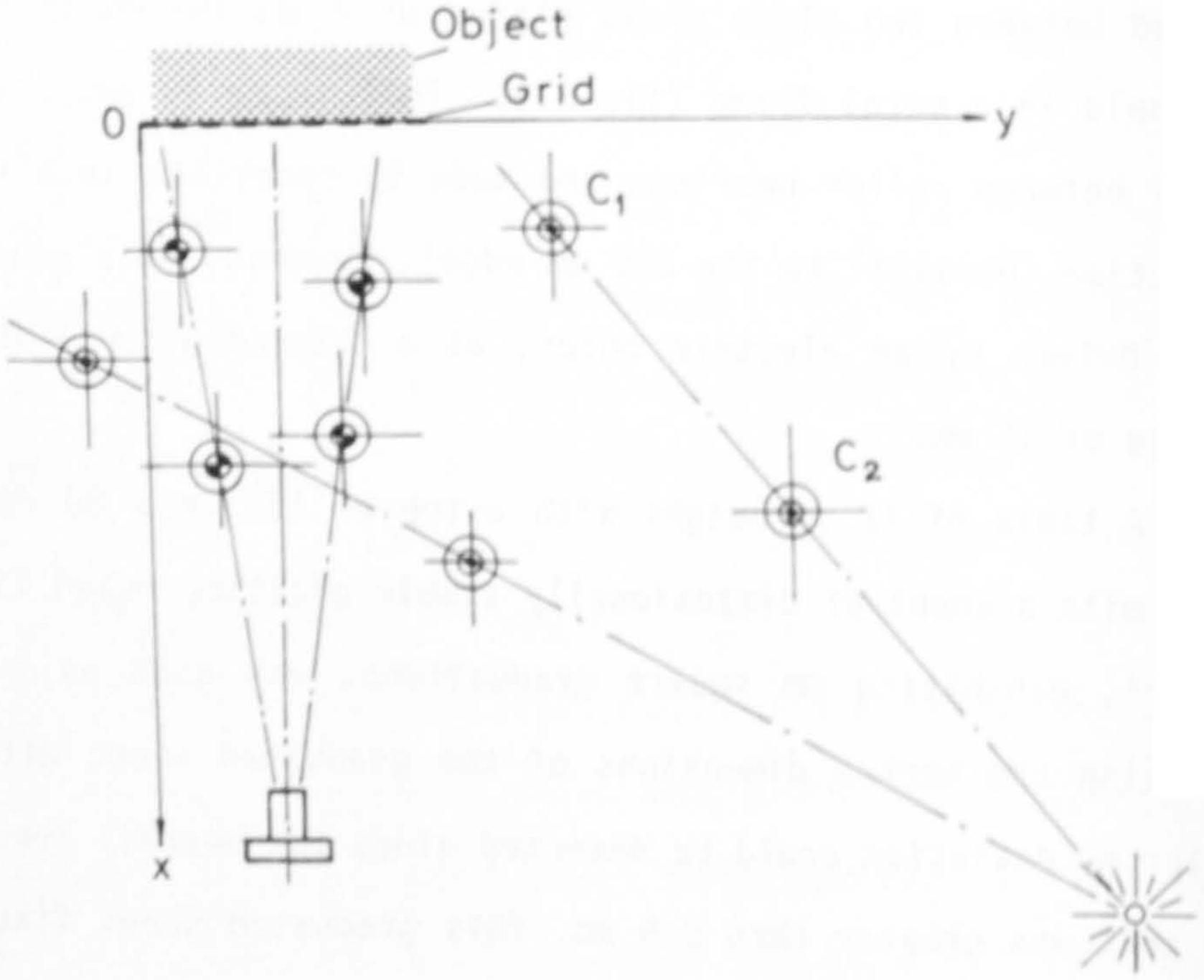

Figure 3·3 Calibration procedure for determining the xy coordinates of camera and light source

to the table top, marks the x-y plane of the coordinate system of reference. The camera used is of the reflex type, a Nikon model F (24 mm x 36 mm) fitted with a Nikkor f/4 lens of 200 mm focal length and placed at a distance of about 1 m from the origin of the x-y system, approximately along the x axis. Black-and-white negative film of 400-ASA sensitivity was found to be ideal.

The light source is a common slide projector placed at x, y coordinates of approximately 2.5 m each.

Two steel columns (C1 and C2) of 8 mm diameter and 150 mm length, each supported in a close-fitting bore located centrally in a cylindrical brass base of 30 mm diameter and 30 mm height, were used for calibrating purposes. Each column is pointed at both ends. One column is painted white, the other grey. Furthermore, a rectangular metal block (B) with a vertical surface of 6 cm x 12 cm covered with mm graph paper, was also used as a calibration requisite.

Finally, a heavy steel slab and a magnetic clamp (such as used for holding dial gauges) were employed for holding the specimen to be measured behind the optical grid. In order to enhance the contrast of the shadow thrown on the cartilaginous surface, the latter was covered by a very thin film of white powder sprayed on, using the 'Developer' of the 'Spot Check' crack detection kit manufactured and supplied by Magnaflux Corporation (materials universally known in mechanical engineering workshop practice).

3.2.2 The calibrating procedure for evaluation of moiré fringes:

To begin with, the whole arrangement is temporarily set up as shown in figure 3.3. The camera is focused on the surface to be measured and the light source (L) moved in a y direction until a suffi-

cient number of fringes (five or more) appear on the surface. Following this, the exact positions of the camera and light source are determined as follows:

The optical grid is now completely removed from the table and the object surface replaced by the vertical face of graph paper attached to the block B. The camera is again carefully focused and a small aperture of value 16 or 22 chosen to permit sufficient depth of sharpness. The camera is fixed rigidly in space by means of a tripod, care being taken not to shift it until the whole experiment has been completed. Adhesive tape is used to fix the focusing arrangement so that no unintentional alteration can occur. A Bowden cable arrangement is advisable to trigger the shutter when taking photographs, to prevent movement of the camera. Now, with the point light source switched off and the room lights turned on, and while looking through the camera view finder, a second person must place the two columns, C1 and C2, on the table top, one behind the other, so that they appear to completely overlap. (Usually a powerful flood light is necessary to illuminate the columns when viewed through the small aperture). Keeping the distance between C1 and C2 as large as possible, the exact position of each of the columns in the xy coordinate system is noted. This procedure is repeated three or more times with C1 and C2 in various parts of the optical field. In this manner, the direction of rays of light that converge at the optical centre of the camera are determined relative to the coordinate system chosen, and the position of the camera is found by finding the point of intersection of these rays. [It is only necessary to find the projection of the point of intersection on the xy plane and therefore a very simple calculation, given the x and y coordinates of two points

(positions occupied by C1 and C2 at a time) through which each ray passes, leads quickly to the solution sought (see Appendix 2(3)). Because of minute errors in determining the exact coordinates of the columns, and because of the narrow field of vision, the estimate of position of the camera thus obtained might vary by a few centimetres, especially in the x direction. Nevertheless, this has insignificant influence on the result if only one selected value is used throughout the subsequent calculations, as has been shown by perturbation of data used in the evaluation of test results].

To determine the position of the light source, the room lights are turned off and the light source (L) alone is switched on. The columns C1 and C2 are now placed on the xy plane so that, with the greatest possible distance between them, the shadow of one falls completely on the other. (The pointed end of the column closer to the light facilitates finding the exact position of its shadow on the one further away). The position of each of the columns in the xy plane is noted and the experiment repeated at least three times. Using the same procedure as described before, the intersection of rays, each given by the position of the two columns C1 and C2, is found. This is the projection of the position of the light source in the xy plane. Care must now be taken not to shift the light source from this position till the experiment is concluded.

Finally, a photograph of the graph paper (mm and cm squares) on the block (B) that occupies the position to be later taken by the object surface is made.

3.2.3 Measurement of the object surface:

The block (B) is now removed and the object brought into position so that the centre of the surface to be measured is approximately in the centre of the view finder and the surface of the object more or less in the plane previously occupied by the graph paper on the face of the block (B). The camera position and adjustments must continue to remain unaltered! The optical grid (G) is put in its original position, that is, along the y axis as shown in figure 3.3. On viewing the object surface through the grid, the moiré pattern will be seen. Final adjustments to the position of the object may now be made to obtain the best possible set of fringes. After the position and direction of anatomical landmarks of the object relative to the plane of grid, and to the table top, have been observed and noted, the grid is set in oscillation and a photograph taken. Leaving the chosen aperture unaltered, several photographs at different exposure times are taken, depending on the sensitivity of film used.

The film is developed and positive copies of the photographs made. All enlargements must be made at the same time with the same settings of the enlargement device. Hence, the dimensions of the object surface parallel to the y-z plane can be determined through direct comparison with the picture of the graph paper attached to the block (B) (neglecting minor projection errors associated with planes at varying distance from the camera). The output of the computer programme "MOIRE" (Appendix 1(3)) gives the distances between points on the object surface through which fringes pass and the plane of the optical grid. By using these values, the difference in the x direction from fringe to fringe, over the whole surface is determined. The profile of the object surface is obtained by selecting a series of

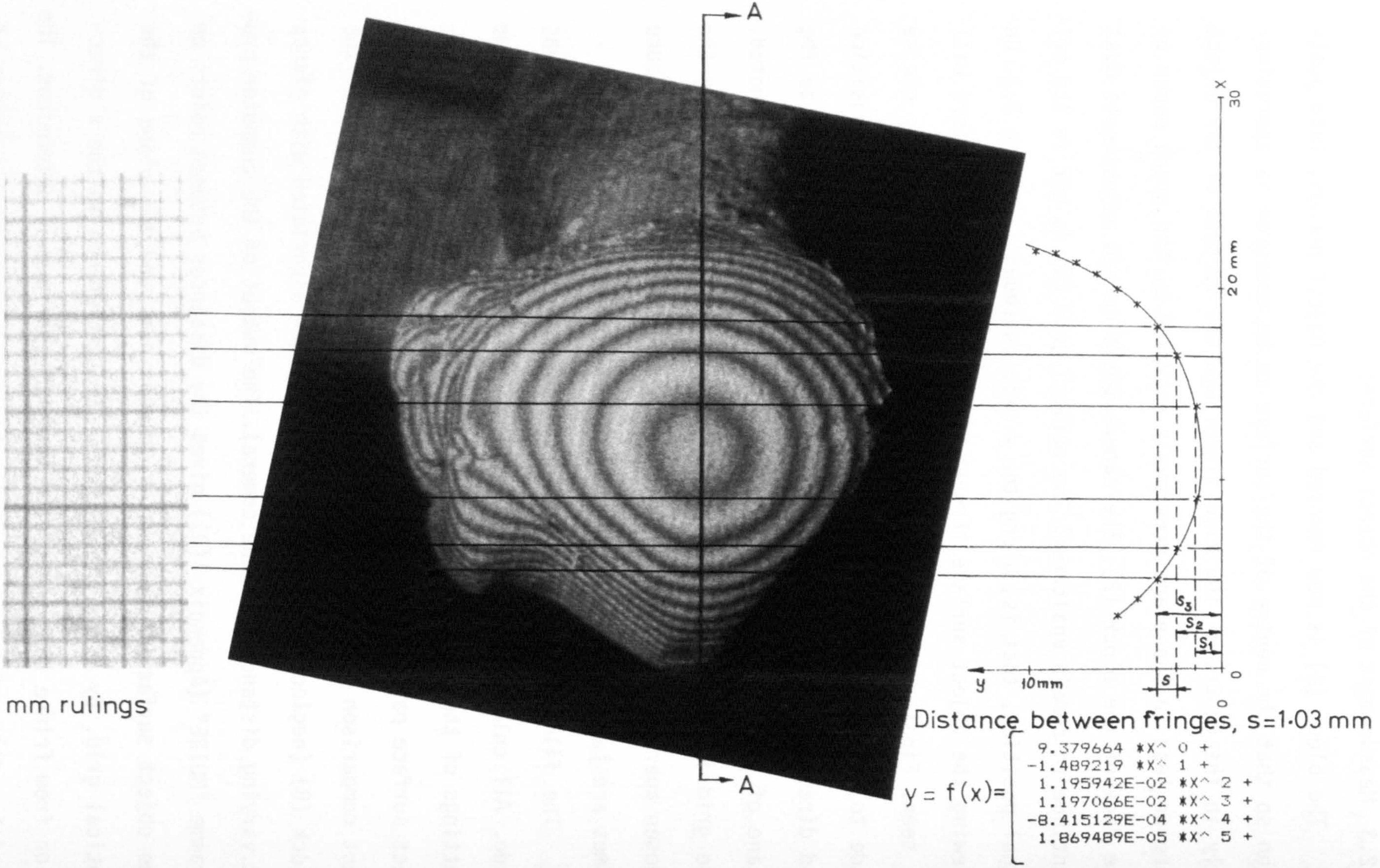

Figure 3·4 Determination of profile of object surface along plane of choice (A-A) from *enlarged moiré photograph*

points on the object that lie in a chosen plane, perpendicular to the photograph, each point lying at the intersection of a fringe with the said plane (fig 3.4). The coordinates of each point are determined as follows: In one direction (parallel to the surface of the photograph) the coordinate is obtained by direct measurement off the object photograph, using the scale obtained from the picture of graph paper, and in the other direction (perpendicular to the surface of the object photograph) the calculated distance between fringes. Figure 3.4 illustrates the method. The contour, or profile, is finally arrived at by finding the best-fitting polynomial which would pass through (or very close to) the points. The process can be substantially simplified by using one mean value for the distances in the x direction between consecutive fringes.

A computer programme was written for the determination of the best-fitting polynomial that could pass through (or close to) a number of given points in a plane, given the coordinate values of each of the points, and after choice of degree (of the required polynomial). The mathematical solution adopted, and details of the programme "AUSGL.POL" are described in Appendix 3(3).

Having found a mathematical expression that describes the contour of the joint surface in a chosen plane, it is now also possible to determine the radius of curvature at any point along the curve.

This is done in the classical manner by differentiation as follows:

Given: $y=f(x)$,

the radius of curvature $r = \dfrac{\sqrt{\left[1+\left(\frac{dy}{dx}\right)^2\right]^3}}{\frac{d^2y}{dx^2}}$

for any chosen value of x.

3.3 Determination of the Axis of Rotation - the Helical or Screw Axis of Motion

When a rigid body A exhibits a planar rotary motion within a cartesian coordinate system S, an instantaneous axis of rotation might be defined by a line passing - at a particular instant - through points of the body A that have zero velocity at that particular instant, parallel to the plane of motion. The instantaneous axis of rotation is therefore oriented normal to the plane of rotation. If, however, particles of the body along the axis of rotation happen to have a velocity other than zero at the instant of observation parallel to the axis of rotation, the rotation movement is no longer strictly planar. This is concisely expressed in Chasles' theorem which states that the most general displacement of a rigid body is a translation plus a rotation. As Goldstein (1950) points out, 'Chasles proved a stronger form of the theorem, namely that it is possible to choose the origin of the body-set of coordinates so that the translation is in the same direction as the axis of rotation. Such a combination of translation and rotation is called a screw motion'. Goldstein goes on to remark that this version of Chasles' theorem presently seems to be but little used.

Indeed, the method commonly employed to determine the instantaneous centre of rotation - when viewing rotation along an axis normal to the assumed plane of rotation - is that attributed to Reuleaux (1900). This consists essentially in tracing the paths taken by at least two points on the object surface and determining the intersection of the normals to the velocity vectors of these two

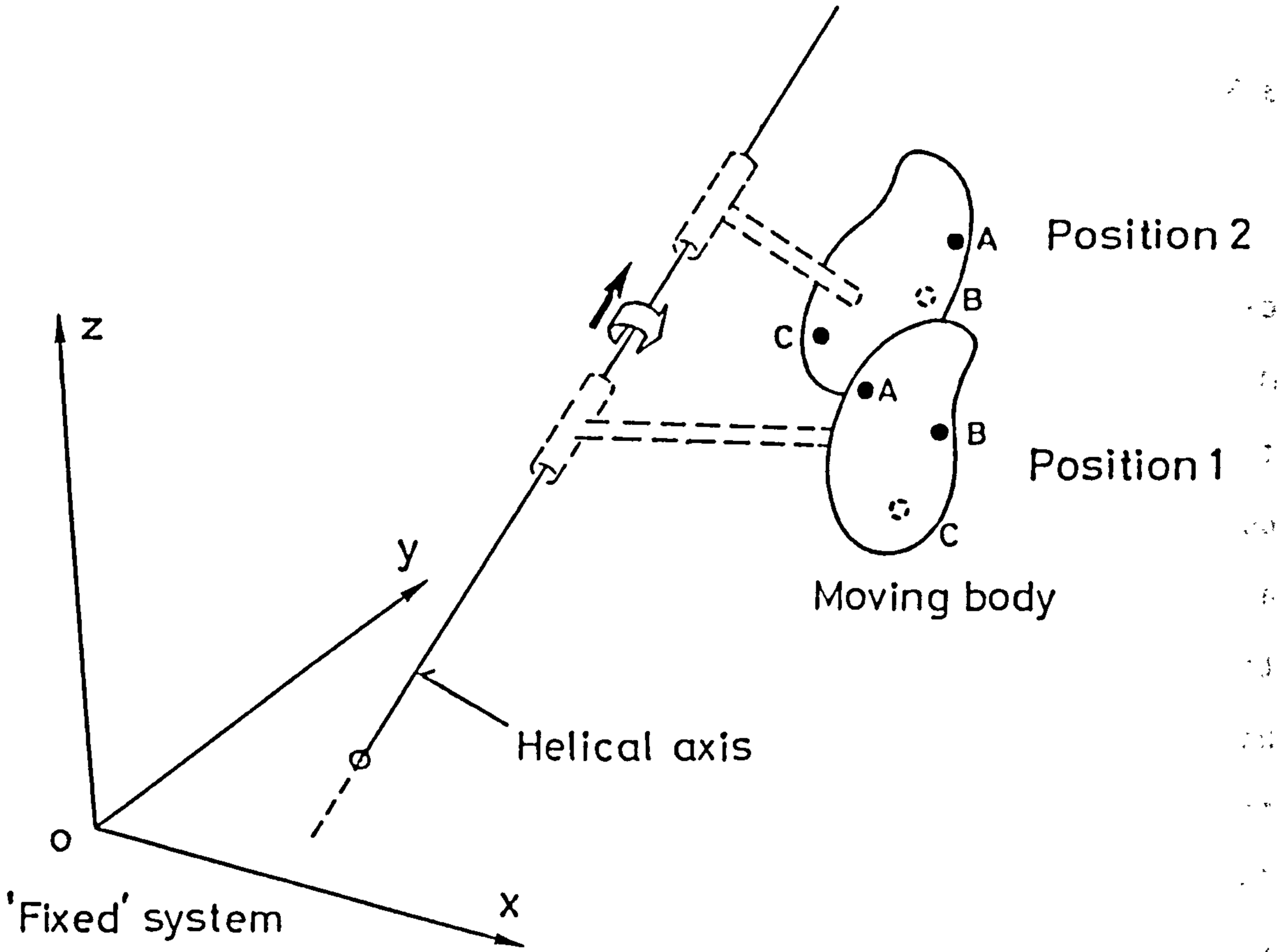

a) Helical axis of motion

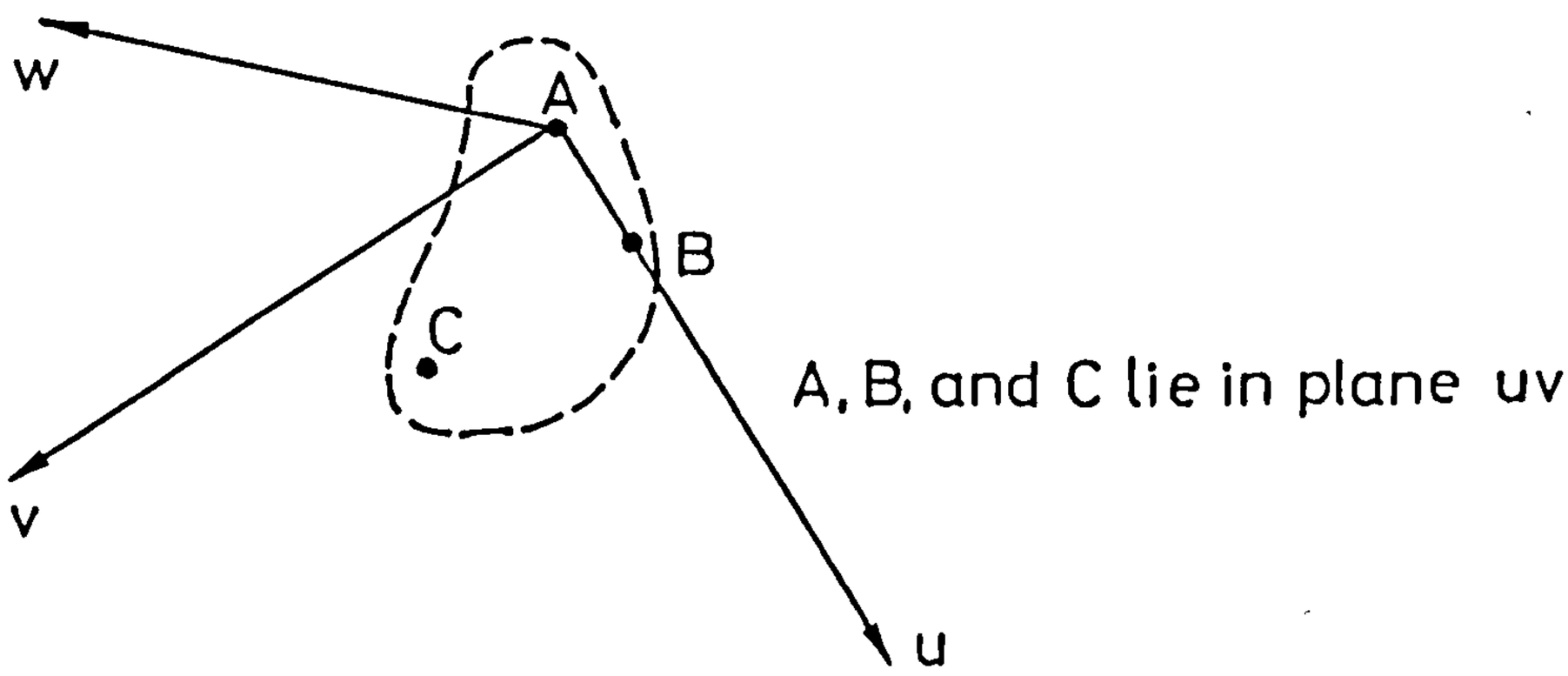

b) Moving system uvw as defined by points A, B, and C

Figure 3.5 General motion as described by the helical axis

points in the plane of motion. The method can, however, lead to appreciable errors if the plane of motion is unknown. Since in biological joints the relative movement between adjacent bodies is often such that the instantaneous axis of rotation moves continuously, accompanied by changes in direction, the so-called Reuleaux method is of very limited application in such cases. [Blacharski et al. (1975) attempted the use of the Rouleaux method in three dimensions but, as Soudan et al. (1979) pointed out, a very bad estimation of the real instantaneous axis results].

Amongst the first to use the 'helical' or 'screw' axis concept (fig 3.5) to describe motion in a biological system were Panjabi and White (1971) and Kinzel et al. (1972). Whereas Kinzel et al. based their method on data obtained from a series of instrumented spatial linkages connecting the two rigid bodies, a description of the relative motion between the two being the aim of the procedure, Panjabi and White derived a description of relative motion by observing the displacement of three vectors (a, b and c) that indicate the position of three arbitrary but non-collinear points (A, B and C) on one of the rigid bodies with reference to a Cartesian coordinate system resident in the second rigid body. In 1981 Panjabi et al. published further details of their computational procedure. Another means of determining the helical axis of motion is based on Rodrigues' formula (Bisshopp, 1969). Brief descriptions of the mathematical details on which these approaches are based are given in the following sections:

3.3.1 The rotation matrix method:

This approach was used by Panjabi et al. (1981) as follows:

Of the two rigid bodies that move relative to each other, one will be referred to as the fixed body with a local coordinate system xyz and the other as the moving body with its local coordinate system uvw (fig 3.5). Definition of the system uvw by means of three non-collinear points A, B and C that are rigidly attached to the moving body follows by declaring A as the origin of the system, AB as lying on the u axis, and the plane containing AB and C as the uv plane. This immediately results in the v and w axes being clearly defined since v lies in the plane determined by A, B and C, and w lies normal to this plane, employing the right-handed convention for positive axis directions. The uvw system is defined in two consecutive spatial positions (pos. 1 and pos. 2) relative to the fixed system xyz*. One position will be referred to as uvw1 and the other as uvw2. Transformation matrices (T1 and T2) are set up for each of the two positions so that any vector $\underline{r}$, in terms of uvw can be transformed to the fixed system xyz. The matrices T1 and T2 are composed of the directional cosines of the axes u, v and w with respect to the xyz system.

Hence, $\underline{r1}_{xyz} = T1 \cdot \underline{r}_{uvw1}$ and $\underline{r2}_{xyz} = T2 \cdot \underline{r}_{uvw2}$

A matrix W is now set up that links T1 with T2, that is, enables $\underline{r1}_{xyz}$ to be transformed directly to $\underline{r2}_{xyz}$.

---

* N.B.: The origins of the uvw and xyz systems are identical.

Since $\underline{r2}_{xyz} = W \cdot \underline{r1}_{xyz}$ it follows that

$W = T1' \cdot T2$ (T1' is the transpose of T1)

W is essentially a rotation matrix.

Now, using Eulerian angles and rotations about the x, y and z axes, a rotation matrix R is set up for transformation of $\underline{r1}_{xyz}$ into $\underline{r2}_{xyz}$, that is:

$$\underline{r2}_{xyz} = R.\underline{r1}_{xyz}$$

where $R = \begin{bmatrix} cy.cz & sx.sy.cz-cx.sz & cx.sy.cz+sx.sz \\ cy.sz & sx.sy.sz+cx.cz & cx.sy.sz-sx.cz \\ -sy & sx.cy & cx.cy \end{bmatrix}$

in which:

sx, sy and sz are the sines of the angles of rotation about the x, y and z axes respectively, and cx, cy and cz are the cosines of the angles of rotation about the x, y and z axes respectively.

By equating the matrices W and R, the Eulerian angles about the x, y and z axes are determined from: R(3,1) = W(3,1), R(3,2) = W(3,2), and R(2,1) = W(2,1).

By definition, a vector $\underline{p}$, describing the helical axes must remain the same for both positions, pos. 1 and pos. 2, of the uvw system. That is:

$$\underline{p2}_{xyz} = \underline{p1}_{xyz}$$

But, $\underline{p2}_{xyz} = R \cdot \underline{p1}_{xyz}$ and therefore

$$(R-I).\underline{p}_{xyz} = NM$$

where I is a unit matrix and NM a null matrix.

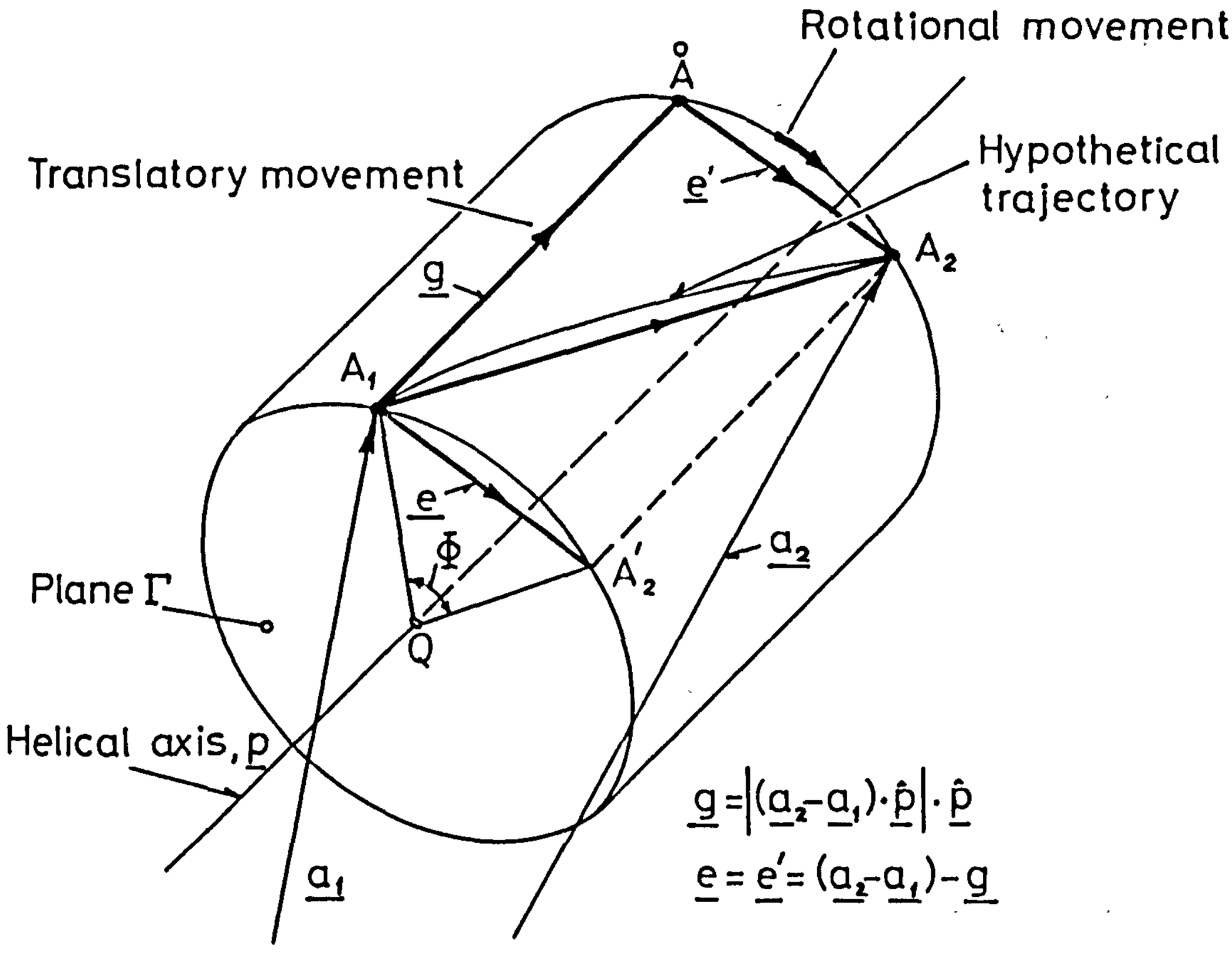

$$\underline{g} = \left|(\underline{a}_2 - \underline{a}_1)\cdot\hat{\underline{p}}\right|\cdot\hat{\underline{p}}$$

$$\underline{e} = \underline{e}' = (\underline{a}_2 - \underline{a}_1) - \underline{g}$$

In plane Γ :

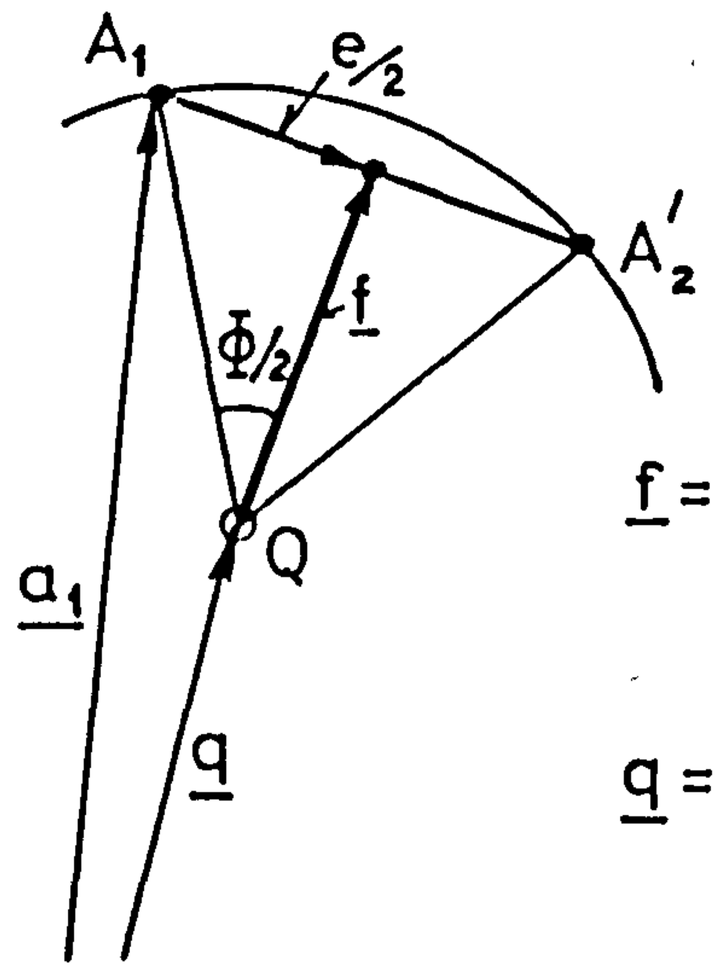

$$\underline{f} = \frac{|e|\cdot(\hat{p}\times\hat{e})}{2\tan(\Phi/2)}$$

$$\underline{q} = \underline{a}_1 - \frac{\underline{e}}{2} - \underline{f}$$

Figure 3.6 Method of obtaining the position vector, $\underline{q}$, for complete description of the helical axis

Hence, the vector $\underline{p}$ describing the direction of the helical axis in the xyz system is determined.

The angle of rotation, Φ, about the helical axis is found from a relation derived by Kinzel (1977) between the vector $\underline{p}_{xyz}$ and the rotation matrix R. It follows that:

$$\cos \Phi = (R(3,3)-\hat{p}_z^2)/(1-\hat{p}_z^2)$$

$$\text{and} \quad \sin \Phi = (R(1,3)-\hat{p}_x.\hat{p}_z(1-\cos \Phi))/\hat{p}_y$$

where $\hat{p}_{xyz}$ is the unit vector.

Now, the system uvw1 moves into position uvw2 by translation parallel to the helical axis, $\underline{p}$, and by rotation through an angle Φ about $\underline{p}$. Knowing the initial and final positions of, for instance, the point A, the direction of $\underline{p}$, and the angle Φ, a point Q can be determined through which $\underline{p}$ must pass. This is done with reference to figure 3.6 as follows:

The projection of the line $\underline{A1\ A2}$ along the helical axis must correspond to the translation, or lead, g, of the screw motion.

Therefore, $$|g| = (\underline{a2}-\underline{a1}) \cdot \underline{p}$$

Now, the total motion of A can be described as a purely translatory motion parallel to $\underline{p}$ of magnitude g, and a purely rotational motion about $\underline{p}$. Allowing the translatory motion to be first performed the position now adopted by A, that is $\mathring{A}$, is found by:

$$\underline{\mathring{a}} = \underline{a1} + g.\underline{p} .$$

It follows that the line $\underline{A1A2'}$ is a chord which is subtended by the angle Φ from a point Q on the helical axis $\underline{p}$.

The above account of the procedure in determining the helical axis of motion as used by Panjabi et al. (1981) is only a very brief

Given:

A_1 B_1 C_1 and A_2 B_2 C_2

Required:
The direction and position
of the helical axis of motion

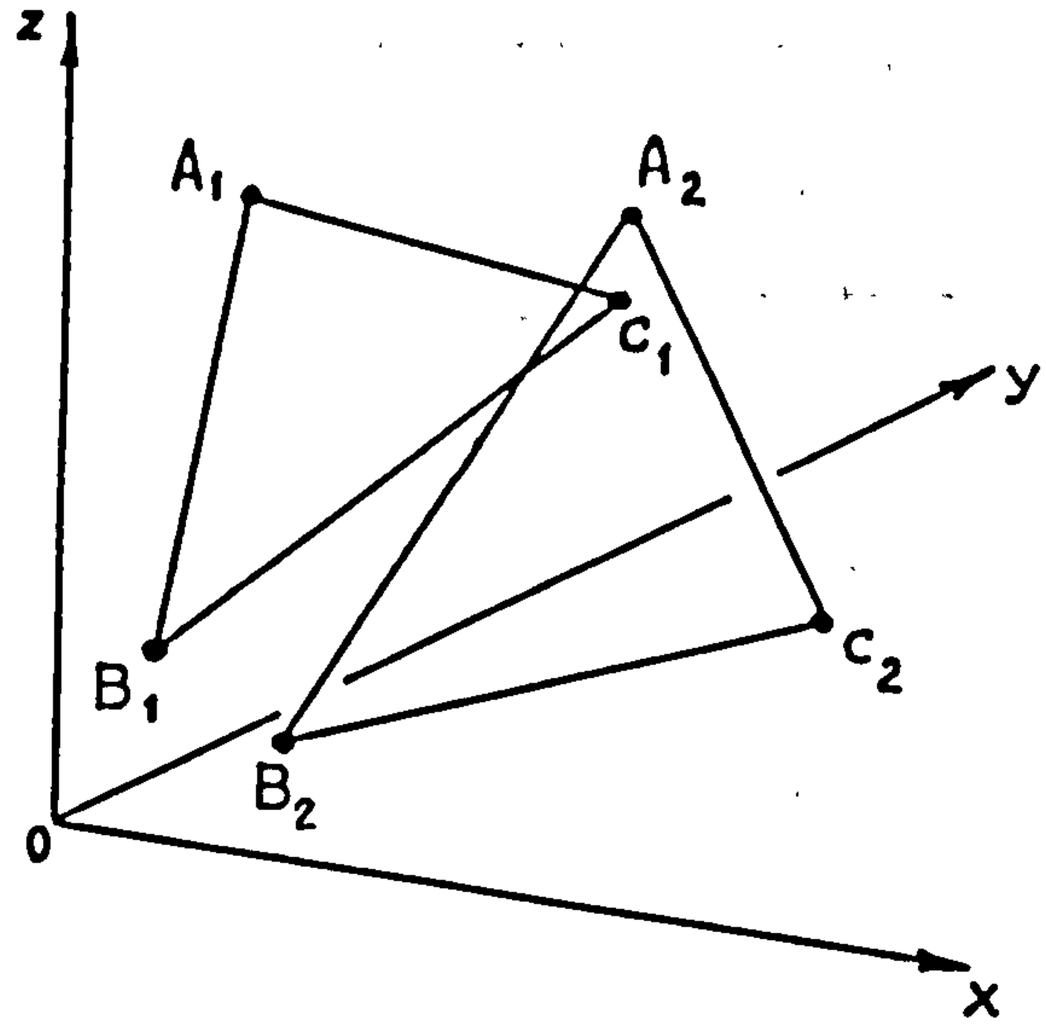

Step 1:

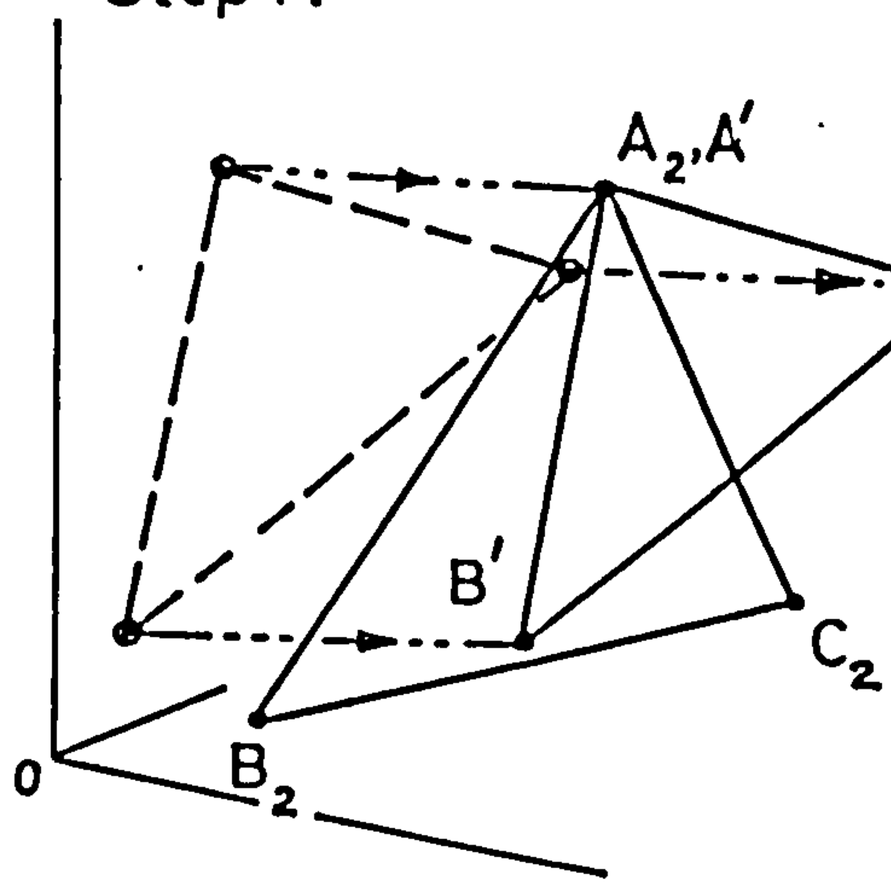

Step 2:

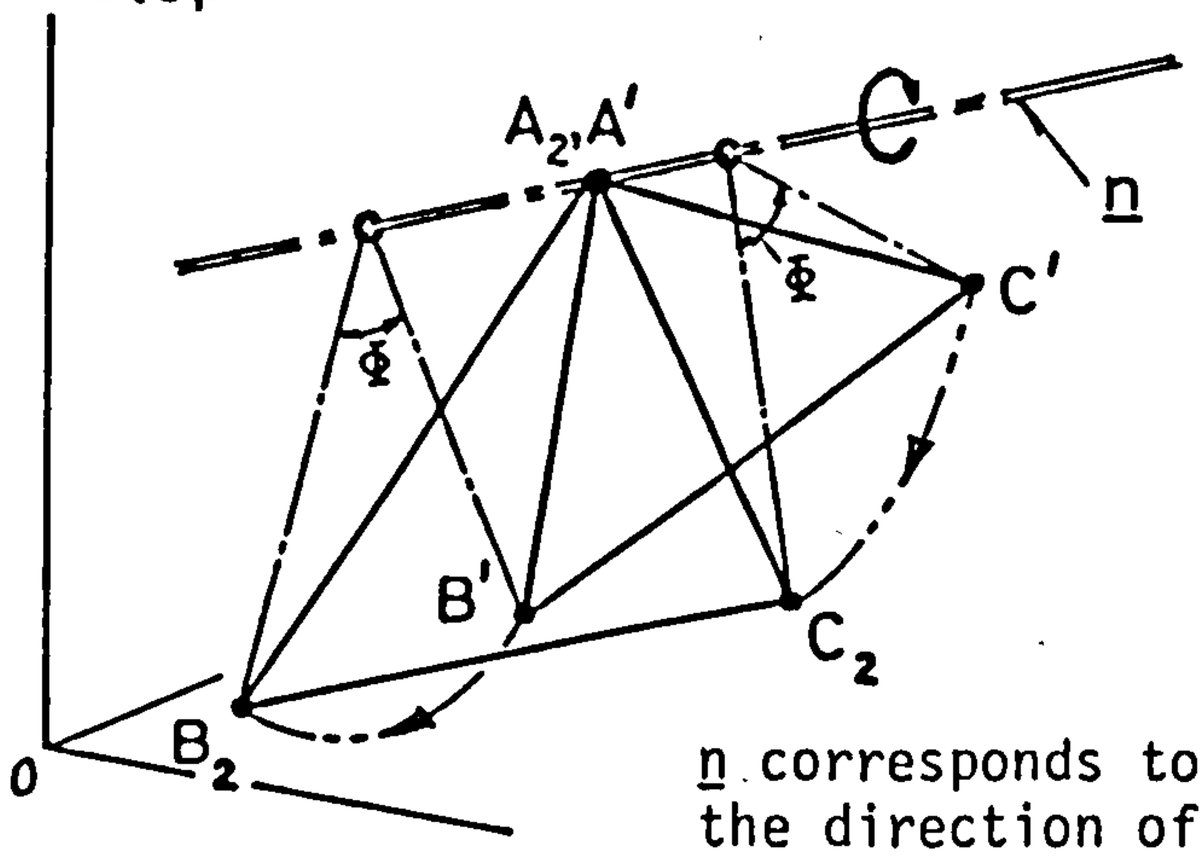

n corresponds to
the direction of
the helical axis

Step 3:

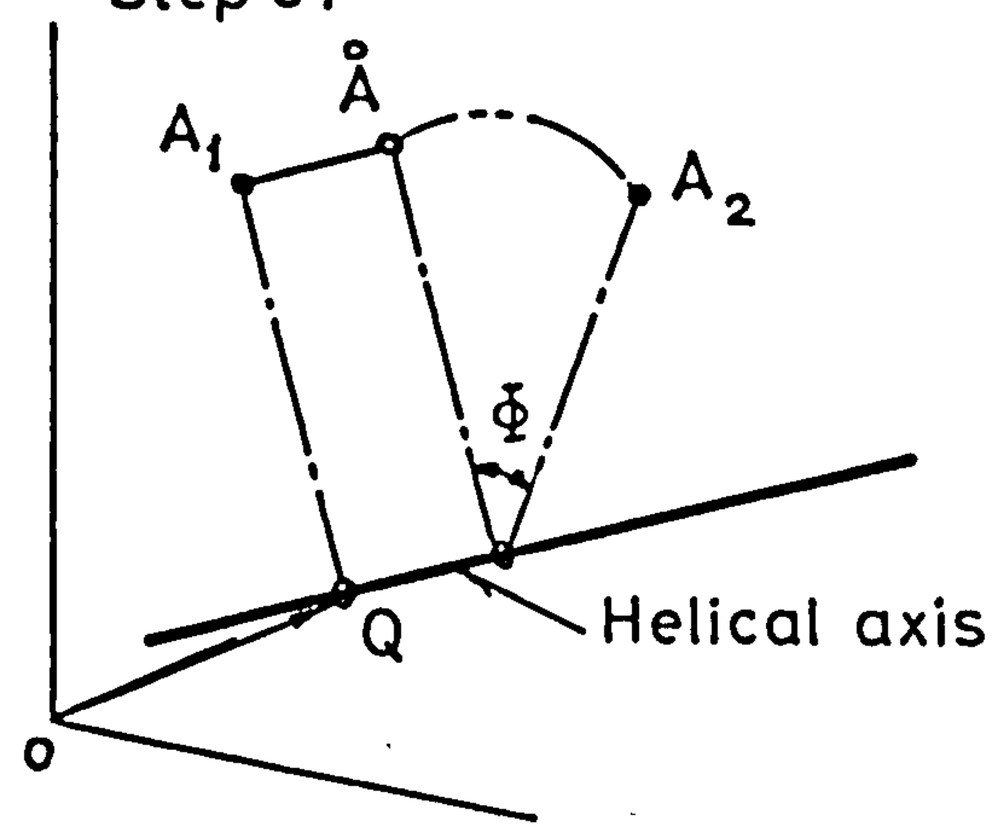

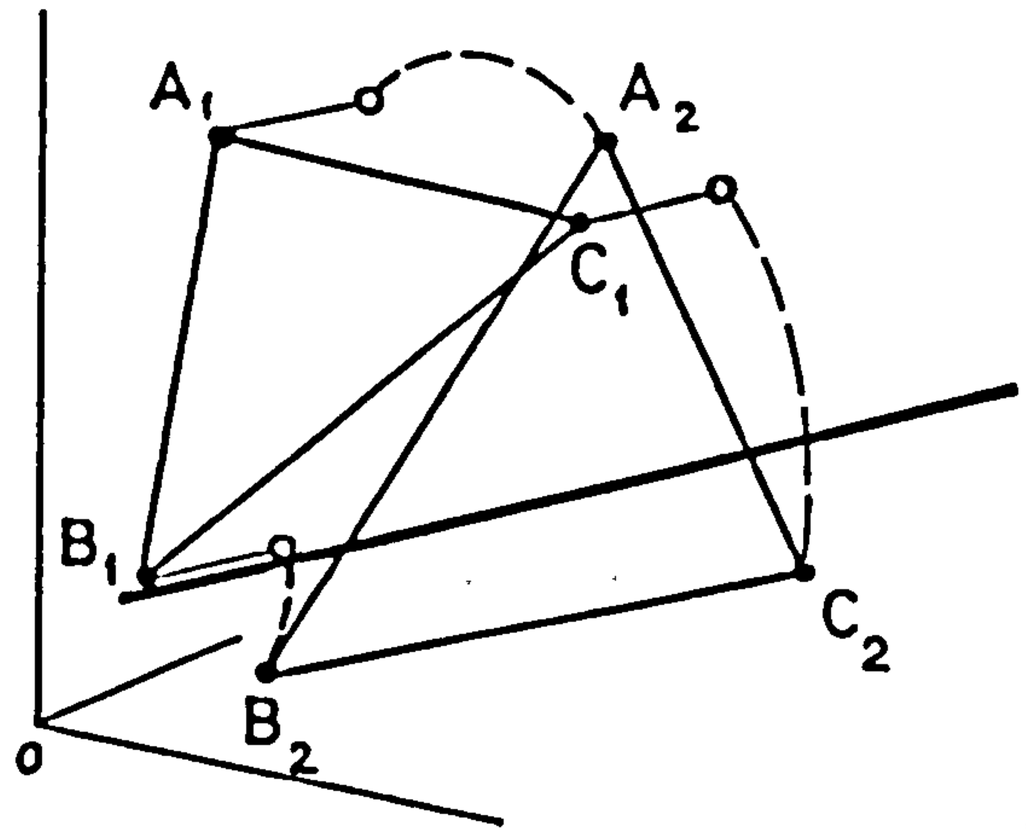

(see figure 3.6)

Figure 3.7 Determination of the helical axis using Rodrigues' formula to obtain Φ

description and for further details reference to the original article is suggested. Appendix 4(3) contains details of the computer programme HELIMAT which was compiled for use in the present investigation.

A limitation of the above method is when dealing with displacements of such minute magnitude that inaccuracies of measurement begin to play a dominant role. Furthermore, rotation angles greater than 90° lead to wrong results. Also, since the method is based on finite differences, the helical axis which results should not be made identical with the true 'instantaneous' axis of rotation.

3.3.2 The Rodrigues' formula method:

Again, the position of a rigid moving body relative to a fixed coordinate system xyz is defined by the position of three non-collinear points A, B and C rigidly attached to the former (fig 3.5). Two consecutive spatial positions (pos. 1 and pos. 2) are denoted by A1, B1, C1 and by A2, B2, C2. Since the total motion of the moving body can be resolved into translation and rotation, these might in fact be considered to take place independent of each other and in any sequence. The rotation is singular, in that it can be accomplished anywhere in space, the direction and magnitude always remaining the same, even if this includes an additional translatory movement when moving the body from its initial position 1 to its final position 2. Hence, the direction of the axis of rotation can be found by first translating A, B, C from position 1 into A', B', C' where A' coincides with A2, and then by rotating B and C about an axis $\underline{n}$ (which passes through A2) so that B and C move from B' and C' to B2 and C2 respectively (fig 3.7). $\underline{n}$ therefore has the same

direction as the helical axis being sought.

$$\underline{n} = (\underline{b2} - \underline{b'}) \times (\underline{c2} - \underline{c'})$$

The angle of rotation, Φ, is obtained from Rodrigues' formula (Bisshopp, 1969) as follows:

$$\tan\frac{\Phi}{2} = \frac{[(\underline{b2} - \underline{a2}) - (\underline{b'} - \underline{a2})] \times \underline{n}}{[(b2 - \underline{a2}) + (b' - \underline{a2})] \times \underline{n}}$$

Having found the angle of rotation, Φ, and the direction of the helical axis, the position of the helical axis and the translatory movement along this axis are determined as outlined in the previous Section 3.3.1 with reference to figure 3.6. Appendix 5(3) shows the computer programme HELIROD.J for determining the helical axis in this manner.

A limitation of the above method, apart from dealing with displacements of such minute magnitude that inaccuracies of measurement begin to play a dominant role and that rotation angles greater than 90° lead to wrong results, is when the chord formed by the rotation of B from B' to B2 happens to be parallel to that formed by C when rotating from C' to C2. Also, since this method too is based on finite differences, the helical axis thus obtained should not be made identical with the true 'instantaneous' axis of rotation.

The latter, however, might be found by tracing the spatial movement of the three markers A, B and C in an xyz coordinate system and expressing their positions as some function of a common parameter (for example: time, flexion-extension angle, or even perhaps

displacement along one of the coordinate axes itself). On obtaining suitable mathematical functions, these are then differentiated and the differential quotient for a particular parameter value determined. The unit vector describing the instantaneous helical axis, $\hat{n}$, is given by:

$$\hat{n} = \frac{\left(\frac{da}{dt} - \frac{db}{dt}\right) \times \left(\frac{da}{dt} - \frac{dc}{dt}\right)}{\left|\left(\frac{da}{dt} - \frac{db}{dt}\right) \times \left(\frac{da}{dt} - \frac{dc}{dt}\right)\right|}$$

and the point P through which the axis passes is:

$$P = \underline{a}(t) + \underline{s}$$

where
$$\underline{s} = \frac{\hat{n} \times \frac{da}{dt} \left|\left[c(t) - b(t)\right] \times \hat{n}\right|}{\left(\frac{db}{dt} - \frac{dc}{dt}\right) \times \hat{n}}$$

The solutions were obtained by F. Barro at the University of Zurich. With this method, however, as can be immediately appreciated, neither the angle of rotation nor the lead of the helix can be computed between two consecutive positions of the moving body. Also, since the method involves the differentiation of mathematical functions, great care must be taken when smoothing curves are fitted to the raw data since the differential quotients that result are extremely sensitive to 'noise'.

Therefore, for the present investigation use has only been made of the earlier described 'incremental' methods rather than the one which gives the true instantaneous helical axis of motion.

3.3.3 The apparatus for determination of the helical axis:

Markers, three in number, are attached to the bone by means of a special arrangement as shown in figure 3.12a. The arrangement consists of a cross formed of 2 mm thick stainless steel rods with each arm of about 7 cm length measured from the point of crossing. At three ends of these cross-rods a coloured plastic sphere of 5 mm diameter with a central hole is slipped over and retained in place with a cyanoacrylate quick-setting adhesive. The end of the fourth arm of the cross, its foot, is brazed to a short pedestal from which two parallel spikes of 2 mm diameter and about 20 mm length project. The spikes are at a distance of about 8 mm from each other. By driving the spikes into corresponding holes drilled into the bone until the pedestal touches the bone surface, a clearly defined marker system that can be even removed and brought back into its previous position relative to the bone, if this be necessary, is obtained.

The spatial position of the three markers now indicating the position of the bone to which they are firmly attached is determined by means of photogrammetry as follows:

A special 'stage' was built consisting of a square floor and two square side walls, or panels, that assemble to form three sides of a cubical space (fig 3.8). While the vertical side walls are rigidly supported by a ground frame, the floor can be readily removed. The three aluminium plates of 4 mm thickness and 450 mm side length are accurate squares that fit exactly. The floor plate is reinforced

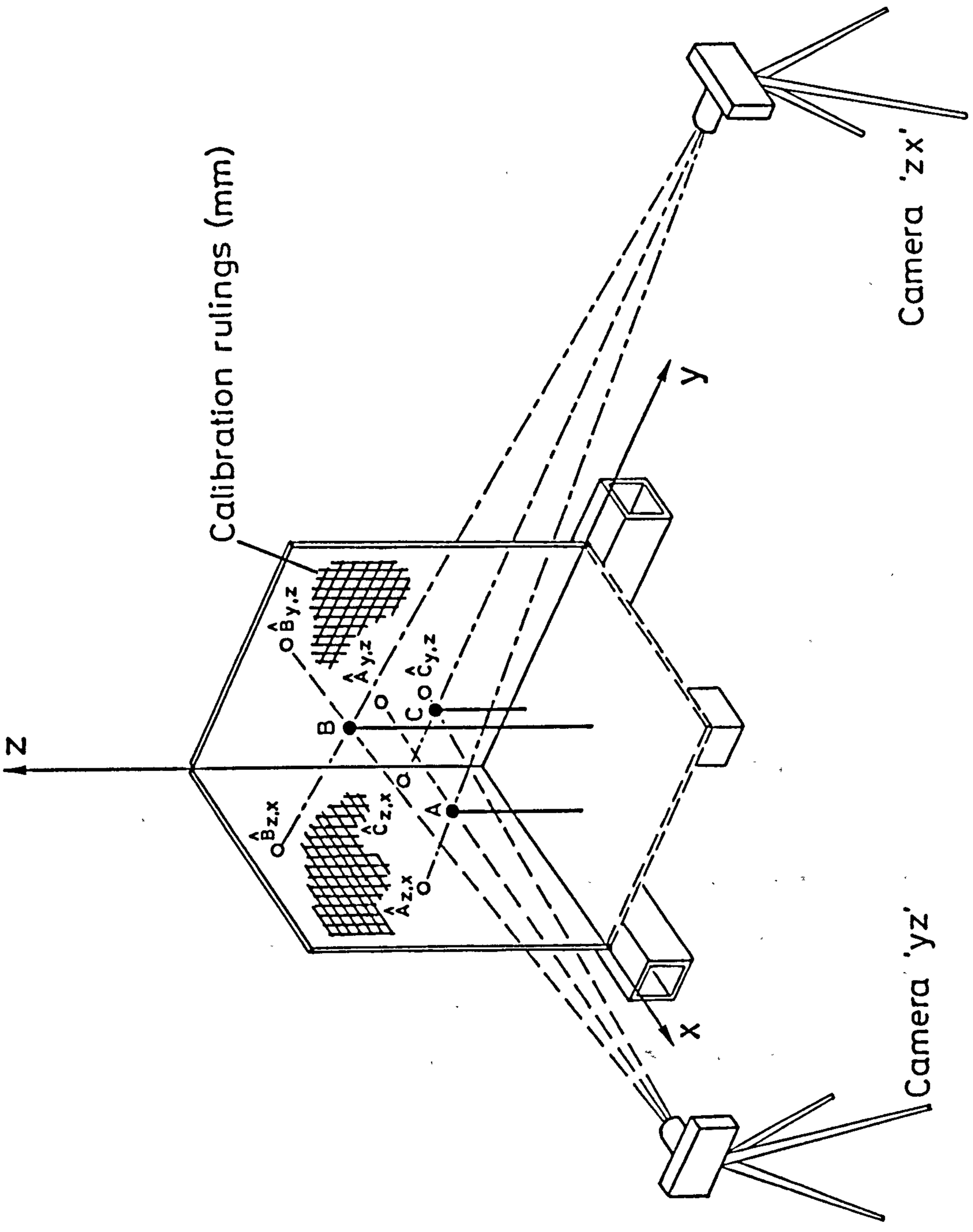

Figure 3.8 Set-up for 3-D measurements

on its underside to minimise sagging and is kept level through an additional support. The corners formed by the plates mark the xyz axes of the Cartesian coordinate system that will hence be referred to as the global system. A number of holes of 1 mm diameter in the plates mark coordinate points at regular intervals of 100 mm on all three planes. These holes were drilled on a precision coordinate drilling machine. Light emitting diodes stationed behind the plates enable these points to be clearly recognised even from a distance of more than 4 m. A dimensionally stable plastic foil with mm and cm rulings (like graph paper) is attached to each of the two vertical planes paying close attention to the origin of the coordinate system.

Two Nikon model F Cameras fitted with Nikkor f/4 lenses of 200 mm focal length mounted on tripods, are placed each at a distance of about 4 m from the yz and zx planes, respectively, as shown in figure 3.8. Using an object placed approximately in the centre of the stage, both cameras are sharply focused and the focusing arrangement thereafter arrested by means of adhesive tape. A small aperture, to permit a maximum of depth of focus, is then chosen. A Bowden cable is used to trigger the shutter of the cameras to prevent them moving when taking pictures. A film for colour slides of ASA-100 sensitivity was found to be quite suitable.

On using the slides to determine the coordinates of the projection of the spherical markers on the yz and zx planes, as seen by the cameras, it proved to be an extremely tedious task to read off the corresponding values directly from the ruled background. To facilitate this and to cope with the large quantity of data that has to be collected, a digitiser is used. Initially a digitising pad, DIGI-PAD, manufactured by GTCO Corporation of Rockville, USA, was

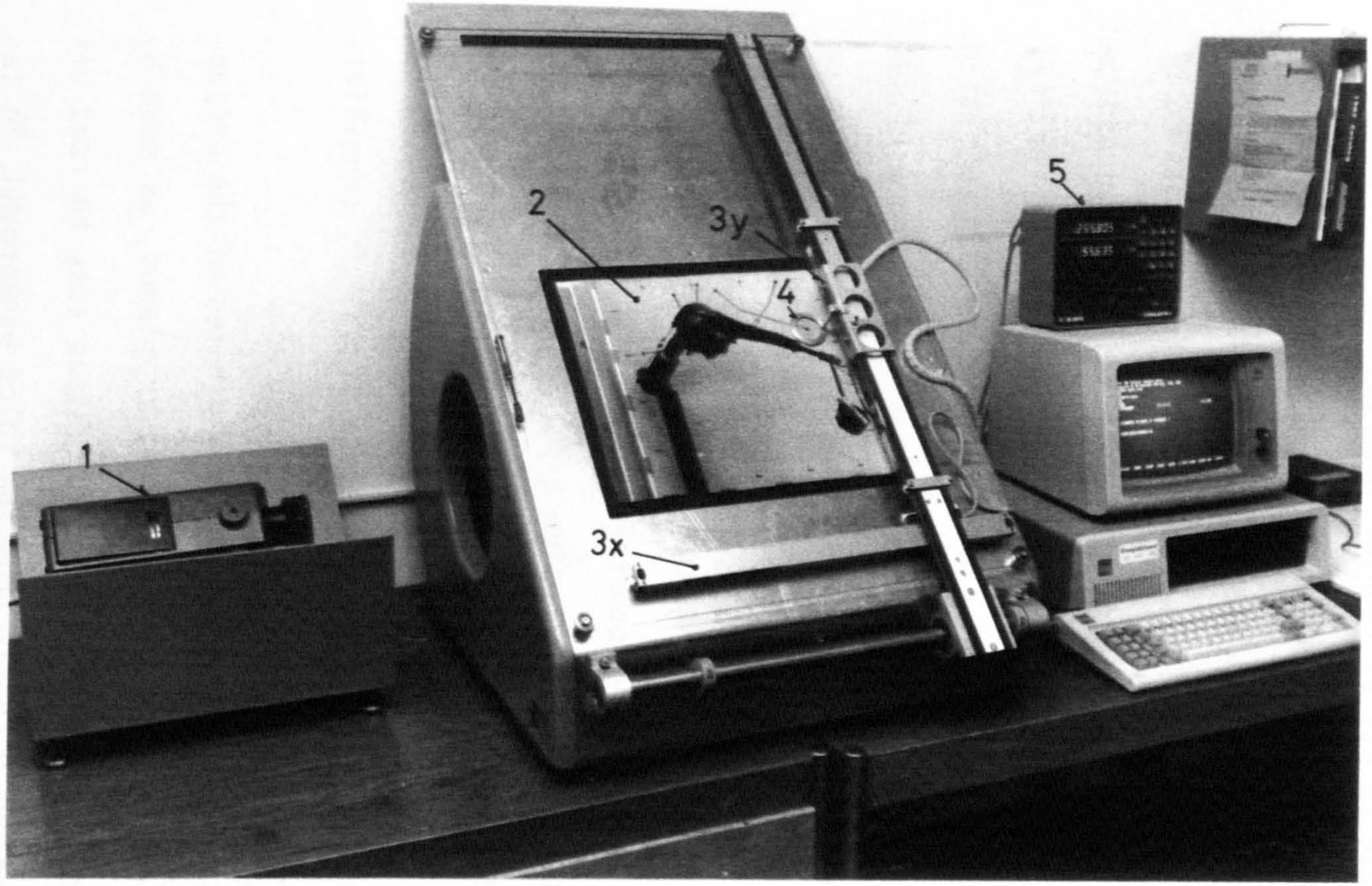

1 Slide or film projector
2 Matt glass screen on which the picture is projected from behind, after reflection by a plane mirror
3x, 3y Linear displacement transducers
4 Cross wires for centring on point target
5 Digital counter (x and y coordinates)

Figure 3.9 The apparatus for obtaining coordinates of picture points

employed but the measuring tolerance was not better than +/- 0.67 mm which proved insufficient for our use and led to gross errors, especially when extrapolations were carried out. A far more accurate device was therefore designed and specially built, based on a linear digital scale as manufactured by Dr. Johannes Heidenhain, Germany, and incorporated in an electronic assessing system manufactured and marketed by ELESTA, Bad Ragaz, Switzerland. The measuring system primarily designed for use in controlling the feed of numerically controlled machine tools, consists of a quartz glass ruler with graduations etched into the surface. A light beam is interrupted by means of the graduations when the former is moved along the ruler so that a digital counter (forwards/backwards) receiving impulses from a photo-cell gives the distance moved. The resolution is 0.0001 mm and the digital counter assesses the displacement to within +/- 0.005 mm. The reading of the counter is fed into a personal computer for storage and further processing. Figure 3.9 shows the device designed and built by the author for digitising the coordinates of points projected from below an obliquely positioned matt glass plate. A cross-wire cursor attached to vertical and horizontal prismatic slides to which the 'electronic rulers' are attached, greatly simplifies centring over the projected image. The cursor moves freely over the whole area of the glass plate which measures 36 cm x 28 cm. To exclude parallax errors, the matt surface of the glass plate, on which the image forms, was brought in contact with the cross-wires of the cursor, the other surface of the glass plate remaining polished.

A special computer programme, DIGXY, was written to transform the digitiser coordinates to picture coordinates. This included var-

ious corrections for linear distortion of the projected image. Distortion occurs through the camera lens, projector lens, and the plane mirror used to deflect the horizontally projected rays onto the obliquely positioned glass plate on which the image is finally formed. This, neglecting other sources of distortion like the film plane within the camera or within the slide projector, and also distortion of the film itself. Finally, projection is not always possible on a plane absolutely normal to the optical axis and therefore, squares tend to become a general quadrilateral when finally viewed on the matt glass plate. Distortion due to the camera lens is negligibly small but, nevertheless, the projection lens first used on a common Kodak-2000 projector gave rise to 'barreling', that is, straight lines close to and parallel to the rectangular picture frame appeared curved. Deviation of up to 5 mm from a straight line was thereby observed! Only after replacing the original lens through a special type, Kodak Retinar S-AV2000 PC with a fixed focal length of 60 mm, was it possible to overcome this problem. Distortion due to oblique projection, however, remains. This is compensated for geometrically as follows:

The four corners of a truly rectangular network, as present on the graduated background of the picture being viewed are digitised. That is, digitiser coordinates are allotted to these four corner points that might now form a general quadrilateral. The true, or picture coordinates of these four corner points are noted. Now, assuming that the scale along each of the four sides of the quadrilateral remains linear along its whole length (each of the four sides could have its own independent scale as seen in the projected view), the true coordinates of any point within the network, or closely

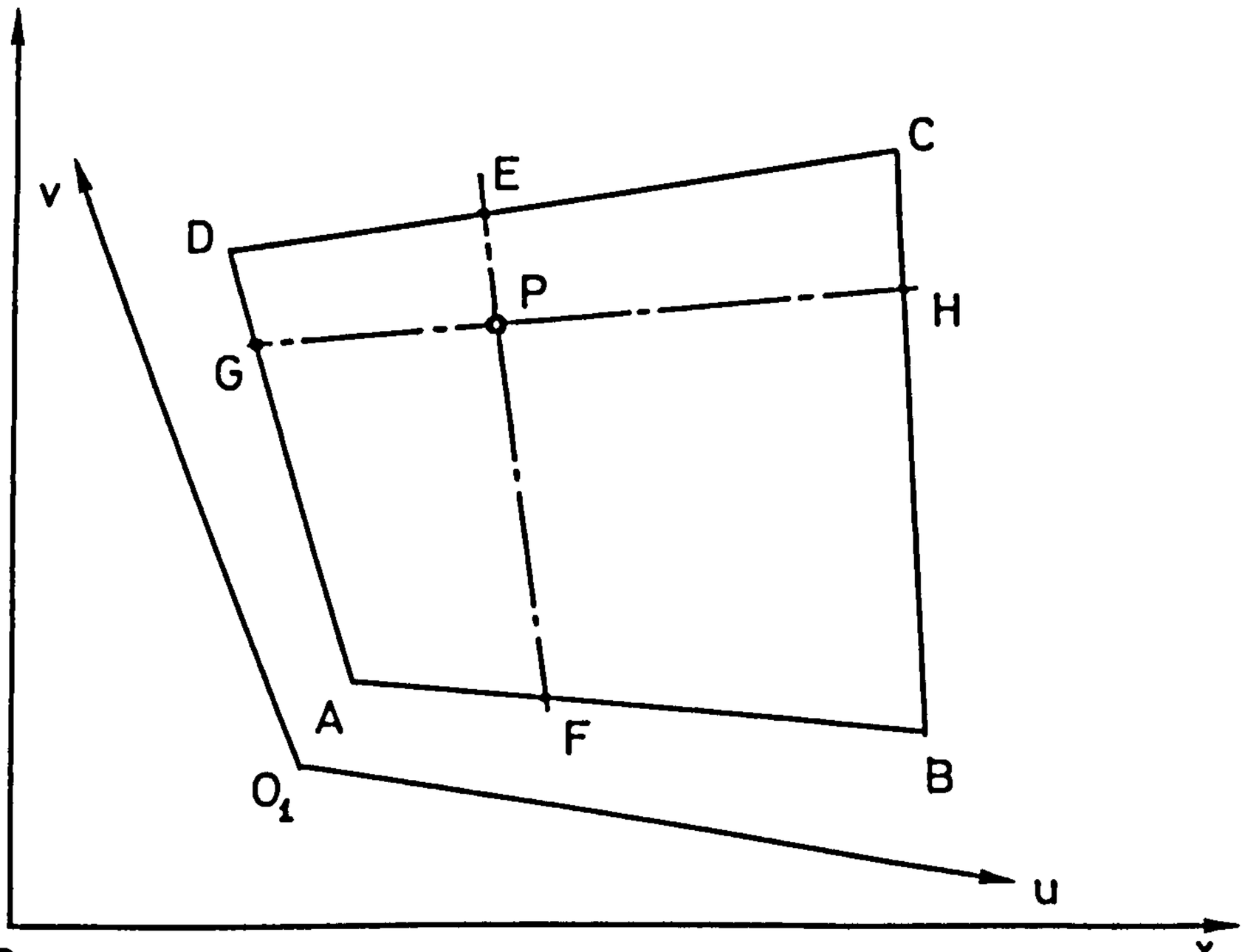

Given: A distorted rectangle ABCD in a plane picture coordinate system, uv, with origin O_1. The uv coordinates of points A, B, C and D are known.

Required: The uv coordinates of a point P.

Digitiser information available: The xy coordinates of points A, B, C, D, and P.

Solution: E_{uv} is determined, where $\frac{DE}{EC} = \frac{AF}{FB}$, and

G_{uv} is determined, where $\frac{DG}{GA} = \frac{CH}{HB}$

$P_u = E_u$ and $P_v = G_v$

Figure 3.10 The problem of determining the coordinates of a point in a distorted picture coordinate system.

situated without, can be calculated from its corresponding digitiser coordinates. Figure 3.10 illustrates the method utilising geometric ratios. Appendix 6(3) gives details of the relevant computer programme DIGXY.

3.3.4 The procedure for determination of the helical axis and its relation to anatomical landmarks:

3.3.4.1 Calibration:

This is necessary to determine the exact position of the two cameras in relation to the global coordinate system xyz (see figure 3.8 and Section 3.3.3). Two columns, each bearing a plastic sphere of 5 mm diameter at their upper extremities, and supported by a cylindrical base of 45 mm diameter, are placed on the floor plate of the xyz 'stage' (fig 3.11). They should be positioned as far apart as possible and still be kept at the largest possible distance from the side walls. Their exact position in the xy plane is determined (usually this is preselected) and the height of the centres of the plastic spheres from the floor plate (the z-position) measured to within +/- 0.1 mm.

On viewing the set-up through the cameras, the spheres are seen projected onto the graduated backgrounds, that is the yz and the zx planes (fig 3.11). Pictures are taken and the true known spatial positions of the spheres noted. Now, by constructing two rays, each of which join the projection of a sphere on one of the background planes (the coordinate values can be read off the 'graph paper' rulings on the picture taken) with the known true spatial position of that sphere, and by extending these two rays toward the camera, they should intersect at a point corresponding to the position adopted by

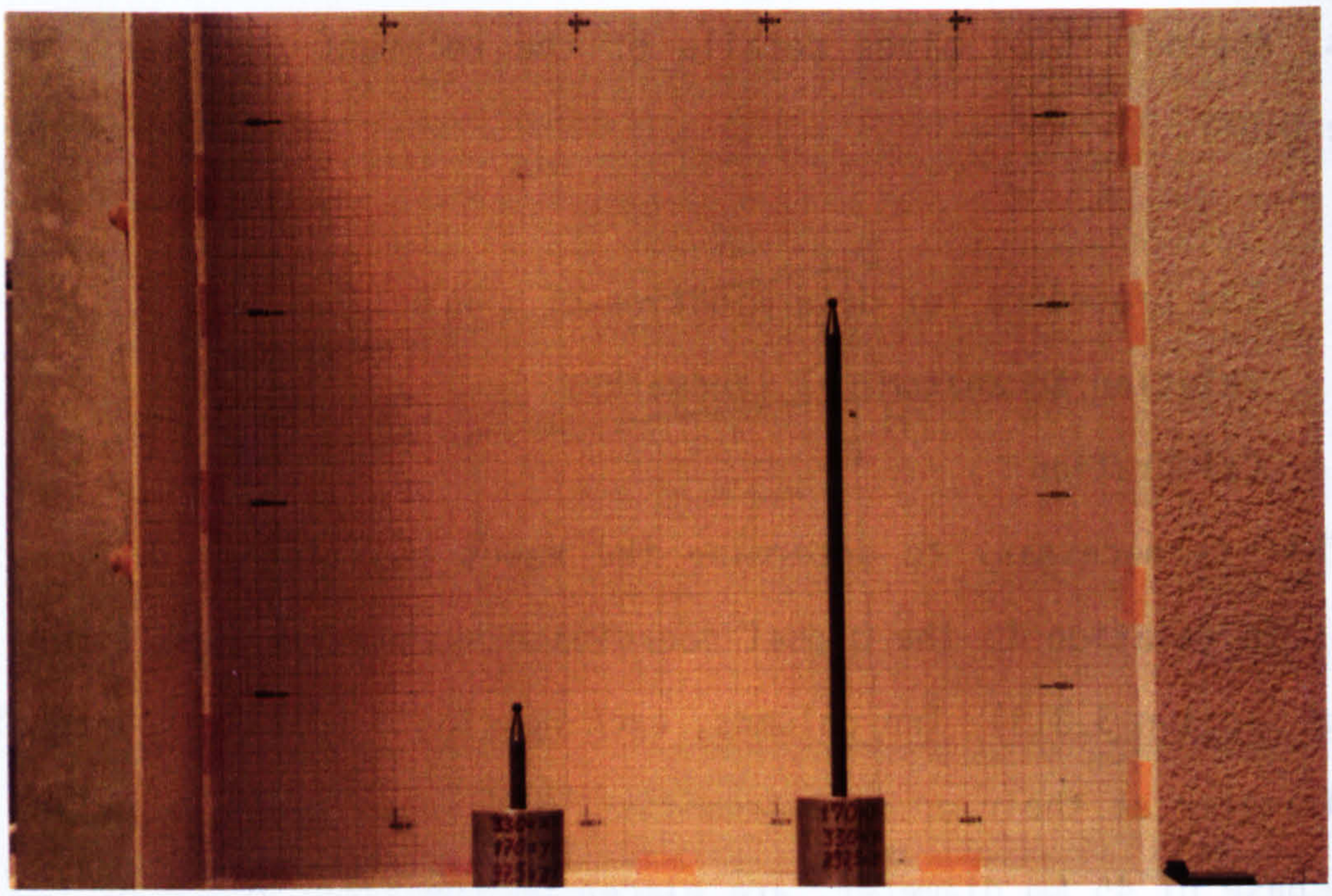

a) Projection of markers on the yz plane, as seen by camera x

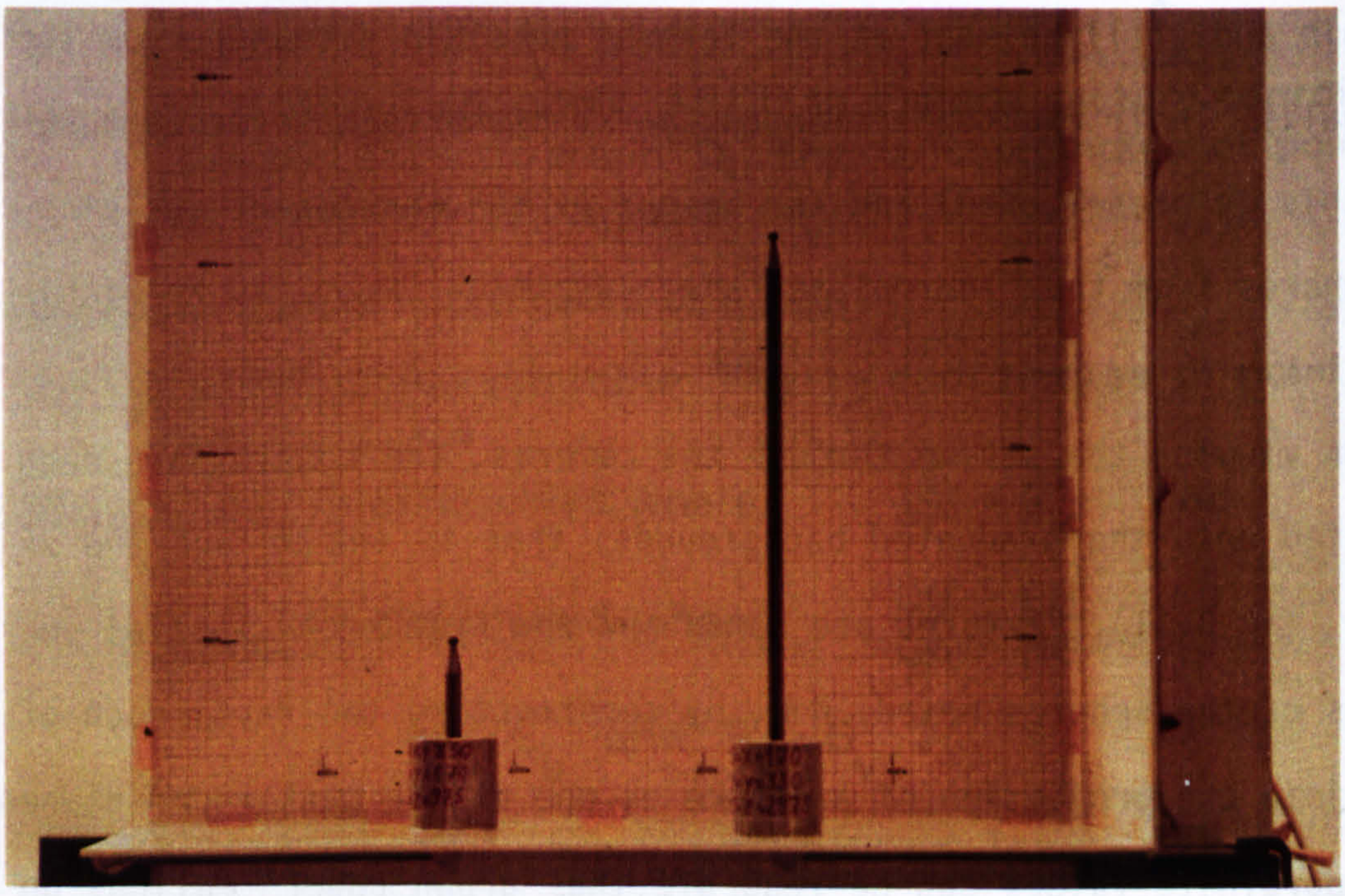

b) Projection of markers on the zx plane, as seen by camera y

Figure 3.11 Calibration procedure for determining the xyz coordinates of the two cameras

the camera itself. This procedure is repeated for the other background plane to obtain the position of the second camera.

The main practical problem that is encountered is that, because of minute unavoidable inaccuracies of measurement, the two rays probably never intersect and are in fact skew lines. One solution would be to determine the intersection of the projection of the two rays on the xy plane (for example) and use this value with the vector equation of one of the rays to find the corresponding z coordinate. The other possibility would be to determine the common perpendicular to the skew lines. This will not only lead to a singular result but, obtaining the length of this perpendicular, the error involved could be expressed in physical terms. Therefore, the latter method was chosen.

The computational procedure involves finding the direction of the common perpendicular, $\underline{n}$, as given by $\underline{n} = \underline{a} \times \underline{b}$, and the length of this perpendicular as obtained from:

$$q = \left| \frac{(\underline{r}-\underline{p})\cdot(\hat{a} \times \hat{b})}{|\hat{a} \times \hat{b}|} \right| \qquad \text{(Faux and Pratt, 1981)}$$

where $\underline{a}$ and $\underline{b}$ are the rays, and $\underline{r}$ and $\underline{p}$ are location vectors for $\underline{a}$ and $\underline{b}$ respectively.

Now, one of the rays is shifted in the direction of $\underline{n}$ and by the amount q, remaining parallel to its original direction, toward the other. In this position the rays must virtually intersect so that the intersection of their projections on the horizontal plane xy immediately leads to the spatial position of one end of the common perpendicular $\underline{n}$. Having found one end, the other follows from q. The computer programme WNSCHF is listed in Appendix 7(3).

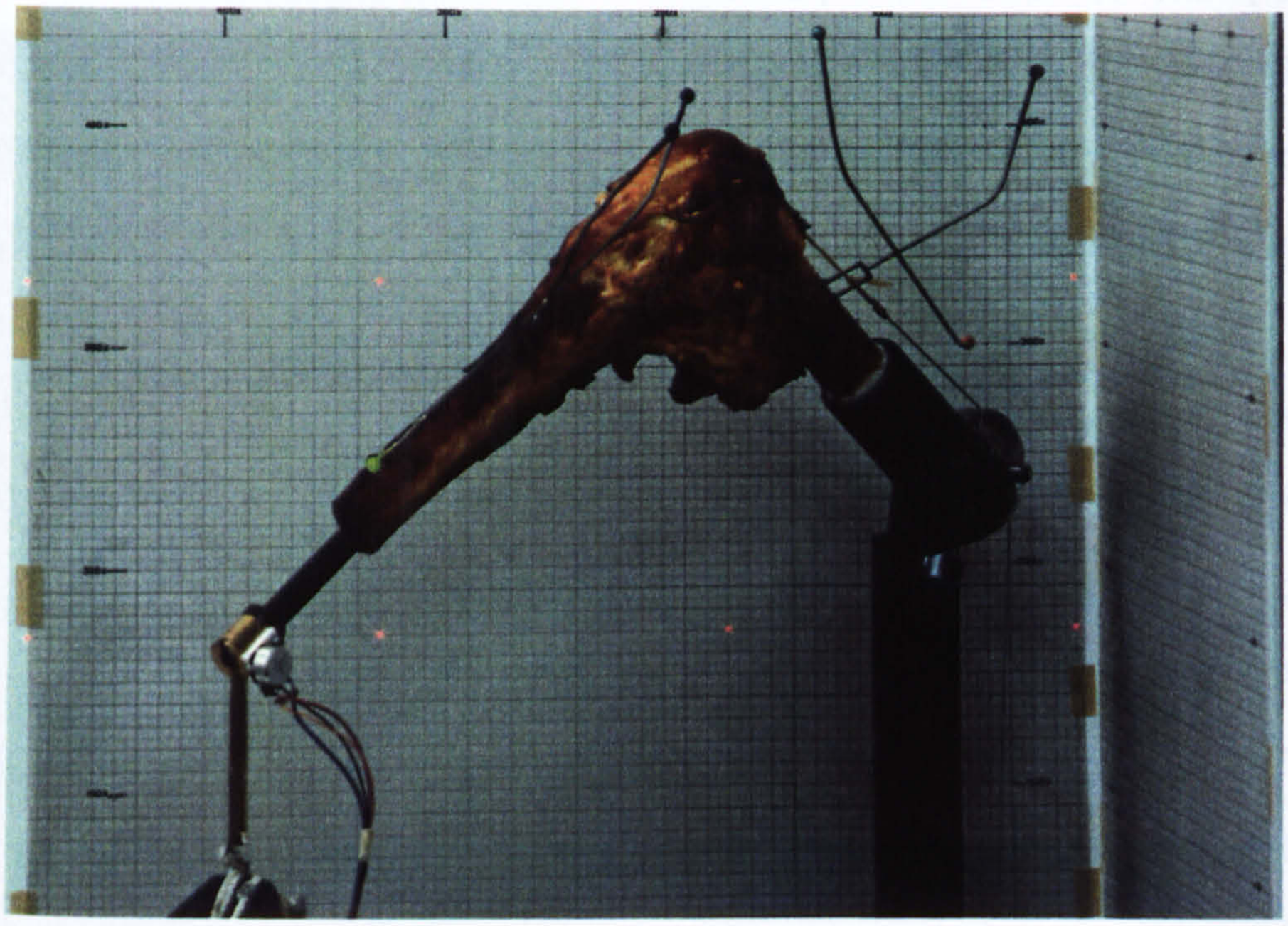

a) A knee joint specimen with a marker triad on the femur and tibia

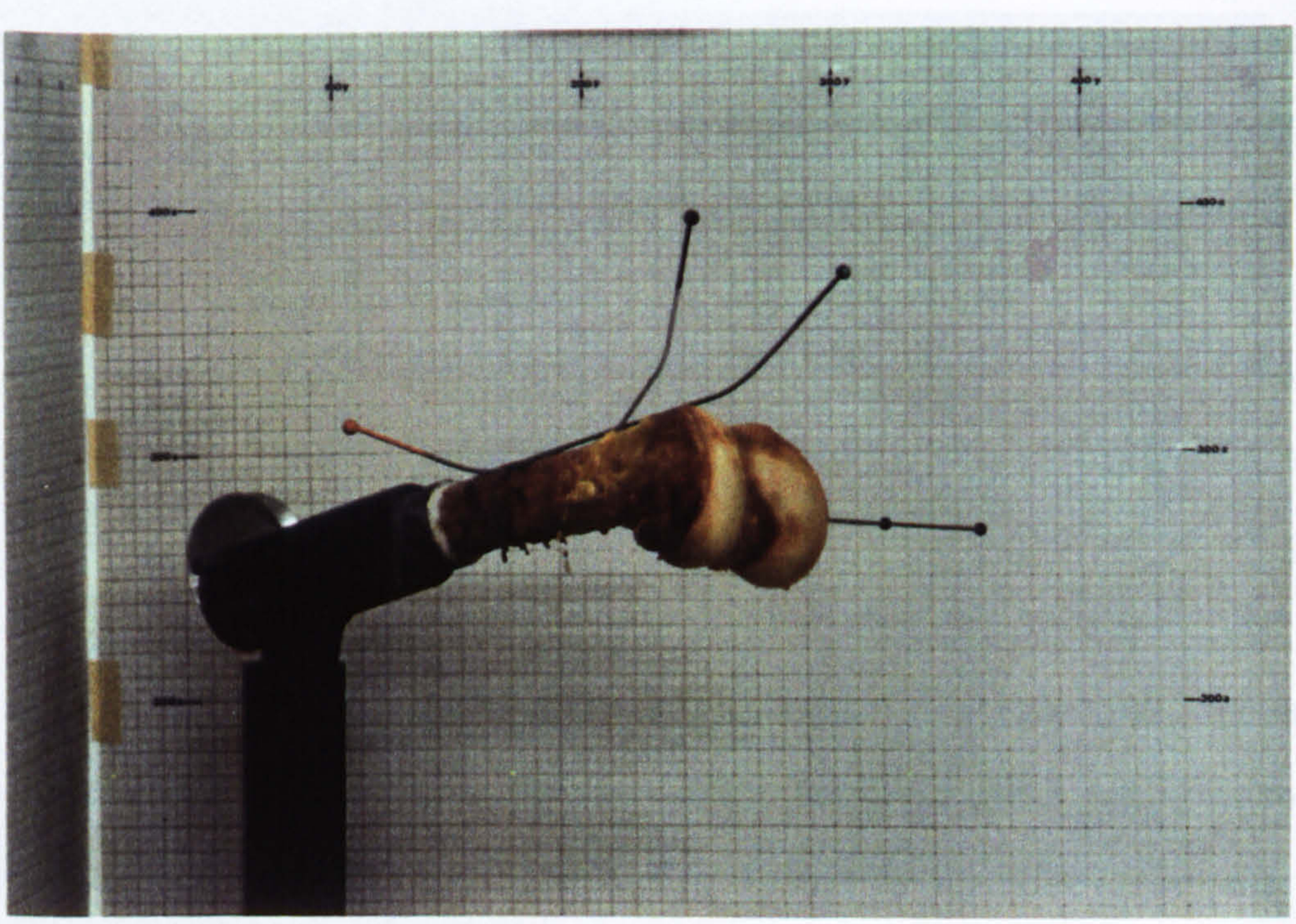

b) Determination of spatial position of an anatomical landmark (origin of med. collat. lig.) in relation to marker triad

Figure 3.12 Markers for determining spatial position

3.3.4.2 Determination of marker coordinates in the global system:

After the calibration procedure has been completed, the floor plate of the 'stage' is removed leaving all other items fixed in their set positions. The articulation to be investigated is now introduced, already fitted with markers as described in Section 3.3.3 and brought into an appropriate position within the cubicle space so that all markers are visible at all times from both cameras during the whole excursion of joint movement to be investigated (fig 3.12a). (The use of spheres of various colours, as markers, greatly facilitates identification). It is usually necessary to apply one set of markers (group of three) to each bone in order to define the position of each in space unless of course, anatomical landmarks or axes are used to specify its spatial location. Pictures are taken with both cameras and with the joint in various degrees of flexion. Determination of the true spatial position of the markers is effected similar to the procedure described in Section 3.3.4.1 only that now the positions of the cameras are known together with the positions of the projections of the spherical markers on the background planes. Again, through intersection of the corresponding rays (fig 3.8) the true spatial coordinates of the markers are found. Since the calculation always involves the same positions of the two cameras for all joint positions, a slightly modified version of programme WNSCHF, called RAUMKO is more suitable for this purpose.

3.3.4.3 Transformation from global coordinates to sub-system coordinates:

Having now obtained the spatial locations of the markers in the global xyz system, it is usually necessary to transform all coordi-

nates into those of a system belonging to one of the bones. This is facilitated through computer programme TRAN-XYZ.UVW (Appendix 8(3)) following this, the helical axis of motion in the chosen Cartesian system is determined as already explained in Section 3.3.

3.3.4.4 Determination of spatial position of anatomical landmarks:

Most often the helical axis of motion has to be finally referred to some anatomical landmarks that are not infrequently uncovered only after the joint has been taken apart. To solve this problem, the markers must be retained in their position relative to the bone until the joint has been disected. Now, a straight K-wire of 2 mm diameter and of 100mm length with two plastic spheres (5 mm diameter) slipped over and glued on, one at the blunt end, the other about 30 mm removed from the pointed end, is so inserted into the bone that the wire literally points towards the landmark, or is in line with the reference axis to be later referred to. Just this bone with its original triad of markers and the now added 'indicators' is brought onto the 'stage' and photographed from both directions (fig 3.12b). The spatial locations of the indicator spheres and the triad of original markers is determined as described in Section 3.3.4.2. The work that remains to be done is now only a matter of transforming coordinates from one Cartesian system to another associated one. Computer programme TRAN-UVW.XYZ (Appendix 9(3)) facilitates the reverse of TRAN-XYZ.UVW. The two indicator spheres on the pointer serve as two points on a vector from which the position of a third point along the same vector can be readily determined.

3.4 Determination of Toe-out

Because of the necessity to observe the toe-out (also: 'foot angle' or 'angle of gait') of individuals among the normal population without them becoming aware of being observed, it was decided to make use of a hidden motion camera to collect the required information. A roofed passage leading to the clinic was selected through which a large number of the employees passed on their way to and from work. This proved particularly convenient because short periods of the day could be chosen during which a large number of people - walking in one direction could be observed. A video technique was preferred to a motion film camera for various reasons: far lower cost of utilized material (photosensitive film), absence of noise, and ability to cope automatically with a wide range of light intensity, down to poor lighting conditions. The low scanning frequency (25/s) and poorer resolution did not impose any limits on the information required. However, since measurements were made directly off a television screen (cathode ray tube) and not with digitised data, probably more error is involved than if photographic film had been used, even though special measures were taken to reduce parallax errors as much as possible.

3.4.1 Video measuring technique and equipment employed:

A video black and white camera, Type BOSCH TNG-9Y, fitted with an Angénieux zoom lens of 15-150 cm focal length, was installed immediately below the ceiling at a height of about 2.6 m from the floor with the optical axis inclined at about 45° to the horizontal (fig 3.13a). The camera was well hidden, but nevertheless on looking upwards when within a horizontal distance of about 5 m from it, the

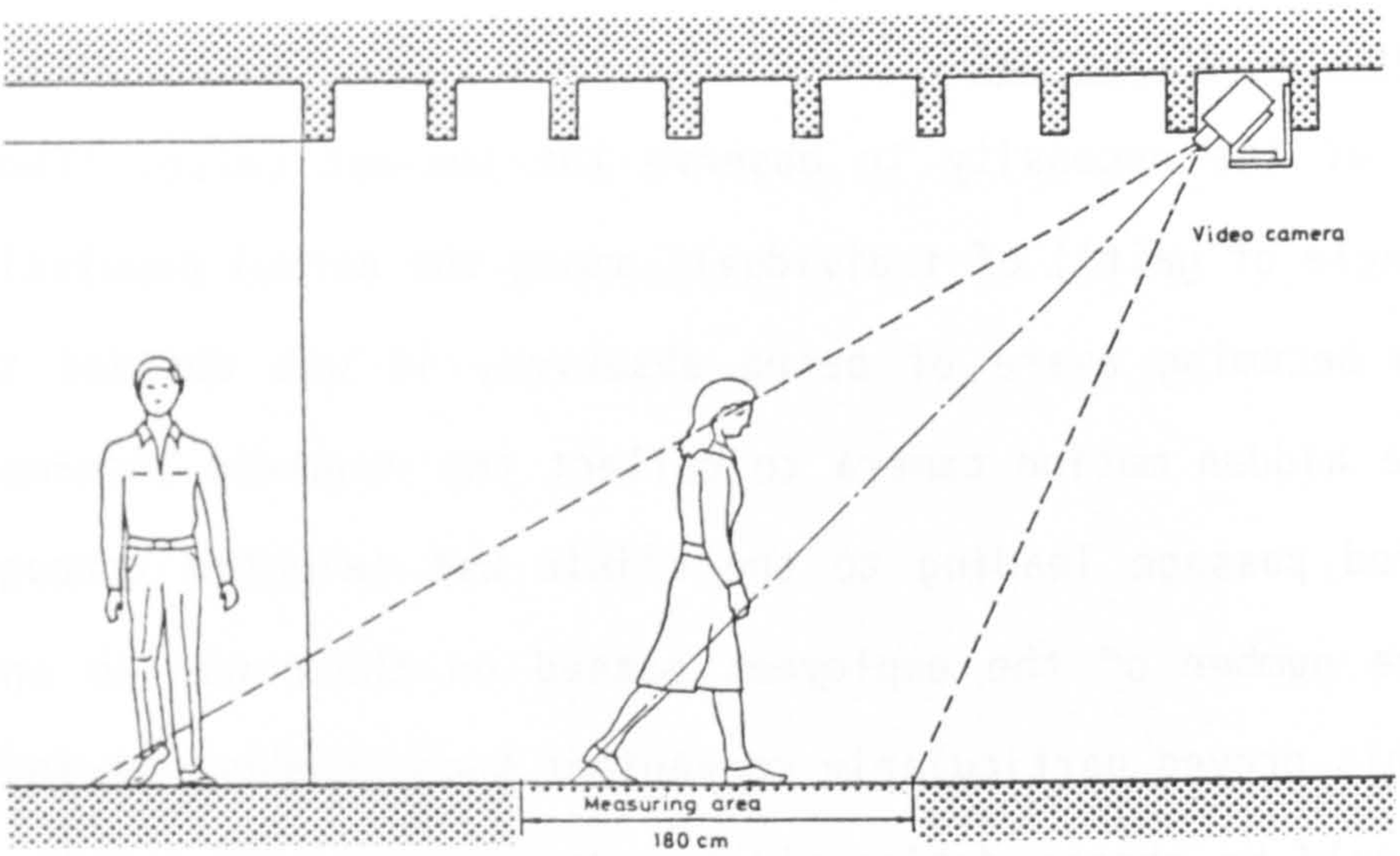

3.13a

3.13b

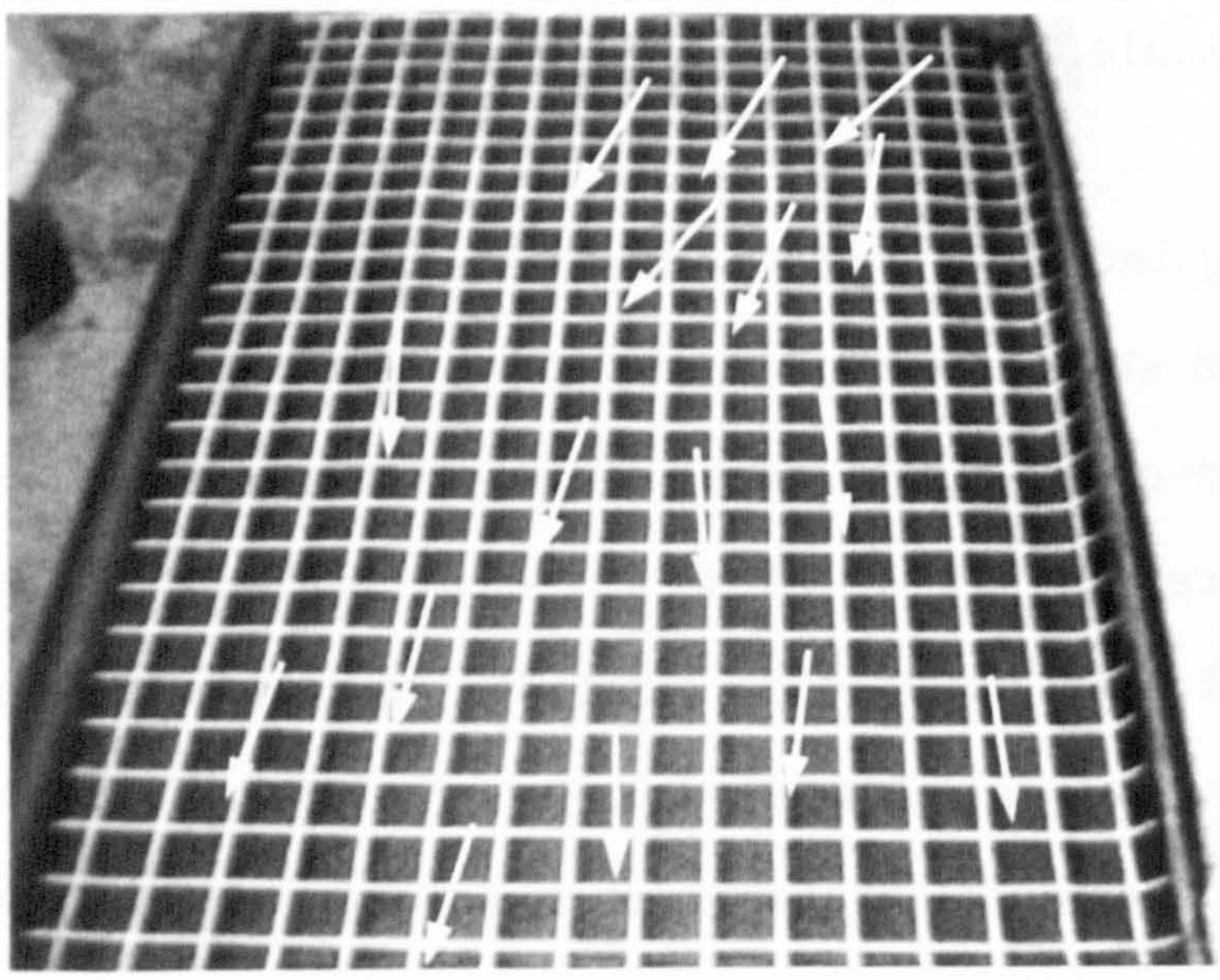

3.13c

Figure 3.13 Determination of toe-out

lens could clearly be seen. This aroused suspicion at the most in some individuals but the purpose of observation remained unknown, thus probably unaffecting their habitual gait pattern.

A reference grating consisting of a regular network of squares drawn with white lines on black cardboard of 1.6 m width and 3 m length was used as a calibration requisite. The meshes formed by the crossing of two sets of parallel lines at right angles to each other measured 10 cm x 10 cm. After having rigidly fixed the camera in the most favourable position (regarding field of vision, asymmetry, etc.) the grating was placed on the floor and the picture of the network recorded. This recorded picture then furnished the reference lines of a Cartesian coordinate system for evaluation of the toe-out later. (The cardboard sheet was removed from the floor when the walking test was performed).

A SONY video cassette recorder, Type VO-2630P, U-Matic, was used to record and reproduce the pictures, even allowing a standing picture to be generated for the purpose of analysis.

The display screen that served best was a SONY PVM-1300 E/AS which measured about 25 cm x 19 cm.

3.4.2 Procedure for determining the toe-out:

A transparent foil was placed over the screen and held in place with adhesive tape. The picture of the reference grating was called up and the network traced onto the foil (fig 3.13c). A simple chin rest enabled the head (eyes) of the investigator to be kept in one constant position relative to the screen so as to maintain the same degree of parallax throughout the whole drawing procedure. With the head in the same position and without altering the position of the

foil on the display screen, standing picture sequences showing the feet of individuals in the foot flat position were called up and the tangent to the inner edge of the shoe sole (sole tangent) also drawn onto the foil. It was not always possible to mark the position of both feet in this manner but it was always possible to do so for the same foot in two consecutive foot flat positions (fig 3.13b). This also enabled the direction of gait to be determined, considered as being along the line joining two similar points on the edge of the shoe sole in two consecutive foot flat positions (fig 3.13c).

The true angle between the sole tangent and the line indicating the direction of gait was found from the traces on the foil by using the digitiser and the computer programme DIGXY to correct for distorted projections of a Cartesian coordinate system, as described in Section 3.3.3.

Based on data collected from 19 randomly selected feet (11 men, 8 women), the angle between the longitudinal axis of the foot and the tangent along the inner adge of the shoe sole was determined. The tangent was assumed to lie parallel to a straight edge brought in contact with the medial side of the foot touching the forefoot and the heel, parallel to the ground, and at the level of the metatarsal head of the first ray. This angle was found to measure about 5°.

The toe-out is the sum of this angle and that determined between the sole tangent and the direction of gait, described earlier.

3.5 Measurement of Forces under the Forefoot

Forces acting normal to the plane of the sole under the heads of the metatarsals and beneath the cusps of the toes were measured

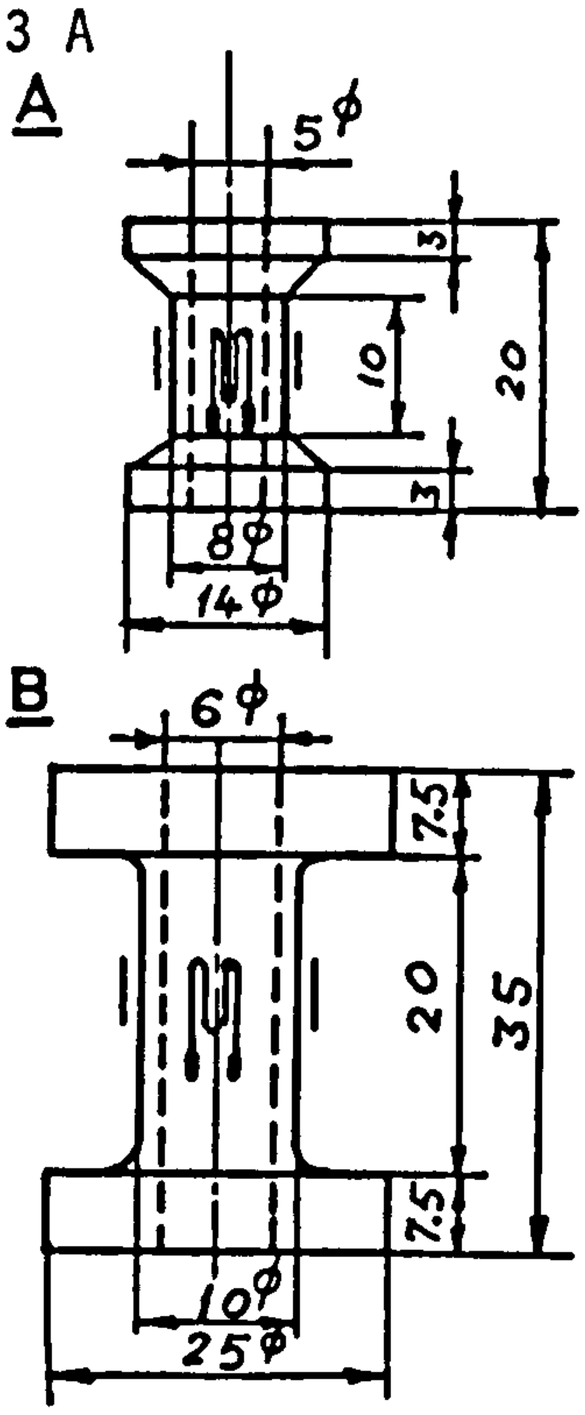

A: For toes

B: For metatarsal heads

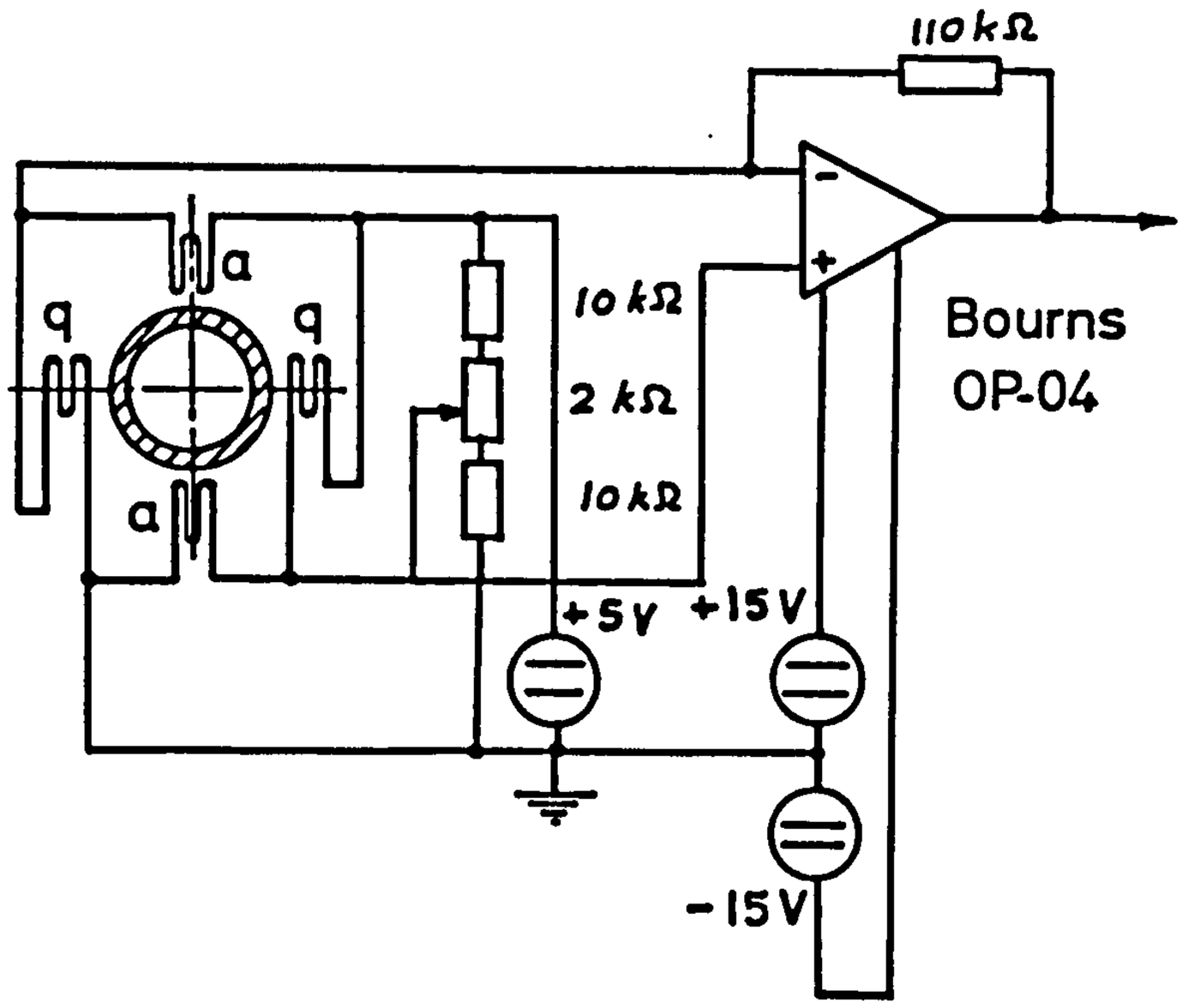

a: Strain gauges in axial direction

q: Strain gauges in circumferential direction

Figure 3.14 Force transducers using strain gauges, with bridge balancing arrangement and amplifier

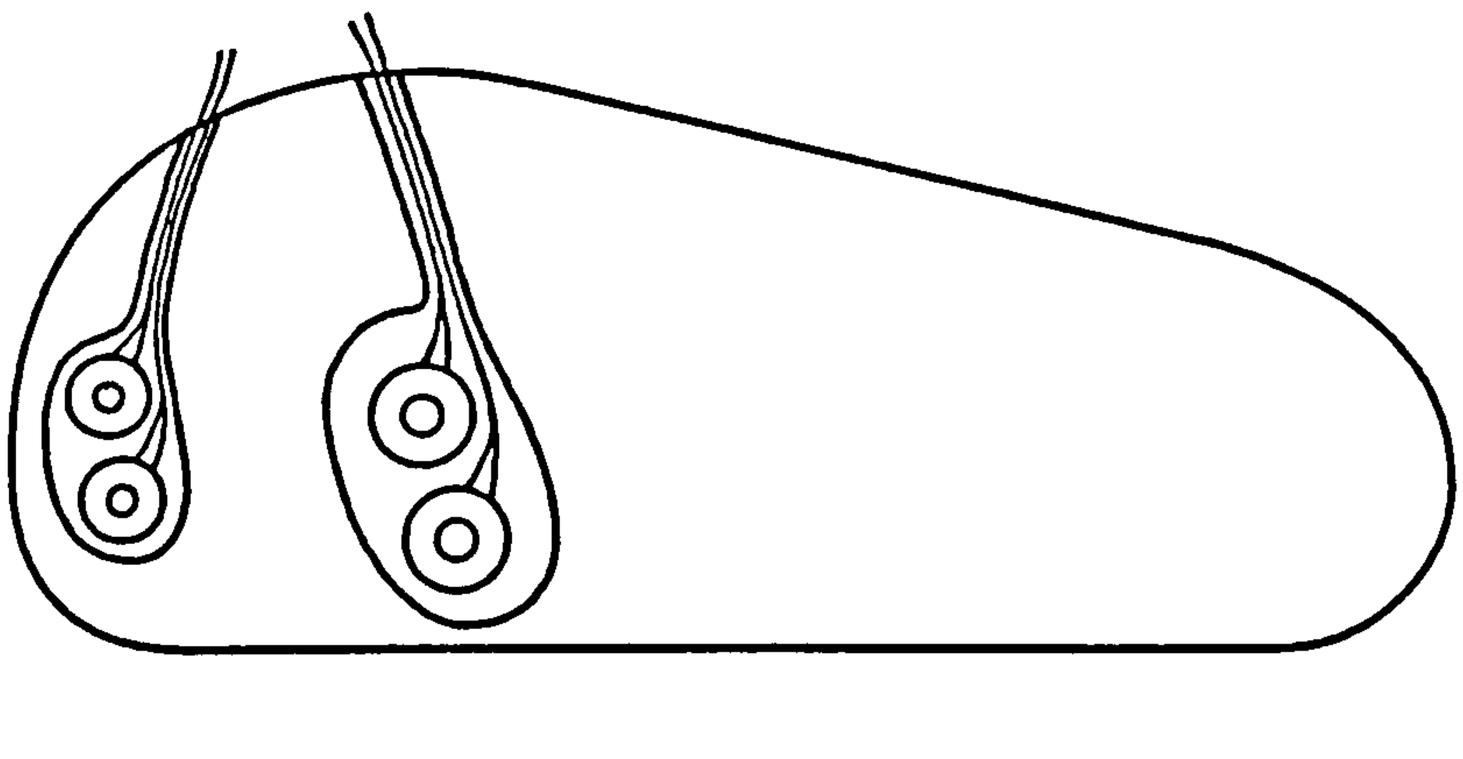

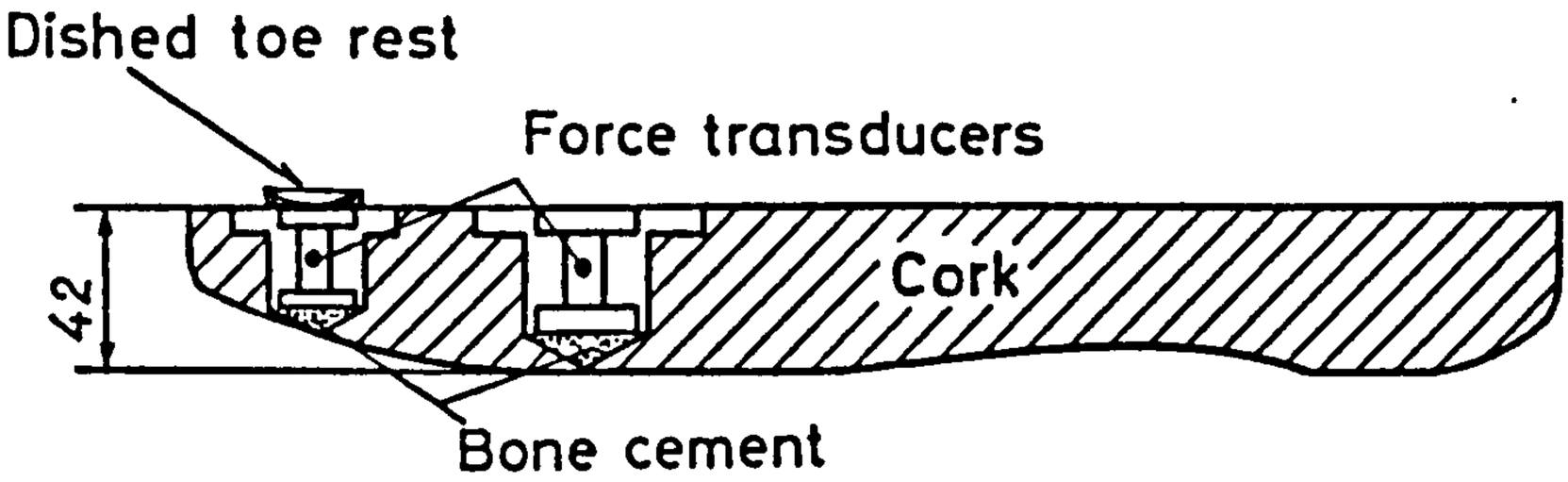

Figure 3.15 Cork sandal with force transducers

in two ways: using strain-gauged force transducers contained in a thick sole of an inflexible cork sandal, and by the use of flat piezo-electric elements (washers) that were accomodated within a foam-rubber foot bed attached to a flexible leather sole.

3.5.1 Measuring arrangement with strain-gauged transducers:

A first series of tests were carried out with force transducers that were made as shown in figure 3.14. Four strain gauges of 3 mm length (Hottinger-Baldwin, Typ LA22, 120ohm, with a k-factor of 2.1) were so applied, that two diametrically opposite gauges were positioned axially while the other two lay in a circumferential direction, also diametrically opposite each other. The Wheatstone bridge wiring was such that the transducer was sensitive only to the axial component of loading.

The main dimensions of the transducer were determined by structural stability under the action of the forces expected. The material of choice was an aluminium alloy (Anticorodal, hard) because of the favourably low modulus of elasticity, compared with that of steel. The height/diameter ratio of at least 2.5:1 was chosen to ensure linear stress distribution in the strain-gauged areas (St. Venant's principle!) which unfortunately called for a rather thick shoe sole.

Because of the height of the transducers, special sandals were made using a cork sole of 42 mm thickness (fig 3.15). The anterior and posterior plantar surfaces of the sole were so rounded, that walking was comfortable and seemed quite natural, without the slightest feeling of bouncing up and down. Circular recesses (counter bores) held the transducers in place so that the upper surface of

the transducers lay flush with the upper surface of the sandal. Only the right sandal was prepared to accept transducers in this manner. Four transducers were so positioned that they came to lie directly under the metatarsal heads and the cusps of the toes of the first and second rays. Channels cut into the upper surface of the cork sole accommodated the wires from the transducers, leading them out laterally.

The transducers were connected to DC bridge balancing and amplifying equipment made by the author (fig 3.14). The output was stored on tape with a RACAL 14DS magnetic tape recorder. Output from the tape was displayed on charts by a Honeywell Visicorder, Type 1858, for evaluation.

Calibration of the transducers along with the measuring equipment was effected by applying an axial load in steps of 100 N up to a maximum of 1000 N in a RUMUL materials testing machine. The greater part of the non-linearity of max. 3% that was observed was due to the visicorder. (This annoying fact was realised when plotting the amplitude in mm against volts. Honeywell guarantees less than +/- 0.4% full scale reading only with reference to the gridlines!). However, because of the large fluctuation of forces measured even with the same test person and under identical gait conditions, no attempt was made to correct for this error. The sensitivity was about 3 N/mm, as measured with a scale.

3.5.2 Measuring arrangement with piezo-electric transducers:

The first series of tests that was performed, as described in the preceding Section, did not allow any flexion in the metatarsophalangeal (MP) joints and, although this situation is perhaps close

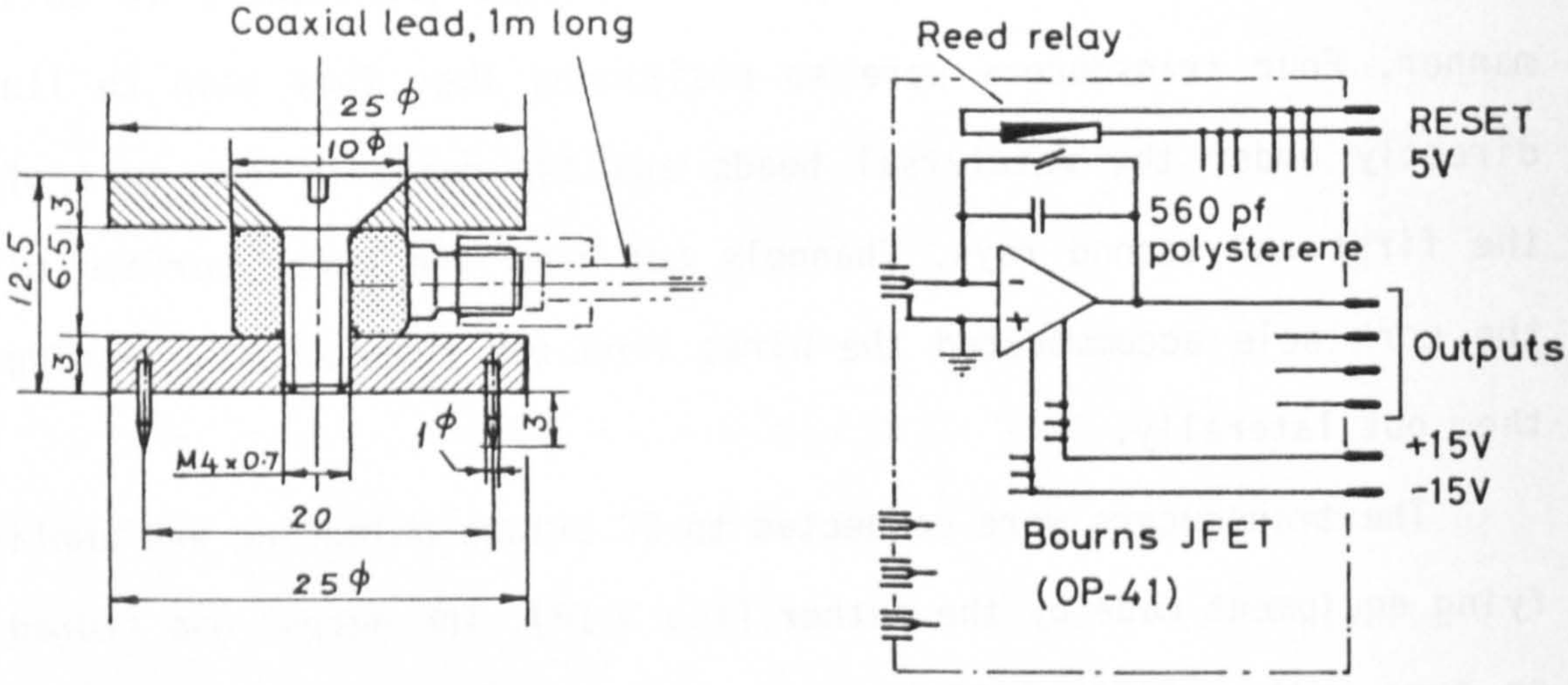

a) Cross section of force transducer

b) Charge amplifier (4 channel)

Figure 3.16 Force transducer incorporating the Kistler P9001 piezo-quartz washer

Figure 3.17 Adjustable, flexible sandal used with force transducers of the piezo-quartz type

to that of wearing shoes with rather stiff soles, it was nevertheless considered necessary to measure forces under the metatarsal heads and under the cusps of toes where flexion in the MP joints could freely take place. Therefore, flat washer-type piezo-electric elements supplied by Kistler were made use of in building miniature force transducers for this purpose.

Figure 3.16a shows the design of the transducer incorporating the Kistler P 9001 piezo-quartz element. Since it is virtually impossible to ensure that the device is at all times centrally loaded, a pre-tensioned arrangement was employed to avoid the end-plates, through which the force is transmitted, from lifting off the piezo-element by tilting.

Four such transducers were introduced into recesses made in the foot bed of a flexible left sandal that was of an adjustable design so as to properly fit any foot within a wide range of sizes (fig 3.17). Four little spikes under the base of each transducer that engaged with the sole proper, prevented lateral movement within the sandal during walking, but also permitted optimal localisation of the transducer to suit individual feet. The transducers could be placed under the metatarsal heads of the first, second and fifth rays or under the cusps of the first and second toes, as required.

Since the piezo-electric effect is made use of by measuring the electric charge that occurs due to deformation of the crystal, or in fact by measuring the potential developed across a condensor, it follows that the capacitor charged must be of constant value and that leakage of the charge must be avoided. For this purpose special coaxial leads of 1 m length, supplied by the manufacturers (Kistler), were used for connecting the piezo-elements to the amplifiers. The

special 'charge amplifiers' that can be bought off the shelf are too voluminous to be easily carried by the test person and therefore a four channel arrangement was made by the author. Figure 3.16b shows the circuitry employed. The principle is based on the original concept by W.P. Kistler in which the charge produced is immediately transferred to a capacitor situated close to the voltage amplifier thus enabling the potential of the lead wire from the piezo-element to the measuring apparatus to be kept constant at ground level. This reduces leakage to a minimum and makes the device insensitive to alterations in the capacitance of the lead wires. The JFET operational amplifier from Bourns (OP-41) was chosen because of the extremely low bias current (3pA) that is typical of it. The capacitor to which the charge is transferred is also of the low leakage polystyrene type. The outputs from the four charge amplifiers are led through a 10 m long flexible cable to further amplifiers before the signals are recorded on magnetic tape and drawn on charts for evaluation as described in the last Section 3.5.1.

Calibration of the piezo transducers is performed exactly in the same manner as in the case of the strain-gauged ones described in the previous section, only that one must be aware that a constant gradual drift of the output signal occurs. This must be taken into account when determining the amplitude of the signal due to force alone. In addition to observing the behaviour under central loading of the device, the effect of eccentric loading was also investigated. It was seen that in extreme cases of eccentric loading an axial force acting at a point removed 8 mm from the centre of the end plate led to a deviation of +/- 7% from the force/voltage relationship obtained with a centrally acting force. Again, considering

fluctuations within 50% about mean values measured, with the same test person and under identical gait conditions, the errors involved due to possible eccentric loading could probably be well neglected.

CHAPTER 4

ANATOMICAL STUDIES

- Anthropometric Measurements and In-Vitro Investigation of the Static Loading of the Forefoot -

4.1 Introduction

Published literature, as discussed in Chapter 2, did not reveal the anthropometric data essential to effect satisfactory determination of forces acting in the structure of the forefoot. The topography of the joint surfaces, for instance, has been described inadequately and the exact direction and location of the tendons that cross the metatarsophalangeal joints, just prior to their insertions, have not been reported at all. An anthropometric study relating to these entitites was therefore undertaken. Also the range of movement in the joints of the forefoot and the limiting effect imposed by the adjacent ligaments and surrounding capsule were noted in order to appreciate the possibility of injury to these structures when a joint is forced against these constraining devices.

Furthermore, static load tests on a fresh cadaver foot were performed to investigate the role played by the plantar aponeurosis in the support of the foot and especially to elucidate the manner in which the first, second, and third metatarsal bones are loaded when subjected to ground forces in the absence of muscular activity. Of the various means available to collect anthropometric data, direct measurement of anatomical structures in cadavers was preferred whenever possible. Also, measurements on wet fresh specimens were performed after treating them with a bactericide that allowed them to be examined for about three weeks (storing them over night at 4°C and over week-ends at -22°C). Some specimens had already been embalmed prior to the start of this investigation. The topography of the joint surfaces was recorded using a moiré technique described in the preceeding Chapter. Photography, using a lens of 105 mm focal length, and a steel scale placed level with the object, was used to

document the form and size of the latter.

This study was restricted to the collection of three complete sets of data - the first two specimens of five produced only a limited amount of data, these having been already embalmed and were therefore used to gain preliminary experience in dissecting. The small number of feet studied precludes the use of statistical measures of variation. All data are therefore presented in the form of mean values and the range observed on either side of the mean.

4.2 Dissection Material

Five feet were dissected for study. Two feet were obtained already embalmed in phenoxotol from the Department of Anatomy of the University of Zurich. The remaining three had been amputated from patients of the Department of Orthopaedic Surgery, Balgrist, two of them because of sarcoma of the leg and one because of a circulatory disorder. None of the feet appeared to be deformed. One showed signs (as seen after dissection) of a damaged joint surface on the plantar aspect of the 1st metatarsal head due to a laterally displaced medial sesamoid, but was otherwise intact. Also, the foot that had been amputated because of a vasculatory disturbance might have been affected by some muscle wasting.

As mentioned, observations on wet, fresh specimens were carried out as far as possible, but when putrefaction set in, a 4% formalin solution was used in one case before proceeding. In this specimen, shrinkage and hardening of the joint capsules and ligaments were observed, and therefore, the two other fresh specimens that followed, were kept conserved by a mixture of 'Mercuryl' (Trade name for a

colourless water-soluble bactericide based on phenylhydrargyrum-boricum and isopropanolum) and glycerine, instead. Care was taken to ensure that the specimens were kept moist all the time.

4.3 Sectioning (Plantar Aponeurosis and Muscles)

The observations made while dissecting the specimens and the measurements taken in the process of doing so are reported. Anthropometric data that were collected and which might be put to use in obtaining a better understanding of the biomechanics of the forefoot are not always presented in the same order in which they were collected as dissection proceeded.

The cross sectional area of tendons was obtained by clamping the tendon between two glass plates (microscope slides) of known thickness and the jaws of a vernier callipers. Simultaneously, the width of the squeezed tendon (the length of which did not increase) was measured with a scale through the transparent glass to the nearest 1/2 mm. The cross sectional area was thus found from the momentary thickness and width.

4.3.1 Structures on the plantar side of the foot:

4.3.1.1 The plantar aponeurosis:

After the skin had been removed from the dorsal and plantar aspects of the foot, leaving the skin in place only distal to the proximal interphalangeal joints, the subcutaneous fat, especially in the area of the sole, was carefully removed. This involved the simultaneous removal of a complex network of ligamentous fibres that ran in the longitudinal, transverse, and vertical directions, connecting the skin to underlying layers of ligamentous structures like septae,

Figure 4.1 The plantar aponeurosis

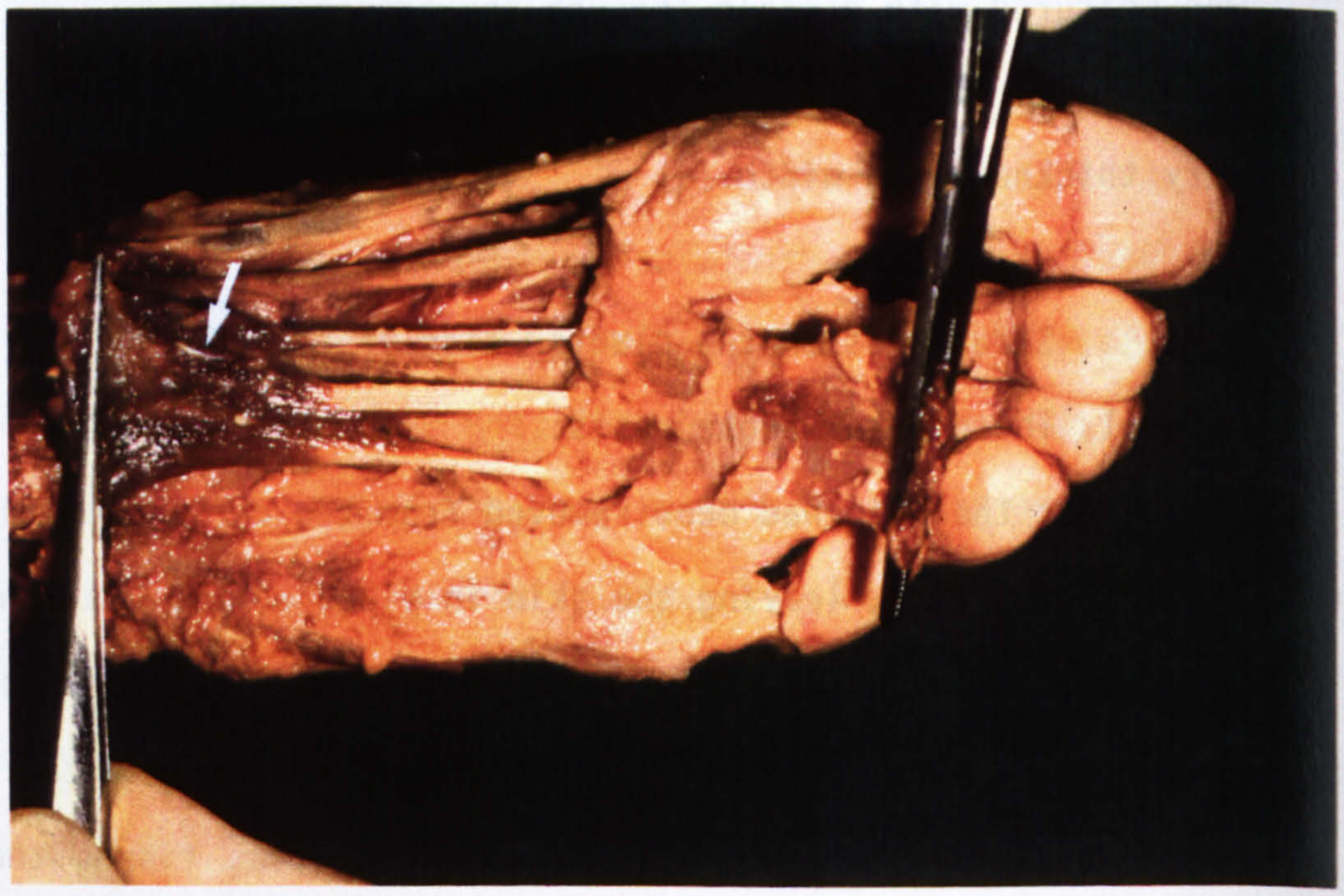

Figure 4.2 The flexor digitorum brevis muscle with only three tendons

and above all, the sheet of plantar aponeurosis. After removal of the interstitial fat and the fibrous matrix that contains it, the plantar aponeurosis was exposed (fig 4.1). The latter was then cut transversely about 5 mm away from its attachment to the calcaneus. Beginning with the posterior end, this fibrous band was then elevated after severing its connections with the underlying flexor digitorum brevis, abductor hallucis, and abductor digiti minimi muscles as well as the underlying septae, up to the region of the metatarsophalangeal joints.

The average thickness of the plantar aponeurosis in the middle of its central area was 1.5 mm and its width measured about 35 mm. On raising it completely off the underlying tissues, the flexor digitorum brevis muscle appeared completely exposed (fig 4.2).

4.3.1.2 Flexor digitorum brevis (flex.digit.brev.):

In one particular specimen as shown in figure 4.2, only three tendons proceeded anteriorly to insert into the bases of the middle phalanx of the 2nd, 3rd and 4th digits. The insertion into the 5th toe was completely absent, as in 21.5% of all cases according to Saraffian (1983). The muscle was detached from its origin and lifted out of its location in the foot leaving the tendons still intact. The muscle was later weighed and the cross sectional areas of the tendons noted (Table 4.1).

Removal of the flex.digit.brev. muscle uncovered all the slips of the flexor digitorum longus tendon and exposed the quadratus plantae muscle that lies beneath the latter.

Table 4.1

Average mass of some muscles of the foot and area of cross section of some of the tendons

Muscle	Cross sectional area of tendon (mm^2)	Muscle mass (g) (contractile tissue)
- Dorsal, intrinsic:		
Ext.hall.brev.	3.5	3.6
Ext.digit.brev.II	2.5	
Ext.digit.brev.III	2.0	6.1
Ext.digit.brev.IV	1.6	
- Dorsal, extrinsic:		
Per.tert.	6.4	
Tib.ant.	22.4	
Ext.hall.long.	6.7	
Ext.digit.long.II	3.4	
Ext.digit.long.III	4.5	
Ext.digit.long.IV	4.7	
Ext.digit.long.V	3.8	
- Plantar, intrinsic:		
Flex.hall.brev. (med. + lat.)	22.0*	6.5
Abd.hall.	18.1*	6.3
Add.hall.obliq.	18.2*	5.8
Add.hall.transv.	15.0*	3.9
Flex.digit.brev.II	3.4	
Flex.digit.brev.III	3.6	5.8
Flex digit.brev.IV	2.5	
Quadratus	2.1	
Lumbricales	2.1 (each)	
Abd.digit.minimi	7.2*	4.2
Interossei II		
- Plantar, extrinsic:		
Flex.hall.long.	13.5	
Flex.digit.long.communis	11.3	
Flex.digit.long.II	6.5	
Flex.digit.long.III	7.2	
Flex.digit.long.IV	5.0	
Flex.digit.long.V	4.2	

* To be accepted with reserve because of difficulty in assessment

4.3.1.3 Flexor hallucis longus (flex.hall.long):

This extrinsic muscle, arising from the posterior surface of the fibula and the interosseus membrane, was only partly present in the specimens examined. The tendon of this muscle was observed to take a surprisingly straight course, after it had emerged from within the groove contained in the talus and calcaneous, up to its passage between the sesamoids under the 1st metatarsal head, before proceeding in an antero-dorsal direction to become inserted into the base of the distal phalanx of the great toe. In fact, the horizontal projection of this thick tendon is practically a straight line from its point of exit from the calcaneus up to its insertion (fig 4.19). Further description of this tendon is to be found in Sections 4.4.2.1 and 4.4.3.1. Table 4.1 shows the cross sectional area determined.

4.3.1.4 Flexor digitorum longus (flex.digit.long):

Also arising from the posterior part of the shank, but from the tibial surface, its tendon closely follows that of the flex.hall. long. until, after following the joint line between the talus and calcaneous just anterior to the flex.hall.long. tendon, it superficially crosses over the latter in the sole of the foot and then splits into four terminal tendons which extend to the terminal phalanges of the lateral four digits. The most direct course appears to be taken by the branches to the 2nd and 3rd toes. Some deviation from a straight course might, however, be effected by the pull of the quadratus plantae muscle on it. Table 4.1 shows the cross sectional area of each of the four branches as well as that of the main stem.

4.3.1.5 Lumbricales:

These very small muscles, four in number, arise from the medial aspect of each of the four branches of the flex.digit.long. tendon, over a length of about 10 to 15 mm, beginning just after the latter divides. After a short length of muscle belly of 10 to 15 mm, each of these semi-pennate muscles leads into a tendon that proceeds anteriorly towards the antero-medially situated web space, and after passing below the deep transverse metatarsal ligament that joins the neighbouring capsules of the MP joints together, turns dorso-anteriorly to spread out into a wing, or hood, that finally inserts into the extensor apparatus over the proximal phalanx of the digit on its lateral side (fig 4.20).

While the tendon crosses the deep transverse ligament to then progress dorso-anteriorly, it comes into close proximity with a neurovascular bundle that is encapsulated in a fat body. These structures appear to be so well attached to each other by means of a fibrous retinaculum, that they seem to move together when the MP joint is moved. However, some relative movement might occasionally take place which could be of importance when considering possible irritation to the nerve and the consequent development of Morton's neuroma.

4.3.1.6 Abductor hallucis (abd.hall.):

The abductor hallucis muscle was removed after cutting through the very short tendon that inserts into the medio-plantar aspect of the base of the proximal digit of the great toe, and releasing its origin from the medial tuberosity of the calcaneus. Some fibres of this muscle were seen to merge with the medial head of the flexor

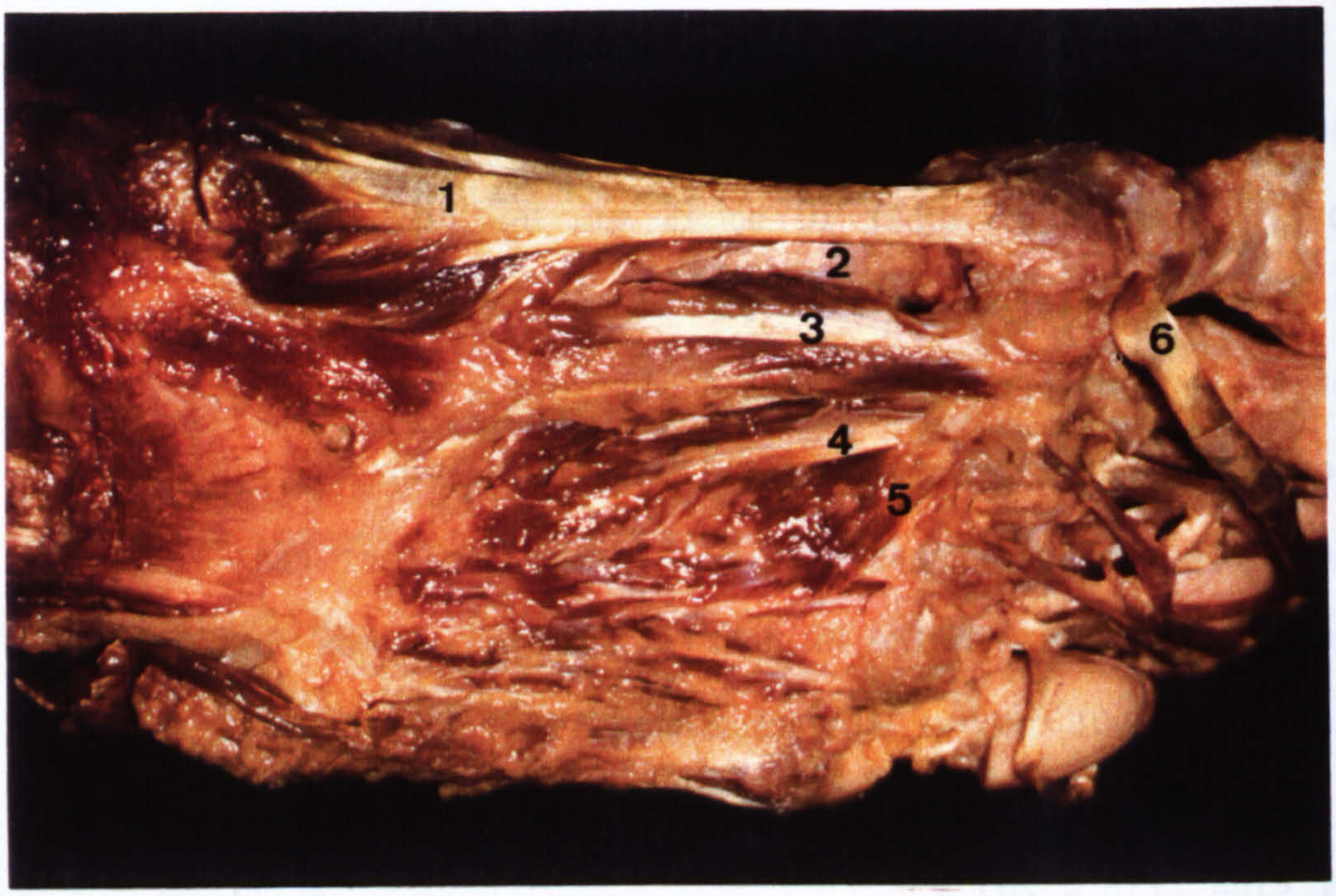

1. Abductor hallucis
2. Flex.hall.brev.(medial head)
3. Flex.hall.brev.(lateral head)
4. Adductor hall.(oblique head)
5. Adductor hall.(transversal head)
6. Tendon of flex.hall.long.

Figure 4.3 Medio-plantar view showing the abductors, the flexors, and the adductors of the great toe

hallucis brevis. The cross sectional area of its tendon and the mass of the muscle were determined and noted (Table 4.1).

4.3.1.7 Abductor digiti minimi:

The abductor digiti minimi was removed after releasing it proximally from the lateral process of the tuber calcanei and from the lower surface of the calcaneous, and distally, from its attachment to the base of the 5th phalanx. Some difficulty was experienced in isolating this muscle from the underlying flexor digiti minimi.

4.3.1.8 Flexor digiti minimi:

The flexor digiti minimi was elevated after releasing its attachment to the base of the metatarsal and to the long plantar ligament. Considerable difficulty was met with when attempting to isolate this muscle from the adjoining plantar interosseus.

4.3.1.9 Flexor hallucis brevis (flex.hall.brev.):

The two heads of this muscle were fairly easily identified at its distal end but it was somewhat difficult to find a continuous line of demarcation between the adjacent abductor, in spite of the clearly separate insertion of the medial head. On the lateral side, there was no clear demarcation between the belly of the flexor and that of the oblique adductor. Only the course taken by the tendons to their source of origin gave some indication of the anatomical differentiation between these entities (fig 4.3).

4.3.1.10 Adductor hallucis (add.hall.):

This muscle which is intimately juxtapositioned to the flexor

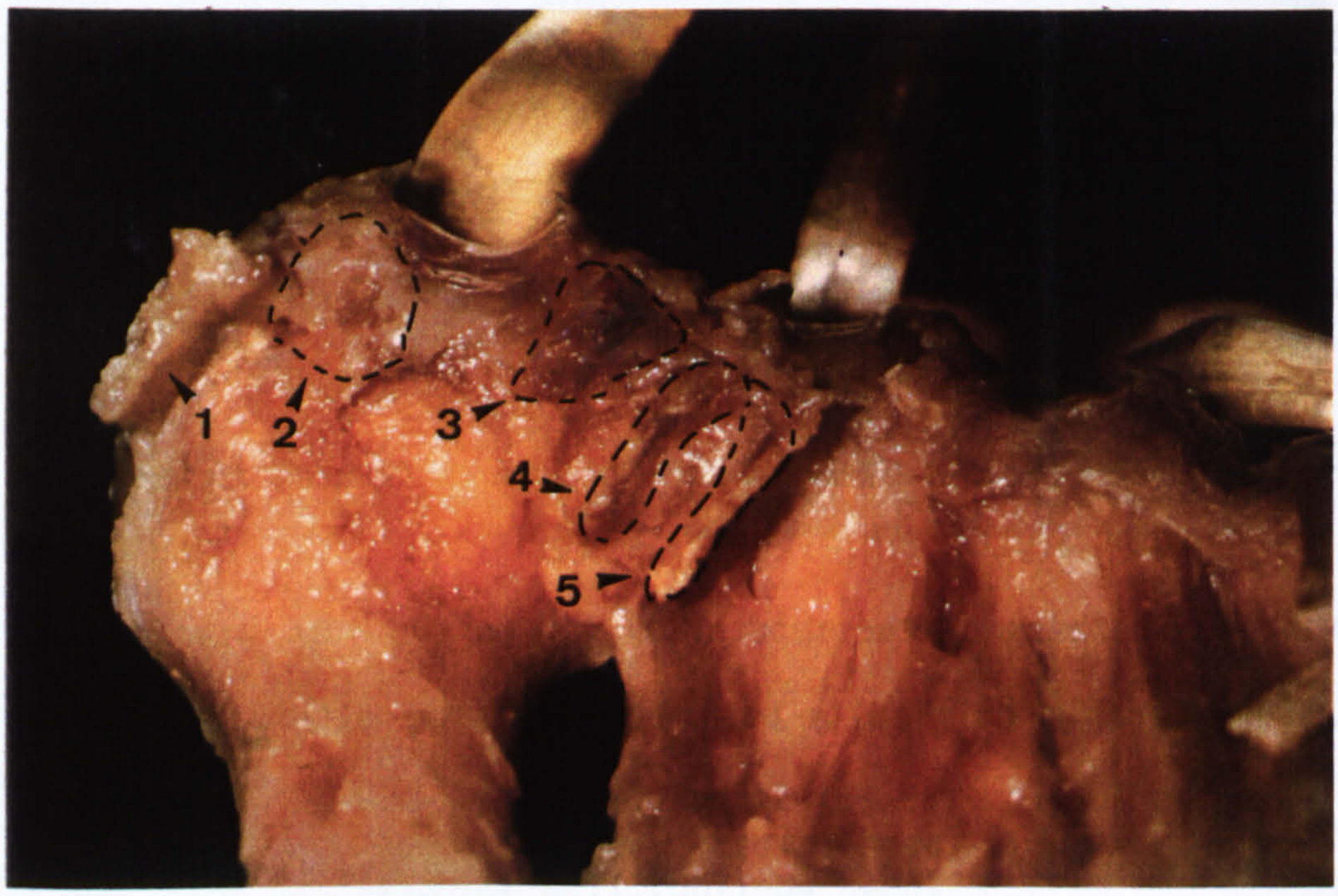

Figure 4.4 Entrance of add. hall. (1), flex. hall. brev. (2+3), and abd. hall. (obliq. 4, transv. 5) into the proximal aspect of the joint capsule

hallucis brevis (fig 4.3) was, as described above, difficult to isolate from the latter. In the feet closely examined in this study, the extremely short tendons were seen to enter the joint capsule just proximal to the lateral sesamoid and immediately lateral to that of the flexor hallucis brevis (fig 4.4).

The oblique head of this muscle arises from the sheath of the peroneus longus tendon that traverses the foot, and from the long plantar ligament, while the comparatively weak transverse head was seen to arise from the medio-plantar aspect of the capsules of the other metatarsophalangeal joints.

4.3.2 Structures on the dorsal side of the foot:

4.3.2.1 Extensor hallucis longus (ext.hall.long.):

Ext.hall.long., arising from the anterior aspect of the upper part of the lower limb, mainly from the interosseus membrane, was only partly present in the specimens studied. After passing underneath the superior and inferior retinaculi, the tendon travels anteriorly, passing over the MP-1 joint, to insert into the dorsum of the base of the distal phalanx of the great toe. While passing over the MP-1 joint and all along its course over the dorsum of the proximal phalanx, a network of fibres connect it to the underlying joint capsule and bone. Nevertheless, movement of the tendon relative to these structures is possible with these 'mooring' fibres complying accordingly. At the area of insertion into the base of the distal phalanx, the tendon merges into the dorsal part of the joint capsule becoming an integral part of it. Table 4.1 shows the area of cross section of the tendon before it enters the extensor aponeurosis.

4.3.2.2 Extensor digitorum longus (ext.digit.long.):

This muscle, arising mainly from the anterior crest of the fibula, was also not completely present in the specimens investigated. The tendon, which also passes beneath the superior and inferior retinaculi in the region of the ankle, is split into four branches that extend to the four lesser digits. The cross sectional areas of these four branches are shown in Table 4.1. In the vicinity of the MP joints, each branch but one comes to lie in close proximity with the tendons of the ext.digit.brev. muscle that insert into the 2nd, 3rd and 4th toes only. The latter lie on the lateral side of the ext.digit.long. tendons (fig 4.5). Over the dorsum of the proximal phalanx of the 2nd, 3rd and 4th digits, the tendons of the long and short extensors unite only to split again into a trifurcation system, the middle slip of which inserts into the dorsal part of the base of the middle phalanx, while the two side-slips proceed anteriorly, converging gradually on the dorsum of the middle phalanx, to insert into the dorsum of the base of the distal phalanx. On their way along the dorsum of the proximal phalanx, the ext.digit. brevis et longus tendons get woven into the retinaculum of the extensor aponeurosis system into which some fibres of the lumbricales tendon, arriving from the medial side, terminate. Because of this interconnection of tendons and fibrous network that moor the former to the underlying bones, individual extension facilities in the proximal and distal interphalangeal joints are indeed very limited.

4.3.2.3 Extensor hallucis brevis (ext.hall.brev.) and extensor digitorum brevis (ext.digit.brev.):

On elevating the ext.digit.long. tendons and the peroneus ter-

Figure 4.5 Extensor hall. brev. and ext. digit. brev. (ext. hall. long and ext. digit. long. tendons elevated)

tius tendon that lie immediately subcutaneously on the dorsum of the foot, free access to the ext.hall.brev. and ext.digit.brev. muscles was gained (fig 4.5). The muscles were detached at their origin along the surface of the calcaneous and from the antero-lateral side of the inferior retinaculum and readily raised off the underlying structures exposing the capsules of the mid-foot bones, the metatarsals, and the interosseus muscles lying in-between the latter. Other details of the ext.digit.brevis tendons have been treated in Section 4.3.2.2. The cross sectional area of the tendons and the mass of the muscles were determined (Table 4.1).

4.4 Joints of the First Ray of the Foot

4.4.1 The tarsometatarsal joint of the first ray:

4.4.1.1 Range of movement and behaviour of capsule and ligaments:

On attempting to move the metatarsals relative to the adjoining cuneiform bones, it became immediately evident that with the exception of the first ray, the bones of the cuneiform-cuboid block and the base of the metatarsals were held rigidly together by the taut ligamentous ties that interconnect these bones. Movement in the 1st metatarsocuneiform joint, although easily detectable, was very limited. Because of the transversal interconnection between the capsules of the 1st and 2nd metatarsophalangeal joints only about 3 mm transversal movement in this region was possible, this amounting to about 3° of abduction. Only after cutting through the deep transverse metatarsal ligament between the 1st and 2nd metatarsophalangeal joints was it possible to abduct the 1st metatarsal to a maximum of about 20°. Details of the force-movement characteristic in the 1st cuneo-

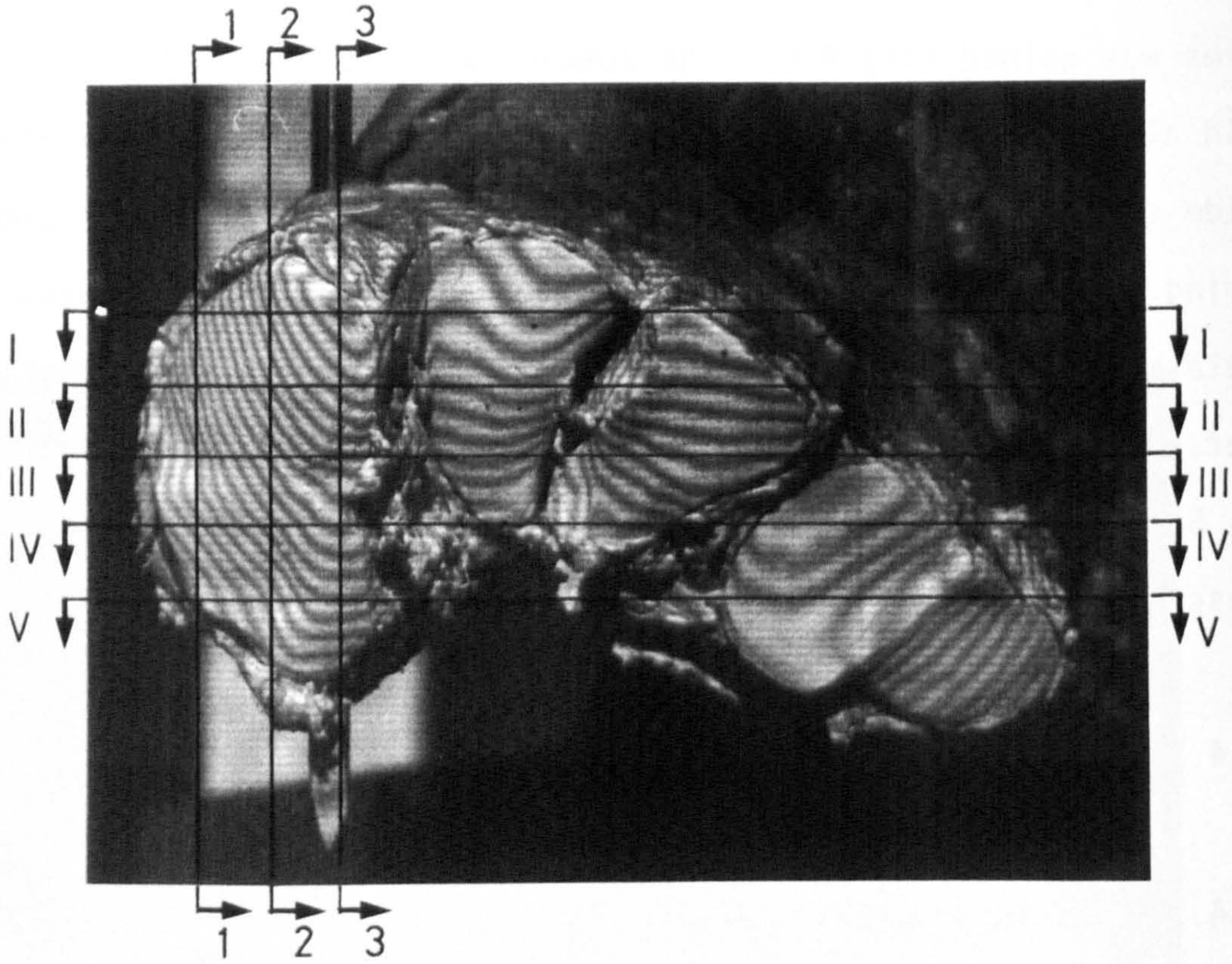

a) Cuneiform and cuboid joint surfaces showing cross-sections chosen

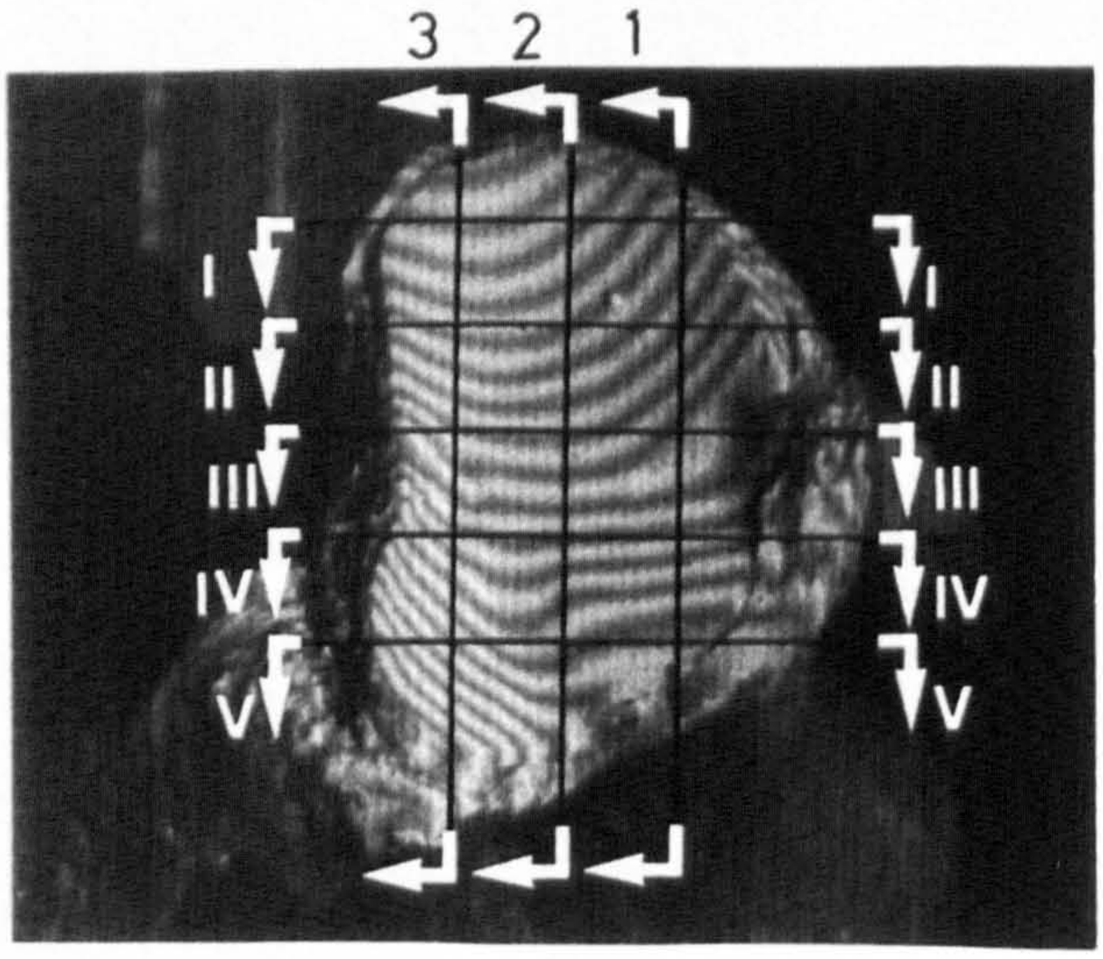

3 2 1

b) Base of metatarsal 1 showing cross-sections chosen

Figure 4.6 Moiré fringes on Lisfranc's joint and base of metatarsal 1

metatarsal joint are given in Section 4.6 that deals with the mode of force transmission through the metatarsal bones in the absence of muscular activity.

4.4.1.2 Topography of the tarsometatarsal joint surfaces:

The foot was divided through Lisfranc's joint and the topography of the joint surfaces determined as described in Chapter 3, Section 3.2. The cuneiform-cuboid block was brought into the 'foot flat' position and viewed in a strictly horizontal direction but at an angle of 20° to the anterior-posterior axis. This was necessary in order to bring all the joint surfaces as close to the optical grid as possible. Geometrical details of the set-up are contained in Appendix 1(4). Following this, the topography of the joint surface of the metatarsal base of the first ray was also determined. Figure 4.6 shows typical moiré patterns obtained and figure 4.7 the contours of the joint surfaces in chosen sagittal and horizontal planes with some of the radii of curvature, as estimated by means of the procedure described in Section 3.2.3, entered in.

4.4.2 The metatarsophalangeal joint of the great toe (MP-1):

4.4.2.1 Range of movement, and observations relating to the capsule, ligaments and tendons:

The range of movement in the MP-1 joint was observed to be about 75° in dorsiflexion, 40° in plantar flexion, 10° in internal rotation (abduction) and 5°in external rotation (adduction) - all measurements being referred to the joint in the physiologically neutral position (foot flat), that is, with the axis of the proximal phalanx at an angle of 25° to the axis of the metatarsal bone. These obser-

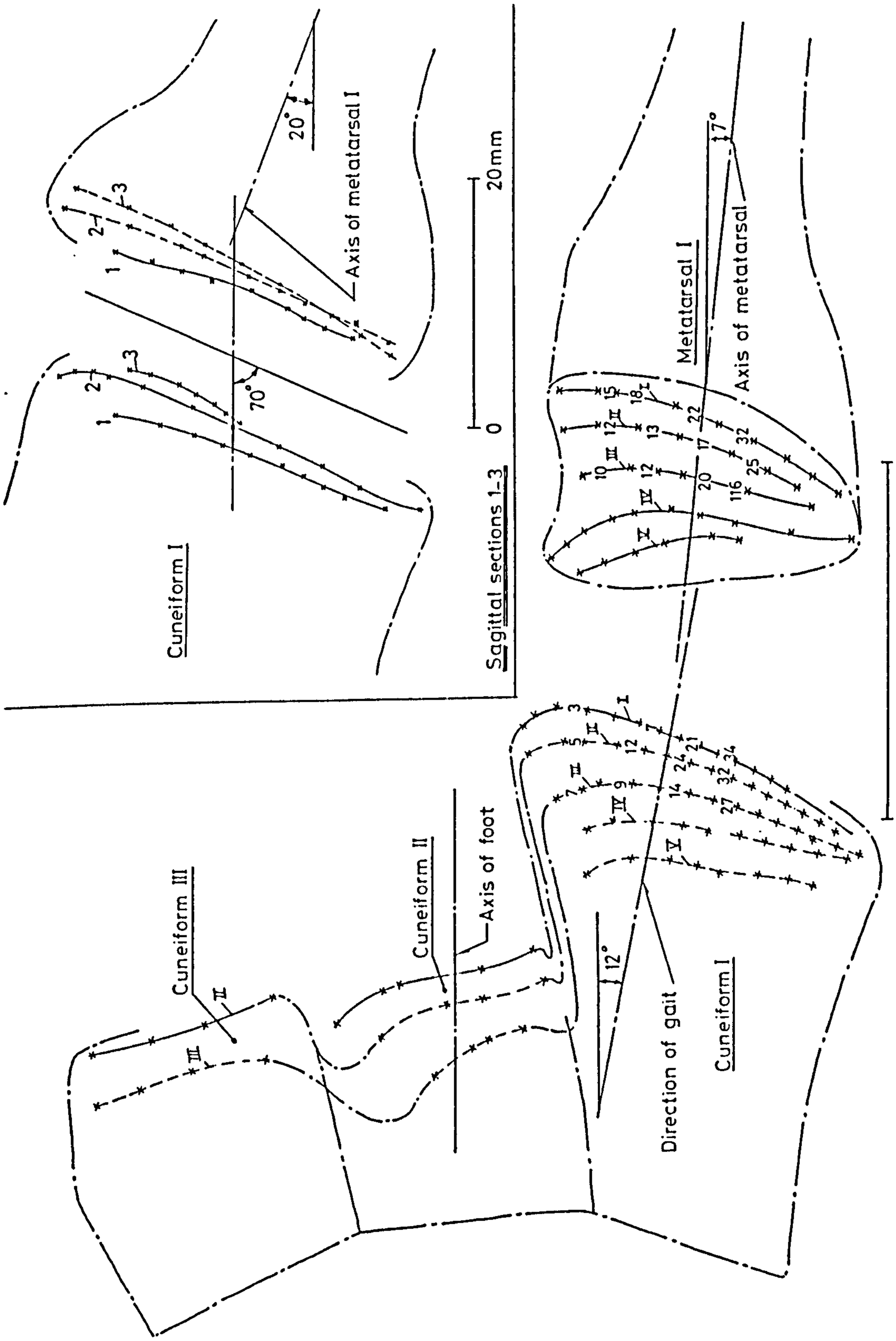

Figure 4.7 Contours of the cuneiform-metatarsal I joint surfaces (left foot) with radii of curvature in mm

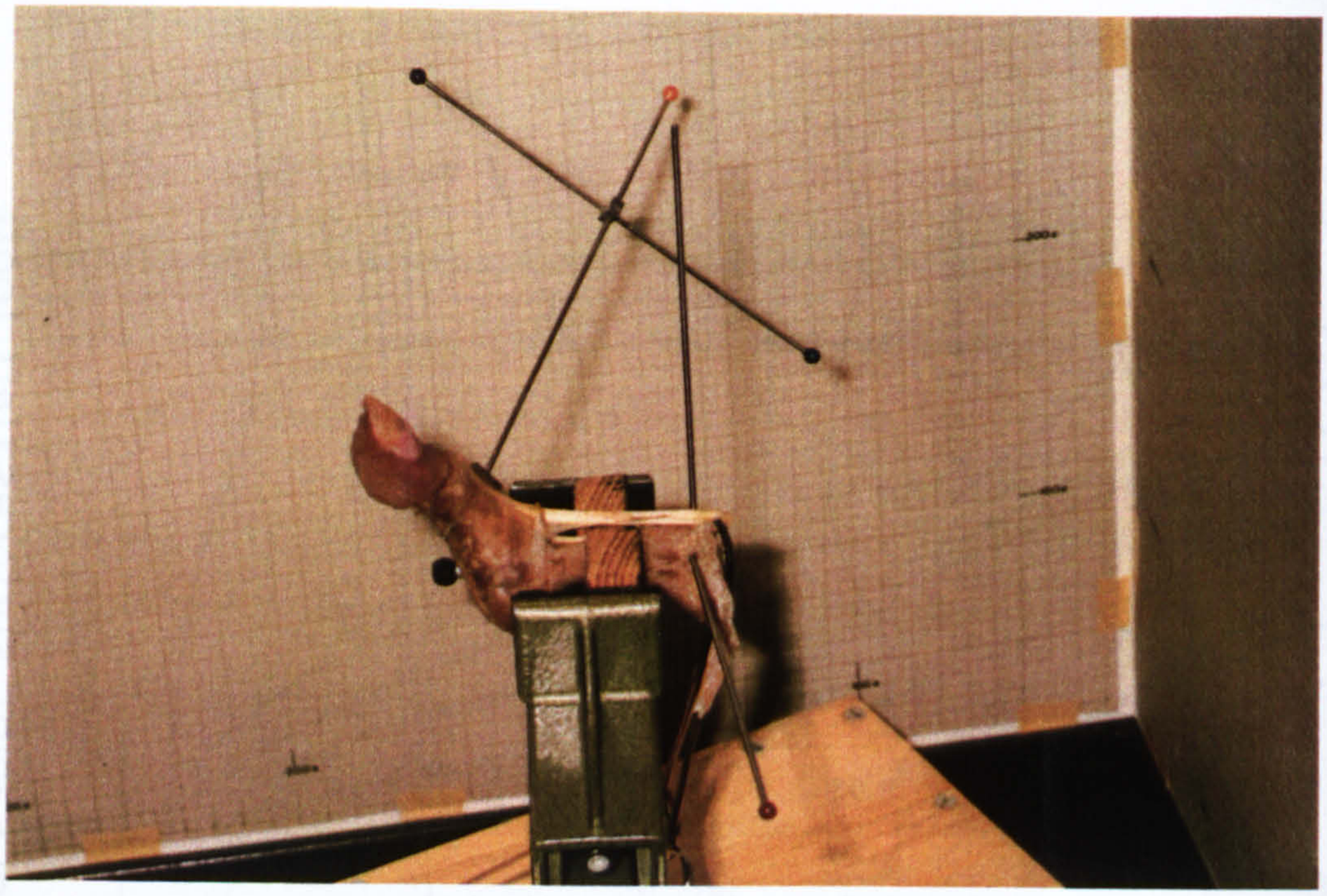

Figure 4.8 Determination of the helical axis of motion in the metatarsophalengeal joint I

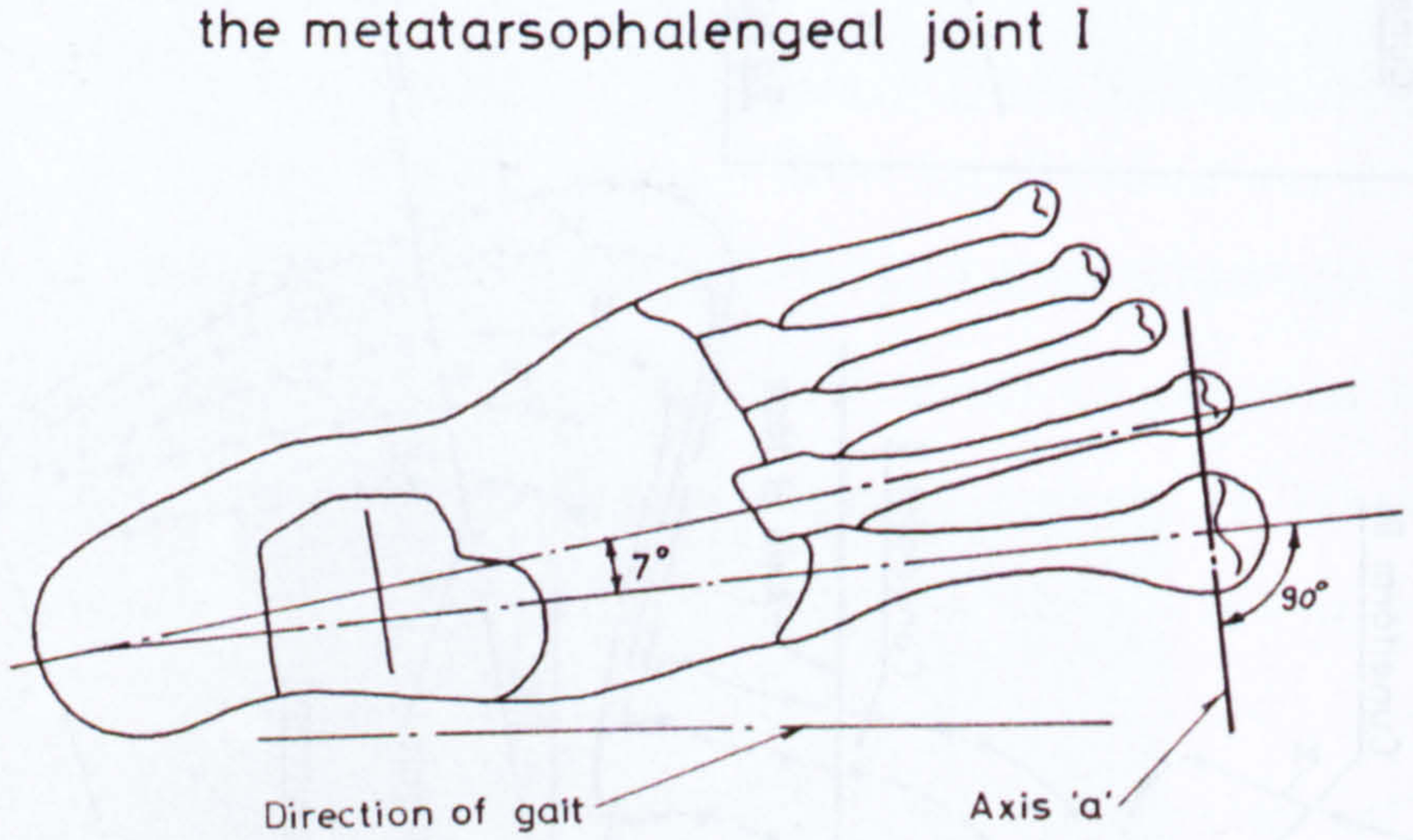

Figure 4.9 Axis `a´ about which the MP-1 joint rotates as enforced by the constraint of the collateral ligaments in the positions of extreme dorsal and plantar flexion.

vations were made with the capsule and ligaments wholly intact.

Before excising the capsule of the MP-1 joint, because of an obviously oblique axis about which motion occurred, it was decided to investigate this motion using the helical axis method described in Chapter 3, Section 3.3. However, due to some extent of freedom of rotational movement in all directions within the extreme limits of dorsiflexion and plantar flexion, that hence precludes any singular description of motion, it was considered interesting to at least describe the axis that would govern the two limiting positions as determined by the constraint offered by the capsule and collateral ligaments against further motion of the joint. The external force applied to fix the joint in extreme dorsiflexion, or in extreme plantar flexion, was introduced over the corresponding tendon (ext. hall. brev. or flex.hall. long.) while gripping the metatarsal bone firmly in a vice (fig 4.8). Figure 4.8 also shows the set of three markers that were rigidly attached to the proximal phalanx bone while the axis of the metatarsal was lined up parallel to the x-axis of the reference coordinate system. A K-wire (Kirschner's wire, used as a marker in bone surgery) of 2 mm diameter was passed through the base of the metatarsal bone to position the latter in respect to the vertical axis (as adopted physiologically). Using the spatial positions of the set of three markers in the two extreme positions of dorsiflexion and plantar flexion, the location and direction of the helical axis was obtained by use of the computer programme HELIROD.J (Appendix 5(3)). After rotating the coordinate system to bring the metatarsal into its physiological position in the foot flat condition, the helical axis was seen to lie in a vertical plane passing through the head of the metatarsal and at right angles to the hori-

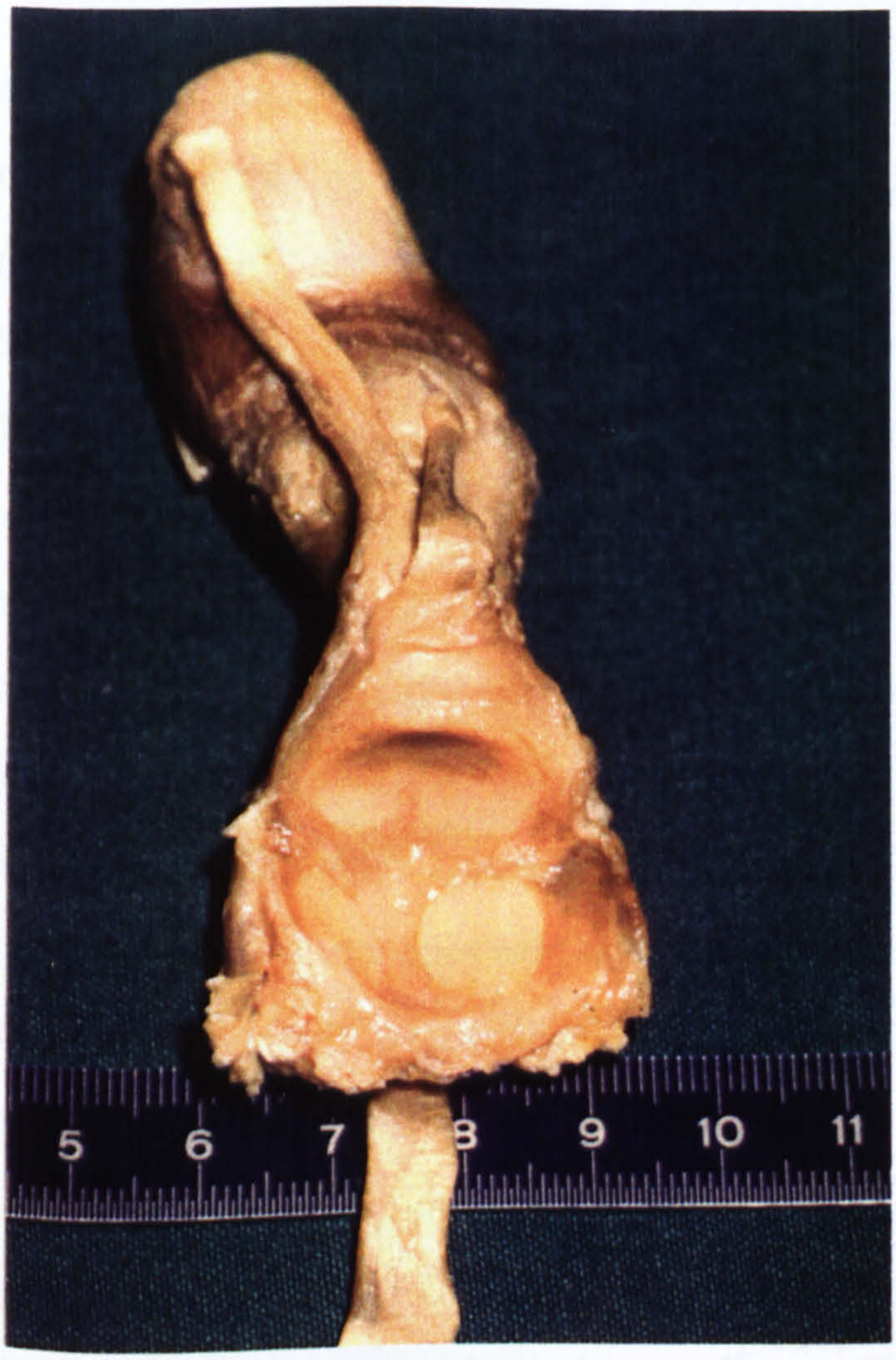

Figure 4.10a

The sesamoid bones embedded in the fibrous plantar plate of the joint capsule (left foot)

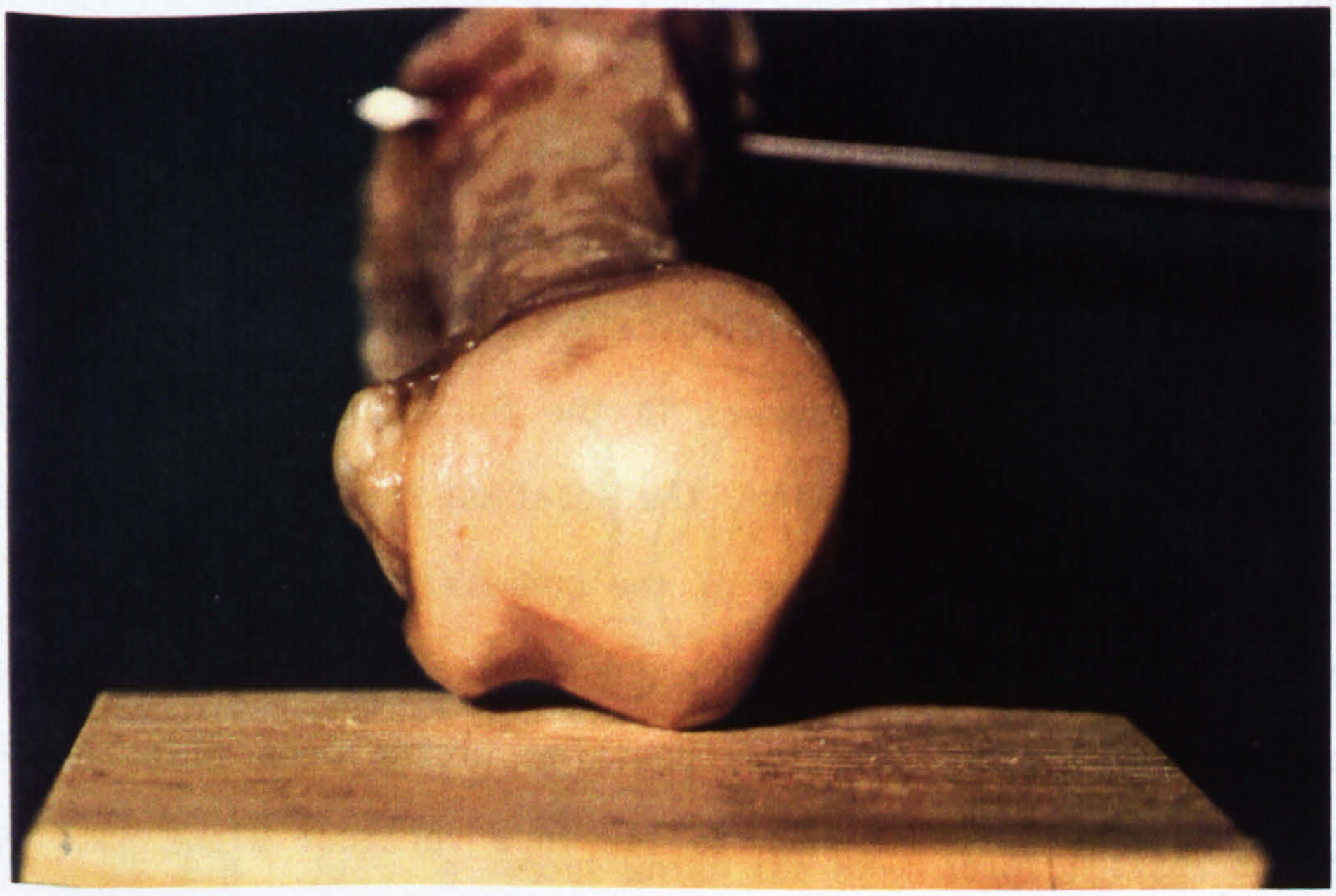

Figure 4.10b Relation of trochlear surface of the metatrsal-1 head to the ground (left foot)

zontal projection of the metatarsal axis. The helical axis passes through the head and lies inclined to the horizontal at an angle of about 12°, sloping downwards medially (fig 4.9). Rotation of 72° is accompanied by a translatory movement along the axis of only 0.4 mm. Observation of the movement of the foot during the toe-off phase in walking shows that the MP-1 joint could indeed move about this axis and hence its determination might be of significant value.

The capsule was then excised at its antero-dorsal and posterio-plantar aspects at its attachment to the metatarsal bone. On examining the medial and lateral sides of the joint capsule, ligamentous fibres can be clearly seen running from an origin about small tubercles situated on the medial and lateral sides of the metatarsal head, fanning out in a triangular manner, and inserting into the base of the proximal phalanx anteriorly as well as into the plantar plate containing the sesamoids directly below. The structures leading to the plantar plate measured about 1.4 x 9 mm^2 on the lateral side and about 1 x 11 mm^2 medially. The lateral and medial collateral ligaments crossing the joint are directed anteriorly and downward, and measure about 1.4 x 8 mm^2 and 1.5 x 8 mm^2, respectively.

On removing the metatarsal head out of its capsular encasement it became immediately apparent that the medial sesamoid was not only slightly larger than the lateral one, but also that the former was more in a plantar position than the latter (fig 4.10a). This fact was also clearly reflected by the position adopted by the medial groove, or trochlear surface under the head of the metatarsal in relation to the ground when the latter was placed in its physiological foot flat position (fig 4.10b). The boat-shaped fibrous capsule with its plantar plate that houses the sesamoid bones is of surpris-

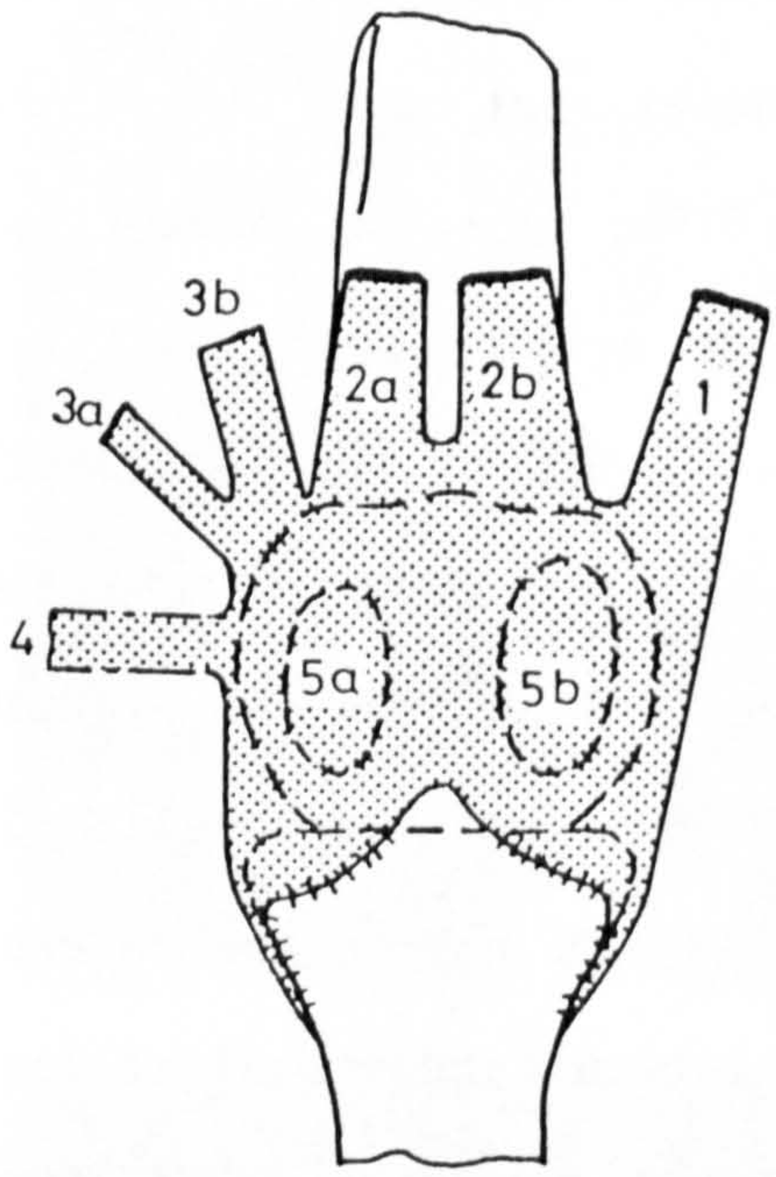

Muscles:
1. Abductor hallucis
2a. Flexor hallucis brevis lateralis
2b. Flexor hallucis brevis medialis
3a. Adductor hallucis transversus
3b. Adductor hallucis obliqus

Other structures:
4. Deep transverse intermetatarsal ligament
5a. Lateral sesamoid
5b. Medial sesamoid

Figure 4.11 Insertion of muscles in the capsule of the MP-1 joint (based on an illustration from Dubois & Levame)

ingly stiff texture so that it seems more reasonable to consider the tendons passing through this area to be firmly interconnected with each other before they reach their ultimate points of insertion into the base of the proximal phalanx than to expect each of them to exhibit a markedly individual action. The abductor of the great toe, for instance, is seen to insert quite proximally on the medial sesamoid in conjunction with the fibres of the medial head of the flexor hallucis brevis. Furthermore, the tendon inserts in a rather plantar location (figs 4.3 and 4.4). Therefore, in spite of some fibres continuing distally to become eventually attached to the medial aspect of the proximal phalanx, it might possibly act more like a plantar flexor than an abductor, especially since very little movement of fibres relative to the compact mass of fibrous cartilage into which they are embedded could be expected, especially in older feet in which the capsule is no longer supple. Figure 4.11 shows the situation, and is based on a sketch from Dubois and Levame (1966). Similar observations apply to the adductor, and considering the direction taken especially by the tendon of the transverse head of this muscle, just prior to its insertion at the level of the lateral sesamoid, its function as inferred from its anatomical designation seems questionable. It probably acts as an adductor in the cuneiform-metatarsal joint.

Also, the functional course taken by the fibres of the plantar flexor tendons prior to their insertion on the base of the proximal phalanx is not very clear. Should they be considered to pass at the level of the sesamoids before taking a sharp upward and anterior course or do they act less inclined to the horizontal by passing more along the lateral and medial sides of the metatarsal head be-

Figure 4.12 Course taken by the fibres of flex. hall. brev. before meeting the base of the proximal phalanx

fore becoming attached to the medio-plantar and latero-plantar borders of the phalanx? In this context it must be remarked that the conditions assumed by Stokes (1979) do indeed appear over-simplified (fig 2.8).

The direction of force application from the short plantar flexor to the base of the phalanx was obtained as shown in figure 4.12 and was found to lie at an angle of about 25° to the horizontal. Also, the tendon of flex.hall.longus that crosses the MP-1 joint was observed to make an angle of about 12° to the horizontal in passing forwards and upwards before following the plantar surface of the proximal phalanx.

The tendon of ext.hall.brevis glides over the cartilagenous surface of the dorso-anterior aspect of the metatarsal head becoming part of the joint capsule before it inserts into the dorsal area of the phalanx base.

4.4.2.2 Topography of the MP-1 joint:

In order to describe the surface geometry of the joint surfaces the moiré method described in Chapter 3, Section 3.2, was used. The metatarsal bone was held in a position corresponding to the foot flat on the ground, and the head viewed along an anterior-posterior axis. Moiré fringes were created and recorded. Following this, the topography of the glenoid mating surface of the proximal phalanx base was recorded in a similar manner. Figure 4.13 shows typical moiré patterns obtained and figure 4.15 the contours of the joint surfaces in sagittal and horizontal planes with some of the radii of curvature entered in.

On attempting to match the corresponding surface contours thus

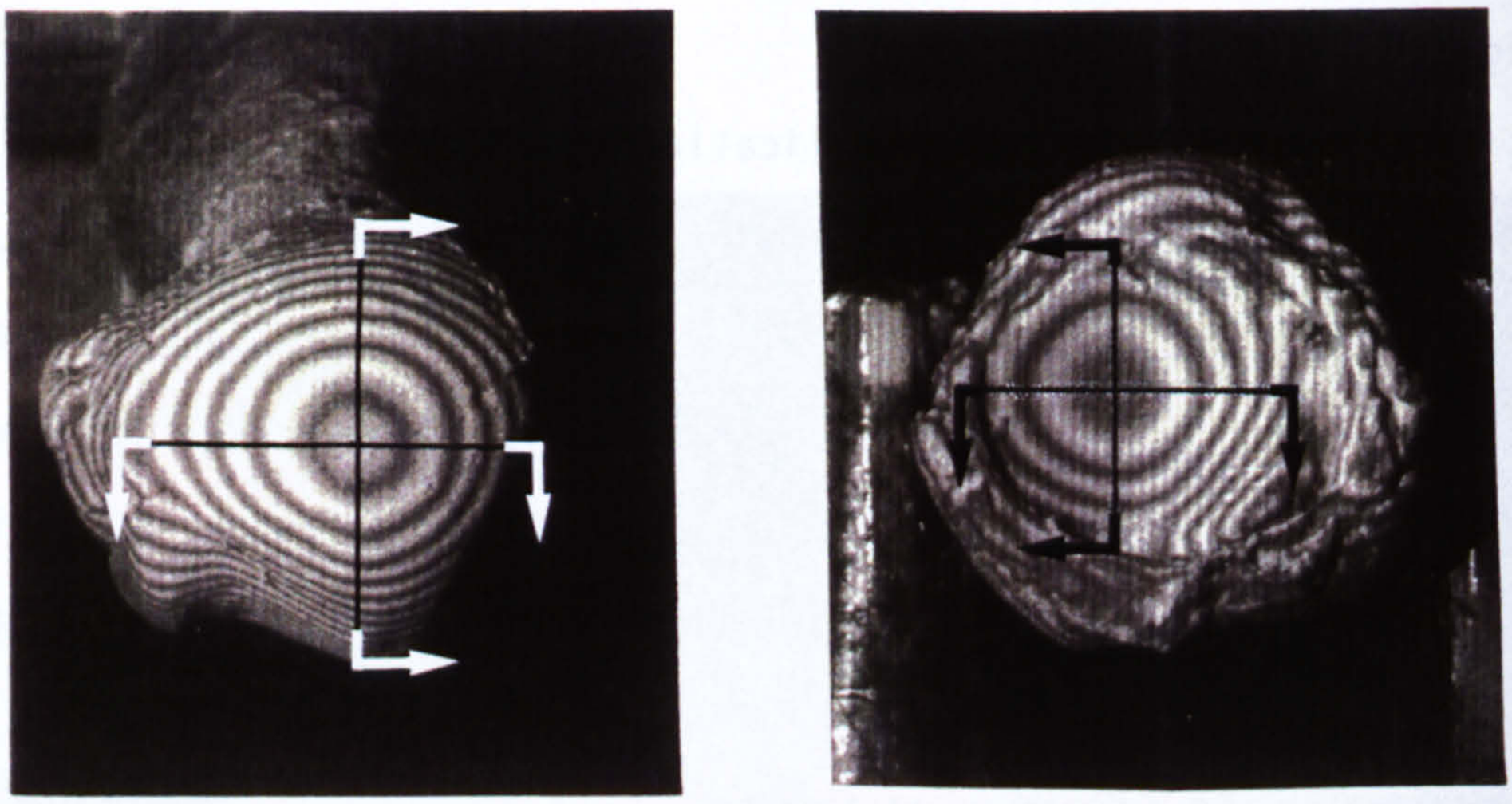

a) Head of metatarsal 1 b) Base of proximal phalanx 1

Figure 4.13 Moiré fringes on the MP-1 joint surfaces (left foot) and cross sections chosen

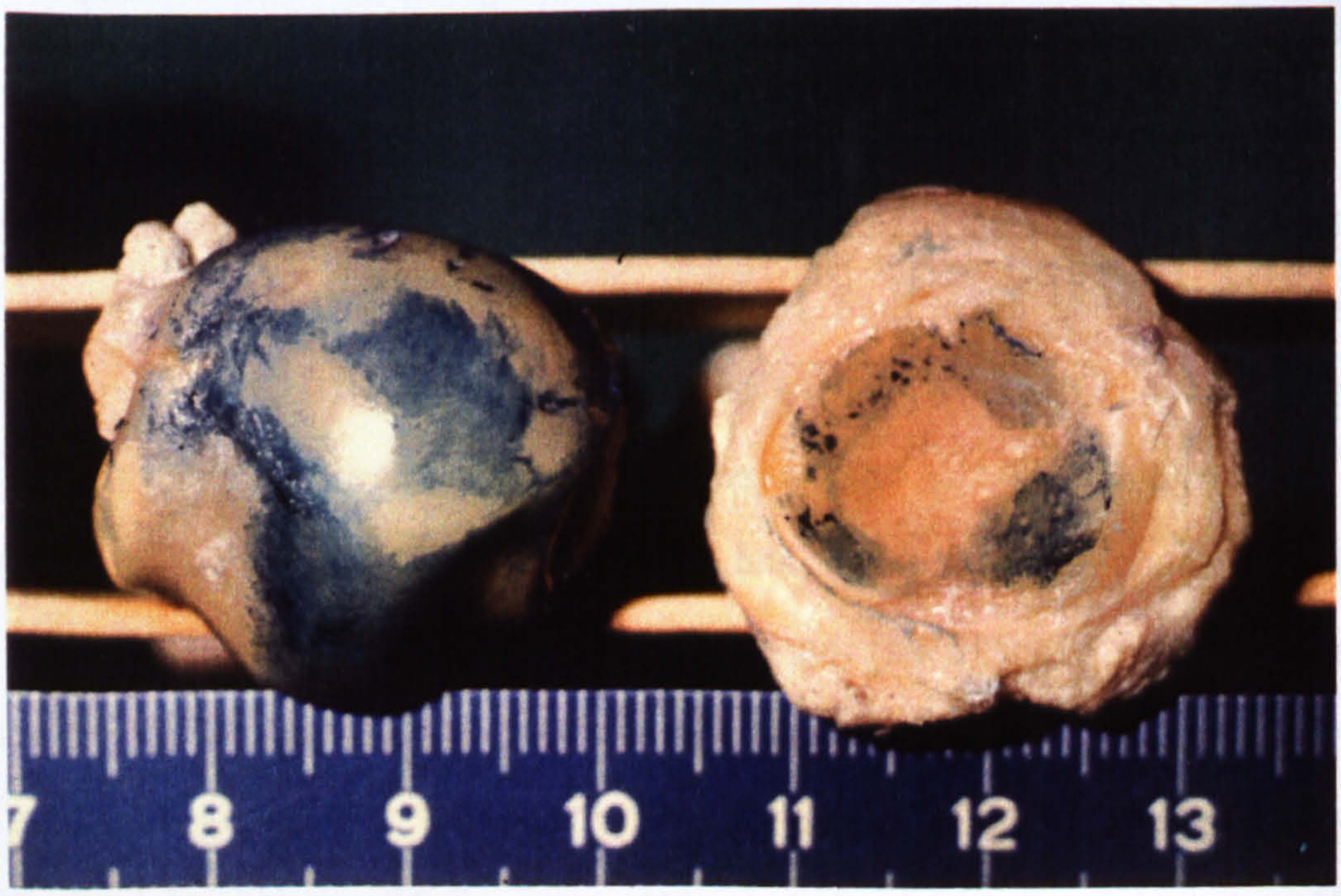

Figure 4.14 Contact areas of the MP-1 joint surfaces illustrated with bearing blue

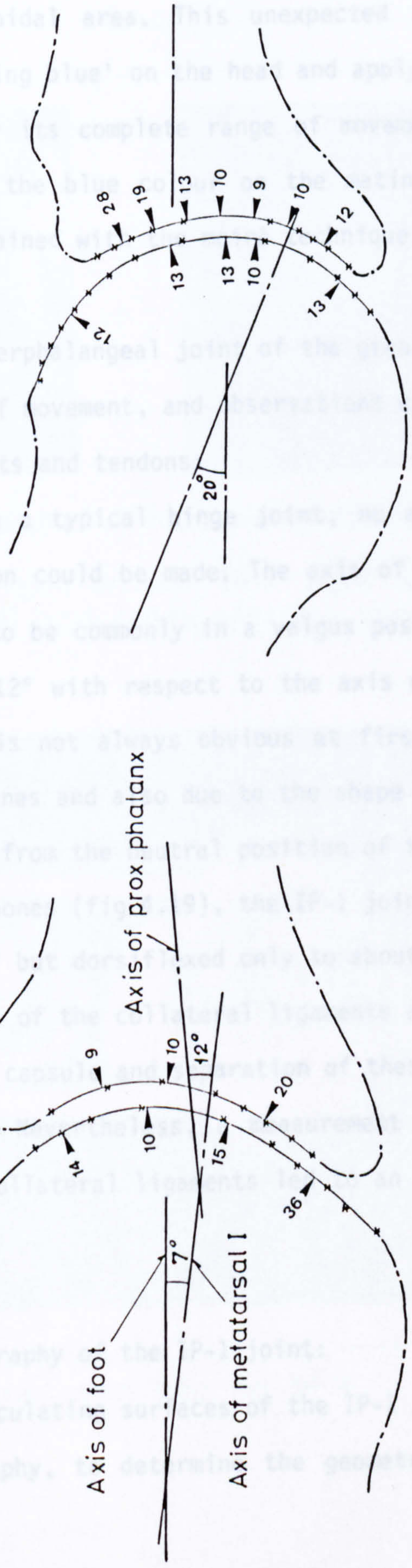

Figure 4.15 Typical contours of the MP-1 joint surfaces (left foot)

obtained, it appeared that surface contact is not maintained over the whole glenoidal area. This unexpected result was checked by spreading 'bearing blue' on the head and applying the glenoidal surface to it over its complete range of movement. Figure 4.14 shows the take-up of the blue colour on the mating surfaces, confirming the results obtained with the moiré technique.

4.4.3 The interphalangeal joint of the great toe (IP-1):

4.4.3.1 Range of movement, and observations concerning the capsule, ligaments and tendons:

This being a typical hinge joint, no appreciable movement in ab- or adduction could be made. The axis of the distal phalanx was however noted to be commonly in a valgus position (externally rotated) by about 12° with respect to the axis of the proximal phalanx although this is not always obvious at first sight because of the rather short bones and also due to the shape and position of the toe nail. Starting from the neutral position of the longitudinal axes of the adjoining bones (fig 4.19), the IP-1 joint can be plantar flexed up to about 80° but dorsiflexed only to about 8°.

The fibres of the collateral ligaments are intimately connected with the joint capsule and separation of these structures is virtually impossible. Nevertheless, a measurement of the cross sectional areas of the collateral ligaments led to an estimation of about 1 x 8 mm^2 each.

4.4.3.2 Topography of the IP-1 joint:

Both articulating surfaces of the IP-1 joint were mapped, using moiré photography, to determine the geometry of the joint. Figure

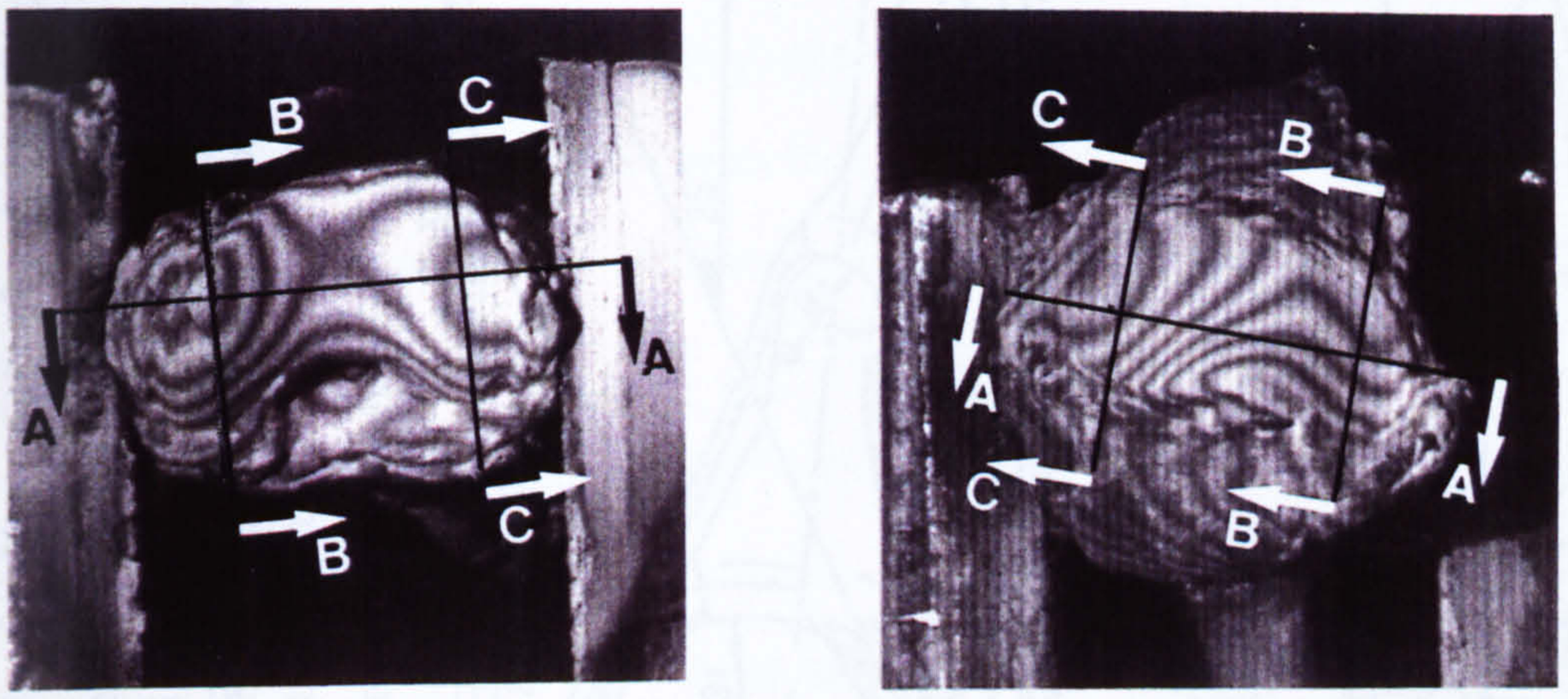

a) Head of prox. phalanx 1 b) Base of distal phalanx 1

Figure 4.16 Moiré fringes on the IP-1 joint surfaces (left foot) and cross sections chosen

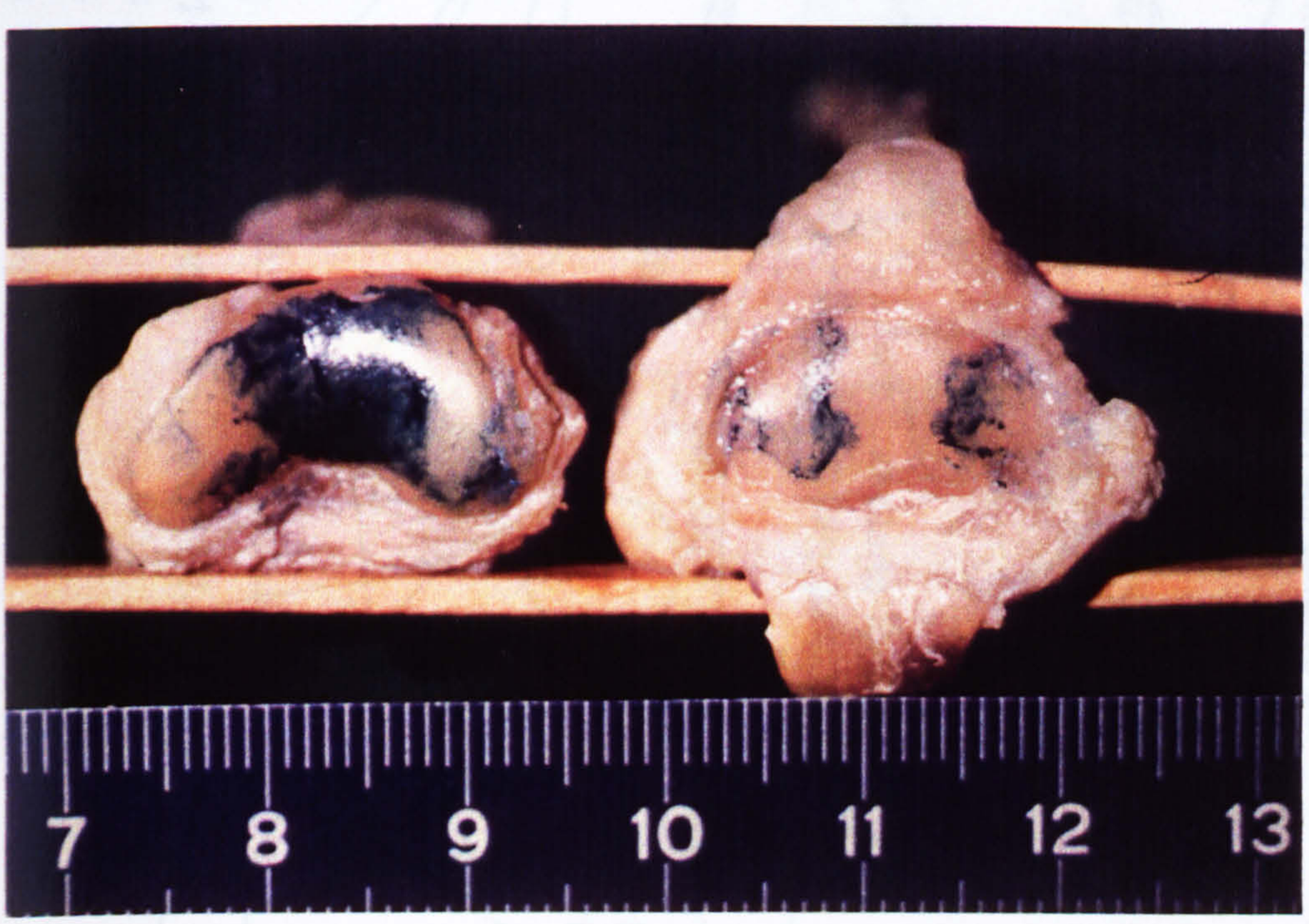

Figure 4.17 Contact areas of the IP-1 joint surfaces illustrated with bearing blue

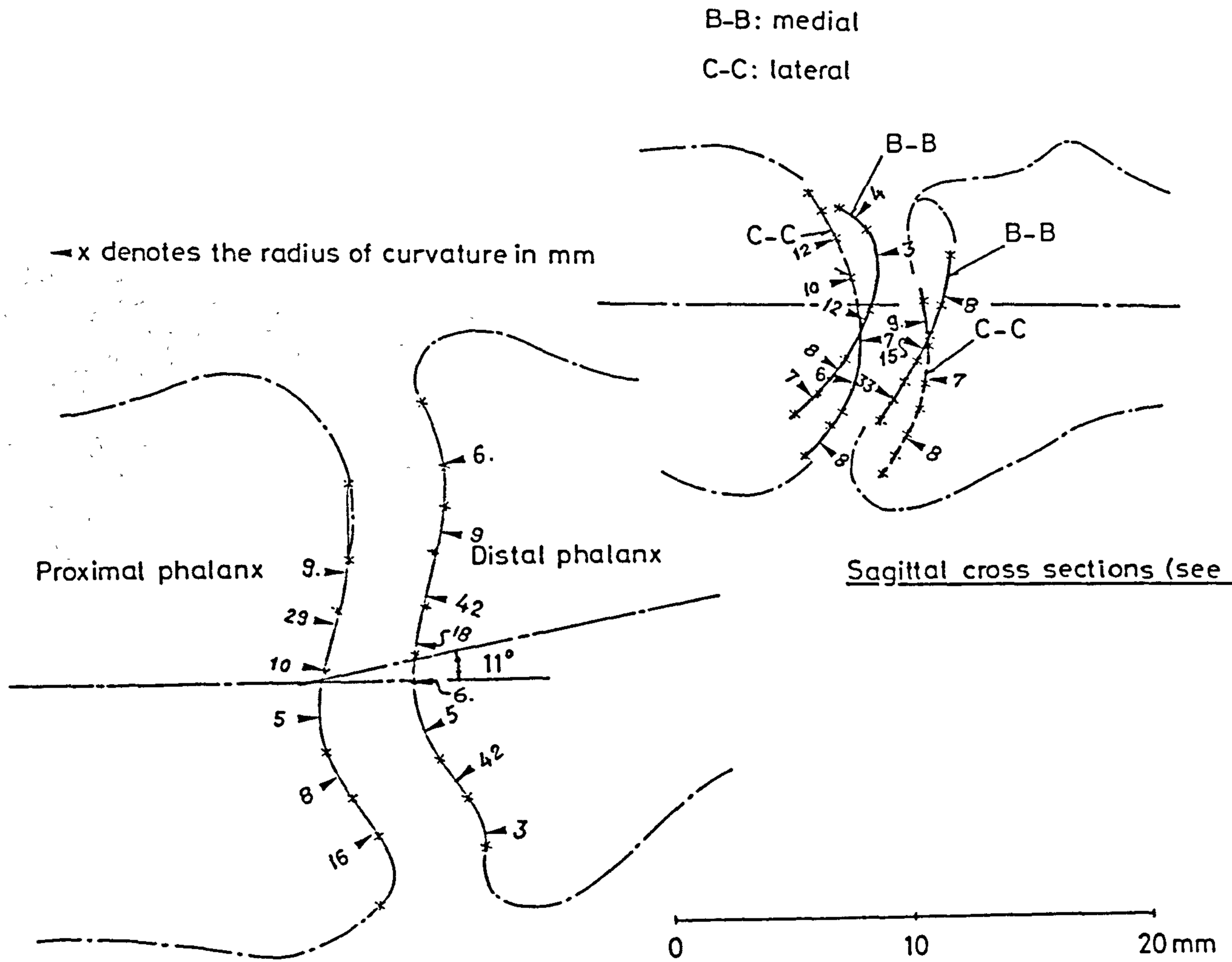

Figure 4.18 Typical contours of the IP-1 joint surfaces (left foot)

* $\left|\begin{array}{|c|}\hline +u \\ \hline v \\ \hline -w \\ \hline\end{array}\right|$ denotes: v is a typical angle in the neutral, foot flat position;

u is the maximum deflection in one direction, the angle now measures v+u;

w is the maximum deflection in the reverse direction, the angle now measures v-w.

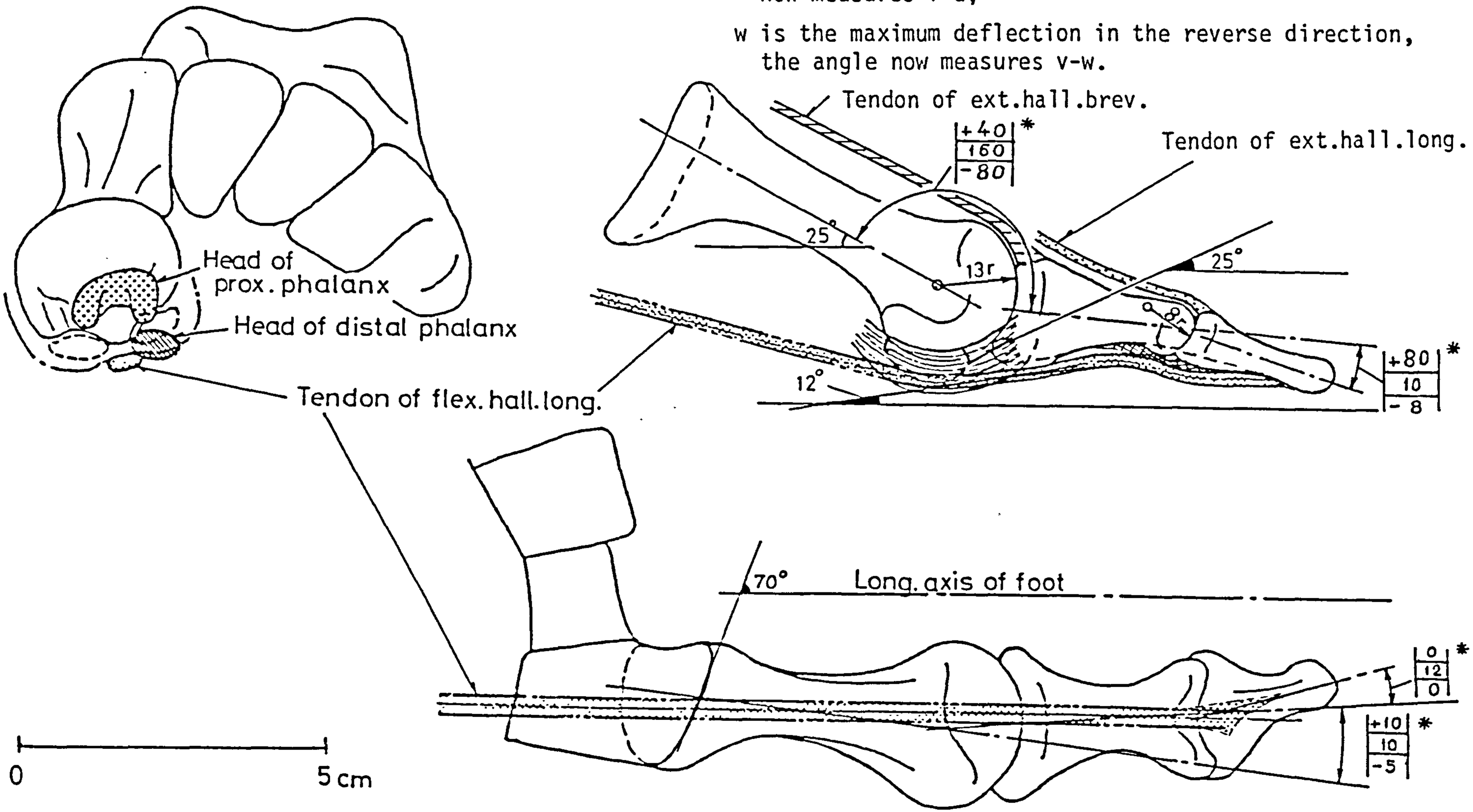

Figure 4·19 Some typical dimensions of the first ray of the foot

4.16 shows typical moiré patterns obtained and figure 4.18 the contours of the joint surfaces in sagittal and horizontal planes. Figure 4.18 also shows some of the calculated radii of curvature that characterise the articulation, details. Also, using 'bearing blue' on the head of the proximal phalanx, the areas of bearing contact between the joint surfaces were observed (fig 4.17).

4.4.4 Overall geometry of the first ray and the course taken by the tendons:

The relevant anthropometric data collected, as described in the preceding sub-sections of 4.4, have been arranged together and is shown in figure 4.19. This data now enables joint forces to be estimated under known conditions of external loading, as undertaken in Chapter 6.

4.5 Joints of the Second Ray of the Foot

4.5.1 The tarsometatarsal joint of the second ray:

4.5.1.1 Range of movement, and behaviour of capsule and ligaments:

The base of the 2nd metatarsal was observed to be very rigidly fastened to the block of cuneiform bones so that no movement, even after cutting the transversal ties between the capsule of its meta-tarsophalangeal joint and the neighbouring capsules had been effected, was readily detectable. Details of the force-movement characteristic in the 2nd cuneometatarsal joint are given in Section 4.6 that treats the mode of force transmission through the metatarsal bones in the absence of muscular activity.

4.5.1.2 Topography of the tarsometatarsal joint surfaces:

Because of the lack of movement in the tenon-and-mortise-joint that characterises the transition from the cuneiform block to the 2nd metatarsal bone, no attempt was made to map the mating surfaces as carried out in the case of the 1st ray. The topography of this amphiarthrosis is described extensively by Sarrafian (1983) and has been briefly treated in Chapter 1 of this thesis.

4.5.2 The metatarsophalangeal joint of the second toe (MP-2):

4.5.2.1 Range of movement, and observations relating to the capsule, ligaments and tendons:

The range of movement in the MP-2 joint was observed to be as follows: 70° in dorsiflexion, 45° in plantar flexion, 25° external rotation, 20° internal rotation - all measurements being referred to the joint in its physiologically neutral position (foot flat) that is, with an angle of about 155° between the longitudinal axis of the proximal phalanx and that of the metatarsal bone. These observations were made with the capsule and ligaments wholly intact.

The capsule was then excised at its antero-dorsal and posterio-plantar aspects at its attachment to the metatarsal bone. On examining the medial and lateral sides of the joint capsule, ligamentous fibres fan out from a tubercle on each side of the flattened head to meet the base (or glenoid) of the proximal phalanx anteriorly and also to pass in a plantar direction so as to form a sling which merges into the plantar capsule plate directly below. The sling passing downwards permits rotation of the head within the encasing capsule about a transversal axis and at the same time prevents the plantar bearing surface from slipping sideways off the convex head.

Lateral aspect of MP-2 joint

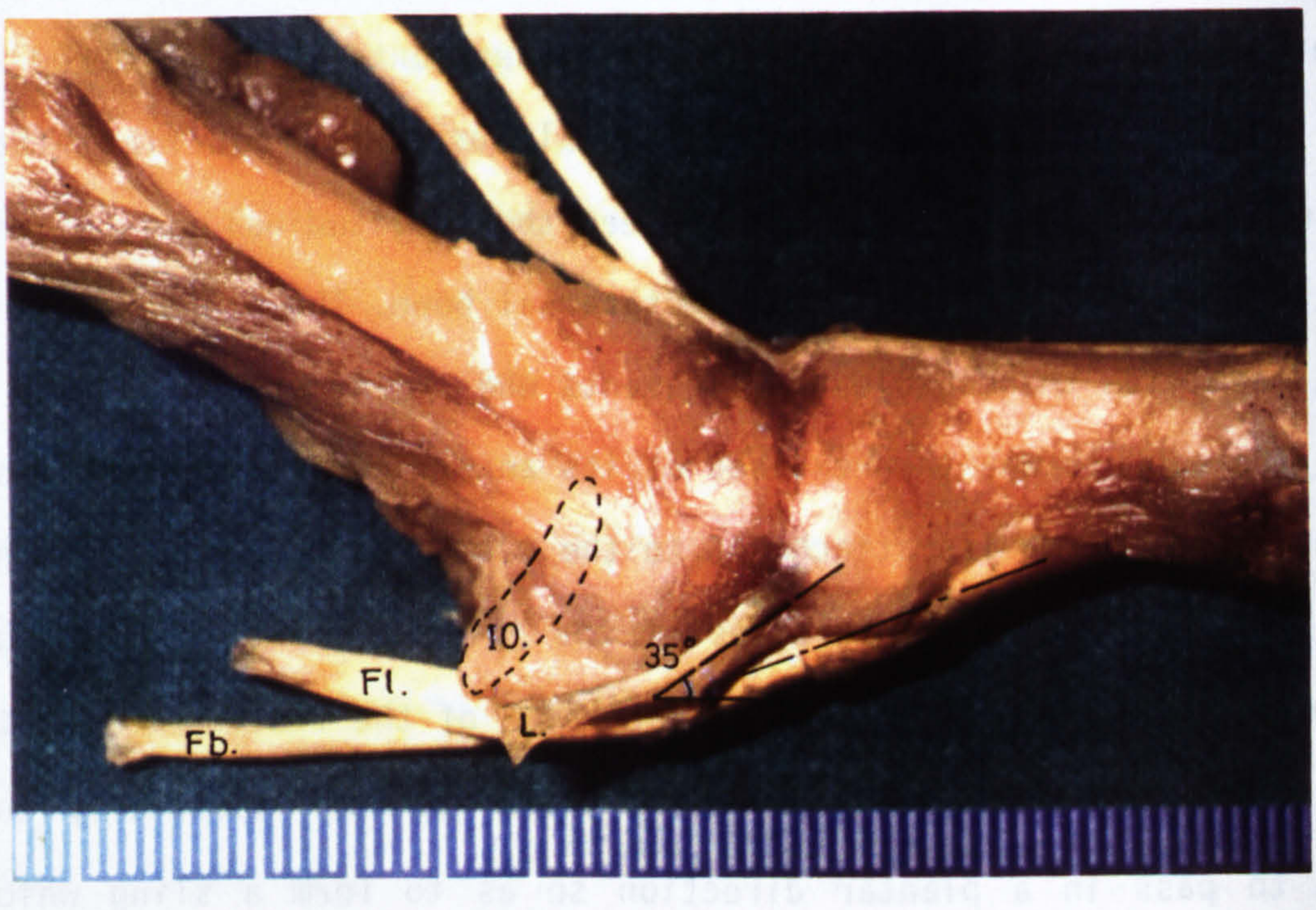

IO: Tendon of dorsal interosseus
Fl: Tendon of flex. digit. long.
Fb: Tendon of flex. digit. brev.
L: Tendon of lumbricales

Medial aspect of MP-2 joint

Figure 4.20 Course taken by the fibres of the interossei before meeting the base of the proximal phalanx

The fibres directed anteriorly and slightly downwards to meet the medio-plantar and latero-plantar aspects of the base of the proximal phalanx limit the range of movement in the metatarsophalangeal joint. Each of these four ligaments has a cross section of about 4 mm x 1 mm.

The boat-shaped fibrous capsule with its plantar plate is of a stiff texture similar to the already described capsule of MP-1 but much thinner and, in the specimens studied, without sesamoidal ossifications. The functional course taken by the fibres of the flexor tendons (interossei dorsalis et plantaris) prior to their insertion on the base of the proximal phalanx is not very clear. However, the direction of force application from these muscles to the base of the phalanx was assumed to be as shown in figure 4.20 and was found to be at an angle of about 35° to the horizontal. The tendons of flex. digit.longus and flex.digit. brevis were observed to make an angle of about 20° to the horizontal in passing forwards and upwards (fig 4.20).

No extensor muscle inserts into the base of the proximal phalanx of the 2nd toe (or of any of the other lesser toes for that matter). Dorsiflexion in the MP-2 joint is effected by the extensor pull on the dorsal aponeurosis along the dorsum of the proximal phalanx and over the proximal interphalangeal joint (see Sections 4.3.2.2 and 4.3.2.3).

4.5.2.2 Topography of the MP-2 joint:

The surface geometry of the joint surfaces was determined by use of moiré photogrammetry as described earlier in Chapter 3, Section 3.2. The metatarsal bone was held in a position corresponding

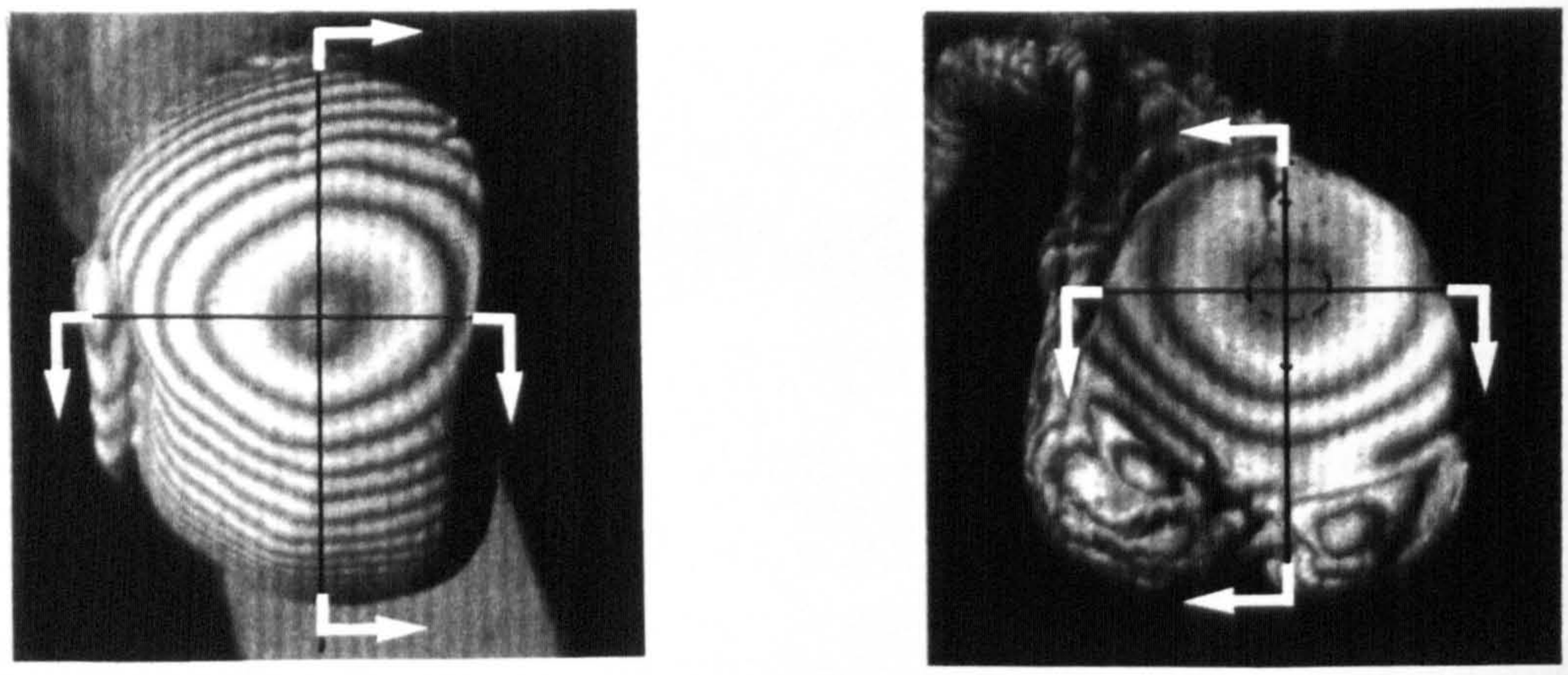

a) Head of metatarsal 2 b) Base of proximal phalanx 2

Figure 4.21 Moiré fringes on the MP-2 joint surfaces (left foot) and cross-sections chosen

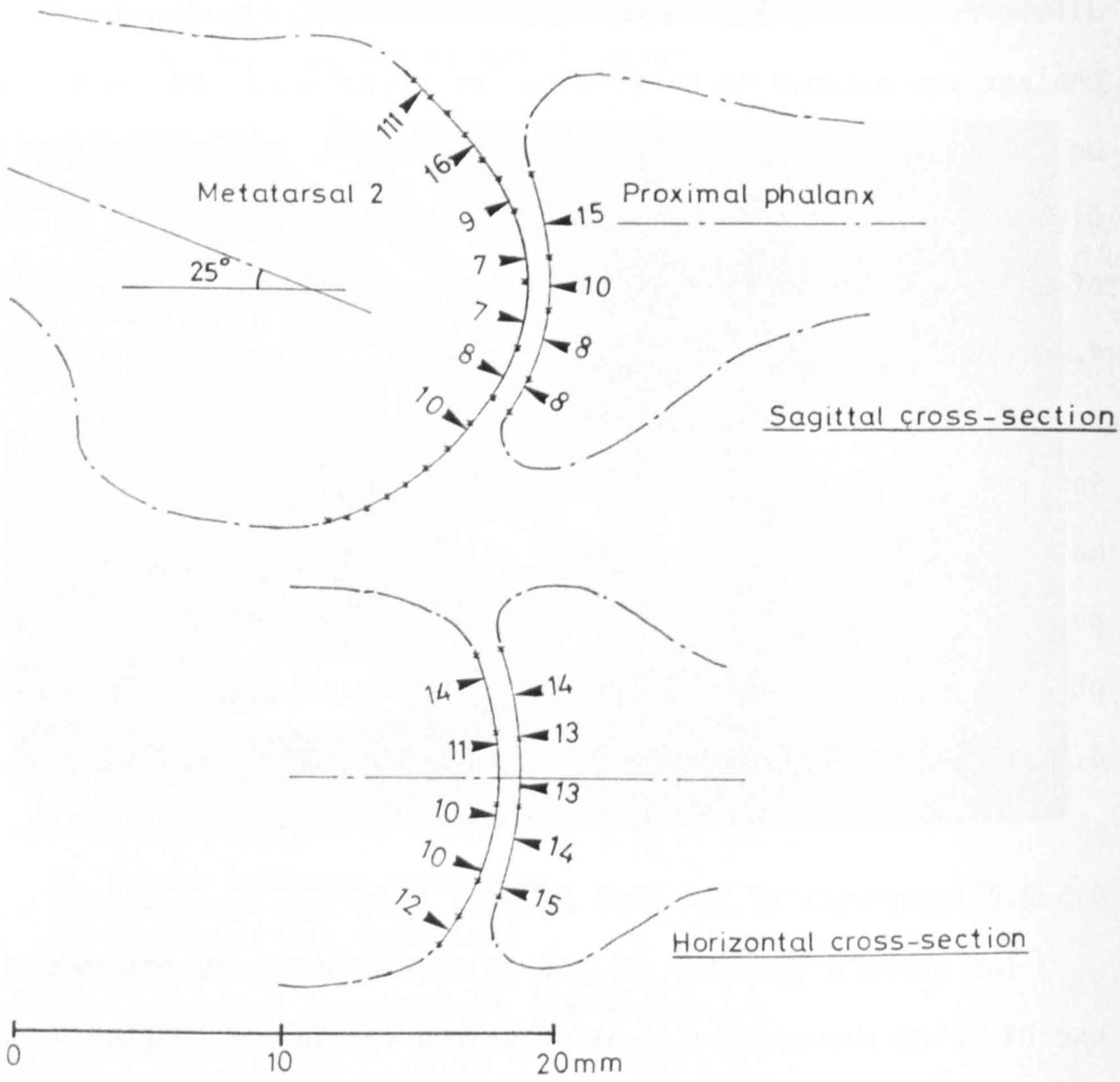

Figure 4.22 Typical contours of the MP-2 joint surfaces (left foot) with radii of curvature in mm

to the foot on the ground, and the head viewed along an anterior-posterior axis. Moiré fringes were produced and recorded. Following this, the topography of the glenoid mating surface of the proximal phalanx base was recorded in a similar manner. Figure 4.21 shows typical moiré patterns obtained and figure 4.22 the contours of the joint surfaces in sagittal and horizontal planes with some of the radii of curvature marked in. It is interesting to note that a maximum of congruence between the joint surfaces issues with about 25° dorsal flexion in the MP-2 joint.

4.5.3 The proximal interphalangeal joint of the second toe (PIP-2):

4.5.3.1 Range of movement, and observations concerning the capsule, ligaments and tendons:

This being a typical hinge joint, no appreciable external or internal rotation can be effected. Starting from the physiologically neutral position (the longitudinal axes of the two bones make an angle in the sagittal plane of about 160° to each other) the PIP-2 joint can be plantarflexed by about 60° but in dorsiflexion movement is limited to about 20° only, that is, up to the point when the longitudinal axes of the proximal and middle phalanges lie parallel to each other (fig 4.27).

The fibres of the collateral ligaments are embedded within the joint capsule and separation of these structures proved to be virtually impossible. Looking through the intact capsule, the fibres of each collateral ligament can be traced from a small tubercle on either side of the head, which, after crossing the joint in an antero-plantar direction, immediately meet the base of the middle phalanx

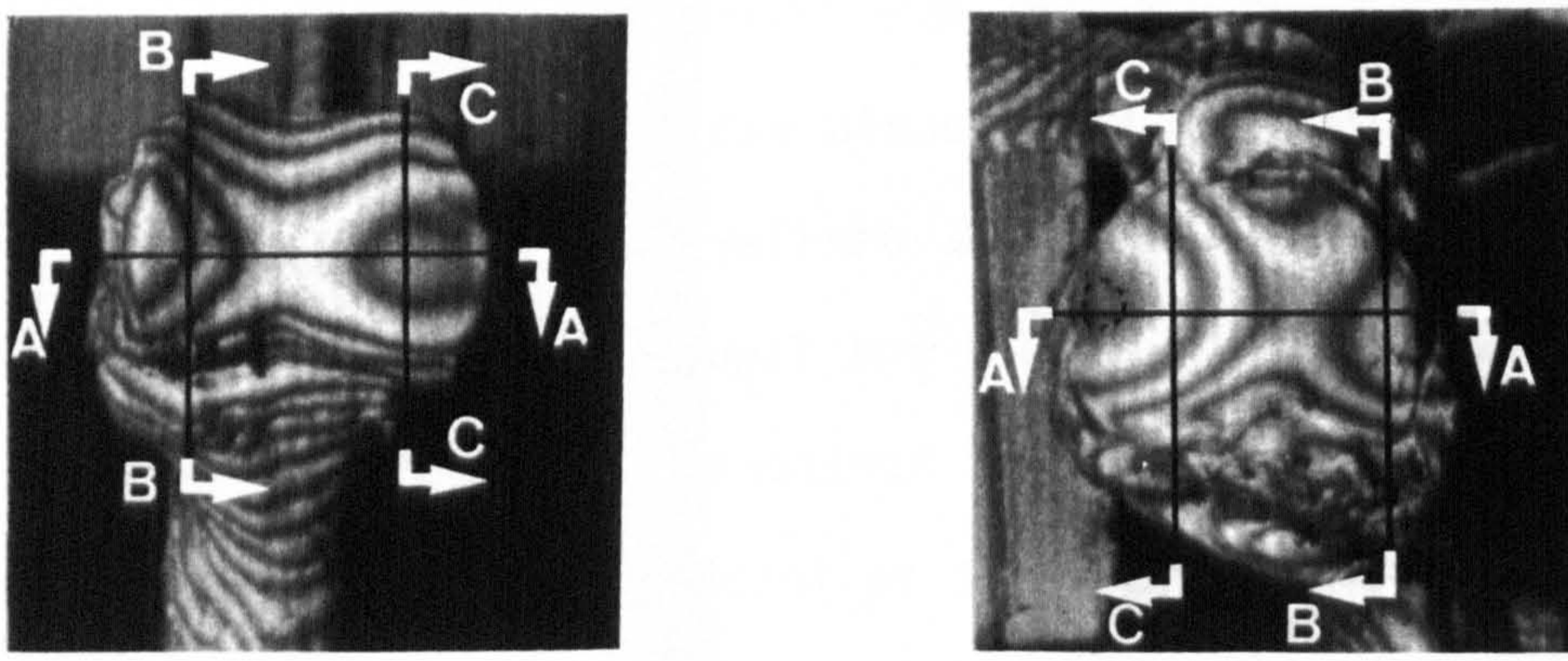

a) Head of prox. phalanx 2 b) Base of middle phalanx 2

Figure 4.23 Moiré fringes on the PIP-2 joint surfaces (left foot) showing cross-sections chosen

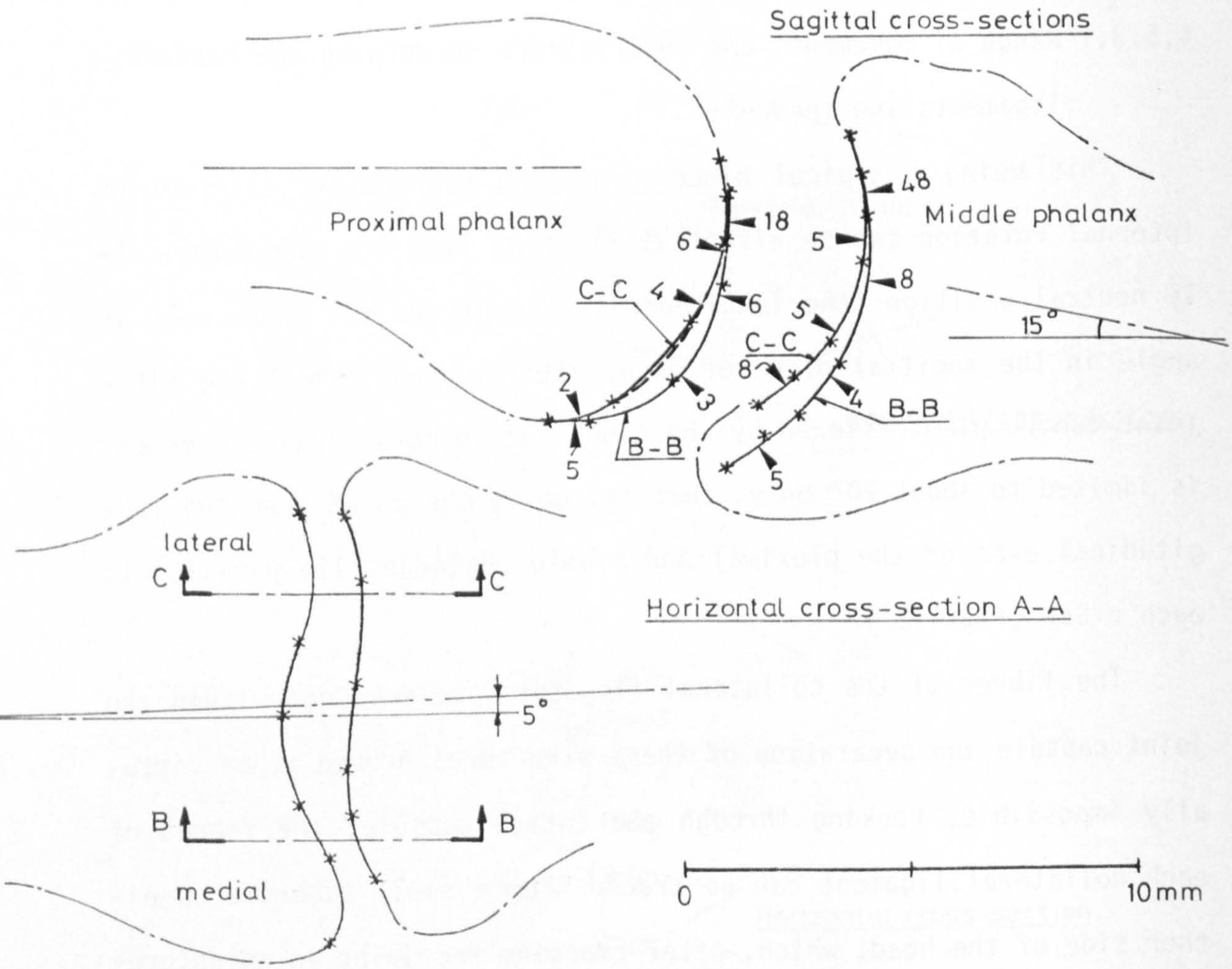

Figure 4.24 Typical contours of the PIP-2 joint surfaces (left foot) with radii of curvature in mm

at its medio-plantar and latero-plantar bearing surface boundaries. On the plantar side, the flex.digit. brevis tendon splits just before crossing the joint, allowing the deeper lying flex.digit.longus tendon to pass through the bifurcation and proceed further distally. The flex.digit.brevis inserts on the medial and lateral parts of the plantar aspect of the base. Figure 4.27 shows the course taken by the flexor and extensor tendons relative to the joint.

4.5.3.2 Topography of the PIP-2 joint:

Both articulating surfaces of the PIP-2 joint were mapped, using moiré photography, to determine the geometry of the joint. Figure 4.23 shows typical moiré patterns obtained and figure 4.24 the contours of the joint surfaces in one horizontal and two sagittal planes. Figure 4.24 also shows some of the calculated radii of curvature that characterise the articulation.

4.5.4 The distal interphalangeal joint of the second toe (DIP-2):

4.5.4.1 Range of movement, and observations relating to the capsule, ligaments and tendons:

This again is also a hinge joint, but in contrast to PIP-2 which is so formed that no transversal movement of the mating parts relative to each other can occur, this articulation does allow for a small amount of translatory movement parallel to the hinge axis. The joint surface of the head only very weakly resembles a saddle and is more like a cylindrical surface instead. The mating part is correspondingly formed. The translatory movement is therefore limited by the soft tissues crossing the joint and is roughly estimated to be in the range of 1 mm. The position of the distal phalanx rela-

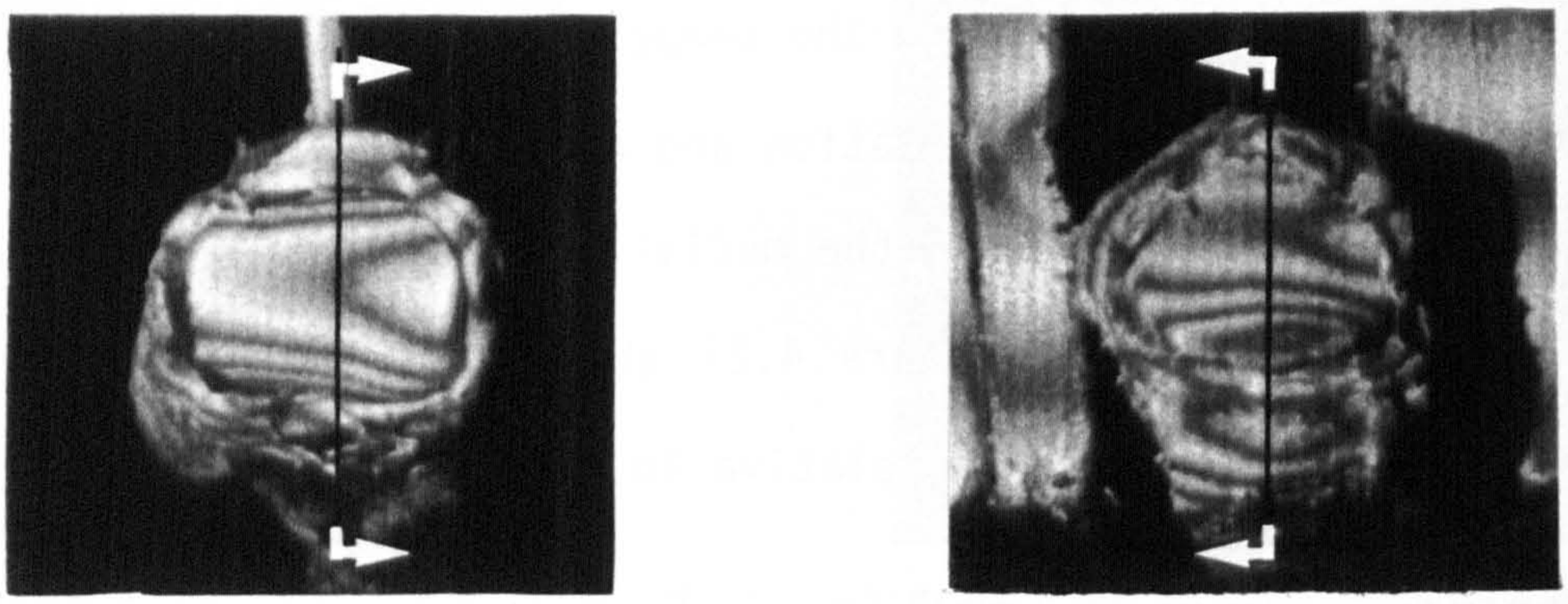

a) Head of middle phalanx 2 b) Base of distal phalanx 2

Figure 4.25 Moiré fringes on the DIP-2 joint surfaces (left foot) and cross-sections chosen

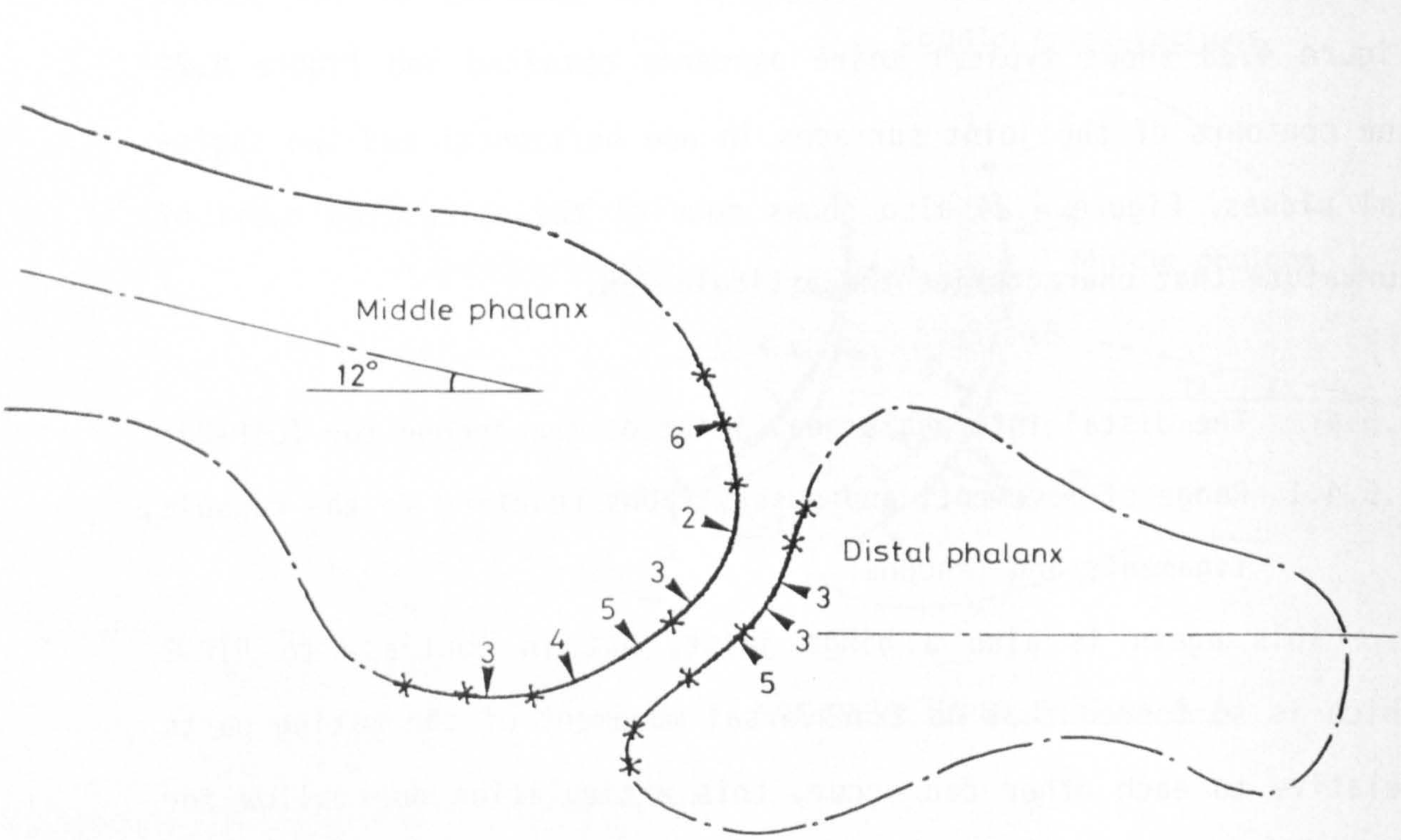

Figure 4.26 Typical profile of the DIP-2 joint surfaces with radii of curvature, in mm

tive to the middle one varies considerably amongst 'normal' feet but was observed in most individuals (as judged by observing the slope of the toe nail) to be as shown in figure 4.27. From this neutral position, the range of movement was found to be about 50° in plantar flexion and 20° in dorsiflexion.

The collateral ligaments and the capsule are even more difficult to separate than in the PIP-2 joint. Nevertheless, the general course taken by the collateral ligament fibres from the head of the middle phalanx to the base of the distal one was observed to be similar, that is, they arise from a tubercle on each side of the head and proceed planto-anteriorly to meet the base at its medio-plantar and latero-plantar aspects. The structure that proceeds along the dorsum of the joint to insert on the distal phalanx is the dorsal aponeurosis which contains fibres of both, the ext.digit. brevis as well as the ext.digit.long. tendons.

On the plantar side, a comparatively well defined tendon of the flex.digit.long. proceeds across the joint to be inserted into the distal phalanx.

4.5.4.2 Topography of the DIP-2 joint:

Both articulating surfaces of the DIP-2 joint were mapped, using moiré photography, to describe the geometry of the articulation. Figure 4.25 shows typical moiré patterns obtained and figure 4.26 the contours of the joint surfaces in a sagittal plane. Figure 4.26 also shows some radii of curvature marked in.

* | + u | v | - w | denotes: v is a typical angle in the neutral, foot flat position;

u is the maximum deflection in one direction, the angle now measures v+u;

w is the maximum deflection in the reverse direction, the angle now measures v-w.

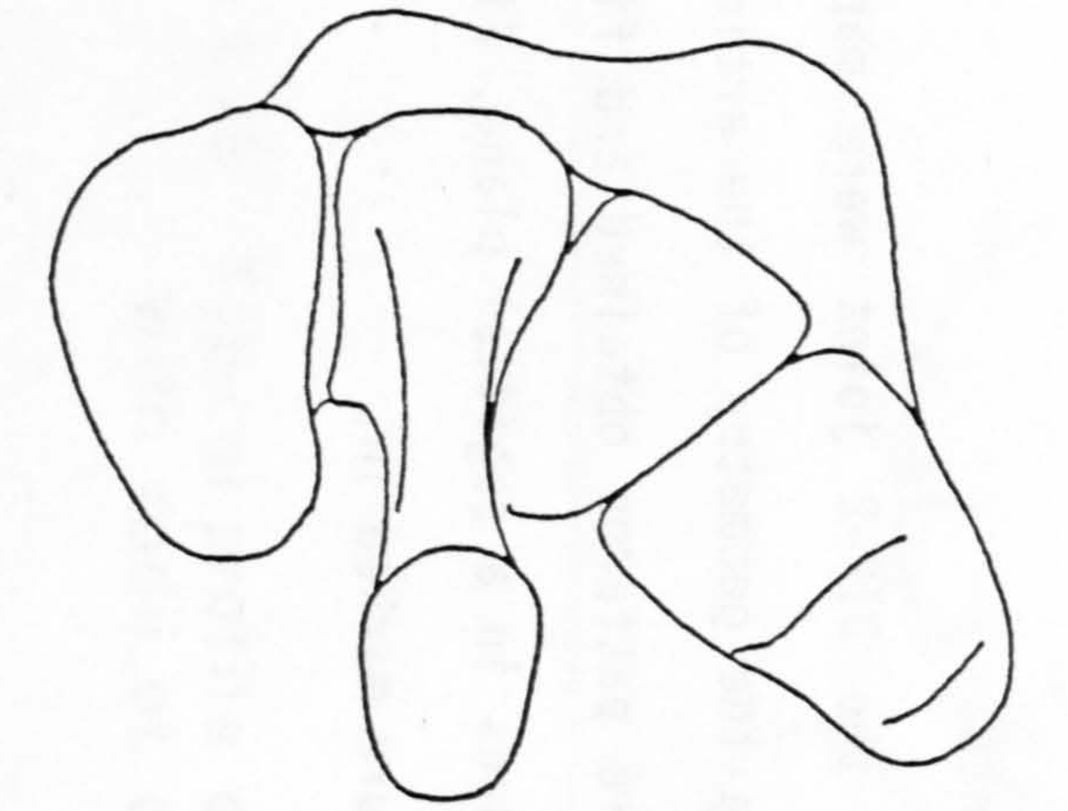

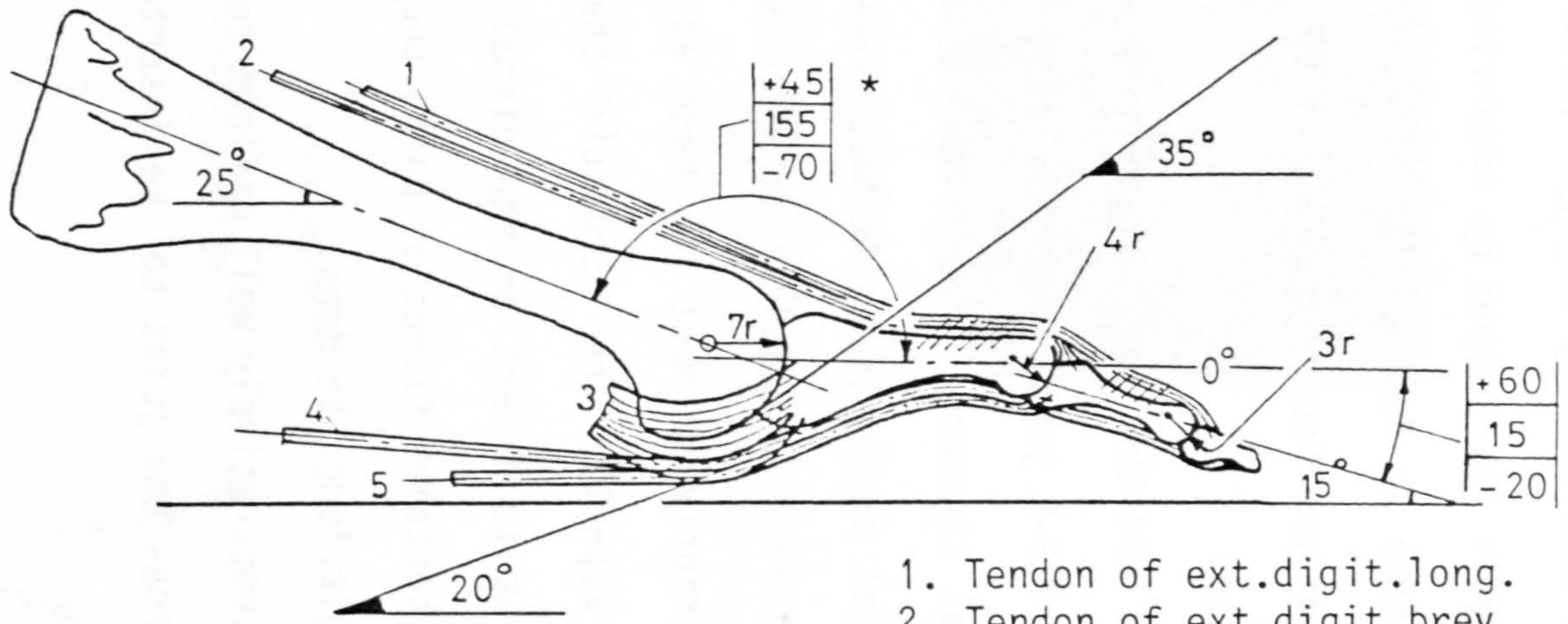

1. Tendon of ext.digit.long.
2. Tendon of ext.digit.brev.
3. Tendons of the interossei
4. Tendon of flex.digit.long.
5. Tendon of flex.digit.brev.

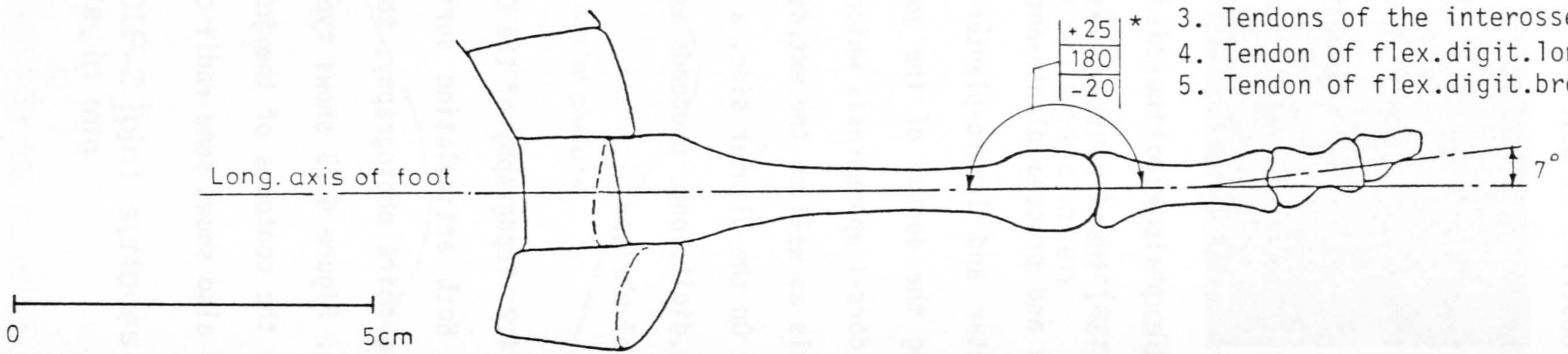

Figure 4.27 Some typical dimensions of the second ray of the foot

4.5.5 Overall geometry of the second ray and the course taken by the tendons:

The relevant anthropometric data collected, as described in the preceding sub-sections of Section 4.5, have been arranged together and is shown in figure 4.27. This data now enables joint forces to be determined under known conditions of external loading, as performed in Chapter 6.

4.6 Statics of the Forefoot in the Absence of Muscular Activity:

4.6.1 Purpose of investigation:

In Chapter 2, Sections 2.5 and 2.8, a detailed account has been given of the various hypotheses that have been advanced regarding the manner in which the metatarsal bones are probably loaded. Although there is no doubt whatever that muscular forces play a paramount role in supporting the dynamic foot, it is still a matter of contention as to whether the structure of the foot behaves like a three bar truss with purely compressive forces acting along the axis of the metatarsal bones, or whether the metatarsal bones behave like a beam, subjected to bending, when the foot is loaded statically in the absence of muscular activity. To investigate this matter further, strain measurements were carried out on a cadaver foot that appeared fully normal.

4.6.2 Method of investigation:

A complete foot with about 30 cm of the shank had been deep-frozen following amputation because of a tumour just below the knee. The foot belonged to a 37 year old man who had been otherwise healthy and had used his feet until shortly before the operation.

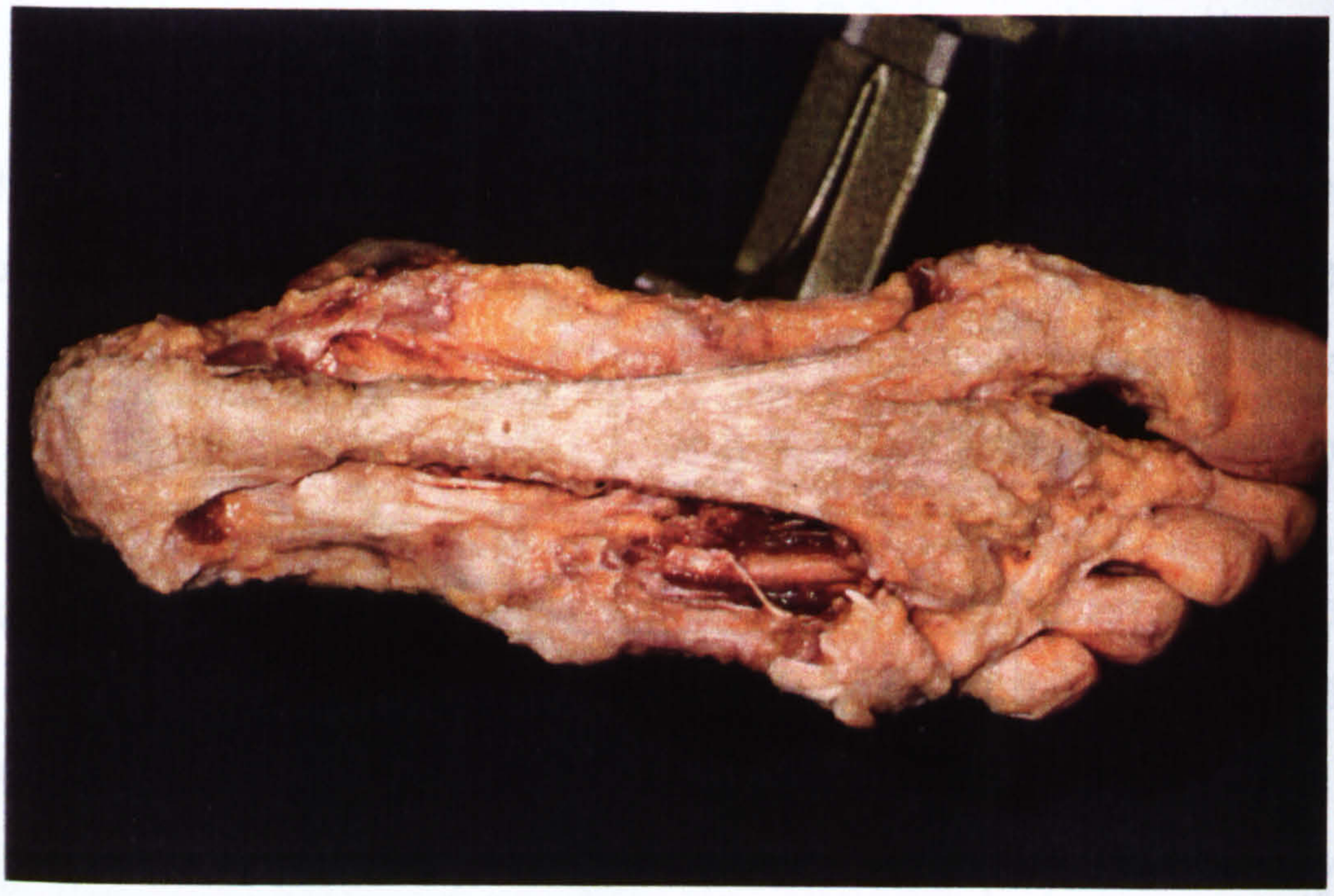

a) Plantar view of the foot with the aponeurosis exposed

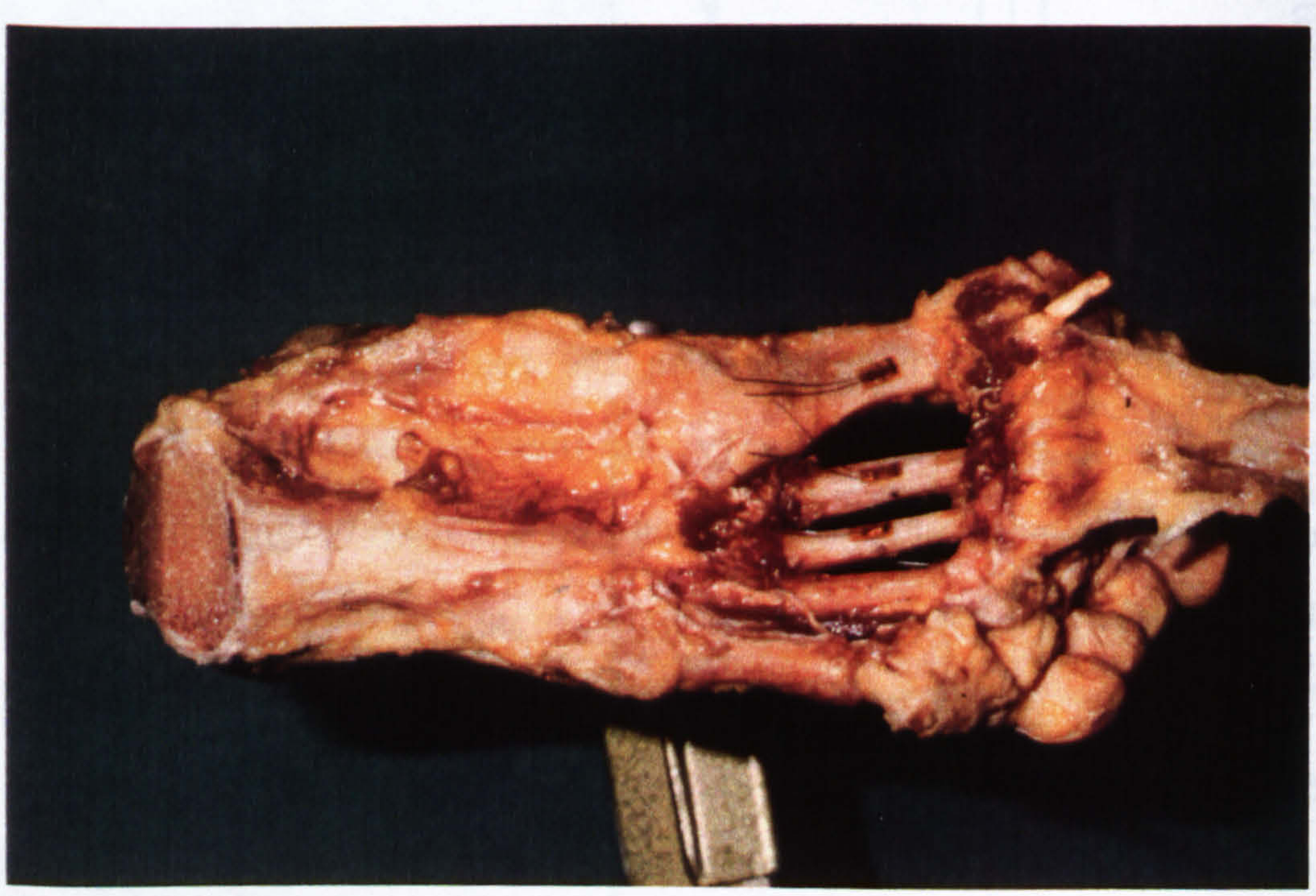

b) Strain gauges applied after elevating the plantar aponeurosis

Figure 4.28 The foot with strain gauges applied

The skin with subcutaneous fat was completely removed to facilitate access to the exposed bones and also in order to observe interosseus movements that might otherwise be masked by the covering skin. The abductor muscles of the great and little toes were removed and the tuberosity of the calcaneus then resected by cutting along two planes while preserving the attachment of the achilles tendon and the plantar aponeurosis to it. In this manner the tuberosity with the achilles tendon and aponeurosis could be lifted off (fig 4.28), after detaching the flexor brevis muscles from the latter, exposing the remaining intrinsic muscles of the plantar foot. It was now possible to remove the flex.hall.brev.muscle, the adductors of the great toe, and such interossei muscles that covered the shafts of the first three metatarsal bones. Great care was taken all the time not to damage any ligamentous structures and it was imperative to work fast so as to avoid any alteration in the elastic properties of the soft tissues that might come about by autodigestion or bacterial decay.

After exposing the middle portion of the first three metatarsal bones, strain gauges were applied (fig 4.28) as follows: The periosteum was scraped off and the bone degreased by a mixture of ether and pure ethyl alcohol (1:1). Strain gauges of 3 mm gauge length (Type HBM-3/120 LY 11) were then glued on, directly opposite each other, one on the dorsal and the other on the plantar side of each bone, using the quick-setting cyano-acrylic glue, Z70, supplied by the manufacturer of the strain gauges (Hottinger-Baldwin). Flexible lead wires with polyvinyl insulation were soldered onto the strain gauge tags and the whole assembly protected against moisture and mechanical damage by a coating of silicone rubber (General Electric

RTV 108). All six strain gauges (from the three first rays) were connected to a Hottinger automatic scanning and measuring unit (UPM60 + UMH3209). Each strain gauge was connected in 1/4 bridge fashion, the Wheatstone bridge being supplied from a source of 0.5 V at a carrier frequency of 225 Hz.

The resected tuberosity of the calcaneous was reattached in its original position with the use of acrylic bone cement after drilling a few shallow holes of about 10 mm dia. to anchor the cement within the two parts to be reunited. Care was taken to bring the tuberosity in its original position (including compensation for the width of the gap made by the saw during the resection procedure). The foot was now held in a jig after anchoring the free ends of the tibia and fibula in a steel tube with acrylic bone cement. The jig (fig 4.29) had the following features:

Basically, a short steel tube of 100 mm length, 60 mm diameter and 3 mm wall thickness that firmly held the shank bones just above the ankle joint was rigidly attached to the end of an arm. By adjusting the position of the arm, the foot could either be brought into the foot-flat position or into any one simulating the condition after heel rise had occurred. A horizontal platform under the foot was forced up against it by means of a special balance arrangement (fig 4.29) thus exerting a vertical ground reaction force on the foot, the magnitude of which remained independent of the position of the foot on the platform. The platform was free to move in a horizontal plane on ball bearings so that no horizontal component of force greater than about 0.006 times the vertical load could inadvertently come into play. Load was applied by means of a lever arrangement and weights (fig 4.29).

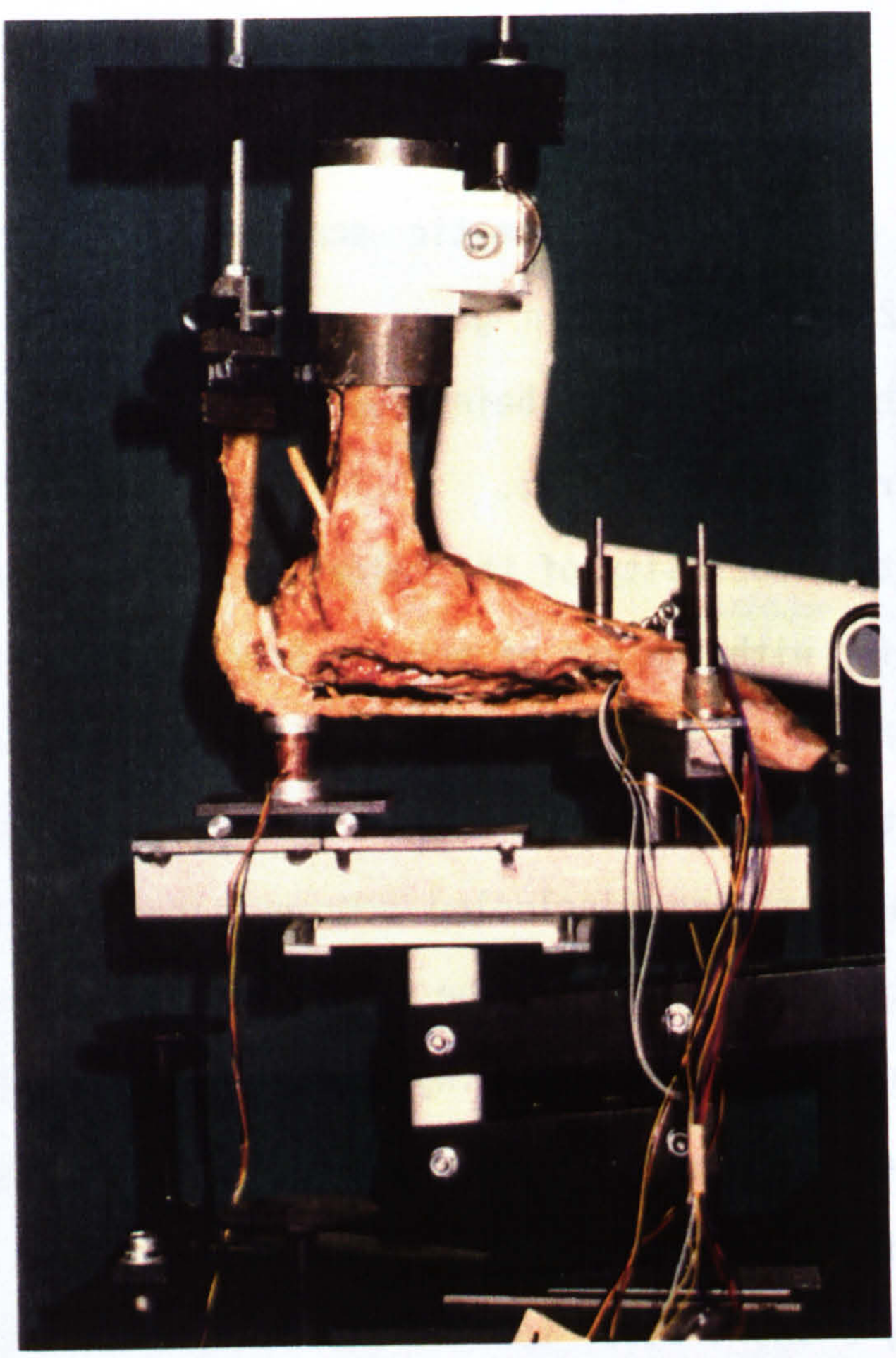

Figure 4.29 Device for loading the foot

A strain-gauged force transducer was placed between the tubercle of the calcaneous and the platform while the heads of the metatarsals all made contact with a flat bar that lay on the same platform (fig 4.29). In the first series of tests the achilles tendon was not fixed and therefore the foot was free to move in the ankle and talocalcanonavicular joints. Hence, the force transmitted upwards from the platform beneath the foot was distributed between the heel and the forefoot inversely proportional to their horizontal distances from the ankle joint. Also, the foot was free to adjust itself on the horizontal plane by eversion or inversion, permitting force distribution across the foot without any external restraint whatever. The strains in the first three metatarsal bones were measured in three steps up to a maximum total load of 324 N under the foot.

After this, a calibration test was performed to determine the relation between strains measured and ground force applied to the individual metatarsal heads. Eyescrews of 3 mm diameter were screwed vertically into the dorsal aspect of each metatarsal head. The achilles tendon was now gripped fast by means of a clamp and attached to the tibial support by a threaded rod. The foot was so positioned that each metatarsal head could in turn be pulled upwards (dorsally) by means of the eyescrew through a cord (fig. 4.30) that was acted upon, after passing over pulleys, by adjustable weights. The transverse metatarsal ligament that links the capsules of the MP joints sideways was severed so that an upward pull on any one head would not force the neighbouring heads to move along too. This necessitated slight longitudinal splitting of the distal fibres of the plantar aponeurosis in a sagittal plane but great care was exercised not to

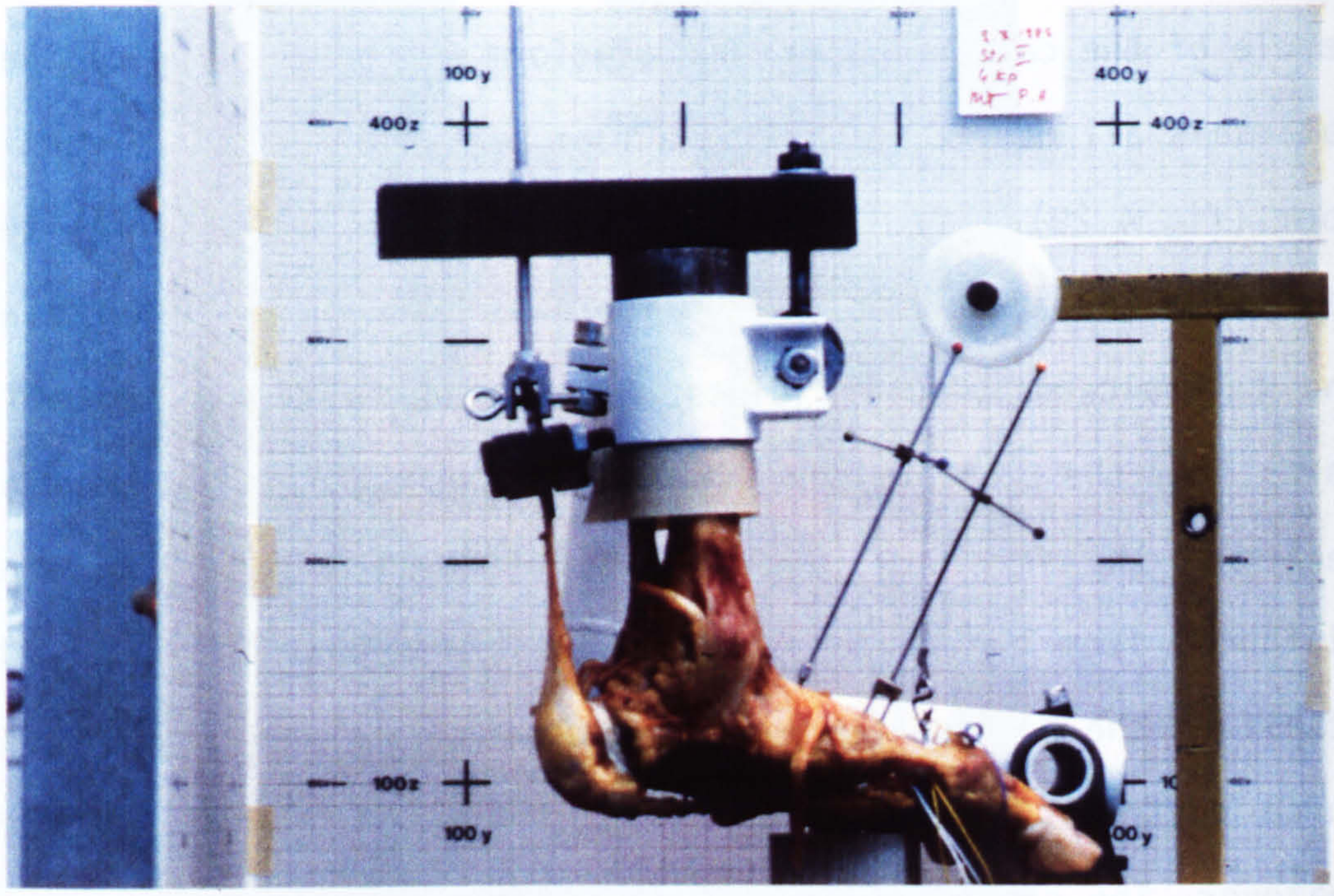

a) Projection of markers on the yz plane

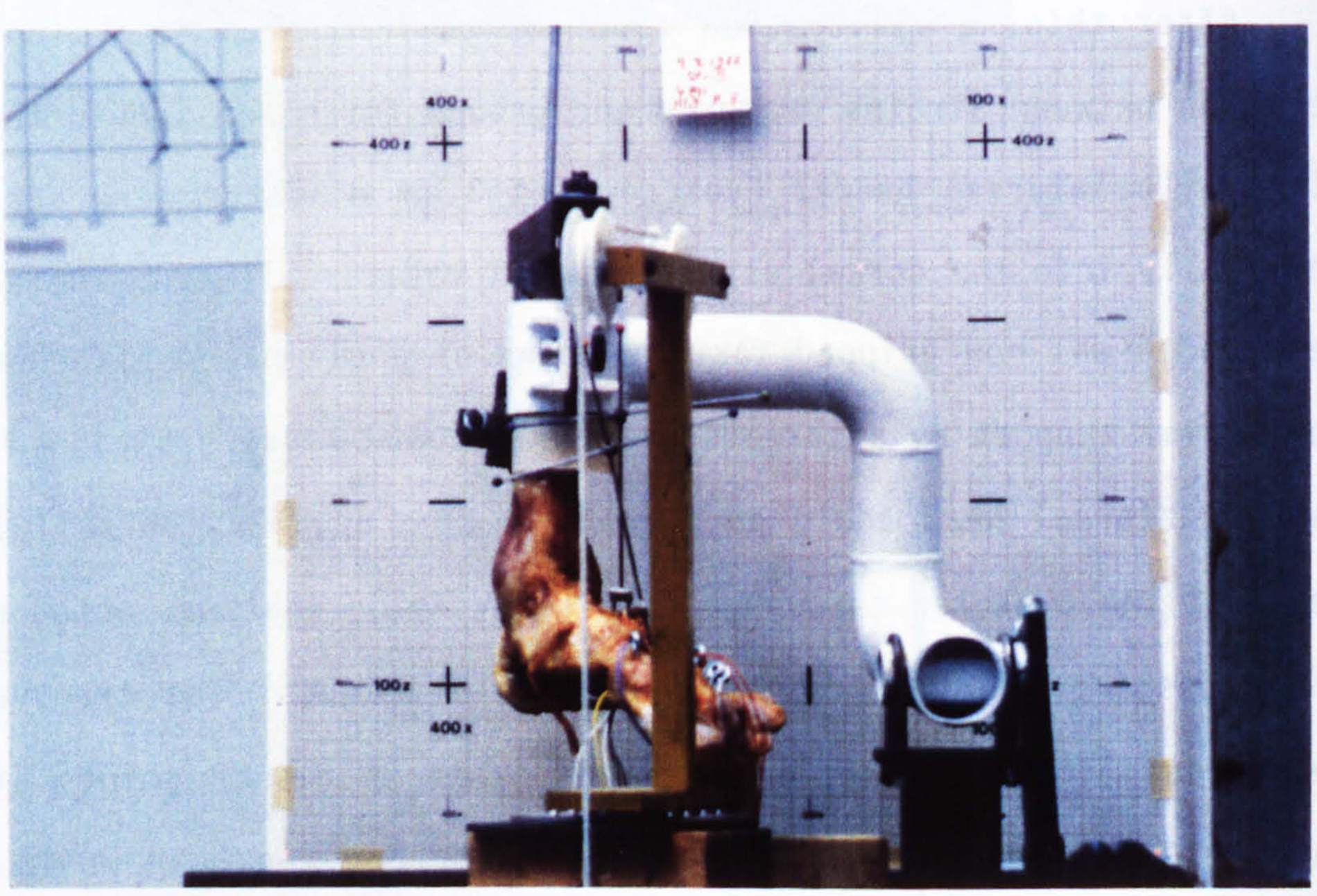

b) Projection of markers on the zx plane

Figure 4.30 Manner of loading individual metatarsals, also showing marker triads (Note: Achilles' tendon is held fast)

cut across any fibres that would otherwise diminish the supporting action of the aponeurosis on the structure of the foot.

Also, marker triads were rigidly fixed to the cuneiform and metatarsal bones of the first two rays (fig. 4.30) so as to determine the exact movement in these tarso-metatarsal joints in the manner described in Section 3.3 of Chapter 3.

After measuring the strains in each metatarsal bone in relation to the upward pull and also photographically recording the positions of the marker triads, the plantar aponeurosis was cut through and the strain and movement measurements as shown in figures 4.29 and 4.30 repeated.

Finally, the whole plantar aponeurosis was removed, and was prepared for testing its elastic properties, being stored in Ringer's solution at 4°C for two days before the test was carried out. The central portion of the aponeurosis of about 50 mm length proved to be of rather constant width and thickness and therefore this section of the specimen was kept free while on either side of this length grips were attached to facilitate tensile loading of the same in a universal materials testing machine (fig 4.36). A "C-clamp"extensometer (furnished with electrical resistance strain gauges) was attached to the aponeurosis over a length of about 40 mm by means of loose sutures into which the ends of the extensometer were hooked.

4.6.3 Results:

4.6.3.1 Strains measured in metatarsals 1, 2 and 3 in the foot flat position, under load:

With the intercapsular connections (ligamentum intermetatarsale transversum) intact and the heel together with all five metatarsal

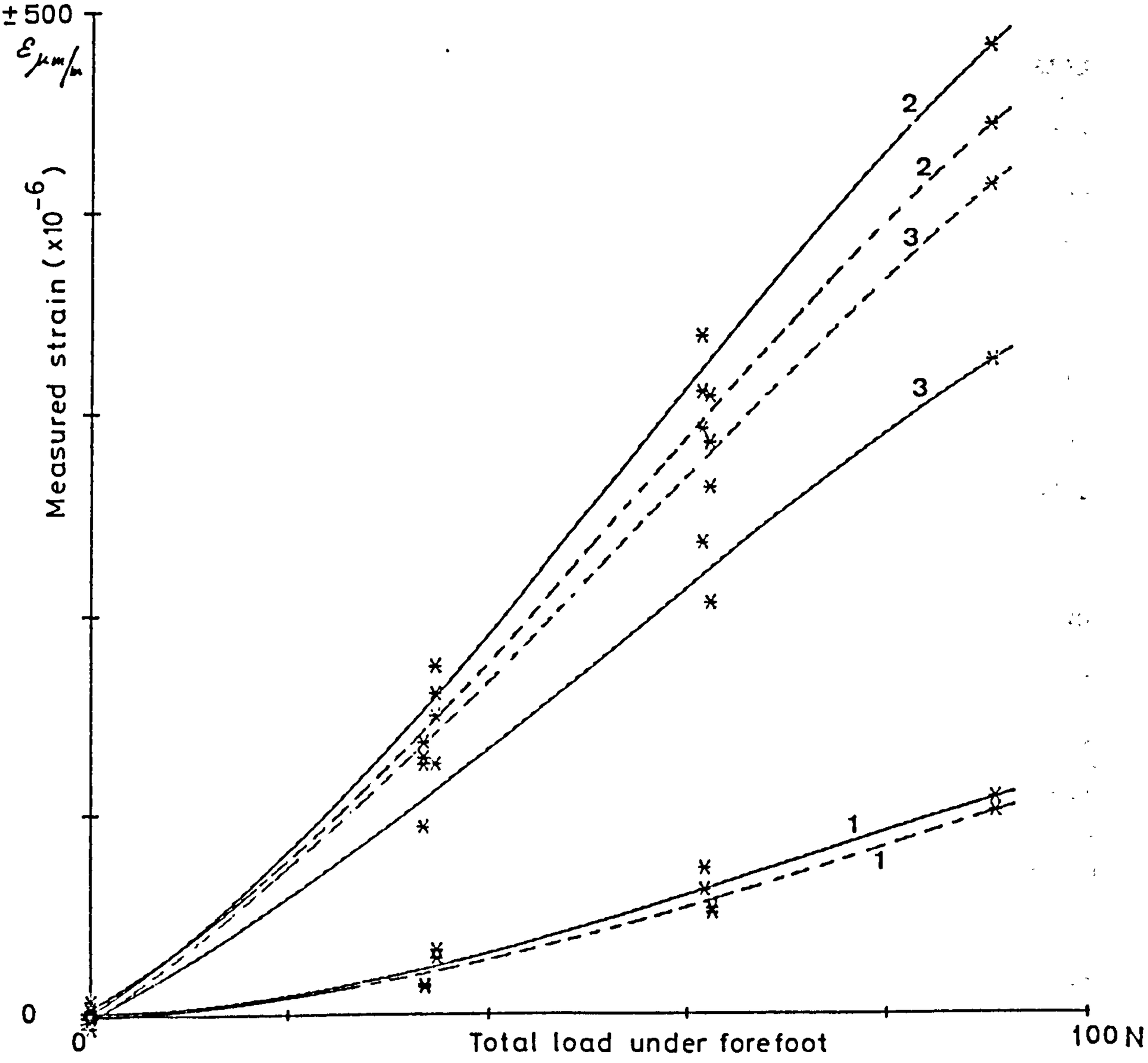

Figure 4.31 Strains measured in metatarsals 1, 2, and 3 versus total forefoot load (foot flat)

heads lying in one horizontal plane, the ankle joint was loaded vertically through the tibia up to a maximum of 324 N in three steps beginning with a pre-load of 30 N. The plantar aponeurosis was wholly intact and the achilles tendon was kept completely relaxed during this test. Figure 4.31 shows the results obtained. The zero-readings of the strain gauges were taken at the total pre-load of 30 N so that the maximum strains shown correspond to a total load difference of 294 N. In the following report only the load differences (taken from the pre-load level) will be discussed. The maximum load on the heel was 203 N, so that the total load under the heads of the metatarsals amounted to 91 N or 31% of the total load. The strain readings which were taken with progressively increasing and decreasing loads were observed to definitely follow a hysteresis loop (the measured points have been entered in figure 4.31) but the graphs plotted represent the best-fitting polynomials of third degree, this being considered sufficient for the present purpose. Repetition of the test several times confirmed the readings.

Section 4.6.3.3 deals with the relationship between strains measured and the forces acting on the individual metatarsal heads. Referring already to these values that are presented later (fig 4.32), it appears that the load under the forefoot is distributed between the 1st, 2nd and 3rd metatarsal heads and the remainder of the forefoot in the ratio of about 1.3:2:1:4 respectively. This in the foot flat position with no force acting along the Achilles tendon.

Furthermore, the relation between the magnitude of positive (tensile) and negative (compressive) strains measured on the planta and dorsum of the metatarsal bones, respectively, clearly indicate that these bones are subjected mainly to bending.

4.6.3.2 Range of movement in the MP joints in the foot flat position with intact plantar aponeurosis and under load:

While the forefoot was bearing load as described in the last section, the position and range of movement of the toes in the MP joints was observed. This, particularly to observe the 'windlass effect' of the plantar aponeurosis as suggested by Hicks (see Chapter 2, Section 2.5).

Although only the heads of the metatarsals rested on the horizontal surface of a bar of 30 mm width and there was no restriction to plantar flexion of the toes whatever, the toes were not observed to move into plantar flexion when the foot was loaded up to a maximum force of 324 N through the ankle joint. However, the range of free movement, especially in dorsiflexion, was markedly reduced. Whereas at no-load free movement in the MP joints (1, 2 and 3) was observed between 25° dorsiflexion up to 20° of plantar flexion at total axial loads above 210 N, the proximal phalanges could not be freely moved in dorsiflexion at all. And yet, free movement was still possible between 0° and 20° of plantar flexion. Probably this is because the point at which the aponeurosis fibres insert into the capsule is such, that with the toes in the neutral position (0° flexion), the 'drum' is practically unwound. The plantar aponeurosis was observed to tauten on loading the ankle joint in the foot flat position.

4.6.3.3 Strains measured in metatarsals 1, 2 and 3 on individual loading, with and without the plantar aponeurosis:

As already described in Section 4.6.2, a series of tests were carried out in which the head of each metatarsal bone was pulled up-

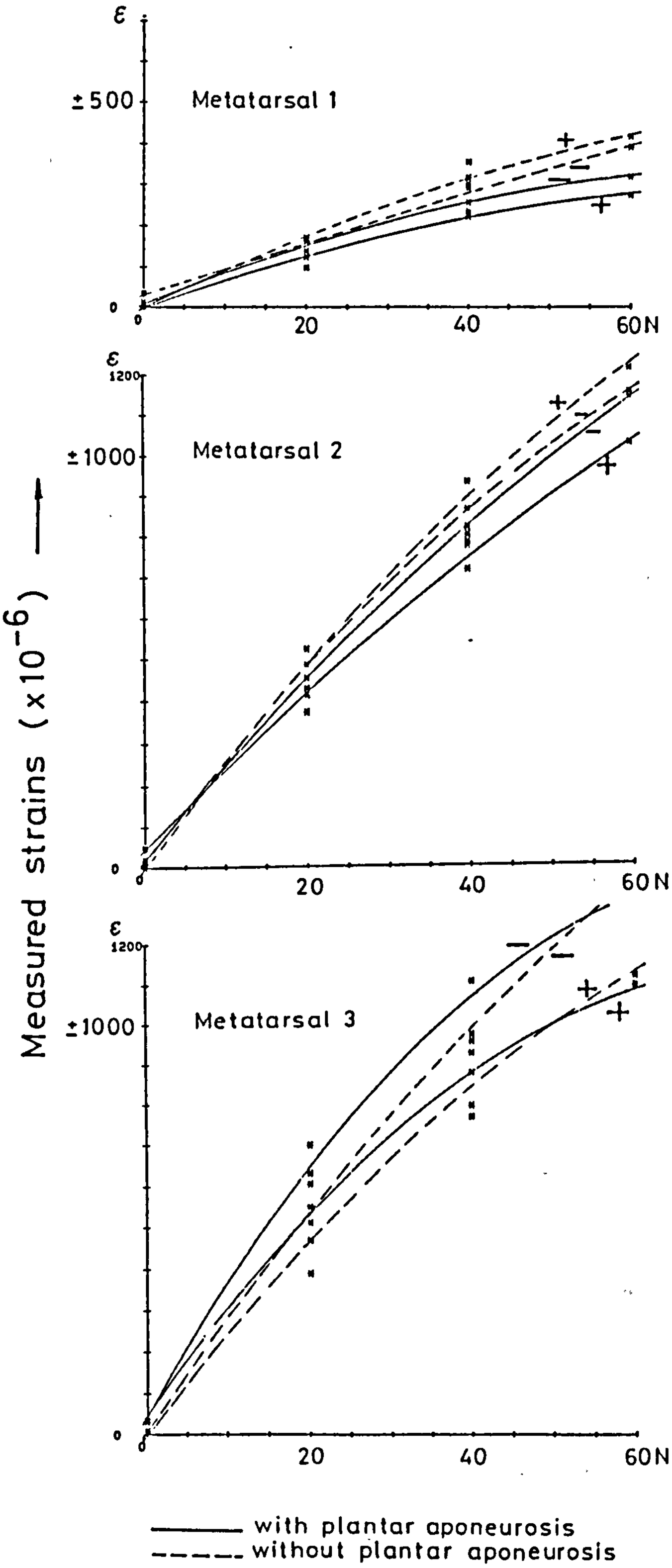

Figure 4.32 Measured strains versus dorsally directed pull on metatarsal head

wards, dorsally, one at a time, while the bones of the shank and the Achilles tendon were held fast (fig 4.30). It was observed that only when the heads of the 2nd or 3rd metatarsals were acted upon was it possible to keep the foot in its original level position without tilting in eversion or inversion, requiring only a minimum 'stabilising' force either under its lateral or medial border. On applying a dorsally directed pull on the 1st metatarsal head, however, the foot readily inverted while action of a similar force on the 4th or 5th metatarsal heads caused the foot to evert. To counteract this movement, either the lateral or the medial aspects of the forefoot had to be additionally supported by introducing shims under the corresponding metatarsal head. This, however, had no effect on the measurements.

Each metatarsal head was acted upon by a force of 20, 40 and 60 N in a progressively increasing and then decreasing order. Hysteresis was evident (the measured points have been entered in figure 4.32) but for practical purposes graphs have been drawn in figure 4.32 representing the best-fitting polynomials of third degree. Only average values of the strains measured were chosen for depicting the results as shown in figure 4.32. The plantar aponeurosis was then cut through and the test repeated. However, before cutting through the aponeurosis, movement in the cuneiform-metatarsal joints was measured as reported in the next Section 4.6.3.4.

On detaching the ties between the plantar aponeurosis and the metatarsal heads, the strain values increased by about 24% in the 1st metatarsal and by about 12% in the 2nd, at a load level of 40 N. The 3rd metatarsal curiously showed a decrease in the strain values up to a load of about 50 N, but above this loading level a slight

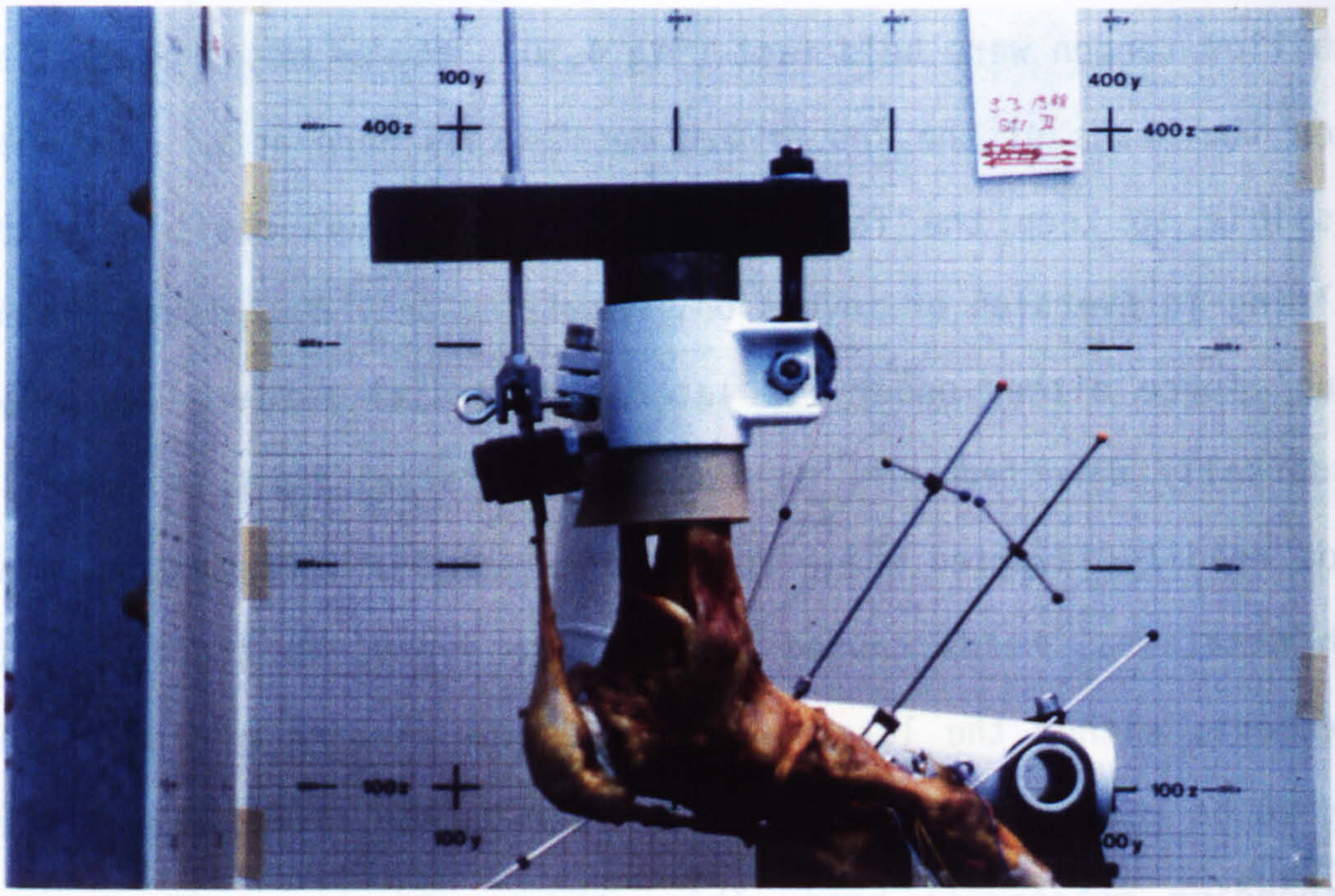

a) Projection of markers on yz plane

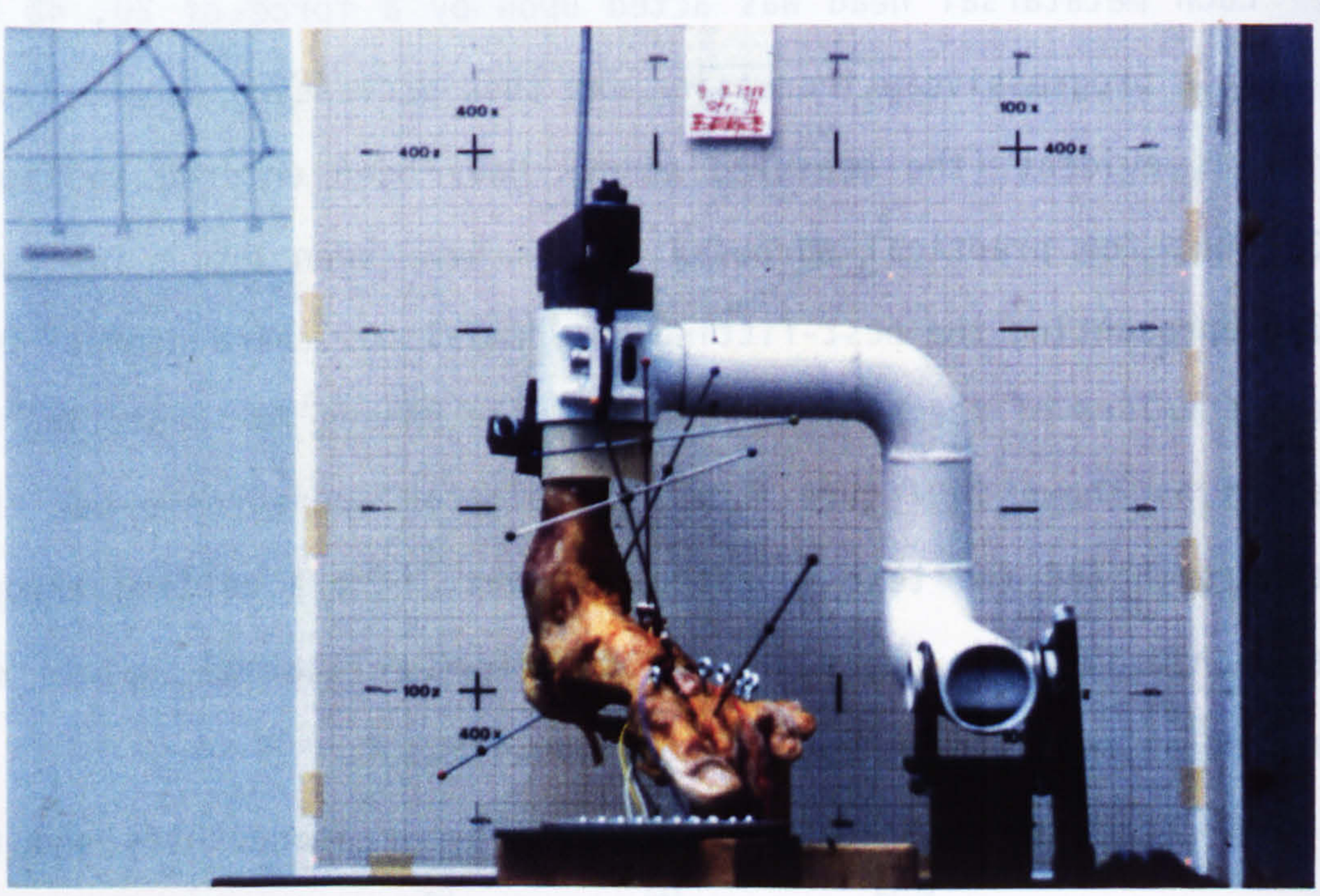

b) Projection of markers on zx plane

Figure 4.33 Marker triads, and pointers to anatomical landmarks

increase in the strains was observed.

4.6.3.4 Movement in the cuneiform-metatarsal joints under load, with and without the plantar aponeurosis:

Movement in the cuneiform-metatarsal joints was observed by attaching a triad of markers to the metatarsal bone and a similar set to the corresponding cuneiform and by applying a dorsally directed load to the metatarsal head (fig 4.30) as in the previous Section 4.6.3.3. The general method adopted for determining the relative movement has been described at length in Chapter 3, Section 3.3. The vertical load applied to the head of the 1st and 2nd metatarsals was 20, 40 and 60 N in magnitude. Figures 4.30a and 4.30b show the set-up for the investigation on the 2nd ray and figures 4.33a and 4.33b the application of pointers to mark the location of prominent anatomical landmarks such as the middle of the 2nd metatarsal head, the apex of the medial calcaneal tuberosity and the middle of the talar trochlear surface, these three points also defining the sagittal plane through the axis of the foot. The procedure adopted to determine and describe the helical axis of motion was, with reference to figure 4.34, as follows:

The location of the two sets of triads in xyz space was first determined with 20, 40 and 60 N load. A Cartesian coordinate system uvw was first assigned to the cuneiform triad and the xyz coordinates of the metatarsal triad transformed to this uvw system. The change in position of the metatarsal triad in the uvw system was then observed to determine the relative movement between the metatarsal and the cuneiform bone. This was done by first determining the position and direction of the helical axis in the uvw system by

Projection of marker triads on YZ and XZ planes are obtained from photographic slides.
Programme DIGXY facilitates reading YZ and XZ coordinates off digitizer. (Appendix 6(3))

↓

Spatial position of markers in the XYZ system are determined from the XYZ position of the cameras and the marker projections on YZ and XZ planes.
Programme: RAUMKO-3 (similar to WNSCHF, Appendix 7(3))

↓

Coordinate system UVW is assigned to a `fixed´ triad (cuneiform). The XYZ coordinates of the `moving´ triad (metatarsal) are now transformed to the UVW system. This is performed for all consecutive positions within the range of movement.
Programme: TRAN-XYZ.UVW (Appendix 8(3))

↓

The helical axis of motion is now determined for any two positions of the `moving´ triad in the UVW system.
Programme: HELIROD.J for large angular movement, otherwise HELIMAT (Appendices 5(3) and 4(3))

↓

Transform UVW coordinates of helical axis vectors (direction and location) into XYZ coordinates.
Programme: TRAN-UVW.XYZ (Appendix 9(3))

↓

Using `pointers´, the XYZ coordinates of three anatomical landmarks are determined. (Vector calculation by hand).

↓

Coordinate system RST is assigned to the anatomical landmarks of the foot. XYZ coordinates of helical axis vectors (direction and location) are transformed to the RST system.
Programme: TRAN-XYZ.UVW (U, V, W, renamed R, S, T, respectively)

Figure 4.34 Flow diagram for computing the helical axis of motion

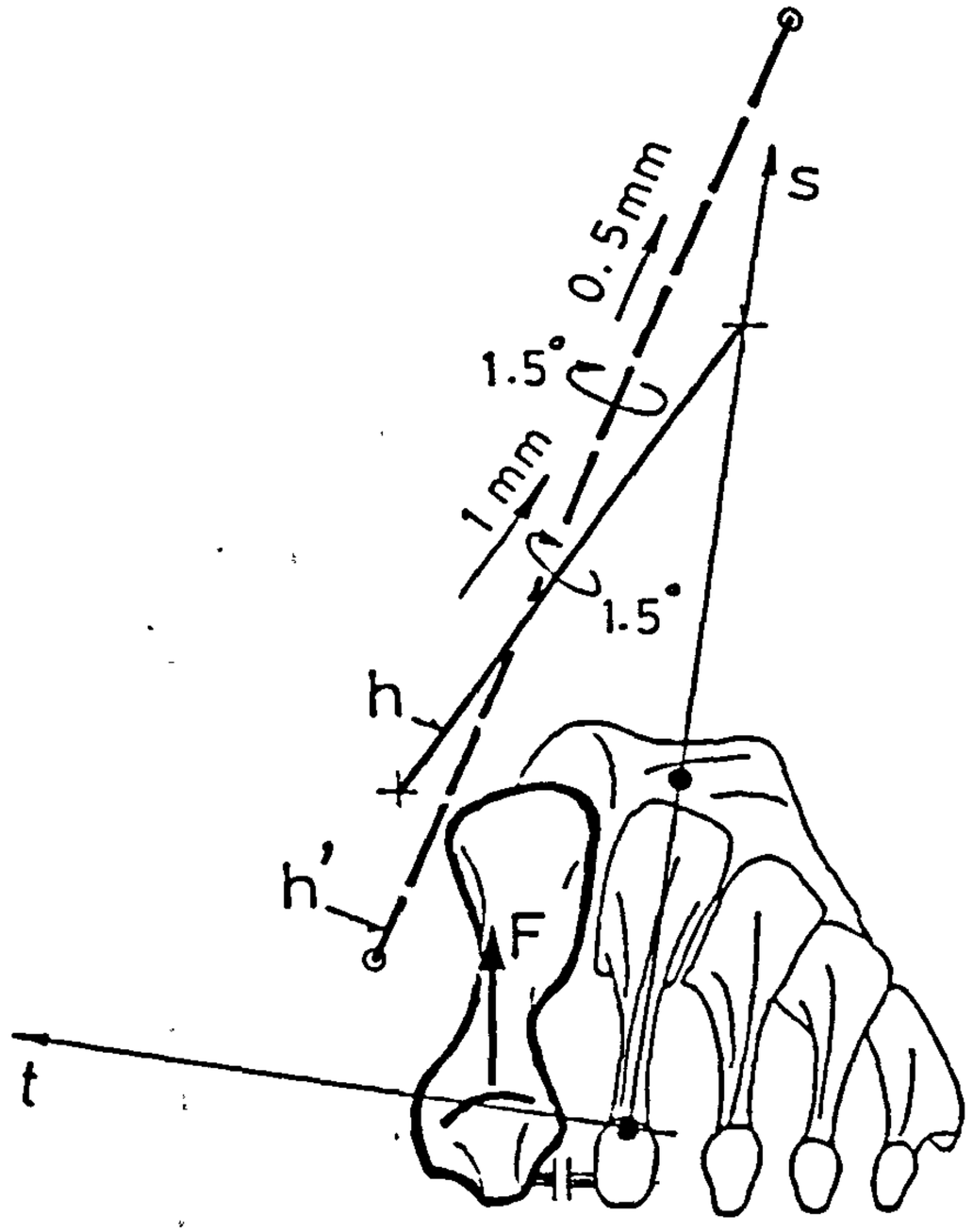

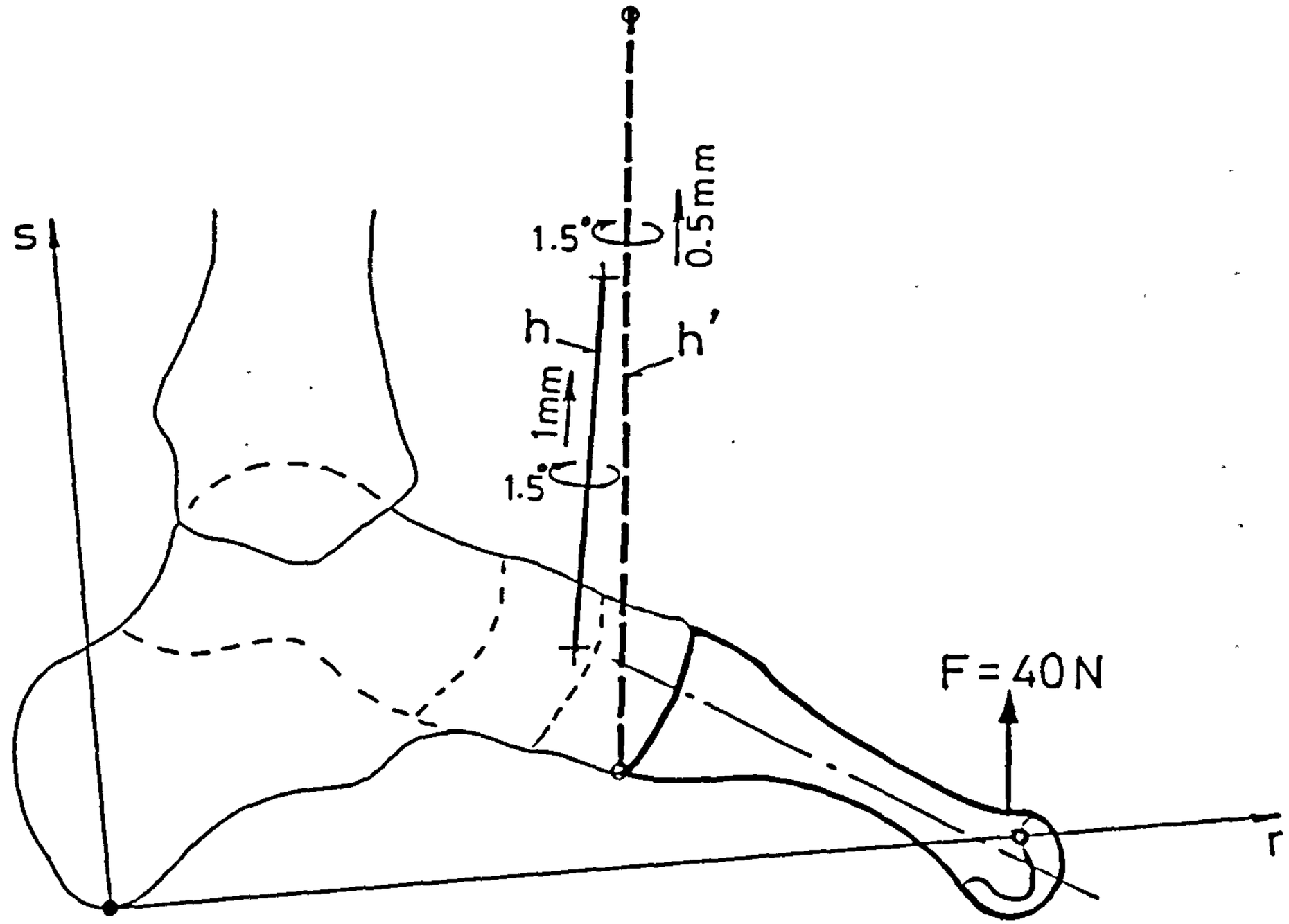

——————— with plantar aponeurosis
— — — — — — without plantar aponeurosis
(Transversal intermetatarsal ligament cut through in both cases)

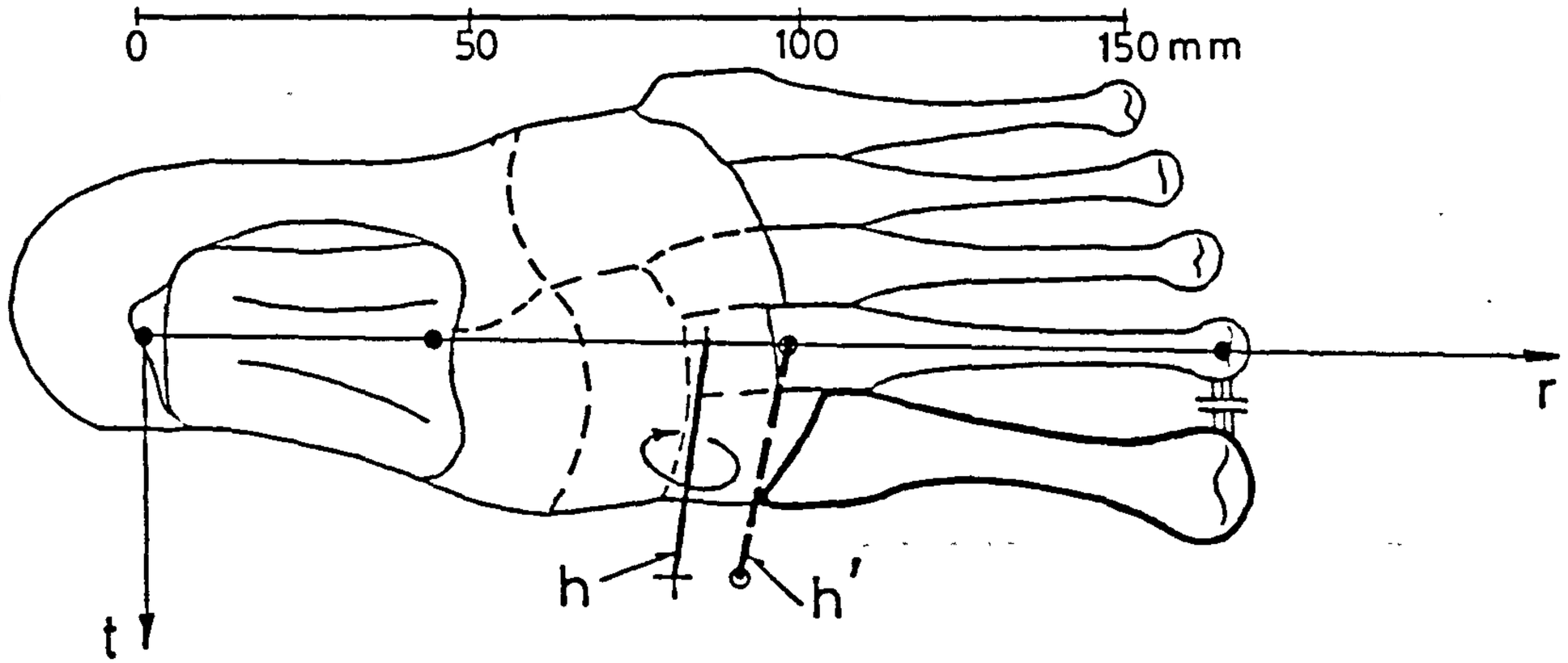

Figure 4.35 Helical axis of movement in the cuneiform-metatarsal 1 joint due to force F

making use of the shift in spa: l values of the marker triad between 20 and 40 N, between 40 and 60 N and between 20 and 60 N. The direction and position of the helical axis (axes) were then transformed to the global xyz system coordinates. Following this, these values were transformed to a third reference coordinate system, rst, defined by the anatomical landmarks of the foot as described earlier. (The apex of the medial calcaneal tuberosity is the origin of system rst, the r axis passes through the head of the 2nd metatarsal and the s axis lies in the sagittal plane, directed upwards. The direction of the t axis follows according to convention). In this manner, and with reference to figure 4.33 from which the position of the relevant anatomical landmarks can be determined, the position and direction of the helical axis relative to the foot is found. Figure 4.35 shows the results obtained for the first ray.

The procedure described above was repeated after the plantar aponeurosis had been severed. Figure 4.35 shows these results too, comparing these with those obtained prior to cutting through the aponeurosis.

The results obtained for the second ray have not been presented since they are probably strongly influenced by the amount of bending of the slender bone. (See next section for further comments).

4.6.3.5 Elastic properties of the plantar aponeurosis:

By means of vernier callipers and scale, the thickness and width of the aponeurosis were first measured, and found to be 1.3 mm and 21 mm, respectively. Beginning with a pre-load of 100 N, the tensile force was increased at an elongation rate of 1.3 mm/min (cross-head speed) until a maximum of 675 N was reached, at which level the spe-

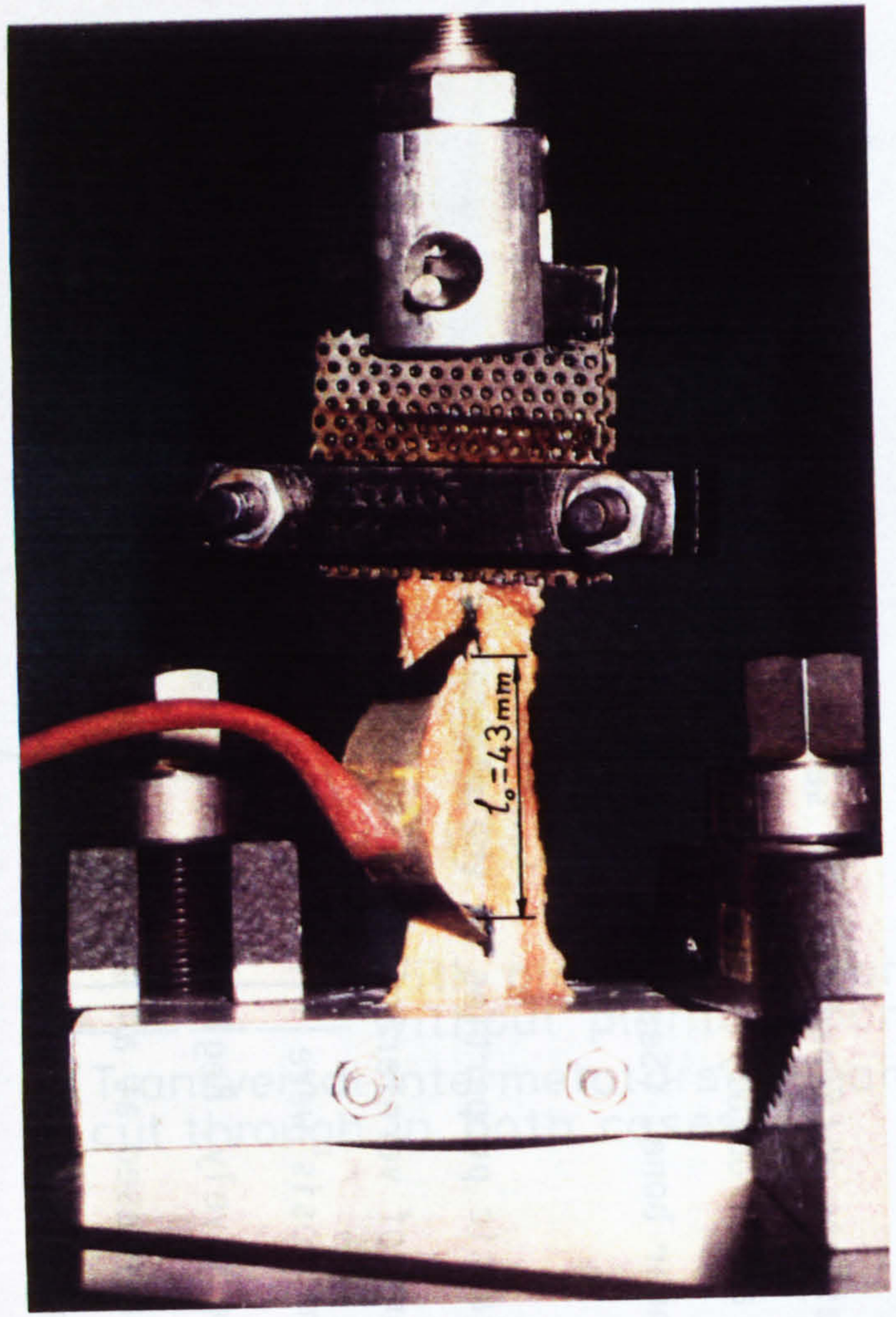

Figure 4·36 Plantar aponeurosis under test

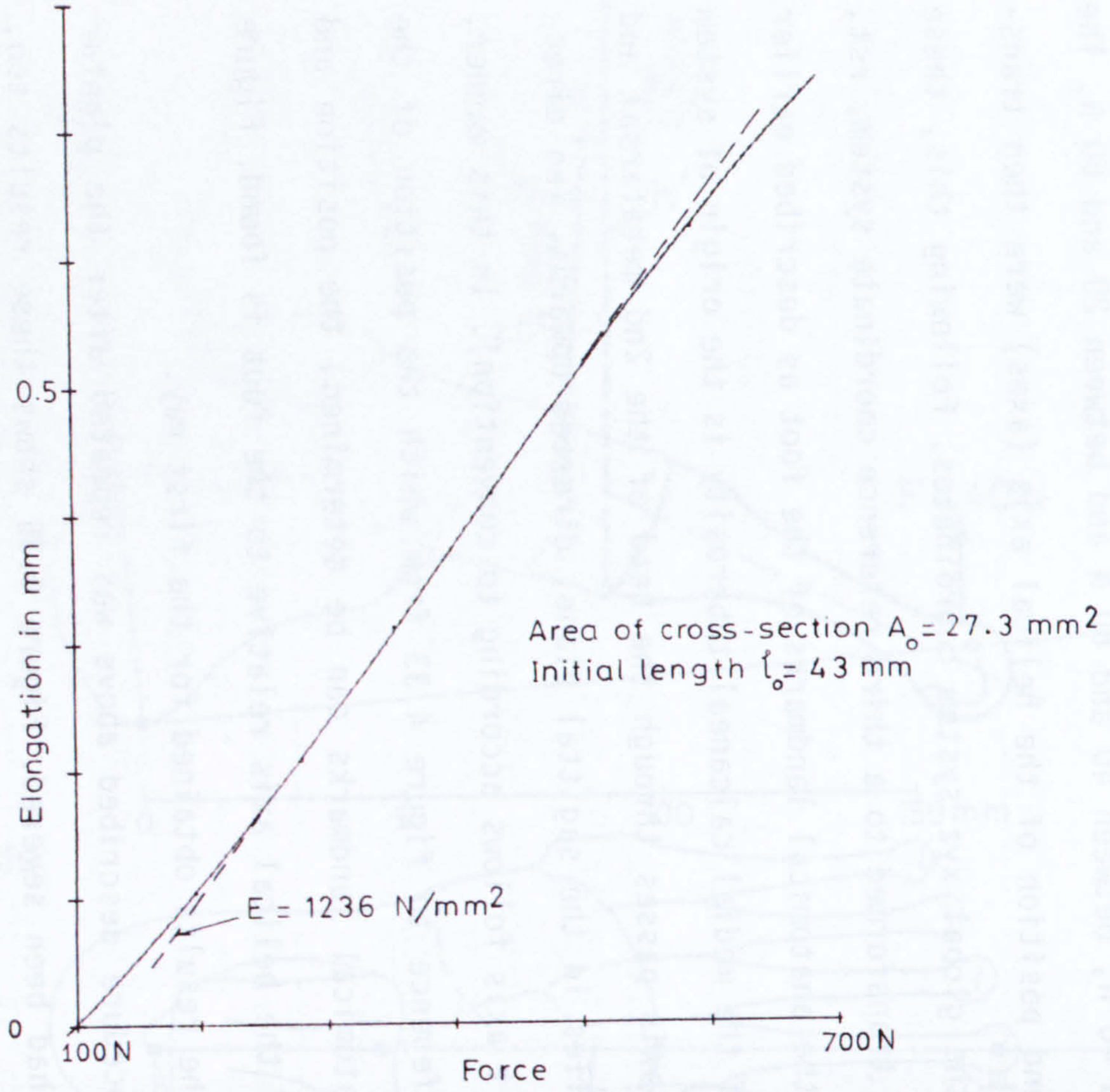

Figure 4·37 Test results obtained with plantar aponeurosis

cimen started to extrude in the area immediately adjacent to the grips. Testing was discontinued at this point. From the load-extension curve plotted, and based on an initial length of specimen of 43 mm that was measured at the pre-load of 100 N, the stress-strain curves presented in figure 4.37 were obtained. This stress-strain relationship corresponds to a Young's modulus of 1236 N/mm^2.

4.6.4 Conclusions:

The results presented in the above Sections 4.6.3.1, 4.6.3.2, 4.6.3.3 , 4.6.3.4 and 4.6.3.5, allow the following conclusions to be drawn:

- Neglecting the possible action of muscle forces, the foot on a horizontal surface bearing a vertical load through the ankle joint is acted upon by ground reaction forces under the medial tuberosity of the calcaneus and under the heads of the metatarsals so that the forefoot carries about 31% of the total load, or is acted upon by about 45% of the force under the heel; the force under the forefoot (metatarsal heads) being distributed in the ratio of about 1.3:2:1:4 amongst the 1st, 2nd and 3rd rays and the rest of the forefoot, respectively. This force distribution pattern is probably explained by freedom of movement in the talocrural and talocalcaneonavicular joints that leads to a fairly symmetrical force distribution across the forefoot with perhaps a slight bias towards the lateral side due to some degree of inversion of the foot, as would be expressed by the ground force acting under the medial tuberosity of the calcaneous.
- The ground reaction forces under the metatarsal heads lead primarily to bending stresses in the diaphysis of the metatarsal bones, even with the plantar aponeurosis intact. On severing the attach-

ment of the plantar aponeurosis to the forefoot, however, the bending stresses were observed to increase by about 24% in the 1st metatarsal and by about 12% in the 2nd metatarsal, thus reflecting the stiffer cuneiform-metatarsal joint of the 2nd ray.

- A vertical load of 60 N under the metatarsal head gave rise to the following bending strains in the diaphysis of the metatarsal bones (at mid-length):

1st metatarsal:	+280/-320 µm/m	µm/m ≡ x 10^{-6}
2nd metatarsal:	+1150/-1030 µm/m	
3rd metatarsal:	+1100/-1320 µm/m	

Positive strains are tensile and were measured on the plantar side whereas negative strains are compressive and were measured on the dorsum of the bone. These values apply to the foot with an intact plantar aponeurosis, with a Young's modulus of 1236 N/mm^2.

- Movement in the cuneiform-metatarsal joint due to the ground reaction force under the metatarsal head is indeed very limited. A difference of force of 40 N (60N-20N) under the head gave rise to an observed rotation of about 1.5° in the case of both, the 1st and 2nd rays. With reference to figure 4.35 it can be seen that the angular movement in the joint of the 1st ray has mainly the character of abduction (internal rotation) rather than dorsal flexion. In the case of the 2nd metatarsal, this experimentally determined value is probably much greater than the true amount of rotation in the joint, since the change in slope of the elastic curve of this slender bone in bending can be expected to have a major influence on the measurement of such small angles of rotation.

4.7 Discussion and Concluding Remarks:

The strain measurements described in Section 4.6 show that in the absence of muscular activity, the 1st, 2nd and 3rd metatarsal bones are mainly loaded in bending (like cantilevers), and as such are stressed to about +/-1.6, +/-7 and +/-5.5 N/mm^2, respectively (assuming a modulus of elasticity of 15 kN/mm^2 for cortical bone) when the forefoot is loaded with a total force of 91 N which corresponds to a total load on the whole foot of 294 N. Also assuming an ultimate tensile strength of 90 N/mm^2 for cortical bone (Evans, 1973) and the same force distribution among the metatarsals, the maximum total load on one foot which could be sustained might then amount to over 3000 N. This shows that as far as only the strength of the metatarsal bones is concerned, the foot may well be able to carry a total load of over 900 N without muscle action (200 pounds according to Basmajian and Stecko, 1963) but certainly not by virtue of the structure behaving like a three bar truss. In fact the high bending moments at the metatarsal bases can in this state only be resisted by corresponding tensile forces in the long plantar ligament and in the short plantar tarsometatarsal ligaments (cuneo-metatarsal 2 and 3, which as noted by Sarrafian, 1983, was considered by Sappey already a century ago to be the key of the tarsometatarsal arch!). Overstressing of these ligaments can alone be prevented by the action of the flexor muscles which would then convert the cantilever beam mechanism of the metatarsals into that of a truss system. The action of the plantar aponeurosis in this sense has probably been overestimated by some others (Hicks, 1954, 1955; Wright and Rennels, 1964). Any doubt as to whether the elastic properties of the plantar aponeurosis had suffered any change and could therefore have been

responsible for inadequate bracing of the arch, might be dismissed on the grounds that the Young's modulus determined (E = 1236 N/mm^2) proved to be even 46% greater than the values given by Wright and Rennels (1964). The considerable discrepancy is probably due to the well-known problems associated with testing soft tissues such as the influence of loading rate, difficulty in determining the area of cross section, errors involved in measuring extension, etc. Nevertheless, the higher modulus of elasticity of the plantar aponeurosis obtained in the present study precludes the objection that a loss of stiffness might have been responsible for the conclusion arrived at above.

Of the several models that have been devised to illustrate the nature of the foot as a mechanical structure, the one presented by R. Fick (1911) seems most appropriate. In this model, the foot is divided into five individual longitudinal arches, each arising from the calcaneus and terminating at a metatarsal head. The in-vitro loading investigations (Section 4.6) have shown that in the foot flat position a vertical load on the ankle joint is carried by the medial tuberosity of the calcaneous, posteriorly, together with all the metatarsal heads, anteriorly. Without any muscle action whatever, the forefoot in the foot flat position was observed to carry about 31% of the total load on the foot; this being distributed in the ratio of about 1.3:2:1:4 amongst the 1st, 2nd and 3rd rays and the rest of the forefoot, respectively. Interestingly, on attaching the Achilles tendon to the tibia support (fig 4.30) so as to load the forefoot alone without subjecting the heel to any ground force, the centre of pressure was found to lie between the heads of the 2nd and 3rd metatarsal bones. This shows the inverting action of the

triceps surae muscle in balance with the eversion caused by a dorsally directed force acting in the region of the 2nd and 3rd metatarsal heads about the talocalcanionavicular joint axis. Hence, with the simultaneous action of the triceps surae muscle a different load distribution across the forefoot might be expected than when the heel is on the ground and no muscular activity whatever is present. As already once mentioned, if the metatarsal bones are to act as individual trusses, it becomes obvious that each must be furnished with its own muscular 'tie rod', as discussed below:

The abductor of the great toe, arising from the heel and inserting into the medio-plantar aspect of the proximal phalanx probably plays a major role in actively sustaining the medial longitudinal arch of the foot, along with the flex.hall.brev. and flex.hall.long. muscles. Considering the foot at about 50% of the walking cycle with about 30° dorsiflexion in the MP-1 joint and with the foot in about 15° of toe-out relative to the direction of progression, the action of the abductor in the MP-1 joint, counteracting external rotation of the toe and simultaneously assisting in imposing resistance to dorsal flexion, is perfectly suited to the situation - taking for granted that an abduction moment across the MP-1 joint can be effected even without evidence in the form of gross joint motion. This would also explain the relatively large mass of this intrinsic muscle. In addition to this, the powerful flex.hall.long. also has a tie rod effect in supporting the arch.

In the other rays of the foot, the flex.digit.brevis and the flex.digit.longus muscles would exhibit a similar bracing effect on the individual longitudinal arches.

Also Carlsöö and Wetzenstein (1968), in a radiologic study of the change of form of the foot skeleton upon momentary weight-bearing, reported no significant variation in the distance between metatarsal heads and the most plantar point of the calcaneous, on weight-bearing. No appreciable change in dimensions in the transverse direction, within the region of the metatarsal heads, could either be observed. This too was apparent during the in-vitro loading experiments described in Section 4.6 even after severing the transverse attachments between the MP joint capsules. Nevertheless, some transversal movement might occur when the transverse ligament is lax, especially between the 1st and 2nd rays, as encountered in some clinically normal feet and in all those with a hallux valgus deformity, due to displacement of subcutaneous tissue in a medial and lateral direction under weight-bearing and also possibly through the action of the abductor hallucis together with perhaps, the abductor digiti minimi.

Finally, it must be mentioned that because of the almost insurmountable difficulty encountered in attempting to measure the angle of pennation of the intrinsic muscles of the foot - this at the best involving a high degree of subjectivity - it was decided not to present any values regarding the physiological cross sectional area (PCSA) of these muscles. Instead, Table 4.1 shows the cross sectional area of tendons, as far as these were able to be measured, and the mass of some of the muscles. It is hoped, however, that this information might be of some value in supporting the estimation of muscle forces called upon to overcome external loads, as undertaken for instance in Chapter 6.

CHAPTER 5

LOCOMOTION STUDIES

5.1 Introduction

In the introductions to the preceding chapters, mention has been made of the information required, but still lacking, to gain a better understanding of the biomechanics of the forefoot. To estimate the forces acting across the joints it is imperative to know the magnitude of the ground reaction forces exerted upon the toes and, of course, the mechanical arrangement of the relevant tendons, in relation to the geometry of the joint surfaces, that serve in producing such forces. While determination of these anatomical details was the subject of Chapter 4, the following sections in this chapter deal with the position of the foot (toe-out) relative to the direction of progression and with the measurement of forces under the toes and heads of the metatarsals while walking.

The investigation relating to toe-out as described in Section 5.2 was considered necessary because of the considerable inconsistency in values reported in the literature, as already discussed at length in Section 2.7.2. These results, together with cinematographic observations of the movement of the foot, especially during the push-off phase of walking, enable the movement in the metatarsophalangeal joints to be described. Furthermore, such information is required to estimate force reactions that might involve even ligamentous structures.

Because an estimation of joint forces can only be arrived at by measuring external reactions, several test series were carried out with various collectives of test subjects to determine the ground forces that act on the heads of the metatarsals and the pads of the toes. This included observations with stiff soles that restricted movement in the metatarsophalangeal joints and with flexible

soles that permitted free flexion. Also, the effect of toe-out, walking at various speeds on a level open floor, walking on a moving belt (tread mill) that was adjustable from walking up-slope (+15°) to down-slope (-15°), and climbing stairs, were observed. Section 5.4 gives details of these tests.

5.2 Determination of Toe-out

5.2.1 Method and Material:

The procedure adopted to observe the toe-out has already been described in details in Section 3.4. In this study a total of 100 feet were evaluated of which two cases with pronounced toe-in, one of which exhibited a definitely pathological gait, were excluded. the remaining 98 feet belonged to an age group of 20 to 60 year-olds with the majority (about 60) between 20 and 40 years of age. The whole collective might be considered as normal and healthy since the individuals observed were employees of the clinic on their way to work. Also, since the majority were not aware of being observed by the hidden camera (see Section 3.4.1) - and those who did detect the camera were certainly not aware of its purpose - it is most improbable that the observed walking style had suffered any alteration whatever.

As described in Section 3.4.2, the angle between the direction of progression and the tangent along the inner edge of the shoe sole was determined. By adding 5° to this value (see Section 3.4.2) the toe-out, or angle of gait, as referred to the anatomical longitudinal axis of the foot was obtained.

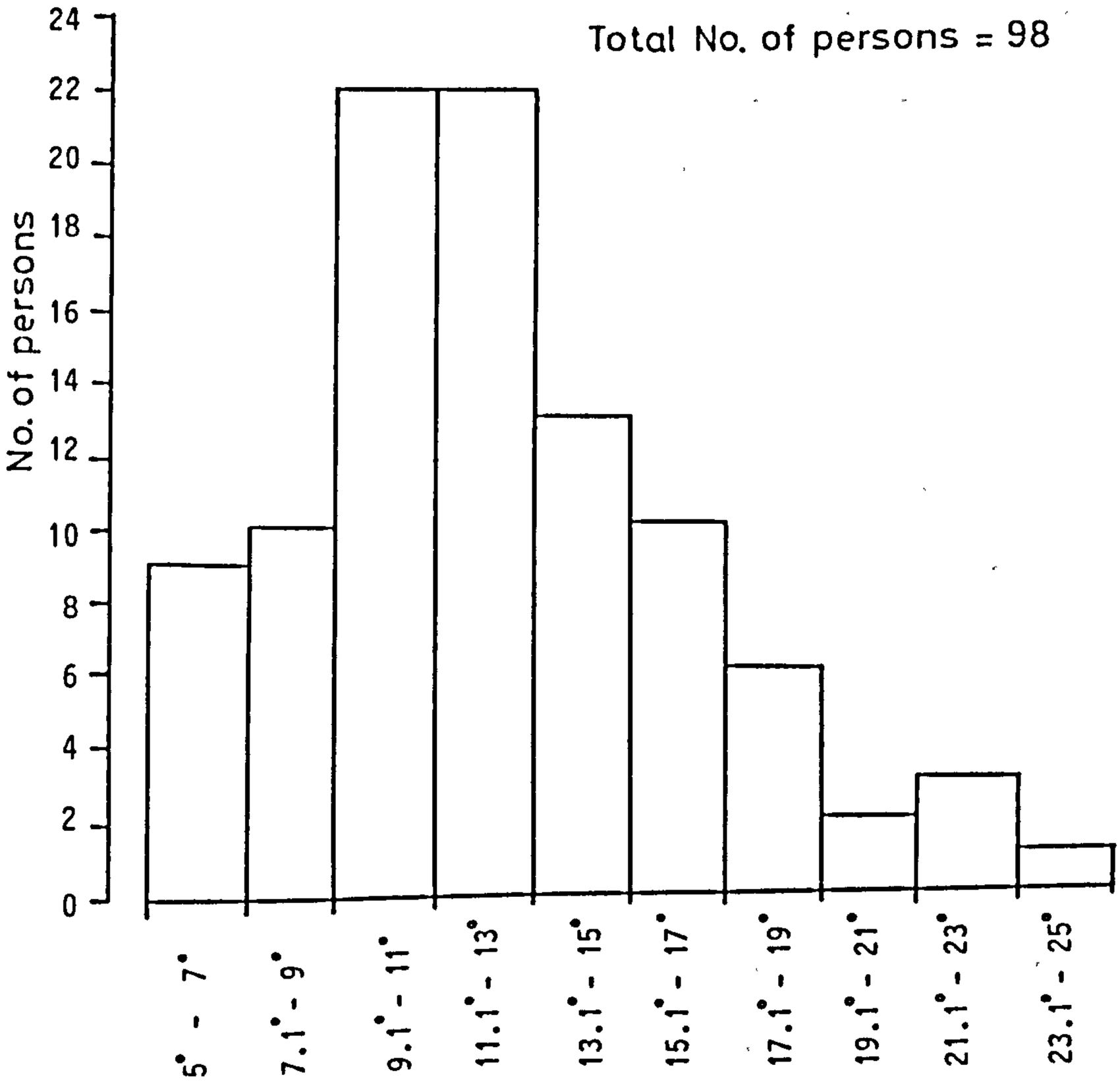

Toe-out mean: 12°

Figure 5.1: Histogram showing distribution of toe-out

5.2.2 Results

Figure 5.1 shows a histogram illustrating the distribution of toe-out angles grouped into 10 grades as observed from the 98 feet studied. The mean value amounted to 12° with the lowest and highest values measuring 5° and 23° respectively.

5.2.3 Discussion and Conclusions:

The relevance of toe-out with respect to load distribution under the ball of the forefoot as pointed out by Elftmann (1934) and as discussed by Bojsen-Møller and Lamoreaux (1979) on considering the importance of the movement of the toes during walking (see Sections 2.7.2 and 2.7.3 of Chapter 2) is a matter which still deserves further investigation. The present study has shown that a randomly selected group of feet of healthy men and women from 20 to 60 years of age, with the majority between 20 and 40, exhibit an average toe-out angle of 12° which corresponds closely to that given by Ducroquet (1965), Frostell (1926) and Klein-Vogelbach (1976), as shown in Table 2.3 of Chapter 2. However, it has also been observed that this value not only can vary by more than +/- 7°amongst individuals with normal gait, but that it varies considerably in a given person too, depending on the speed of progression and on the physical properties of the ground. While some authors have reported a marked difference between the toe-out of the left and right foot (Brinckmann, 1981; Dougan, 1924; Frostell, 1926) no such difference was observed in the present study. However, it has been noticed with test subjects on a moving belt (treadmill) that the foot closer to the person conducting the test, and who stood beside the moving belt, most often exhibited a greater toe-out angle than that of the other

foot. Also, it has been observed that footprints in soft soil (slush) or snow definitely show a greater amount of toe-out than on firm ground; this probably to increase the stability in stance by virtue of the greater transversal bearing area, and also possibly to aid forward propulsion of the body by employing a thrust normal to the broad side of the whole foot instead of rolling over the ball of the forefoot and using the push-off afforded by the metatarsal heads and toes only.

Even though in this study it was not possible to measure the change in toe-out with change in speed of progression, the average value of 12° obtained was a useful confirmation of the toe-out angle given by some investigators in contrast to that given by some others. Also, it might be maintained that, as reported by Frostell (1926), the toe-out or angle of gait, decreases with increase of walking speed and that, as pointed out by Murray et al. (1964), increases in the aged.

5.3 Cinematographic Studies of Foot Movement

5.3.1 Method and Material:

In order to especially observe the movement in the metatarso-phalangeal joints during the 'push-off' phase, when walking bare-foot, cinematographic investigations were carried out to document the movement of the mid-foot relative to the ground. This was done by observing the movement of marker triads that had been attached to the foot, from two directions.

Since only one high-speed camera was available, a mirror was

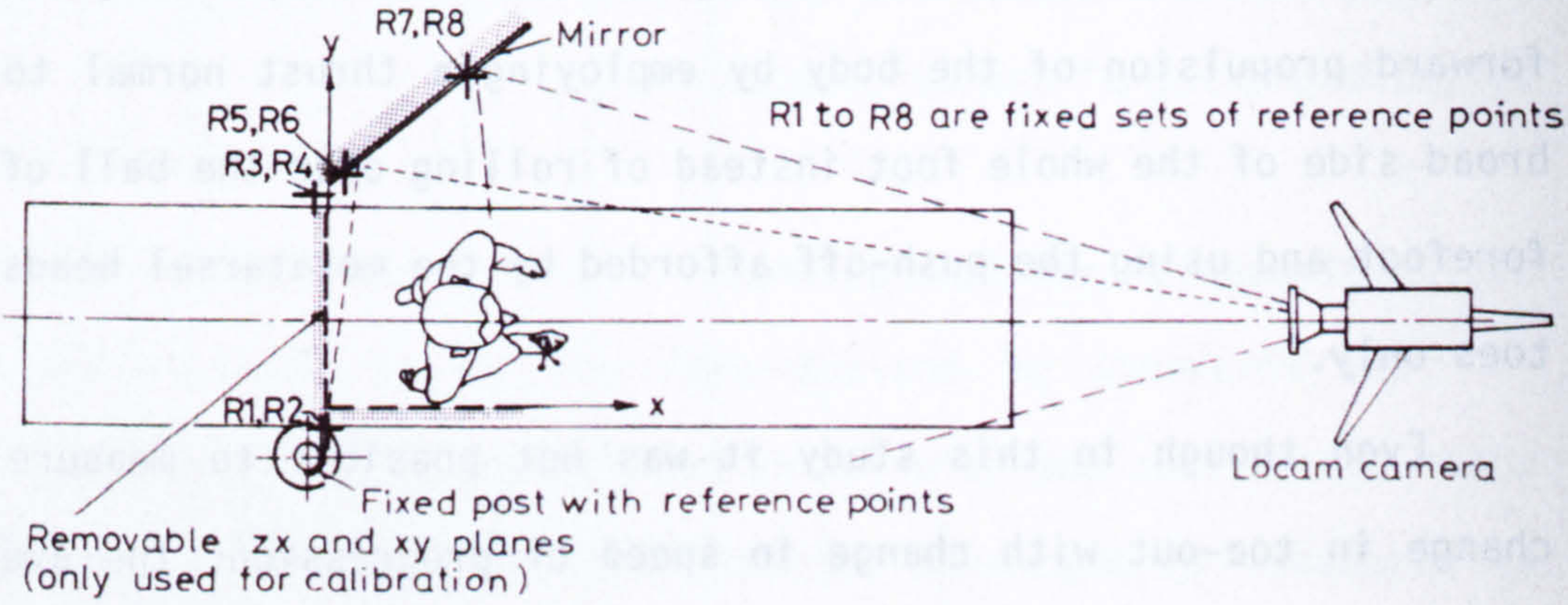

Figure 5·2a Arrangement for determining movement of the foot (MP joints) when walking

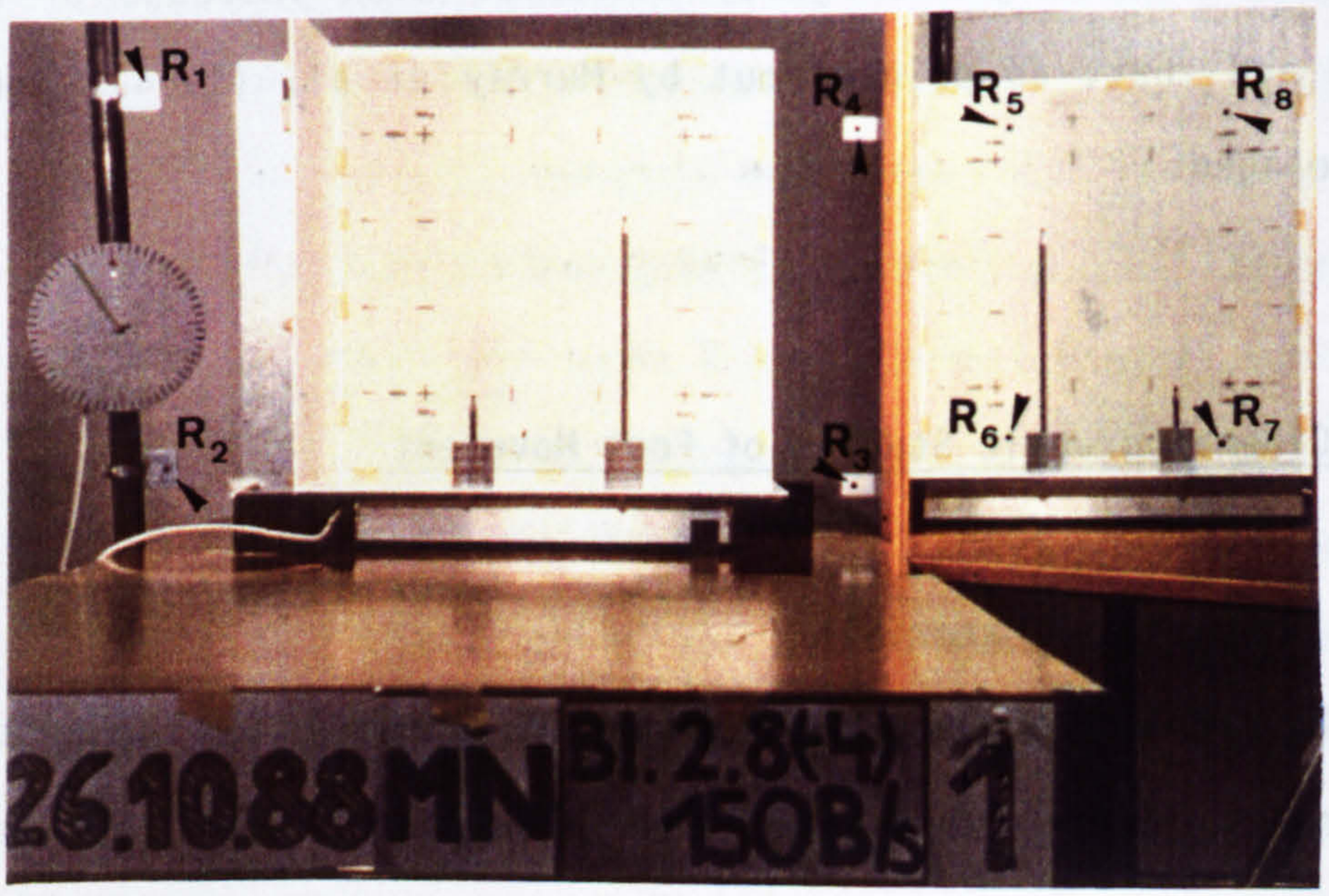

Figure 5·2b View through the camera lens showing calibration markers and stationary reference points

used to form a split picture, one part of which was as observed directly from the front, while the other part was observed from the side, as reflected by the mirror. Figures 5.2a and 5.2b show the arrangement. A walkway of 80 cm width and 480 cm length, 60 cm above floor level, was used for the test subject to walk along. The LOCAM film camera fitted with a 'KERN Vario Switar' zoom lens of 12.5 to 100 mm focal length was located about 250 cm away from the end of the long walkway. A mirror of 60 cm breadth and 120 cm height was placed vertically at an angle of about 45° to the longitudinal axis of the walkway as shown in Figure 5.2a. On both sides of the walkway, in the immediate vicinity of the mirror, two vertical posts that carried markings (fig 5.2b) were placed. The mirror surface too carried four spots arranged approximately at the corners of a square of 50 cm side length (fig 5.2b). On looking through the camera lens, the central part of the walkway is seen with the two posts on either side of it, and the whole width of mirror (at a slant of about 45°), too. Also to be seen are the four markings R1 to R4 on the posts as well as the four similar markings R5 to R8 on the mirror surface.

To calibrate the set-up, an xyz-stage (fig 5.2b), as described and shown in Section 3.3.3 was used. The stage is so placed, that either the yz or the zx plane (depending on which side of the walkway the mirror is located) comes to lie between the two vertical posts. The calibration procedure remains the same as described in Section 3.3.4.1, only that the whole picture seen must first be split into two parts - the one seen directly, and the other seen in the mirror - before treating each part separately. This results in the determination of the location of two cameras in xyz space, one real and one virtual. At the same time, the yz (or zx) coordinates of the

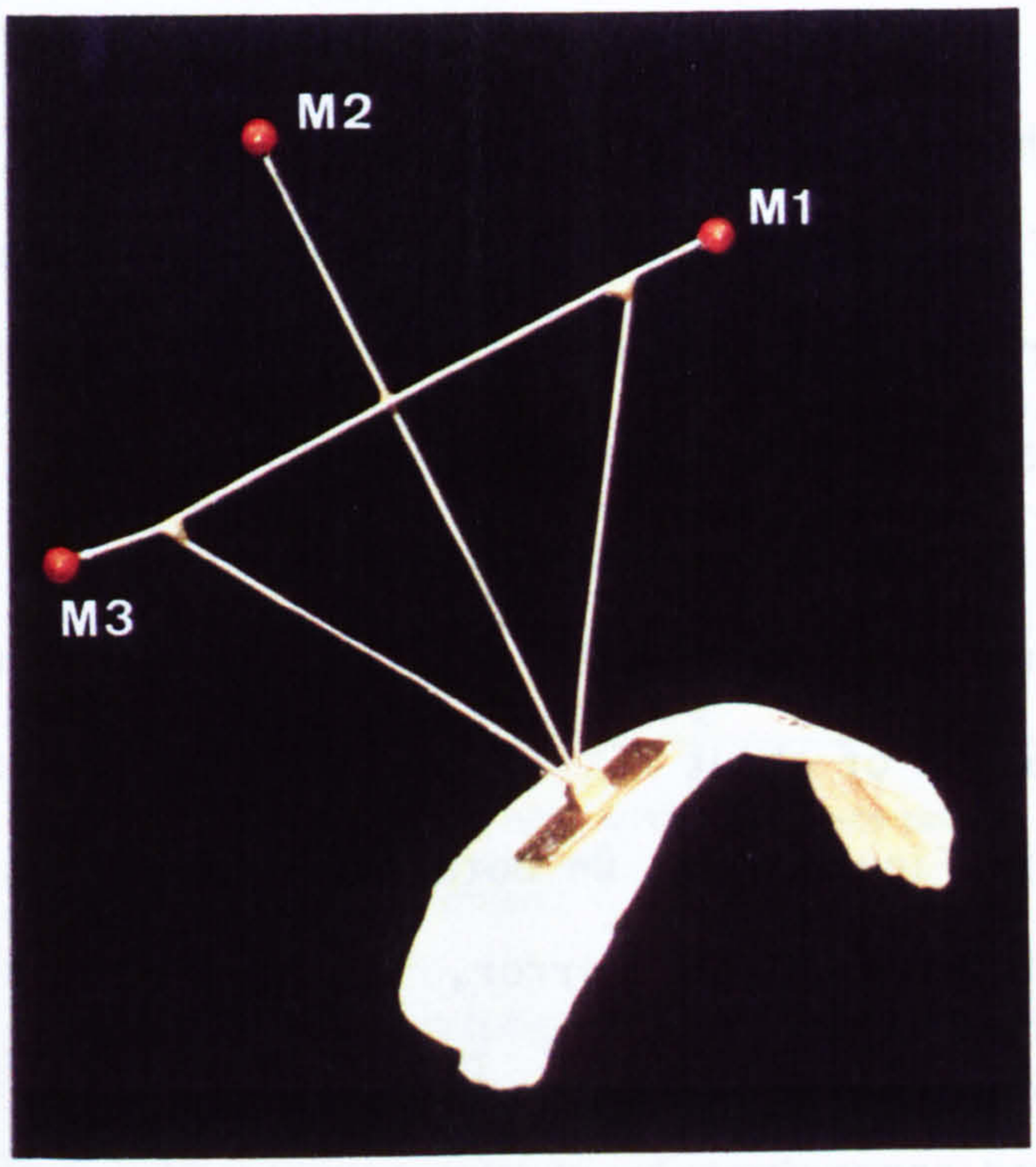

Figure 5·3a

The marker triad fixed to a saddle of bone cement

Figure 5·3 b View through camera lens showing marker triad on foot and stationary reference points on split picture

four markings R1 to R4 on the two posts, and the zx (or yz) coordinates of the four markings R5 to R8 on the mirror surface, as seen by the camera are noted. After this, the xyz stage is removed and the test subject filmed while walking along the walkway, from the far end towards the camera. [As mentioned in Section 3.3.3, the camera adjustments must remain absolutely unaltered from the instant the calibration pictures are taken up to the end of the test]. It is important to observe that the two sets of four reference points (R1 to R4 and R5 to R8) do not represent the four corner points of a rectangle in the yz or zx planes as had been called for in the procedure described in Section 3.3.3 of Chapter 3 (fig 3.10). Therefore, a method was further developed allowing the known coordinates of four corner points of a general quadrilateral (as in the present case) to be used in order to determine the true picture coordinates of any other point projected onto the same plane (zx or yz), even when the final projection is distorted. Appendix 1(5) gives details of the procedure and describes the relevant programme DIGXY.FLM. Apart from this, the same procedure is followed as described in Sections 3.3.3 and 3.3.4].

Marker triads (M1, M2, M3) were placed over the cuneiform and cuboid bones of the test subject by the aid of a saddle moulded from acrylic bone cement and made to fit the dorsum of the foot exactly (fig 5.3a), taking care to ensure no burns occurred due to the exothermal heat generated on curing. The saddle was then strapped firmly onto the foot by means of elastic bandage. [Initially, a marker triad had also been attached to the toe nail of the 1st digit by using a fast-setting cyano-acrylic cement to fix a light-weight paper cone that carried the cross-wires with coloured beads. It was, how-

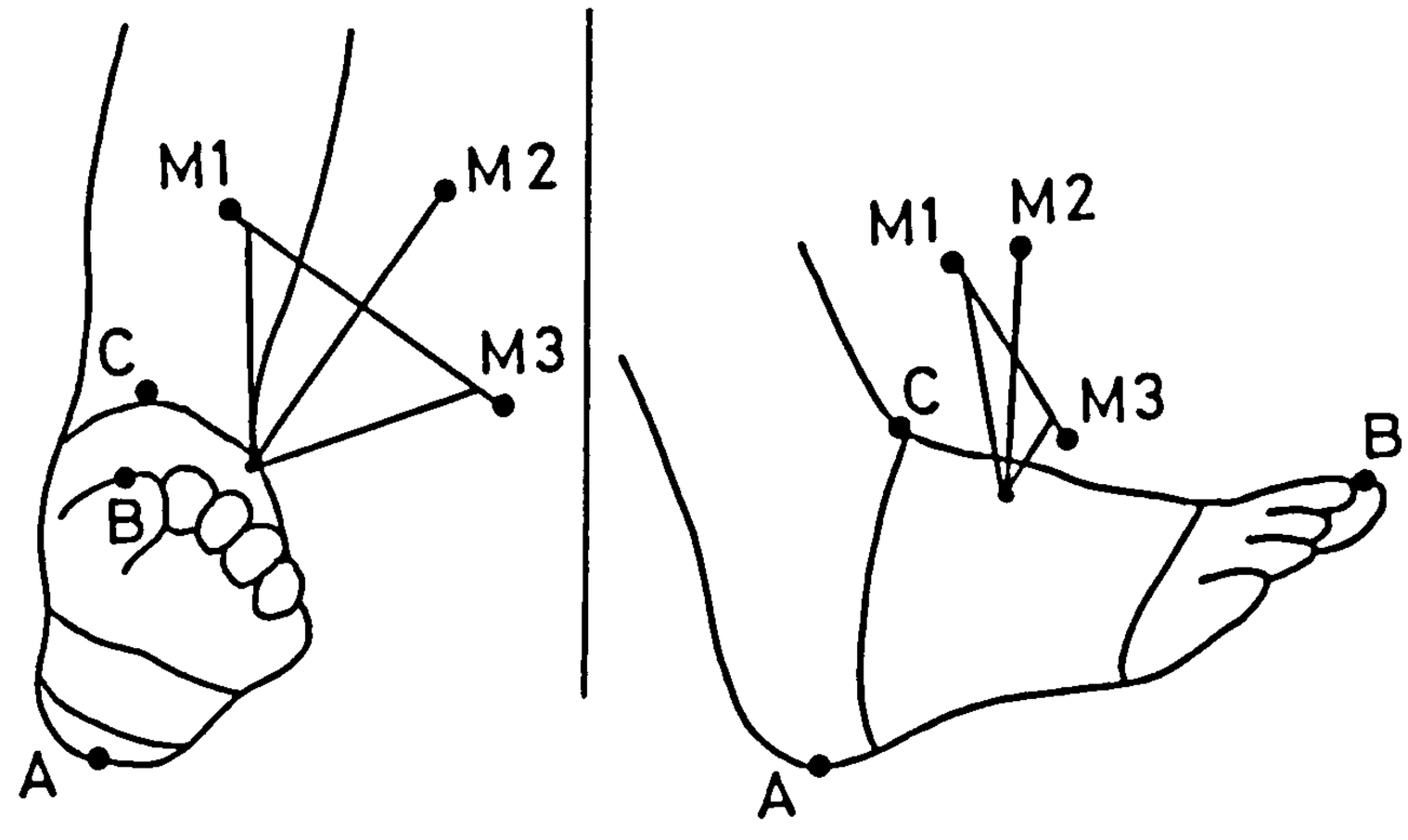

Figure 5.4 View of anatomical landmarks as indicated by points A, B and C in relation to the markers M1, M2, M3

ever, seen that movement in the interphalangeal joint precluded the assumption that movement of the distal phalanx (toe nail) could approximate that of the whole toe, and therefore this arrangement was abandoned].

As the test subject walked along the walkway, the foot movement could be seen through the mirror only for a short time, and therefore to ensure the foot in walking had been placed in front of the mirror so that the whole event from heel-strike to toe-off had been captured, it was necessary to repeat the performance several times. Walking was always maintained at a comfortable pace of about 60 m/min while filming at a rate of usually 150 frames/s.

Evaluation was performed by first reading off the projections of the markers M1, M2 and M3 on the yz and zx planes with the aid of the stationary reference points R1 to R4 and R5 to R8, respectively, the virtual yz and zx coordinates of which are known (fig 5.3b). Furthermore, since any description of spatial movement of the foot, as determined by the marker triad (M1, M2, M3) will still bear no direct relation to anatomical landmarks of the foot, the latter had to be first defined. This was done by selecting three points on the foot: point A in the middle of the plantar surface of the heel, point B on the medio-distal corner of the great toe nail and point C on the ventro-dorsal aspect of the ankle, just below the superior extensor retinaculum and over the tibialis anterior tendon (fig 5.4).

As mentioned earlier, in Section 3.3 of Chapter 3, the helical axis of motion gives a complete description of the general motion of a body in space, and therefore the spatial positions of the markers M1, M2 and M3 were recorded at particular moments during the stance phase. These were:

- t1, when the heel had just contacted the walkway and the plantar aspect of the foot could still be seen (only at this instant were the positions of A, B and C also registered!);
- t2, when the heel was just about to rise off the walkway;
- t(45%), corresponding to 45% GC (gait cycle);
- t(55%), corresponding to 55% GC;
- t(62%), corresponding to 62% GC;
- t3, when the ball of the foot (head of metatarsal 5) was just about to lift off the walkway. (This instant sometimes coincided with t(62%), but occurred on an average at 65% GC).

These instants were chosen for the following reasons:

The recordings at instant t1 are of necessity because only at this moment are all three anatomical landmarks (A, B and C) on the foot simultaneously visible along with the marker triad (M1, M2, M3). At this instant, each of the points A, B and C can be related to a Cartesian sub-system uvw defined by M1, M2 and M3. Thereafter, the spatial positions occupied by A, B and C can always be determined in the global coordinate system xyz with the help of the positions adopted by M1, M2, M3 even when the former cannot be seen. The instants t_2 and t_3 are obviously of prime interest because they mark the beginning and end of the range of movement in the MP joints with the toes still practically in a horizonal position ('digitigrade' phase as termed by Bojsen-Møller, 1979). At about 45% GC the ground forces under the metatarsal heads reach their peak values and at about 62% the forces under the metatarsal heads drop to zero (see Section 5.4). The t(55%) instant was of interest because trajectorial traces of M1, M2 and M3 between t_2 and t_3 showed a change in direction about the instant which might have been an indication of a change in direc-

tion, or position, of the helical axis. In Appendix 2(5) a trace of the marker M2 is shown to illustrate this. Furthermore, t(55%) approximately halves the interval between t(45%) and t_3. The picture frames on the film that corresponded to the above mentioned instants in the gait cycle were found by dividing the total number of frames from heel-strike to heel-strike, accordingly.

Acopting the procedure described in detail in Sections 3.3.2 and 3.3.3 of Chapter 3, helical axes were determined for the intervals t_2 to t(45%), t_2 to t(55%), t_2 to t(62%) and t_2 to t_3. Programme HELIROD.J (Appendix 5(3)) was employed. Only in two test cases were helical axes determined during the intervals t_2 to t(55%) and from t(55%) to t_3. Appendix 2(5) gives some details of the procedure.

Transformation of the coordinates of points A, B and C at instant t_1 from the xyz system to the sub-system uvw was performed with programme TRAN-XYZ.UVW, and the re-conversion into xyz coordinates at instant t_2 (foot-flat), with programme TRAN-UVW.XYZ (Appendices 8(3) and 9(3).

In this manner the location and direction of the helical axis relative to the anatomical landmarks A, B and C were arrived at. An outline of the test subject's foot on a sheet of plain paper, that included the anatomical landmarks A and B, enabled allocation of the axis of rotation to the foot contour as shown in figure 5.5. [The anatomical landmark C was occasionally used together with A and B to define a further cartesian coordinate sub-system, rst, to facilitate quicker comparison of the position and direction of the helical axis relative to the foot, amongst the feet investigated. This was done by transforming the helical axis from the xyz into the rst system which then provided a common and convenient base for com-

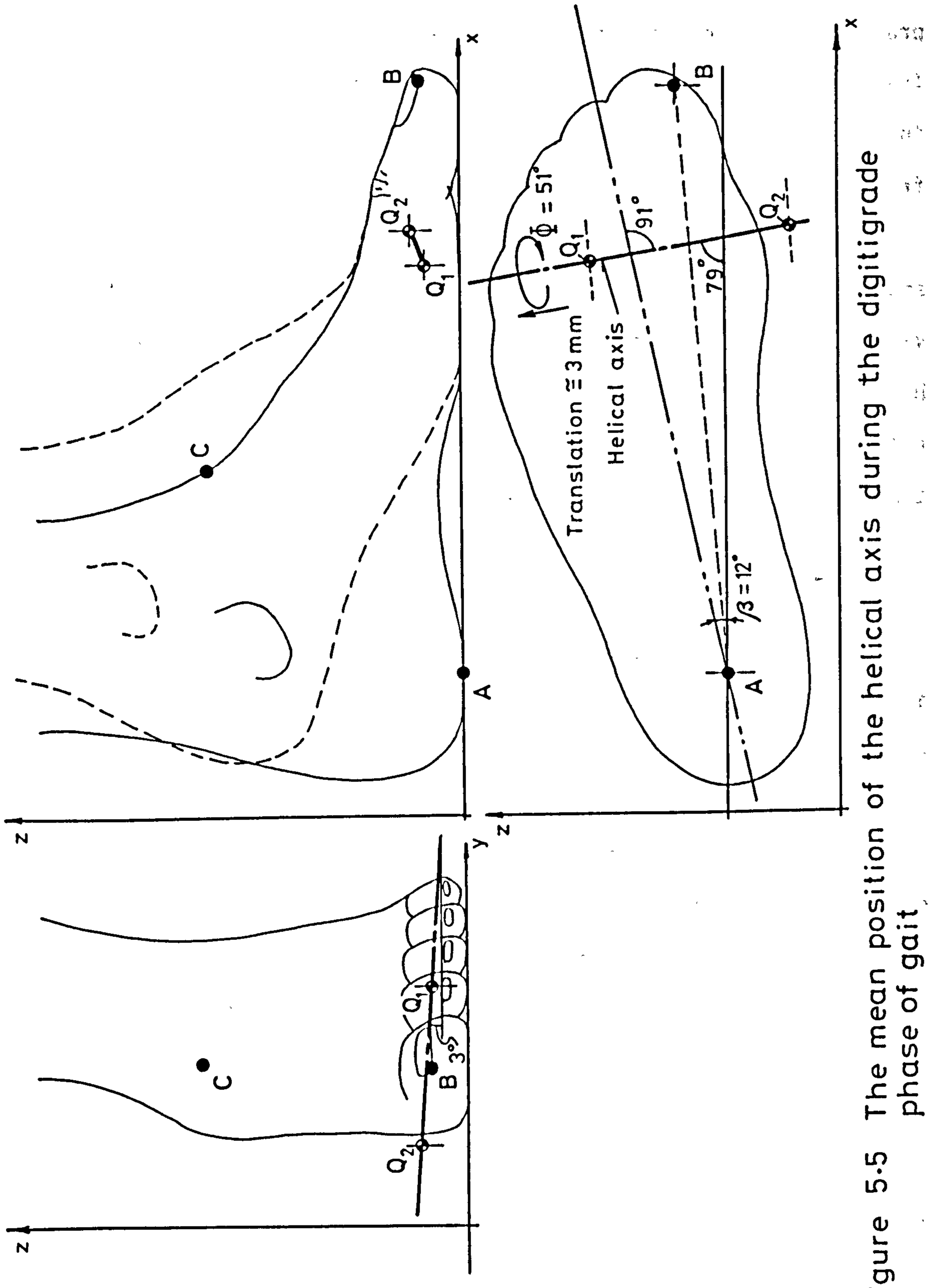

Figure 5.5 The mean position of the helical axis during the digitigrade phase of gait

parison. No further use was made of C].

Ten 'normal' feet (six females and four males) were investigated in this manner. Appendix 2(5) gives some relevant details. The tests were generally performed with habitual toe-out.

However, to observe the effect of exaggerated toe-out (36° to 43°) or toe-in (-5° to -30°) on the movement of the foot during the push-off phase of walking, four cases (one female and three males) were investigated in this manner.

Finally, as already mentioned, to observe whether the direction of the helical axis describing movement of the mid-foot relative to the ground (which approximately equals movement in the MP-joints) changes its direction appreciably during the push-off phase of walking, or not, the trajectories of the markers M1, M2 and M3 were plotted in 40 ms intervals (every 6th frame) in two test cases. [One of these test subjects (E.W.) had been chosen because of an habitual toe-out of as much as 20°]. Subsequently, helical axes were determined in each case for the intervals t(45%) to t(55%), and t(55%) to t(62%).

5.3.2 Results:

Figure 5.5 shows the mean position of the helical axis of motion as determined on ten subjects with 'normal feet'. Table 5.1 gives further details, including the range of values observed with all ten subjects walking in their habitual manner. Table 5.2, on the other hand, shows the results with the four test subjects who were requested to walk with exaggerated toe-in and toe-out.

In the two cases closely examined to observe whether the position and direction of the helical axis changes appreciably during the

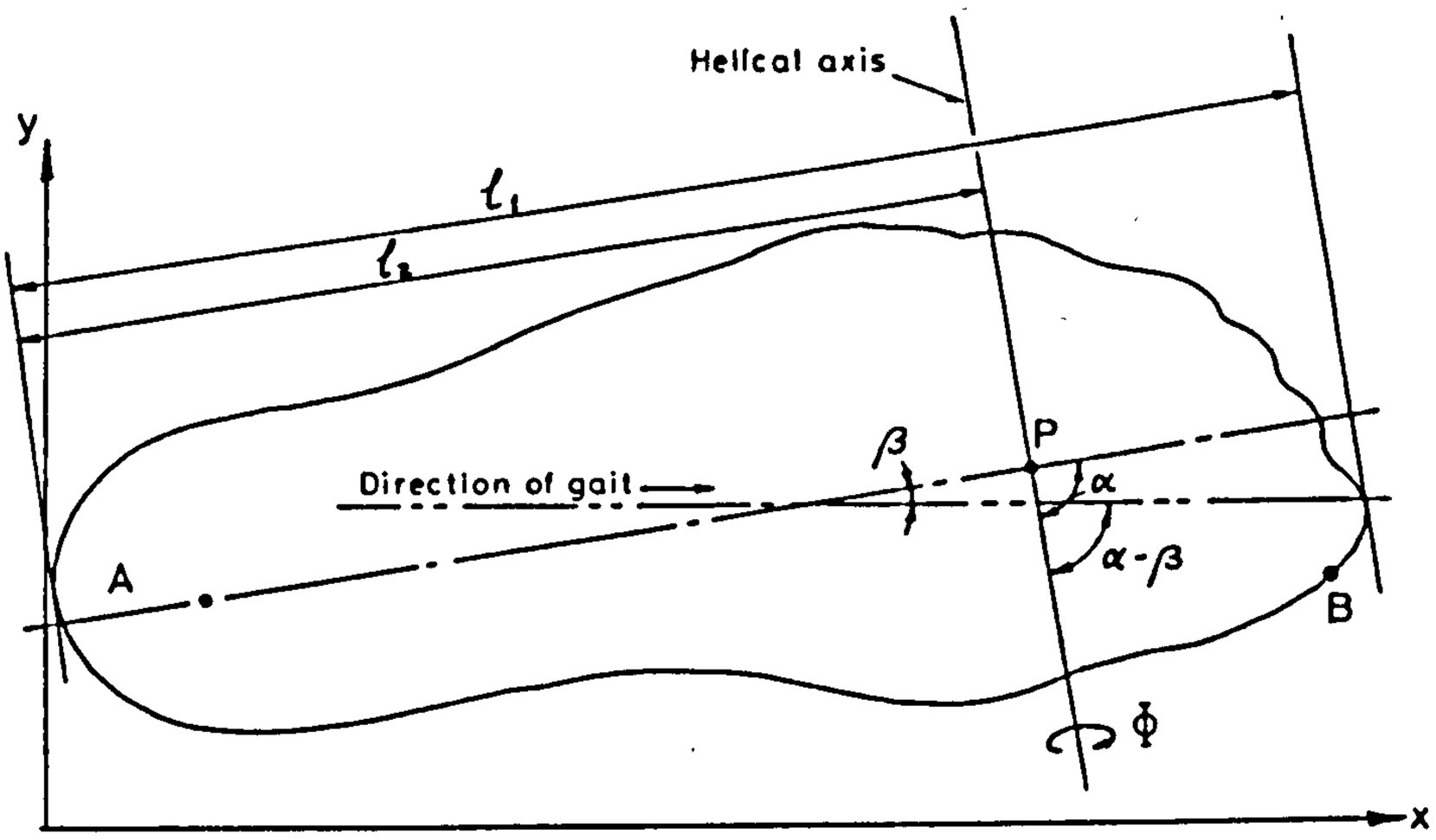

	Measured range	Mean value
Toe-out, β	3° - 25°	12°
α	81° - 102°	91°
$\alpha-\beta$	73° - 87°	79°
Dorsiflexion, Φ_{max} (from t2 to t3)	37° - 56°	51°
Translation along helical axis	0 - 4.5 mm	3.5 mm
Position of P ($l_2 . 100 / l_1$)	72% - 77% FL	75% FL
Instant t2	33% - 44% GC	38% GC
Instant t3	57% - 71% GC	62% GC

FL: Foot length

GC: Gait cycle (heel-strike to heel-strike)

Table 5.1 Some details of test results with six females and four males relating to movement of the mid-foot relative to the ground during the digitigrade phase of normal gait.

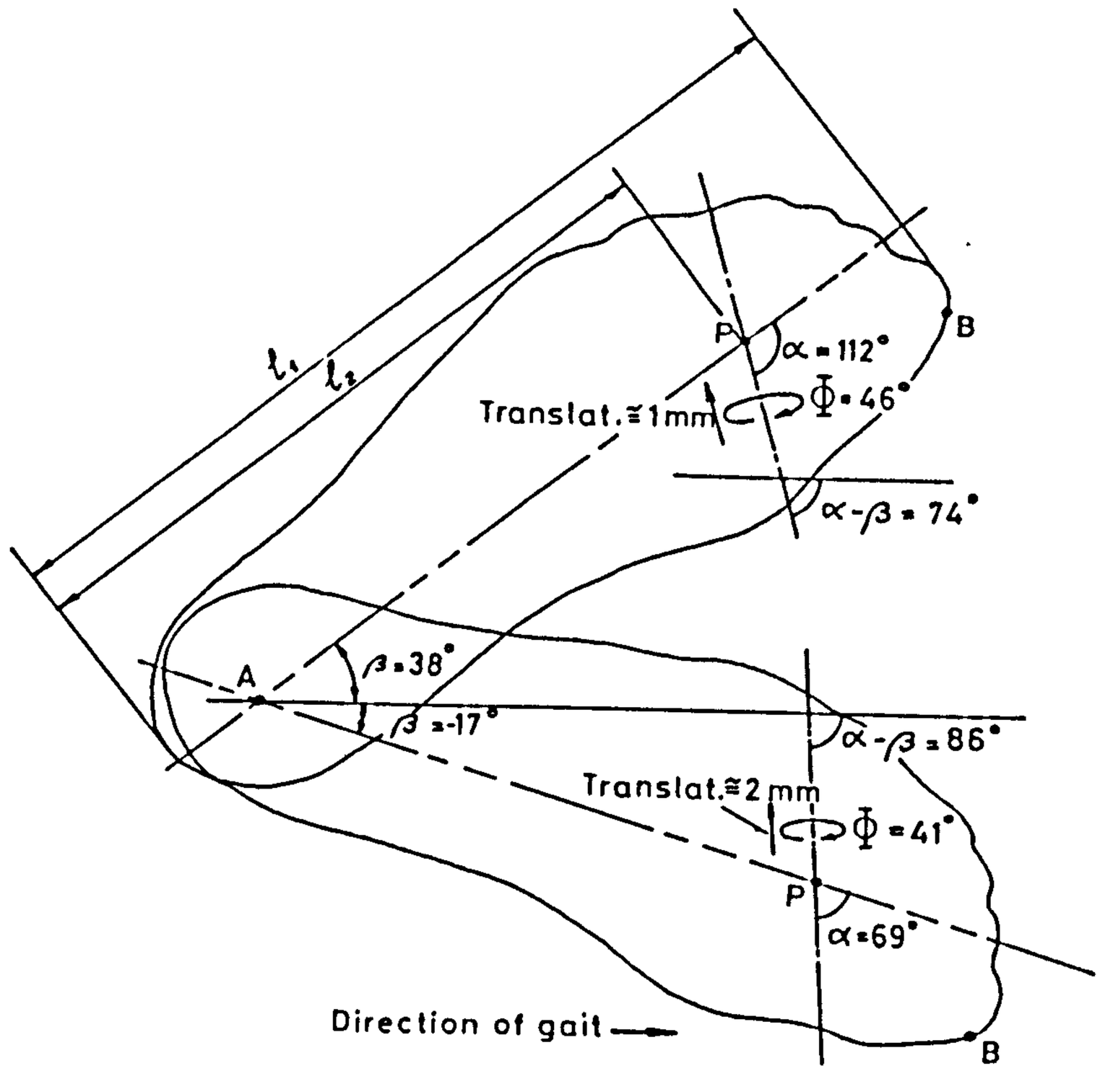

	Exaggerated toe-out		Exaggerated toe-in	
	Measured range	Mean value	Measured range	Mean value
Toe-out, β	36° - 43°	38°	-5° - -30°	-17°
α	102° - 126°	112°	51° - 90°	69°
$\alpha - \beta$	66° - 89°	74°	81° - 91°	85°
Dorsiflexion, Φ_{max} (from t2 to t3)	42° - 53°	46°	27° - 54°	41°
Translation along helical axis	-5 - +8.2mm	0.6mm	-0.5 - +4.3mm	2.2mm
Position of P ($l_2 . 100 / l_1$)	75 - 85% FL	79% FL	73 - 81% FL	76% FL

FL: Foot length

Table 5.2 Some details of test results with one female and three males relating to movement of the mid-foot relative to the ground during the digitigrade phase of walking with exaggerated toe-out and toe-in.

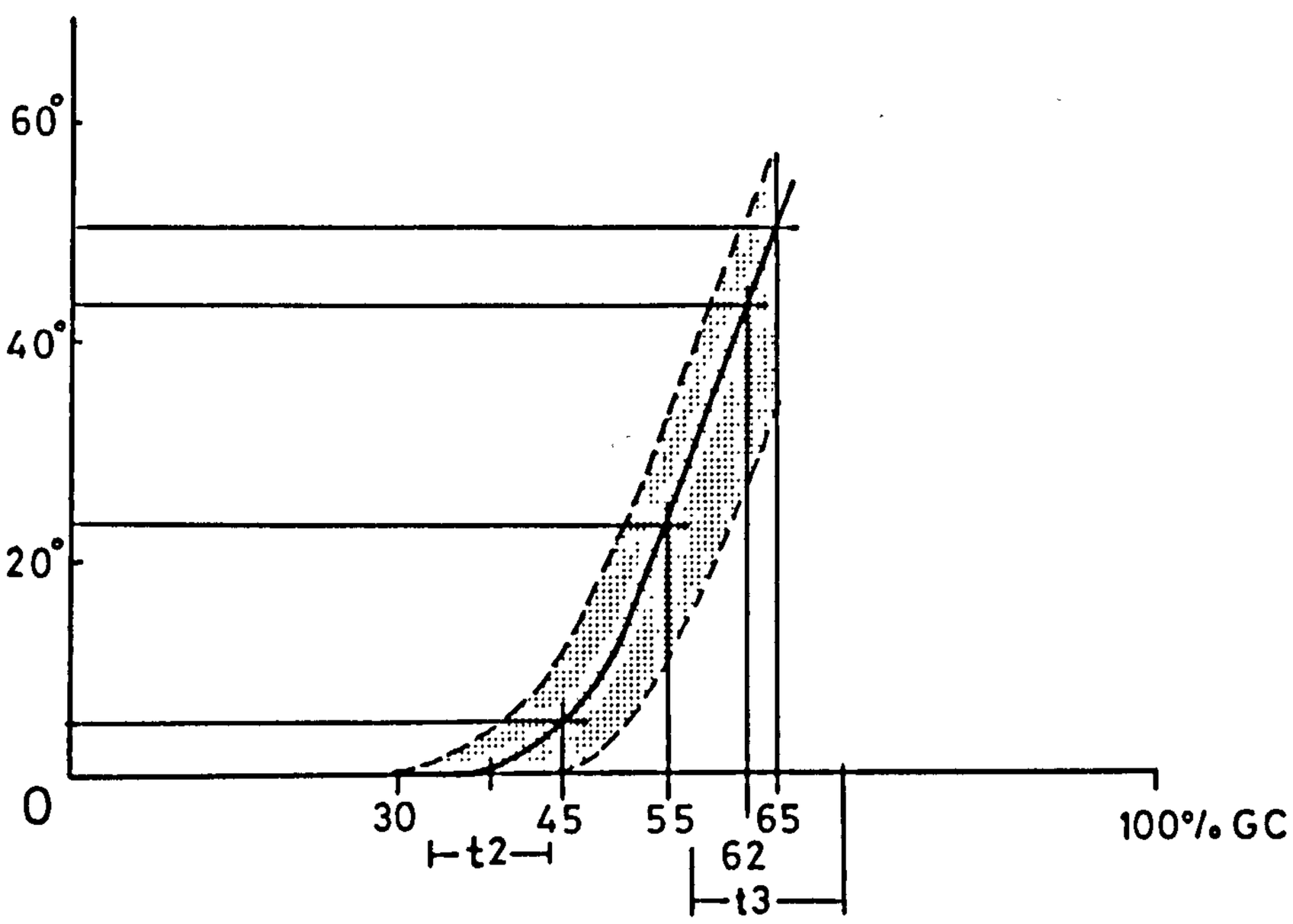

Figure 5.6 Dorsal flexion in the MP joints during the digitigrade phase of gait

interval t_2 to t_3, it was seen that from 45% GC to 55% GC the axis passes through the heads of metatarsals 1, 2 and 3 at an angle of about 76° (74° in one case and 78° in the other) to the direction of gait. Following this phase, between 55% GC and 62% GC, the helical axis was seen in both cases to move distal to the MP joints by about 18 mm and adopt a slightly altered position of 82° to the direction of progession.

Finally, figure 5.6 shows the observed angular movement of the dorsum of the foot (corresponds approximately to the movement in the MP joints) during the 'digitigrade' phase of gait. This angular movement was accompanied by a small amount of translation along the helical axis of about 3.5 mm.

5.3.3 Discussion and conclusions:

Referring to figure 5.5 it can be clearly seen that the helical axis of motion during the 'push-off' phase, or from the moment the heel has left the ground to the instant the metatarsal heads also do so, passes approximately through the heads of metatarsals 1 and 3, at an angle of about 80° to the direction of progression, directed postero-laterally in the horizontal projection. In the transversal vertical plane its projection slopes at an angle of about 3° to the horizontal. The mean value of dorsiflexion in the MP joints at 45% GC is only about 5°, but at 55% GC already reaches 24°, thereafter rapidly increasing to 43° at 62% GC, until finally at about 65% GC a maximum value of 51° is attained (fig 5.6). In this connection, attention must be drawn to the small amount of translation of only about 3.5 mm that resulted along the helical axis, thereby showing the basically 'hinge' nature of movement of the mid-foot in the MP

joints as referred to the ground.

The observation made in two cases, in which the axis of rotation appeared to move distal to the MP joints during the angular movement between 55% GC and 62% GC (while the direction of the axis changed from 76° to 82° relative to the direction of gait) is probably explained by changes that occur in the thickness of soft plantar tissues interposed between the bones and the ground as the ground forces are redistributed over the bearing surface of the forefoot. It must be borne in mind that the movement of the dorsum of the foot is being described relative to the ground, and not in relation to the proximal phalanges.

Also, no matter whether an exaggerated toe-out (38°) or toe-in (-17°) was assumed, the direction of the helical axis remained within ±6° the same as in normal gait.

In none of the five cases investigated could movement about an oblique axis passing through heads of the second to the fifth metatarsal bones as hypothesized by Bojsen-Møller and Lamoreux (1979) be observed. [On careful reading of the above mentioned reference, it will be noted that the authors do not insist on dorsiflexion of the toes about an oblique axis occurring regularly at some time in the push-off phase, but merely mention that: 'The two axes can be used for different mechanical purposes as their distances to the ankle joint complex, and thus the resistance arms of the foot, are different.'].

It might therefore be concluded that in level walking at a rate of about 60 m/min, the axis of rotation about which dorsiflexion in the MP joints takes place, passes through the 1st metatarsal head, lying at an angle of about 80° to the direction of progression, slop-

ing posteriorly and lateralwards, while remaining almost in a horizontal plane. Also, it was observed that the heel begins to rise from the ground at about 35% of the gait cycle (GC) and that the ball of the foot follows suit at about 65% GC. The observed angle of rotation (dorsiflexion) ranged from 37° to 56° (mean 51°) during this period.

5.4 Measurement of Ground Reaction Forces under the Forefoot

5.4.1 Methods and Material:

Two methods of measuring the ground reaction forces under the metatarsal heads and the pads of the toes were employed in the course of this study. At the beginning, only strain-gauge measuring equipment was available and therefore transducers were designed and built accordingly. This, however, necessitated such proportions and dimensions of the transducer elements in view of eliminating errors due to eccentric force application (St. Venant's priniple!) that a sole of at least 40 mm thickness in the region of the metatarsal heads was required to contain the transducers. Light-weight cork sandals (2.8 N each) were therefore specially made for this purpose, as described in detail in Section 3.5.1. It must be expressly mentioned that in spite of the 42 mm thick sole which allowed no flexion whatsoever in the MP joints, walking was very comfortable and felt natural because of the rocker shape given to the heel and forefoot region of the sandals (fig 3.15). After a first series of tests had been completed (Jacob et al., 1985, 1987) miniature piezo-quartz washers were used to build smaller and flatter transducers that could easily be accommodated within the 15 mm thick foam-rubber

insole of flexible leather sandals (fig 3.17). Thus, whereas the earlier series of experiments were performed with stiff-soled sandals that did not allow any dorsal flexion in the metatarsophalangeal joints when walking, the later series permitted practically unhampered movement in these joints.

The measuring equipment used including the self-made force transducers and signal amplifiers, have already been described at length in Sections 3.5.1 and 3.5.2, but as a matter of detail, the general method adopted in processing the analogue data may be briefly mentioned as follows: The visicorder graphs (voltage/time) were digitised with the aid of an 'Absolute x/y Electromagnetic Digitiser' (DIGI - PAD) using a manually controlled stylus. The x and y coordinates were read into an IBM-PC computer and were further processed by use of the appropriate calibration factors relating to each particular signal. By also considering the weight of the test subject, 'normalised' graphs were drawn with a Hewlett-Packard plotter with forces shown as percentage of body weight over one complete gait cycle (heel-strike to heel-strike as simultaneously recorded by means of a microswitch attached to the heel). In each test, from six to fifteen complete gait cycles were evaluated and the normalised graphs all drawn on the same diagram. Also, the arithmetical mean was determined and drawn on the same illustration too.

Since two measuring systems were adopted, one with stiff soles and the other in which dorsiflexion in the MP joints was possible, the further details of the test procedure will be split into two corresponding sub-sections, 5.4.1.1 and 5.4.1.2, as follows:

5.4.1.1 Force measurements with stiff soles (cork sandals) and strain-gauged transducers:

As shown in Figure 3.15 of Section 3.5.1, allowance was made for positioning four transducers inside the sole of the right cork sandal. Only the ground forces under the metatarsal heads and the pads of the 1st and 2nd rays were measured. The decision to locate the transducers in this manner was strongly influenced by the clinical question regarding the aetiology of an occasionally observed idiopathic necrosis of the metatarsal heads (Morbus Koehler-Freiberg II) that affects the 2nd ray more often than the 1st. The force under the metatarsal head of the 5th ray was measured in the second series of experiments (Section 5.4.1.2). The flexible lead wires from the transducers were led along the shank up to the waist of the test person so that free movement of the lower limbs was not impaired in any way.

Five test persons (Group A: four males and one female between 25 and 45 years of age) with no obvious evidence of a pathological disorder of the feet were investigated on a moving belt (treadmill) of 1.9 m usable length at walking rates of 30, 40 and 50 m/min. A heel switch incorporated within the sandal gave an indication of the instant the heel struck the ground. The four signals from the force transducers and the heel-strike switch signal were simultaneously recorded after the test subject had been given some time to get accustomed to walking on the moving belt. Recordings usually lasted about 15 s. Results of this investigation have been published before (Jacob et al. 1985, 1987) and are shown in Section 5.4.2.1.

Following a first series of measurements with flexible leather sandals and with piezo-quartz transducers, some uncertainty arose

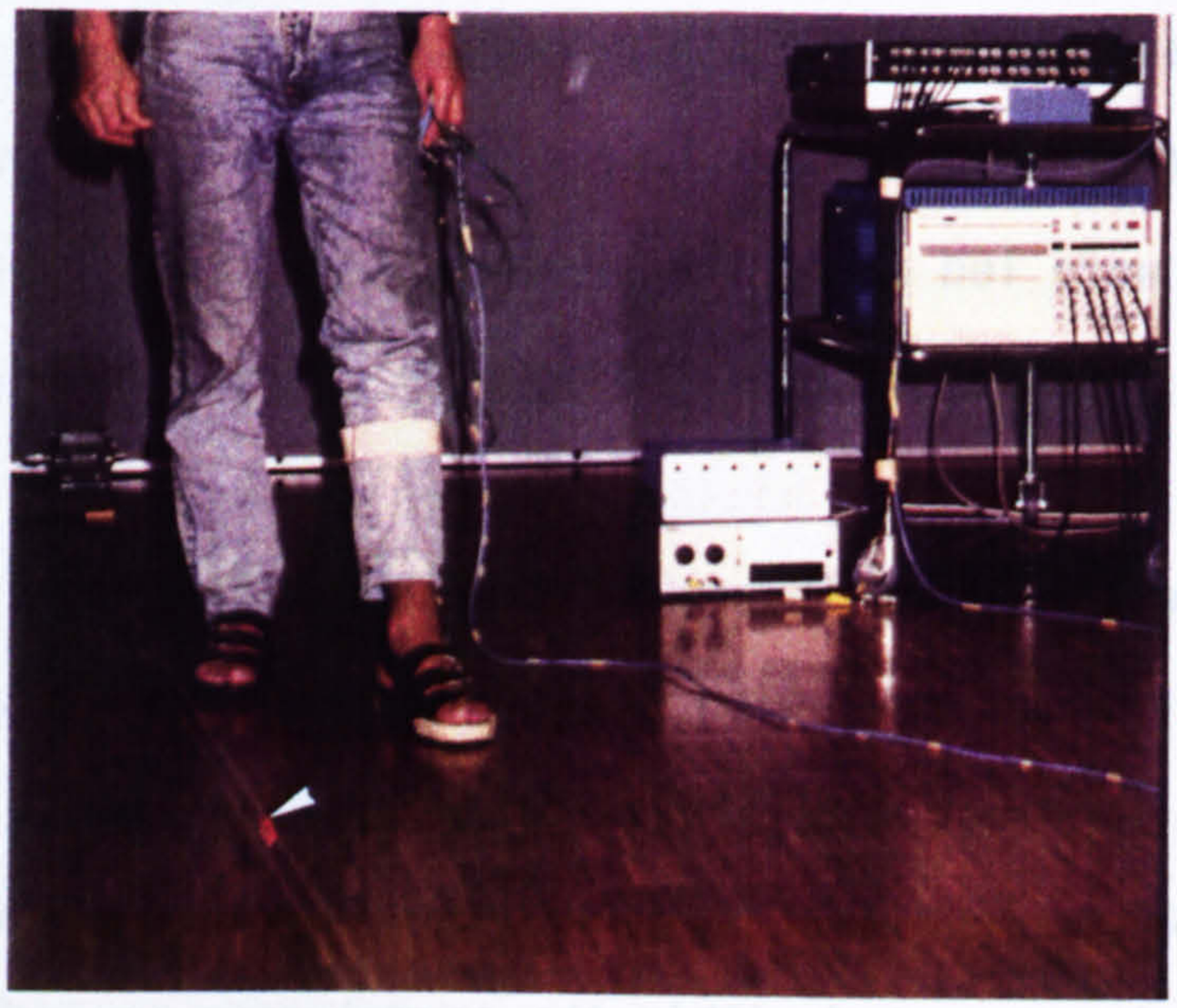

Figure 5·7: Walking on an open floor at a constant pace by following a pace-maker

because of discrepancy in the results hitherto obtained. This necessitated repeating the former tests, both with stiff and flexible sandals, under identical environmental conditions, and with identical test subjects.

Therefore, with another batch of five test persons - Group C - (not all identical with those of the first batch) the test was repeated, but this time on the open floor. Walking at a constant predetermined pace was facilitated by a 'pace-maker'. This consisted of an endless cord that passed horizontally over two small pulleys kept at a distance of about 10 m from each other. One of the pulleys (of a stepped form exhibiting two different diameters) was driven by a squirrel-cage motor, and moved the cord at a constant speed (50 or 80 m/min). A small flag attached to the cord was followed some distance away by the test subject across the floor (fig 5.7). Because of the rocker-shape given to the sole of the stiff cork sandals, walking was smooth and comfortable, and felt 'natural' with normal toe-out. On increasing the toe-out angle to about 30°, however, walking became constrained and jolty, and therefore no tests were performed with toe-out other than normal.

The results of the tests performed with this second batch of test subjects (Group C) is also given in Section 5.4.2.1.

5.4.1.2 Force measurements with flexible leather sandals and piezo-quartz transducers:

In this series of tests, two batches of test subjects were involved. The first batch of six persons (Group B: 3 males and 3 females from 24 to 46 years of age) produced results that, as mentioned before, were surprisingly different to those earlier obtained with

Test No.	Stiff sole MP-1, MP-2,* T-1, T-2	Flexible sole T-1, MP-1, * MP-2, MP-5	Toe-out	Mode	Results (fig No.)
1	A		normal	30, 40 and 50 m/min	5.8
2		Only 2 of B** MP-1, T-1, T-2, T-3	normal	50 m/min	5.11
3		Only 1 of B**	normal	50 m/min	5.12
4	C		normal	50 m/min	5.9
5	C		normal	80 m/min	5.10
6		Only 2 of B** MP-1, T-1, T-2, T-3	" "	about 50 m/min	5.11
7		Only 1 of B**	"	"	5.12
8		C	"	50 m/min	5.23
9		B	"	80 m/min	5.13
10		C	"	"	5.20
11		B	~ 5°	"	5.14
12		C	~ 5°	"	5.21
13		B	~ 30°	"	5.15
14		C	~ 45°	"	5.22
15		C MP-1, MP-2, T-1, T-2	normal	"	5.24
16		B	normal	up stairs	5.16
17		B	"	down stairs	5.17
18		B	"	up slope	5.18
19		B	"	down slope	5.19

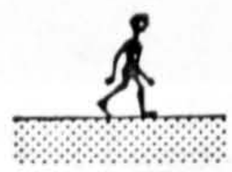

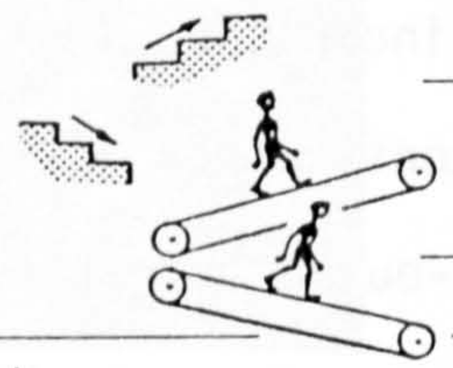

* Configuration of transducers unless otherwise specified

** Preliminary tests

Test groups: A: 3 males + 1 female
B: 3 males + 3 females
C: 3 males + 2 females

TABLE 5.3 Overview of gait tests performed

the stiff cork sandals by Group A. Therefore, the tests were repeated with a batch of five test persons, Group C (not all identical with those of Group B) but, however, identical with the second batch mentioned in Section 5.4.1.1.

The general arrangement of force transducers under the forefoot was changed from that used with the stiff cork sandal (Section 5.4.1.1) following preliminary tests with the transducers under the pads of the 1st, 2nd and 3rd toes and under the head of MP-1 (fig 5.11). In the general arrangement finally chosen, the four piezo-quartz transducers were placed as follows: one directly under each head of the metatarsals 1, 2 and 5, and one under the pad of the great toe. Figure 3.17 shows this arrangement. The transducers were furnished with three small spikes that protruded from their bases and which engaged with the underlying sole. By this means, sideways slipping of the transducers was prevented. Exact location of the transducers relative to the anatomical target area was determined through palpation of the metatarsal heads and use of a marking dye to check the positioning that resulted. The strapping arrangement (fig 3.17) afforded good hold of the foot over a wide range of foot sizes.

The test programmes for the batch of six (Group B) and batch of five (Group C) are shown schematically in Table 5.3. Basically, information was sought on the loading of the foot when dorsiflexion in the MP-joints was free to take place. Furthermore, the effect of toe-out angle and rate of progression were of interest. In addition to this, the load on the pad of the 3rd toe in level walking, and on the forefoot when walking up and down stairs of 16 cm height, and up and down a ramp of 15° inclination (moving belt), were observed. Also, forces and force-time graphs obtained when walking on

an open floor were compared with those resulting from walking on a moving belt. All these results are presented in Section 5.4.2.2.

5.4.2 Results:

The results of the measurements of ground reaction forces under the forefoot during walking, as undertaken according to Section 5.4.1, are presented in two main sub-sections. The first, Section 5.4.2.1, deals with the series of tests performed with the stiff cork sandal and strain-gauged transducers, while the second, Section 5.4.2.2, presents the results obtained with the flexible leather sole and transducers of the piezo-quartz type.

5.4.2.1 Results obtained with stiff sandals and strain-gauged transducers:

This sub-section will be further split into two parts: a) measurements taken with Group A (five subjects) and b) those taken later with Group C (also five subjects, but not identical with those of Group A).

a) The ground reaction forces under the metatarsal heads and toe pads of the 1st and 2nd rays were measured in the case of each of the five test subjects of Group A on a moving belt at speeds of 30, 40 and 50 m/min. Although the force/time graphs showed uniqueness that was characteristic of each test subject (rise time, wave form, and relation of amplitude to those of the other forces simultaneously measured), the variation of amplitude observed even at a given walking pace was, however, so large that it was not possible to singularly define either the shape of the curve, or the magnitude of force under given conditions. This, even when consecutive walking

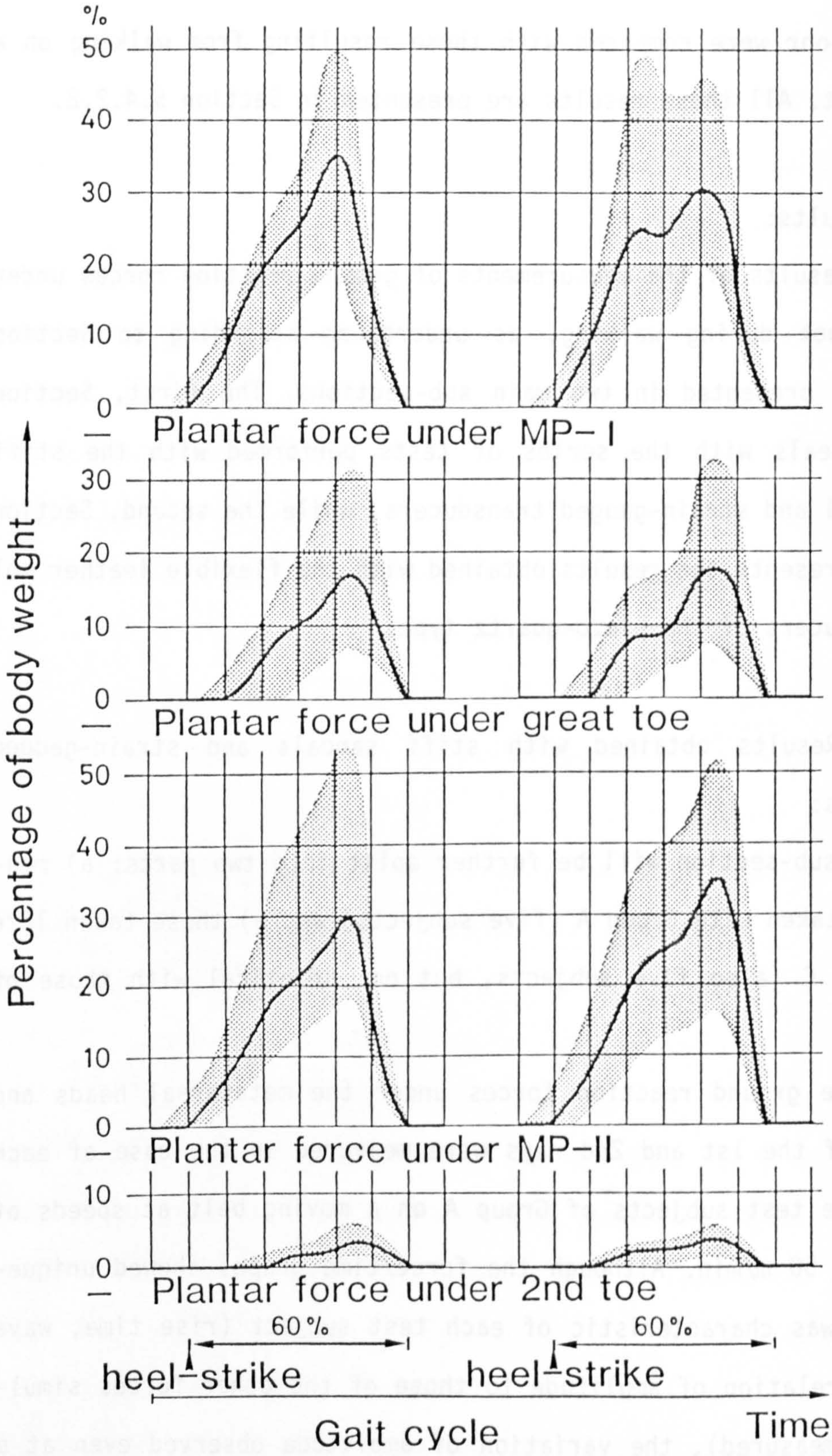

Figure 5.8 : Ground reaction forces with stiff soles
(test subjects of Group A)

cycles were compared. Also, although a definite relationship was observed between the speed of progression and the magnitude of ground reaction force, the scatter of values obtained was so great that an attempt to formulate a relationship between walking speed and ground force was considered futile, and the idea therefore abandoned. Figure 5.8 shows the results obtained as percentage of body weight (BW) against time (percentage of walking cycle), at a walking speed of 50 m/min. The shaded areas indicate the scatter, and the bold curves show the arithmetical mean.

In all five test subjects two shapes of curves were generally observed (fig 5.8), a single-humped and a double-humped shape. [In the single-humped curve, a vague manifestation of the second hump was always present]. One of the five subjects showed a distinct deviation from the general pattern with a maximum average ground force under the 1st metatarsal head of only 18% BW, and of only 14% BW under the great toe. The maximum average values under the 2nd metatarsal head and under the pad of the 2nd toe were 15% BW and 8% BW in this case, respectively. On subjecting the foot to closer examination, it was noticed that the range of movement in the MP-1 joint was considerably reduced (hallux rigidus?) in this individual. Subsequently, the force data obtained from this person was completely excluded from that used to arrive at the average values that are presented in figure 5.8.

b) With the five test subjects of Group C, ground reaction forces under the metatarsal heads and toe pads of the 1st and 2nd rays were measured while walking on the open level floor at 50 and 80 m/min, in contrast to walking on the travelling belt as described previously. Figures 5.9 and 5.10 show the total distribution of

185 A

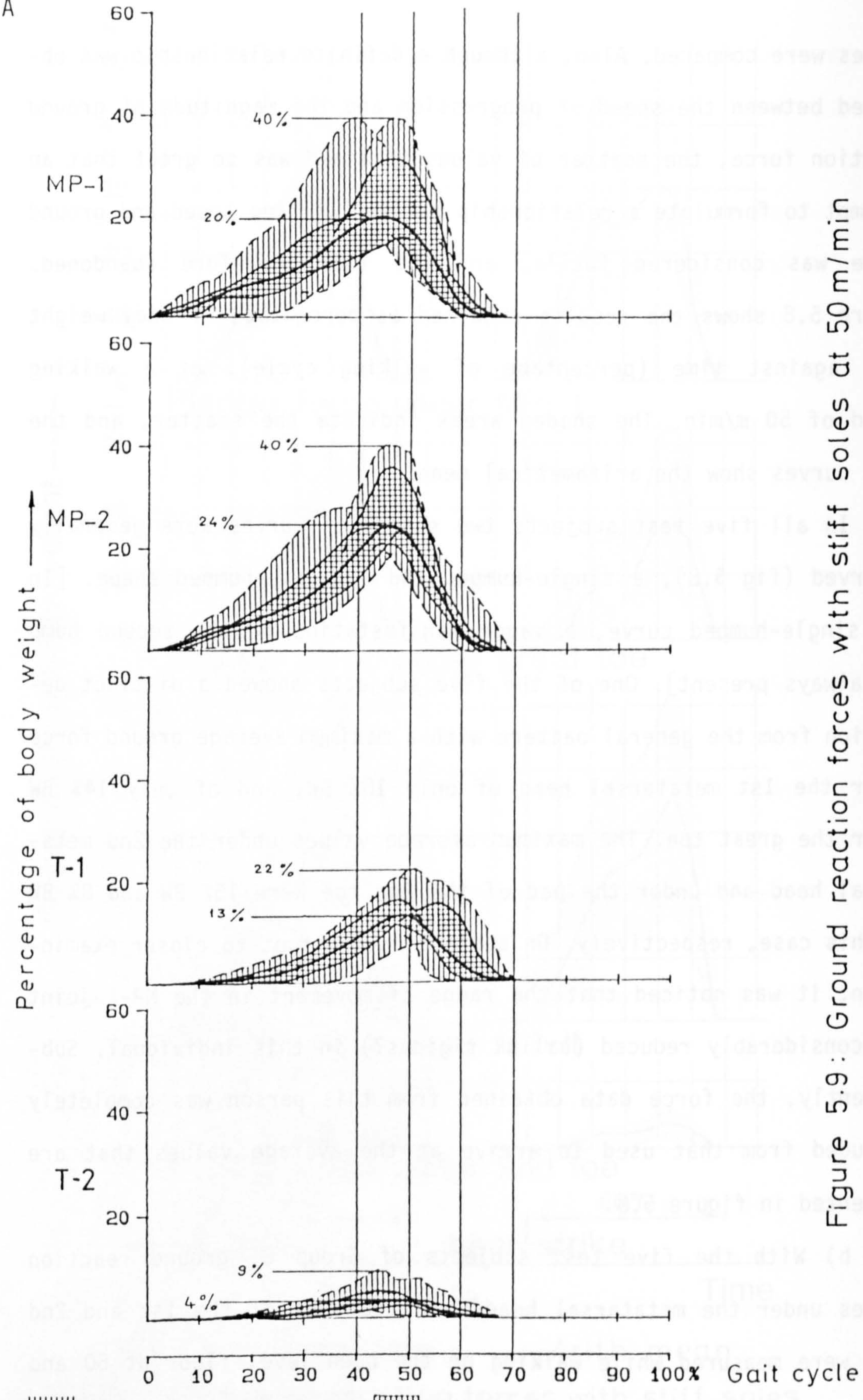

Figure 5.9: Ground reaction forces with stiff soles at 50 m/min
(Group C on open floor)

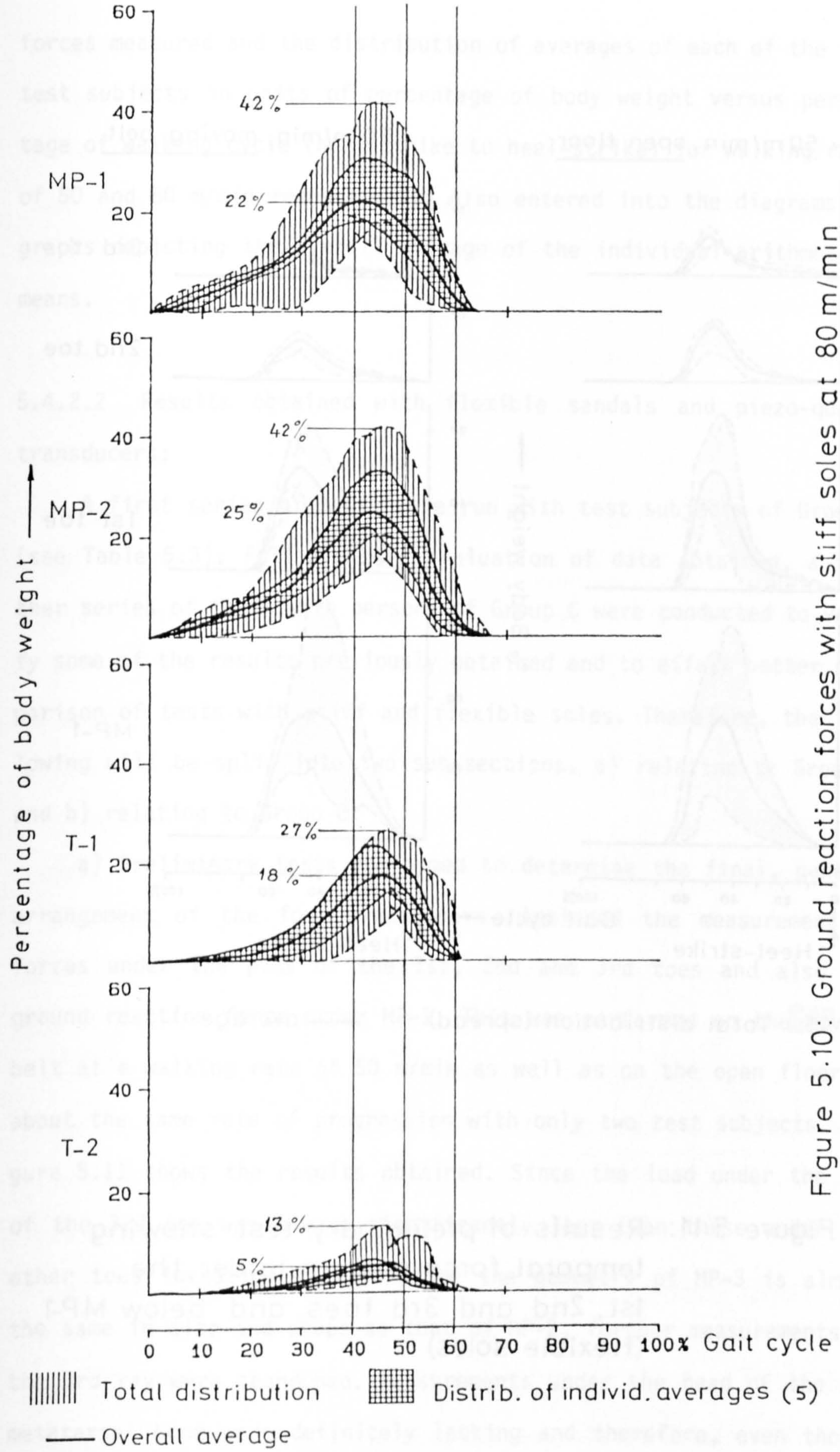

Figure 5.10: Ground reaction forces with stiff soles at 80 m/min
(Group C on open floor)

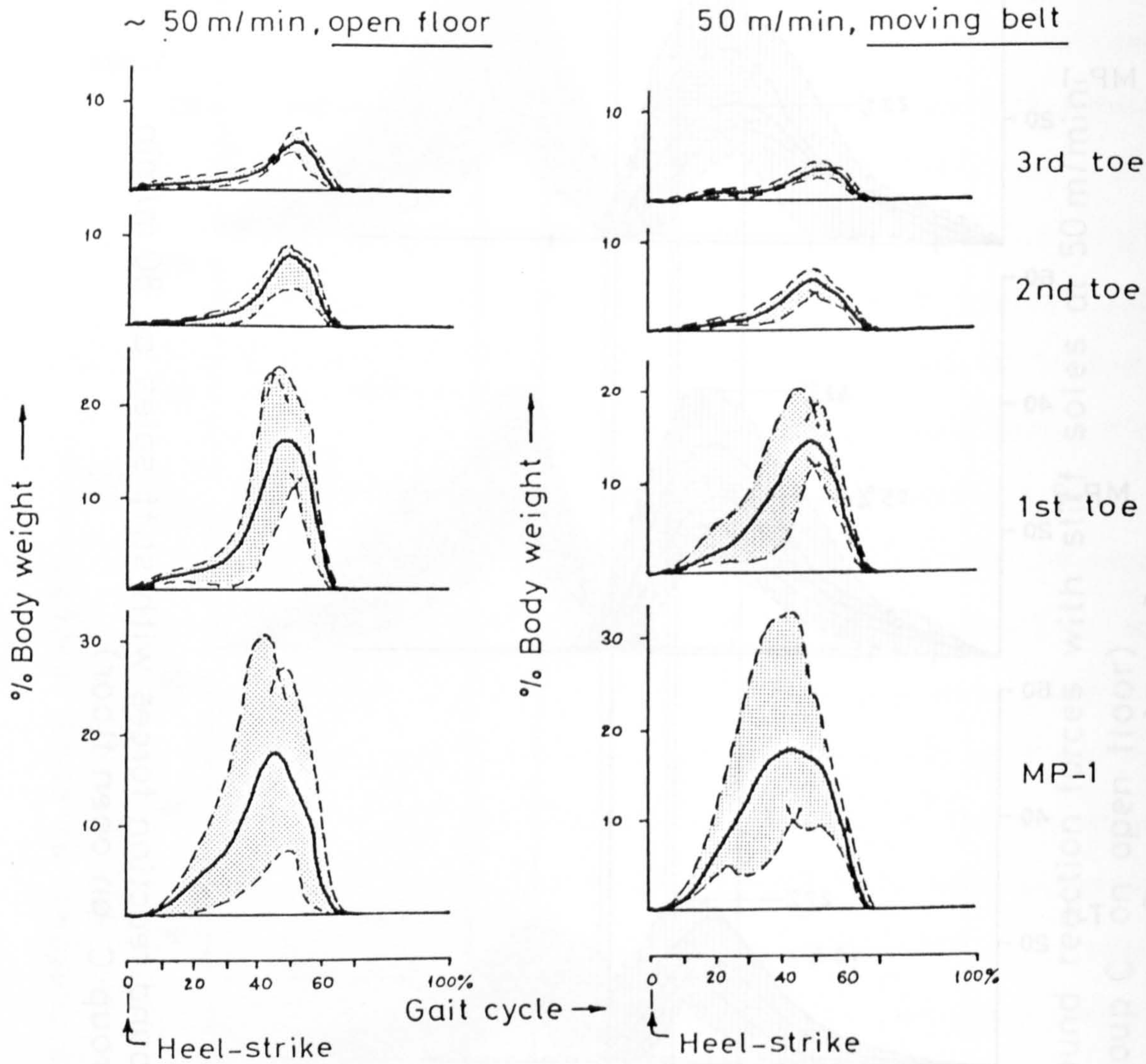

Figure 5.11: Results of preliminary test showing temporal force pattern under the 1st, 2nd and 3rd toes and below MP-1 (flexible soles)

forces measured and the distribution of averages of each of the five test subjects in units of percentage of body weight versus percentage of walking cycle (heel-strike to heel-strike) for walking rates of 50 and 80 m/min respectively. Also entered into the diagrams are graphs depicting the overall average of the individual arithmetical means.

5.4.2.2 Results obtained with flexible sandals and piezo-quartz transducers:

A first series of tests were run with test subjects of Group B (see Table 5.3). Following the evaluation of data obtained, a further series of tests with persons of Group C were conducted to verify some of the results previously obtained and to effect better comparison of tests with stiff and flexible soles. Therefore, the following will be split into two sub-sections, a) relating to Group B and b) relating to Group C.

a) Preliminary tests performed to determine the final, general arrangement of the four transducers, included the measurement of forces under the pads of the 1st, 2nd and 3rd toes and also the ground reaction force under MP-1. This was performed on the moving belt at a walking rate of 50 m/min as well as on the open floor at about the same rate of progression with only two test subjects. Figure 5.11 shows the results obtained. Since the load under the pad of the 3rd toe was always significantly less than those under the other toes investigated, and since the geometry of MP-3 is almost the same in size and shape as that of MP-2, further measurements on the 3rd ray were abandoned. Measurements under the head of the 5th metatarsal bone were definitely lacking and therefore, even though

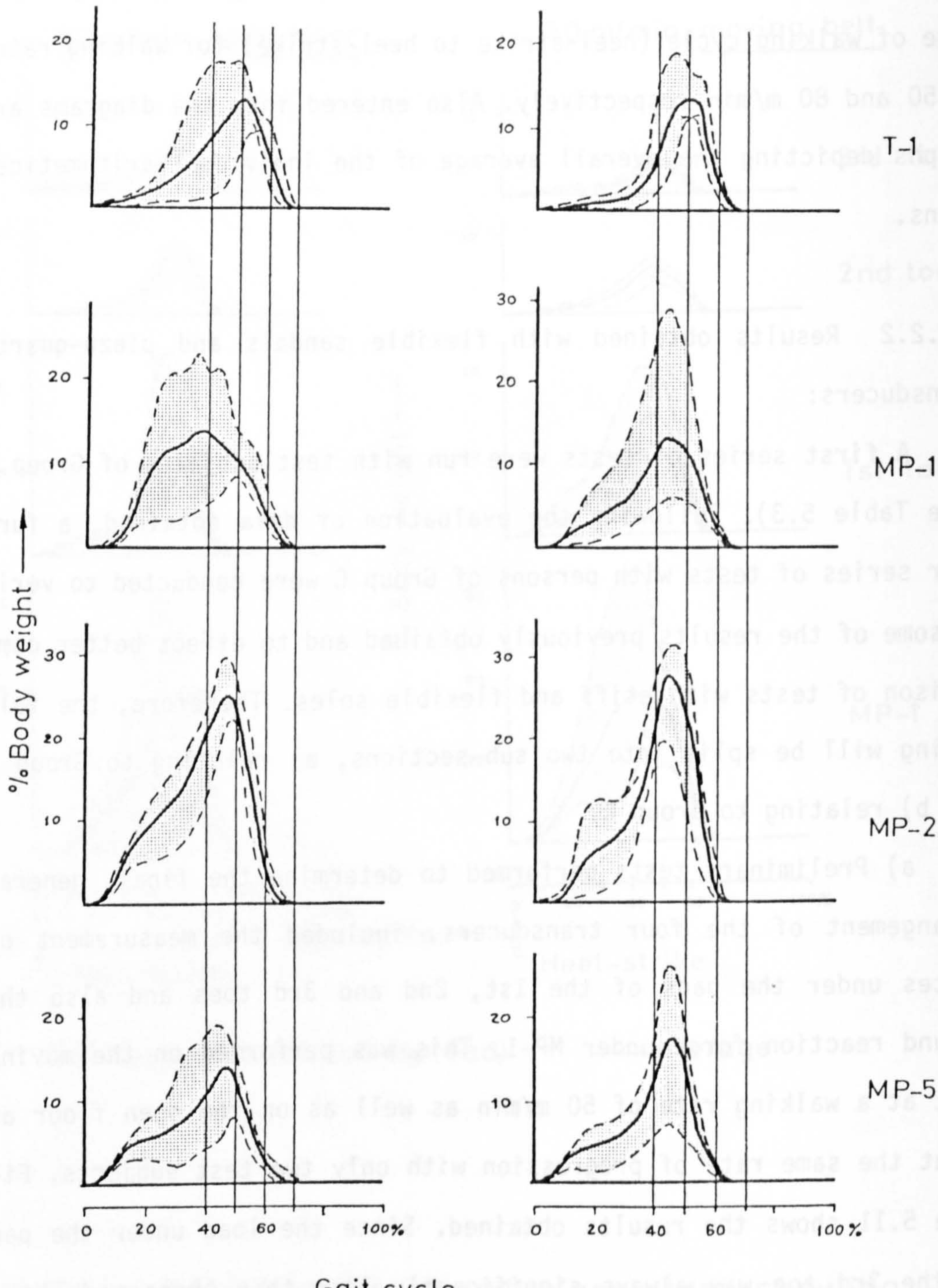

Figure 5.12: Ground reaction forces of a single test subject on a moving belt and on the open floor (preliminary test, ~50 m/min, flexible soles)

it would have been very interesting to further follow the loading of the 2nd toe pad, the force distribution under the metatarsal heads across the foot was given preference, however, at the same time retaining the force transducer under the pad of the geat toe. This led to the final arrangement of the only four available transducers. Further preliminary tests on the moving belt at 50 m/min and on the open floor at about the same progression rate were performed. The results of these tests - that also compare walking on the moving belt with walking on the open floor under otherwise nearly identical conditions, but with only one test subject - are shown in figure 5.12. Because walking on the open floor at 50 m/min was found uncomfortably slow, it was decided to carry out further measurements at a walking pace of 80 m/min instead. Figure 5.13 shows the results obtained with Group B with normal toe-out, and figures 5.14 and 5.15 with toe-out of about 5° and 30° respectively.

Following these tests, investigations were carried out with the same group of six persons (Group B) when climbing up and down stairs (16 cm height) and when walking up and down a slope of 15°. The last mentioned tests were performed on the moving belt at a speed of 50 m/min. Figures 5.16 to 5.19 show the results obtained.

As already mentioned, on considering the data obtained from the above mentioned tests, the marked difference in forces measured under MP-1 between that of Group A with stiff soles (fig 5.8), and that of Group B with flexible leather sandals (fig 5.11 or 5.12) was so striking, that it was decided to repeat some of the tests, both with stiff as well as flexible sandals, using a common group of test subjects in both cases under otherwise identical conditions. The following sub-section b) presents the results obtained with this

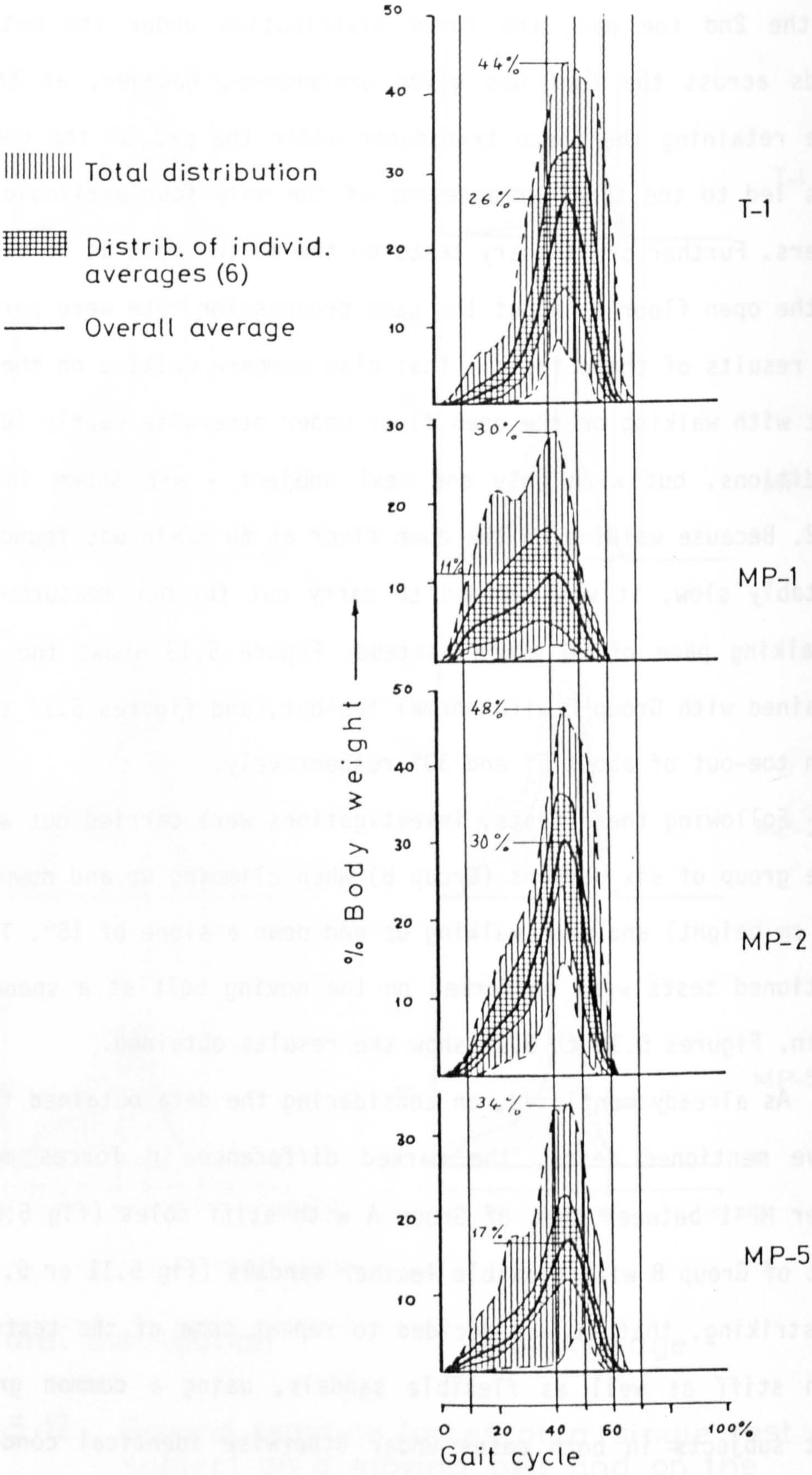

Figure 5·13: Ground reaction forces at 80 m/min
(Group B, normal toe-out, flexible soles)

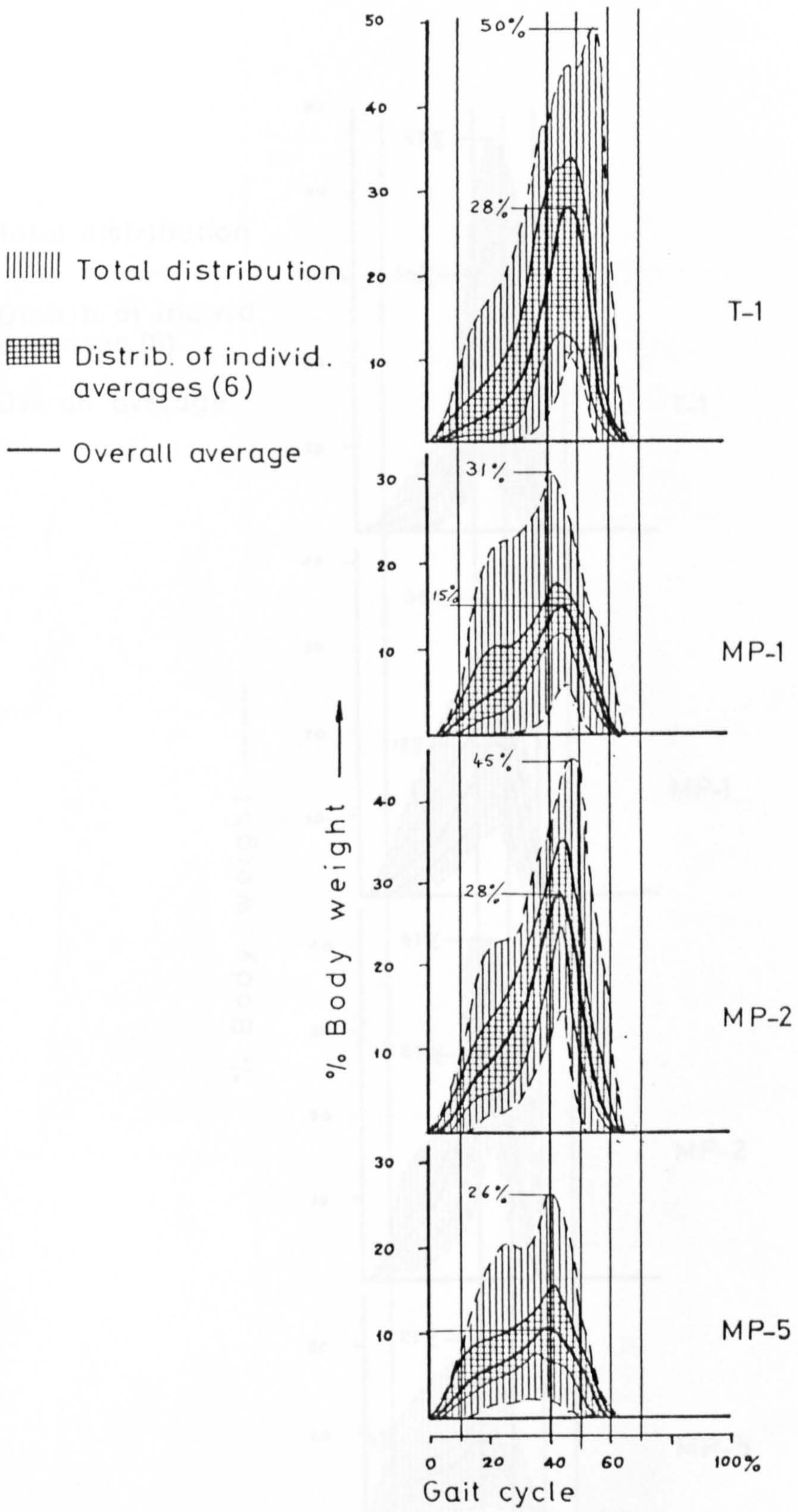

Figure 5.14: Ground reaction forces at 80 m/min (Group B, ~5° toe-out, flexible soles)

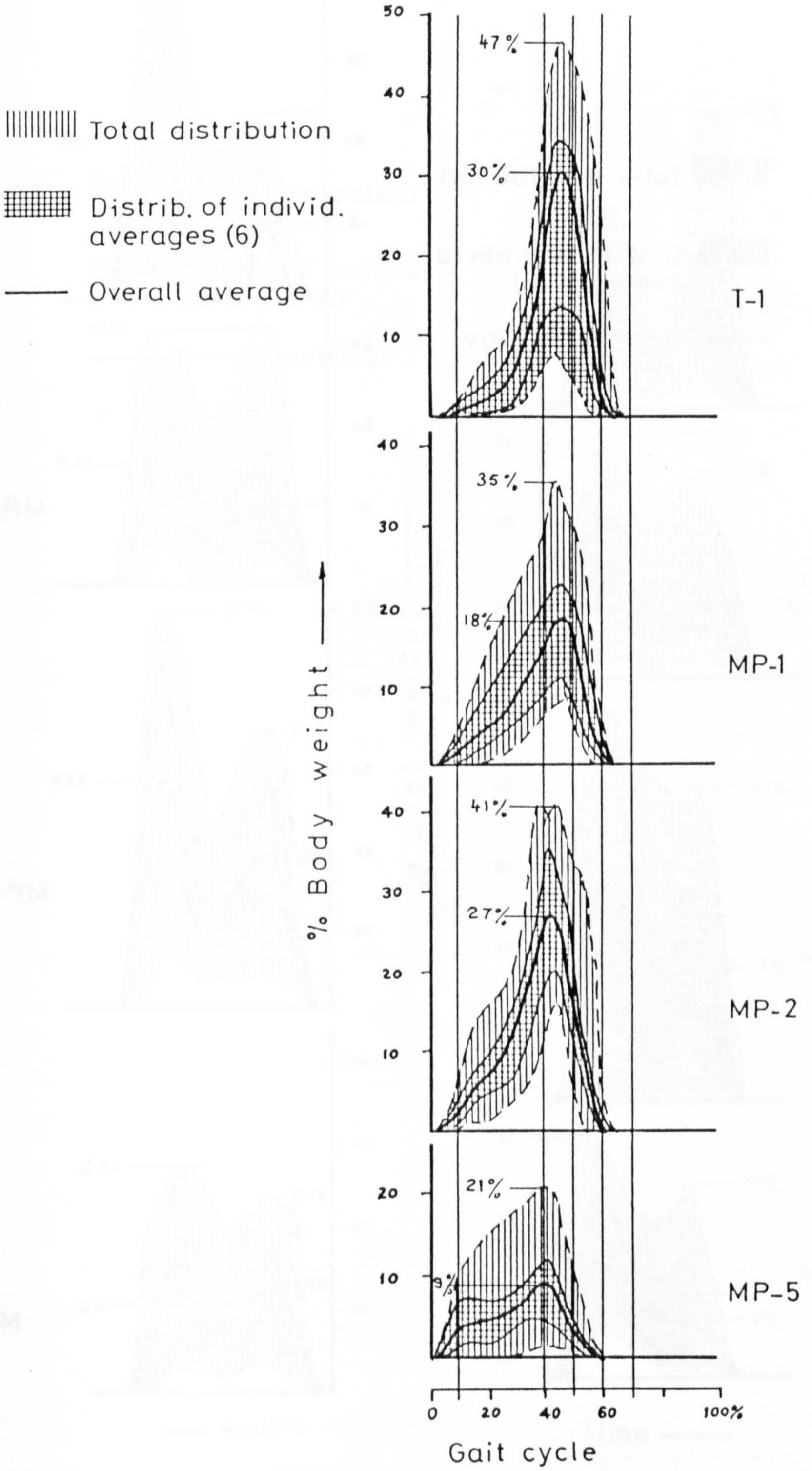

Figure 5.15: Ground reaction forces at 80 m/min (Group B, ~ 30° toe-out, flexible soles)

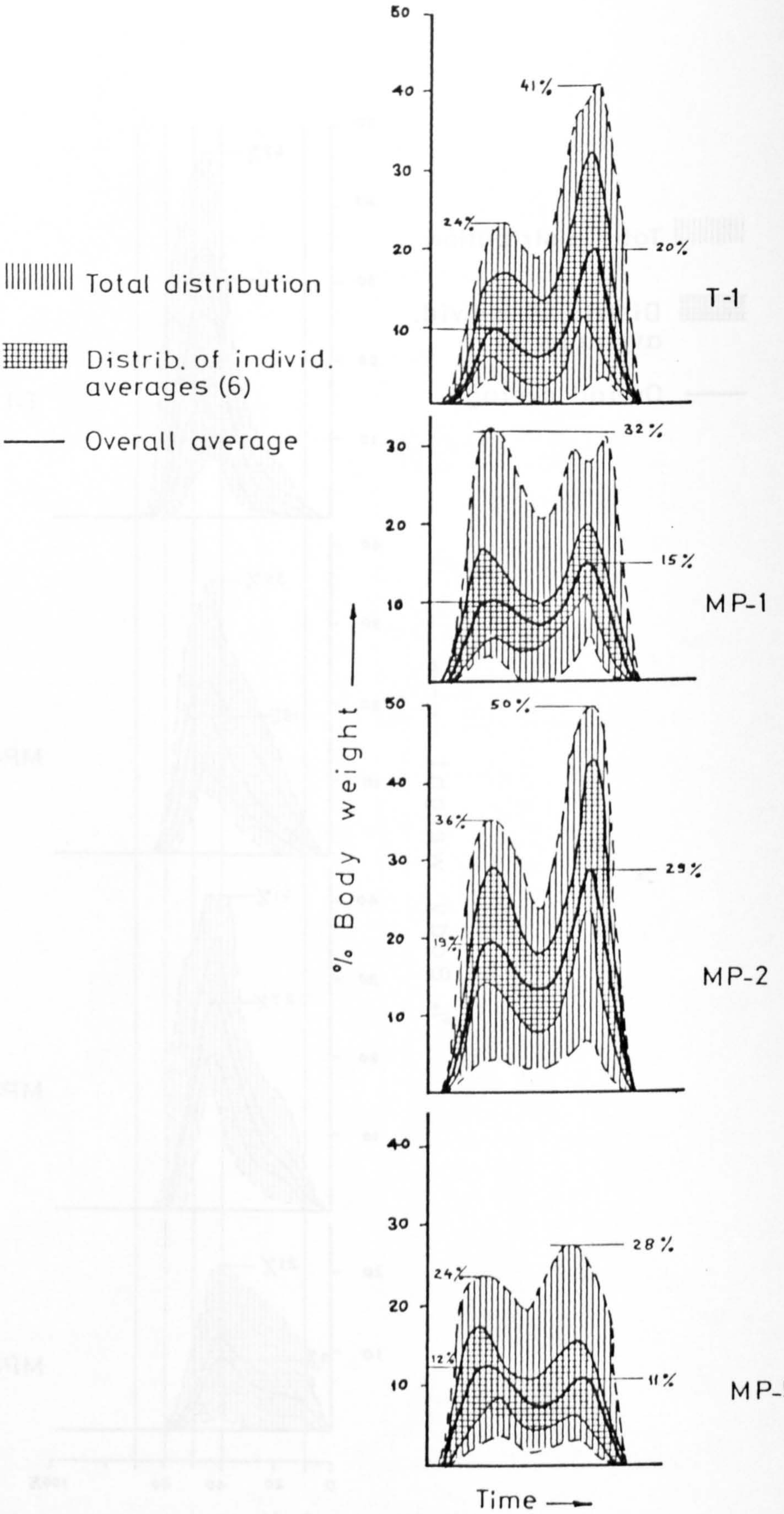

Figure 5.16: Ground reaction forces on ascending stairs (Group B, flexible soles)

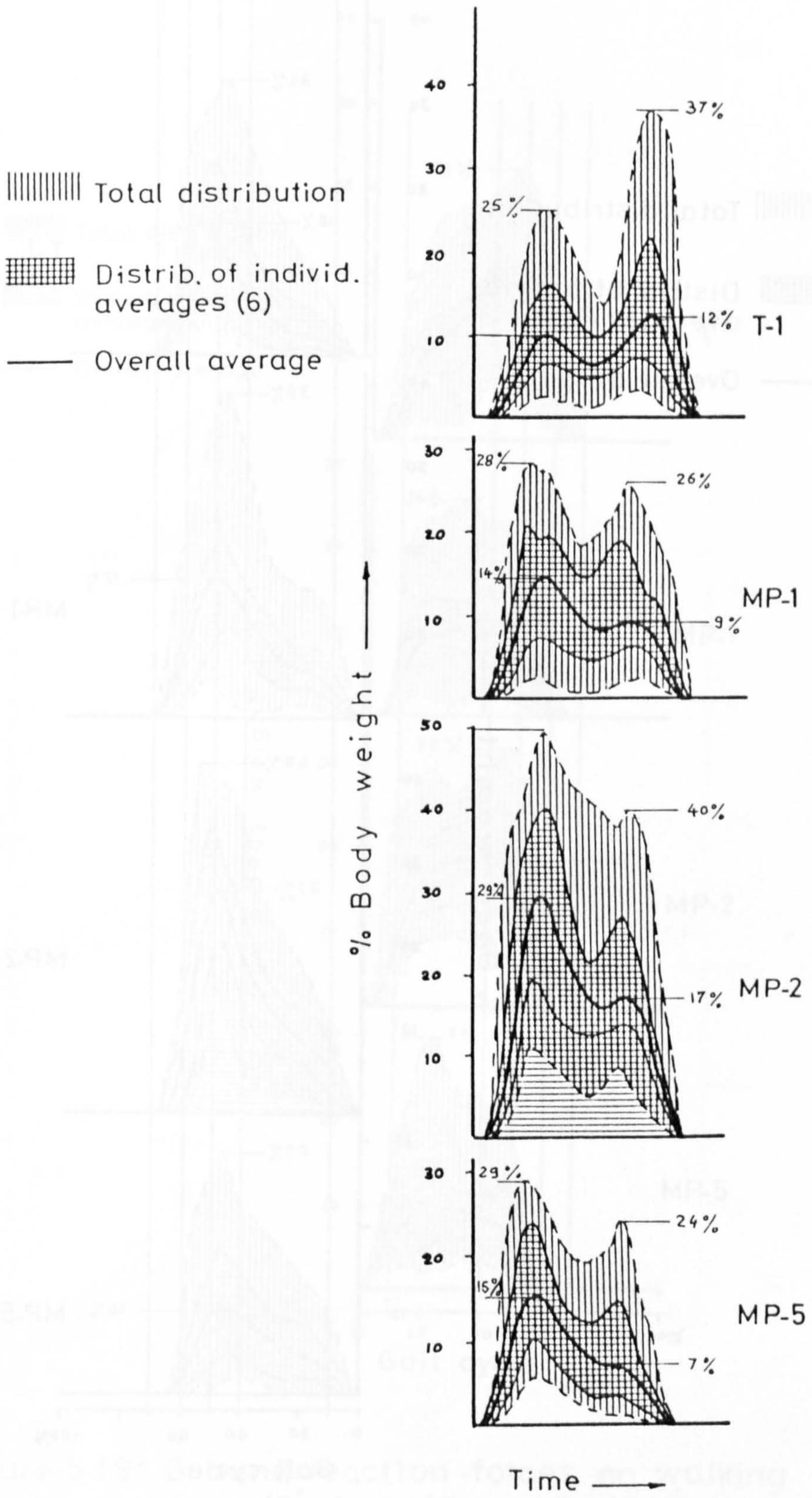

Figure 5·17: Ground reaction forces on descending stairs (Group B, flexible soles)

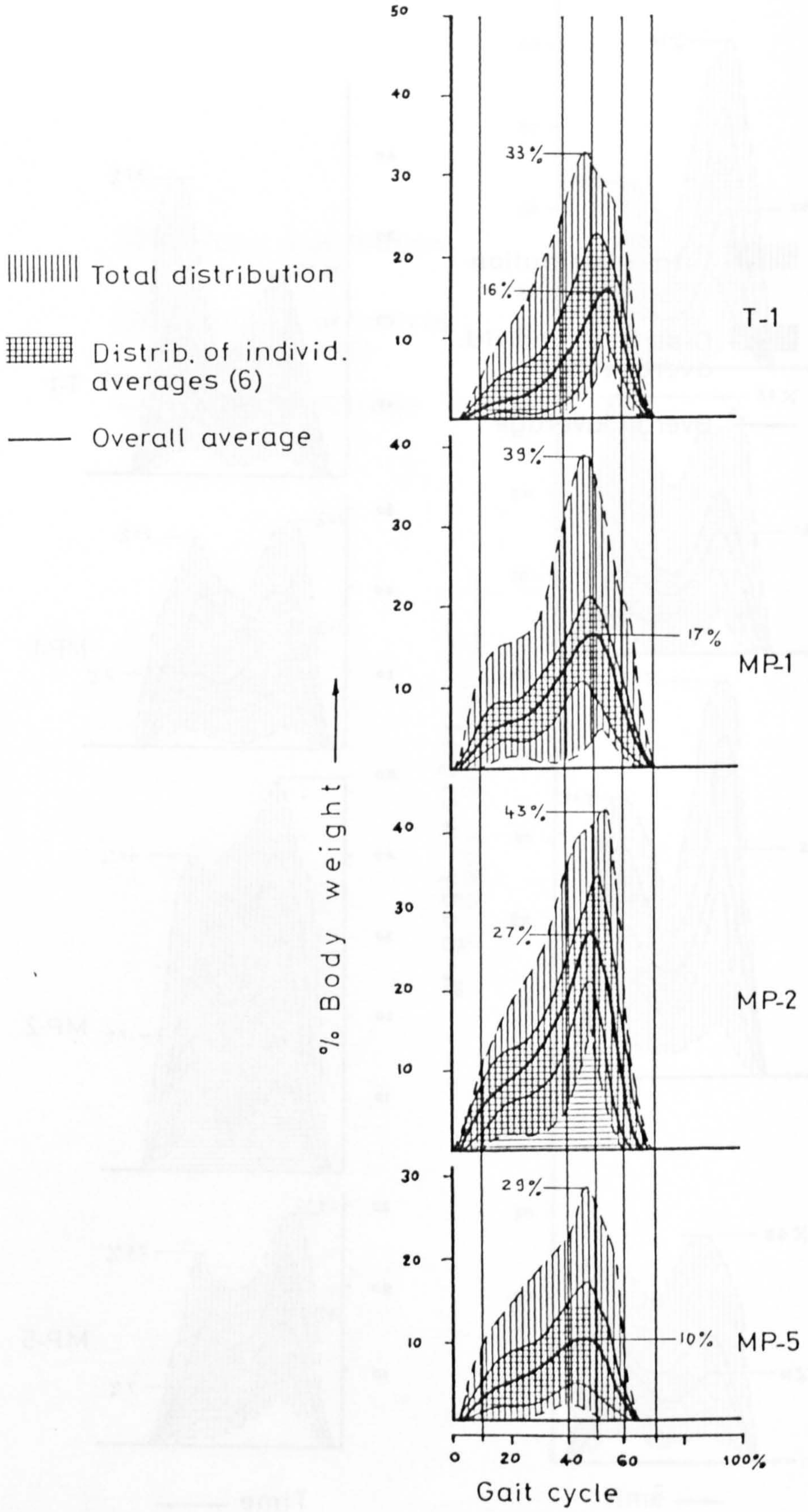

Figure 5.18 : Ground reaction forces on walking up 15° slope (Group B, flexible soles 50 m/min, moving belt)

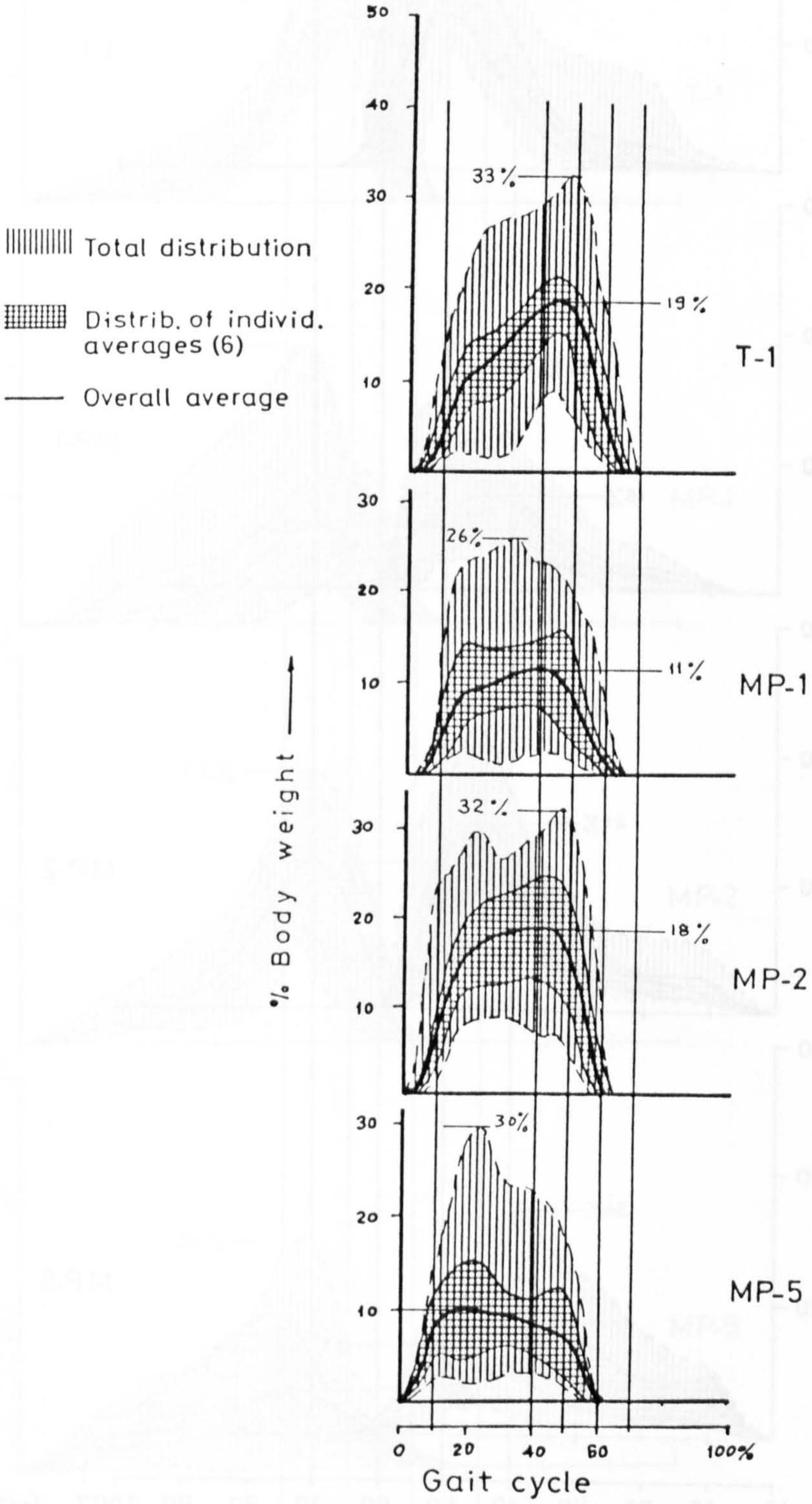

Figure 5.19: Ground reaction forces on walking down 15° slope (Group B, flexible soles 50 m/min, moving belt)

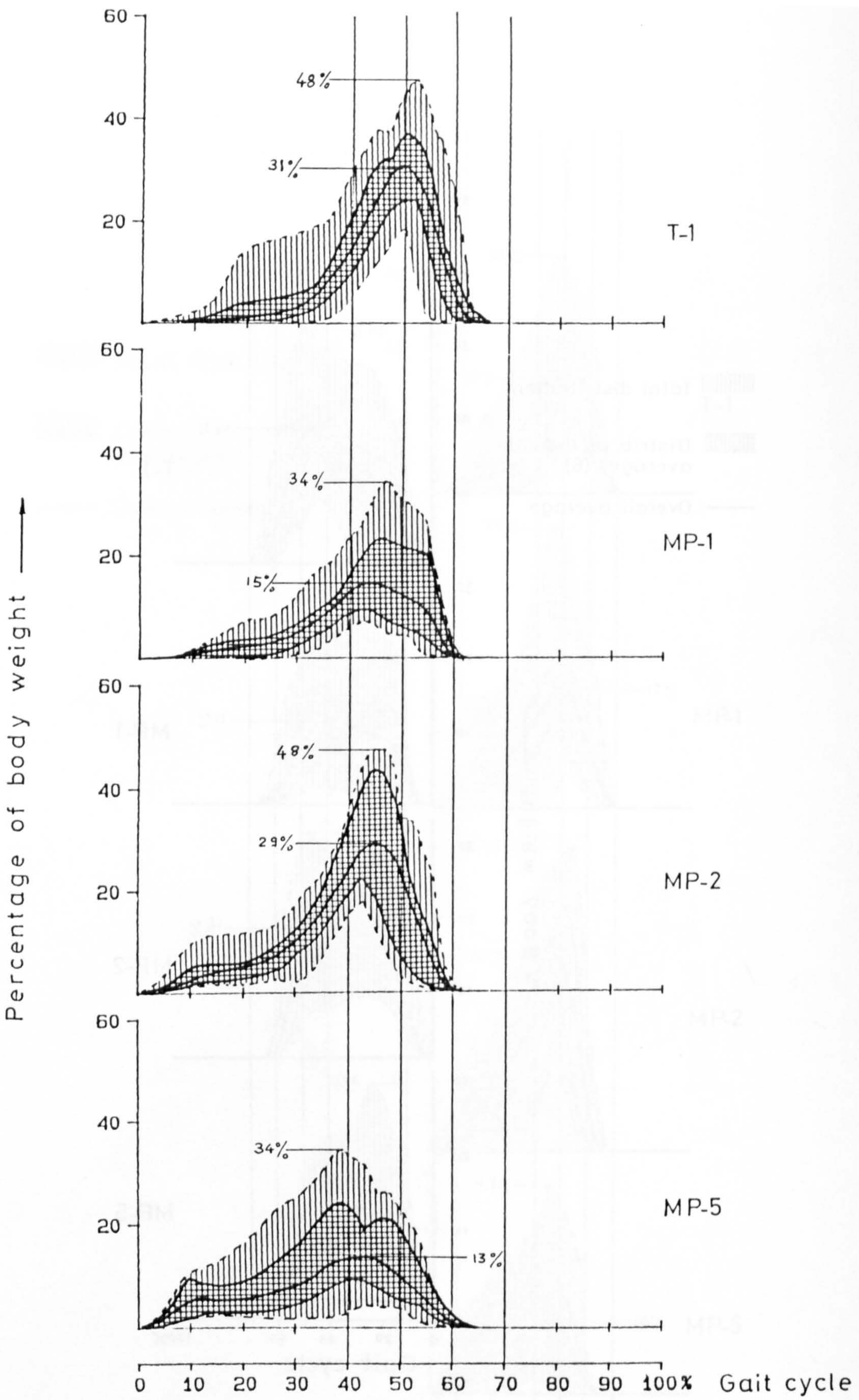

Figure 5.20: Ground reaction forces at 80 m/min
(Group C, normal toe-out, flexible soles)

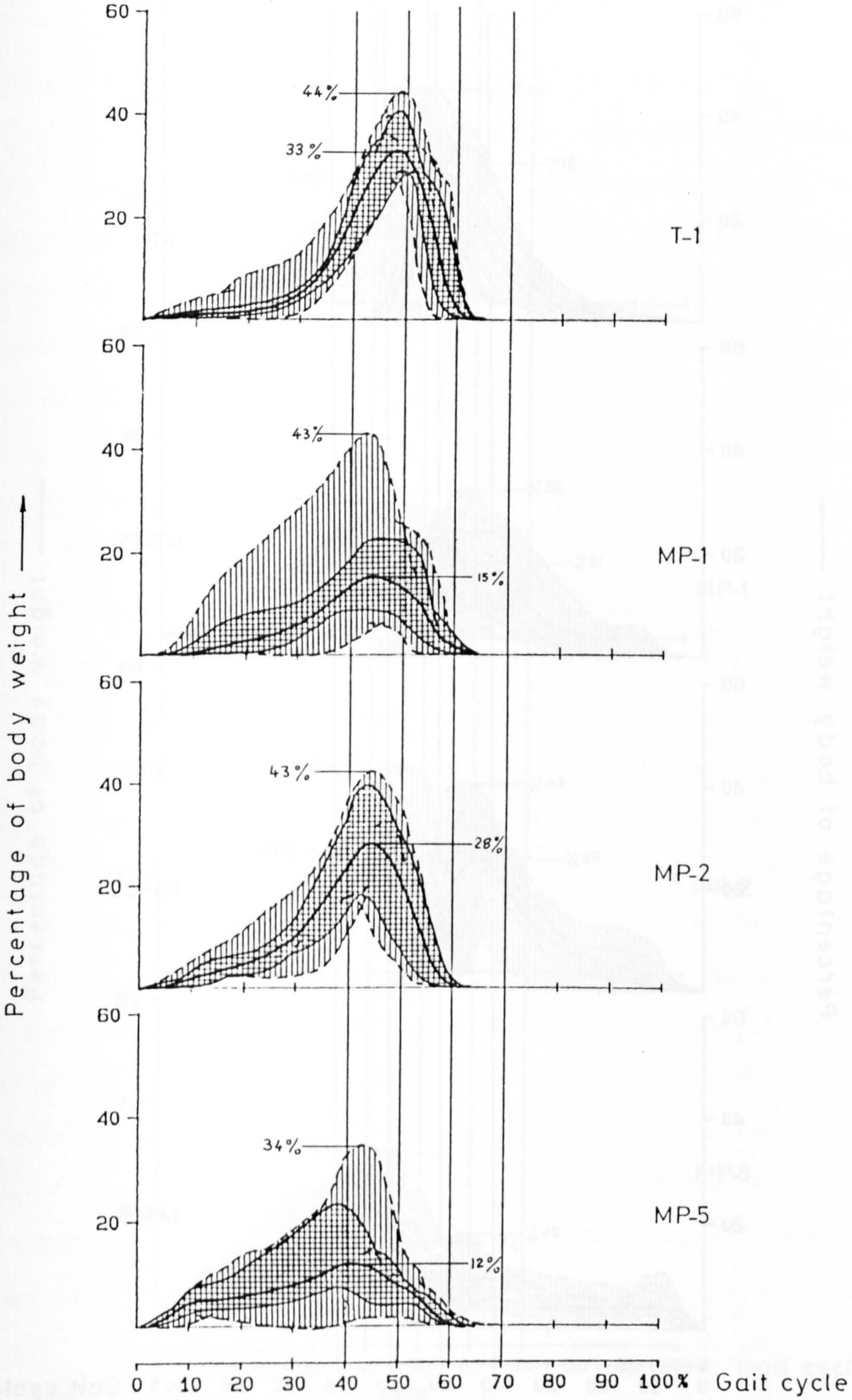

Figure 5·21: Ground reaction forces at 80 m/min (Group C, ~5° toe-out, flexible soles)

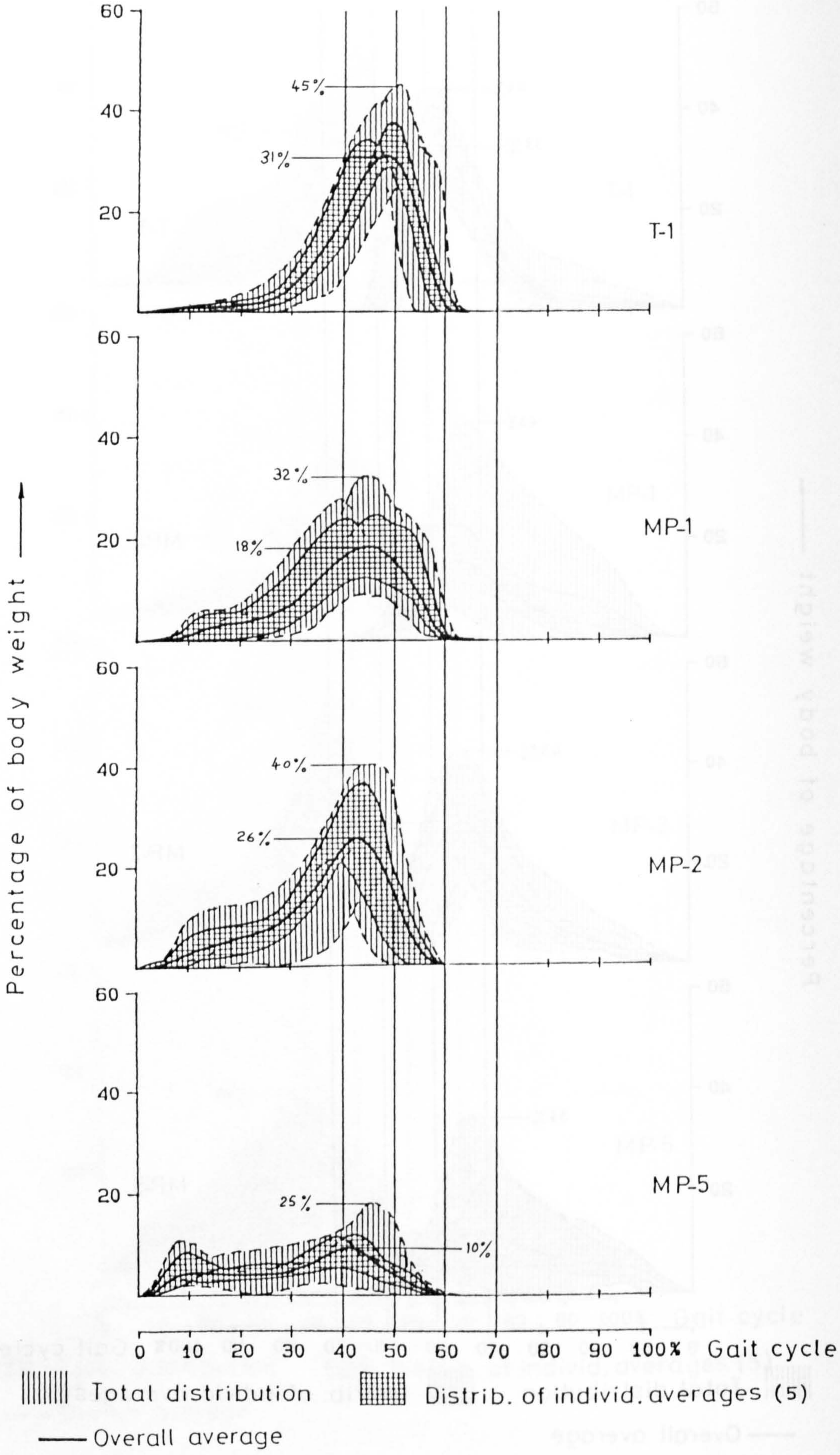

Figure 5.22: Ground reaction forces at 80 m/min
(Group C, ~45° toe-out, flexible soles)

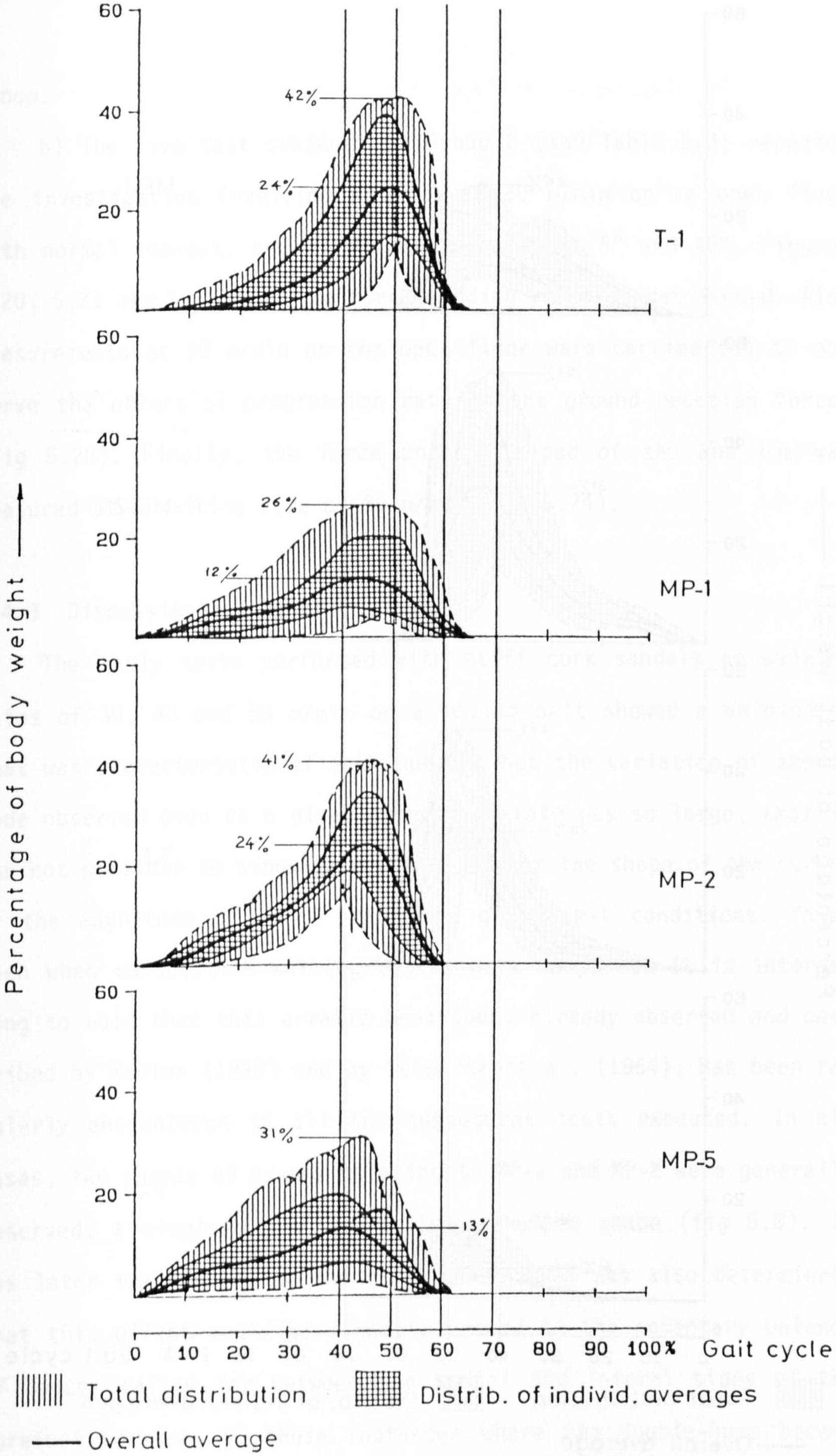

Figure 5·23 : Ground reaction forces at 50 m/min
(Group C, normal toe-out, flexible soles)

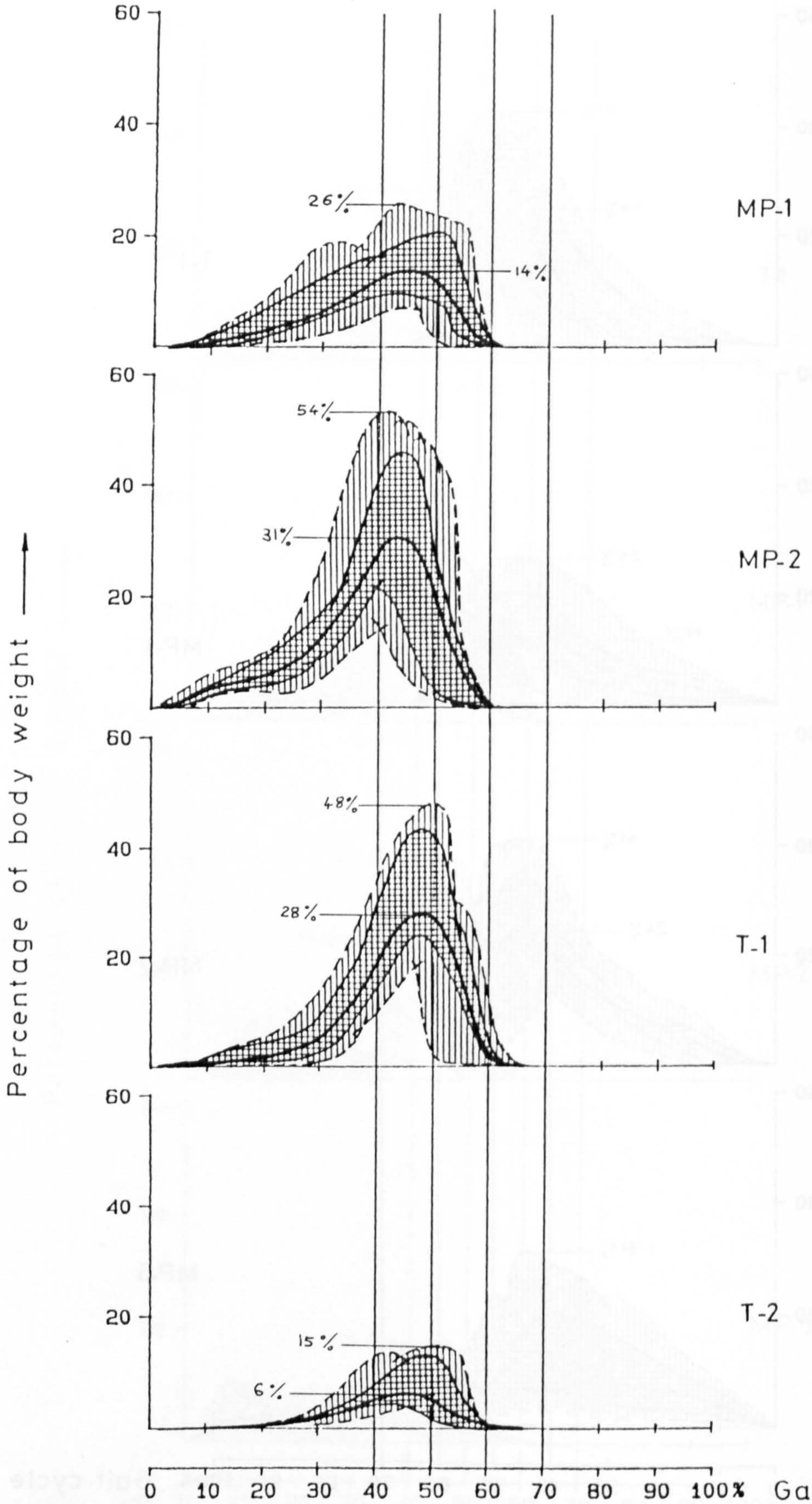

Figure 5·24 : Ground reaction forces at 80 m/min (Group C, normal toe-out, flexible soles)

group.

b) The five test subjects of Group C (see Table 5.3) repeated the investigation involving walking at 80 m/min on an open floor with normal toe-out, and with toe-out of about 5° and 45°. Figures 5.20, 5.21 and 5.22 show the corresponding results that issued. Also measurements at 50 m/min on the open floor were carried out to observe the effect of progression rate on the ground reaction forces (fig 5.28). Finally, the force under the pad of the 2nd toe was measured at a walking rate of 80 m/min (fig 5.24).

5.4.3 Discussion and Conclusions:

The early tests performed with stiff cork sandals at walking rates of 30, 40 and 50 m/min on a moving belt showed a uniqueness that was characteristic of each person, but the variation of amplitude observed even at a given progession rate was so large, that it was not possible to singularly define either the shape of the curve, or the magnitude of force under the given test conditions. This, even when consecutive walking cycles were compared. It is interesting to note that this erratic behaviour, already observed and described by Morton (1935) and by Schwartz et al. (1964), has been regularly encountered in all the subsequent tests executed. In all cases, two shapes of graphs relating to MP-1 and MP-2 were generally observed, a single-humped and a double-humped shape (fig 5.8). It was later realised, when the force under MP-5 was also determined, that this effect could be directly traced to the momentary balance of forces called for between the medial and lateral sides of the forefoot because, in those instances where the double-hump became most pronounced, actually due to the appearance of a trough in the

curve, there was invariably a particularly high peak of the MP-5 force/time graph corresponding exactly to the trough between the above mentioned humps; this at about 30% of the walking cycle. Hence, the continuous balancing required in the frontal plane while weight is being transferred from the heel towards the forefoot is obviously accomplished by inversion/eversion movements in the talocalcanonavicular joint.

Due to the vast scatter in results obtained and the relatively small number of walking cycles closely examined (up to 15 per test subject) it was considered futile to attempt searching for an algebraical expression that would show the dependency of the ground reaction forces on the speed of walking. However, as figures 5.9 and 5.10 that show results at 50 and 80 m/min respectively illustrate, there appears to be a definite tendency at the higher walking rate for the force under the great toe to increase (by 30% in the given example) followed by a relatively small and less ascertainable rise in the other forces measured.

Striking differences, especially in the forces measured under the head of the 1st metatarsal head, between the results of Group A with stiff cork sandals and those of Group B with flexible leather soles, made investigations with a further Group C necessary. The results with Group C completely confirmed those obtained with Group B (compare figures 5.13 and 5.20, 5.14 and 5.21, and 5.15 and 5.22). On the other hand, results of tests earlier performed with Group A were not confirmed by Group C (compare figures 5.8 and 5.9). Therefore, it could only be concluded that the results procured with Group A were not representative probably because of the small number of participants (only the results of four participants had been finally

evaluated) and possibly because an unusual, individual gait pattern had a much too dominating effect on the averages that resulted. Hence, for the purpose of further discussion relating to walking with stiff soles, only the results shown in figures 5.9 and 5.10 will be considered.

- General remarks concerning discussion of results:

Because walking with flexible soles is more usual and also approaches the physiological bare-foot gait closer than when dorsiflexion in the metatarsophalangeal joints is restricted through use of stiff soles, the results obtained when walking with normal toe-out at a pace of 80 m/min as shown in figure 5.20 will be presently discussed and used as standard reference when comparing the results of other investigations. A glance at figure 5.20 will, however, show the wide scatter in forces measured (from +160% to -70% of overall average in the case of MP-5!) and therefore the overall average values only will be considered. The <u>overall average</u> is defined here as the arithmetical mean of the average values obtained for each individual test subject and is entered into the graphs as a heavy line. The cross-hatched area envelopes all the <u>individual averages</u> and the vertically hatched field encompasses all results that were obtained during the investigation. No attempt was ever made during the evaluation to exclude a particular tracing just because it seemed to deviate too much from an expected pattern. Furthermore, the abreviation '% GC' will be used to denote an absolute temporal point in the gait cycle, and also '% BW' to denote the force in terms of percent body weight.

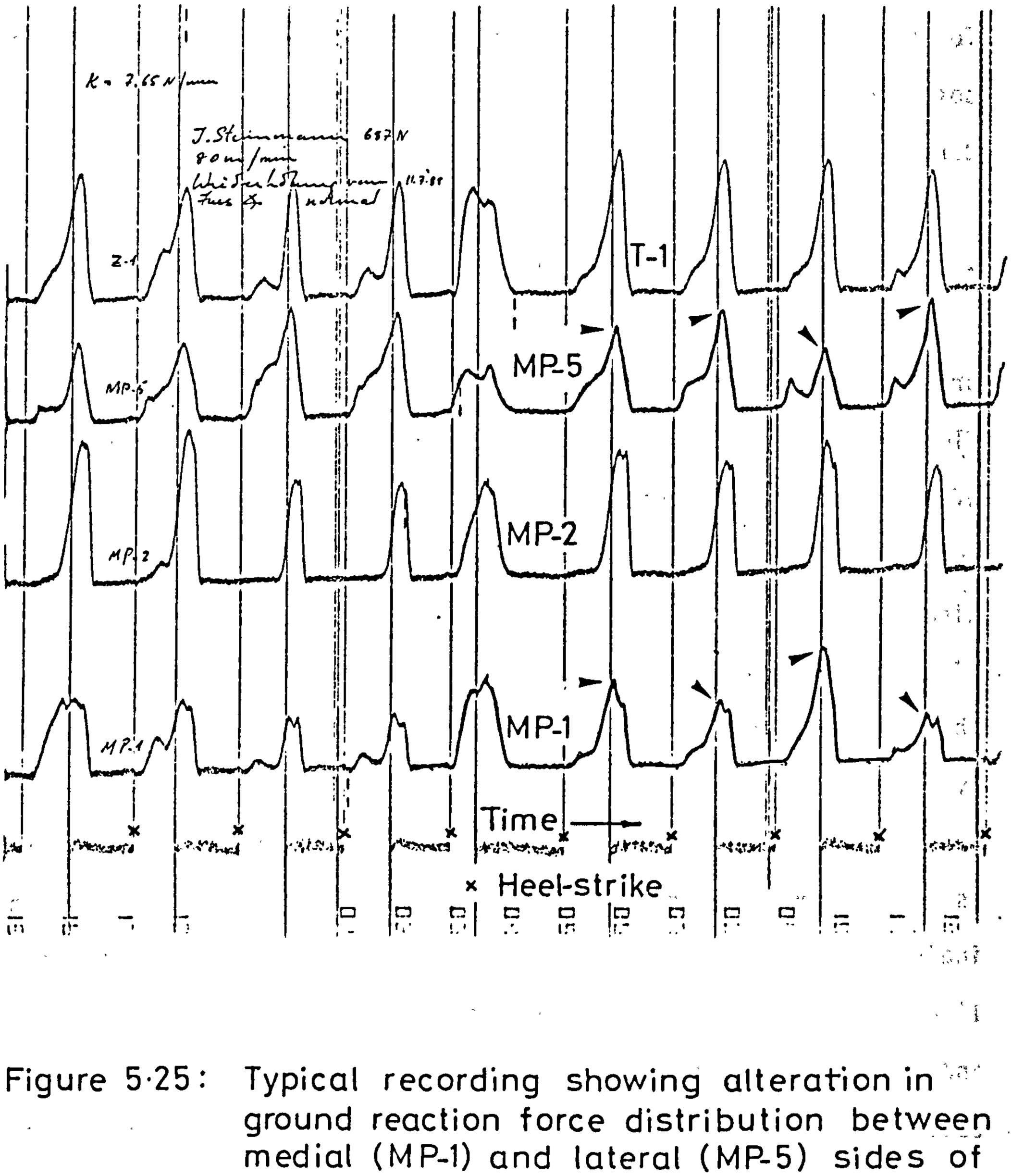

Figure 5·25: Typical recording showing alteration in ground reaction force distribution between medial (MP-1) and lateral (MP-5) sides of the forefoot when walking.

- Observations with flexible soles at 80 m/min walking pace:

The first impression gained on viewing figure 5.20 (or 5.13) is that all the measured forces in the area of the forefoot seem to show roughly the same temporal pattern: rising from zero shortly after heel-strike to about 5% BW at 10% GC, then with a lower rise rate to about 30% GC, after which a steeper rise occurs until the peak is reached in the vicinity of 45% GC before quickly returning to zero around 62% GC. Closer inspection shows slight, but characteristical differences. Whereas the above mentioned applies closely to the MP-2 and MP-5 areas, the diagram of the MP-1 ground force shows a delay of 5 to 10% of gait cycle in commencing to rise. Also, there is a definite tendency for the peak value to be maintained for a longer period of time (about 10% of the gait cycle) before falling off rapidly to zero at 62% GC. On the other hand, the force under the great toe after beginning to rise at about 10% GC, reaches its maximum only at about 50% GC, and then drops to zero as late as 65% GC. It must finally be expressly mentioned that the deviation of measured ground forces from the average loading pattern was highest in the MP-5 area, probably related to weight-balancing activities during walking, involving inversion/eversion movements in the talo-calcanonavicular joint. This effect is clearly reflected in the temporal pattern of the ground reaction force under MP-1 which not only often exhibits a relatively large deviation from the average trace, but also shows a strikingly alternating behaviour when compared with the momentary deviation of the force under MP-5 (fig 5.25).

- Stiff soles vs. flexible soles:

Comparing walking at the same rate of 80 m/min but with stiff soles (fig 5.10), it has been observed that the overall average force under MP-1 increases from about 14% BW (flexible sole) to 22% BW (stiff sole). At the same time, however, the force under the great toe diminishes from 28% BW (flexible sole) to 18% BW (stiff sole). The ground reaction force under MP-2 is also reduced from 31% BW (flexible sole) to 25% BW (stiff sole). A peak overall average force under the pad of the 2nd toe of about 5% BW was obtained. Regarding the temporal characteristics of the forces measured, it is interesting to note that with a stiff sole the force under MP-1 tends to appear earlier in the gait cycle by about 5%, reaching a peak at about 40% GC; all the other peaks were observed to appear at approximately 45% GC. Also remarkable is the duration of the forces under MP-1 and MP-5; they return to zero usually at 65% GC, compared to 62% GC with flexible soles.

- Effect of toe-out:

The effect of walking with the feet parallel to each other (about 5° toe-out) as shown in figure 5.21 is practically the same as when walking with normal toe-out. A slight reduction in the forces under MP-5, and increase under MP-1 and T-1 might occur, but the differences are insignificant. Also, a lengthening of the duration of forces until about 65% GC can be observed. On increasing the toe-out angle to about 45°, however, (fig 5.22) some slightly more obvious differences can be observed as follows: The peak force under MP-1 increases from 15% BW to 18% BW, that under MP-2 decreases from 29% BW to 26% BW and the peak group average force under MP-5 falls

from 13% BW to 10% BW; but no great differences are apparent. The temporal characteristics are similar to walking with the feet parallel to each other (toe-out of about 5°).

- Walking up and down stairs:

In walking upstairs (a flight of stairs of 1.5 m breadth with steps of 16 cm height each was used for the investigation) it was observed that generally two distinct force peaks characterise a complete stepping cycle. The first peak in the force graphs (fig 5.16) appears on the upper foot when the lower one is just about to leave the step surface. It is obviously the moment when weight is transferred to the upper foot completely. The knee above the upper foot is still flexed at this instant. The second peak arrives when the knee is extended and the foot plantar flexed in the ankle joint propelling the body upwards and forwards. At this moment the foot that had just been swung has already contacted a step further ahead and is itself in a position shortly before experiencing the 'first peak' as described before. On climbing stairs at a rate of about 2 steps per second (1 complete cycle per second) it was observed that the first peak occurred on all the force/time graphs at the same instant. The first peak was smaller than the second in the case of MP-1, MP-2 and the great toe. The overall average values of this first force peak wereas follows: 10% BW under MP-1, 20% BW under MP-2, 10% BW under the great toe, and 13% BW under MP-5. The second force peak appeared under MP-5 first, then simultaneously under MP-1 and MP-2, and finally under the great toe, with an amplitude of 11% BW, 15% BW, 29% BW and 20% BW, respectively.

In walking downstairs, it was again observed that two distinct force peaks characterise a stepping cycle (fig 5.17). The first peak appears when the ball of the foot that is on the lower step takes over the total weight of the body, at the same time decelerating the descending mass, while the second one is similar to the push-off peak seen at about 45% of the normal gait cycle. The first peak was found to be much greater than the second in the case of MP-1, MP-2 and MP-5, this first peak measuring on an overall average 15% BW, 30% BW and 15% BW, respectively. Under the great toe it measured 10% BW. The values of the second peak for MP-1, MP-2, MP-5 and the great toe were 9% BW, 18% BW, 8% BW and 12% BW, respectively.

- Walking up and down a slope of 15° (belt moving at 50 m/min!):

Compared with level walking at the same speed on the open floor (fig 5.23), the most significant difference in walking up slope (fig 5.18) appears in the peak average ground reaction force under MP-1, which increased from 11% BW to 17% BW. This is accompanied by a smaller increase of the peak average value under MP-2 from 24% BW to 27% BW but, on the other hand, by a remarkable decrease under T-1 and MP-5 that now measured only 16% BW and 10% BW, respectively. Obviously the medial side of the foot takes a greater share of the load but interestingly the force under the great toe is markedly reduced even though more dorsiflexion in the MP-1 joint might be expected due to progression up the 15° inclined plane. Walking up-slope might be characterised by a prolongated stance-phase and a correspondingly shortened swing phase of the gait cycle, the former lasting up to about 70% GC. The toe-out was observed to increase when walking upwards, but had not been recorded. Walking down a slope of 15° (fig

5.19) produced results with peak values that were generally lower than those observed in level walking under otherwise comparable conditions (fig 5.23). Also, the temporal force pattern is markedly changed, the graphs being very much flattened between about 20 and 50% GC.

- Effect of walking speed:

A comparison of figures 5.20 and 5.23 that show the respective results at 80 m/min and 50 m/min, but otherwise under identical test conditions, clearly indicate an increase in the peak values of the average ground reaction forces under T-1 (from 24% BW to 31% BW), MP-1 (from 12% BW to 15% BW) and MP-2 (from 26% BW to 29% BW), with increase of walking speed. The peak average force value under MP-5, however, was observed to remain unchanged at 13% BW. This also reflects a tendency for the 'centre of pressure' in the forefoot to move more towards the medial border of the foot with increase in walking rate.

- Gait pattern on moving belt vs. walking on open floor:

From figure 5.12 which shows the results obtained from a preliminary test that involved only a single test subject, it can be seen that no significant difference in the overall average values is present. It may, however, be remarked that the stance phase appears to be extended by about 3 to 5% of the gait cycle, while the swing phase becomes correspondingly shorter. Whether this is a typical characteristic of gait on a moving belt is not known. However, since this detail is probably of no great importance for the present purpose, it has not been pursued any further.

The results of the investigations performed in this study approach the observations made by Hutton, Stott and Stokes (1982) most closely (see Sections 2.3.2 and 2.3.3). In contrast, however, the present results that were obtained through a different measuring technique give discrete quantitative information on the ground reaction forces acting specifically on the heads of the 1st, 2nd and 5th metatarsals and on the pad of the great toe in several modes of walking. In some limited tests, the forces under the pads of the 2nd and 3rd toes too were measured. The present findings that are quite in agreement with observations made by Hutton et al. (1982), especially regarding the function of the toes in walking, whereby the great toe alone can be subjected to as much as 48% BW in normal walking (fig 5.20), are in sharp contrast to those of Mann and Hagy (1979) who maintain:'during walking there is no ankle plantar flexion or intrinsic muscle of the foot which causes push-off to propel the body forward'; nor could the observation of Fujita et al. (1983) be confirmed who also are of the opinion that 'the toes do not participate in the action of push-off in regular level walking'.

Apart from the measured forces under the great toe (T-1) that occasionally reached values of about 50% BW, the 2nd toe (T-2) was also seen to be exposed to forces of about 15% BW in maximum (Table 5.4 shows the peak values measured for easy reference and comparison). The 3rd toe (fig 5.11) too was observed to be acted upon by about 80% of the peak load under T-2.

Summarizing the results of the investigations performed, with reference to Table 5.4, it might be stated that:

- In habitual walking on the level floor at about 80 m/min (a comfortable walking speed) with flexible soles, the ground reaction

TEST				GROUP	MEASURED PEAK FORCES* (GROUP AVERAGE / HIGHEST) T= toe MP= metatarsophalangeal joint					FIGURE
Sole F=flex. S=stiff	Walking speed m/min	Toe-out (n= normal)	Further details		T-1	T-2	MP-1	MP-2	MP-5	
F	80	n	Level walking	B	26 / 44		11 / 30	30 / 48	17 / 34	5.13
				C	31 / 48		15 / 34	29 / 48	13 / 34	5.20
				C	28 / 48	6 / 15	14 / 26	31 / 54		5.24
S	80	n	"	C	18 / 27	5 / 13	22 / 42	25 / 42		5.10
S	50	n	"	C	13 / 22	4 / 9	20 / 40	24 / 40		5.9
F	80	~5°	"	B	28 / 50		15 / 31	28 / 45	10 / 26	5.14
				C	33 / 44		15 / 43	28 / 43	12 / 34	5.21
F	80	30 to 45°	"	B	30 / 47		18 / 35	27 / 41	9 / 21	5.15
				C	31 / 45		18 / 32	26 / 40	10 / 25	5.22
F			Ascending stairs	B	20 / 41		15 / 32	29 / 50	11 / 28	5.16
F			Descending strs.	B	12 / 37		14 / 28	29 / 50	15 / 29	5.17
F	50		Walking up slope	B	16 / 33		17 / 39	27 / 43	10 / 29	5.18
F	50		Walkg down slope	B	19 / 33		11 / 26	18 /32	10 /30	5.19
F	50	n	Level walking	C	24 / 42		12 / 26	24 / 41	13 / 31	5.23

* in percentage of body weight (% BW)

TABLE 5.4 Peak ground reaction forces measured (overall, or group average, and highest individual) under various gait conditions

force under the head of the 2nd metatarsal is the highest, and has been observed to attain a maximum value of 54% BW. The overall average (group average) peak was found to be about 30% BW. The ground reaction forces under MP-1 and MP-5 were seen to be very similar to each other, the overall average peak measuring about 15% BW and the highest peak value ever measured being 34% BW in both cases. The overall average peak force determined under the great toe was about 30% BW, while the highest peak measured 48% BW.

- On forcing the foot to adopt a small toe-out angle of about 5° (feet parallel) when walking, no significant difference in the loads measured under the forefoot could be observed when compared to walking in a habitual manner at the same speed. On adopting an exaggerated toe-out of 30° to 45°, however, a distinct tendency for the centre of pressure in the forefoot to move more medially during push-off was observed. This was evident through a slight reduction of the peak forces under MP-5 and a simultaneous increase under MP-1. Also, the peak value under T-1 increased slightly. The shift in the measured values amounted to about 3% BW in each case (Table 5.4).

- Walking up a slope of 15° loaded the heads of the 1st and 2nd metatarsals more, and at the same time, caused reduction of the ground force under MP-5 (Table 5.4) when compared with walking on the level at the same speed of 50 m/min (fig 5.23). The difference in peak average values were 5, 3 and 3% BW, respectively. Interestingly, the peak force under the great toe was reduced to only 67% of its value when walking on a level floor at the same speed of 50 m/min. On walking down the same slope, a general reduction in all the measured forces resulted (Table 5.4).

- Ascending and descending stairs cause a marked difference in the shape of the force/time graphs. They all now show a distinct double-humped form. On ascending, the second peak was generally higher than the first. Peak average values obtained when walking up 16 cm high steps were: 15% BW, 29% BW, 11% BW and 20% BW under MP-1, MP-2, MP-5 and T-1, respectively. Descending stairs causes the first peak to become greater than the second in the graphs of the forces acting under the metatarsal heads. The peak values observed are of about the same magnitude as those obtained on climbing, with the exception of the great toe; in which case only 12% BW was measured (Table 5.4) on descending.

- An increase in walking speed results in higher forces under MP-1, MP-2 and T-1 (15% BW, 29% BW and 31%BW at 80 m/min, compared with 12% BW, 24% BW and 24% BW at 50 m/min, respectively). The average force peak under MP-5 remains unchanged, so that it might be inferred that the centre of pressure in the forefoot moves more towards the medial border of the foot when the speed of walking is increased.

- The gait pattern on a moving belt of 1.5 m usable length is similar to that on the open floor. However, the stance phase is possibly lengthened by about 3 to 5% of the gait cycle, with a corresponding shortening of the swing phase, but this point was not investigated any further.

- Stiff soles, even when furnished with a rocker bar in the region of the forefoot, were observed to alter the distribution of ground reaction forces under T-1 and MP-1 considerably. Under otherwise identical test conditions and at a walking rate of 80 m/min, a decrease in the peak loads under MP-2, T-1 and T-2 was observed with

stiff soles, that under T-1 dropping from 28% BW to only 18% BW (Table 5.4). Only the force under MP-1 showed an increase from 14% BW to 22% BW when stiff soles were worn.

Generally in normal walking, the forces under the forefoot appear immediately after heel strike and remain for about 62% of the walking cycle with the great toe leaving the ground a little later, at about 65% GC. As soon as the habitual gait style is altered, e.g. through changing the toe-out angle, walking on a relatively short (1.5 m long) moving belt, walking at an uncomfortably low speed, or through wearing stiff soles, the duration of contact between forefoot and ground becomes lengthened by about 3% of the gait cycle, with a corresponding reduction in the duration of the swing phase. It is interesting to note that Schwartz and Heath (1947) also observed lengthening of the stance phase when comparing locomotion characteristics of functionally disabled feet with normal ones.

CHAPTER 6

THEORETICAL ANALYSIS OF FORCES AND STRESSES IN THE FOREFOOT

6.1 Introduction:

Having determined the principal dimensions of the bones of the forefoot and the topography of the joint surfaces, observed the exact direction and location of the tendons that cross the joints of the forefoot with respect to the joint contours, and also having measured the external forces that act on the forefoot, it is now possible to proceed with an estimation of the muscle forces that act along the tendons and to determine the forces that come into play at the joint surfaces. As is most often customary with such evaluations, it will be assumed that only synergetic muscles (agonists) come into action at a particular moment to overcome external forces and that the simultaneous action of antagonists can be completely disregarded. This assumption might not be true, as the EMG recordings of the extensor digitorum brevis and flexor digitorum brevis in figure 2.6a suggest, but because of the problem of predicting muscle forces (see Section 2.4.1 of Chapter 2) and because, on the other hand, there even might not be simultaneous activity, as shown by the EMG plots in figure 2.5a, the action of the agonists alone will be considered in determining joint forces.

Furthermore, some pathological affections like 'march' fractures, or like the idiopathic necrosis of the metatarsal heads (Koehler-Freiberg's disease) with the characteristic necrotic zone lying just underneath the plate of subchondral bone of the metatarsal head, so much resembling the mechanical fatigue phenomenon resulting in 'pitting' (fatigue of ball and roller bearings, for example), compel one to examine the state of stress in the relevant structures. This is presented in Section 6.4.

Finally, it must be mentioned that these analytical procedures

have been presently applied only to the first and second rays of the foot, this being considered of prime importance because these two structures differ functionally most from each other, each being exposed to pathological conditions peculiar to itself.

6.2 Forces Exerted by the Flexor Muscles, and Joint Forces in the First Ray:

Locomotion studies as reported in Chapter 5 have shown that the plantar pad of the great toe is exposed to forces that could amount to as much as 50% body weight (BW) in normal, level walking. In running, jumping, etc., even higher forces might well occur. Also, the plantar surface just underneath the 1st metatarsal head was observed to transmit up to about 40% BW on walking up a slope or when using shoes with stiff soles (MP-1 in Table 5.4). By now applying these known external forces to the mechanical structure, which can be geometrically described as shown in figures 4.7, 4.15, 4.18 and 4.19, the magnitude and direction of the internal forces crossing the joint surfaces can be estimated.

6.2.1 Method of analysis:

The forces exerted by agonist muscles and the reaction forces acting across joint surfaces are basically determined by using free-body diagrams, according to the principles of statics of rigid bodies, to satisfy the conditions necessary to equilibrate the external forces that had been measured. That is, the masses of the distal elements of the foot and the accelerations to which they are exposed are considered to be so small, that inertia forces due to their movement might be neglected totally. The possible action of the plantar

aponeurosis has also been totally disregarded since, as shown in Chapter 4, the metatarsal bones are loaded mainly in bending (like cantilevers) even with the plantar aponeurosis intact. Totally disregarding any supporting action of this structure leads to relatively unfavourable results and therefore this approach was decided upon. Furthermore, the assumption is made that the coefficient of friction of the cartilaginous joint surfaces is so low that the force vector crossing the joint surface could always be drawn normal to the latter. [The coefficient of friction as determined by Charnley (1960) on cartilaginous joint surfaces was observed to be lower than 0.02 so that the vector would be displaced by only about 1°]. And finally, for the sake of convenience, some minor adjustments to linear dimensions (e.g. smoothing of radii of curvature along joint contours) have been carried out - this being justified by anthropometric variability always encountered.

Beginning with the ground force under the pad of the great toe, the force in the flexor hallucis longus (flex.hall.long.) tendon is determined and also the force across the interphalangeal (IP-1) joint. In a second step, the force exerted by the flexor hallucis brevis (flex.hall.brev.) muscles is estimated, not neglecting the force applied by flex.hall.long. simultaneously, to obtain equilibrium in the first metatarsophalangeal (MP-1) joint. On considering the action of the flex.hall.brev. muscles, it must be borne in mind that these are strongly supported by that of the abductor hallucis (abd.hall.) muscle, as evident from the EMG recordings shown in figures 2.6a-e. Nevertheless, because of the difficulty in ascertaining the share of load taken by this muscle, it will be totally disregarded in the analysis, so that the flex.hall.brev. muscles will

be considered to exert the whole force necessary to satisfy equilibrium conditions in the MP joint. This approach has been chosen, since it leads to 'worst case' results. However, when relevant, it is possible to judge what influence the action of the abd.hall. could have had on the results, had it also been taken into consideration as an entity of its own.

The calculation and results do not use absolute units of force but units relative to the ground force F, acting on the pad of the great toe, instead. It must therefore be borne in mind, that F is not a unit of constant magnitude (not even of constant relationship to the total body weight, BW) but varies during the gait cycle from instant to instant.

The following Sections show details of the procedure and the results obtained.

6.2.2 Analysis and results:

Referring to figure 4.19 of Chapter 4, it will be immediately recognised that the projections of the axes of the bones of the first ray in a horizontal plane do not coincide to produce a continuous straight line but that the three axes are more like chords along a circular arc. Each bone axis may be described as being positioned in about 10° external rotation with respect to the more proximal immediate neighbour. Also considering the path taken by the flex.hall.long. tendon in relation to these axes, and the location of the pad of the great toe through which the ground force is transmitted, it becomes obvious that the structure cannot strictly be treated as a two-dimensional problem lying in a vertical plane. Nevertheless, the vector projections in the vertical plane along the

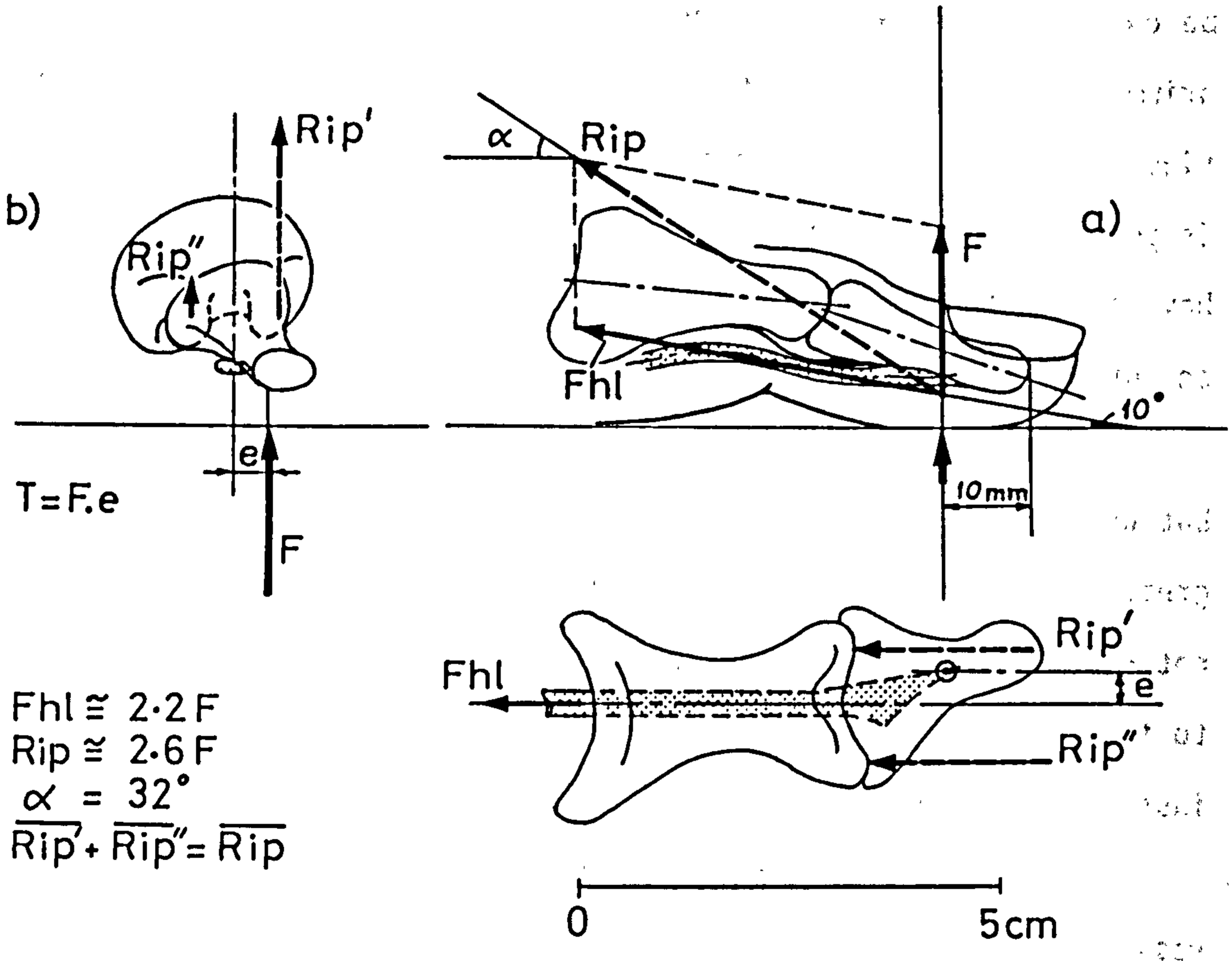

(Left foot)

Figure 6.1 Muscle force ($\overline{Fhl}$) and resultant ($\overline{Rip}$) in the IP-1 joint due to a vertical ground reaction $\overline{F}$

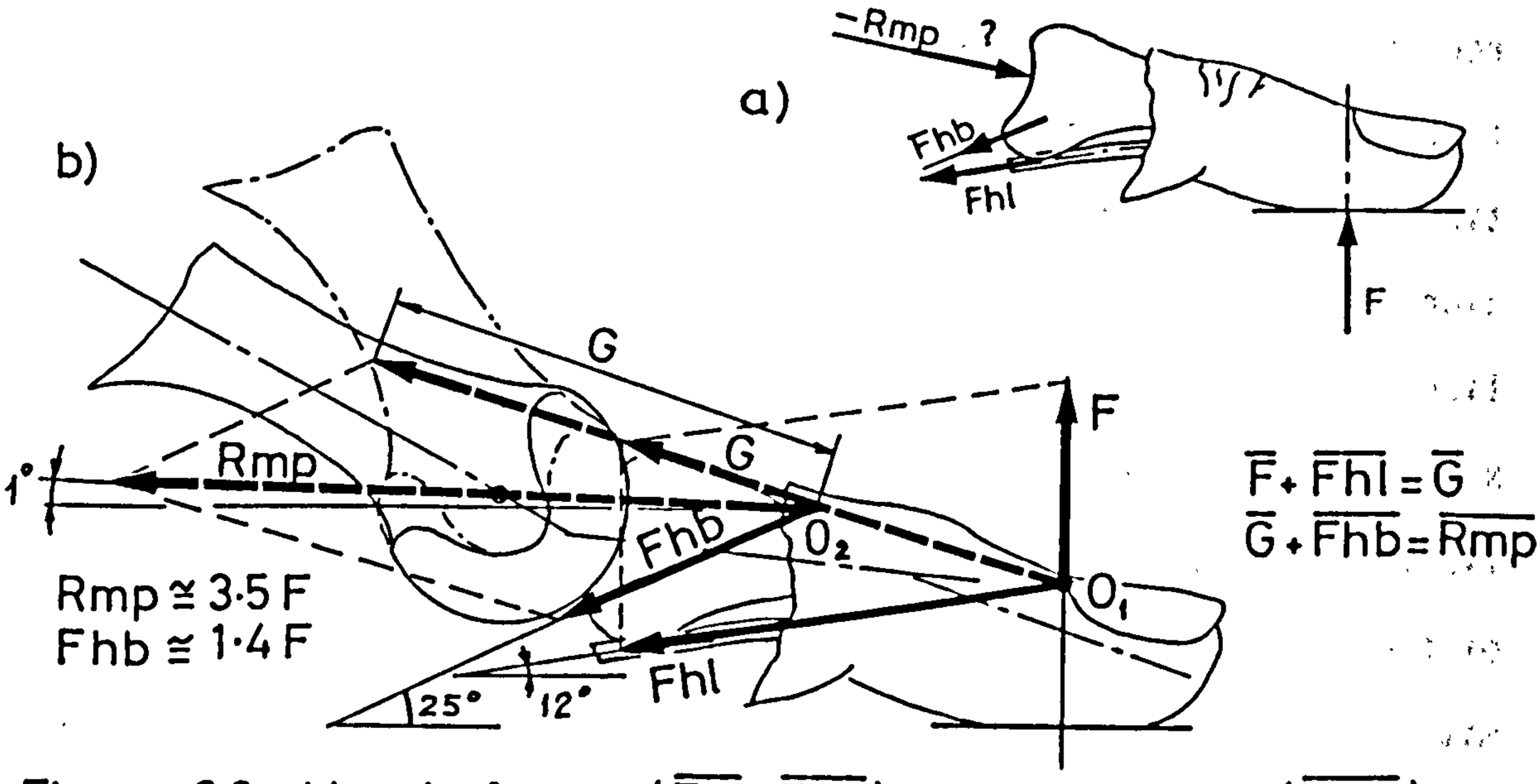

Figure 6.2 Muscle forces ($\overline{Fhl}$, $\overline{Fhb}$) and resultant ($\overline{Rmp}$) in the MP-1 joint due to force $\overline{F}$

longitudinal axis of the foot must still comply with equilibrium conditions and therefore two-dimensional analysis will first be performed before the effects of forces acting outside the chosen plane are considered.

6.2.2.1 The interphalangeal joint of the great toe (IP-1):

Figure 6.1a shows the situation for the distal phalanx in a vertical plane passing through the axis of the flexor tendon. Because of the large contact area between toe and ground, it has been assumed that the centre of ground pressure acts about 10 mm proximal to the distal tip of the bone. The distal phalanx, according to conditions assumed in figure 6.1a which do not include any restraint effected by the joint capsule or collateral ligaments, requires a muscle force of about 2.2F, resulting in a joint force of about 2.6F, to sustain the ground force F. The resultant in the IP-1 joint may be described as acting in an antero-plantar (or dorso-posterior) direction at an angle of about 32° to the horizontal.

Observing the same structure projected onto a transversal vertical plane, that is, one normal to the axis of the foot as shown in figure 6.1b, it becomes immediately apparent that a turning couple (T) would exist because the vector $\underline{F}$ lies outside the longitudinal, vertical plane previously chosen. Keeping the proximal phalanx fixed, the torque thus applied to the distal phalanx must be transmitted to the saddle, or hinge joint. This, however, allows no freedom of rotation about the longitudinal axis and therefore, the joint resultant $\underline{Rip}$ must be resolved into two components, $\underline{Rip'}$ and $\underline{Rip''}$, each acting on a medial and lateral condyle of the saddle joint (cross sections B-B and C-C in figure 4.18) such that their combined action

constitutes the turning couple, T. This of course holds true only for the case in which the ground reaction force is strictly vertical. Any additional horizontal component facilitated by friction between toe and ground will lead to a different situation, possibly even negating the torque mentioned above. This will be discussed later.

6.2.2.2 The metatarsophalangeal joint of the first ray (MP-1):

Considering the free body situation of the whole extremity distal to the MP-1 joint, as figure 6.2a shows, the dorsally directed ground force F is counteracted by the pull of the flex.hall.long. tendon (already estimated to be about 2.2F) together with the pull of the flex.hall.brevis muscles (this including contribution from the abd.hall. muscle), and the joint resultant Rmp that appears normal to the joint surfaces. The vector diagram in figure 6.2b, based on the dimensions shown in figures 4.15 and 4.19, shows the manner in which the unknowns have been determined; by first adding F and Fhl to obtain the vector sum G, and by then applying G to the direction of the flex.hall.brev. pull (Fhb) before constructing the final parallelogram of forces, the diagonal of which must necessarily pass through the centre of curvature of the joint surfaces. The diagonal represents the magnitude and direction of the joint resultant, Rmp. With reference to figure 6.2, it might be concluded that the force exerted by the flex.hall.brev. muscles would amount to about 1.4F while the joint resultant, Rmp, measures about 3.5F, the latter acting at approximately 1° to the horizontal in an antero-posterior direction.

An earlier analysis (Jacob et al., 1985) in which it was assumed that the combined effect of the flex.hall.brev. et long. mus-

a)

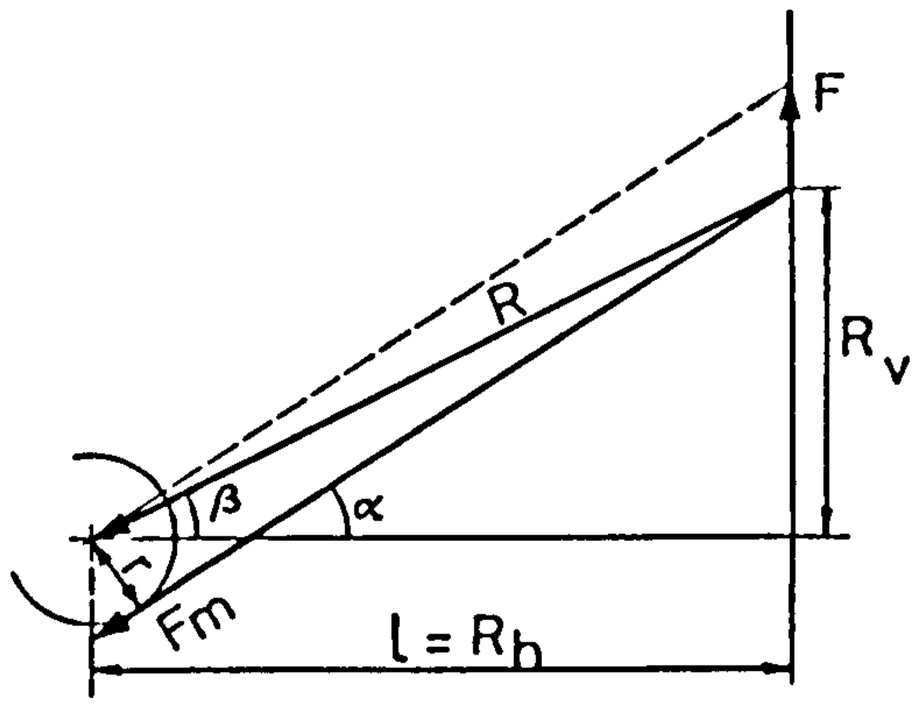

b)

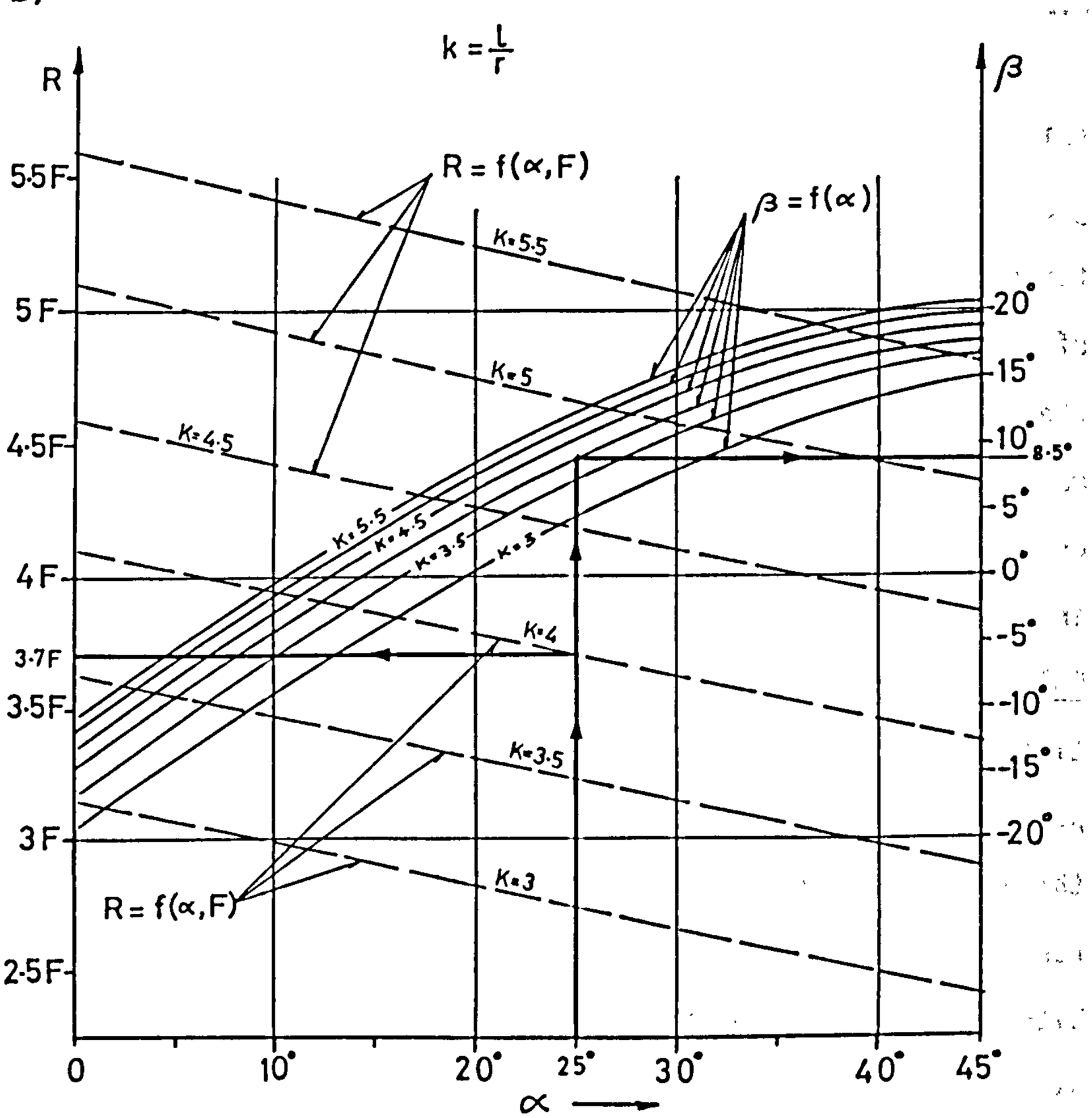

Figure 6·3 Dependence of joint resultant R on l/r (=k) and α

cles acted at an angle of abc . 22° to the horizontal showed that the joint resultant could attain a magnitude of about 5F. This considerable discrepancy from the result obtained in the present model (3.5F) calls for a closer examination of the factors governing the result.

Taking the generalised case as shown in figure 6.3a, it follows that:

$Fm = \frac{F.l}{r}$ where F is the ground reaction and Fm the muscle force

$R_v = Fm \cdot \sin\alpha - F = \frac{F.l}{r} \cdot \sin\alpha - F = F\,(\frac{l}{r}\sin\alpha - 1)$

$R_h = Fm \cdot \cos\alpha = \frac{F.l}{r} \cdot \cos\alpha$

Let $k = \frac{l}{r}$, then:

$R = \sqrt{R_v^2 + R_h^2} = F\sqrt{k^2\sin^2\alpha - 2k\sin\alpha + 1 + k^2\cos^2\alpha}$

$R = F\sqrt{1-2k\sin\alpha + k^2}$ (I)

$\beta = \arctan\frac{1-k\sin\alpha}{k\cos\alpha}$ (II)

Using parameter values of 3, 3.5, 4, 4.5, 5, and 5.5 for k, that is 1/r, graphs of R and β of the equations (I) and (II) are shown in figure 6.3b for α between 0° and 45°.

Figure 6.3b clearly indicates that R, the magnitude of the resultant, highly depends on the ratio 1/r and to a far lesser extent on the angle α. Figure 6.4 shows the assumptions that had been made earlier (Jacob et al., 1985) in which the ratio 1/r amounted to 5. It will be readily appreciated that the course taken by the flex. hall.long. tendon, as now marked by wires in figure 6.4, is diffi-

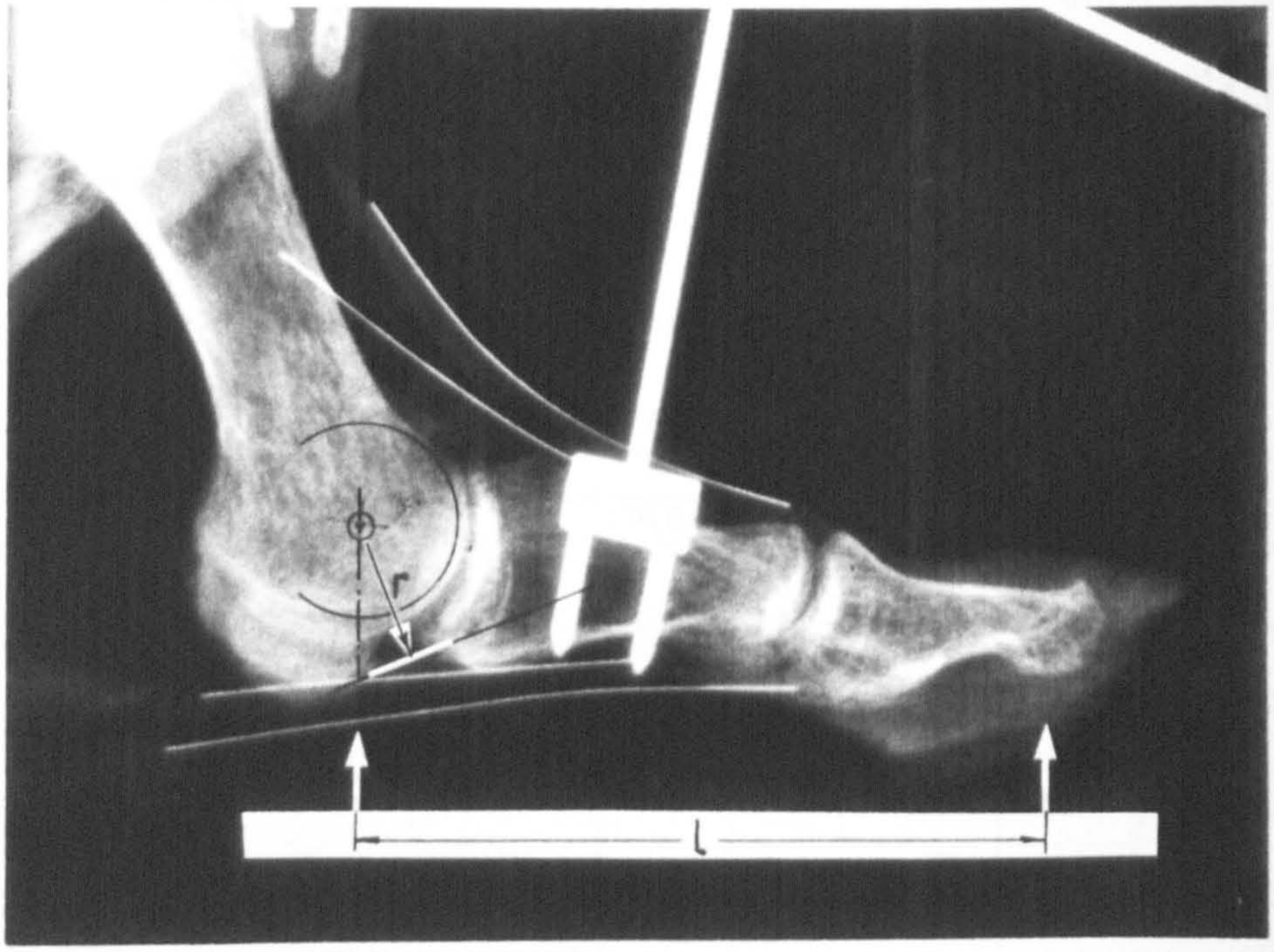

(Wires were introduced between the tendons and their sheaths to observe the paths followed)

Figure 6.4 A first ray with an l/r ratio of about 5

cult to establish precisely and could therefore easily lead to assumptions of length r that would markedly affect the results.

It must also be mentioned that only forces acting in a vertical plane have been considered and that, as in the case of the interphalangeal joint treated before, the off-set of the line of action of the vertical ground reaction force F with respect to the chosen vertical plane containing the flexor tendons and the joint centres, would induce rotation about a longitudinal axis, causing the toe to pronate in the MP-1 joint. This pronation would be resisted by the medial collateral ligament and by the fibrous ties that join the medial tubercle of the metatarsal head to the plantar plate containing the sesamoid bones. However, the magnitude of the torque depends very much on whether a horizontal component, enabled by friction between ground and toe pad, is present in the ground reaction vector under the toe. This will be considered in the discussion later.

6.2.2.3 The tarsometatarsal joint of the first ray (TM-1):

Again, observing the action of all principal external forces with regard to the first ray distal to the tarsometatarsal joint (fig 6.5a and b), it will be seen that these are: the ground reaction forces F and Fmp under the pad of the toe and under the metatarsal head, respectively, and the action of the flex.hall.long. (Fhl), flex.hall.brev. (Fhb), abd.hall. (Fabh) and peroneus longus muscles. Apart from these 'active' entities, there are of course the so-called 'passive' structures which consist of the capsule and ligaments attached to the base of the first metatarsal bone. However, for the moment, only those elements which allow their activity to be

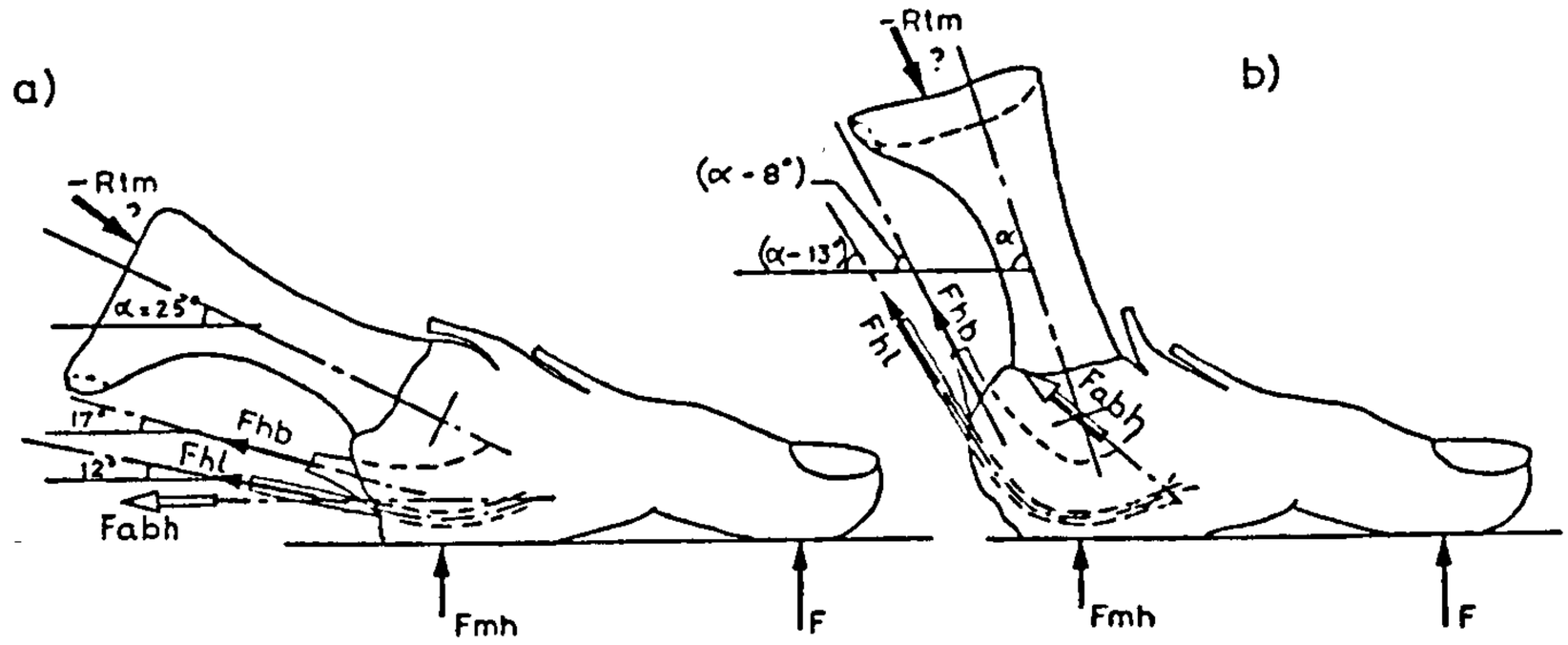

The relative positions of Fhb and Fhl remain unaltered with respect to the metatarsal axis. a) in the foot-flat position, b) with the foot at about 50% of the gait cycle.

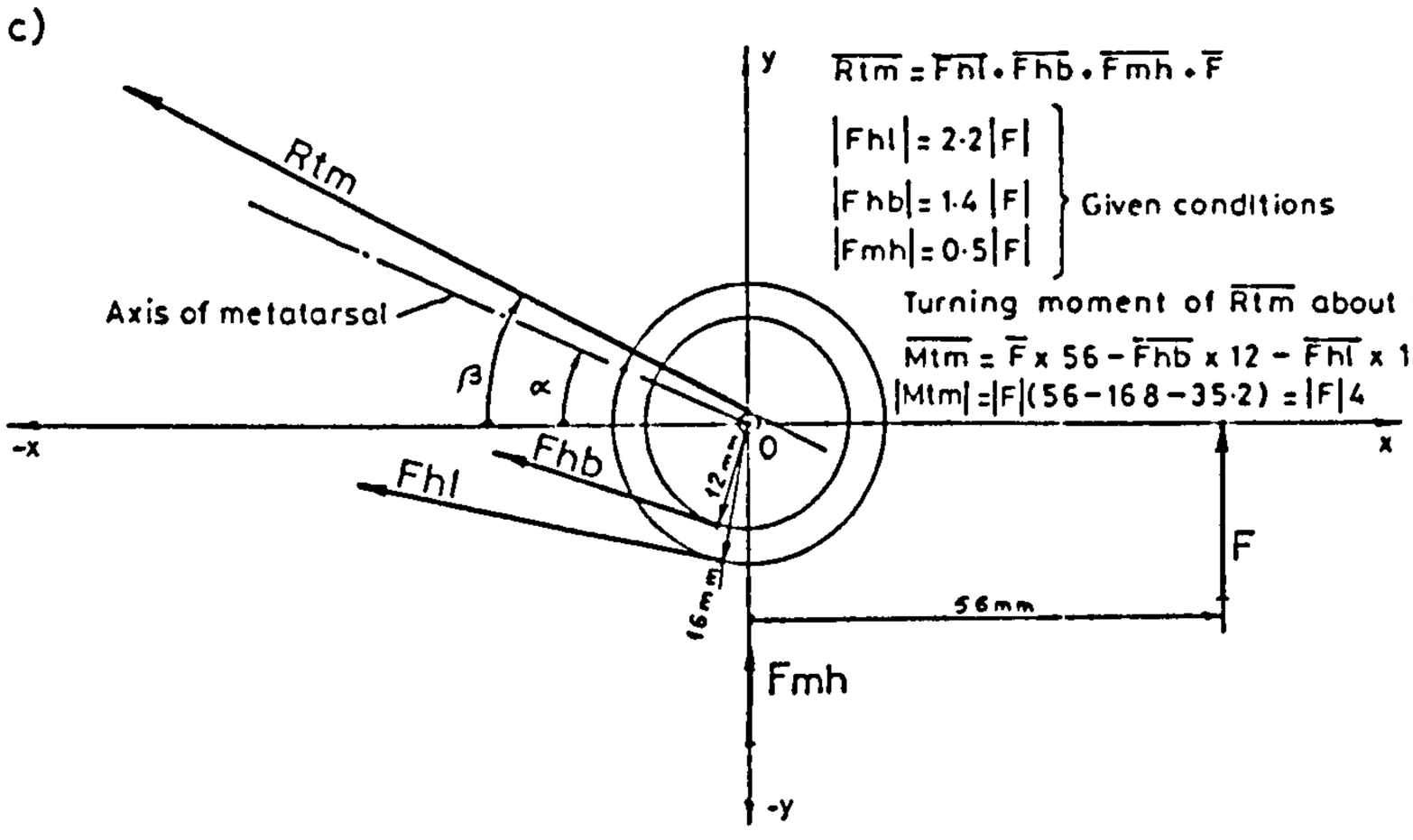

On rotating $\overline{Fhb}$ and $\overline{Fhl}$ about the z axis ($25° \leqq \alpha \leqq 85°$):

$$|Rtm| = k \cdot |F|$$

α	25°	35°	45°	55°	65°	75°	85°
k	4.2	4.43	4.61	4.76	4.89	4.98	5.05
β	34°	42°	50°	57°	64°	72°	79°
(β-α)	9°	7°	5°	2°	-1°	-3°	-6°

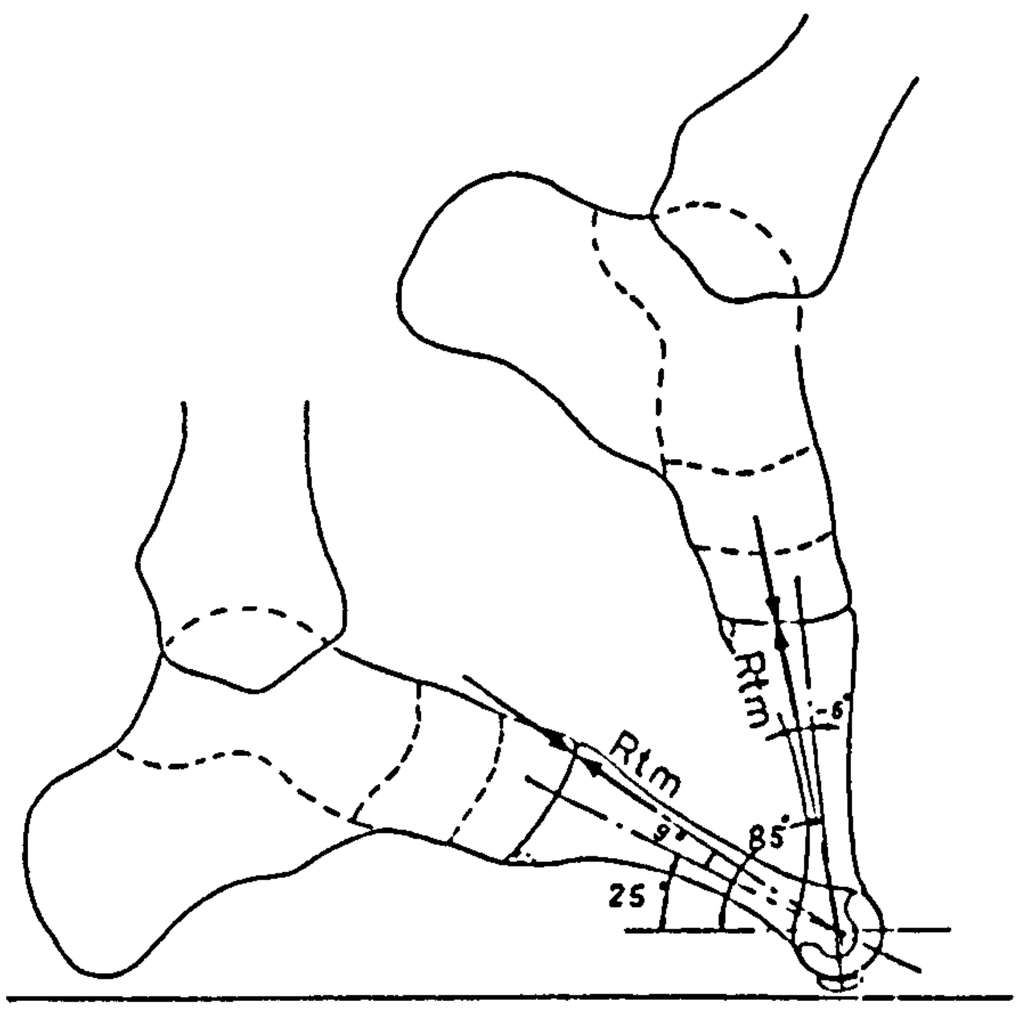

Rtm is the resultant of all forces acting at the distal end of the metatarsal bone.

Figure 6·5 Resultant (Rtm) in the tarsometatarsal joint of the first ray, disregarding the effect of the abductor hallucis muscle (Fabh).

quantitatively estimated will be taken into consideration and their combined action on the tarsometatarsal joint observed. As already mentioned, the action of the abd.hall. muscle will be completely disregarded in the analysis. Instead, the flex.hall.brev. muscles are considered to exert the whole force necessary to satisfy equilibrium conditions in the MP joint, bearing in mind that the course taken by the flex.hall.brev. muscles is less favourable than that taken by the abd.hall. for support of the longitudinal arch. Also, the action of the peroneus longus muscle - for want of quantitative force data - will be totally disregarded too.

With reference to figure 6.5 it will be noted that the magnitude of the ground force (Fmh) under the metatarsal head has been chosen to be half that acting under the toe pad (F), as observed from gait investigations (see figures 5.13 and 5.20, and Table 5.4 of Chapter 5). The gait investigations showed that the peak force under the metatarsal head (MP-1 in figures 5.13 and 5.20) usually appears at 40 to 45% of the gait cycle (GC), whereas the peak force under the great toe (T-1) follows slightly later, at about 50% GC. Since obviously the force F under the great toe influences the forces in the first ray to a greater extent than Fmh, this point in the gait cycle, that is 50% GC, will be especially considered. At 50% GC the heel is well off the ground but the actual amount of dorsiflexion in the MP-1 joint varies considerably; this being very individual, and also dependent on the type of foot wear used. Cinematographic investigations described in Section 5.3.3 showed a range of dorsiflexion in the MP joints ranging from 37° to 56°. As already reviewed at length in Section 2.7.3 of Chapter 2, Bojsen-Møller and Lamoreux (1979) as well as Mann and Hagy (1979) have reported on their obser-

vations regarding movement in this joint. Also Inmann et al. (1981) describes the movement between the hindfoot-midfoot and forefoot during gait. Following these observations, an analysis of the forces relevant to the tarsometatarsal joint is now described to cover a total range of dorsiflexion of 60° (0° dorsiflexion is the neutral, foot-flat position).

With reference to the drawings a) and b) of figure 6.5 it will be appreciated that the positions of the vectors Fhb and Fhl remain unchanged with respect to the metatarsal axis. Therefore, beginning with their initial position as shown in sketch a), they were rotated about a z axis, along with the metatarsal axis, from $\alpha = 25°$ to $\alpha = 85°$ in steps of 10°, in a Cartesian coordinate system as shown in diagram c). From:

$$\begin{bmatrix} x' \\ \\ y' \end{bmatrix} = \begin{bmatrix} \cos\alpha & -\sin\alpha \\ \\ \sin\alpha & \cos\alpha \end{bmatrix} \cdot \begin{bmatrix} x \\ \\ y \end{bmatrix}$$

the rotated directions of Fhb and Fhl were calculated for the chosen values of α.

The sum of all force vectors, Rtm, and the sum of all turning moments, Mtm, about the origin O were determined for each value of α. It is interesting to note that Mtm turns out to be very small (fig 6.5c), which implies that the resultant Rtm passes very close to the centre of the MP-1 joint. The shortest distance between Rtm and the centre of the joint is given by 4F/Rtm in mm. The magnitude of Rtm is defined in units of F, the factor being expressed by k in

the table shown in figure 6.5. The direction of Rtm is given by β.

6.2.3 Discussion and conclusions:

The analysis of muscle forces and joint reactions acting in a vertical plane that contains the flexor hallucis longus tendon has shown that a very strict balance between each of the forces exerted by the flex.hall.long (Fhl) and flex.hall.brev. (Fhb) muscles must be provided for if the relative positions of the adjoining members of the first ray are to be maintained in equilibrium while the pad of the great toe is acted upon by a ground force F. While considering the effect of load sharing between these muscles it must be borne in mind that the main purpose served by them is to enable the pad of the great toe to transmit force to the ground and, as will be shown later, to actively support the longitudinal arch of the foot. As figures 6.1 and 6.2 show, under the geometrical assumptions made (figs 4.15, 4.18 and 4.19), the ratio of Fhl:Fhb:F is about 2.2 : 1.4 : 1.

If, for instance Fhb would take a larger share, then the IP-1 joint would be forced into dorsiflexion until movement is either arrested by taughtening of the collateral ligaments and the plantar aspect of the joint capsule, or until a position on the joint surface is reached where the radius of curvature is now such that the increased lever arm of the flex.hall.long. tendon satisfies equilibrating conditions. The last mentioned 'self-stabilising' effect seems, however, unlikely with the joint topography observed and therefore it is more probable that the IP-1 joint would move into hyper-dorsiflexion until the capsule and collateral ligaments arrest further movement. On the other hand, if Fhb would fall short of

taking its share, then the great toe would 'curl' into a clawing position, forcing the IP-1 into plantar flexion while the MP-1 joint dorsiflexes correspondingly.

With the geometrical configuration that has been assumed, the resultant in the IP-1 joint measures about 2.6 F while that in the MP-1 joint amounts to about 3.5 F. It must be emphasized that the results are very dependent on the assumptions made regarding the position of the ground force and the tendon with respect to the centre of rotation (lever arms) and that therefore these values should only be accepted and used with due caution.

Observing the magnitude of forces that were measured under the pad of the great toe during gait (as shown in figures 5.13 and 5.20, and Table 5.4 of Chapter 5) the tensile stress produced in the flex. hall.long. tendon, assuming a cross-sectional area of 13.5 mm^2 (Table 4.1) and total body weight of 700 N, amounts to about 35 N/mm^2 with the average peak load measured under the pad of the great toe. Since the maximum peak force under the great toe could amount to about 1.7 times the average peak value, the highest tensile stress that develops in the tendon would be correspondingly higher. The UTS of this tendon as determined by Yamada (1970) is about 66 N/mm^2 and therefore at maximum peak loads, the stress in the tendon would approach 85% of the rupture limit. [A flex.hall.long. tendon of 13.6 mm^2 initial cross sectional area was tested by the author. The rupture limit (failure at the edge of the grips) proved to be 990 N which gives a UTS of about 73 N/mm^2].

In the analysis performed, the force vector $\underline{F}$ has been assumed to act strictly in a vertical direction. However, because of friction between the foot and the ground, especially in barefoot gait,

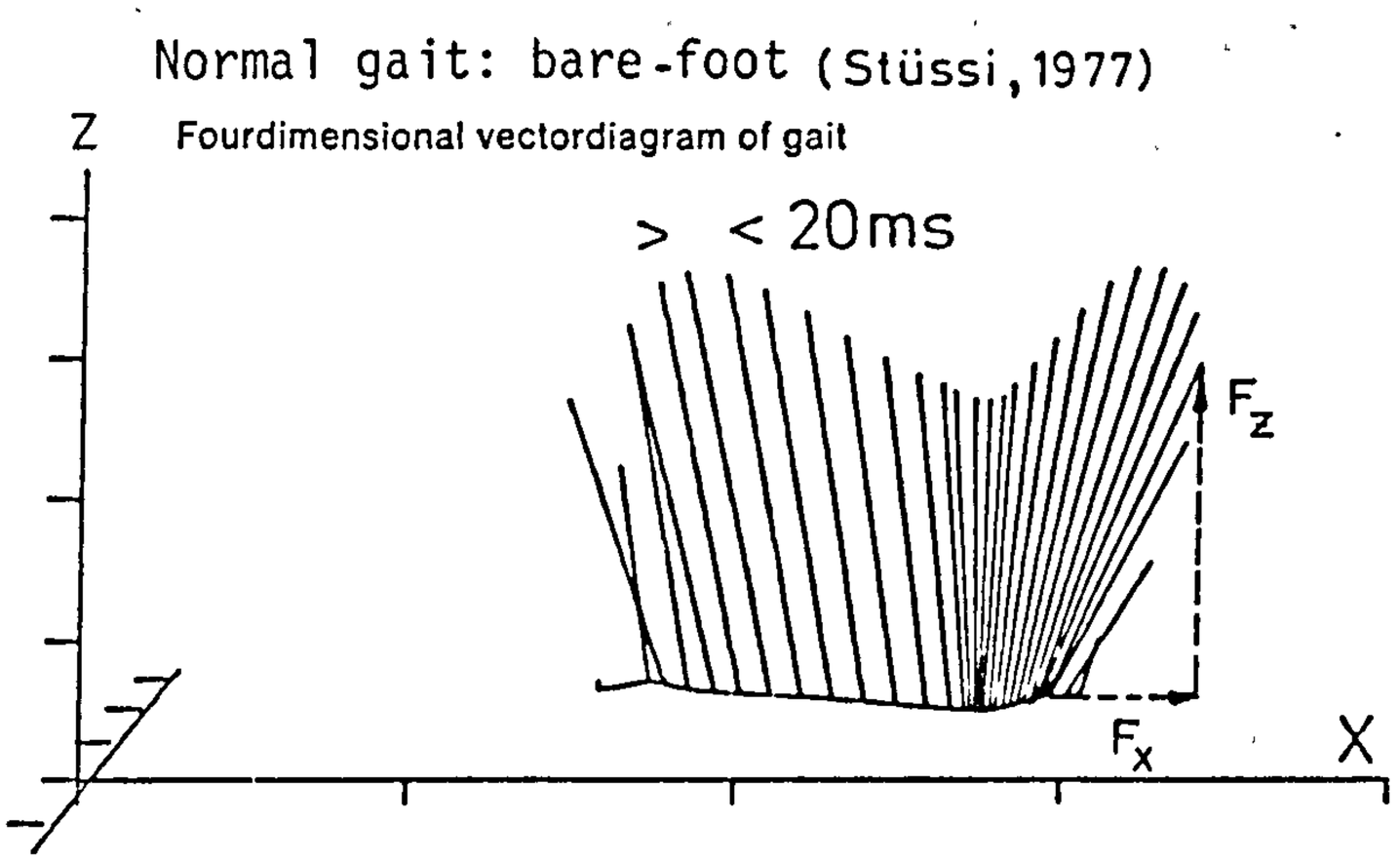

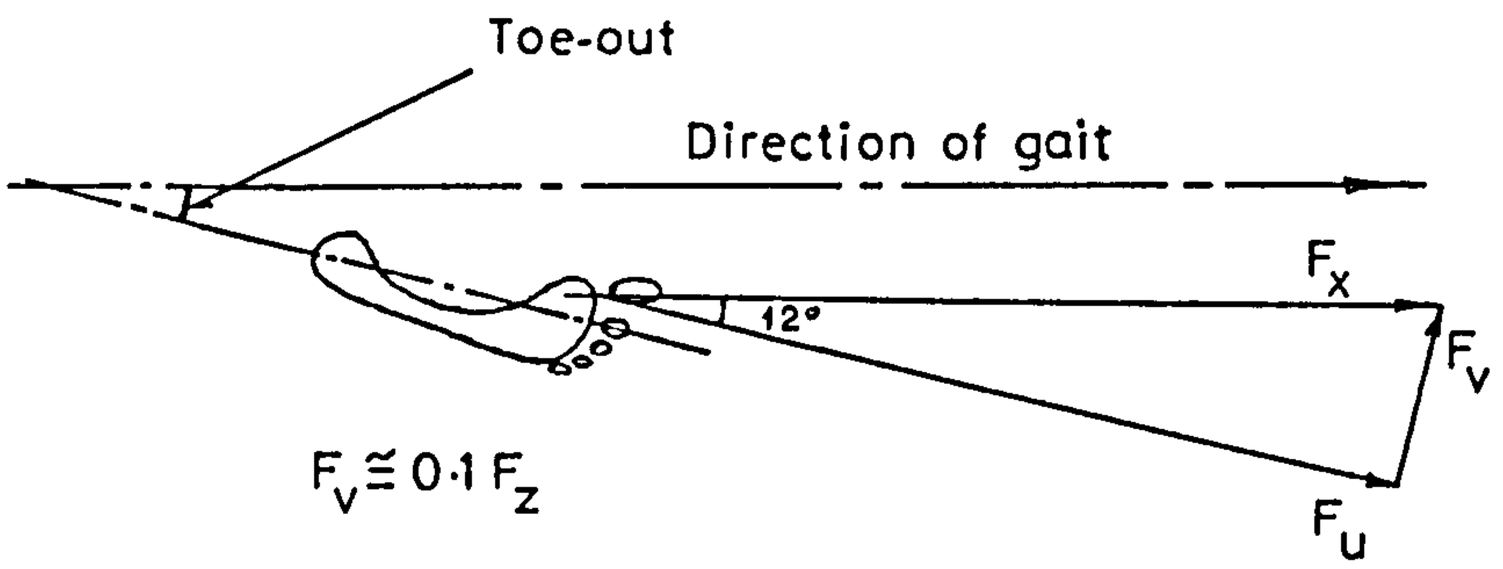

Figure 6·6 Horizontal force components acting from the ground on the forefoot during gait

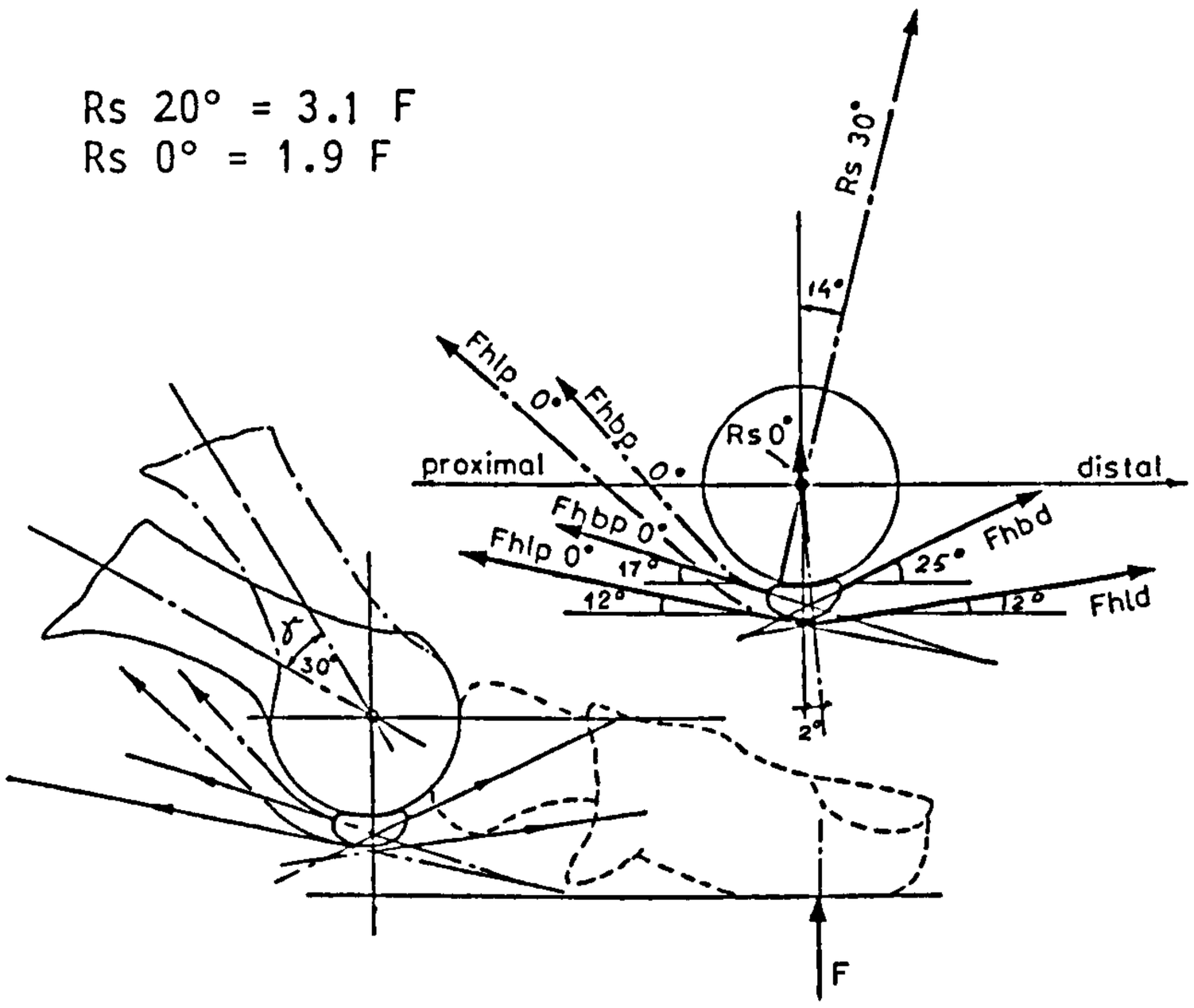

Figure 6·7 Force acting between the sesamoid bones and the metatarsal head in the neutral, foot-flat position (Rs 0°) and in 20° dorsiflexion (Rs 20°). The resultant (Rs 0°, or Rs 20°) does not include the ground force acting beneath the sesamoids.

horizontal components of force appear: one directed anteriorly and parallel to the axis of the foot, the other, due to toe-out, at right angles to the former and directed medially (fig 6.6). A diagram published by Stüssi (1977) in which the horizontal and vertical components of force measured on a Kistler foot-force platform in 20 ms intervals are indicated, shows that the postero-anterior component could amount to approximately 46% of the vertical value Fz at about 59% of the gait cycle. As figure 6.6 shows, this could be resolved into a component Fu parallel to the foot axis, and one at right angles to this, Fv. Fu therefore amounts to 45% and Fv to 10% of the vertical value, Fz. According to Bojsen-Møller and Lamoreux (1979), dorsiflexion of the toes tightens the framework of fibres in the ball of the foot, thereby restricting passive movements of the skin, enabling shear forces to be transferred to the skeleton. It is therefore probable that the greater part of the horizontal forces are transmitted through the ball of the foot but certainly, when this has been raised off the ground, the great toe is left fully exposed to the action of such shear forces.

Fortunately, when this happens (at about 60% of the gait cycle as shown in figures 5.13 and 5.20) the vertical ground force exerted on the great toe has fallen to less than 10% BW and because of this, no attempt will be made to estimate additional stresses that could be imposed on the flex.hall.long. tendon due to horizontal force components.

While still considering the effect of horizontal force components between ground and foot, it might once again be mentioned that the torque produced by the slight off-set of the contact area of the toe with respect to the medial longitudinal plane containing

the joint centres and the flex.hall.long. tendon (T = F.e in figure 6.1) might well be compensated for - at least to some extent - by the horizontal ground force component Fv.

While making use of muscle forces in the free-body diagrams, it must be mentioned that the direction of force exerted by a tendon (e.g. flex.hall.long.) changes from joint to joint. Therefore, the vector Fhl in figure 6.1 is not identical with the vector Fhl in figure 6.2. Only the magnitudes of these vectors are the same! The change in direction is brought about by the tendon running along a curved path through a sheath that is moored to the bone by fibres. This change in direction gives rise to radial forces that act between the bone and the tendon through the sheath and mooring elements and which are therefore of local character, not perceptible outside the closed system. The same applies to the flex.hall.brev. tendonous fibres that form the capsule of the MP-1 joint before inserting into the base of the proximal phalanx. Action of the flex.hall.brevis and flex.hall.long. muscles causes the sesamoid bones to be forced up against the metatarsal head. This local action is shown in figure 6.7, which is a maximum when the magnitudes of Fhl and Fhb are great and when simultaneously dorsiflexion in the MP-1 joint is effected. This happens at about 55% GC, when dorsiflexion in the MP-joint measures approximately 20°. Under such conditions, the flexor tendons proximal to the sesamoid bones tend to somewhat wrap around the rotated metatarsal head so that some of the reaction force Rs 20° (figure 6.7) might possibly pass directly from the capsule to the head without loading the sesamoids. The magnitude of the resultant Rs 20° measures about 6.2 F. Considering the external ground force Fmh which also must be transmitted to the metatarsal head, the total force bet-

ween the plantar aspect of the capsule and the metatarsal head would then amount to roughly 6.7 F. Obviously, the sesamoid bones serve primarily the purpose of furnishing the flexor tendon with an efficient gliding surface capable of transmitting high radial forces to the metatarsal head that arise from the diversion of tendon pull, and only to a far lesser extent for the ground forces that pass through the ball of the foot.

Finally, the analysis of forces passing through the tarsometatarsal joint, as shown in figure 6.5, reveals dramatically that the resultant, Rtm, passes through the base of the metatarsal bone, almost perpendicular to the joint surfaces as geometrically defined in figures 4.7 and 4.19 of Chapter 4. The exact direction of Rtm relative to the metatarsal bone is somewhat dependent on the extent of dorsiflexion in the MP joint as shown by (β-α) in the table in figure 6.5. It must again be pointed out that the individual action of the abductor hallucis muscle which takes a course parallel to the plantar aponeurosis has not been taken into consideration in the analysis performed. Action of this muscle would cause the resultant Rtm to adopt a position slightly removed in an anti-clockwise direction to that shown in figure 6.5d. However, the direction of Rtm (fig 6.5d) which is the resultant of the flex.hall.brevis and flex. hall.long. muscles together with the ground reaction forces F and Fmh, even on excluding the action of the abd.hall. muscle, clearly indicates that the metatarsal bone of the first ray is subjected mainly to compressive forces and that the tarsometatarsal joint is probably not exposed to much shear in normal gait. This obviously by virtue of the flexor hallucis muscles that primarily effect force transmission between the pad of the great toe and the ground. It has

	45% GC α = 30° θ = 5°	50% GC α = 37° θ = 12°	55% GC α = 45° θ = 20°
F	26% BW	30% BW	20 % BW
Fmh	14% BW*	12% BW*	
Fhl	2.2 F ≙ 57% BW	2.2 F ≙ 66% BW	
Fhb	1.4 F ≙ 36% BW	1.4 F ≙ 42% BW	
Rip	2.6 F ≙ 68% BW	2.6 F ≙ 78% BW	
Rmp	3.5 F ≙ 91% BW	3.5 F ≙ 105% BW	
Rtm	4.3 F ≙ 112% BW	4.5 F ≙ 135% BW	
Rs	2.2 F ≙ 57% BW	2.6 F ≙ 78% BW	3.1 F ≙ 62% BW

* For convenience Fmh = 0.5 F has been assumed throughout

BW : Body weight

F : Ground force under toe pad

Fmh: Ground force under metatarsal head

Fhl: Force exerted by flex.hall.long.

Fhb: Force exerted by flex.hall.brev.

Rip: Resultant in the IP-1 joint

Rmp: Resultant in the MP-1 joint

Rtm: Resultant in the tarsometatarsal joint

Rs : Force between sesamoids and metatarsal head (does not include the ground reaction Fmh !)

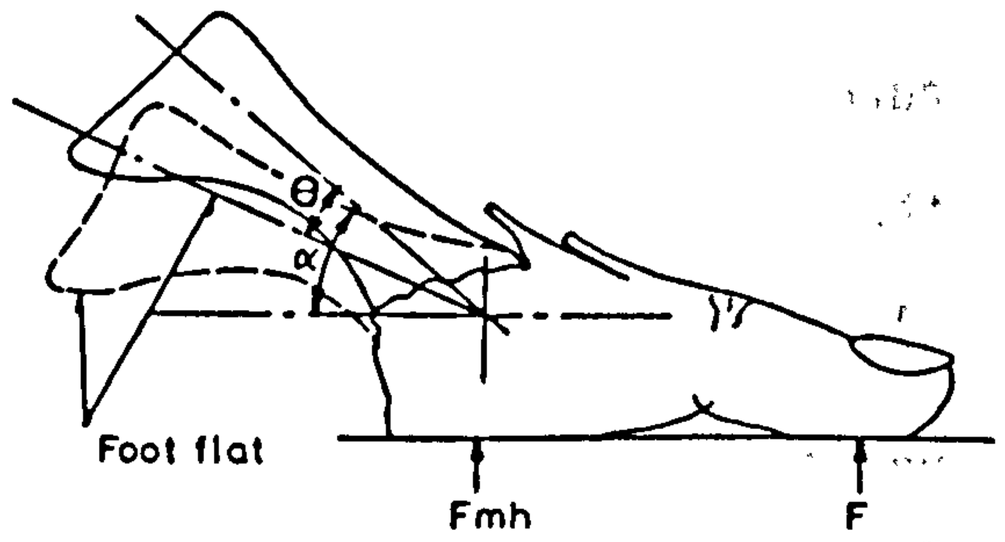

Actually, Rtm is the resultant of all forces acting at the distal end of the metatarsal bone. Since Rtm is not necessarily normal to the tarsometatarsal joint surface, the true resultant across the joint might also include forces that are exerted by ligamentous structures that cross the joint.

TABLE 6.1 Average peak values of forces in the first ray during level walking at 80 m/min (maximum peak values are about 1.7 times the values shown)

already been suggested in Chapter 4, that the action of flex.hall. long. together with the intrinsic abductor muscle possibly plays a major role in sustaining the medial longitudinal arch of the foot, rather than the plantar aponeurosis. This view has certainly found support in the analysis just discussed.

The results of the analysis performed on the first ray have been collected and are presented in Table 6.1 for convenience.

6.3 Forces Exerted by the Flexor Muscles and Joint Forces in the Second Ray:

The second ray of the foot differs basically in several respects from the first, and although the plantar forces observed during gait under the pad of the second toe are only about 20% the magnitude of those that appear under the great toe, the joints of the second ray are nevertheless subject to functional disorders that could also probably be traced to mechanical factors; in some diseases this ray being affected to an even greater extent than the first (e.g. Koehler-Freiberg's disease, an idiopathic necrosis of the metatarsal head). On the other hand, the head of this metatarsal bone is exposed to about twice the ground force acting under the head of the first metatarsal during normal gait, which, considering the slender shank form and the relatively rigid fixation to the bones of the middle foot, might well predispose this bone to mechanical failure.

Furthermore, the second toe is more adapted to the purpose of grasping (prehension) than the first, and with its additional phalanx and corresponding flexor-extensor mechanism, the second toe is liable to such deformities as mallet-toe, hammer toe and claw toe. To investigate the biomechanics of the second ray, a similar proce-

dure to that adopted in the preceding Section 6.2, has been followed. External ground forces reported in Chapter 5 (Table 5.4 and figure 5.24) have been applied to the mechanical structure as described in figures 4.22, 4.24, 4.26 and 4.27, to estimate the magnitude and direction of the internal forces acting across the joints.

6.3.1 Method of analysis

The forces exerted by agonist muscles and the reaction forces acting across joint surfaces have been determined by using free-body diagrams, to satisfy the conditions necessary to equilibrate the external forces that were measured. The same assumptions as mentioned in Section 6.2.1 regarding inertia forces and coefficient of friction of the joint surfaces have been made, and minor adjustments to linear dimensions have also been carried out as described before.

Beginning with the ground force under the pad of the second toe, the force in the corresponding flexor digitorum longus (flex. digit.long.) tendon is determined and also the force across the distal interphalangeal (DIP-2) joint. In a second step, the force exerted by the flexor digitorum brevis (flex.dig.brev.) muscle is estimated, not neglecting the force applied by flex.digit.long. simultaneously, to obtain equilibrium in the proximal interphalangeal (PIP-2) joint. Similarly, while considering the simultaneous actions of flex.digit.long. and flex.digit.brev. across the metatarsophalangeal (MP-2) joint, the force required from the interossei muscles to maintain equilibrium in this joint is then determined.

As in the analysis of forces in the first ray performed earlier, the calculation and results do not use absolute units of force but units relative to the ground force F, acting on the pad of the se-

cond toe, instead. F is therefore not an absolute unit of constant magnitude (not even of constant relationship to the total body weight, BW) but varies during the gait cycle continuously.

The following Sections show details of the procedure and the results obtained.

6.3.2 Analysis and results:

With reference to figure 4.27 of Chapter 4, it is obvious that the projections of the axes of the bones of the second ray in a horizontal plane do not coincide to produce a continuous straight line, but that the axes are arranged like chords along a circular arc. Because of the very short distal phalangeal bone, it was difficult to define its longitudinal axis and therefore it can only be said with certainty, that the middle phalanx is positioned in about 7° external rotation with respect to the more proximal neighbour. Therefore, the second ray as an entity can also not be strictly treated as a two-dimensional problem lying in a vertical plane. Nevertheless, the vector projections in the vertical plane that contains the longitudinal axis of the foot must still comply with equilibrium conditions and therefore, in the case of this ray too, two-dimensional analysis will first be carried out before the effects of forces acting outside the chosen plane are considered.

6.3.2.1 The distal interphalangeal joint of the second toe (DIP-2):

The distal phalanx of the second toe is depicted with its flexor tendon and ground reaction force $\underline{F}$ in figure 6.8. Because of its small size, the difficulty of locating a 'centre of pressure' arising from the ground reaction beneath it, within reasonable tolerances as

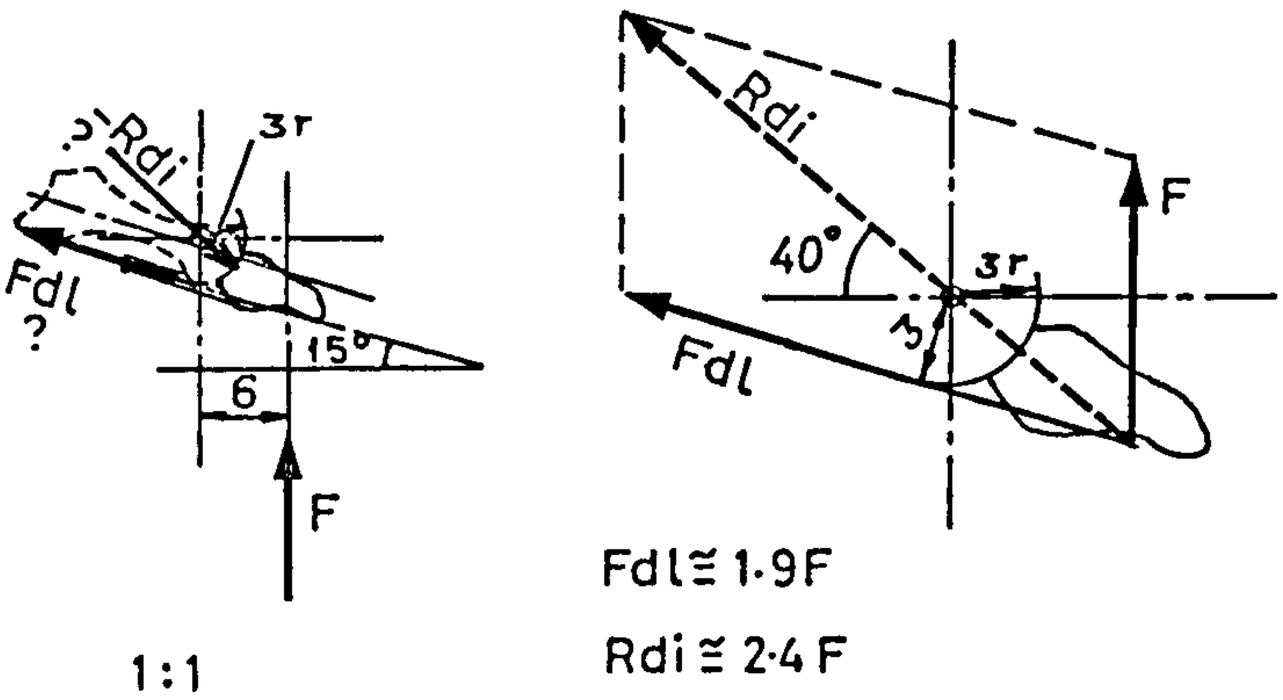

Figure 6·8 Muscle force ($\overline{Fdl}$) and resultant ($\overline{Rdi}$) in the DIP-2 joint due to a vertical ground reaction $\overline{F}$

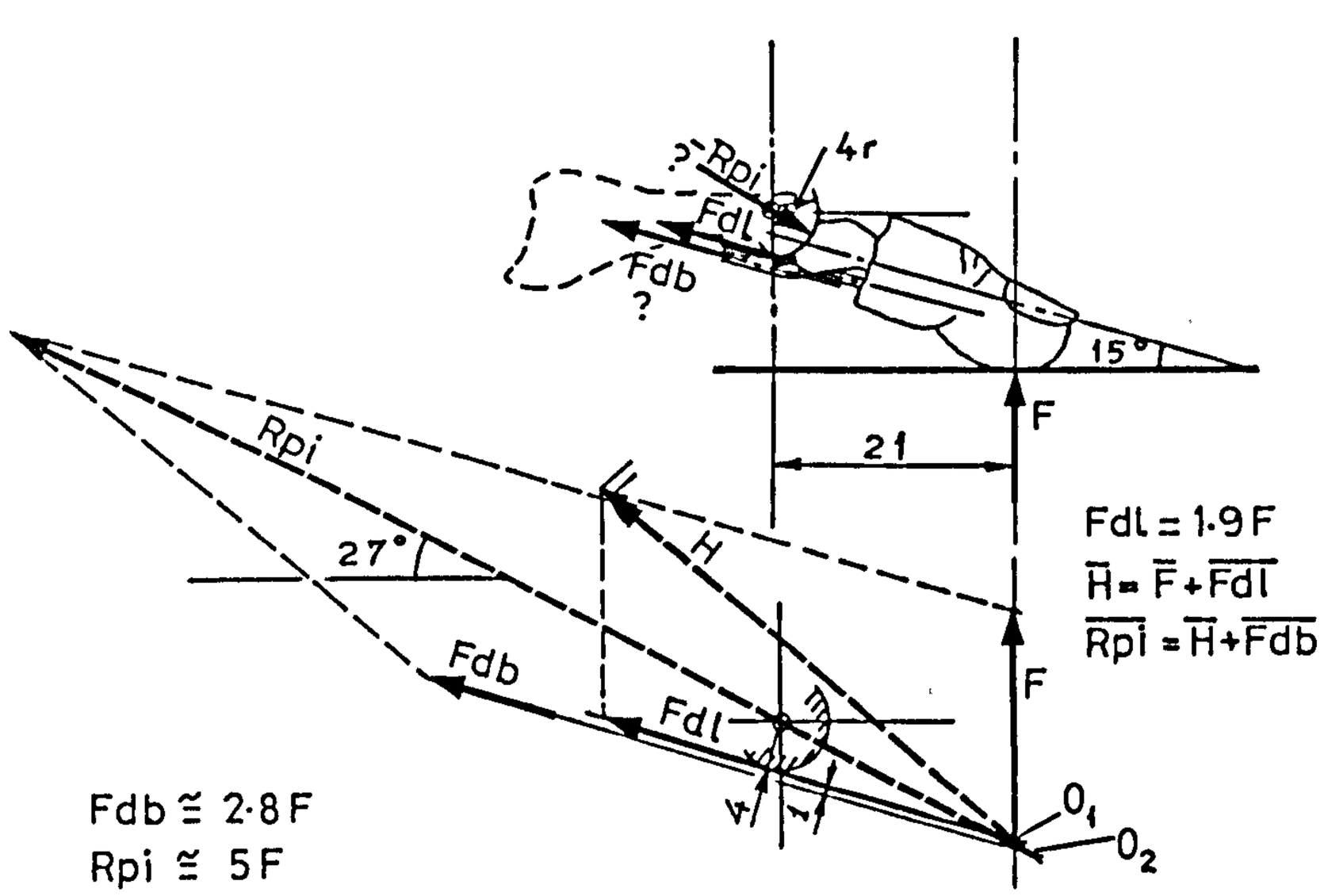

Figure 6·9 Muscle force ($\overline{Fdb}$) and resultant ($\overline{Rpi}$) in the PIP-2 joint due to the vertical ground reaction $\overline{F}$

called for by the small dimensions involved, will be readily appreciated. Therefore, the position of F as assumed in figure 6.8 could well lead to a tendon force Fdl which might either be an over- or underestimate of the true value. Nevertheless, the effect of an increase or decrease of the presently obtained magnitude on the joint reactions can be observed and the corresponding behaviour of the joints of this ray deduced.

According to the assumption made, and based on the dimensions obtained from figures 4.26 and 4.27 of Chapter 4, the vector diagram in figure 6.8 shows that the tendon force Fdl would amount to about 1.9 F while the resultant across the joint surfaces Rdi measures about 2.4 F. The latter is inclined at an angle of approximately 40° to the horizontal. If the line of action of F be assumed to act closer to the centre of curvature of the bearing surfaces, the angle of inclination of Rdi would increase and the value of Fdl would correspondingly decrease. The opposite is true if F be taken further away from the joint.

6.3.2.2 The proximal interphalangeal joint of the second toe (PIP-2):

Considering the free body situation of the whole extremity distal to the PIP-2 joint, as figure 6.9 shows, the dorsally directed ground force F is counteracted by the pull of the flex.digit.long. tendon (already estimated to be about 1.9 F) together with the pull of the flex.digit.brev. muscle, and the joint resultant Rpi that appears normal to the joint surface. The vector diagram in figure 6.9, based on the dimensions shown in figures 4.24 and 4.27, shows the manner in which the unknowns have been determined; by first adding F to Fdl to obtain the vector sum H, and by then applying H to

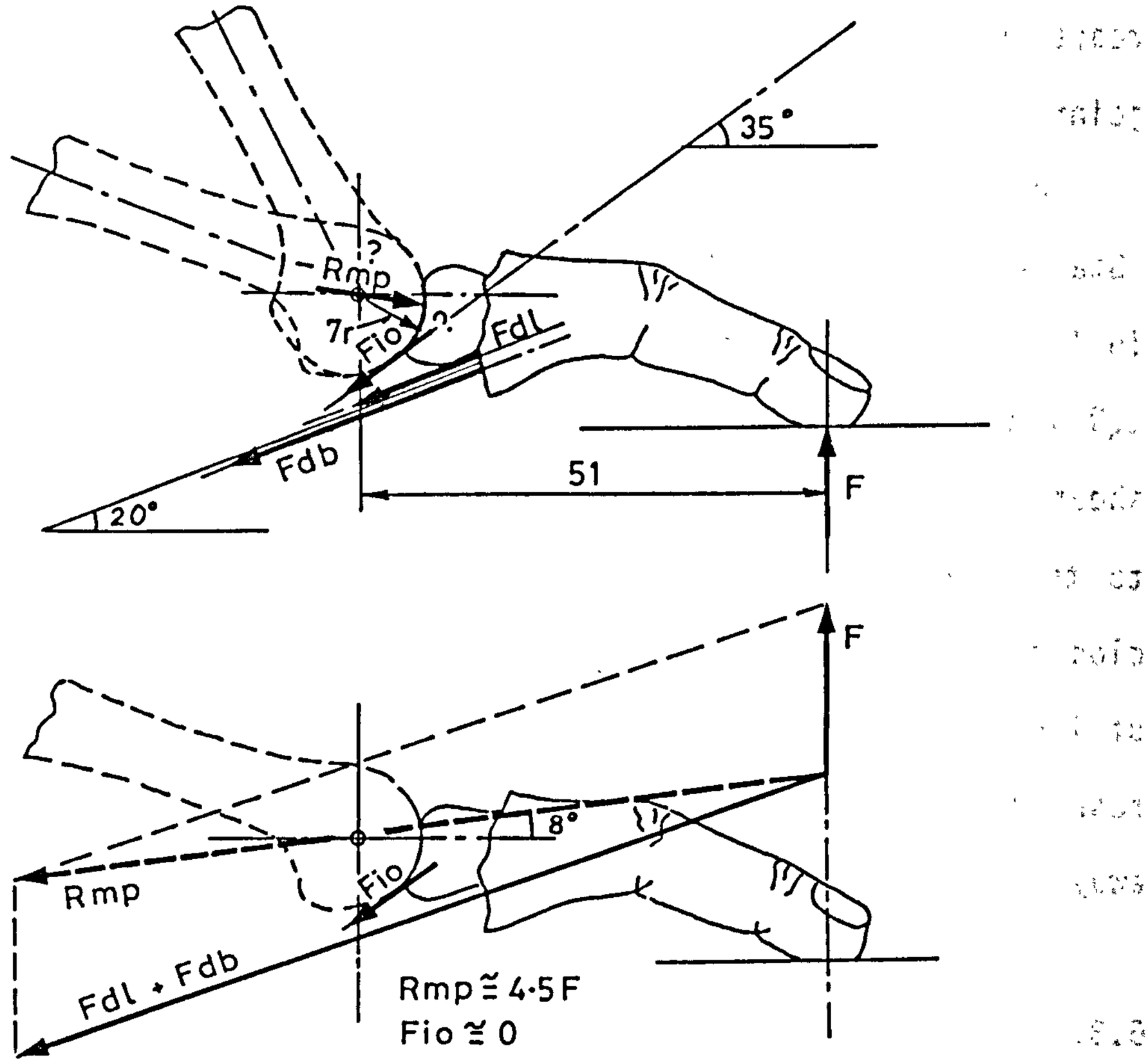

Figure 6·10 Muscle force ($\overline{Fio}$) and resultant ($\overline{Rmp}$) in the MP-2 joint due to $\overline{F}$

the direction of the flex.digit.brev. pull (Fdb) before constructing the final parallelogram of forces, the diagonal of which must necessarily pass through the centre of curvature of the joint surface. The diagonal represents the magnitude and direction of the joint resultant, Rpi. With reference to figure 6.9, it might be concluded that the force exerted by the flex.digit.brev. tendon would amount to about 2.8 F while the resultant, Rpi, measures about 5 F, the latter acting at approximately 27° to the horizontal.

6.3.2.3 The metatarsophalangeal joint of the second ray (MP-2):

Again, as in the previous cases, considering the free body situation of the entity distal to the metatarsophalangeal joint (MP-2), the dorsally directed ground force F is now counteracted by the pull of the flex.digit.long. and flex.digit.brev. muscles (already estimated to be about 1.9 F and 2.9 F, respectively) together with the pull of the interosseus muscles, and the joint resultant Rmp that acts normal to the joint surface. The vector diagram in figure 6.10, based on the dimensions shown in figures 4.22 and 4.27, shows the manner in which the unknowns have been determined; by first finding the sum F + Fdl + Fdb and then using the direction of insertion of the interossei muscles to obtain a parallelogram of forces, the diagonal of which must pass normal to the joint surfaces. However, as figure 6.10 shows, the resultant of F + Fdl + Fdb already passes through the centre of curvature of the joint surfaces, making simultaneous action of the interossei unnecessary. Therefore, the joint resultant Rmp amounts to about 4.5 F, acting at approximately 8° to the horizontal, passing close to the dorsal rim of the glenoid bearing surface.

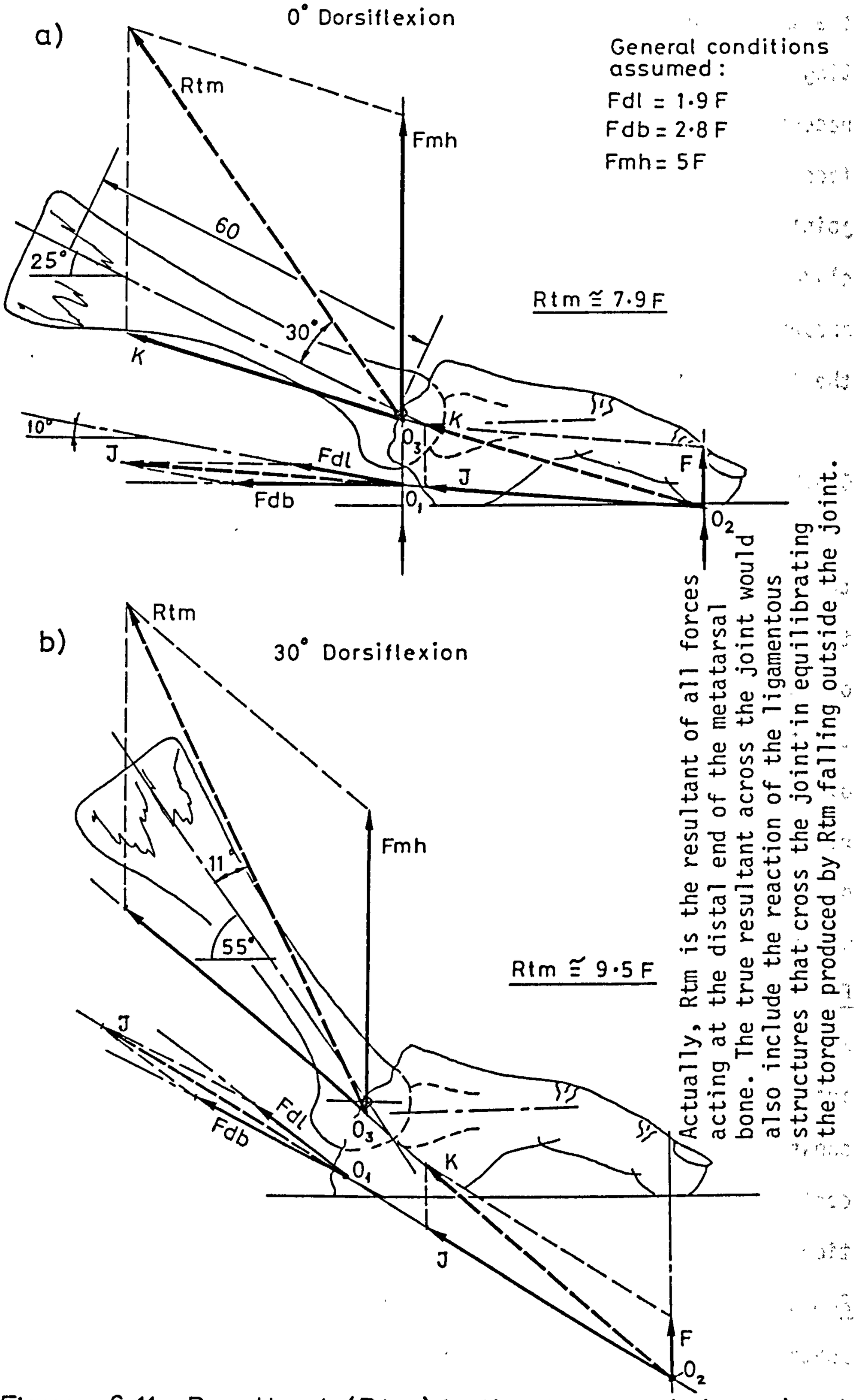

General conditions assumed :

Fdl = 1·9 F

Fdb = 2·8 F

Fmh = 5 F

Actually, Rtm is the resultant of all forces acting at the distal end of the metatarsal bone. The true resultant across the joint would also include the reaction of the ligamentous structures that cross the joint in equilibrating the torque produced by Rtm falling outside the joint.

Figure 6·11 Resultant (Rtm) in the tarsometatarsal joint of the second ray

It must be mentioned that the direction and magnitude of the resultant, Rmp, relative to the ground, is independent of the position adopted by the metatarsal bone relative to the ground, that is, the degree of dorsiflexion in the MP joint is irrelevant.

6.3.2.4 The tarsometatarsal joint of the second ray (TM-2):

Observing the action of all principal external forces with regard to the second ray distal to the tarsometatarsal joint (fig 6.11), it will be seen that these are: the ground reaction forces F and Fmp under the pad of the toe and under the metatarsal head, respectively, together with the action of the flex.digit.long. (Fdl) and flex.digit.brev. (Fdb) muscles. While with respect to the metatarsal bone it might be assumed that the direction of action of the flexor tendons throughout the whole range of movement remains practically constant, the positions of the ground vectors, F and Fmh, however, vary with dorsiflexion in the MP joint. Therefore, the resultant has been determined in two extreme positions of the foot: a) in the foot-flat position, and b) in 30° dorsiflexion, as shown in figure 6.11. Reference to fig 5.24 shows that the average load under the metatarsal head of the second ray (MP-2) is about five times that under the toe pad. Although the absolute values of the ground forces acting on the second ray vary during the gait cycle, it has been assumed for convenience that the ratio of these forces remain constant at 5 : 1 and therefore, Fmh has been allotted a corresponding magnitude of 5 F in figure 6.11.

The resultant Rtm passes close to the tarsometatarsal joint at its dorsal extremity, making an angle of about 11° to the axis of the metatarsal when the latter is at 55° to the horizontal (30° dor-

siflexion). The magnitude of Rtm is about 9.5 F in this position. In the foot-flat position, the direction of Rtm lies at an angle of about 30° to the metatarsal, lying far dorsal to the tarsometatarsal joint. The resultant Rtm now measures 7.9 F.

6.3.3 Discussion and conclusions:

The analysis of muscle forces and joint reactions of the second ray acting in a vertical plane along the axis of the foot shows the conditions that must be provided for in order to resist an external vertical ground force F acting under the pad of the toe. Under given geometrical circumstances, a strict balance between each of the forces exerted by the flex.digit.long. (Fdl) and flex.digit.brev. (Fdb) muscles must be maintained if neither the DIP-2 nor the PIP-2 joint is to be forced into hyperflexion or hyperextension. Figures 6.6 and 6.9 show that with the geometrical data presently used, Fdl and Fdb must measure 1.9 F and 2.8 F, respectively. The DIP-2 joint resultant measures 2.4 F while across the PIP-2 joint, a force of 5 F appears.

Most surprising, however, are the results pertaining to the forces across the MP-2 joint. As figure 6.10 shows, the pull of the flex.digit.long. and flex.digit.brev. tendons appear to exactly fulfill the requirements for equilibrium in this joint so that no force from the interossei muscles whatever is called for. This is, however, a semistable condition leaving no room for regulation of dorsiflexion in the MP-2 joint and therefore it is most probable that some force is exerted by the interossei while a simultaneous compensating moment is provided for by the extensor digitorum brevis muscle, as observed in EMG recordings presented by Mann and Inman in 1984 (see

figure 2.6a of Chapter 2). Therefore, it might be deduced that the interossei muscles primarily serve as ab- and adductors of the metatarsalia and only to a lesser extent as plantar flexors in the corresponding MP joints.

The results of the analysis of forces acting across the tarsometatarsal joint are also rather surprising. Figure 6.11a shows a vast deviation of the resultant Rtm of about 30° from the axis of the metatarsal bone when the forefoot is loaded in the foot-flat position. Because of the considerable transversal force component (Rtm.sin30°) that ensues, high bending moments in the shank of the metatarsal and a correspondingly high torque about a transverse, horizontal axis passing through the base of the metatarsal bone are to be expected. In the course of the locomotion studies described in Section 5.3 it was observed that at 45% GC the MP joints had dorsiflexed by about 5° only (observation on ten test subjects showed a range extending from 0° to 12°), and at this instant in the gait cycle the force under the head of the 2nd metatarsal reaches its peak value. Therefore, this position of the foot is of prime importance when considering the stresses in the metatarsal bones, as presented later in Section 6.4.1.2. The torque about a transverse, horizontal axis passing through the base of the metatarsal bone in this position of the foot could amount at average peak loads to about 14xBW (Nmm), assuming a bone length of 60 mm (fig 6.11a).

To illustrate the effect of a substantial amount of dorsiflexion in the MP joint on the position adopted by the resultant Rtm relative to the metatarsal bone, an angle of 30° was arbitrarily assumed, and as figure 6.11b shows, Rtm now makes an angle of only about 11° to the bone axis, passing close to the dorsal extremity

of the tarsometatarsal joint. The magnitude of Rtm has however increased from 7.9 F in the foot-flat position to 9.5 F in 30° dorsiflexion, where F is the ground reaction under the 2nd toe and the ground force under the metatarsal head is assumed to be 5xF. The torque to be resisted at the base of the metatarsal now measures only 6.5xBW (Nmm) at average peak loads.

It must be pointed out that in considering the effect of the resultant Rtm on the loading of the shank and on the torque produced at the cuneiform-metatarsal joint in the sagittal plane, any supporting action from the interossei muscles has been completely disregarded. There might in fact be some load sharing among neighbouring bones by means of the muscular interconnections, but this has not been taken into account at the moment.

On examining the tensile stresses that are produced in the flexor tendons, it will be observed that, assuming a total body weight of 700 N and the cross sectional areas of the tendons to be as shown in Table 4.1, the average peak stress in the flex.digit.long. tendon would amount to about 12 N/mm^2 while that in the flex.digit.brev. tendon approaches 35 N/mm^2 (figs 6.8, 6.9 and 5.24). Since the maximum peak force observed under the pad of the 2nd toe could amount to 2.5 times the average peak value (fig 5.24), the highest tensile stresses that develop in the flexor tendons would be correspondingly higher than the values given above.

It is indeed peculiar that the flex.digit.long. tendon with a cross sectional area of about 6.5 mm^2 should take only 68% of the load carried by the weaker flex.digit.brev. tendon which exhibits a cross sectional area of only about 3.4 mm^2. This was thought to reflect incorrect assumptions made either with respect to the position

adopted by the ground force F relative to the interphalangeal joints, or in regard to the distances between the centres of rotation and the tendons, or both. However, even after making geometrical adjustments as far as tolerable, the most favourable ratio of Fdl:Fdb that could be arrived at is about 1:1, which still cannot justify the ratio in cross sectional areas of 1.9:1 (Table 4.1) of the tendons involved. Therefore, the question arises as to whether this can be explained by requirements called upon when performing grasping functions. This matter, however, will not be pursued any further in this thesis, but must be left for another opportunity.

Nevertheless, a further fresh autopsy specimen was investigated to check the strength and dimensional characteristics of the flex. digit.long. and flex.digit. brevis tendons of the 2nd toe. The cross sectional areas measured 7.7 and 4 mm^2, respectively, thus closely approaching the values already given in Table 4.1. Tensile tests on the same specimens showed a rupture limit of 387 and 267 N, respectively. Since the specimens always failed at the edge of the grips, it could be assumed that the UTS was more than 55 N/mm^2 in the case of the flex.digit.long. tendon and also more than 66 N/mm^2 in the case of the flex.digit.brevis one. Therefore, it also cannot be explained how, with the geometrical layout that has been assumed, a ground force of 2.5 times the average peak value can occur (Table 5.4). At present, it can only be surmised that the toe might have adopted a claw form, thus shortening the lever arm and correspondingly increasing the ground force. There is also the vague possibility of the great toe having inadvertently moved over the transducer surface, adding to the force exerted by the 2nd toe. [As mentioned in Chapter 5, no attempt was ever made to select only particular

tracings of the force/time graphs. All tracings were evaluated without disqualifying even those that seemed to show a sudden erratic behaviour]. The ratio of maximum peak load to average peak load under MP-2 (Table 5.4) appears to be about 1.6 to 1 (as in the case of the ground forces measured under the 1st ray) and therefore it seems more reasonable to assume a maximum peak force under the pad of the 2nd toe of also 1.6 times the average value, that is, of about 10% BW.

On considering the slight off-set of the contact area of the toe with respect to the medial longitudinal plane containing the metatarsal bone axis (fig 4.27), a strictly vertical ground force would induce a torque about an antero-posterior axis in the joints. This torque can suitably be transmitted by virtue of the saddle forms of the DIP-2 and PIP-2 joints and in the MP-2 joint by means of the collateral ligaments that form a sling beneath the metatarsal head, the former forming an integral part of the capsule which is firmly attached to the base of the proximal phalanx. However, as in the case of the great toe, the second toe also is exposed to the effect of horizontal ground reaction forces which, taking the 'toe-out' of the foot during gait into consideration, impose a transverse component of force onto the toe tip. This, together with the vertical component of ground force, might well compensate for the torque expected (as described above) so that finally very little torque might indeed result.

In conclusion, attention must be drawn to the difference in loading conditions to which the first and second rays of the foot are exposed: In the case of the first ray, the great toe transmits up to 50% BW and the head of the metatarsal about 30% BW while in

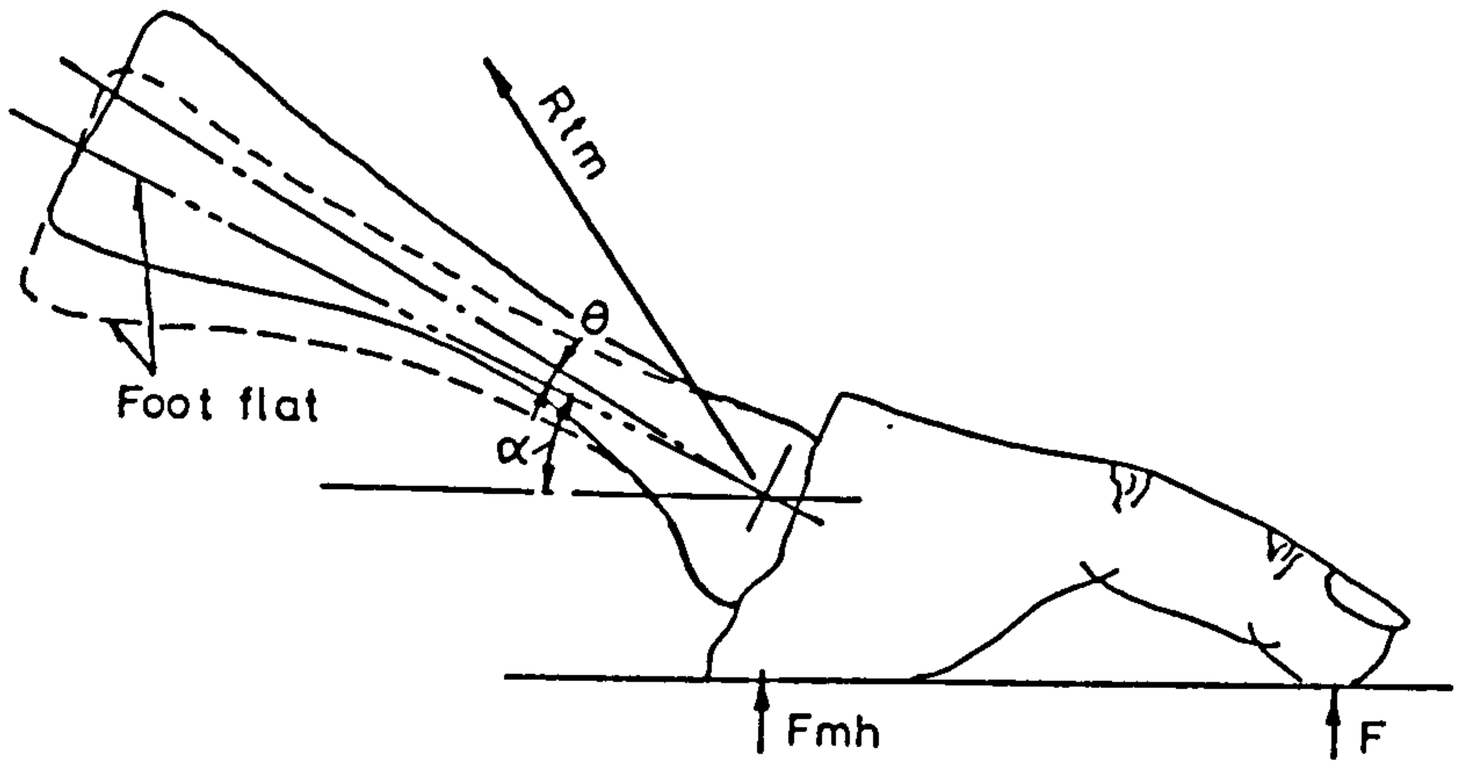

		45% GC α = 30° Θ = 5°
Body weight: BW		
Ground force under toe pad:	F	6% BW
Ground force under metatarsal head:	Fmh	30% BW
Force exerted by flex.digit.long.:	Fdl	1.9 F ≙ 12% BW
Force exerted by flex.digit.brev.:	Fdb	2.8 F ≙ 17% BW
Force exerted by interossei:	Fio	0 F
Resultant in the DIP-2 joint:	Rdi	2.4 F ≙ 14% BW
Resultant in the PIP-2 joint:	Rpi	5 F ≙ 30% BW
Resultant in the MP-2 joint:	Rmp	4.5 F ≙ 27% BW
Resultant in the Tarsometatarsal joint: *	Rtm	8.3 F ≙ 50% BW

*The direction of Rtm deviates by about 26° from the axis of the metatarsal bone.

Actually, Rtm is the resultant of all forces acting at the distal end of the metatarsal bone. The true resultant across the tarso-metatarsal joint would include the action of the ligamentous structures that equilibrate the torque produced by Rtm falling beyond the joint surfaces.

TABLE 6.2 Average peak values of forces in the second ray during level walking at 80 m/min (maximum peak values are about 1.6 times the values shown)

the second, the toe transmits up to 10% BW and the metatarsal head even as much as about 55% BW to the ground. Having seen that loading of the toes generally effects bracing of the longitudinal arch of the foot, thereby ensuring that the metatarsals are loaded like struts (as indeed in the case of the first ray), the manner in which the second metatarsal bone is exposed to bending stresses demands further inspection. This is treated in Section 6.4.1.2.

Table 6.2 shows the results of the analysis performed on the second ray, arranged conveniently.

6.4 Estimation of Stresses in the Metatarsal Bones:

Probably the first to have investigated the state of stress in the metatarsal bones while 'standing on ones toes' was E. Abramson (1927). Having estimated the static ground force under each metatarsal head by observing the depth of indentation of steel balls in a lead sheet, these values were applied to the corresponding bone and the stresses in the bone shank computed, assuming that the resultant force acted between the plantar tip of the bone and the centre of the tarsometatarsal joint, as shown in figure 2.13 of Chapter 2. Muscular force was assumed to resist movement in the said joint. Abramson determined the moments of inertia of various cross sections of metatarsal bones, presenting average values of five specimens each. These values have now been used to calculate the stresses in the shanks of the first and second metatarsals with the forces that were obtained in the previous sections of this chapter.

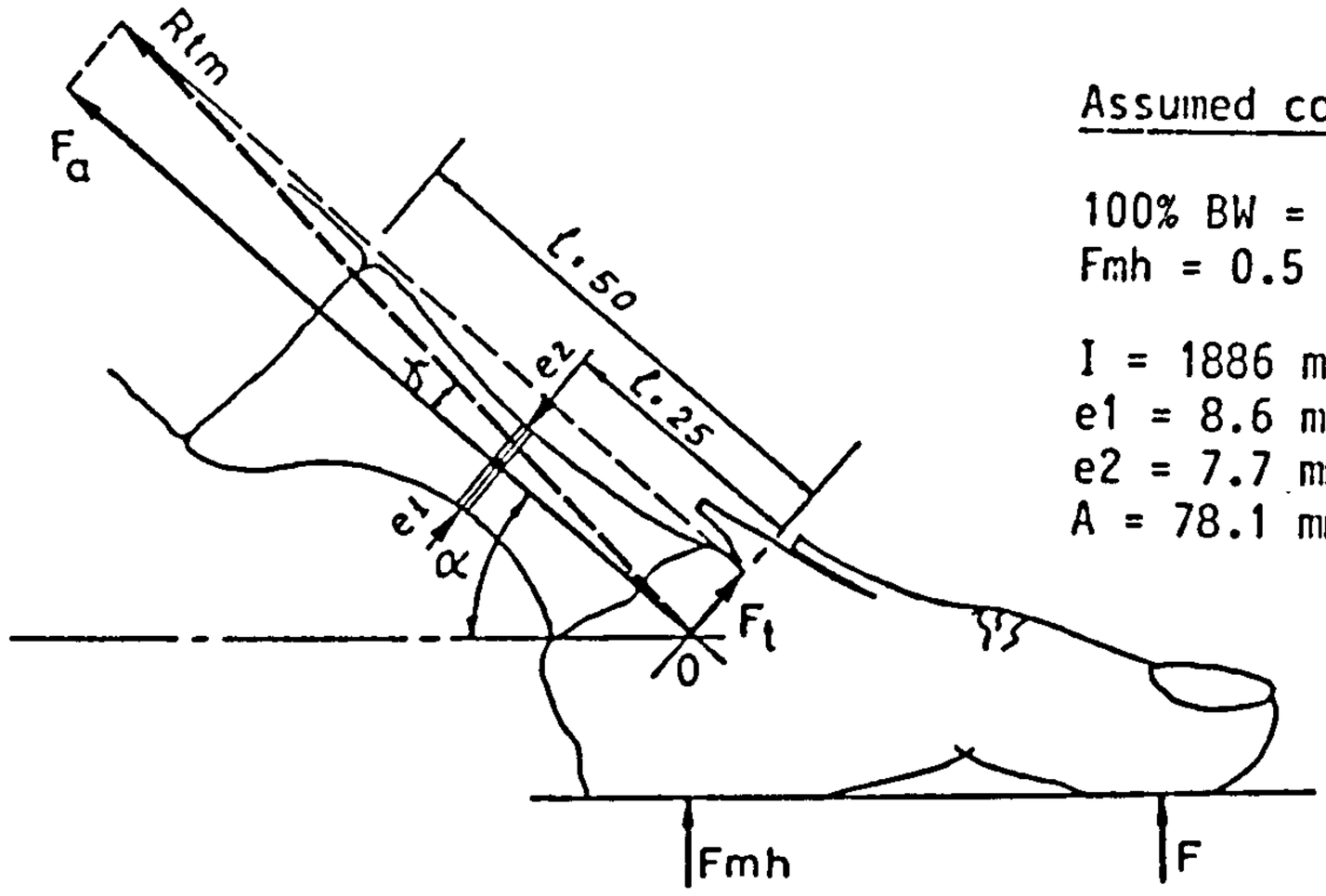

Assumed conditions :

100% BW = 700 N
Fmh = 0.5 F

I = 1886 mm^4
e1 = 8.6 mm
e2 = 7.7 mm_2
A = 78.1 mm^2

$F_t = \sin \gamma . Rtm$ $\quad F_a = \cos \gamma . Rtm$

$M_b = F_t . l$ $\quad M_{bm} = F_t . 25$ (Nmm) ; $M_{bj} = F_t . 50$ (Nmm)

$\sigma_{b1} = + M_b . e_1 / I$ (I = moment of inertia of cross section)

$\sigma_{b2} = - M_b . e_2 / I$

$\sigma_a = - F_a / A$ (A = area of cross section)

$\sigma_{tot} = \sigma_a + \sigma_b$

	At 45% GC $\alpha = 30°$; $\gamma = 8°$		At 50% GC $\alpha = 37°$; $\gamma = 6°$	
F	++ 22% BW	+++ (38% BW)	++ 31% BW	+++ (48% BW)
Rtm	662 N	(1143 N)	977 N	(1512 N)
M_{bm}	2303 Nmm		2553 Nmm	
σ_{b1}	10 *		11.6 *	
σ_{b2}	-9.4 *		-10.4 *	
σ_a	-8.4 *		-12.4 *	
σ_{tot1}	1.6 *	(2.8 *)	-0.8 *	(-1.2 *)
σ_{tot2}	-17.8 *	(-30.7 *)	-22.8 *	(-35.3 *)

* N/mm^2 ++ average peak values +++ (maximum peak values)

Figure 6·12 Stresses in the shank of the first metatarsal bone

6.4.1 Stresses in the shanks:

6.4.1.1 Stresses in the shank of the first metatarsal bone:

Two positions of the foot have been taken into consideration, the first when the heel has just left the ground (45% GC), and the second when the great toe sustains the heaviest load during the gait cycle (50% GC). In both cases, stresses have been estimated for average peak forces measured (fig 5.20). Results based on the highest forces are presented in parenthesis in figure 6.12.

As shown in figure 6.12, which makes use of previously obtained results shown in figures 5.20 and 6.5, the stresses in the middle of the metatarsal shank were calculated using values for the moment of inertia, area of cross section and position of the neutral axis that were estimated by Abramson as mentioned earlier. Also, a total body weight of 700 N was assumed. Under these conditions, the average peak stresses amount to about -18/+2 N/mm^2 with the MP joint in 5° dorsiflexion (45% GC), and about -23/-1 N/mm^2 with the MP joint in 12° dorsiflexion (50% GC), the highest compressive stresses occurring on the dorsal aspect.

Under the same conditions mentioned above, the tarsometatarsal joint is acted upon simultaneously by a compressive load of 656 N and bending moment of 4607 Nmm at 45% GC (5° dorsiflexion), and by a compressive load of 971 N and bending moment of 5106 Nmm at 50% GC (12° dorsiflexion in the MP joint).

6.4.1.2 Stresses in the shank of the second metatarsal bone:

Figure 6.11 shows the vast difference in the direction exhibited by the resultant Rtm between the foot-flat and dorsiflexed positions of the foot. Even though the magnitude of the resultant, for a given

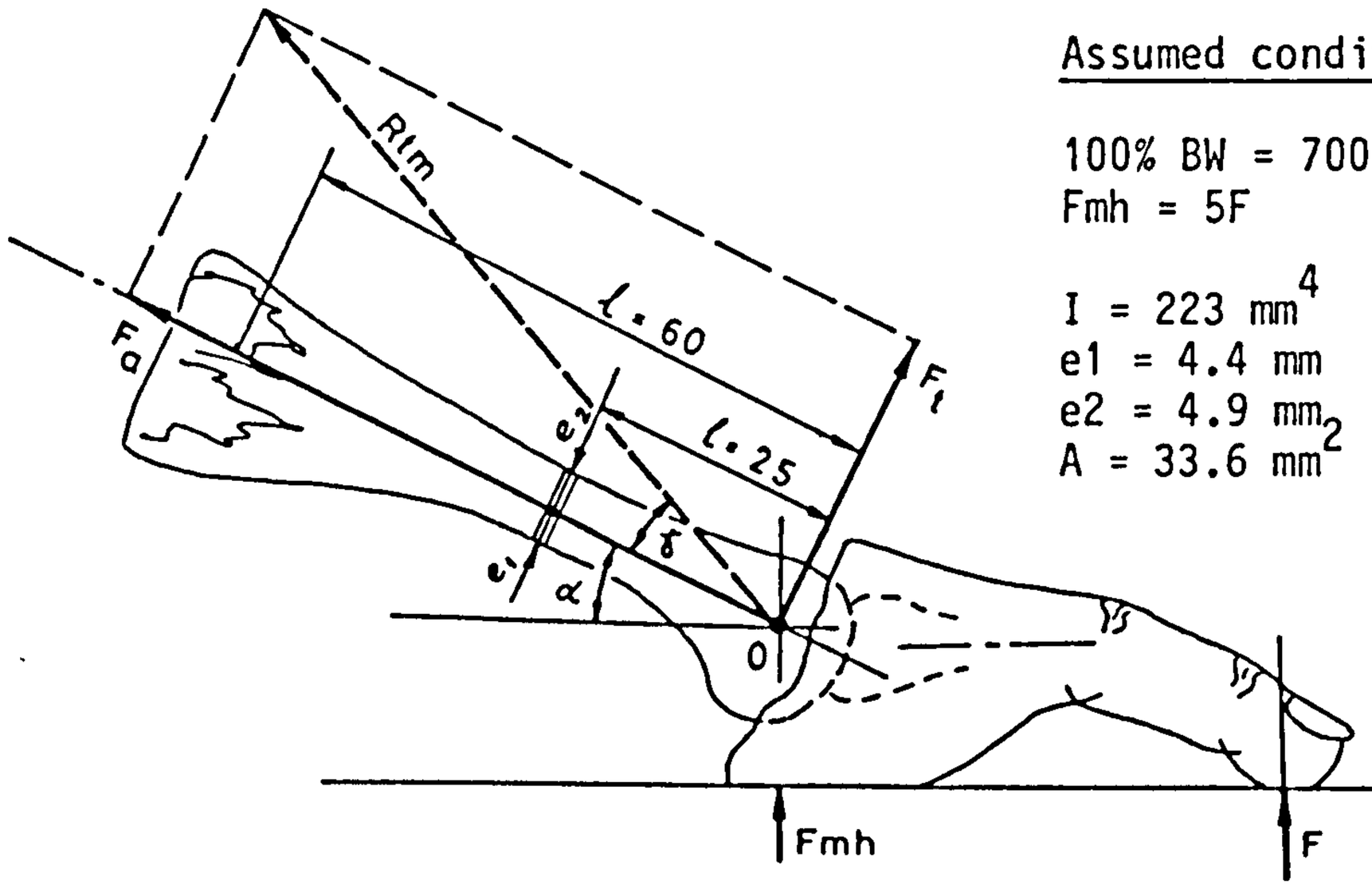

Assumed conditions :

100% BW = 700 N
Fmh = 5F

I = 223 mm^4
e1 = 4.4 mm
e2 = 4.9 mm
A = 33.6 mm^2

$F_t = \sin \gamma . Rtm$ $\qquad F_a = \cos \gamma . Rtm$

$M_b = F_t . l$ $\qquad M_{bm} = F_t . 25$ (Nmm) ; $M_{bj} = F_t . 50$ (Nmm)

$\sigma_{b1} = + M_b . e_1 / I$ $\qquad$ (I = moment of inertia of cross section)

$\sigma_{b2} = - M_b . e_2 / I$

$\sigma_a = - F_a / A$ $\qquad$ (A = area of cross section)

$\sigma_{tot} = \sigma_a + \sigma_b$

	At 45% GC $\alpha = 30°$; $\gamma = 26°$	
F	++ 6% BW	+++ (10% BW)
Rtm	350 N	(583 N)
M_{bm}	3835 Nmm	
σ_{b1}	75.7 *	
σ_{b2}	-84.4 *	
σ_a	-9.4 *	
σ_{tot1}	66.3 *	(110.5 *)
σ_{tot2}	-93.8 *	(-156.3 *)

* N/mm^2 $\qquad$ ++ average peak values $\qquad$ +++ (maximum peak values)

Figure 6·13 Stresses in the shank of the second metatarsal bone

magnitude of the toe force F, is lower in the foot-flat position, much higher bending stresses are nevertheless to be expected than with the foot flexed in the MP-joints. For the estimation of stresses in the shank of the second metatarsal bone, the values originally determined by Abramson (1927) for the area of cross section, moment of inertia, and position of the neutral axis, have again been employed. As in the case of the first metatarsal, stresses have been estimated for average peak forces measured and also for the highest forces ever observed during the locomotion tests that were performed earlier (fig 5.24). Results based on the highest peak forces are presented in parenthesis in figure 6.13.

Figure 6.13 shows the procedure in determining the stresses in the shank of the second metatarsal, using values for the resultant Rtm that had been estimated earlier (fig 6.11). The worst case arises when the head of the metatarsal is heavily loaded with the foot almost flat on the ground. This happens at 45% GC, when only about 5° dorsiflexion in the MP joints has occurred. This position was therefore chosen to observe the state of stress. As the table in figure 6.13 shows, the average peak stresses amount to about -94/+ 66 N/mm^2 when the heel has just begun to leave the ground (45% GC). Compressive stress appears on the dorsal aspect while tensile stress occurs on the plantar side.

Under the same conditions mentioned above, the tarsometatarsal joint of the second ray is acted upon simultaneously by a compressive load of 315 N, and a bending moment of 9206 Nmm in the sagittal plane, assuming a lever arm of 60 mm length (fig 6.13).

6.4.2 Stresses in the metatarsal heads:

Koehler-Freiberg's disease, an idiopathic necrosis of the metatarsal head, most commonly occurs in the 2nd, sometimes in the 3rd and relatively seldom in the other rays of the foot. Investigations regarding the possible causes of this disorder have led to an enquiry into the biomechanics of the metatarsophalangeal articulations by the author that was started in 1983. A report on the investigations performed, giving details of a finite element stress analysis that was carried out with the assistance of the Research and Development Laboratories of Sulzer Bros. Ltd. in Winterthur, Switzerland, was first published in 1987 (Jacob et al.). The following is a detailed description of the procedure adopted and the results that issued, preceded by an explanation of why this investigation had been done.

The changes in the bone structure and form of the metatarsal heads as they appear on x-rays that show Koehler-Freiberg's disease raise the question as to whether the action of mechanical forces could play an important part in the development of this ailment, or not. The vascular situation, which certainly plays a decisive role in bone necrosis, has been studied by Zollinger and Kubik (1984) but no quantitative indication was found to explain why, for instance, the disease attacks usually the 2nd and 3rd metatarsals and less commonly the 1st. Also, although it has been shown that wide-spread bone necrosis could be caused by deficiency of the blood supply, necrosis of the localised type, such as in osteochondrosis dissecans, in which a small portion of the joint surface becomes detached from the rest and eventually floats as a separate entity within the articulation, is difficult to explain. This type of lesion,

a) Osteonecrosis dissecans

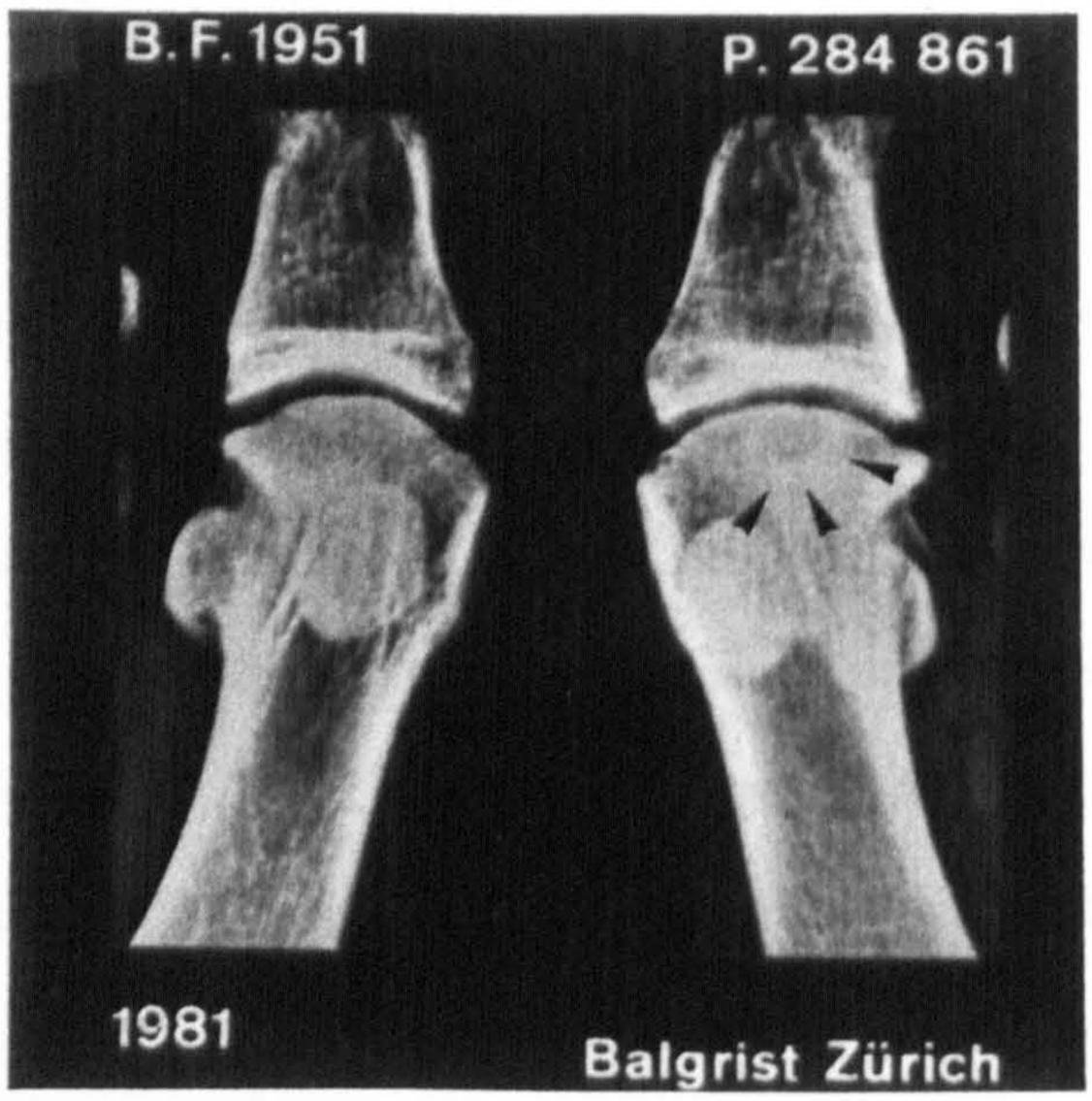

b) Alteration in bone structure

Figure 6·14 Two cases of idiopathic necrosis of the 1st metatarsal head

also sometimes encountered in the 1st ray (fig 6.14a), is almost exclusively seen in the heads of the 2nd and 3rd metatarsals, in which cases it is more dorsally located than the position observed when present in the head of the 1st. The appearance of these subchondral bone lesions is indeed very reminiscent of the surface fatigue phenomenon commonly known as "pitting", which is due to the repeated action of concentrated loading on the surface of an object at almost a point. Having already observed that the resultant in the MP-2 joint acts more dorsally than the one in the MP-1 articulation (see Rmp in figures 6.2 and 6.10), this matching well with the location of necrosis as seen in radiographs and also observing that the resultant Rmp passes very close to the boundary of the glenoid surface of the proximal phalanx in the case of the 2nd ray (fig 6.10) thus probably giving rise to edge loading, it became pressing to investigate the state of stress that develops within the head of the metatarsal when a load is transmitted over a very small area of the spherical surface.

6.4.2.1 Finite element models

Basically, two models were investigated, one with a hemispherical head and with force introduced over a small circular area, and the other with a flattened head and the external force acting over a ring surface. Figure 6.15 shows the first model and figure 6.16 the second, both showing the subdivision into finite elements. Both models are rotationally symmetrical. The cortex of 0.2 mm thickness was divided into 4 layers and again into $\pi/48$ radians. The cancellous bone and cartilage were divided into almost square meshes with a side length of $\pi/48$ radians. In the first model (fig 6.15) a

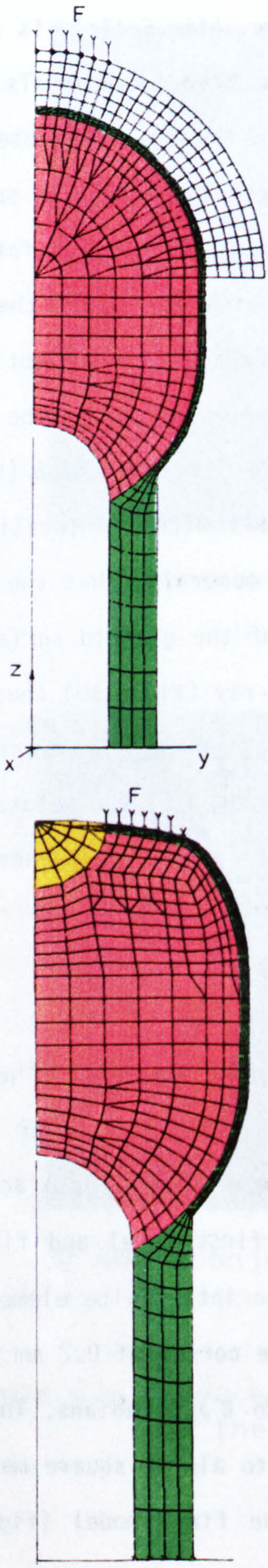

Figure 6·15

Subdivision of model 1 into finite elements

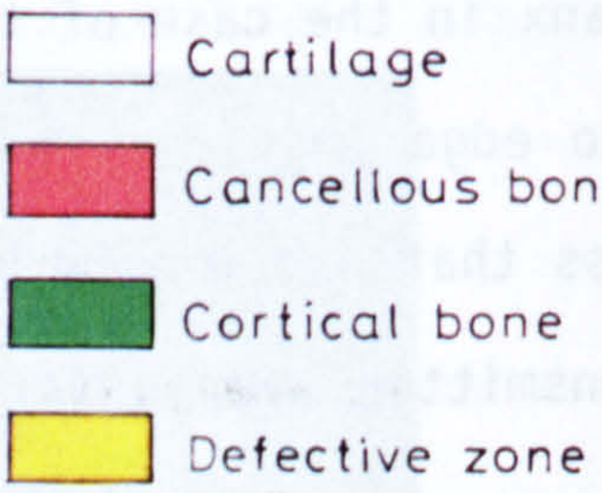

Figure 6·16

Subdivision of model 2 into finite elements

force of 200 N was uniformly distributed in an axial direction over a circular area of 4 mm diameter on the head of 12 mm diameter. In the second model (fig 6.16), the same force was uniformly distributed over a ring of 4 mm inner diameter and 8 mm outer diameter. Young's moduli of 15000, 1500 and 50 N/mm^2 were assigned to cortex, cancellous bone and cartilage, respectively. In the second model (figs 6.16, 6.18, 6.19a and 6.19b) a hemispherical volume of material at the joint surface was considered to have become discontinuous with its surroundings and was therefore attributed Young's moduli corresponding to various assumptions made (see next section 6.4.2.2). A Poisson's ratio of 0.3 was assumed throughout.

The isotropic finite element models were run on an ANSYS (Swanson Analysis Systems, USA) computer programme at Sulzer Bros. Ltd., Winterthur.

6.4.2.2 Results of FE analysis:

Figure 6.17 shows the stress intensities as determined by the Tresca criterion (maximum stress difference) within the metatarsal head. This manner of presentation was chosen because plots showing the magnitude and direction of the principal stresses tended to become cluttered with information making the drawing difficult to read. On examining figure 6.17 it becomes immediately apparent that not only is the thin layer of cortical bone highly stressed, but also the cancellous material directly below the area of force application too. The form of the most highly stressed area in the cancellous bone bears a striking resemblance with the necrotic defect seen in early stages of the disease (fig 6.14b) and it is suggested that the high shearing stresses in this area give rise to

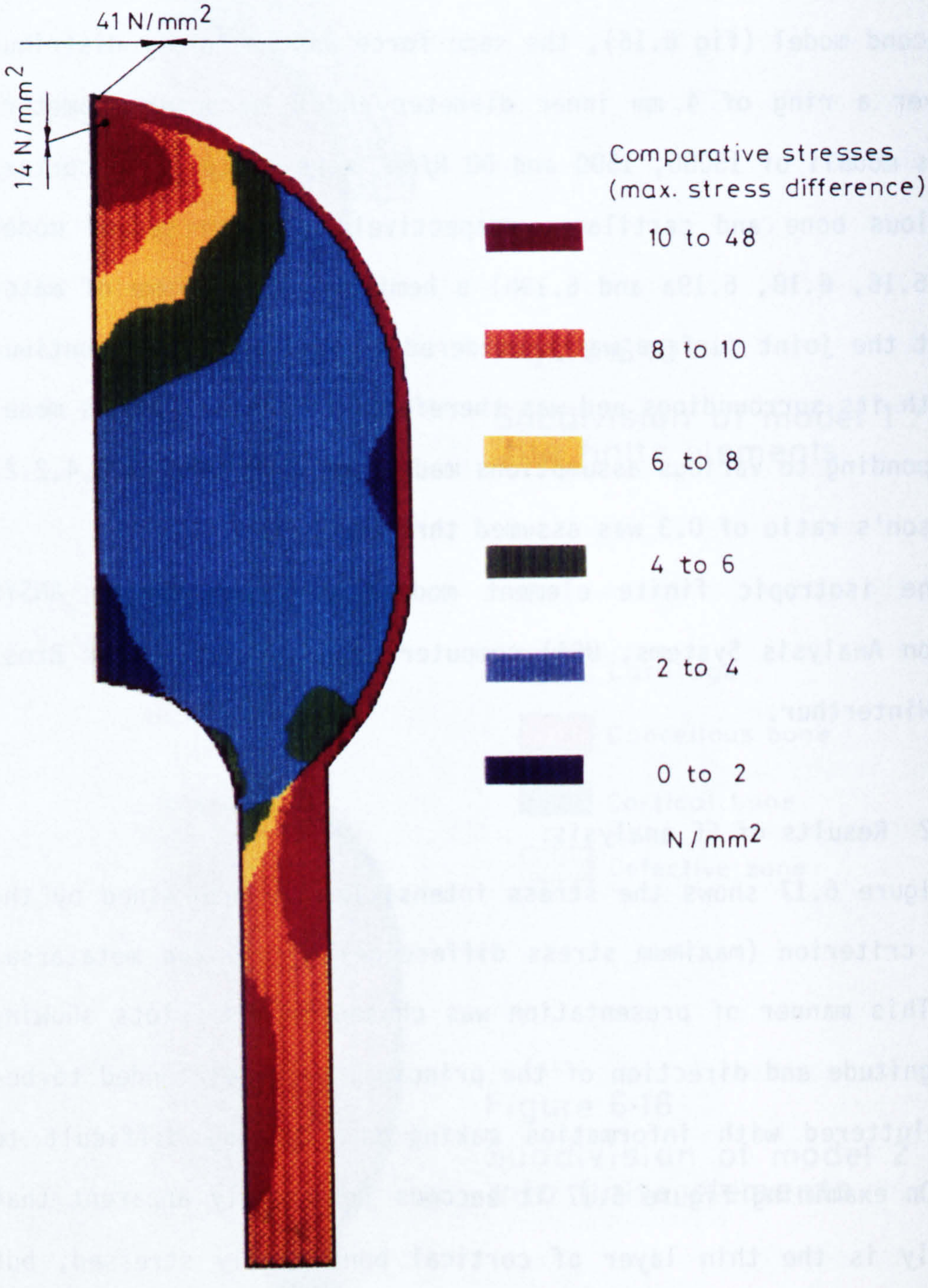

Figure 6·17 Stress intensity pattern with load of 200 N acting on small circular area of hemispherical head

micro-fractures of the bone that then result in an interruption of the local blood supply. Once this has happened, the bone becomes necrotic, and until the vascularisation of the disturbed zone becomes reorganised, healing of the fractures cannot take place. In this necrotic state, the bone is particularly subject to fatigue failure under repeated loading so that further bone destruction in this area might occur leading eventually to physical collapse of the structure. Flattening of the head, which possibly results, would cause re-distribution of the bearing contact pressures and therefore, it became interesting to furthermore investigate whether after this has happened, the stress intensity drops off to generally low values, or not. This has been tested by means of the second model (figs 6.16, 6.18, 6.19a and 6.19b).

It might also be hypothesised that following the development of bone necrosis, the biological repair mechanism becomes manifest by a gradual re-vascularisation of the adjoining necrotic zone which must then be resorbed prior to the formation of new, viable bone tissue. Just at this stage, when some resorbtion along the boundary has occurred, due to the continued action of forces on the metatarsal head, the whole affected volume of bone might begin to move relative to the surrounding material. This movement could in turn provoke the formation of soft connective tissue instead of bone and thus a sequester might form. Therefore, because of the intermediate layer of soft tissue of very low stiffness (compared to bone), it has been assumed that the resultant force in the MP joint would be transmitted now only through the surrounding surface and therefore a ring area of force input would again be appropriate (fig 6.16). Since the sequester will not contribute to the structural strength

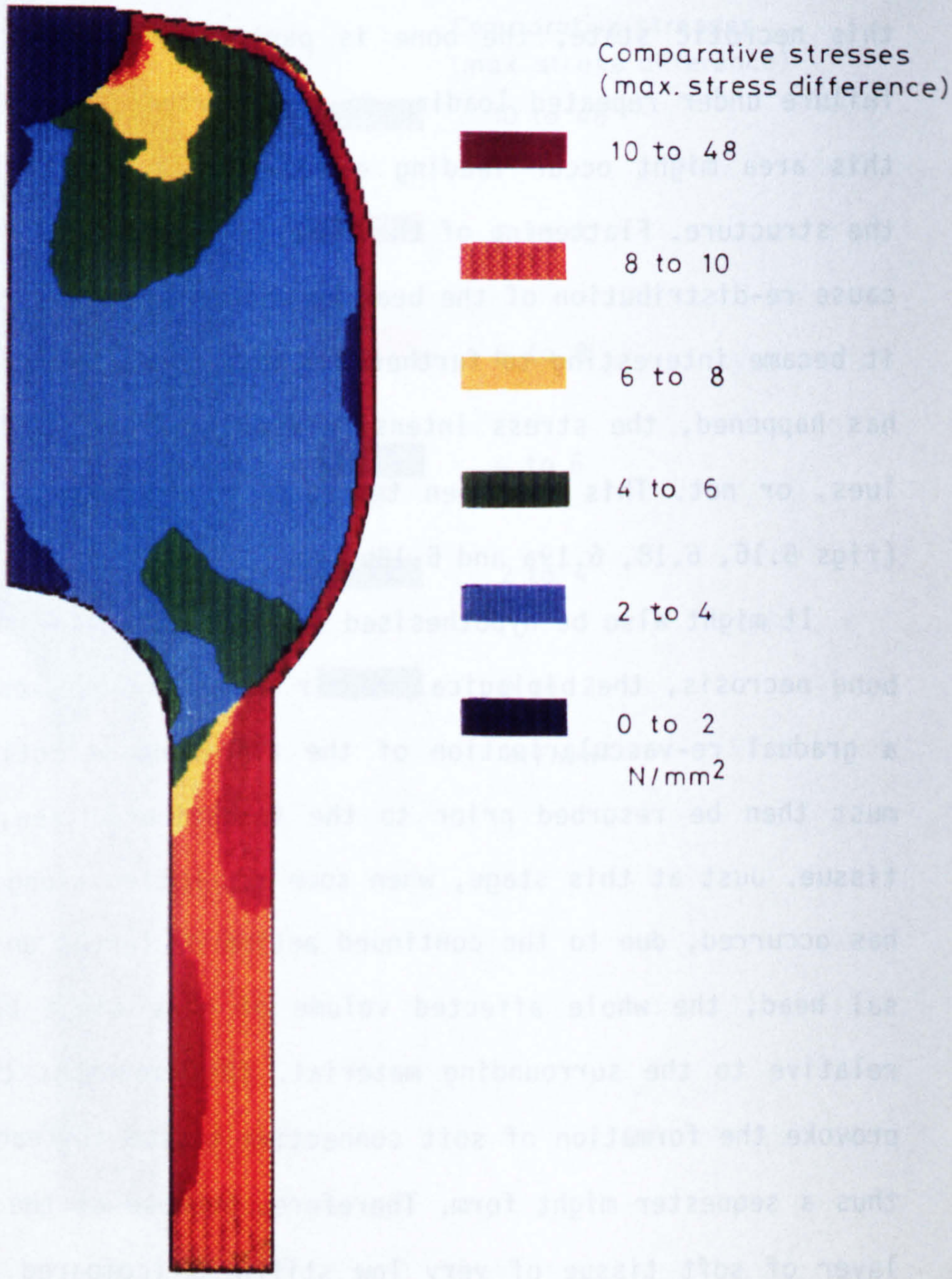

Figure 6·18 Stress intensity pattern with load of 200 N acting on ring surface of flattened head, with defective zone sequestered ($E_{def} = 1\ N/mm^2$)

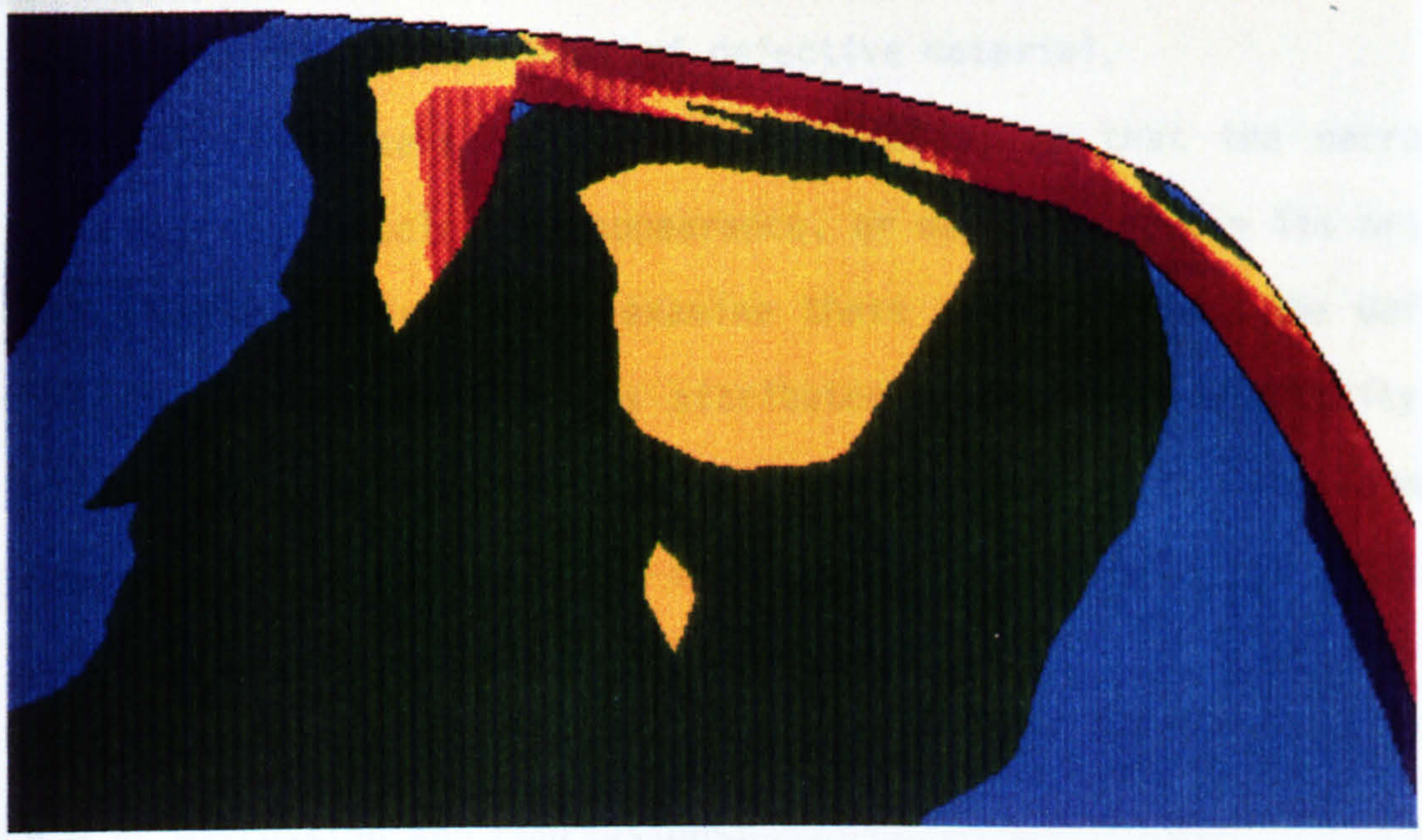

a) $E_{def} = 3000\ N/mm^2$

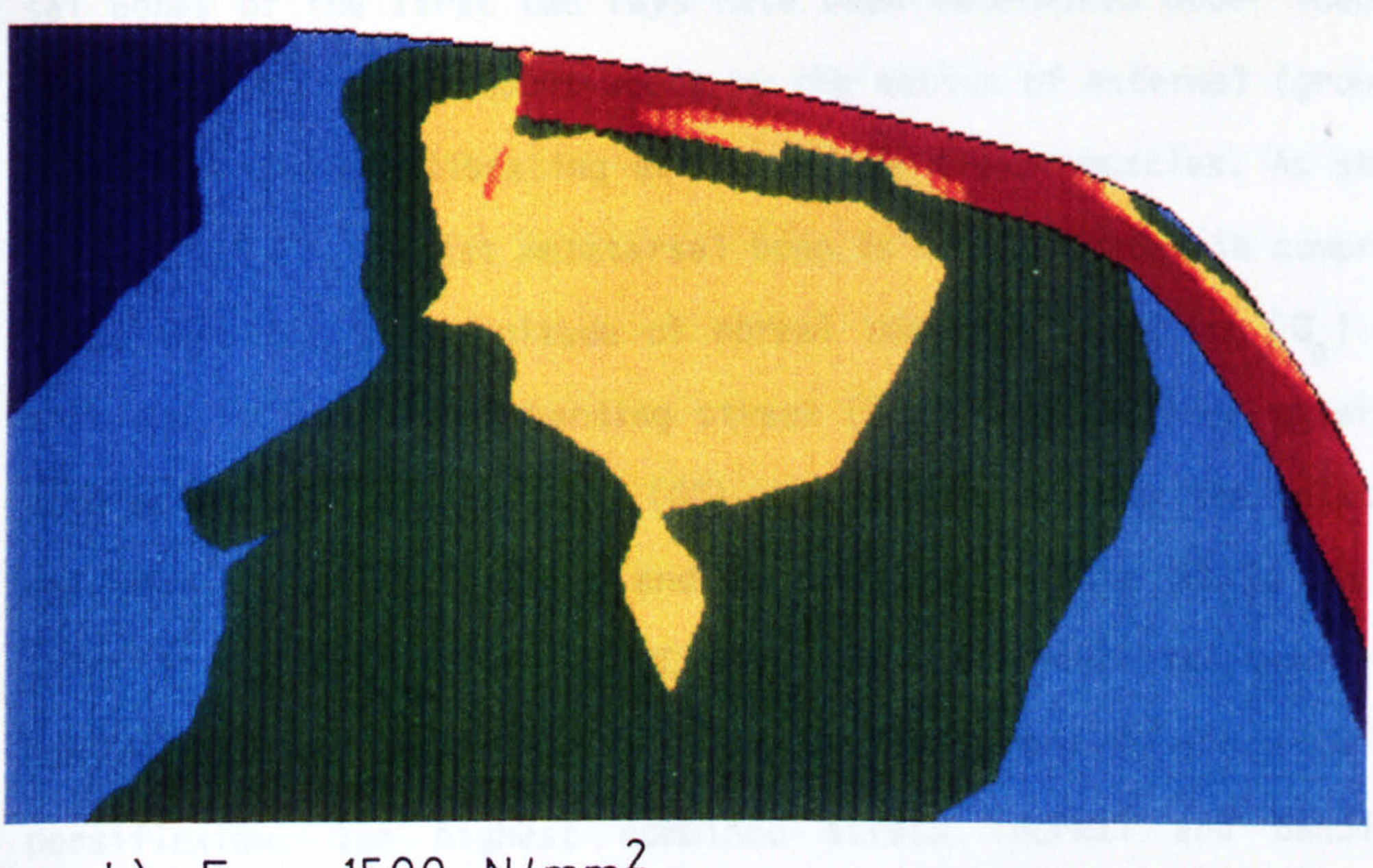

b) $E_{def} = 1500\ N/mm^2$

10 to 48 | 8 to 10 | 6 to 8 N/mm^2

4 to 6 | 2 to 4 | 0 to 2

Comparative stresses (max. stress difference)

Figure 6·19 Stress intensity pattern with load of 200 N acting on ring surface of flattened head, with defective zone of various stiffnesses

of the environment, a fictive modulus of elasticity of only 1 N/mm^2 was attributed to the volume of defective material.

But, sequesters do not always develop, so that the necrotic area may show a sclerotic appearance, or may even retain its original elastic properties. To examine these possibilities, the defective zone in figure 6.16 was attributed a modulus of elasticity of either 3000 N/mm^2 (sclerotic bone) or 1500 N/mm^2 (cancellous bone). Figures 6.18, 6.19a and 6.19b show the stress distributions obtained under these circumstances.

6.4.3 Discussion and conclusions:

The stresses that develop in the shank and head of the metatarsal bones of the first two rays have been determined under loading conditions that are brought about by the action of external (ground) forces and the equilibrating action of the flexor muscles. As shown in figure 6.12, the 1st metatarsal bone is mainly loaded in compression, that is, the magnitude of normal compression stress (σ_a) almost equals that of the bending stress (σ_b). This has been observed both at 45% of the gait cycle (GC) when the force under the metatarsal head is at its highest and dorsiflexion in the MP joints is about 5°, as well as at 50% GC when the force under the great toe has reached its peak value and the MP joints are in about 12° of dorsiflexion. The highest combined stress (normal and bending) estimated in the middle of the shank amounts to about -23 N/mm^2 at an average. However, maximum peak values of up to -35 N/mm^2 might sometimes occur when walking on the level ground at a pace of 80 m/min (fig 6.12). It is interesting to note that the stress on the plantar aspect of the bone varies from about +1.6 N/mm^2 to

-0.8 N/mm^2 between 45% GC and 50% GC.

On examining the stresses in the middle of the shank of the 2nd metatarsal bone, it has been observed that the bending component is predominant and gives rise to a combined stress of +66/-94 N/mm^2 at 45% GC, when the force under the metatarsal head has reached its average peak (fig 6.13). Under maximum peak loads measured, the stress could even attain a value of as much as +106/-150 N/mm^2 (!). This enormously high value (the average ultimate bending strength of cortical bone given by Yamada (1970) is about 157 N/mm^2) throws some doubt on the estimation. However, it must be pointed out that the metatarsal bone of the 2nd ray was assumed to bear the ground loads acting on it all by itself, without sharing any part of the load with the neighbouring bones. It is quite conceivable that some support is afforded by the interconnection to the 3rd metatarsal by means of the interossei muscles and also through the transversal ligamentous attachment between the MP joint capsules. Also, it is a common opinion amongst foot surgeons that the bone of the 2nd metatarsal is particularly difficult to cut, which might be an indication of bone with higher strength properties than as reported by Yamada (1970). This point too should be taken up and examined at another opportunity. Nevertheless, the results have indeed shown that the shaft of the 2nd metatarsal bone is more vulnerable to fractures than that of the first, a fact which is regularly observed in clinical practice.

A further point of interest is that with increase of dorsiflexion in the MP joints, the action of the ground force under the head of the 2nd metatarsal bone together with that of the flexor tendons results in a corresponding decrease in the bending moment in the

shank as the resultant Rtm approaches the metatarsal axis (fig 6.11b). This might be an advantage in wearing high-heeled shoes and must certainly be taken into consideration when investigating the feet of ballet dancers.

In view of the changes in bone structure and alteration in form of the metatarsal heads as they appear on radiographs that are characteristic of Koehler-Freiberg's disease (an idiopathic necrosis of the metatarsal heads), the semi-quantitative finite element stress analysis that has been performed showed that under local bearing conditions (edge loading) the cancellous bone of the bearing area can be exposed to such stresses that fractures might occur, sometimes resulting in collapse of the bone and flattening of the head (fig 6.17). Fractures in the trabecular bone would interrupt the microvascular system that in turn would lead to necrosis. In this state the bone is even more vulnerable to fatigue failure since fracture healing mechanisms cannot come into play. In the meantime, as necrotic bone resorbtion along the boundary of the defective zone occurs prior to deposition of new viable bone, the whole necrotic bone mass might be induced to move under the continued action of joint forces, thus preventing bone growth at the boundary and resulting in a sequester embedded in soft connective tissue as shown in figure 6.14a.

The question however arises, as to whether - following some initial destruction with perhaps flattening of the head - the magnitude of stress drops to such an extent that further spreading of damage is arrested. Using a second finite element model (fig 6.16) in which a slightly flattened head with force input over a ring surface has been assumed, three cases were considered:

a) the defective area sequestered and therefore not forming an

integral part of the structure (E_{def} = 1 N/mm^2)

b) the defective area sclerotic (E_{def} = 3000 N/mm^2)

c) the defective area unaltered (E_{def} = 1500 N/mm^2)

The results in figures 6.18, 6.19a and 6.19b show that in some regions of the head, high stresses continue to persist so that spreading of the damaged area is to be expected.

It must be expressly mentioned that the results of the finite element investigations are to be accepted only in a semi-quantitative sense since no details are known of the actual form and size of the bearing area nor of the pressure distribution over the area of edge contact. Nevertheless, it was considered appropriate to observe the manner of stress distribution that follows when the joint resultant acts within a very small surface area.

Finally, it must be pointed out that even though the magnitude of the resultant in MP-2 is only 27% BW compared with 105% BW in MP-1 (Tables 6.2 and 6.1), the bearing pressures could be almost the same when considering the diameters of the heads that are in a ratio of about 1:2; the contact areas being therefore in a ratio of 1:4 when geometrical similarity is assumed. In addition, the 2nd metatarsal head is more exposed to edge loading conditions than the head of the 1st (compare positions of the resultants Rmp in figures 6.2 and 6.10) which therefore suggests that the 2nd metatarsal head is more vulnerable to damage than that of the 1st. Also, it will be observed that Rmp acts more dorsally on the 2nd metatarsal head than on the 1st. These findings coincide well with clinical observations regarding the occurrence of idiopathic necrosis of the metatarsal heads (Zollinger, 1988).

CHAPTER 7

SUMMARY AND FINAL REMARKS

7.1 Introduction:

The observations made with respect to the kinematics and dynamics of the forefoot, as described in the previous chapters, might broadly be classified into two groups: those relating to the forefoot in standing, and those relating to the forefoot during gait. Hence, a recapitulation of the results of the investigations performed in the course of this thesis are presented under these headings in the following sections.

This last chapter closes finally with the author's recommendations for further elaboration of particular investigations since, on viewing the significance of the results in the light of the whole context - a matter which can only be accomplished retrospectively - it has been recognised that some of these investigations deserve closer attention and call for observations on a much larger collective of specimens than was possible during this study.

Also, the relationship between the results of this study and clinical problems are indicated in the process of this final summary.

7.2 The Foot in Standing:

Observations made on a fresh autopsy specimen of the foot, especially with regard to the mechanical function of the plantar aponeurosis, showed that in the absence of muscular activity, the 1st, 2nd and 3rd metatarsal bones are mainly loaded in bending, like cantilevers. On severing the plantar aponeurosis, the bending stresses were observed to increase by about 24% in the 1st metatarsal bone and by only about 12% in the 2nd, thus reflecting the stiffer cuneiform-metatarsal joint of the 2nd ray. Therefore, if the slight supporting action of the plantar aponeurosis be completely

neglected, it becomes apparent that only the long plantar ligaments together with the short plantar ones that cross the cuneiform-metatarsal joints (2 and 3) resist the bending action at the metatarsal bases. In the case of the first ray this is probably effected by the plantar joint capsule and the distal fibres of the tibialis anterior and, perhaps in some cases, by those of the tibialis posterior tendon, too.

A rough estimate of the total load which the foot might bear without muscular activity until fracture of bone occurs (not taking into consideration the strength of the ligaments) amounted to over 3000 N, so that the load of about 900 N (200 pounds) that had been applied to a foot in vivo without calling for muscular force, as reported by Basmajian and Stecko (1963), is quite conceivable.

The distribution of force between the 1st, 2nd and 3rd metatarsal heads and the remainder of the forefoot in the foot-flat position with no force acting along the Achilles tendon, was observed to be in the ratio of about 1.3:2:1:4 respectively. This force distribution pattern is probably explained by freedom of movement in the talocrural and talocalcaneonavicular joints that leads to a fairly symmetrical force distribution across the forefoot, with perhaps a slight bias towards the lateral side due to some degree of inversion of the foot, as would be expected through the ground force acting under the medial tuberosity of the calcaneus. The forefoot carries about 31% of the vertical force acting on the ankle joint, the remainder being taken by the heel.

On holding the Achilles tendon and the bones of the shank fast, the forefoot alone could be subjected to ground forces with the heel off the ground. It was observed that only when the heads of the 2nd or 3rd metatarsals were acted upon, was it possible to keep the

foot in a level position without tilting in eversion or inversion, requiring only a minimum stabilising force either under its medial or lateral border. On applying a dorsally directed load to the 1st metatarsal head, however, the foot readily inverted while similar action on the 4th or 5th metatarsal heads caused the foot to evert. This shows the inverting action of the triceps surae muscle in balance with the eversion caused by a dorsally directed force acting in the region of the 2nd or 3rd metatarsal heads, about the talo-calcaneonavicular joint axis. Hence, with the simultaneous action of the triceps surae muscle, a different load distribution across the forefoot results than when the heel is on the ground and no muscular activity whatever is present.

7.3 The Foot during Gait:

7.3.1. Movement in the metatarsophalangeal joints:

Motion studies of the physiological foot during gait as described in Chapter 5 have shown that the heel begins to rise off the ground at about 35% of the gait cycle (GC) and that the ball of the foot follows suit at about 65% GC. During this period, the positions of the phalanges relative to the ground remain practically unaltered (the 'digitigrade' phase of gait as termed by Bojsen-Møller and Lamoreux, 1979). During this period, dorsiflexion of about 51° in the MP joints is effected. The axis of rotation during this movement was observed to remain almost in a horizontal plane, passing through the heads of metatarsals 1, 2 and 3 at an angle of about 80° to the direction of progression, directed postero-laterally. Also, no matter whether an exaggerated toe-out (38°) or toe-in (-17°) was adopted, the direction of this axis continued to remain within $\pm$6° the

same as in normal gait, in which the average toe-out was found to measure 12°. The mean value of dorsiflexion in the MP joints at 45% GC is only about 5°, at 55% GC it measures 22°, then rapidly increases to 43° at 62% GC, until finally at about 65% GC the maximum value of 51° is attained.

7.3.2 External forces acting on the forefoot:

Force measurements under the heads of metatarsals 1, 2 and 5, and under the pads of the 1st and 2nd toes have shown the following peak values when walking on the open floor at a pace of about 80 m/min with flexible soles:

The ground force under the 2nd metatarsal head (MP-2) is usually the highest, and has been observed to exhibit an average peak value of about 30% body weight (BW). The forces under the 1st and 5th metatarsal heads (MP-1 and MP-5) were seen to be very similar to each other, the average peak measuring about 15% BW. It was furthermore observed that the deviation of measured ground forces from the average loading pattern was highest under MP-5, probably related to balancing activities during walking, involving inversion/eversion movements in the talocalcanionavicular joint. This effect was clearly reflected in the temporal pattern of the ground reaction force under MP-1 which also often exhibited a corresponding deviation from the average trace, showing a strikingly alternating behaviour with respect to the force pattern under MP-5.

The average peak force measured under the great toe amounted to about 30% while the corresponding value determined under the pad of the 2nd toe was 6% BW.

Maximum peak values of the forces mentioned above were seen to be about 1.7 times the average.

The temporal force graphs under the investigated areas of the forefoot exhibited roughly the same form: rising from zero shortly after heel-strike to about 5% BW at 10% GC, then with a lower rise rate to about 30% GC, after which a steeper rise occurs until the peak is reached in the vicinity of 45% GC before quickly returning to zero around 62% GC. Closer inspection, however, shows slight, but characteristical differences. Whereas the above mentioned applies closely to the MP-2 and MP-5 areas, the diagram of the MP-1 ground force showed a delay of 5 to 10% of the gait cycle in commencing to rise. Also, there was a definite tendency for the peak value to be maintained for a longer period of time (about 10% of the gait cycle) before falling off rapidly to zero at 62% GC.

On the other hand, the force under the great toe, after beginning to rise at about 10% GC, reached its maximum only at about 50% GC, thereafter declining to zero as late as 65% GC.

Apart from the gait conditions (80 m/min on a level, open floor) during which the results presented above were observed, the following locomotion activities were also investigated:
walking with stiff soles versus flexible soles, the effect of toe-out, walking up and down stairs, and walking up and down a slope of 15°. To repeat all the results that have been described and discussed in detail in Chapter 5 again in this section would be carrying this final review beyond its purpose and therefore the reader is invited to refer to the corresponding sections and to Table 5.4 for relevant details. Nevertheless, it is again worthy of mention that as soon as the habitual gait style is altered, e.g. through

changing the toe-out angle, walking on a relatively short moving belt (treadmill of 1.5 m length), walking at an uncomfortably low speed, or through wearing shoes with stiff soles, etc., the duration of contact between foot and ground becomes lengthened by about 3% of the gait cycle, with a corresponding reduction in the duration of the swing phase.

7.3.3 Internal forces acting within the structure of the forefoot (1st and 2nd rays):

Having investigated the geometry of the forefoot, as described in Chapter 4, and also having determined the external (ground) forces acting on the structure, the succeeding step was to estimate the internal forces that come into play during gait. This involves the muscle forces acting through the tendons, and the forces that result at the joint surfaces. Analytical procedures were applied only to the first and second rays of the foot, this being considered of prime importance because these two structures differ functionally most from each other, thereby being exposed to pathological conditions peculiar to themselves. It must be emphasized that the results obtained are very dependent on the assumptions made regarding the positions of the ground forces (centres of pressure at the ground contact areas) and also on individual anthropometric differences. Therefore the values presented should be accepted with due caution.

7.3.3.1 Forces in the first ray:

The analysis of muscle forces and joint reactions acting in a vertical longitudinal plane has shown that a very strict balance

between each of the forces exerted by the flexor hallucis longus (flex.hall.long.) and flexor hallucis brevis (flex.hall.brev.) muscles must be provided for if the relative positions of the adjoining members of the 1st ray are to be maintained in equilibrium while the pad of the great toe is acted upon by a ground force F. While the prime purpose served by these muscles is to enable the pad of the great toe to transmit force to the ground, it has also been seen that they actively support the longitudinal arch of the foot. This, to the extent that the resultant force across the tarsometatarsal (cuneometatarsal) joint, Rtm, falls within the mating joint surfaces (fig 6.5), thus preventing cleavage of this amphiarthrosis at its plantar aspect without requiring the assistance of ligamentous ties such as the plantar joint capsule or the distal fibres of the tibialis anterior or tibialis posterior tendons. On considering the additional passive bracing effect afforded by the plantar aponeurosis and the active support given by the abductor hallucis muscle, it will be immediately appreciated that the vector Rtm would adopt an even more favourable position for the transmission of compressive forces across the tarsometatarsal joint as shown in figure 6.5.

This observation might be of importance when considering the advantages and disadvantages of certain surgical methods in the treatment of hallux valgus that could adversely effect the transmission of force to the great toe. It might also be advisable to consider this in cases of metatarsalgia of the first ray.

The magnitude of the resultant compressive force acting across the tarsometatarsal joint has been estimated to be about 112% BW at 45% GC, reaching about 135% BW at 50% GC when the great toe exerts its peak force on the ground during gait. Maximum peak values could

be about 1.7 times the average values given above (Table 6.1).

The joint force that results across the metatarsophalangeal (MP) articulation has been observed to measure about 91% BW at 45% GC, and about 105% BW at 50% GC (Table 6.1). The direction of this force vector is practically horizontal.

Forces in the flexor tendons and the corresponding forces in the articulations of the first ray are shown in Table 6.1. It must, however, be remembered that the abductor hallucis muscle has not been taken into consideration as an entity of its own, but that the adjoining flex.hall.brev. muscles have been assumed to effect the total force required at the base of the proximal phalanx, instead. This might particularly affect the force RS estimated between the sesamoid bones and the metatarsal head which under the present assumption attains higher values, because of 'wrapping around' of the tendon (capsule) fibres, than would otherwise be the case.

In connection with forces acting across the MP-1 joint it must finally be mentioned that because the ground force acting under the pad of the great toe is off-set with respect to the vertical plane containing the flexor tendons and the joint centre, rotation about a longitudinal axis would be induced, causing the toe to pronate in the MP-1 joint (fig 6.1b). This pronation would be resisted by the medial collateral ligament and by the fibrous ties that join the medial tubercle of the metatarsal head to the plantar plate containing the sesamoid bones. Also, a transversal, horizontal component of force that might eventually be present under the pad of the toe due to friction between ground and toe (as probably is the case in bare-foot gait) could effect compensation - at least to some extent - of the pronating torque just discussed (fig 6.6).

Again, when considering various surgical methods in the treatment of hallux valgus, these observations might be of value too.

7.3.3.2 Forces in the second ray:

The analysis of muscle forces and joint reactions of the second ray acting in a vertical longitudinal plane has shown that under given geometrical circumstances, a strict balance between each of the forces exerted by the flex.digit.long. (Fdl) and flex.digit.brev. (Fdb) muscles must be maintained if neither the distal (DIP-2) nor the proximal (PIP-2) interphalangeal joint is to be forced into hyperflexion or hyperextension. As shown in Table 6.2, the average peak forces exerted by Fdl and Fdb during normal gait have been estimated to be about 12% BW and 17% BW, respectively; this at 45% GC. Maximum peak forces could be as much as 1.6 times the values mentioned above.

Most surprising, however, are the results pertaining to the forces across the MP-2 joint and the conditions required for equilibrium in this articulation. As figure 6.10 shows, the pull of the flex.digit.long. and flex.digit.brev. tendons appear to exactly fulfill the requirements for equilibrium in this joint so that no force from the interossei muscles is called for whatever. This, however, is a semistable condition leaving no room for regulation of dorsiflexion in the MP-2 joint and therefore it is most probable that some force is exerted by the interossei while a simultaneous compensating moment is provided for by the extensor digitorum brevis muscle, as observed in EMG recordings presented by Mann and Inman in 1964 (see figure 2.6a of Chapter 2). Therefore, it might be deduced that the interossei muscles primarily serve as ab- and adduc-

tors of the metatarsalia and only to a lesser extent as plantar flexors in the corresponding MP joints.

The tarsometatarsal joint of the 2nd ray, unlike that of the 1st, is subjected to a considerable torque about a transverse, horizontal axis passing through the base of the metatarsal bone. Figure 6.11a shows the vast deviation of the resultant Rtm of about 30° from the axis of the metatarsal bone when the forefoot is loaded in the foot-flat position. The magnitude of torque would be given by Rtm.sin30°l, where l is the length of the metatarsal bone (fig 6.11a), thereby reaching a value of about 14xBW (Nmm) under the geometrical conditions assumed.

It is interesting to note that with the MP joint in dorsiflexion (fig 6.11b), the resultant Rtm approached the axis of the metatarsal bone so that the torque about the tarsometatarsal joint is reduced. In 30° dorsiflexion the torque drops to 46% of the value previously mentioned, in spite of the magnitude of Rtm increasing. This is mainly due to the set direction of the dominating ground force under the head of the metatarsal head, and should be given thought when considering the effect of wearing high-heeled shoes.

Table 6.2 presents a list of the average peak forces in the tendons, and the corresponding forces in the joints of the 2nd ray during normal gait. Maximum forces of about 1.6 times the values mentioned have been observed to occur.

7.3.4 Stresses in the first and second rays of the foot:

Finally, the stresses that occur in the tendons and metatarsals of the 1st and 2nd rays during normal gait have been estimated. Also, it has been hypothesized how, under the action of repeated

loading, fatigue fractures within the cancellous bone of the metatarsal heads could occur leading to a local form of necrosis that becomes clinically manifest as Koehler-Freiberg's disease.

7.3.4.1 Stresses in the flexor tendons:

The tensile stress produced in the flex.hall.long. tendon, observing the magnitude of forces that were measured under the pad of the great toe during gait (figures 5.13 and 5.20 and Table 5.4 of Chapter 5) and on assuming a cross-sectional area of 13.5 mm^2 (Table 4.1) and total body weight of 700 N, amounts to about 35 N/mm^2 at average peak load. Since the maximum peak force under the great toe could amount to about 1.7 times the average peak value, the highest tensile stress will be about 60 N/mm^2. Thus, the highest stress would approach 85% of the rupture limit of 66 N/mm^2 as given by Yamada (1970). No attempt has been made to estimate the tensile stresses in the flex.hall.brev. tendons for the following reasons: a) the difficulty in ascertaining the areas of cross section and b) the uncertainty of load sharing, not only amongst the two heads of the flex.hall.brev.muscles, but also with the abductor hallucis that adjoins them.

On examining the tensile stresses produced in the flexor tendons of the 2nd ray, it has been observed that, assuming a total body weight of 700 N and the cross sectional areas of the tendons to be as shown in Table 4.1, the average peak stress in the flex. digit.long. tendon amounts to about 12 N/mm^2 while that in the flex.digit.brev. tendon approaches 35 N/mm^2. Since the maximum peak force observed under the pad of the 2nd toe could amount to about 1.6 times the average peak value, the highest tensile stresses that

develop in the flexor tendons would be correspondingly higher. It is indeed strange that the flex.digit.long. tendon with a cross sectional area of about 6.5 mm^2 should take only 68% of the load carried by the weaker flex.digit.brev. tendon which exhibits a cross sectional area of only about 3.4 mm^2. This might be because of other activities expected of it, like clawing, grasping, etc., which, however, have not been examined in this study.

7.3.4.2 Stresses in the metatarsal shanks:

The stresses in the middle of the metatarsal shanks of the 1st and 2nd rays were calculated using values for the moment of inertia, area of cross section and position of the neutral axis that were estimated by Abramson (1927). Also assuming again a total body weight of 700 N, the average peak combined stresses (bending and normal) in the 1st ray amounted to -23/-1 N/mm^2, the highest compressive stress occurring on the dorsal aspect of the bone. Under the same assumptions, the stresses in the 2nd metatarsal bone measured -94/+66 N/mm^2 (compressive stress appearing on the dorsal aspect and tensile stress on the plantar). Under maximum peak loads measured, the stresses could even amount to as much as -150/+106 N/mm^2. This enormously high value (the average ultimate bending strength of cortical bone given by Yamada (1970) is about 157 N/mm^2) does throw some doubt on the estimation. However, it must be pointed out that there might be some load sharing with the neighbouring bones, by virtue of the interconnection to the 3rd metatarsal by means of the interossei muscles and also through the transversal ligamentous attachment between the MP joint capsules, that would reduce these figures. Also, this particular bone might well exhibit

higher strength properties than other bones since it is a common opinion amongst foot surgeons that the bone of the 2nd metatarsal is particularly difficult to cut. Nevertheless, the results have indeed shown that the shaft of the 2nd metatarsal bone is more vulnerable to fractures than that of the 1st, a fact which is regularly observed in clinical practice, especially in the form of so-called 'march' fractures. This is probably a material fatigue phenomenon in which healing of initiated fractures cannot keep pace with fracture propagation under repeated loading conditions.

7.3.4.3 Stresses in the metatarsal heads:

The analysis described in detail in Section 6.4.2 shows that especially under edge loading conditions, the resultant in the metatarsophalangeal joints could cause over-loading and collapse of the cancellous bone just below the area of force transmission. In the discussion which follows (Section 6.4.3) it is also shown why the head of the 2nd metatarsal bone is more prone to this kind of damage than that of the 1st. This, and the observation that the joint resultant acts more dorsally on the 2nd metatarsal head than on the 1st (figs 6.2 and 6.10), coincide well with the clinical findings regarding the occurrance of idiopathic necrosis of the metatarsal heads (Zollinger, 1988).

It must be expressly mentioned that the results of the finite element investigations are to be accepted only in a semi-quantitative sense since no details are known of the actual form and size of the bearing areas nor of the pressure distribution over the areas of edge contact. Nevertheless, it was considered appropriate to observe the manner of stress distribution that follows when the joint

resultant acts within a very small surface area.

7.4 Final Remarks:

It is recognised that the observations made on the anatomy of only three fresh autopsy specimens of feet would not justify the results presented in this thesis to be readily applicable to every foot. The wide degree of anthropometric variability and the individual manner of using these 'walking implements' (as termed by the Weber brothers, 1836) would certainly make such an attempt questionable. Nevertheless, even the observations made on a single specimen with regards to the much discussed supporting action of the longitudinal arch through the plantar aponeurosis prompts one to reconsider the function ascribed to the latter, and in the light of present views on muscle control systems involving propreoceptive mechanisms (Schultz et al., 1984), the question arises as to whether the plantar aponeurosis - like probably several other ligamentous structures - is substantially part of a sensoring device.

Also, as repeatedly mentioned, the geometrical dimensions of the bones of the forefoot and the spatial relationship of the tendons to the joint surfaces, which are major factors in determining the internal forces that act within the structure of the foot, must be confirmed on a much larger number of specimens than studied during this work.

The present study has shown that the 2nd ray of the foot needs to be investigated further. An analysis involving clawing and grasping actions might explain some of the anatomical features like a flex.digit.long. tendon that is stronger than the flex.digit.brev. one. The bending strength of the 2nd metatarsal bone and the resis-

tance to bending in the tarsometatarsal 'mortise and tenon' joint should be examined too. Finally, is it possible that soft structures like transversal ligaments, intercapsular connections and the interossei muscles enable the four lateral metatarsals of the foot to be so linked together that they form an integral high-strength shell structure, as suggested by Szymanowski (1860/1861)?

In spite of this and many other unanswered questions, it is hoped that the work presented in this thesis would be a useful contribution towards a further understanding of the biomechanics of the human foot.

BIBLIOGRAPHY

Abramson E (1927), Zur Kenntnis der Mechanik des Mittelfusses. Skand Arch Physiol 51:175-234.

Alexander R McN & Vernon A (1975), The dimensions of knee and ankle muscles and the forces they exert. J Human Movemt Stud 1:115-123.

Amis AA, Dawson D & Wright V (1980), Elbow joint force predictions for some strenuous isometric actions. J Biomech 13:765-775.

Arcan M & Brull MA (1976), Fundamental characteristics of the human body and foot, the foot-ground pressure pattern. J Biomech 9:453-457.

Barnett CH (1956), The phases of human gait. Lancet ii:617-621.

Basler A (1927), Ueber die Ausdehnung und Belastung der Sohlenstürz-punkte beim Stehen. Z orthop Chir 48:98-124.

Basmajian JV & Stecko G (1963), The role of muscles in arch support of the foot. J Bone Joint Surg 31B:1184-1190.

Basmajian JV (1978), Muscles Alive, ed Williams and Wilkins.

Bauman JH & Brand PW (1963), Measurement of pressure between foot and shoe. Lancet 1:629-632.

Beely F (1882), Zur Mechanik des Stehens. Langenbeck's Arch f Chir 27:457-471.

Bisshopp KE (1969), Rodrigues' Formula and the Screw Matrix, in "Journal of Engineering for Industry". Transactions of the ASME, pp 179-185.

Blacharski PH, Somerset JH & Murray DG (1975), A 3-D study of the kinematics of the human knee. J Biomech 8:375-384.

Blauth W (1986), Hallux Valgus. Springer-Verlag, Berlin.

Bojsen-Møller F (1979), Anatomy of the forefoot, normal and patho-logic. Clin Orthop Rel Res 142:10-18.

Bojsen-Møller F & Lamoreux L (1979), Significance of free dorsi-flexion of the toes in walking. Acta orthop scand 50:471-479.

Borelli GA (1685), De Mortu Animalium. Editio Altera.

Brand RA, Pedersen DR & Friederich JA (1986), The sensitivity of muscle force predictions to changes in physiologic cross-sectional area. J Biomech 19:589-596.

Braune W & Fischer O (1895), Der Gang des Menschen, 1. Teil, in "Abhandlung der math. phys. Classe der königl. sächsischen Gesell-schaft der Wissenschaften", vol XXI.

Brinckmann P (1981), Die Richtung der Fusslängsachse beim Gehen. Z Orthop 119:445-448.

Carlet M (1872), Essai expérimental sur la locomotion humaine, in "Annales de Science Naturelles, Section Zoologique", vol XV.

Carlslöö SL & Wetzenstein H (1968), Change of form of the foot and the foot skeleton upon momentary weight-bearing. Acta orthop scand 39:413-423.

Cavanagh PR & Michiyoshi A (1980) A technique for the display of pressure distributions beneath the foot. J Biomech 13:69-75.

Cavanagh PR & Rodgers MM (1985), Pressure distribution underneath the human foot, in "Biomechanics - Current interdisciplinary research", ed SM Perren & E Schneider, Martinus Nijhoff Publishers.

Charnley J (1960), The lubrication of animal joints in relation to surgical reconstruction by arthroplasty. Ann rheum Dis 19:10-19.

Chodera J (1957), Examination methods of standing in man. F U CSAV, Praha 1:3.

Collis WJMF & Jayson MIV (1972), Measurement of pedal pressures. Ann rheum Dis 31:215-217.

Debrunner HU (1982), Orthopädisches Diagnostikum. Georg Thieme Verlag.

Debrunner HU (1985), Biomechanik des Fusses, in "Bücherei des Orthopäden", vol 49. Enke.

Diebschlag W (1982), Die Druckverteilung an der Fusssohle des Menschen im Stehen und Gehen, barfuss und im Schuh. Z Orthop 120: 814-820.

Dubois J-P & Levame J-H (1966), Anatomie descriptive du pied humain. Librairie Maloine SA, Paris.

Duckworth T, Betts RP, Franks CI & Burke J (1982), The measurement of pressures under the foot. Foot & Ankle, vol 3, pp 130-141.

Ducroquet RJ & Ducroquet P (1965), La marche et les boiteries. Masson & Cie, Paris.

Elftman, H (1934), A cinematic study of the distribution of pressure in the human foot. Anat Rec, vol 59.

Evans FG (1973), Mechanical properties of bone. Charles C Thomas, Illinois.

Faux ID & Pratt MJ (1981), Computational geometry for design and manufacture. Ellis Horwood Ltd.

Fick R (1910), Handbuch der Anatomie und Mechanik der Gelenke, II. Teil. Gustav Fischer, Jena.

Fick R (1911), Handbuch der Anatomie und Mechanik der Gelenke, III. Teil. Gustav Fischer, Jena.

Fischer O (1900), Der Gang des Menschen, III. Teil, in "Abhandlung der màth. phys. Classe der königl. sächsischen Gesellschaft der Wissenschaften" vol XXVI.

Fischer O (1904), Der Gang des Menschen, VI. Teil, in "Abhandlung der math. phys. Classe der königl. sächsischen Gesellschaft der Wissenschaften", vol XXVIII.

Francillon MR (1957), Myokinesigraphie, in "Handbuch der Orthopädie", vol 1, ed Hohmann, Hackenbroch & Lindemann. Georg Thieme.

Frostell G (1926), Beitrag zur Kenntnis der vorderen Stützpunkte des Fusses, sowie des Fusswinkels beim Stehen und Gehen. Z orthop Chir 47:3-54.

Fujita M, Matsusaka N, Norimatsu T, Chiba G, Hayashi T, Miyasaki M, Yamaguchi K, Suzuki R & Hani T (1983), Motion and role of the MP joints in walking. Biomechanics VIIIa:467-470.

Goldstein H (1950), Classical mechanics. Addison-Wesley.

Gray's Anatomy (1973), 35th edition, ed R Warwick & PL Williams. Longman.

Grundy M, Tosh PA, McLeish & Smidt L (1975), An investigation of the centres of pressure under the foot while walking. J Bone Joint Surg 57:98-103.

Haxton HA (1944), Absolute muscle force in the ankle flexors of man. J Physiol 103:267-273.

Henke W (1858), Die Contracturen der Fusswurzel. Z. für rationelle Med. 3. Reihe, Vol. V:44 - 82.

Hicks JH (1953), The mechanics of the foot. J Anat 87:345-357.

Hicks JH (1954), The mechanics of the foot, J Anat 88:25-31.

Hicks JH (1955), The foot as a support. Acta anat 25:34-45.

Hohmann G (1939), Fuss und Bein. JF Bergmann, München.

Houghton S (1867), On some elementary principles in animal mechanics. Proc Roy Soc London 16:19-24.

Hutton WC, Stott JRR & Stokes IAF (1982), The mechanics of the foot, in "The Foot and its Disorders", ed L Klenermann. Blackwell Scientific Publications, pp 31-47.

Ikai M & Fukunaga T (1968), Calculation of muscle strength per unit cross sectional area of human muscle by means of ultrasonic measurement. Int Z angew Physiol einschl Arbeitsphysiol 26:26-32.

Inman VT (1976), The joints of the ankle. Williams & Wilkins, Baltimore.

Inman VT, Ralston HJ & Todd F (1981), Human walking. Williams & Wilkins, Baltimore.

Jacob HAC, Huggler AH, Dietschi C & Schreiber A (1976), Mechanical function of subchondral bone as experimentally determined on the acetabulum of the human pelvis. J Biomech 9:625-627.

Jacob HAC, Zollinger H & Georgiev S (1985), Untersuchungen zur Biomechanik der Zehengrundgelenke. Z Orthop 123:929-938.

Jacob HAC, Zollinger H & Georgiev S (1987), Could Koehler-Freiberg's disease be caused by biomechanical factors?, in "Biomechanics: Basic and Applied Research", ed G Bergmann, R Kölbel & A Röhlmann. Martinus Nijhoff Publishers.

Jones RL (1941), The human foot. An experimental study of its mechanics and the role of its muscles and ligaments in the support of the arch. Am J Anat 68:1-39.

Joseph J (1954), Range of movement of the great toe in men. J Bone Joint Surg 36B:450-457.

Keith A (1929), The history of the human foot and its bearing on orthopaedic pracitce. J Bone Joint Surg 11: 10-32.

Kewenter Y (1936), Die Sesambeine des 1. Metatarsophalangealgelenks des Menschen. Acta Orthop Scand, Suppl II

Kimizuko M, Kurosawo H & Fukubayashi T (1980), Load bearing pattern of the ankle joint. Contact area of pressure direction. Arch Orthop Traum Surg 96:45-49.

Kinzel GL, Hall AS & Hillberry BM (1972), Measurement of the total motion between two body segments. Analytical development. J Biomech 5:93-105.

Klein-Vogelbach (1976), Funktionelle Bewegungslehre, 3rd ed. Springer Verlag.

Kubik ST (1982), Vergleichende Anatomie und Entwicklungsgeschichte des Fusses. Orthop Praxis 18/7:513-529.

Kummer B (1984), Biomechanik des Vorfusses. Orthop Praxis 7:521-527.

Lake N (1937), The arches of the foot. Lancet: 872-873.

Lanz T von, Wachsmuth W (1972), Praktische Anatomie, Bein und Statik. Springer.

Last RJ (1984), Anatomy, regional and applied, 7th ed. Churchill Livingstone.

Mann R & Inman VT (1964), Phasic activity of intrinsic muscles of the foot. J Bone Joint Surg 46A:469-481.

Mann RA & Hagy JL (1979), The function of the toes in walking, jogging and running. Clin Orthop Rel Res 142:24-29.

Manter JT (1946), Distribution of compression forces in the joints of the human foot. Anat Rec 96:313-321.

Meyer H von (1853), Das aufrechte Stehen. Arch Anat, Physiol, wiss Med. Müller's Archiv, pp 9-44.

Meyer H von (1873), Die Statik und Mechanik des menschlichen Knochengerüstes. Wilhelm Engelmann Verlag, Leipzig.

Milatz WFJ (1921), Ein Koordinatenmesser und Goniometer. Z orthop Chir 41:351-356.

Morrison JB (1970), The mechanics of muscle function in locomotion. J Biomech 3:431-451.

Morton DJ (1930), Structural factors in static disorders of the foot. Am J Surg 9:315-326.

Morton DJ (1935), The human foot. Columbia University Press.

Murray MP, Drought AB & Kory RC (1964), Walking patterns of normal men. J Bone Joint Surg 46A:335-360.

Nicol AC (1987), A new flexible electrogoniometer with widespread applications, in "International Series on Biomechanics", ed Bengt Jonsson. Human Kinetic Publishers Inc., Champaign, IL, vol. 6B.

Nicol K & Hennig EM (1978), Measurement of pressure distribution by means of a flexible, large-surface mat, in "Biomechanics VI-A, Proc 6th Int Congr Biomech", ed E Asmussen & K Jorgenssen. Univ Park Press, pp 374-380.

Panjabi M & White AA (1971), A mathematical approach for 3-D analysis of the mechanics of the spine. J Biomech 4:203-211.

Panjabi MM, Krag MH & Goel VK (1981), A technique for measurement and description of three dimensional six degree-of-freedom motion of a body joint with an application to the human spine. J Biomech 14: 447-460.

Paul JP (1967), Forces at the human hip joint. Ph D Thesis, University of Glasgow.

Paul JP (1971), Comparison of EMG signals from leg muscles with corresponding force actions calculated from walkpath measurements. Conf Human Locomotor Engineering, University of Sussex.

Platzer W (1984), Colour Atlas and Textbook of Human Anatomy, Locomotor System, vol 1, 2nd ed. Georg Thieme Stuttgart.

Preuschoft H (1970), Statische Untersuchungen am Fuss der Primaten. Z Anat Entwickl-Gesch 131:156-192.

Preuschoft H (1971), Body posture and mode of locomotion in early pleistocene hominids. Folia primat 14:209-240.

Procter PH (1980), Ankle Joint Biomechanics. Ph D Thesis, University of Strathclyde.

Rouleaux F (1900), Lehrbuch der Kinematik. F Vieweg & Sohn, Brunswick.

Salathé Jr EP, Arangio GA & Salathé EP (1986), A biomechanical model of the foot. J Biomech 19:989-1001.

Sarrafian SK (1983), Anatomy of the foot and ankle. Lippincott.

Scherb R (1926), Ein Vorschlag zur kinetischen Diagnostik in der Orthopädie in "Verhdlg Dtsch orthop Ges", pp 462-472.

Scherb R & Arienti A (1945), Ist die Myokinesigraphie als Untersuchungsmethode objektiv zuverlässig? Schweiz med Wschr 49:1077-1079.

Schultz RA, Miller DC, Kerr CS & Micheli L (1984), Mechanoreceptors in human cruciate ligaments. J Bone Joint Surg 66A:1072-1076.

Schwartz RP & Heath AL (1947), The definition of human locomotion on the basis of measurement. J Bone Joint Surg 29A:203-214.

Schwartz RR, Heath AL, Morgan DW & Towns RC (1964), A quantitative analysis of recorded variables in the walking pattern of "normal" adults. J Bone Joint Surg 46A:324-334.

Scranton PE & McMaster JH (1976), Momentary distribution of forces under the foot. J Biomech 9:45-48.

Simkin A & Stokes IAF (1982), Characterisation of the dynamic vertical force distribution under the foot. Med Biol Eng and Comput 20:12-18.

Soudan K, van Audekercke R & Martens M (1979), Methods, difficulties and inaccuracies in the study of human joint kinematics and pathokinematics by the instant axis concept. J Biomech 12:27-33.

Staudinger (1933), Eine neue Mess- bzw. Untersuchungsmethode des Fusses, in "Verhandlungen der Deutschen Orthopädischen Gesellschaft" 58:219-225.

Stokes IAF, Hutton WC & Stott JRR (1979), Forces acting on the metatarsals during normal walking. J Anat 129:579-590.

Stott JRR, Hutton WC & Stokes IAF (1973), Forces under the foot. J Bone Joint Surg 55B:335-344.

Strasser H (1908), Lehrbuch der Muskel- und Gelenkmechanik. Springer, Berlin.

Stüssi E (1977), Vierdimensionale Vektordatstellung der Bodenkräfte beim Gehen. MOT 6:

Szymanowski (1860/61), Kritik der partiellen Fussamputationen, gestützt auf eine neue anatomische Deutung der Architektur des Fusses. Arch f klin Chir I.

Trott AW (1980), The normal human foot - what is it?, in "The foot and Ankle", ed Bateman & Trott. BC Decker, New York.

University of California (1953), The pattern of muscular activity in the lower extremity during walking. Prosth Dev Res Project Inst Engng Res U California, Berkeley, Ser 11, Iss 25.

Weber W & Weber E (1836), Mechanik der menschlichen Gehwerkzeuge. Dieterichsche Buchhandlung, Göttingen.

Weidenreich (1921), Der Menschenfuss. Z Morph Anthrop 22:

Weil S & Weil UH (1966), Mechanik des Gehens. G. Thieme, Stuttgart.

Wickiewicz TL, Roy RR, Powell PL & Egerton VR (1983), Muscle architecture of the human lower limb. Clin Orthop Rel Res 179:275-283.

Wood-Jones F (1944), Structure and function as seen in the foot. Baillière, Trindall and Cox, London.

Wright DG & Rennels DC (1964), A study of the elastic properties of plantar fascia. J Bone Joint Surg 46A:482-492.

Wright DB, Desai SM & Henderson WH (1964), Action of the subtalar and ankle-joint complex during the stance phase of walking. J Bone Joint Surg 46A:361-

Yamada H (1970), Strength of biological materials. Williams & Wilkins, Baltimore.

Zitzlsperger S (1960), The mechanics of the foot based on the concept of the skeleton as a statically indeterminate space frame. Clin Orthop 16:47-63.

Zollinger H & Kubik S (1984), Ein seltener Fall von Osteonekrose der Metatarsaleköpfchen 1 und 2 beidseits. Chir del Piede 8:121-124.

Zollinger H (1988), Osteonekrosen der Metatarsaleköpfchen, in "Bücherei des Orthopäden", vol 53. Enke.

Zurmühl R (1965), Praktische Mathematik für Ingenieure und Physiker. Springer.

APPENDIX 1(3)

Determination of position of moiré fringes

Given:

- Location of grid along the y axis
- Pitch of grid, t
- Position of light source, C_x, C_y
- Position of camera, A_x, A_y

Required:

- Distances s_0--- s_n (for any choice of `n´) within the interval y = E to y = F.

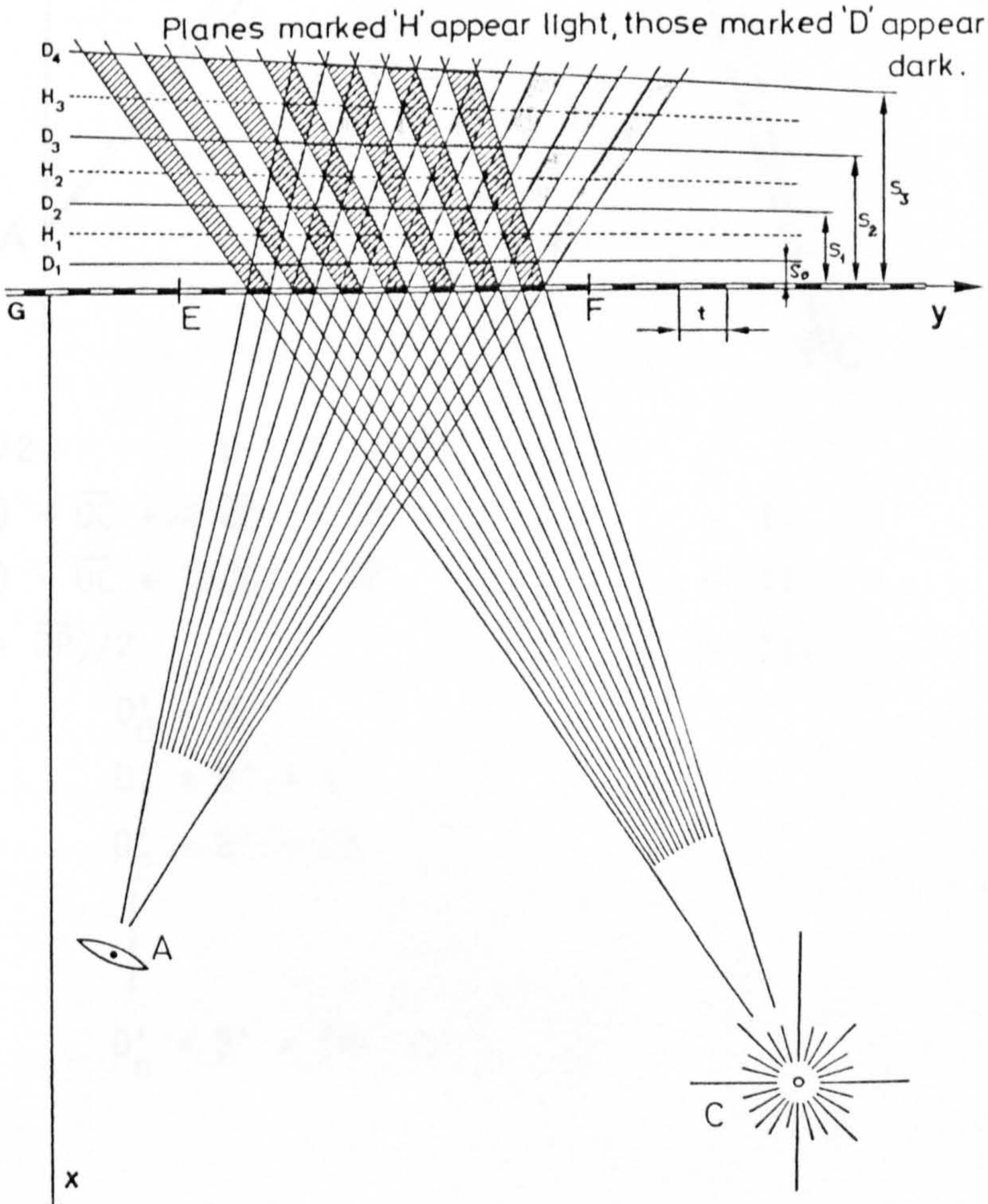

Solution:

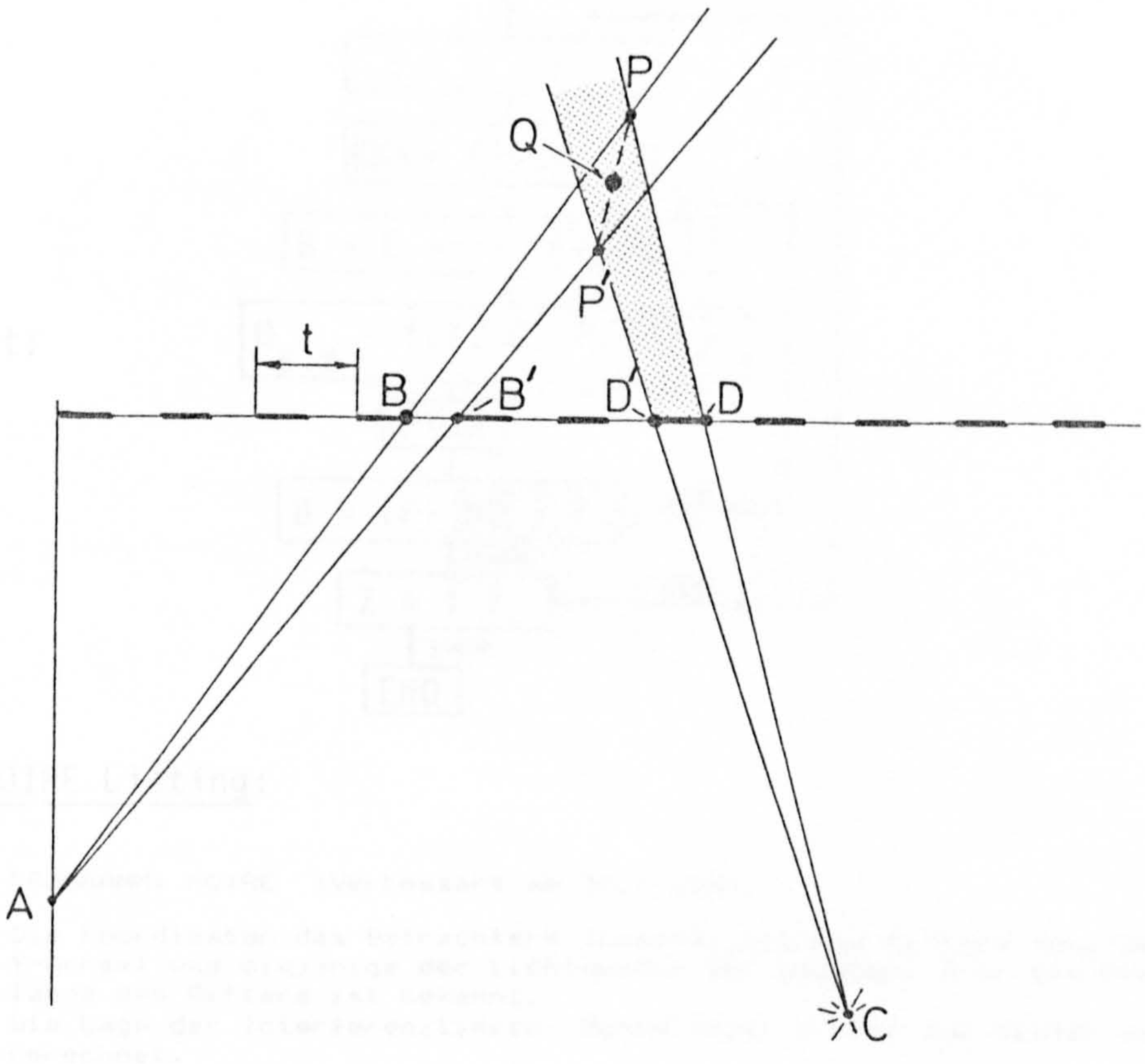

$B' = B + t/2$ $\qquad D = D' + t/2$

$\overline{OA} + \alpha(\overline{AB}) = \overline{OC} + \beta(\overline{CD}) = \overline{OP}$ — I

$\overline{OA} + \gamma(\overline{AB}) = \overline{OC} + \delta(\overline{CD}) = \overline{OP}$ — II

$\overline{OQ} = (\overline{OP'} + \overline{OP})/2$ — III

For s_0 : $D'_0 = B'$

For s_1 : $D'_1 = B' + t$

For s_2 : $D'_2 = B' + 2t$

For s_n : $D'_n = B' + (n-1)t$

Flow diagram of programme MOIRE:

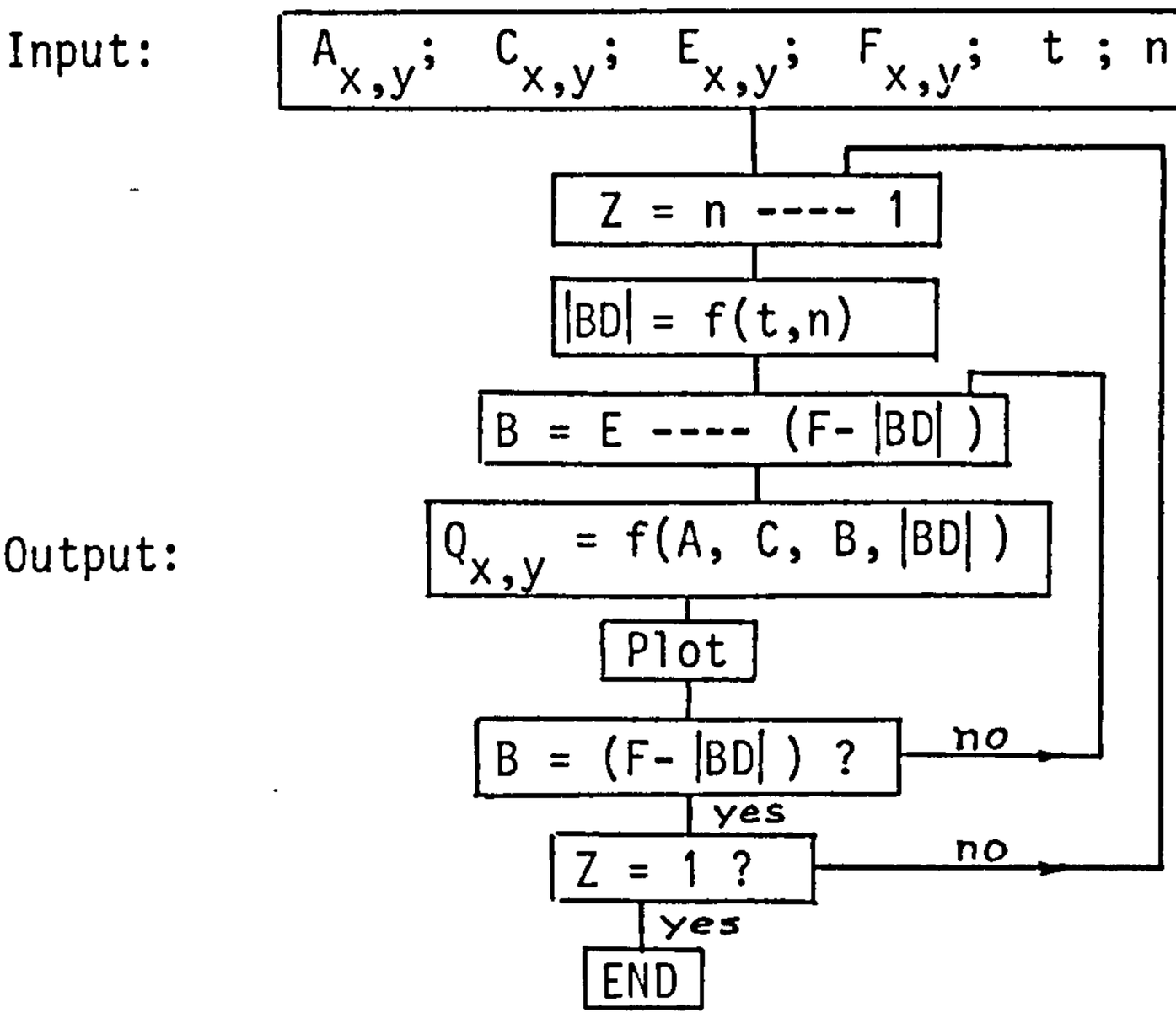

Programme MOIRE Listing:

```
2 REM:      PROGRAMM: MOIRE  (Verbessert am 30.7.1985)
5 CLS
10 REM:    Die Koordinaten des Betrachters (Kamera),und des Gitters (entlang der
20 REM:    Y-Achse) und diejenige der Lichtquelle sei gegeben. Auch die Perioden-
30 rem:    länge des Gitters ist bekannt.
30 REM:    Die Lage der Interferenzlinien (Dunkelfeld) hinter dem Gitter wird
40 REM:    berechnet.
50 BEEP
60 INPUT "Lage der Kamera: Ax=";A1
70 BEEP
80 INPUT "Lage der Kamera: Ay=";A2
90 BEEP
100 INPUT "Lage der Lichtquelle: Cx=";C1
110 BEEP
120 INPUT "Lage der Lichtquelle: Cy=";C2
130 BEEP
140 INPUT "Lage des Gitteranfangs: Ey=";E2
150 BEEP
160 INPUT "Lage des Gitterendes: Fy=";F2
170 BEEP
180 INPUT "Periodenlänge des Gitters: t="; T
190 BEEP
200 INPUT "Anzahl Interferenzlinien: n=";N
205 INPUT "Schrittweite der Berechnung in der Y-Richtung: Sch.W = t*F,  F =";F
207 LPRINT " PROGRAMM:          MOIRE ":LPRINT :LPRINT
210 LPRINT "Lage der Kamera: Ax =";A1;"          Ay =";A2
220 LPRINT "Lage der Lichtquelle: Cx =";C1;"          Cy =";C2
230 LPRINT "Lage des Gitteranfanges: Ey =";E2;"  Lage des Gitterendes: Fy =";F2
240 LPRINT "Periodenlänge des Gitters: t =";T
250 LPRINT "Anzahl Interferenzlinien: n =";N
260 C2=C2-A2
270 E2=E2-A2
280 F2=F2-A2
290 PRINT
300 PRINT
310 B2=E2
320 Z=N
330 GOSUB 690
```

```
340 B2=F2-T/2-N*T
350 U1=Q1
360 U2=Q2
370 GOSUB 690
380 IF ABS(Q1)>=ABS(U1) THEN  410
390 S=U1
400 GOTO  420
410 S=Q1
420 CLS
430 SCREEN 2
440 KEY OFF
450 O=1
460 X=Q2
470 Y=-Q1
480 YT=347-Y*300/(-S)-27
490 XT=(X-E2)*680/(F2-E2)+20
500 IF O=2 THEN 650
510 LINE(20,320)-(700,320)
520 FOR Z=N TO 1 STEP -1
530 B2=E2
540 GOSUB 690
550 X=Q2
560 Y=-Q1
570 GOSUB 830
580 PRESET(XT,YT)
590 LPRINT "y(";Z;")=";Q2+A2,"X(";Z;")=";Q1
600 B2=B2+T*F
610 IF B2>(F2-T-N*T) THEN 670
620 GOSUB 690
630 O=2
640 GOTO 460
650 LINE -(XT,YT)
660 GOTO 590
670 NEXT Z
680 GOTO 860
690 D2=B2+T/2+Z*T
700 M1=B2/(-A1)
710 R=(A1*M1-M1*C1+C2)/(M1*(-C1)-(D2-C2))
720 P1=C1+R*(-C1)
730 P2=C2+R*(D2-C2)
740 B3=B2+T/2
750 D3=D2-T/2
760 M1=B3/(-A1)
770 R=(A1*M1-M1*C1+C2)/(M1*(-C1)-(D2-C2))
780 P3=C1+R*(-C1)
790 P4=C2+R*(D2-C2)
800 Q1=(P1+P3)/2
810 Q2=(P2+P4)/2
820 RETURN
830 YT=347-Y*300/(-S)-27
840 XT=(X-E2)*680/(F2-E2)+20
850 RETURN
860 END
```

APPENDIX 2(3)

Determination of point of intersection of two non-parallel rays in a plane to which Cartesian coordinates have been ascribed

Given:

- Each ray is defined by two points on it.
  $A_{x,y}$ and $B_{x,y}$ describe one ray, and $C_{x,y}$ and $D_{x,y}$ the other.

Required:

- The x and y coordinates of the point of intersection P.

Solution:

$$\overline{OP} = \overline{OA} + \alpha(\overline{OB}-\overline{OA}) = \overline{OC} + \beta(\overline{OD} - \overline{OC})$$

(where O is the origin of the coordinate system)

Programme SCHNITT.PKT Listing:

```
  5 PRINT "PROGRAMM:       SCHNITT.PKT                              17.05.85 "
  7 LPRINT "PROGRAMM:       SCHNITT.PKT   "
 10 REM:   Der Schnittpunkt zweier Strahlen in einer Ebene wird berechnet.
 20 REM:   Jeder Strahl ist durch 2 Punkte (A und B, bzw. C und D) gegeben)
 30 INPUT "Ax =";A1
 40 INPUT "Ay =";A2
 50 INPUT "Bx =";B1
 60 INPUT "By =";B2
 70 INPUT "Cx =";C1
 80 INPUT "Cy =";C2
 90 INPUT "Dx =";D1
100 INPUT "Dy =";D2
110 PRINT "Ax =";A1,"Bx =";B1
120 PRINT "Ay =";A2,"By =";B2
130 LPRINT "Ax =";A1,"Bx =";B1
140 LPRINT "Ay =";A2,"By =";B2
150 PRINT
160 LPRINT
170 PRINT "Cx =";C1,"Dx =";D1
180 PRINT "Cy =";C2,"Dy =";D2
190 LPRINT "Cx =";C1,"Dx =";D1
200 LPRINT "Cy =";C2,"Dy =";D2
210 PRINT
220 PRINT
230 LPRINT
240 LPRINT
250 F=(B2-A2)/(B1-A1)
260 A=(A1*F-A2-C1*F+C2)/(F*(D1-C1)-(D2-C2))
270 P1=C1+A*(D1-C1)
280 P2=C2+A*(D2-C2)
290 PRINT "Der Schnittpunkt ist gegeben durch :"
300 PRINT "Px =";P1,"Py =";P2
310 LPRINT "Der Schnittpunkt ist gegeben durch :"
320 LPRINT "Px =";P1,"Py =";P2
330 PRINT
340 LPRINT
350 PRINT
360 LPRINT
370 GOTO 30
380 END
```

APPENDIX 3(3)

Curve fitting (best-fitting polynomial of n^{th} degree)
- Programme AUSGL.POL -

Given:

- A data set of j values such that y_1, y_2, y_3,----y_j correspond to x_1, x_2, x_3,----x_j.

Required:

- A function $y = f(x)$ of the polynomial form $C_0 + C_1x + C_2x^2$+--- --+ C_nx^n which approaches the given set of j values so closely that the square of the deviation (error) is a minimum; for any value of the integer n chosen between $n = 1$ and $n = (j-1)$.

Solution:

- An algorithm according to Zurmühl (1965), based on a series of linear equations that give the required coefficients C_0, C_1, C_2,-- --- C_n. These linear equations are as follows:

$$j\,C_0 + [x]\,C_1 + [x^2]\,C_2 + \text{---------} + [x^n]\,C_n = [y]$$
$$[x]\,C_0 + [x^2]\,C_1 + [x^3]\,C_2 + \text{--------} + [x^{n+1}]\,C_n = [xy]$$
$$\text{----------}$$
$$\text{----------}$$
$$[x^n]\,C_0 + [x^{n+1}]\,C_1 + [x^{n+2}]\,C_2 + \text{--------} + [x^{2n}]\,C_n = [x^n y]$$

The quantities in brackets denote sums as follows:

$$[x] = x_1 + x_2 + x_3 + \text{----------} + x_j$$
$$[y] = y_1 + y_2 + y_3 + \text{----------} + y_j$$
$$[x^2] = x_1^2 + x_2^2 + x_3^2 + \text{----------} + x_j^2$$
$$[x^2y] = x_1^2y_1 + x_2^2y_2 + x_3^2y_3 + \text{----} + x_j^2y_j$$

etc.

Flow diagram of programme AUSGL.POL:

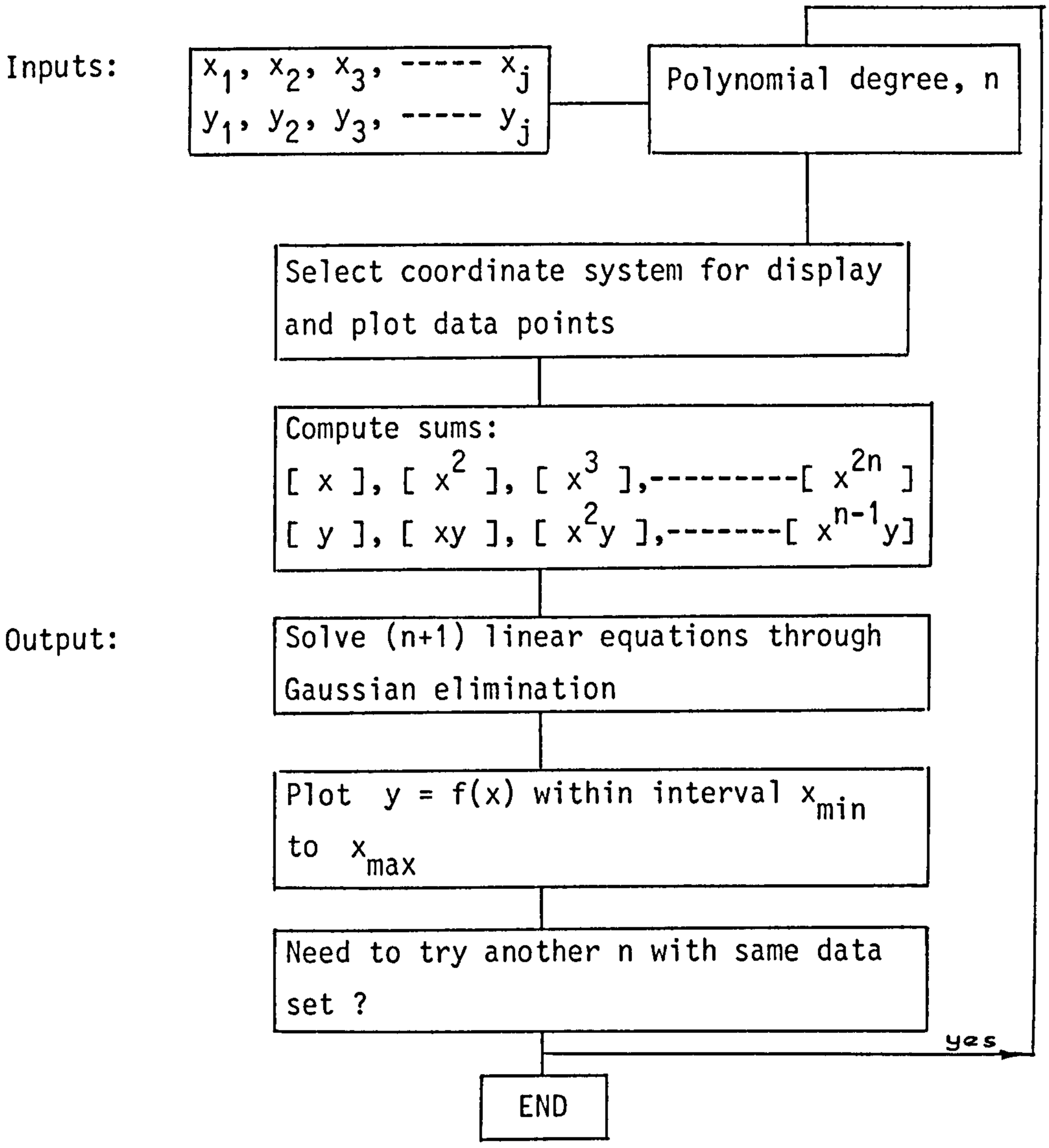

Programme AUSGL.POL Listing:

```
10  REM  " Programm 'AUSGL.POL' ergänzt für HP-Plotter seit 15.7.86 "
11 CLS
13 DIM X(100)
14 DIM Y(100)
15 DIM A(100,20)
16 DIM B(20)
17 DIM C(100,20)
18 CLS
20 BEEP :PRINT "Benütze Programm 'AUSGLJ.POL' wenn keine Achsen aufgezeichnet we
rden müssen !!!"
30 KEY OFF
40 LPRINT CHR$(18)
50 LPRINT "                AUSGLEICHSPOLYNOM: AUSGL.POL"
55 BEEP
60 INPUT "ANZAHL MESSPAARE  = ";N
65 BEEP
70 INPUT "GRAD DES AUSGLEICHSPOLYNOMS = ";G
```

```
80 LPRINT "ANZAHL MESSPAARE  = ";N
90 LPRINT
100 PRINT
110 LPRINT "GRAD DES AUSGLEICHSPOLYNOMS = ";G
120 LPRINT
170 BEEP
180 FOR Z=1 TO N STEP 1
190 PRINT "X(";Z;")=";
200 INPUT X(Z)
210 PRINT "Y(";Z;")=";
220 INPUT Y(Z)
230 NEXT Z
240 Z=1
250 PRINT "X";Z;"=";X(Z),"Y";Z;"=";Y(Z)
260 LPRINT "X";Z;"=";X(Z),"Y";Z;"=";Y(Z)
270 Z=Z+1
280 IF Z>N THEN 300
290 GOTO 250
300 PRINT
310 LPRINT
320 GOTO 360
330 INPUT "Grad des Ausgleichspolynoms = ";G
340 LPRINT "Grad des Ausgleichspolynoms = ";G
350 LPRINT "--------------------------------"
360 P=1
370 FOR Z=1 TO N STEP 1
380 FOR K=1 TO 2*G STEP 1
390 P=X(Z)*P
400 A(Z,K)=P
410 NEXT K
420 P=1
430 NEXT Z
440 S=0
450 FOR K=1 TO 2*G STEP 1
460 FOR Z=1 TO N STEP 1
470 S=S+A(Z,K)
480 NEXT Z
490 B(K+1)=S
500 S=0
510 NEXT K
520 FOR Z=1 TO N STEP 1
530 FOR K=1 TO G STEP 1
540 C(Z,K)=A(Z,K)*Y(Z)
550 NEXT K
560 NEXT Z
570 S=0
580 FOR K=1 TO G STEP 1
590 FOR Z=1 TO N STEP 1
600 S=S+C(Z,K)
610 NEXT Z
620 E(K+1)=S
630 S=0
640 NEXT K
650 FOR Z=1 TO N STEP 1
660 S=Y(Z)+S
670 NEXT Z
680 E(1)=S
690 B(1)=0
700 FOR Z=1 TO G+1 STEP 1
710 FOR K=1 TO G+1 STEP 1
720 Q=1-Z
730 D(Z,K)=B(K-Q)
740 NEXT K
750 NEXT Z
760 D(1,1)=N
770 FOR Z=1 TO G+1 STEP 1
780 D(Z,G+2)=E(Z)
790 NEXT Z
800 FOR P=2 TO G+1 STEP 1
810 FOR Z=P TO G+1 STEP 1
820 F=D(Z,P-1)/D(P-1,P-1)
830 FOR K=1 TO G+2 STEP 1
840 D(Z,K)=D(Z,K)-D(P-1,K)*F
850 NEXT K
860 NEXT Z
870 NEXT P
880 FOR Z=1 TO G+1 STEP 1
890 M(Z)=0
900 NEXT Z
910 FOR Z=G+1 TO 1 STEP-1
920 Q=0
```

```
930 FOR P=G+1 TO Z STEP-1
940 Q=M(P)*D(Z,P)+Q
950 NEXT P
960 M(Z)=(D(Z,G+2)-Q)/D(Z,Z)
970 NEXT Z
980 PRINT "AUSGLEICHSFUNKTION Y ="
990 LPRINT "AUSGLEICHSFUNKTION Y ="
1000 FOR K=1 TO G+1 STEP 1
1010 PRINT M(K);"*X^";K-1;"+"
1020 LPRINT M(K);"*X^";K-1;"+"
1030 NEXT K
1040 PRINT
1050 LPRINT
1060 S=0
1070 FOR Z=1 TO N STEP 1
1080 S=S+Y(Z)^2
1090 NEXT Z
1100 FOR Z=1 TO G+1 STEP 1
1110 S=S-M(Z)*E(Z)
1120 NEXT Z
1130 M=SQR(ABS(S/(N-G-1)))
1140 PRINT "MITTLERER FEHLER m=";M
1150 LPRINT "MITTLERER FEHLER m=";M
1160 PRINT
1170 LPRINT
1180 CLS
1190 SCREEN 2
1200 BEEP
1210 INPUT "X-MAX=";B
1220 BEEP
1230 INPUT "X-MIN=";A
1240 BEEP
1250 INPUT "Y-MAX=";F
1260 BEEP
1270 INPUT "Y-MIN=";E
1280 U=B-A
1290 V=F-E
1300 CLS
1310 GOTO 1400
1320 IF U=V THEN 1340
1330 IF U>V THEN 1370
1340 YT=347-((Y-E)*300/V)-27
1350 XT=((X-A)*300*1.659/V)+20
1360 GOTO 1390
1370 XT=((X-A)*680/U)+20
1380 YT=347-((Y-E)*680/U/1.659)-27
1390 RETURN
1400 LINE (20,320)-(700,320)
1410 LINE (20,20)-(20,320)
1420 FOR Z=1 TO N STEP 1
1430 X=X(Z)
1440 Y=Y(Z)
1450 GOSUB 1320
1460 PRESET(XT,YT)
1470 LINE (XT-2,YT)-(XT+2,YT)
1480 LINE (XT,YT-2)-(XT,YT+2)
1490 NEXT Z
1500 K=X(1)
1510 FOR L=2 TO N STEP 1
1520 IF K>X(L) THEN 1540
1530 GOTO 1550
1540 K=X(L)
1550 NEXT L
1560 Q=K
1570 K=X(1)
1580 FOR C=2 TO N STEP 1
1590 IF K<X(C) THEN 1610
1600 GOTO 1620
1610 K=X(C)
1620 NEXT C
1630 D=K
1640 I=0
```

```
1650 FOR Z=1 TO G STEP 1
1660 I=M(Z+1)*Q^Z+I
1670 NEXT Z
1680 I=I+M(1)
1690 X=Q
1700 Y=I
1710 GOSUB 1320
1720 PRESET(XT,YT)
1730 S=(D-Q)/100
1740 FOR K=(Q-S) TO (D+S*2) STEP S
1750 I=0
1760 FOR Z=1 TO G STEP 1
1770 I=M(Z+1)*K^Z+I
1780 NEXT Z
1790 I=I+M(1)
1800 X=K
1810 Y=I
1820 GOSUB 1320
1830 LINE -(XT,YT)
1840 NEXT K
1850 BEEP
1860 LOCATE 25,1 :PRINT "HP-PLOT ?    Ja(1) / Nein(0)"
1870 INPUT " ",Q
1880 IF Q=1 GOTO 1910
1890 IF Q=0 GOTO 2630
1900 GOTO 1860
1910 OPEN "com1:9600,S,7,1,rs,cs65000,ds,cd" AS #1
1915 INPUT "X-Achse Einteilung";J1
1917 INPUT "Y-Achse Einteilung";J2
1920 GOTO 1990
1930 IF U=V GOTO 1950
1940 IF U>V GOTO 1970
1950 YPT=500+(Y-E)*6700/V : XPT=500+(X-A)*6700/V
1960 GOTO 1980
1970 XPT=500+(X-A)*6700/U : YPT=500+(Y-E)*6700/U
1980 RETURN
1990 PRINT #1,"in;sp2;pa500,7200,pd500,500,7200,500;pu;"
2000 X=A : Y=E
2010 IF X>B GOTO 2060
2020 GOSUB 1930
2030 PRINT #1,"pa";XPT,YPT;"pd;xt;pu;"
2040 X=X+J1
2050 GOTO 2010
2060 Y=E :X=A
2070 IF Y>F GOTO 2120
2080 GOSUB 1930
2090 PRINT #1,"pa";XPT,YPT;"pd;yt;pu;"
2100 Y=Y+J2
2110 GOTO 2070
2120 X=A : Y=E
2130 GOSUB 1930
2140 PRINT #1,"pa";XPT,YPT;"cp-5,-.25;LB";E;""+CHR$(3)
2150 X=A : Y=F
2160 GOSUB 1930
2170 PRINT #1,"pa";XPT,YPT;"pd,yt,pu;cp-5,-.25;LB";F;""+CHR$(3)
2180 PRINT #1,"pa500,7200;cp-.5,1;LBY"+CHR$(3)
2190 X=A : Y=E
2200 GOSUB 1930
2210 PRINT #1,"pa";XPT,YPT;"cp-2,-1;LB";A;""+CHR$(3)
2220 X=B : Y=E
2230 GOSUB 1930
2240 PRINT #1,"pa";XPT,YPT;"pd,xt,pu;cp-2,-1;LB";B;""+CHR$(3)
2250 PRINT #1,"pa7200,500;cp1,-.25;LBX"+CHR$(3)
2260 FOR Z=1 TO N
2270 X=X(Z) : Y=Y(Z)
2280 GOSUB 1930
2290 PRINT #1,"sm*;pa";XPT,YPT;";pd;pu;"
2300 NEXT Z
2310 PRINT #1,"df;"
2320 K=X(1)
2330 FOR L=2 TO N
2340 IF K>X(L) GOTO 2360
```

```
2350 GOTO 2370
2360 K=X(L)
2370 NEXT L
2380 D=K :K=X(1)
2390 FOR C=2 TO N
2400 IF K<X(C) GOTO 2420
2410 GOTO 2430
2420 K=X(C)
2430 NEXT C
2440 D=K : I=0
2450 FOR Z=1 TO G
2460 I=M(Z+1)*Q^Z+I
2470 NEXT Z
2480 I=I+M(1) : X=Q : Y=I
2490 GOSUB 1930
2500 PRINT #1,"pa";XPT,YPT;";pd;"
2510 S=(D-Q)/100
2520 FOR K=(Q-S) TO (D+S*2) STEP S
2530 I=0
2540 FOR Z=1 TO G
2550 I=M(Z+1)*K^Z+I
2560 NEXT Z
2570 I=I+M(1) : X=K : Y=I
2580 GOSUB 1930
2590 PRINT #1,"pa";XPT,YPT;";"
2600 NEXT K
2610 PRINT #1,"pu;sp0;"
2620 CLOSE
2630 BEEP
2640 LOCATE 25,1:PRINT "FORTFAHREN ------> 1                    "
2650 INPUT " ",Q
2660 IF Q=1 THEN  GOTO 2680
2670 GOTO 2640
2680 CLS
2690 INPUT "weitere Ausführung mit gleicher Datei gewünscht? ja(1) / nein(0)",Z
2700 IF Z=0 THEN GOTO 18
2710 IF Z=1 THEN GOTO 330
2720 GOTO 2690
2730 END
```

APPENDIX 4(3)

Determination of the helical axis of motion using a rotation matrix method described by Panjabi et al.(1981)

- Programme HELIMAT -

Given:

- The spatial position of three non-collinear points A, B and C on a rigid moving body at two instants, t_1 and t_2; that is, $A_{1(xyz)}$, $B_{1(xyz)}$, $C_{1(xyz)}$; and $A_{2(xyz)}$, $B_{2(xyz)}$, $C_{2(xyz)}$.

Required:

- The direction and location of the helical axis
- The angular motion about this axis
- The translation along this axis

Solution:

- See Chapter 3, Section 3.3.1

Flow diagram of programme HELIMAT:

contd.

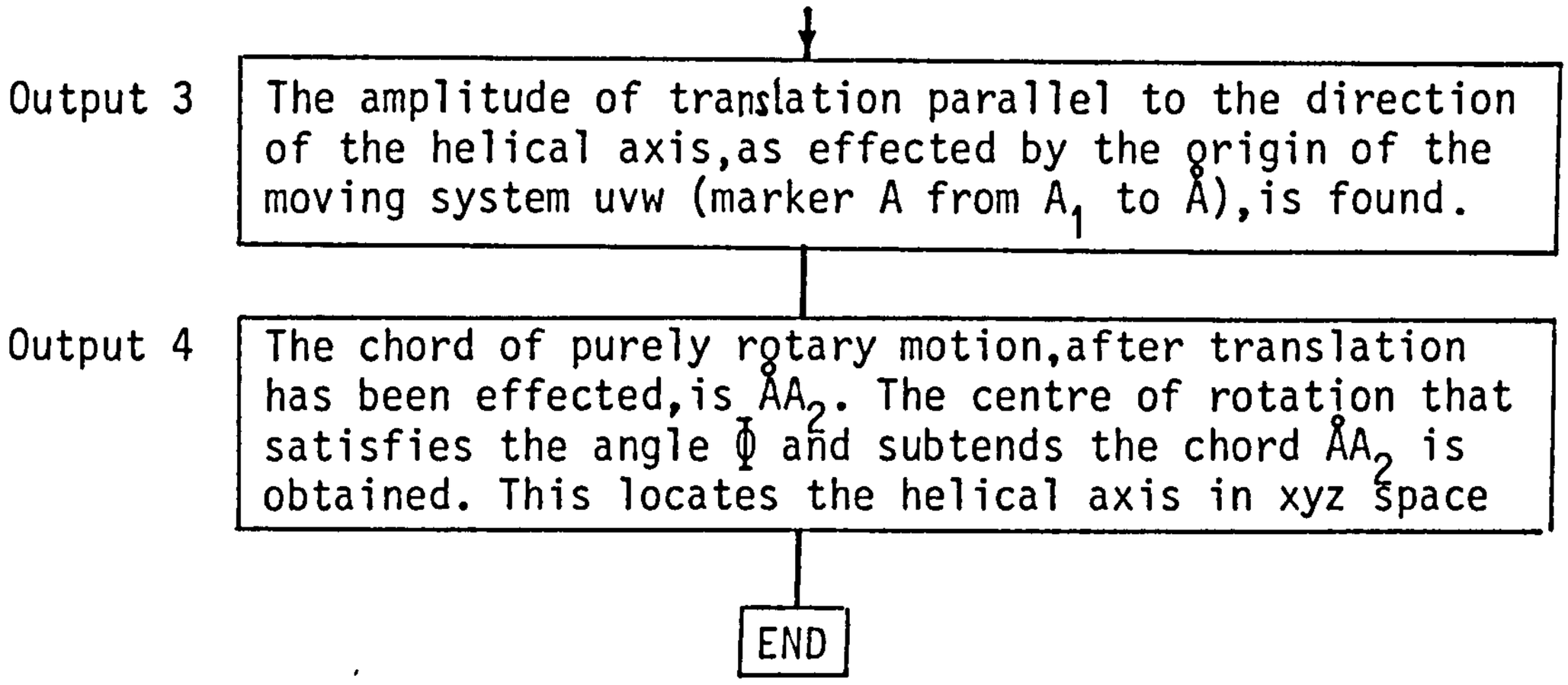

Programme HELIMAT Listing:

```
10 REM "Programm: HELIMAT                                          3.Dez.1986"
20 LPRINT  "Programm:                HELIMAT ":LPRINT :LPRINT
30 REM Bestimmung der Schraubenachse eines Körpers im Raum.
40 REM ---------------------------------------------
50 REM Der Körper ist gekennzeichnet durch 3 beliebige Punkte (A, B, C).
60 REM Die Koordinaten der Punkte (A, B, C), entsprechend 2 sukzessiven
70 REM Positionen (1 und 2), sind einzugeben.
80 INPUT "AX1="; A(1)
90 INPUT "AY1="; A(2)
100 INPUT "AZ1="; A(3)
110 INPUT "BX1="; B(1)
120 INPUT "BY1="; B(2)
130 INPUT "BZ1="; B(3)
140 INPUT "CX1="; C(1)
150 INPUT "CY1="; C(2)
160 INPUT "CZ1="; C(3)
170 INPUT "AX2="; A(4)
180 INPUT "AY2="; A(5)
190 INPUT "AZ2="; A(6)
200 INPUT "BX2="; B(4)
210 INPUT "BY2="; B(5)
220 INPUT "BZ2="; B(6)
230 INPUT "CX2="; C(4)
240 INPUT "CY2="; C(5)
250 INPUT "CZ2="; C(6)
260 LPRINT "AX1="; A(1),"AY1=";A(2),"AZ1=";A(3)
270 LPRINT "BX1="; B(1),"BY1=";B(2),"BZ1=";B(3)
280 LPRINT "CX1="; C(1),"CY1=";C(2),"CZ1=";C(3)
290 LPRINT
300 LPRINT "AX2="; A(4),"AY2=";A(5),"AZ2=";A(6)
310 LPRINT "BX2="; B(4),"BY2=";B(5),"BZ2=";B(6)
320 LPRINT "CX2="; C(4),"CY2=";C(5),"CZ2=";C(6)
330 LPRINT
340 FOR P=1 TO 4 STEP 3
350 N1=B(P)-A(P)
360 N2=B(P+1)-A(P+1)
370 N3=B(P+2)-A(P+2)
380 N4=C(P)-A(P)
390 N5=C(P+1)-A(P+1)
400 N6=C(P+2)-A(P+2)
410 N7=N2*N6-N3*N5
420 N8=N1*N6-N3*N4
430 N9=N1*N5-N2*N4
440 N0=-N8*N3-N9*N2
450 M1=N7*N3-N9*N1
460 M2=N7*N2+N8*N1
470 U=SQR(N1^2+N2^2+N3^2)
```

contd.

```
480 U(P)=N1/U
490 U(P+1)=N2/U
500 U(P+2)=N3/U
510 V=SQR(N0^2+M1^2+M2^2)
520 V(P)=N0/V
530 V(P+1)=-M1/V
540 V(P+2)=M2/V
550 W=SQR(N7^2+N8^2+N9^2)
560 W(P)=N7/W
570 W(P+1)=-N8/W
580 W(P+2)=N9/W
590 NEXT P
600 S2=-(U(1)*U(6)+V(1)*V(6)+W(1)*W(6))
610 QQ=ABS(S2)
620 W=ATN(QQ/SQR(1-QQ*QQ))
630 C2=COS(W)
640 S1=U(2)*U(6)+V(2)*V(6)+W(2)*W(6)
650 S1=S1/C2
660 PP=ABS(S1)
670 W=ATN(PP/SQR(1-PP*PP))
680 C1=COS(W)
690 S3=U(1)*U(5)+V(1)*V(5)+W(1)*W(5)
700 S3=S3/C2
710 RR=ABS(S3)
720 W=ATN(RR/SQR(1-RR*RR))
730 C3=COS(W)
740 R1=S1*S2*C3-C1*S3
750 R2=C1*S2*C3+S1*S3
760 R3=S1*S2*S3+C1*C3
770 R4=C1*S2*S3-S1*C3
780 Q=C2*S3/(C2*C3-1)
790 K1=(R4-Q*R2)/(Q*R1-R3+1)
800 K2=-(R1*K1+R2)/(C2*C3-1)
810 P3=SQR(1/(K1^2+K2^2+1))
820 P2=K1*P3
830 P1=K2*P3
840 C=(C1*C2-P3^2)/(1-P3^2)
850 S=(-S2-P1*P3*(1-C))/P2
860 W=ATN(S/SQR(1-S*S))
870 G=(A(4)-A(1))*P1+(A(5)-A(2))*P2+(A(6)-A(3))*P3
880 E1=A(4)-A(1)-G*P1
890 E2=A(5)-A(2)-G*P2
900 E3=A(6)-A(3)-G*P3
910 E=SQR(E1^2+E2^2+E3^2)
920 F1=P2*E3-P3*E2
930 F2=-(P1*E3-P3*E1)
940 F3=P1*E2-P2*E1
950 F=SQR(F1^2+F2^2+F3^2)
960 F1=F1/F
970 F2=F2/F
980 F3=F3/F
990 Q1=A(1)+E1/2+E*F1/(2*TAN(W/2))
1000 Q2=A(2)+E2/2+E*F2/(2*TAN(W/2))
1010 Q3=A(3)+E3/2+E*F3/(2*TAN(W/2))
1020 Q4=A(1)+E1/2-E*F1/(2*TAN(W/2))
1030 Q5=A(2)+E2/2-E*F2/(2*TAN(W/2))
1040 Q6=A(3)+E3/2-E*F3/(2*TAN(W/2))
1050 T1=INT(Q1*100)/100
1060 T2=INT(Q2*100)/100
1070 T3=INT(Q3*100)/100
1080 T4=INT(Q4*100)/100
1090 T5=INT(Q5*100)/100
1100 T6=INT(Q6*100)/100
1110 PRINT
1120 PRINT  "Ortsvektor der Schraubenachse :"
1130 PRINT  "QX1="; T1, "QY1="; T2, "QZ1="; T3
1140 PRINT  "oder:"
1150 PRINT  "QX2="; T4, "QY2="; T5, "QZ2="; T6
1160 PRINT
1170 PRINT  "Einsvektor der Schraubenachse :";P1;"I + ";P2;"J +";P3;"K"
1180 PRINT
1190 PRINT  "Ganghöhe : ";G
1200 PRINT
1210 PRINT  "PHI= +/-"; ABS(W*180/3.141592); "Grad"
1220 PRINT
END
```

APPENDIX 5(3)

Determination of the helical axis of motion using Rodrigues' formula (Bisshopp,1969)

- Programme HELIROD.J -

Given (same as in Appendix 4(3)):

- The spatial position of three non-collinear points A, B and C on a rigid moving body at two instants, t_1 and t_2; that is, $A_{1(xyz)}$, $B_{1(xyz)}$, $C_{1(xyz)}$, and $A_{2(xyz)}$, $B_{2(xyz)}$, $C_{2(xyz)}$.

Required (same as in Appendix 4(3)):

- The direction and location of the helical axis
- The angular motion about this axis
- The translation along this axis

Solution:

- See Chapter 3, Section 3.3.2

Flow diagram of programme HELIROD.J:

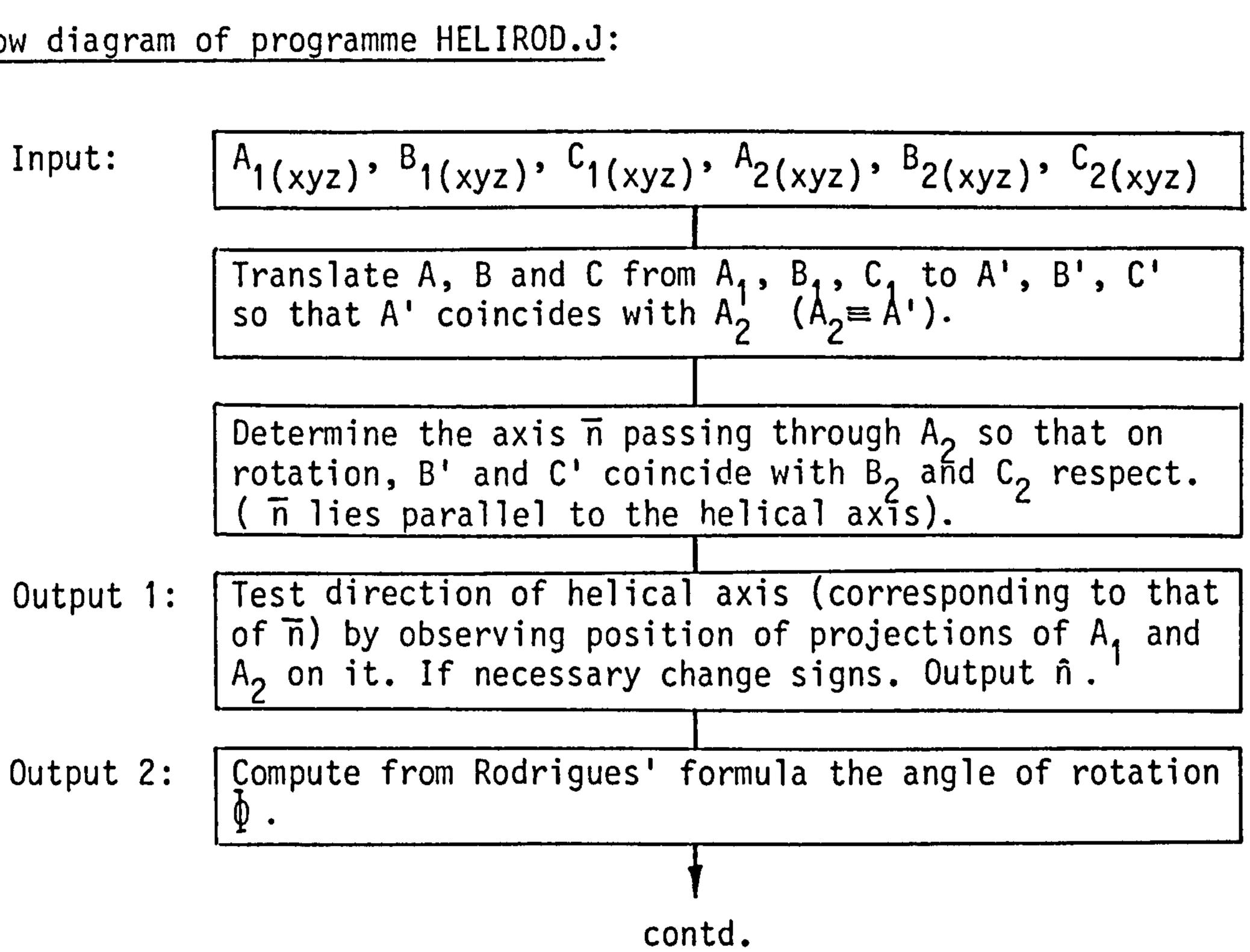

contd.

Output 3: Determine the amplitude of translation, $|g|$, required to move A parallel to $\bar{n}$, from A_1 to $\mathring{A}$, so that its projection on n coincides with A_2.

Output 4: The chord of purely rotary motion, after translation has been effected, is $\mathring{A}A_2$. The centre of rotation that satisfies the angle Φ and subtends the chord $\mathring{A}A_2$ is obtained. Test whether the center obtained is on the correct side of the chord. If not, re-do correctly. This locates the helical axis in xyz space.

END

Programme HELIROD.J Listing:

```
10 CLS
20 PRINT " PROGRAMM                          HELIROD.J2                    3.Nov.1988"
30 LPRINT "                                  HELIROD.J2"
40 REM  DAS PROGRAMM "HELIROD.J" BERECHNET AUFGRUND VON 2 KOORDINATENWEISE VOR-
        GEGEBENEN PUNKTETRIPPELN (A1, B1, C1) UND (A2, B2, C2): DIE SCHRAUBUNGS-
        ACHSE, DEN DREHWINKEL SOWIE DIE GANGHOEHE BEI DER BEWEGUNG AUS EINER
50 REM  AUSGANGSPOSITION 1 IN EINE ENDPOSITION 2.
60 REM  ACHTUNG !  Das Programm ist ungeeignet für den Fall wo die Schraubungs-
                   achse in der Ebene A1,B1,C1 bzw. A2,B2,C2 liegt.(Die Punkte
                   B und C dürfen sich nicht parallel bewegen ! Auch darf die
70 REM             Schraubungsachse nicht durch B und C gehen !).In einem solchen
                   Fall ist Programm "HELIMAT" zu benützen.
80 LPRINT :LPRINT
90 INPUT "AX1=";A1
100 INPUT "AY1=";A2
110 INPUT "AZ1=";A3
120 INPUT "BX1=";B1
130 INPUT "BY1=";B2
140 INPUT "BZ1=";B3
150 INPUT "CX1=";C1
160 INPUT "CY1=";C2
170 INPUT "CZ1=";C3
180 INPUT "AX2=";A4
190 INPUT "AY2=";A5
200 INPUT "AZ2=";A6
210 INPUT "BX2=";B4
220 INPUT "BY2=";B5
230 INPUT "BZ2=";B6
240 INPUT "CX2=";C4
250 INPUT "CY2=";C5
260 INPUT "CZ2=";C6
270 PRINT "AX1=";A1,"AY1=";A2,"AZ1=";A3
280 PRINT "BX1=";B1,"BY1=";B2,"BZ1=";B3
290 PRINT "CX1=";C1,"CY1=";C2,"CZ1=";C3
300 PRINT
310 PRINT "AX2=";A4,"AY2=";A5,"AZ2=";A6
320 PRINT "BX2=";B4,"BY2=";B5,"BZ2=";B6
330 PRINT "CX2=";C4,"CY2=";C5,"CZ2=";C6
340 PRINT
350 D1=A4-A1
360 D2=A5-A2
370 D3=A6-A3
380 A7=A4
390 A8=A5
400 A9=A6
410 B7=B1+D1
420 B8=B2+D2
430 B9=B3+D3
440 C7=C1+D1
450 C8=C2+D2
460 C9=C3+D3
```

```
470 R1=B4-A4
480 R2=B5-A5
490 R3=B6-A6
500 R4=B7-A7
510 R5=B8-A8
520 R6=B9-A9
530 SB1=B4-B7 : SB2=B5-B8 : SB3=B6-B9
540 SC1=C4-C7 : SC2=C5-C8 : SC3=C6-C9
550 NN1=SB2*SC3-SB3*SC2
560 NN2=-(SB1*SC3-SB3*SC1)
570 NN3=SB1*SC2-SB2*SC1
580 NN=SQR(NN1^2+NN2^2+NN3^2)
590 NN1=NN1/NN : NN2=NN2/NN : NN3=NN3/NN
600 AB=ABS(R1*NN1+R2*NN2+R3*NN3)
610 BB1=A4+AB*NN1 : BB2=A5+AB*NN2 : BB3=A6+AB*NN3
620 BB=SQR((B4-BB1)^2+(B5-BB2)^2+(B6-BB3)^2)
630 RR=SQR(R1^2+R2^2+R3^2)
640 IF (BB/RR)=<1 GOTO 660
650 NN1=-NN1 : NN2=-NN2 : NN3=-NN3
660 DD1=R1-R4 : DD2=R2-R5 : DD3=R3-R6
670 SS1=R1+R4 : SS2=R2+R5 : SS3=R3+R6
680 DN1=DD2*NN3-DD3*NN2
690 DN2=-(DD1*NN3-DD3*NN1)
700 DN3=DD1*NN2-DD2*NN1
710 DN=SQR(DN1^2+DN2^2+DN3^2)
720 SN1=SS2*NN3-SS3*NN2
730 SN2=-(SS1*NN3-SS3*NN1)
740 SN3=SS1*NN2-SS2*NN1
750 SN=SQR(SN1^2+SN2^2+SN3^2)
760 T=DN/SN  : PHI=2*ATN(T)
770 PRINT "PHI= +/-";PHI*180/3.141592;"Grad" : PRINT
780 PRINT "Einsvektor der Scraubungsachse :"
790 PRINT NN1 TAB(12)"*i +";TAB(20)NN2 TAB(32)"*j +";TAB(40)NN3 TAB(52)"*k"
800 G=NN1*D1+NN2*D2+NN3*D3
810 PRINT "Ganghöhe = ";G
820 A10 =A1+G*NN1 : B10 =B1+G*NN1
830 A11=A2+G*NN2  : B11 =B2+G*NN2
840 A12=A3+G*NN3  : B12 =B3+G*NN3
850 AA1=SQR(D1^2+D2^2+D3^2) :AA2=SQR((A4-A10)^2+(A5-A11)^2+(A6-A12)^2)
860 IF AA1/AA2=>1 GOTO 900
870 A10 =A1-G*NN1 : B10 =B1-G*NN1
880 A11=A2-G*NN2  : B11 =B2-G*NN2
890 A12=A3-G*NN3  : B12 =B3-G*NN3
900 S1=A4-A10 : S2=A5-A11 : S3=A6-A12 : U1=B4-B10 : U2=B5-B11 : U3=B6-B12
910 S=SQR(S1^2+S2^2+S3^2) : U=SQR(U1^2+U2^2+U3^2)
920 F1=NN2*S3-NN3*S2  : H1=NN2*U3-NN3*U2
930 F2=-(NN1*S3-NN3*S1) : H2=-(NN1*U3-NN3*U1)
940 F3=NN1*S2-NN2*S1 : H3=NN1*U2-NN2*U1
950 F=SQR(F1^2+F2^2+F3^2) : H=SQR(H1^2+H2^2+H3^2)
960 F1=F1/F : F2=F2/F : F3=F3/F :H1=H1/H : H2=H2/H : H3=H3/H
970 F1=F1*S*.5/T :F2=F2*S*.5/T :F3=F3*S*.5/T :H1=H1*U*.5/T :H2=H2*U*.5/T :H3=H3*
U*.5/T
980 P1=A10+.5*S1-F1 : P4=B10+.5*U1-H1 : P7=P4-P1
990 P2=A11+.5*S2-F2 : P5=B11+.5*U2-H2 : P8=P5-P2
1000 P3=A12+.5*S3-F3 : P6=B12+.5*U3-H3 : P9=P6-P3
1010 P=SQR(P7^2+P8^2+P9^2) :P7=P7/P :P8=P8/P :P9=P9/P
1020 IF (ABS(NN1)-ABS(P7))>.1 GOTO 1060
1030 IF (ABS(NN2)-ABS(P8))>.1 GOTO 1060
1040 IF (ABS(NN3)-ABS(P9))>.1 GOTO 1060
1050 GOTO 1070
1060 P1 =A10+.5*S1+F1 : P2 =A11+.5*S2+F2 : P3 =A12+.5*S3+F3
1070 PRINT "Ortsvektor der Schraubungsachse :"
1080 PRINT P1 TAB(12)"*i +";TAB(20)P2 TAB(32)"*j +";TAB(40)P3 TAB(52)"*k"
1090 ZZ=ZZ+1
1100 LPRINT :LPRINT "Variante ";ZZ;":":LPRINT
1110 LPRINT "AX1=";A1,"AY1=";A2,"AZ1=";A3
1120 LPRINT "BX1=";B1,"BY1=";B2,"BZ1=";B3
1130 LPRINT "CX1=";C1,"CY1=";C2,"CZ1=";C3
1140 LPRINT
1150 LPRINT "AX2=";A4,"AY2=";A5,"AZ2=";A6
1160 LPRINT "BX2=";B4,"BY2=";B5,"BZ2=";B6
1170 LPRINT "CX2=";C4,"CY2=";C5,"CZ2=";C6
1180 LPRINT
1190 LPRINT "PHI= +/-";PHI*180/3.141592;"Grad" : LPRINT
1200 LPRINT "Einsvektor der Schraubungsachse :"
1210 LPRINT NN1 TAB(12)"*i +";TAB(20)NN2 TAB(32)"*j +";TAB(40)NN3 TAB(52)"*k"
1220 LPRINT "Ganghöhe = ";G
1230 LPRINT "Ortsvektor der Schraubungsachse :"
     END
```

APPENDIX 6(3)

Determination of coordinates of a point in a distorted picture coordinate system *

- Programme DIGXY -

Given:

- The true u,v coordinates of four corner points of a known rectangular field (the rectangular field probably appears like a quadrilateral on the projection screen)*
- The x,y coordinates of the same corner points as read off a measuring device
- The x,y coordinates of any other points P1 --- Pn either within or immediately outside the known rectangular field, also read off the measuring device.

Required:

- The true u,v coordinates of the points P1 --- Pn on the picture.

Solution:

- See Chapter 3, Section 3.3.3 and figure 3.10.

* A special programme, DIGXY.FLM, that allows the u,v coordinates of a point to be determined from known u,v coordinates of the corner points of a distorted general quadrilateral, and not necessarily from a rectangle, is described in Appendix 1(5).

Flow diagram of programme DIGXY:

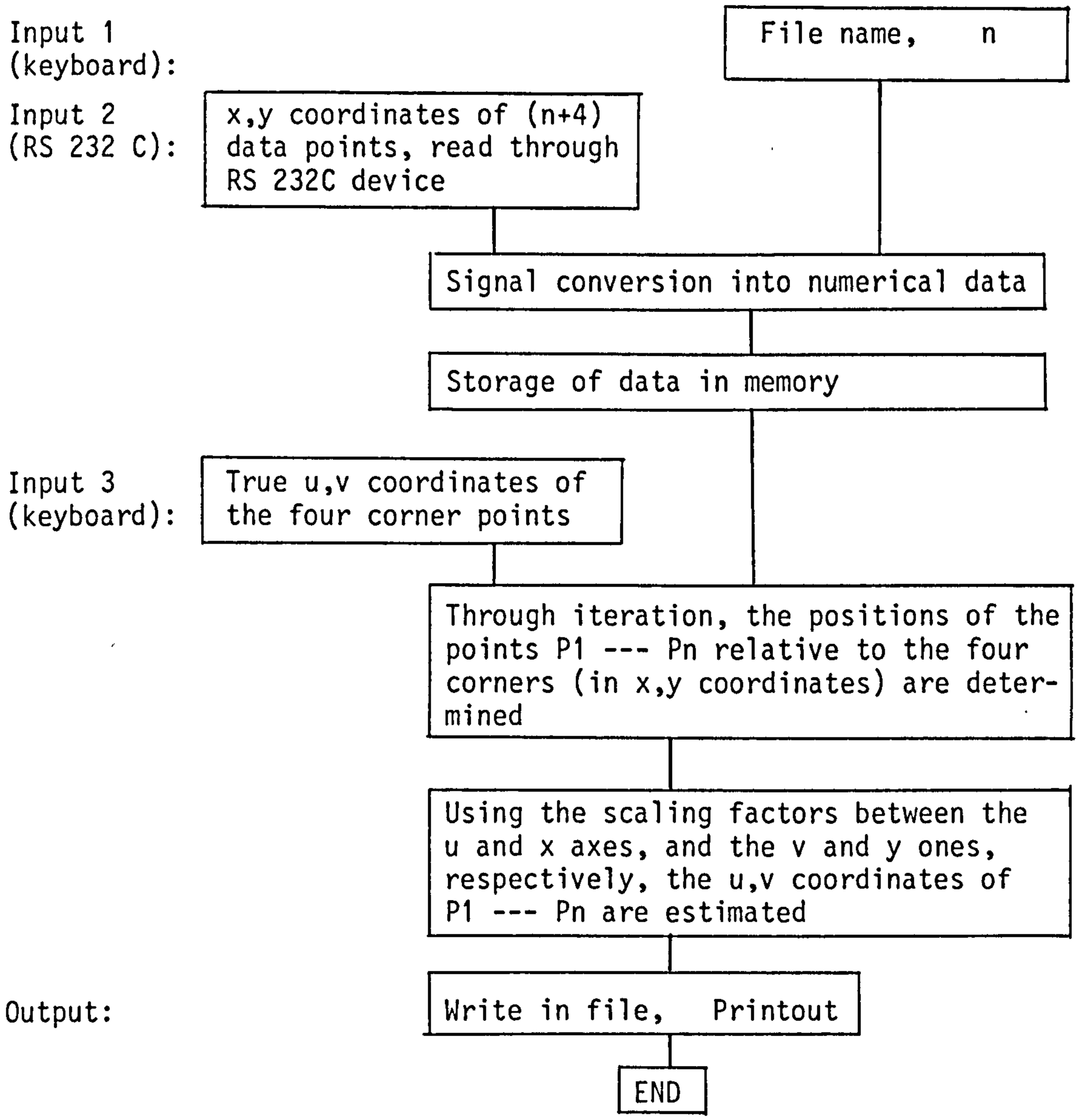

Programme DIGXY Listing:

```
10 PRINT "PROGRAMM:          D I G X Y                    17.6.1986"
20 LPRINT "PROGRAMM:          D I G X Y                  17.6.1986"
30 LPRINT "                   ---------"
33 BEEP
35 PRINT :BEEP :BEEP :PRINT "DATEI-DISKETTE IN DRIVE 'A' EINLEGEN  !":PRINT :PRI
NT
40 LPRINT
50 REM    Das auszuwertende Bild darf schiefstehende X-Y-Koordinaten aufweisen.
60 REM    Das Messfeld darf dementsprechend ein beliebiges Viereck darstellen.
70 REM    Vor Beantwortung der Fragen (Linien 1030-1060) mussten die Messwert-
          paare in folgender Reihenfolge eingelesen worden sein:
80 REM    1. die linke, untere Ecke des definierten Messfeldes (entsprechend
          "Messfeldursprung")
90 REM    2. die rechte, untere Ecke des defenierten Messfeldes (entsprechend
          "Ende des X-Bereiches")
100 REM    3. die rechte, obere Ecke des definierten Messfeldes (entsprechend
           "Ende des X-Y-Bereiches")
110 REM   4. die linke, obere Ecke des definierten Messfeldes (entsprechend "Ende
          des Y-Bereiches), und dann:
```

```
120 REM  5. die auszuwertende Markierungen innerhalb des Messfeldes in gewählter
         Reihenfolge.
130 REM   Zur Beginn müssen die Anzahl Messpunkte (auszuwertende Markierungen)
         die zu einem Messfeld gehören, angegeben werden.
140 INPUT "DATEIBEZEICHNUNG:";D$
150 INPUT "ANZAHL MARKIERUNGEN =";Z
160 DIM X(Z+4),Y(Z+4),PX(Z),PY(Z)
170 Q=0
180 ON ERROR GOTO 1010
190 FOR M=1 TO (Z+4) STEP 1
200 Q=Q+1
210 OPEN "com1:2400,e,7,2,cs,ds" AS#1
220 SOUND 1200,10
230 IF LOC(1)>26 GOTO 260
240 FOR T=1 TO 500 : NEXT T
250 GOTO 230
260 A$=INPUT$(LOC(1),#1): A$=MID$(A$,1,25)
270 CLOSE:PRINT (M-4),A$
280 X$=MID$(A$,3,10)
290 XS$=MID$(X$,1,1):XS=ASC(XS$)
300 XT$=MID$(X$,3,1):XT=ASC(XT$)
310 IF XT=32 GOTO 330
320 XT=(XT-48)*1000:GOTO 340
330 XT =0
340 XH$=MID$(X$,4,1):XH=ASC(XH$)
350 IF XH=32 GOTO 370
360 XH=(XH-48)*100:GOTO 380
370 XH=0
380 XZ$=MID$(X$,5,1):XZ=ASC(XZ$)
390 IF XZ=32 GOTO 410:XZ=(XZ-48)*10
400 XZ=(XZ-48)*10:GOTO 420
410 XZ=0
420 XE$=MID$(X$,6,1):XE=ASC(XE$)
430 IF XE=32 GOTO 450
440 XE=XE-48:GOTO 460
450 XE=0
460 X1$=MID$(X$,8,1):X1=ASC(X1$)
470 IF X1=32 GOTO 490
480 X1=(X1-48)/10:GOTO 500
490 X1=0
500 X2$=MID$(X$,9,1):X2=ASC(X2$)
510 IF X2=32 GOTO 530
520 X2=(X2-48)/100:GOTO 540
530 X2=0
540 X3$=MID$(X$,10,1):X3=ASC(X3$)
550 IF X3=32 GOTO 570
560 X3=(X3-48)/1000:GOTO 580
570 X3=0
580 X(Q)=XT+XH+XZ+XE+X1+X2+X3
590 IF XS=45 GOTO 620
600 IF XS=43 GOTO 630
610 SOUND 1200,40:PRINT "ERROR IN DATENUEBERTRAGUNG !!":STOP
620 X(Q)=-X(Q)
630 Y$=MID$(A$,15,10)
640 YS$=MID$(Y$,1,1):YS=ASC(YS$)
650 YT$=MID$(Y$,3,1):YT=ASC(YT$)
660 IF YT=32 GOTO 680
670 YT=(YT-48)*1000:GOTO 690
680 YT =0
690 YH$=MID$(Y$,4,1):YH=ASC(YH$)
700 IF YH=32 GOTO 720
710 YH=(YH-48)*100:GOTO 730
720 YH=0
730 YZ$=MID$(Y$,5,1):YZ=ASC(YZ$)
740 IF YZ=32 GOTO 760
750 YZ=(YZ-48)*10:GOTO 770
760 YZ=0
770 YE$=MID$(Y$,6,1):YE=ASC(YE$)
780 IF YE=32 GOTO 800
790 YE=YE-48:GOTO 810
800 YE=0
810 Y1$=MID$(Y$,8,1):Y1=ASC(Y1$)
820 IF Y1=32 GOTO 840
830 Y1=(Y1-48)/10:GOTO 850
840 Y1=0
850 Y2$=MID$(Y$,9,1):Y2=ASC(Y2$)
860 IF Y2=32 GOTO 880
870 Y2=(Y2-48)/100:GOTO 890
880 Y2=0
```

```
890 Y3$=MID$(Y$,10,1):Y3=ASC(Y3$)
900 IF Y3=32 GOTO 920
910 Y3=(Y3-48)/1000:GOTO 930
920 Y3=0
930 Y(0)=YT+YH+YZ+YE+Y1+Y2+Y3
940 IF ASC(YS$)=45 GOTO 970
950 IF ASC(YS$)=43 GOTO 980
960 SOUND 1200,40:PRINT "ERROR IN DATENUEBERTRAGUNG !!":STOP
970 Y(0)=-Y(0)
980 BEEP
990 NEXT M
1000 GOTO 1020
1010 IF ERR=57 THEN CLOSE:GOTO 210:RESUME
1020 CLS
1030 INPUT "X-Koordinate des Messfeldursprungs";A1
1040 INPUT "Y-Koordinate des Messfeldursprungs";A2
1050 INPUT "X-Koordinate des Messfeldendes";C1
1060 INPUT "Y-Koordinate des Messfeldendes";C2
1070 LPRINT "Dateibezeichnung: ";D$:LPRINT
1080 PRINT "Messfeldursprung: X0= ";A1,"Y0= ";A2
1090 LPRINT "Messfeldursprung: X0= ";A1,"Y0= ";A2
1100 PRINT "Messfeldende: X'= ";C1,"Y'= ";C2
1110 LPRINT "Messfeldende: X'= ";C1,"Y'= ";C2
1120 PRINT :PRINT
1130 LPRINT :LPRINT
1140 OPEN D$ FOR OUTPUT AS#1
1150 FOR N=5 TO (Z+4)
1160 AX=X(1):BX=X(2):CX=X(3):DX=X(4):PX=X(N)
1170 AY=Y(1):BY=Y(2):CY=Y(3):DY=Y(4):PY=Y(N)
1180 LX=PX:MX=AX:NX=DX:QX=AX:RX=BX:SX=AX
1190 LY=PY:MY=AY:NY=DY:QY=AY:RY=BY:SY=AY
1200 IF MX=NX GOTO 1230
1210 GOSUB 2320
1220 GOTO 1240
1230 FX=PX
1240 IF FX><AX GOTO 1270
1250 PX(N-4)=A1:PY(N-4)=A2+(C2-A2)*(PY-AY)/(DY-AY)
1260 GOTO 2230
1270 MX=BX:NX=CX
1280 MY=BY:NY=CY
1290 IF MX=NX GOTO 1320
1300 GOSUB 2320
1310 GOTO 1330
1320 FX=PX
1330 IF FX><BX GOTO 1360
1340 PX(N-4)=C1:PY(N-4)=A2+(C2-A2)*(PY-BY)/(CY-BY)
1350 GOTO 2230
1360 DPX=PX-DX:DPY=PY-DY
1370 M=SQR(DPX^2+DPY^2)
1380 DPX=DPX/M:DPY=DPY/M
1390 DCX=CX-DX:DCY=CY-DY
1400 M=SQR(DCX^2+DCY^2)
1410 DCX=DCX/M:DCY=DCY/M
1420 IF DCX><DPX GOTO 1460
1430 IF DCY><DPY GOTO 1460
1440 PX(N-4)=A1+(C1-A1)*(PX-DX)/(CX-DX)
1450 PY(N-4)=C2:GOTO 2230
1460 APX=PX-AX:APY=PY-AY
1470 M=SQR(APX^2+APY^2)
1480 APX=APX/M:APY=APY/M
1490 ABX=BX-AX:ABY=BY-AY
1500 M=SQR(ABX^2+ABY^2)
1510 ABX=ABX/M:ABY=ABY/M
1520 IF APX><ABX GOTO 1560
1530 IF APY><ABY GOTO 1560
1540 PX(N-4)=A1+(C1-A1)*(PX-AX)/(BX-AX)
1550 PY(N-4)=A2:GOTO 2230
1560 KTR=1
1570 EX=PX:EY=DY+(CY-DY)*(EX-DX)/(CX-DX)
1580 IF PY>=(AY+DY)/2 GOTO 2240
1590 FX=EX
1600 V1=(EX-DX)/(CX-DX):V2=(FX-AX)/(BX-AX)
1610 IF V1=V2 GOTO 2130
1620 IF V1>V2 GOTO 1710
1630 EX=EX+10:EY=DY+(CY-DY)*(EX-DX)/(CX-DX)
1640 LX=EX:MX=PX:NX=EX
1650 LY=EY:MY=PY:NY=EY :IF MX=NX GOTO 1630
1660 GOSUB 2320
```

```
1670 V1=(EX-DX)/(CX-DX):V2=(FX-AX)/(BX-AX)
1680 IF V1=V2 GOTO 2130
1690 IF V1>V2 GOTO 1790
1700 GOTO 1630
1710 EX=EX-10:EY=DY+(CY-DY)*(EX-DX)/(CX-DX)
1720 LX=EX:MX=PX:NX=EX
1730 LY=EY:MY=PY:NY=EY :IF MX=NX GOTO 1790
1740 GOSUB 2320
1750 V1=(EX-DX)/(CX-DX):V2=(FX-AX)/(BX-AX)
1760 IF V1=V2 GOTO 2130
1770 IF V1<V2 GOTO 1790
1780 GOTO 1710
1790 IF V1>V2 GOTO 1880
1800 EX=EX+1:EY=DY+(CY-DY)*(EX-DX)/(CX-DX)
1810 LX=EX:MX=PX:NX=EX
1820 LY=EY:MY=PY:NY=EY :IF MX=NX GOTO 1800
1830 GOSUB 2320
1840 V1=(EX-DX)/(CX-DX):V2=(FX-AX)/(BX-AX)
1850 IF V1=V2 GOTO 2130
1860 IF V1>V2 GOTO 1960
1870 GOTO 1800
1880 EX=EX-1:EY=DY+(CY-DY)*(EX-DX)/(CX-DX)
1890 LX=EX:MX=PX:NX=EX
1900 LY=EY:MY=PY:NY=EY :IF MX=NX GOTO 1960
1910 GOSUB 2320
1920 V1=(EX-DX)/(CX-DX):V2=(FX-AX)/(BX-AX)
1930 IF V1=V2 GOTO 2130
1940 IF V1<V2 GOTO 1960
1950 GOTO 1880
1960 IF V1>V2 GOTO 2050
1970 EX=EX+.1:EY=DY+(CY-DY)*(EX-DX)/(CX-DX)
1980 LX=EX:MX=PX:NX=EX
1990 LY=EY:MY=PY:NY=EY :IF MX=NX GOTO 1970
2000 GOSUB 2320
2010 V1=(EX-DX)/(CX-DX):V2=(FX-AX)/(BX-AX)
2020 IF V1=V2 GOTO 2130
2030 IF V1>V2 GOTO 2130
2040 GOTO 1970
2050 EX=EX-.1:EY=DY+(CY-DY)*(EX-DX)/(CX-DX)
2060 LX=EX:MX=PX:NX=EX
2070 LY=EY:MY=PY:NY=EY :IF MX=NX GOTO 2130
2080 GOSUB 2320
2090 V1=(EX-DX)/(CX-DX):V2=(FX-AX)/(BX-AX)
2100 IF V1=V2 GOTO 2130
2110 IF V1<V2 GOTO 2130
2120 GOTO 2050
2130 IF KTR =2 GOTO 2220
2140 PX(N-4)=A1+(C1-A1)*(FX-AX)/(BX-AX)
2150 AX=Y(1):BX=Y(4):CX=Y(3):DX=Y(2)
2160 AY=X(1):BY=X(4):CY=X(3):DY=X(2)
2170 SWAP PX,PY
2180 LX=PX:MX=AX:NX=DX:QX=AX:RX=BX:SX=AX
2190 LY=PY:MY=AY:NY=DY:QY=AY:RY=BY:SY=AY
2200 KTR=2
2210 GOTO 1570
2220 PY(N-4)=A2+(C2-A2)*(FX-AX)/(BX-AX)
2230 GOTO 2360
2240 SWAP AX,DX
2250 SWAP AY,DY
2260 SWAP BX,CX
2270 SWAP BY,CY
2280 LX=PX:MX=AX:NX=DX:QX=AX:RX=BX:SX=AX
2290 LY=PY:MY=AY:NY=DY:QY=AY:RY=BY:SY=AY
2300 EX=PX
2310 GOTO 1590
2320 H=(MY-NY)/(MX-NX)
2330 V=(H*(LX-QX)+QY-LY)/(H*(RX-SX)-(RY-SY))
2340 FX=QX+V*(RX-SX)
2350 RETURN
2360 PRINT TAB(15)"Px(";N-4;")=";:PRINT USING "#####.##";PX(N-4),
2370 LPRINT TAB(15)"Px(";N-4;")=";:LPRINT USING "#####.##";PX(N-4),
2380 PRINT TAB(45)"Py(";N-4;")=";:PRINT USING "#####.##";PY(N-4)
2390 LPRINT TAB(45)"Py(";N-4;")=";:LPRINT USING "#####.##";PY(N-4)
2400 WRITE #1,PX(N-4),PY(N-4)
2410 NEXT N
```

APPENDIX 7(3)

Determination of the point closest to two given skew lines in space

- Programme WNSCHF -

Given:

- Two non-parallel rays in space, each described by two points through which the corresponding ray passes ($A_{1(xyz)}$, $A_{2(xyz)}$ and $B_{1(xyz)}$, $B_{2(xyz)}$)

Required:

- The point $Q_{(xyz)}$ that is closest to both the rays (or, the mid-point along the shortest distance between the rays)

Solution:

- See Chapter 3, Section 3.3.4.1

Flow diagram of programme WNSCHF:

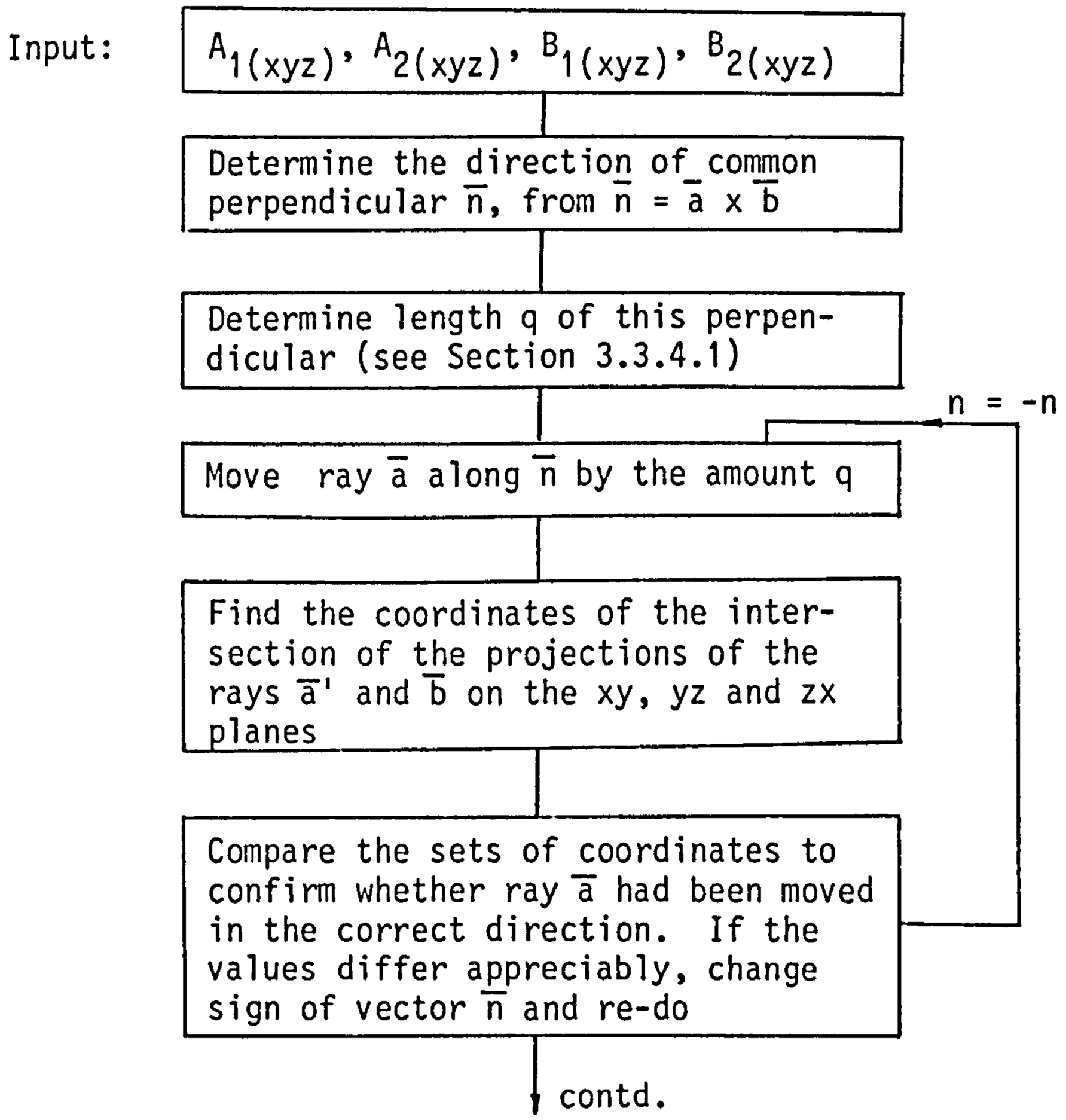

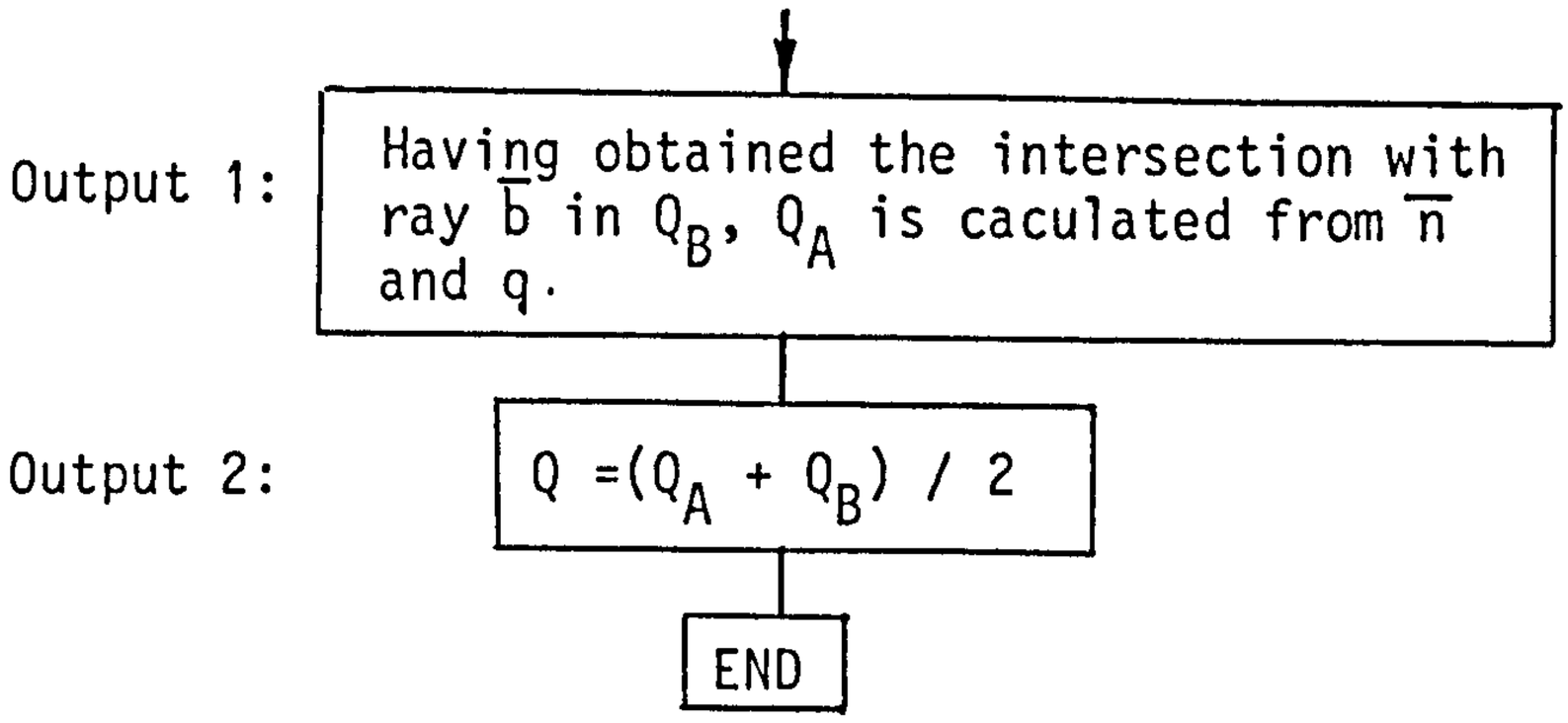

Programme WNSCHF Listing:

```
10 REM          Programm 'WNSCHF' (verbessert am 13.1.1986)
20 CLS
25 LPRINT "                    Programm WNSCHF:"
30 LPRINT "Bestimmung der kürzeste Verbindung zwischen 2 windschiefen Strahlen"
50 LPRINT "-------------------------------------------------------"
60 REM Die Strahlen A und B sind je durch 2 Punkte bezeichnet
70 REM Die kürzeste Verbindungsstrecke ist durch QA und QB gegeben
80 REM Die Mitte der Verbindungsstrecke ist Q
90 INPUT "A1(X)=";P1
100 INPUT "A1(Y)=";P2
110 INPUT  "A1(Z)=";P3
120 INPUT  "A2(X)=";A1
130 INPUT  "A2(Y)=";A2
140 INPUT  "A2(Z)=";A3
150 INPUT  "B1(X)=";R1
160 INPUT  "B1(Y)=";R2
170 INPUT  "B1(Z)=";R3
180 INPUT  "B2(X)=";B1
190 INPUT  "B2(Y)=";B2
200 INPUT  "B2(Z)=";B3
210 CLS
220 PRINT "A1(X)= ";P1 TAB(30)"A1(Y)= ";P2 TAB(60)"A1(Z)= ";P3
230  LPRINT    "A1(X)= ";P1 TAB(30)"A1(Y)= ";P2 TAB(60)"A1(Z)= ";P3
240 PRINT "A2(X)= ";A1 TAB(30)"A2(Y)= ";A2 TAB(60)"A2(Z)= ";A3
250 LPRINT "A2(X)= ";A1 TAB(30)"A2(Y)= ";A2 TAB(60)"A2(Z)= ";A3
260 PRINT
270 LPRINT
280 PRINT"B1(X)= ";R1 TAB(30)"B1(Y)= ";R2 TAB(60)"B1(Z)= ";R3
290 LPRINT"B1(X)= ";R1 TAB(30)"B1(Y)= ";R2 TAB(60)"B1(Z)= ";R3
300 PRINT"B2(X)= ";B1 TAB(30)"B2(Y)= ";B2 TAB(60)"B2(Z)= ";B3
310 LPRINT"B2(X)= ";B1 TAB(30)"B2(Y)= ";B2 TAB(60)"B2(Z)= ";B3
320 IF P1<>A1 THEN 360
330 IF A1<>R1 THEN 360
340 IF R1<>B1 THEN 360
350 GOTO 440
360 IF P2<>A2 THEN 400
370 IF A2<>R2 THEN 400
380 IF R2<>B2 THEN 400
390 GOTO 440
400 IF P3<>A3 THEN 460
410 IF A3<>A3 THEN 460
420 IF R3<>B3 THEN 460
430 GOTO 440
440 PRINT :BEEP:PRINT "     PROGRAMM  ' SCHNITT.PKT ' verwenden
450 GOTO 1430
460 LPRINT
470 PRINT
480 A1=A1-P1
490 A2=A2-P2
500 A3=A3-P3
510 A=SQR(A1^2+A2^2+A3^2)
520 A1=A1/A
530 A2=A2/A
540 A3=A3/A
```

```
550 B1=B1-R1
560 B2=B2-R2
570 B3=B3-R3
580 B=SQR(B1^2+B2^2+B3^2)
590 B1=B1/B
600 B2=B2/B
610 B3=B3/B
620 C1=A2*B3-A3*B2
630 C2=-A1*B3+A3*B1
640 C3=A1*B2-A2*B1
650 C=SQR(C1^2+C2^2+C3^2)
660 C4=C1/C
670 C5=C2/C
680 C6=C3/C
690 Q=ABS(((R1-P1)*C1+(R2-P2)*C2+(R3-P3)*C3)/C)
700 Z=.1
710 N=1
720 K1=P1+C4*Q
730 K2=P2+C5*Q
740 K3=P3+C6*Q
750 IF A1=0 THEN GOTO 810
760 E=A2/A1
770 B=(K2-R2+E*(R1-K1))/(B2-B1*E)
780 Q1=R1+B*B1
790 Q2=R2+B*B2
800 GOTO 830
810  Q1=K1
820 Q2=R2+B2*(K1-R1)/B1
830 IF A2=0 THEN GOTO 890
840 E=A3/A2
850 B=(K3-R3+E*(R2-K2))/(B3-B2*E)
860 Q3=R2+B*B2
870 Q4=R3+B*B3
880 GOTO 910
890 Q3=K2
900 Q4=R3+B3*(K2-R2)/B2
910 IF A3=0 THEN GOTO 970
920 E=A1/A3
930 B=(K1-R1+E*(R3-K3))/(B1-B3*E)
940 Q5=R3+B*B3
950 Q6=R1+B*B1
960 GOTO  990
970 Q5=K3
980 Q6= R1+B1*(K3-R3)/B3
990 IF ABS(Q1-Q6)>Z THEN GOTO 1030
1000 IF ABS(Q2-Q3)>Z THEN GOTO 1030
1010 IF ABS(Q4-Q5)>Z THEN GOTO 1030
1020 GOTO  1110
1030 IF N=-1 THEN GOTO 1090
1040 K1=P1-C4*Q
1050 K2=P2-C5*Q
1060 K3=P3-C6*Q
1070 N=-1
1080 GOTO  750
1090 Z=Z+.1
1100 GOTO  710
1110 Q1=(Q1+Q6)/2
1120    Q2=(Q2+Q3)/2
1130 Q3=(Q4+Q5)/2
1140 Q4=Q1-K1+P1
1150 Q5=Q2-K2+P2
1160 Q6=Q3-K3+P3
1170 Q7=(Q1+Q4)/2
1180 Q8=(Q2+Q5)/2
1190 Q9=(Q3+Q6)/2
1200 PRINT
1210 LPRINT
1220 Q1=INT(Q1*100)/100
1230 Q2=INT(Q2*100)/100
1240 Q3=INT(Q3*100)/100
1250 Q4=INT(Q4*100)/100
1260 Q5=INT(Q5*100)/100
1270 Q6=INT(Q6*100)/100
```

```
1280 PRINT "QA(X)= ";Q4 TAB(30)"QA(Y)= ";Q5 TAB(60)"QA(Z)= ";Q6
1290 LPRINT "QA(X)= ";Q4 TAB(30)"QA(Y)= ";Q5 TAB(60)"QA(Z)= ";Q6
1300 PRINT"QB(X)= ";Q1 TAB(30)"QB(Y)= ";Q2 TAB(60)"QB(Z)= ";Q3
1310 LPRINT"QB(X)= ";Q1 TAB(30)"QB(Y)= ";Q2 TAB(60)"QB(Z)= ";Q3
1320 PRINT "Abweichung Z < ";Z
1330 LPRINT "Abweichung Z < ";Z
1340 Q7=INT(Q7*100)/100
1350 Q8=INT(Q8*100)/100
1360 Q9=INT(Q9*100)/100
1370  PRINT "Q(X)= ";Q7 TAB(30)"Q(Y)= ";Q8 TAB(60)"Q(Z)= ";Q9
1380 LPRINT "Q(X)= ";Q7 TAB(30)"Q(Y)= ";Q8 TAB(60)"Q(Z)= ";Q9
1390 PRINT
1400 LPRINT
1410 LPRINT "_____________________________________________________________"
1420 LPRINT
1430 END
```

APPENDIX 8(3)

Transformation of Cartesian coordinates from a system xyz to system uvw

- Programme TRAN-XYZ.UVW -

Given:

- A point P_{xyz} in system xyz
- A second coordinate system uvw determined by a triplet of non-collinear points A, B and C. Point A is the origin of the system. uvw. $\overline{AB}$ coincides with the u axis. C is contained in the uv plane. $\overline{w} = \overline{AB} \times \overline{AC}$. A_{xyz}, B_{xyz} and C_{xyz} are known.

Required:

- P_{uvw} [NB: In transforming a vector p_{xyz}, the uvw coordinates of the xyz system must be considered !]

Solution:

- The directional cosines of the u, v and w axes are found in the xyz system. Then:

$$\begin{bmatrix} P_u \\ P_v \\ P_w \end{bmatrix} = \begin{bmatrix} \hat{u}_x & \hat{u}_y & \hat{u}_z \\ \hat{v}_x & \hat{v}_y & \hat{v}_z \\ \hat{w}_x & \hat{w}_y & \hat{w}_z \end{bmatrix} \cdot \begin{bmatrix} P_x - A_x \\ P_y - A_y \\ P_z - A_z \end{bmatrix} \qquad \text{--- I}$$

Flow diagram of programme TRAN-XYZ.UVW:

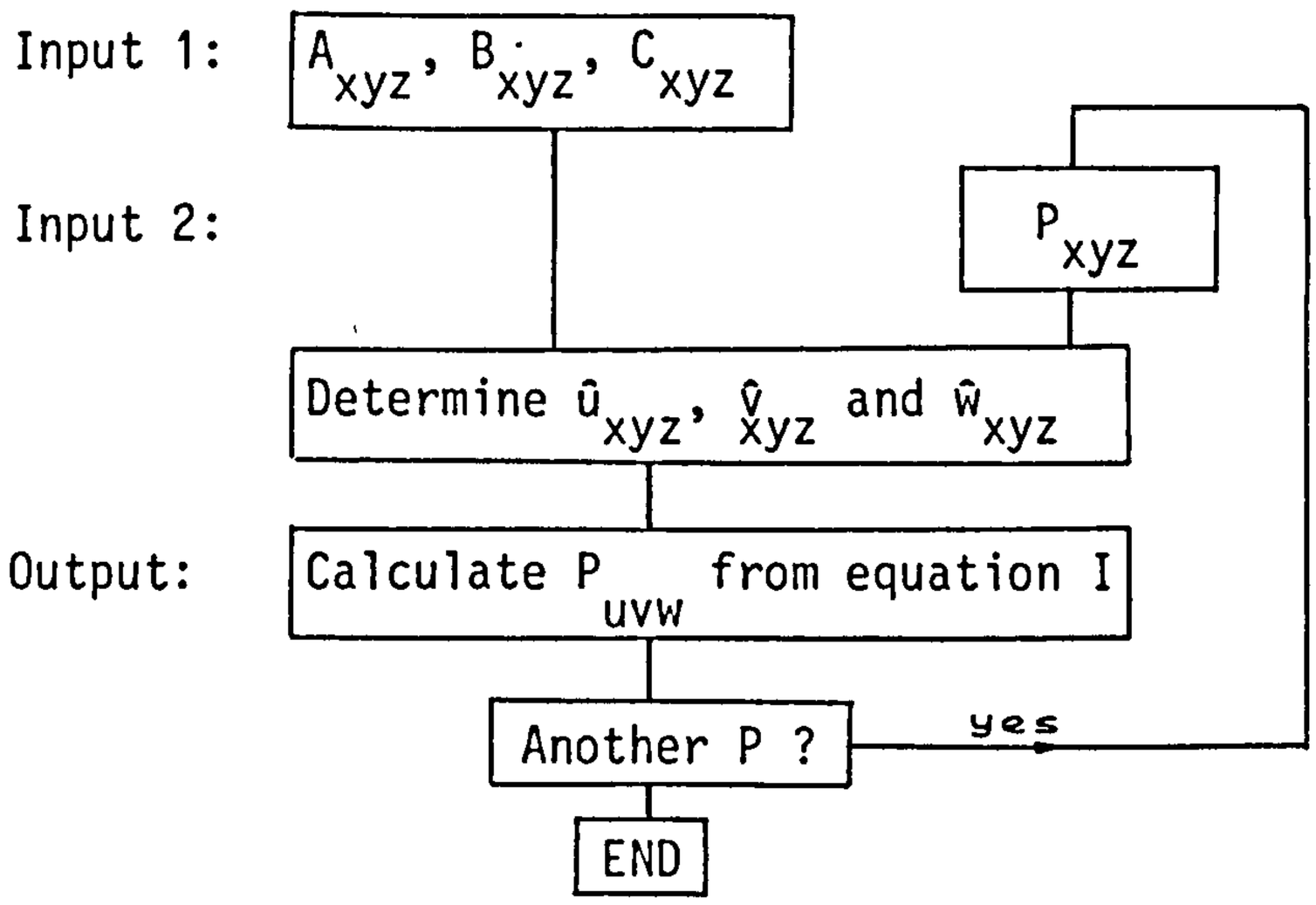

Programme TRAN-XYZ.UVW Listing:

```
10 REM    Das Programm TRAN-XYZ.UVW berechnet die Transformation der Koordina-
20 REM   ten eines im XYZ-System angegebenen Punktes in die einem aus 3 Punkten
30 REM   A,B,C, bestimmten Koordinatensystem UVW zugeordneten Koordinaten.
40 REM   Das erwähnte Koordinatensystem wird dabei wie folgt aus den einzelnen
50 REM   Punkten A,B,C, berechnet:
60 REM    Der Punkt A ist der Ursprung des neuen Koordinatensystems, der Vektor
70 REM   von A nach B bestimmt die Richtung der U-Achse. Der Vektor von A nach
80 REM   C zusammen mit dem Vektor AB bilden die U-V-Ebene. Damit sind die
90 REM   Richtungen der V- und W-Achsen des rechtwinkligen Koordinatensystems
100 REM   bestimmt. Die Längeneinheiten des XYZ-Systems werden ins UVW-System
110 REM   übernommen.
120 LPRINT "          PROGRAMM:      TRAN-XYZ.UVW"
130 LPRINT
140 LPRINT "       Transformation der Koordinaten eines Punktes P von einem"
150 LPRINT "                  System XYZ in einem System UVW."
160 LPRINT "                 ------------------------------------"
170 PRINT "AX= ";
180 INPUT AX
190 PRINT "AY= ";
200 INPUT AY
210 PRINT "AZ= ";
220 INPUT AZ
230 PRINT "BX= ";
240 INPUT BX
250 PRINT "BY= ";
260 INPUT BY
270 PRINT "BZ= ";
280 INPUT BZ
290 PRINT "CX= ";
300 INPUT CX
310 PRINT "CY= ";
320 INPUT CY
330 PRINT "CZ= ";
340 INPUT CZ
350 PRINT
360 PRINT
370 LPRINT
380 LPRINT "AX= ";AX TAB(30) "AY= ";AY TAB(60) "AZ= ";AZ
390 LPRINT "BX= ";BX TAB(30) "BY= ";BY TAB(60) "BZ= ";BZ
400 LPRINT "CX= ";CX TAB(30) "CY= ";CY TAB(60) "CZ= ";CZ
410 LPRINT
420 LPRINT
430 Z=1
440 PRINT "P";Z;"X= ";
450 INPUT PX
460 PRINT "P";Z;"Y= ";
470 INPUT PY
480 PRINT "P";Z;"Z= ";
490 INPUT PZ
500 PRINT
510 LPRINT "P";Z;"X= ";PX TAB(30) "P";Z;"Y= ";PY TAB(60) "P";Z;"Z= ";PZ
520 UX#=BX-AX
530 UY#=BY-AY
540 UZ#=BZ-AZ
550 U#=SQR(UX#^2+UY#^2+UZ#^2)
560 UX#=UX#/U#
570 UY#=UY#/U#
580 UZ#=UZ#/U#
590 CX#=CX-AX
600 CY#=CY-AY
610 CZ#=CZ-AZ
620 C#=SQR(CX#^2+CY#^2+CZ#^2)
630 CX#=CX#/C#
640 CY#=CY#/C#
650 CZ#=CZ#/C#
660 WX#=UY#*CZ#-UZ#*CY#
670 WY#=-UX#*CZ#+UZ#*CX#
680 WZ#=UX#*CY#-UY#*CX#
```

```
690 W#=SQR(WX#^2+WY#^2+WZ#^2)
700 WX#=WX#/W#
710 WY#=WY#/W#
720 WZ#=WZ#/W#
730 VX#=WY#*UZ#-WZ#*UY#
740 VY#=-WX#*UZ#+WZ#*UX#
750 VZ#=WX#*UY#-WY#*UX#
760 V#=SQR(VX#^2+VY#^2+VZ#^2)
770 VX#=VX#/V#
780 VY#=VY#/V#
790 VZ#=VZ#/V#
800 PXX#=PX-AX
810 PYY#=PY-AY
820 PZZ#=PZ-AZ
830 PU=PXX#*UX#+PYY#*UY#+PZZ#*UZ#
840 PV=PXX#*VX#+PYY#*VY#+PZZ#*VZ#
850 PW=PXX#*WX#+PYY#*WY#+PZZ#*WZ#
860 PRINT "P";Z;"U= ";PU TAB(30) "P";Z;"V= ";PV TAB(60) "P";Z;"W= ";PW
870 LPRINT "P";Z;"U= ";PU TAB(30) "P";Z;"V= ";PV TAB(60) "P";Z;"W= ";PW
880 LPRINT
890 BEEP
900 INPUT "Noch ein P? ja(1)/nein(0)";Q
910 IF Q=0 THEN GOTO 960
920 IF Q=1 THEN GOTO 940
930 GOTO 900
940 Z=Z+1
950 GOTO 440
960 END
```

APPENDIX 9(3)

Transformation of Cartesian coordinates from system uvw to system xyz

- Programme TRAN-UVW.XYZ -

Given:

- A point P_{uvw} in system uvw. (The sub-system uvw is defined through a triplet of non-collinear points A, B and C. Point A is the origin of the system uvw. C is contained in the uv plane. $\overline{w} = \overline{AB} \times \overline{AC}$. A_{xyz}, B_{xyz} and C_{xyz} are known.

Required:

- P_{xyz} [NB: in transforming a vector p_{uvw}, the coordinates of the origin A_{xyz} must also be considered !]

Solution:

- The directional cosines of the u, v and w axes are found in the xyz system. Then:

$$\begin{bmatrix} P_x \\ P_y \\ P_z \end{bmatrix} = \begin{bmatrix} \hat{u}_x & \hat{v}_x & \hat{w}_x \\ \hat{u}_y & \hat{v}_y & \hat{w}_y \\ \hat{u}_z & \hat{v}_z & \hat{w}_z \end{bmatrix} \cdot \begin{bmatrix} P_u + A_x \\ P_v + A_y \\ P_w + A_z \end{bmatrix} \qquad \text{----- I}$$

Flow diagram of programme TRAN-UVW.XYZ:

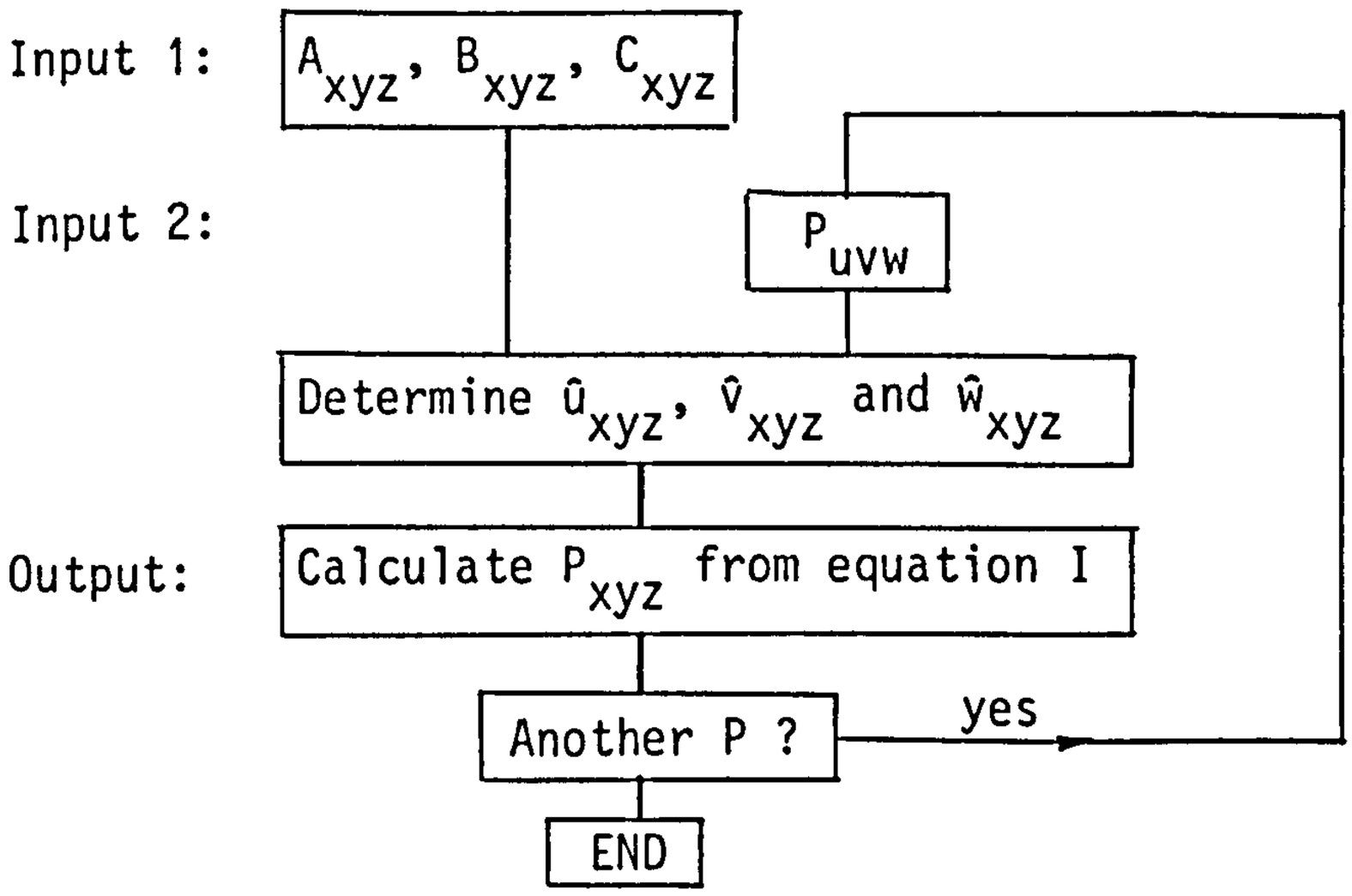

Programme TRAN-UVW.XYZ Listing:

```
10 REM    Das Programm TRAN-UVW.XYZ berechnet die Transformation der Koordina-
20 REM   ten eines im UVW-System angegebenen Punktes in Koordinaten eines
30 REM   XYZ-Systems. Die Lage des UVW-Systems relativ zum XYZ-System ist
40 REM   durch 3 bezügliche Referenzpunkte des UVW-Systems gegeben.
50 REM   Die XYZ-Koordinaten der Punkte A,B,C sind bekannt. Das erwähnte
60 REM   koordinatensystem wird dabei wie folgt aus den einzelnen Punkten
70 REM   A,B,C erkannt:
80 REM    Der Punkt A ist der Ursprung des neuen Koordinatensystems, der Vektor
90 REM   von A nach B bestimmt die Richtung der U-Achse. Der Vektor von A nach
100 REM   C zusammen mit dem Vektor AB bilden die U-V-Ebene. Damit sind die
110 REM   Richtungen der V- und W-Achsen des rechtwinkligen Koordinatensystems
120 REM   bestimmt. Die Längeneinheiten des XYZ-Systems und die des UVW-Systems
130 REM   sind dieselben.
140 LPRINT "              PROGRAMM:   TRAN-UVW.XYZ"
150 LPRINT
160 LPRINT "      Transformation der Koordinaten eines Punktes P von einem"
170 LPRINT "                 System UVW in einem System XYZ."
180 LPRINT "                 ------------------------------"
190 PRINT "AX= ";
200 INPUT AX
210 PRINT "AY= ";
220 INPUT AY
230 PRINT "AZ= ";
240 INPUT AZ
250 PRINT "BX= ";
260 INPUT BX
270 PRINT "BY= ";
280 INPUT BY
290 PRINT "BZ= ";
300 INPUT BZ
310 PRINT "CX= ";
320 INPUT CX
330 PRINT "CY= ";
340 INPUT CY
350 PRINT "CZ= ";
360 INPUT CZ
370 PRINT
380 PRINT
390 LPRINT
400 LPRINT "AX= ";AX TAB(30) "AY= ";AY TAB(60) "AZ= ";AZ
410 LPRINT "BX= ";BX TAB(30) "BY= ";BY TAB(60) "BZ= ";BZ
420 LPRINT "CX= ";CX TAB(30) "CY= ";CY TAB(60) "CZ= ";CZ
430 LPRINT
440 LPRINT
450 Z=1
460 PRINT "P";Z;"U= ";
470 INPUT PU
480 PRINT "P";Z;"V= ";
490 INPUT PV
500 PRINT "P";Z;"W= ";
510 INPUT PW
520 PRINT
530 LPRINT "P";Z;"U= ";PU TAB(30) "P";Z;"V= ";PV TAB(60) "P";Z;"W= ";PW
540 UX#=BX-AX
550 UY#=BY-AY
560 UZ#=BZ-AZ
570 U#=SQR(UX#^2+UY#^2+UZ#^2)
580 UX#=UX#/U#
590 UY#=UY#/U#
600 UZ#=UZ#/U#
610 CX#=CX-AX
620 CY#=CY-AY
630 CZ#=CZ-AZ
640 C#=SQR(CX#^2+CY#^2+CZ#^2)
650 CX#=CX#/C#
660 CY#=CY#/C#
670 CZ#=CZ#/C#
680 WX#=UY#*CZ#-UZ#*CY#
690 WY#=-UX#*CZ#+UZ#*CX#
700 WZ#=UX#*CY#-UY#*CX#
710 W#=SQR(WX#^2+WY#^2+WZ#^2)
720 WX#=WX#/W#
730 WY#=WY#/W#
740 WZ#=WZ#/W#
```

```
750 VX#=WY#*UZ#-WZ#*UY#
760 VY#=-WX#*UZ#+WZ#*UX#
770 VZ#=WX#*UY#-WY#*UX#
780 V#=SQR(VX#^2+VY#^2+VZ#^2)
790 VX#=VX#/V#
800 VY#=VY#/V#
810 VZ#=VZ#/V#
820 PXX=PU*UX#+PV*VX#+PW*WX#
830 PYY=PU*UY#+PV*VY#+PW*WY#
840 PZZ=PU*UZ#+PV*VZ#+PW*WZ#
850 PX=PXX+AX
860 PY=PYY+AY
870 PZ=PZZ+AZ
880 PRINT "P";Z;"X= ";PX TAB(30) "P";Z;"Y= ";PY TAB(60) "P";Z;"Z= ";PZ
890 LPRINT "P";Z;"X= ";PX TAB(30) "P";Z;"Y= ";PY TAB(60) "P";Z;"Z= ";PZ
900 LPRINT
910 BEEP
920 INPUT "Noch ein P? ja(1)/nein(0)";Q
930 IF Q=0 THEN GOTO 980
940 IF Q=1 THEN GOTO 960
950 GOTO 920
960 Z=Z+1
970 GOTO 460
980 END
```

APPENDIX 1(4)

Details of procedure involved in determining the topography of the cuneiform-metatarsal joint surfaces (Specimen No.2)

(N.B.: All linear dimensions in the following presentation are in mm)

1. The photographic set-up:

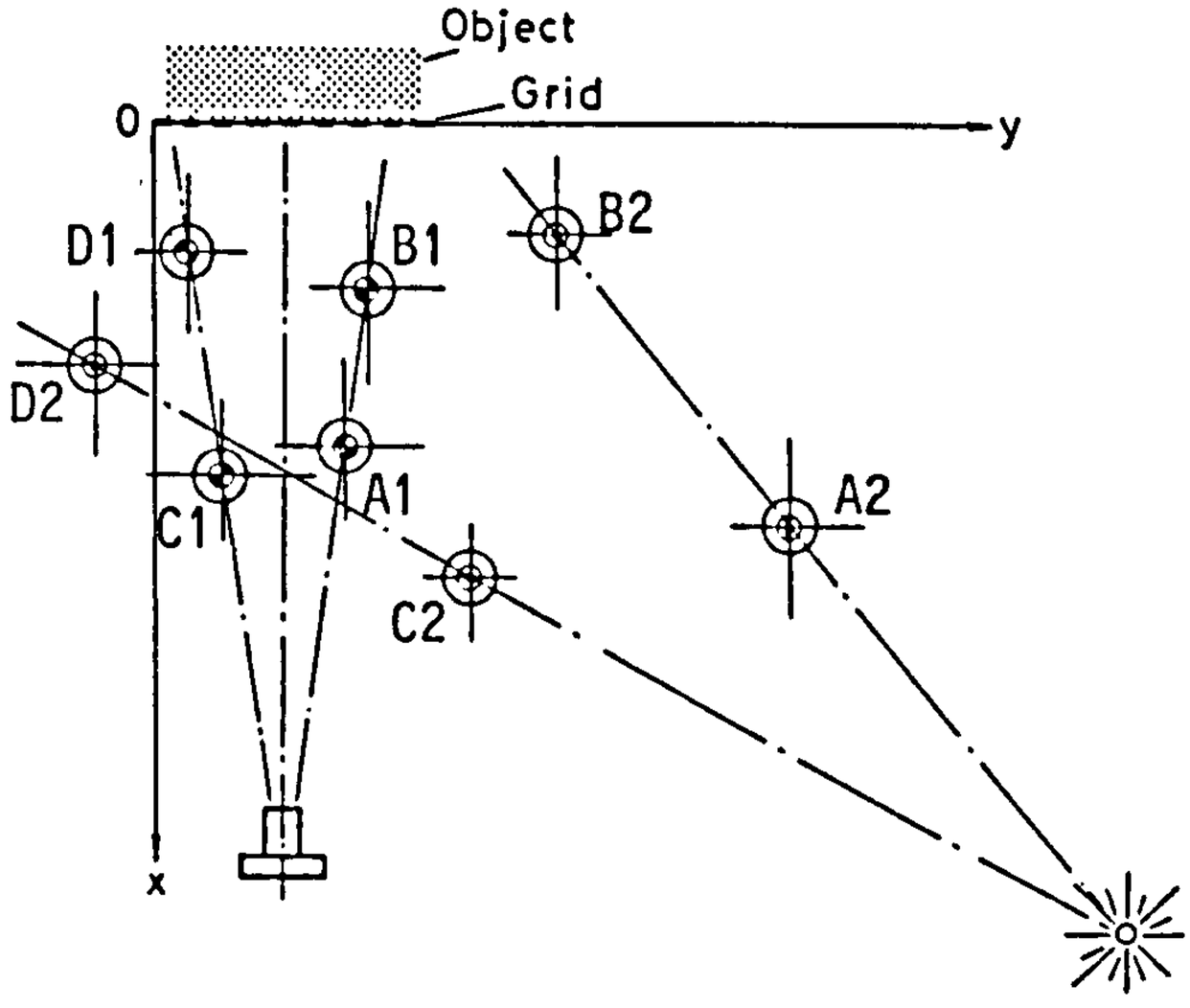

a) Calibration procedure for determining the xy coordinates of camera and light source

1.1 Calibration (see CHapter 3, Section 3.2.2):

	Test 1		Test 2	
	x	y	x	y
A1	350	130	350	120
B1	100	142.5	100	129.5
C1	350	60	350	75
D1	100	50.5	100	71
A2	350	450	500	450
B2	100	274.5	100	143.5
C2	500	60	500	0
D2	220	-222	240	-272

Camera

Light source

Using programme SCHNITT.PKT (Appendix 2(3)), the position of the

camera was found to be:

x = 1145.5 y = 90.2 (test 1)
or x = 1183.3 y = 88.3 (test 2)

Similarly, the position of the light source was found to be:

x = 2123.1 y = 1694.7 (test 1)
or x = 2107.7 y = 1681.9 (test 2)

The results obtained from each of the two tests confirm each other within reasonable limits and from a practical point of view any of the sets of results may be used. Therefore, considering the pair of rays with a maximum deviation (smallest error) the following values were decided upon:

Camera: x = 1145 y = 90 (test 1)

Light source: x = 2113 y = 1688 (A2,B2 of test 1 with C2,D2 of test 2)

[See foot note * at end of appendix].

1.2 Position of object in measuring system:

The object was brought close to the optical grid with the whole surface to be mapped so tilted that a sufficiently large number of fringes appeared. Surface contours later mapped are always contained in planes normal to the plane of the grid ! Therefore, due care was taken in positioning the object correspondingly.

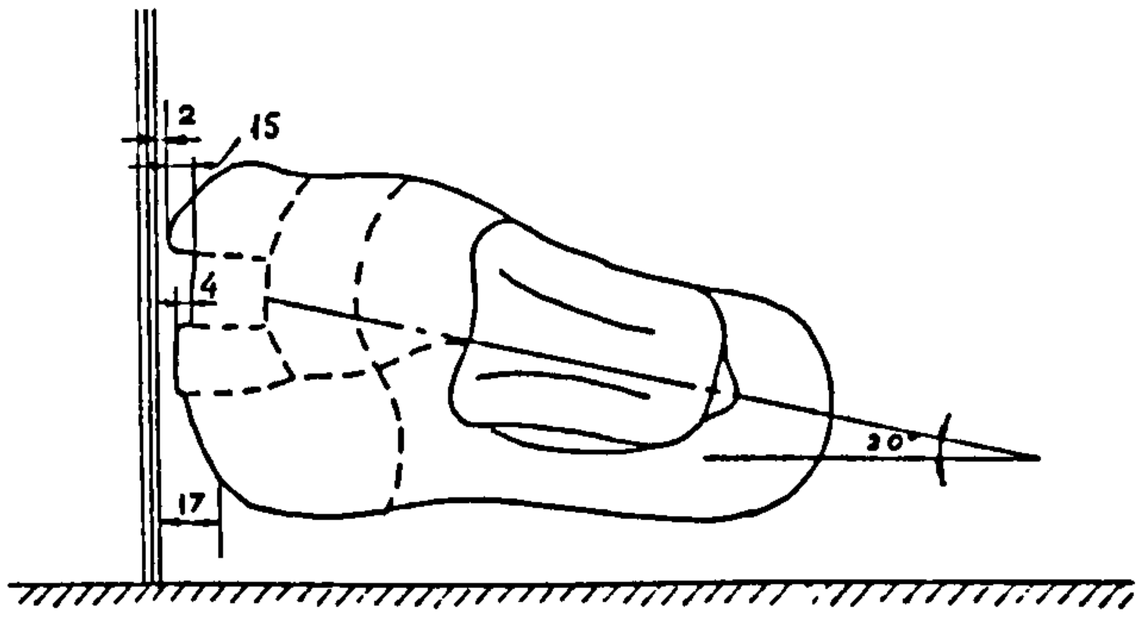

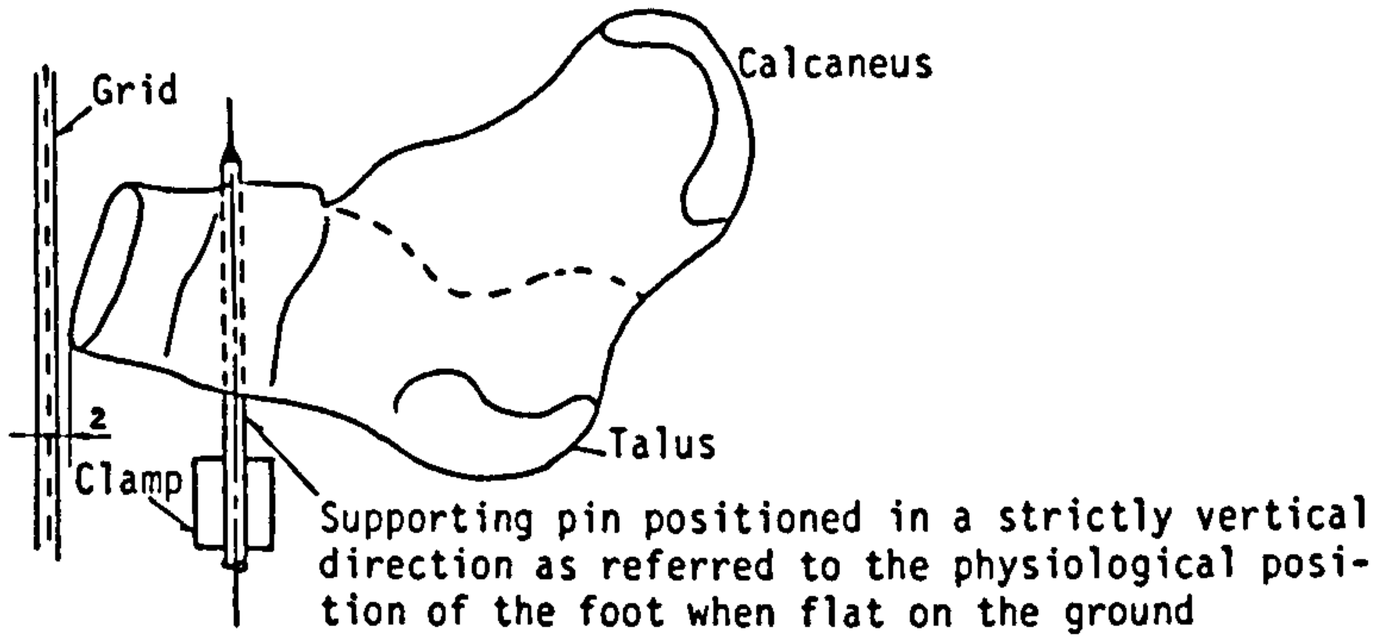

b) Position of the tarsus relative to the optical grid

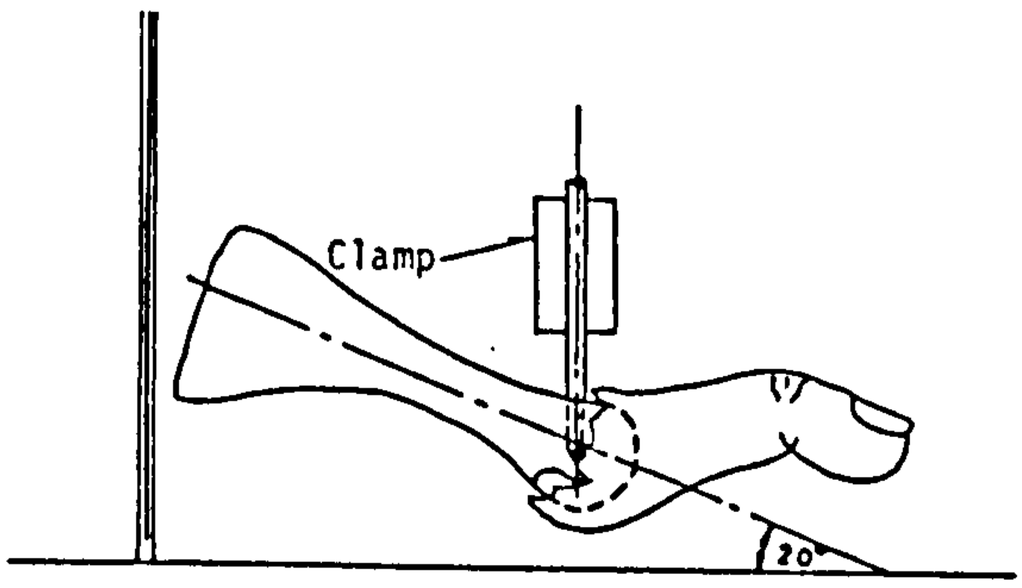

c) Position of the 1st metatarsal bone relative to the optical grid

2. Determination of distance between fringes:

Using programme MOIRE (Appendix 1(3)), results were obtained for up to n = 20 fringes, and between E_y = 60mm and F_y = 130 mm, this interval being divided into 5 parts. In the following sketch, only some of the results are illustrated:

Pitch of grid: 0.6 mm

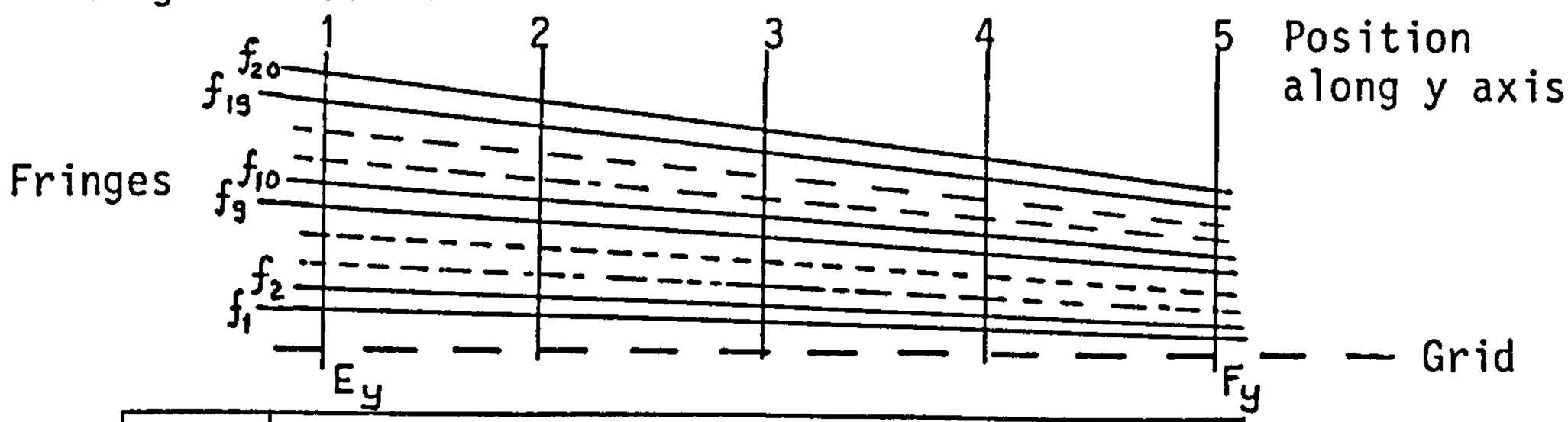

	Distance of fringe from grid				
	Pos.1	Pos.2	Pos.3	Pos.4	Pos.5
f_{20}	16.474	16.367	16.263	16.159	16.057
f_{19}	15.654	15.553	15.453	15.355	15.258
f_{10}	8.307	8.253	8.200	8.148	8.097
f_9	7.493	7.445	7.397	7.351	7.304
f_2	1.818	1.806	1.795	1.783	1.772
f_1	1.010	1.003	0.997	0.990	0.984

Therefore, for the middle 30 mm of space between E_y and F_y that had been occupied by the object surface, the mean value used for the distance between fringes (from (f_2-f_1)= 0.798 to $(f_{20}-f_{19})$= 0.810) was 0.804 mm. [See foot note*]

3. Determination of topography:

On selecting planes of intersection with the object surface as shown in figures 4.6a and 4.6b, and using the picture of mm graph paper that had been photographed and enlarged in the same way as the object surface (see Chapter 3, Section 3.2.2 and figure 3.4) the true dimensions of the object surface in the plane of the photograph were determined.

Programme AUSGL.POL (Appendix 3(3)) was used to find the best fitting polynomial that passes through a set of points lying on an intersecting plane of choice. Most often a polynomial of 3rd degree was found adequate, but occasionally one of up to 5th degree was found necessary. Figure 4.7 illustrates the computer plottings. Knowing the coefficients of the polynomial, differentiation was performed after which substitution of x in the following equation was made to arrive at the radius of curvature at any desired point corresponding to x:

$y = f(x)$:

$$r = \frac{\sqrt{\left[1 + \left(\frac{dy}{dx}\right)^2\right]^3}}{\frac{d^2y}{dx^2}}$$

---

* If the other values that were obtained for the positions of camera and light source had been employed instead (for example: camera x=1183, y=88; light source x=2107, y=1682), (f_2-f_1) would have resulted in 0.7961 and $(f_{20}-f_{19})$ in 0.8068 mm. Certainly of negligible difference to the values that were used !

APPENDIX 1(5)

Determination of coordinates of a point in a distorted picture coordinate system *

- Programme DIGXY.FLM -

Given:

- The true u,v coordinates of four corner points of a known, general quadrilateral on the distorted picture
- The x,y coordinates of the same corner points as read off a measuring device
- The x,y coordinates of any other points P1---Pn,either within or immediately outside the known quadrilateral field, also read off the measuring device.

Required:

- The true u,v coordinates of the points P1 ---- Pn on the picture.

Solution:

Section 3.3.3 (fig 3.10) and Appendix 6(3) show the procedure adopted when the true u, v coordinates of corner points of a rectangle in the distorted picture are known.

The method to be presently described is based on first finding the x,y coordinates of the distorted rectangle that would share some common coordinates with the given, distorted quadrilateral.

Having found the x,y coordinates of the rectangle (in a non-distorted system uv) ABCD, the same procedure as described in Appendix 6(3) is followed to obtain the u,v coordinates of any point P. Therefore, the second part of programme DIGXY.FLM is identical with the already described DIGXY (Appendix 6(3)).

* See Appendix 6(3) for the special case in which the coordinates of all four corner points of a rectangle are known.

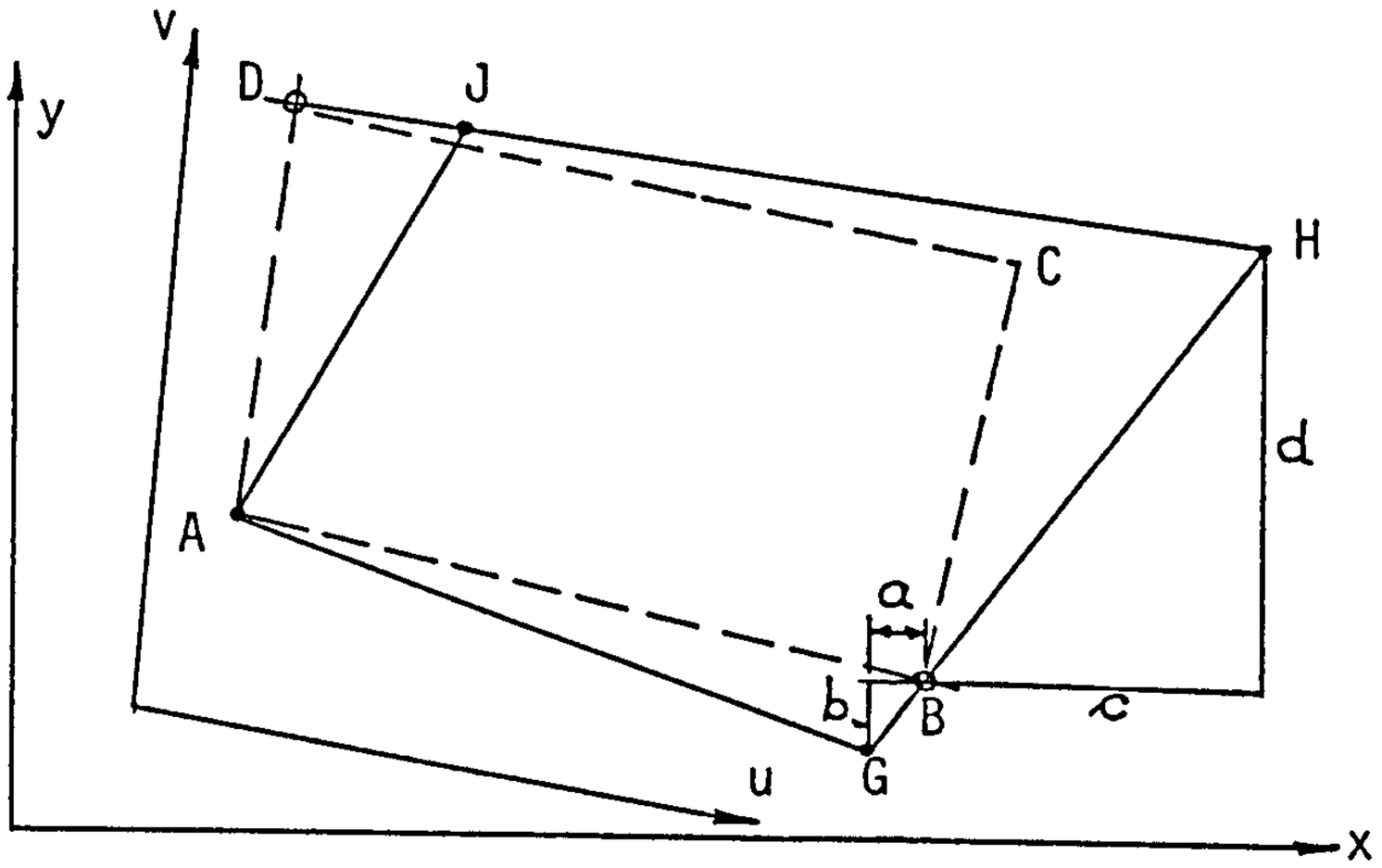

u, v : axes of linearly distorted picture system

x, y : axes of measuring device system

AGHJ is a given quadrilateral in the non-distorted uv system

ABCD would be a rectangle in the non-distorted uv system

The problem:

If $B_v = A_v$ and $D_u = A_u$

$B_u = ?$ $D_v = ?$

$B_x = ?$ $D_x = ?$

$B_y = ?$ $D_y = ?$

Also, if $C_u = B_u$ and $C_v = D_v$

$C_x = ?$ $C_y = ?$

Remark:

- In the following text, indices are typed on the same line in small letters, that is, for example: Av instead of the conventional A_v. Multiplication is always denoted by a point (.).

Procedure:

Scaling factors (f) are made use of to relate u with x coordinates, and v with y coordinates along lines HG, HJ, etc.

Step 1:

$$f1 = (Hy-Gy)/(Hv-Gv)$$

$$By = Gy + f1.(Av-Gv)$$

a = ?

$$\frac{a}{c} = \frac{b}{d} = K1 = (By-Gy)/(Hy-By)$$

$$c = \frac{a}{K1}$$

$$a + c = K2$$

$$a + \frac{a}{K1} = K2 = Hx-Gx$$

$$a = \frac{K1.K2}{K1+ 1} = K3$$

Bx = Gx + K3

f2 = (Gx-Ax)/(Gu-Au)

Bu = Gu + (K3/f2)

Step 2:

Similarly, f3 = (Hx-Jx)/(Hu-Ju)

Dx = Jx + f3.(Au-Ju)

K1 = (Dx-Jx)/(Hx-Dx)

K2 = Hy-Jy

K3 = (K1.K2)/(K1+ 1)

Dy = Jy + K3

f4 = (Jy-Ay)/(Jv-Av)

Dv = Jv + (K3/f4)

Step 3:

f5 = (Hy-By)/(Hv-Bv)

Cy = Hy + f5.(Dv-Hv)

f6 = (Hx-Dx)/(Hu-Du)

Cx = Hx + f6.(Bu-Hu)

As already mentioned, the results derived above serve to furnish the programme DIGXY with relevant information. The above procedure being readily adaptable for computer use, no flow diagram or listing is included.

APPENDIX 2(5)

Some details of the procedure followed in investigating movement of the mid-foot relative to the ground (approximates movement in the MP joints during the digitigrade phase) as described in Section 5.3 of Chapter 5.

The age, sex, weight and height of the ten test subjects were as follows:

No.	Initials	Sex	Age	Weight (N)	Height (cm)
1	E.B.	f	25	670	172
2	M.B.	f	27	540	163
3	S.B.	f	22	650	166
4	S.D.	f	27	690	170
5	H.J.	m	50	580	172
6	M.Sch.	m	27	720	176
7	U.Sch.	f	26	530	168
8	J.S.	m	33	700	176
9	E.W.	m	31	710	180
10	K.Z.	f	28	580	172

As mentioned in Section 5.3, in the case of two subjects (E.W. and K.Z.) the positions of the markers M1, M2 and M3 were recorded about every 40 ms (every 6th frame). Figure a) shows the path taken by the projections of marker M2 in the zx and yz planes with time as parameter in the case of test subject E.W. Also marked in are the instants 45% GC, 55% GC and 62% GC. Polynomials of 7th degree were used to fit curves to the series of points measured.

Figure b) shows how the spatial positions of the markers were determined from their projections on the zx and yz planes at instants t(45%), t(55%) and t(62%). Also shown in figure b) are the outputs of programme HELIROD.J for the intervals t(45%) to t(55%) and t(55%) to t(62%),

giving details of the corresponding helical axes.

Finally, figure c) shows an outline of E.W.'s foot with the anatomical landmarks A and B marked in, and also the positions of the helical axes as obtained above. Note must be particularly taken of the small amount of translation along the helical axis (0.7 mm from t(45%) to t(55%) and 4.8 mm from t(55%) to t(62%). [See Section 5.3.3 for comment on the position of the helical axis during the phase t(55%) to t(62%)].Furthermore, note that the helical axes are practically normal to the z axis,as can be judged by the extremely small values of the 'k' components of the direction vectors (output of HELIROD.J in figure b)).

(Appendix 2(5))

Projection of marker 'M2' in the ZX plane:

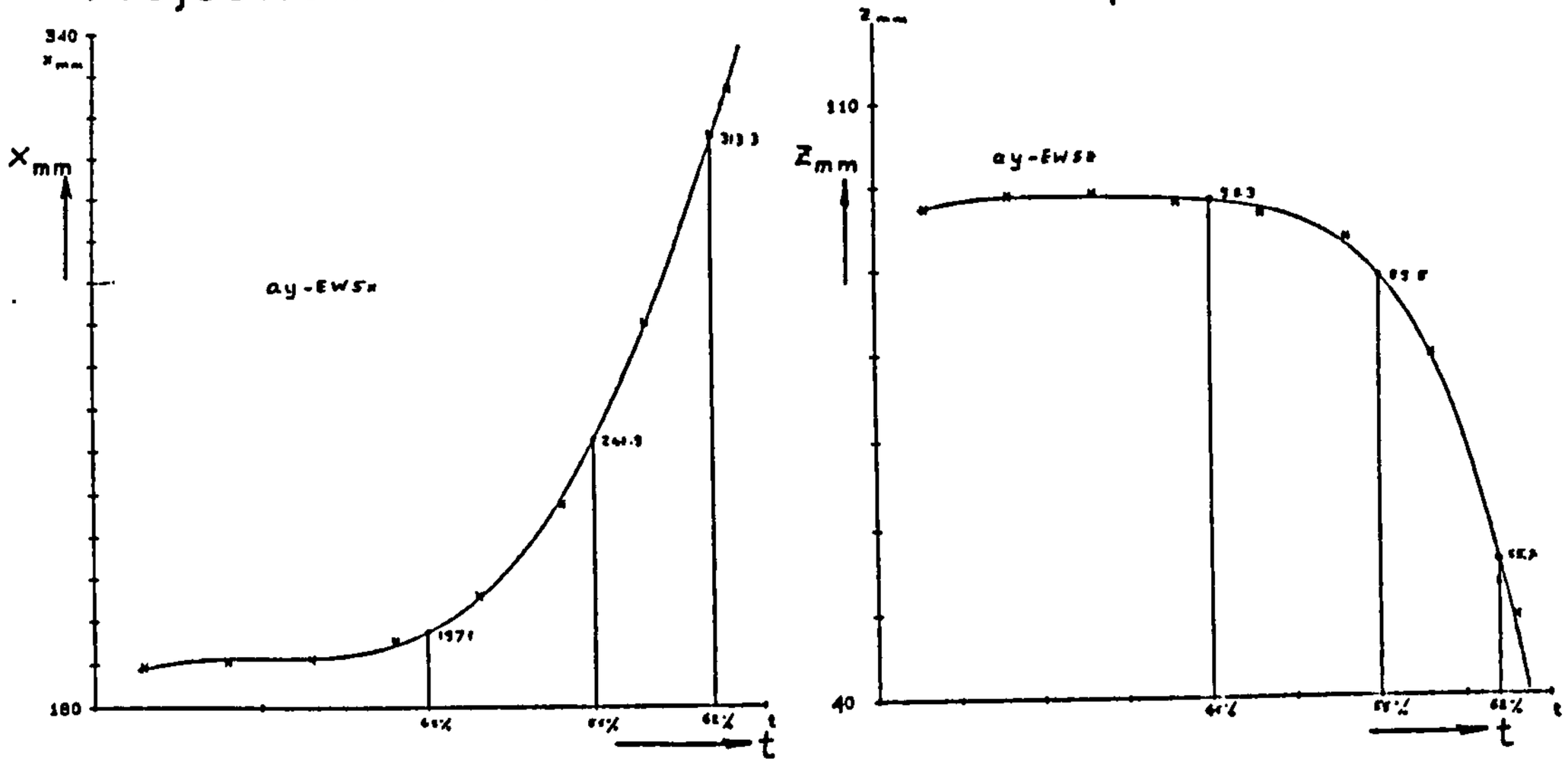

Projection of marker 'M2' in the YZ plane:

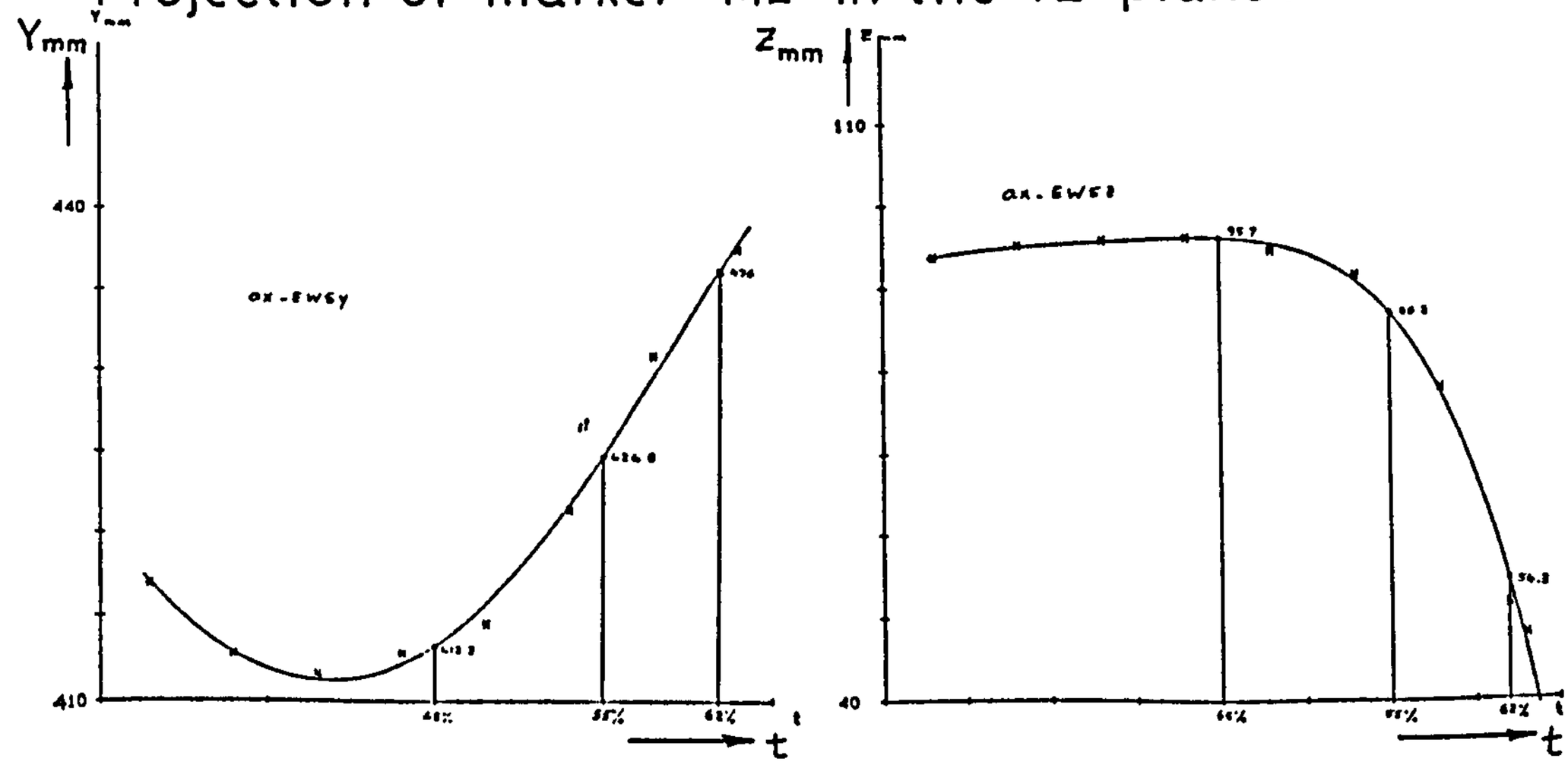

a): Coordinates of projections of a single marker versus time. Three points on each graph have been chosen corresponding to 45%, 55%, and 62% of the gait cycle.

Marker No.	Coordinates of projections in ZX plane		in YZ plane		True spatial coordinates*			
	Z	X	Y	Z	X	Y	Z	
M1	32.4	196.1	443.1	31.5	158.37	429.27	36.24	at 45% GC
M2	98.3	197.1	413.3	95.7	161.78	400.51	96.69	
M3	85.7	161.4	344.8	83.8	134.49	336.7	85.19	
M1	25.2	221.1	449.3	24.5	180.51	433.23	29.96	at 55% GC
M2	89.5	241.9	424.8	86.2	201.67	408.22	88.33	
M3	90.7	204.3	355	88.1	173.38	344.08	89.72	
M1	10	262.1	453.6	9.3	217.32	434	16.46	at 62% GC
M2	55.7	313.3	436	54.3	265.73	413.34	58.53	
M3	77.1	282.9	366	74.3	245.11	349.82	77.33	

* Calculated from positions of cameras (one camera is virtual, the other true), as follows:
- camera opposite YZ plane at: 3636 x, 126 y, 118 z
- camera opposite ZX plane at: -184 x, 4322 y, 81 z

Table showing derivation of spatial coordinates from those of the projections

HELIROD.J

AX1= 158.37 AY1= 429.27 AZ1= 36.24
BX1= 161.78 BY1= 400.51 BZ1= 96.68999
CX1= 134.49 CY1= 336.7 CZ1= 85.18999

Between 45% GC and 55% GC

AX2= 180.51 AY2= 433.23 AZ2= 29.96
BX2= 201.67 BY2= 408.22 BZ2= 88.33
CX2= 173.38 CY2= 344.08 CZ2= 89.72

FHI= +/- 17.29861 Grad **R**

Einsvektor der Schraubungsachse :
.2056771 *i + -.9785776 *j + -9.100088E-03 *k **D**

Ganghöhe = .7356792 **T**

Ortsvektor der Schraubungsachse :
149.1973 *i + 427.3067 *j + -40.79496 *k **P**

AX1= 180.51 AY1= 433.23 AZ1= 29.96
BX1= 201.67 BY1= 408.22 BZ1= 88.33
CX1= 173.38 CY1= 344.08 CZ1= 89.72

Between 55% GC and 62% GC

AX2= 217.32 AY2= 434 AZ2= 16.46
BX2= 265.73 BY2= 413.34 BZ2= 58.53
CX2= 245.11 CY2= 349.82 CZ2= 77.33

FHI= +/- 30.03019 Grad **R**

Einsvektor der Schraubungsachse :
.1417003 *i + -.9895362 *j + -.0271858 *k **D**

Ganghöhe = 4.821052 **T**

Ortsvektor der Schraubungsachse :
174.316 *i + 429.5292 *j + -44.95704 *k **P**

Print-outs of programme HELIROD.J :

D= direction of helical axis (unit vector)
P= position vector
R= angular motion in degrees
T= translatory motion in mm

(Appendix 2(5))

b) An example of the procedure in determining the helical axis of motion

(Appendix 2(5))

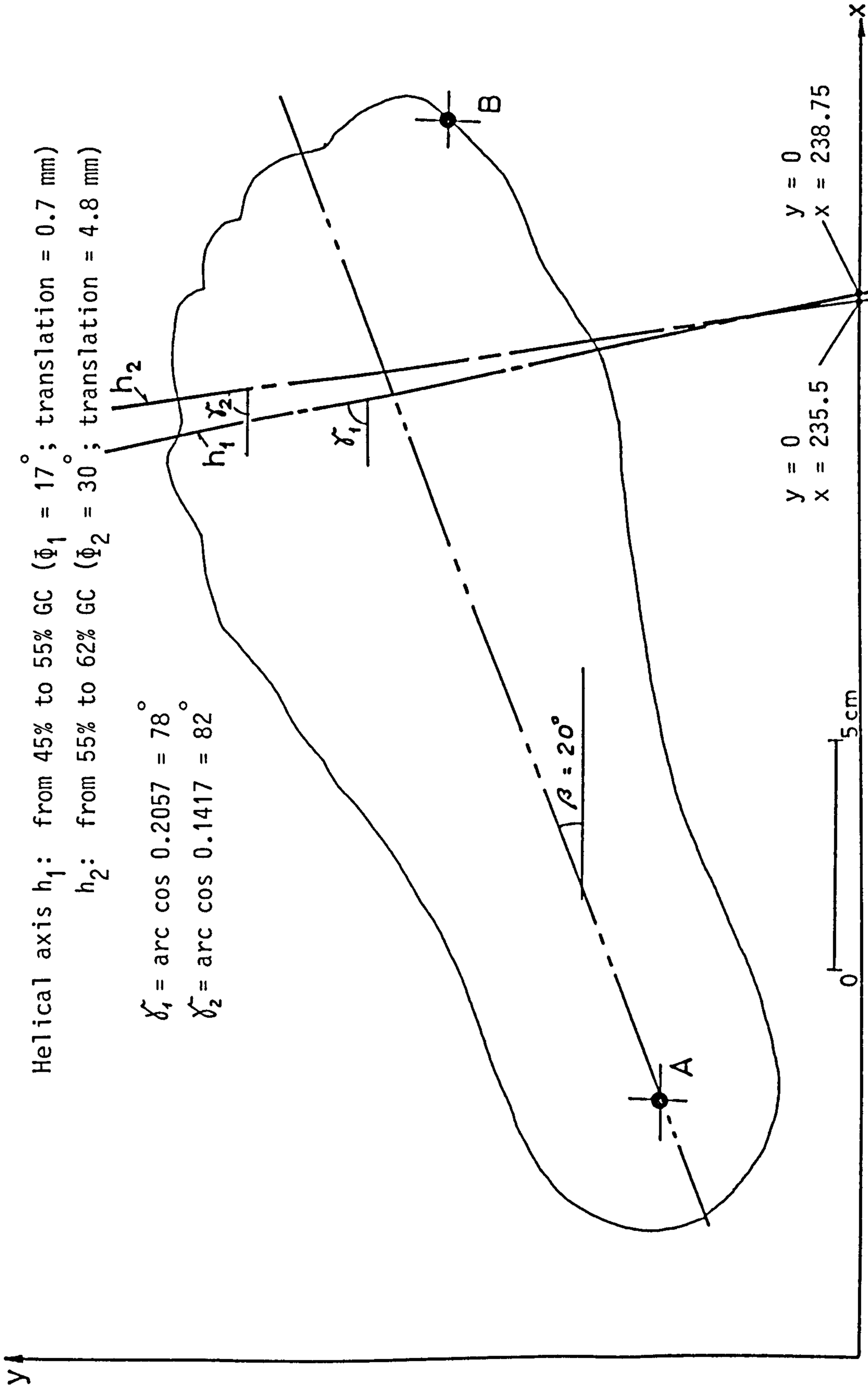

c) Outline of E.W.'s foot with A and B positioned in the xy plane. The positions of the helical axes in the xy plane were determined by finding the corresponding x values when y = 0, using the vector equations obtained from HELIROD.J.